Predation in the Cambrian

Stephen Pates

(OSS Student ID: 847244)

St Catherine's College

Department of Zoology

University of Oxford

Thesis submitted for the degree of Doctor of Philosophy

Submitted November 2018

Examined January 2019

Resubmitted February 2019

Acknowledgements

I have been extremely fortunate to have met, worked with, and enjoyed the company of very kind, generous, and intelligent people over the 3+ years of this DPhil. Without this network of support, both academic and personal, there is no way in which I would have managed to complete my thesis, let alone have enjoyed it so much.

I am immensely grateful to Allison Daley, for her mentorship, positivity, and sharing the knowledge from her giant brain, and Peter Holland, for his additional support and advice. The friendship and camaraderie of the ANOM, Holland, and Shimeld labs, alongside the Oxford Palaeoclub, made my working environments in Lausanne and Oxford incredibly positive and supportive. In particular I would like to thank Harrie Drage for sharing the ups, downs, and emigrations.

One of my favourite aspects of this research was the collaborative network of local and international researchers I had the privilege to work with. I would like to thank all of you for involving me in projects, and contributing to those that I was leading. I would also like to thank the support of staff at the Department of Zoology in Oxford, ISTE in UNIL, and at all the museums and institutes I visited, and acknowledge my funding, an Oxford-St Catherine's Brade-Natural Motion Scholarship.

I would like to recognise the support of my friends and family. From the Cambridge diaspora, Catz MCR Football, and Pri's Pals, you have provided distractions, entertainment, and empathy, when I really needed them. Finally heartfelt thanks are due to Heather Plumpton for the countless ways you have made my life better over more than just the last 3 years.

Table of contents

List of figures

Chapter 7: Systematics, preservation, and biogeography of radiodonts from the southern Great Basin, USA, during the upper Dyeran (Cambrian Series 2, Stage 4)

Chapter 8: The hurdiid *Ursulinacaris* nov. identifies two ancestral characters of radiodont frontal appendages

Chapter 9: The evolution of the hurdiid frontal appendage, and a novel phylogenetic hypothesis for radiodont families

Chapter 10: Analysis of the diversity and disparity of Radiodonta reveals two phases of evolution within the group

Chapter 12: Quantitative analysis of repaired and unrepaired damage to trilobites from the Cambrian (Stage 4-Drumian) Iberian Chains, NE Spain

Chapter 13: Elongated thoracic spines as potential predatory deterrents in olenelline trilobites from the lower Cambrian of Nevada

Abstract

Although predation has been suggested repeatedly as a force shaping the diversification of animals during the Cambrian period, studies of the evolutionary dynamics of predation are lacking from this time period. Radiodonta, the largest Cambrian nektonic animals, and repaired injuries on trilobites, a diverse and disparate group of prey animals, provide study systems to assess predation dynamics at this time. Radiodont fossils were first discovered over 100 years ago, but are now known worldwide from early Palaeozoic deposits which preserve soft-bodied material. Intense research on radiodonts from the Chengjiang biota (China) and Burgess Shale (Canada) since 2009 recently greatly improved our knowledge of the group, outdating previous interpretations of USA specimens, which are needed for large-scale analyses. Anecdotal reports of repaired injuries on trilobites are common in the literature, but quantitative studies on the role of morphology, behaviour, or geography have not been conducted.

I restudied radiodonts from the USA, placed them into an up to date taxonomic and taphonomic context, and revealed that these deposits hold a much higher diversity and disparity than previously reported. Findings include the first and last appearances of a number of families worldwide, and eight taxa not known from any other deposit. I used this new data to undertake the most comprehensive phylogenetic analysis and the first diversity and disparity analyses of Radiodonta, which showed two phases of evolution in the group, and that the ancestral radiodont was likely not a raptorial predator. I also performed the first quantitative measurements of predation pressure on trilobites, showing that morphology, geography, and behaviour, effect on the location and frequency of repaired injuries. These results suggest that predation pressure was a complex and changeable ecological influencing the early evolution of animals.

Chapter 1

Introduction: Predation in the Cambrian

Introduction: Predation in the Cambrian

The rapid diversification of animals during the Cambrian period, over 540 million years ago, dramatically transformed the functioning of the biosphere. This event, called the Cambrian Explosion, saw the emergence of stem and crown groups (Budd & Jensen 2000) and is recorded in the fossil record by a rapid and large increase in metazoan diversity and disparity (Marshall 2006; Lee et al. 2013; Na & Kiessling 2015) alongside the convergent development of mineralised exoskeletons in a number of groups (Murdock & Donoghue 2011; Wood & Zhuravlev 2012). Explanations for the Cambrian explosion include environmental changes, modification of genetic or developmental capacity of taxa, and ecological interactions (Marshall 2006), though it was likely a combination of these interlinked and codependent factors (e.g. Erwin et al. 2011; Smith & Harper 2013; Zhang et al. 2014).

Escalation (Vermeij 1987) and coevolution (Slatkin & Maynard Smith 1979) offer theoretical explanations for the role that predation played in shaping the Cambrian Explosion (Vermeij 1989; Bengtson 2002; Babcock 2003; Knoll 2003; Wood & Zhuravlev 2012; Erwin & Valentine 2013; Sperling et al. 2013). Escalation proposes that the most important agents of natural selection among organisms are enemies (competitors, predators, and prey that pose a danger to their predators) (Vermeij 1987, 1994). Responses to enemies can lead to adaptations and longer-term evolutionary trends in the morphology and behaviour of animals (Vermeij 1987, 1994). If two interacting parties are mutual enemies, then escalation and coevolution are equivalent (Vermeij 1994). Broadly, coevolution requires the reciprocal evolution of two interacting parties

(enemies or mutual beneficiaries). Many examples of specialised offensive, defensive, and sensory features in predators and prey animals are evident by Cambrian Series 2, around 520 million years ago (e.g. Lee et al. 2011; Murdock & Donoghue 2011; Paterson et al. 2011; Wood & Zhuravlev 2012) offering support for the role of predation in shaping morphological innovations as part of the Cambrian radiation.

Cambrian-aged predation traces are well known (reviewed in Bicknell & Paterson 2018; Vinn 2018) and consist of qualitative observations and descriptions of gut contents, coprolites, and isolated examples of repaired injuries or drill-holes. These provide direct support for Cambrian predation and/or scavenging, but cannot provide systematically-collected quantitative measurements that can be used to test hypotheses with statistical analyses (Harper 2016). The frequency of drilled or repaired prey offer the best opportunity for quantitative data for testing predation-related hypotheses (Harper 2016). In the Cambrian period, there are few suitable studies providing such data, despite the repeated invocation of predation as a primary influence on evolution during this time period (Leighton 2011). These few studies have used brachiopods (e.g. Zhang et al. 2011; Peel 2015) and helcionellid molluscs (Vendrasco et al. 2011) as study animals. Despite having been used to explore stereotypy (clustering of attack locations on prey exoskeletons) (Babcock & Robison 1989; Babcock 1993, 2003), Cambrian trilobites have never before been used to study predation intensity in the fossil record, but have been suggested as a highly suitable system (Leighton 2011). This absence of data on trilobite predation intensity is striking, because the group has a high diversity, disparity, and abundance of fossils in the early Palaeozoic (Foote 1991; Adrain et al. 1998; Webster 2007), and there are numerous anecdotal reports of trilobites with repaired injuries (reviewed in Owen 1985; Babcock

1993; Bicknell & Paterson 2018). Asymmetric ‘U’, ‘V’ and ‘W’ shaped injuries dominate the trilobite record, alongside shortened single spines, and are known in the Cambrian from Series 2 (the oldest trilobites) to the Furongian (Bicknell & Paterson 2018).

I provide the first quantitative measurements of predation intensity on trilobites (Chapters 12 and 13), by developing a new method to compare repair frequencies of different sample sizes (Chapter 12) and testing the role of morphology (spines) as a predator deterrent (Chapter 13). These case-studies provide novel methods that can be used to provide comparative data on predation intensity on trilobites across the Palaeozoic, for the testing of longer-scale macro evolutionary hypotheses.

Cambrian examples of injured trilobites and fragments in coprolites are often attributed to radiodonts (e.g. Rudkin 1979; Conway Morris & Jenkins 1985; Babcock & Robison 1989; Nedin 1999; English & Babcock 2010; Zamora et al. 2011; Kimmig & Strotz 2017 – see Bicknell & Paterson 2018, tables 1, 4 for summary), a diverse group of stem-lineage euarthropods best known from the Burgess Shale animal *Anomalocaris canadensis* (e.g. Whittington & Briggs 1985; Daley et al. 2009; Daley & Edgecombe 2014). To determine whether radiodonts were responsible for trilobite injuries and coprolites, and to understand their potential role in shaping Cambrian ecosystems, radiodont diversity and disparity needs to be fully explored and quantified.

Radiodonts are known from soft-bodied deposits (*Lagerstätten*) worldwide, and include the largest nektonic Cambrian apex raptorial predators (e.g. Whittington & Briggs 1985; Chen et al. 1994; Hou et al. 1995; Daley & Edgecombe 2014), but also sediment sifters (e.g. Daley et al. 2009, 2013) and filter feeders (e.g. Vinther et al. 2014; Van Roy et al. 2015; Lerosey-Aubril & Pates 2018). Most studies on this group have focussed on taxa from the Series 2, Stage 3-aged Chengjiang biota, South China (e.g.

Chen et al. 1994; Hou et al. 1995; Cong et al. 2014, 2016, 2017, 2018; Guo et al. 2018; Liu et al. 2018) and the Miaolingian, Wulian aged Burgess Shale, British Columbia, Canada (e.g. Whittington & Briggs 1985; Collins 1996; Daley et al. 2009; Daley & Budd 2010; Daley et al. 2013; Daley & Edgecombe 2014). This uneven geographic and temporal sampling has presented an incomplete view of this major stem-euarthropod group, which can be distinguished by the presence of arthropodised paired frontal appendages, radial mouthparts constructed of large and small plates, a frontal carapace, and metameric body with paired lateral flaps. The uneven sampling has also produced uncertainty relating to the root cause for the differences in the constituent taxa of these two well-studied fossil *Lagerstätten* (e.g. time, geography). Other Cambrian-aged fossil *Lagerstätten*, such as the Great Basin (southwestern USA) and Kinzers Formation (eastern USA), provide opportunities to explore the diversity of Radiodonta at a higher temporal resolution within a constrained geographic area. These deposits therefore provide a potential basis for studies of the diversity and disparity of this group through time. However, these radiodonts (first described by: Briggs 1979; Briggs & Mount 1982; Conway Morris & Robison 1988; Lieberman 2003; Briggs et al. 2008) have not been taxonomically revised to align with the past 10 years of intense research on radiodonts, and so require restudy.

In this thesis I review the history of research, taxonomic identification, and potential of USA *Lagerstätten* for the study of radiodonts (Chapter 2), and place material from the Kinzers Formation (Pennsylvania, USA) (Chapter 3) and Great Basin (southwestern USA) (Chapters 4-8) into an up-to-date taxonomic, taphonomic, and ecological context. I use these new findings to provide a more comprehensive group of taxa for a phylogenetic analysis (Chapter 9) and a novel disparity analysis of the clade

(Chapter 10). These chapters show the stark differences in the diversity and disparity histories of individual radiodont families, and provide new evidence for how the frontal appendages of different families evolved.

References

Adrain, J. M., Fortey, R. A., & Westrop, S. R. (1998). Post-Cambrian trilobite diversity and evolutionary faunas. *Science*, 280(5371), 1922-1925.

Babcock, L. E., & Robison, R. A. (1989). Preferences of Palaeozoic predators. *Nature*, 337, 695-696.

Babcock, L. E. (1993). Trilobite malformations and the fossil record of behavioral asymmetry. *Journal of Paleontology*, 67(2), 217-229.

Babcock, L. E. (2003). Trilobites in Paleozoic predator-prey systems, and their role in reorganization of early Paleozoic ecosystems. *In* Predator—prey interactions in the fossil record (pp. 55-92). Springer, Boston, MA.

Bengtson, S. (2002). Origins and early evolution of predation. *The Paleontological Society Papers*, 8, 289-318.

Bicknell, R. D., & Paterson, J. R. (2018). Reappraising the early evidence of durophagy and drilling predation in the fossil record: implications for escalation and the Cambrian Explosion. *Biological Reviews*, 93(2), 754-784.

Briggs, D. E. (1979). *Anomalocaris*, the largest known Cambrian arthropod. *Palaeontology*, 22(3), 631-664.

Briggs, D. E., & Mount, J. D. (1982). The occurrence of the giant arthropod *Anomalocaris* in the Lower Cambrian of southern California, and the overall distribution of the genus. *Journal of Paleontology*, 56(5), 1112-1118.

Briggs, D. E., Lieberman, B. S., Hendricks, J. R., Halgedahl, S. L., & Jarrard, R. D. (2008). Middle Cambrian arthropods from Utah. *Journal of Paleontology*, 82(2), 238-254.

Budd, G. E., & Jensen, S. (2000). A critical reappraisal of the fossil record of the bilaterian phyla. *Biological Reviews*, 75(2), 253-295.

Chen, J. Y., Ramsköld, L., & Zhou, G. Q. (1994). Evidence for monophyly and arthropod affinity of Cambrian giant predators. *Science*, 264(5163), 1304-1308.

Collins, D. (1996). The "evolution" of *Anomalocaris* and its classification in the arthropod class Dinocarida (nov.) and order Radiodonta (nov.). *Journal of Paleontology*, 70(2), 280-293.

Cong, P., Ma, X., Hou, X., Edgecombe, G. D., & Strausfeld, N. J. (2014). Brain structure resolves the segmental affinity of anomalocaridid appendages. *Nature*, 513(7519), 538.

Cong, P., Daley, A. C., Edgecombe, G. D., Hou, X., & Chen, A. (2016). Morphology of the radiodontan *Lyrarapax* from the early Cambrian Chengjiang biota. *Journal of Paleontology*, 90(4), 663-671.

Cong, P., Daley, A. C., Edgecombe, G. D., & Hou, X. (2017). The functional head of the Cambrian radiodontan (stem-group Euarthropoda) *Amplectobelua symbrachiata*. *BMC Evolutionary Biology*, 17(1), 208.

Cong, P. Y., Edgecombe, G. D., Daley, A. C., Guo, J., Pates, S., & Hou, X. G. (2018). New radiodonts with gnathobase-like structures from the Cambrian Chengjiang biota and implications for the systematics of Radiodonta. *Papers in Palaeontology*, 4(4), 605-621.

Conway Morris, S., & Jenkins, R. J. F. (1985). Healed injuries in early Cambrian trilobites from South Australia. *Alcheringa*, 9(3), 167-177.

Conway Morris, S., & Robison, R. A. (1988). More soft-bodied animals and algae from the Middle Cambrian of Utah and British Columbia. *University of Kansas Paleontological Contributions*, 122, 1-48.

Daley, A. C., Budd, G. E., Caron, J. B., Edgecombe, G. D., & Collins, D. (2009). The Burgess Shale anomalocaridid *Hurdia* and its significance for early euarthropod evolution. *Science*, 323(5921), 1597-1600.

Daley, A. C., & Budd, G. E. (2010). New anomalocaridid appendages from the Burgess Shale, Canada. *Palaeontology*, 53(4), 721-738.

Daley, A. C., Budd, G. E., & Caron, J. B. (2013). Morphology and systematics of the anomalocaridid arthropod *Hurdia* from the Middle Cambrian of British Columbia and Utah. *Journal of Systematic Palaeontology*, 11(7), 743-787.

Daley, A. C., & Edgecombe, G. D. (2014). Morphology of *Anomalocaris canadensis* from the Burgess Shale. *Journal of Paleontology*, 88(1), 68-91.

English, A. M., & Babcock, L. E. (2010). Census of the Indian Springs Lagerstätte, Poleta Formation (Cambrian), western Nevada, USA. *Palaeogeography, Palaeoclimatology, Palaeoecology*, 295(1-2), 236-244.

Erwin, D. H., Laflamme, M., Tweedt, S. M., Sperling, E. A., Pisani, D., & Peterson, K. J. (2011). The Cambrian conundrum: early divergence and later ecological success in the early history of animals. *Science*, 334(6059), 1091-1097.

Erwin, D. H., & Valentine, J. W. (2013). The Cambrian Explosion: the construction of animal biodiversity. Greenwood Village, Colorado: Roberts and Company. 406pp.

Foote, M. (1991). Morphologic patterns of diversification: examples from trilobites. *Palaeontology*, 34(2), 461-485.

Guo, J., Pates, S., Cong, P., Daley, A. C., Edgecombe, G. D., Chen, T., & Hou, X. (2018). A new radiodont (stem Euarthropoda) frontal appendage with a mosaic of characters from the Cambrian (Series 2 Stage 3) Chengjiang biota. *Papers in Palaeontology*. Online early view, doi: 10.1002/spp2.1231

Harper, E. M. (2016). Uncovering the holes and cracks: from anecdote to testable hypotheses in predation studies. *Palaeontology*, 59(5), 597-609.

Hou, X-G., Bergström, J., & Ahlberg, P. (1995). *Anomalocaris* and other large animals in the Lower Cambrian Chengjiang fauna of southwest China. *GFF*, 117(3), 163-183.

Kimmig, J., & Strotz, L. C. (2017). Coprolites in mid-Cambrian (Series 2-3) Burgess Shale-type deposits of Nevada and Utah and their ecological implications. *Bulletin of Geosciences*, 92(3).

Knoll, A. H. (2003). Biomineralization and evolutionary history. *Reviews in mineralogy and geochemistry*, 54(1), 329-356.

Lee, M. S., Jago, J. B., García-Bellido, D. C., Edgecombe, G. D., Gehling, J. G., & Paterson, J. R. (2011). Modern optics in exceptionally preserved eyes of Early Cambrian arthropods from Australia. *Nature*, 474(7353), 631.

Lee, M. S., Soubrier, J., & Edgecombe, G. D. (2013). Rates of phenotypic and genomic evolution during the Cambrian explosion. *Current Biology*, 23(19), 1889-1895.

Leighton, L. R. (2011). Analyzing predation from the dawn of the Phanerozoic. *In* Quantifying the Evolution of Early Life (pp. 73-109). Springer, Dordrecht.

Lerosey-Aubril, R., & Pates, S. (2018). New suspension-feeding radiodont suggests evolution of microplanktivory in Cambrian macronekton. *Nature Communications*, 9(1), 3774.

Lieberman, B. S. (2003). A new soft-bodied fauna: the Pioche Formation of Nevada. *Journal of Paleontology*, 77(4), 674-690.

Liu, J., Lerosey-Aubril, R., Steiner, M., Dunlop, J. A., Shu, D., & Paterson, J. R. (2018). Origin of raptorial feeding in juvenile euarthropods revealed by a Cambrian radiodontan. *National Science Review*, nwy057. doi.org/10.1093/nsr/new057.

Marshall, C. R. (2006). Explaining the Cambrian "explosion" of animals. *Annual Review of Earth and Planetary Science*, 34, 355-384.

Murdock, D. J., & Donoghue, P. C. (2011). Evolutionary origins of animal skeletal biomineralization. *Cells Tissues Organs*, 194(2-4), 98-102.

Na, L., & Kiessling, W. (2015). Diversity partitioning during the Cambrian radiation. *Proceedings of the National Academy of Sciences*, 112(15), 4702-4706.

Nedin, C. (1999). *Anomalocaris* predation on nonmineralized and mineralized trilobites. *Geology*, 27(11), 987-990.

Owen, A. W. (1985). Trilobite abnormalities. *Earth and Environmental Science Transactions of The Royal Society of Edinburgh*, 76(2-3), 255-272.

Paterson, J. R., García-Bellido, D. C., Lee, M. S., Brock, G. A., Jago, J. B., & Edgecombe, G. D. (2011). Acute vision in the giant Cambrian predator *Anomalocaris* and the origin of compound eyes. *Nature*, 480(7376), 237.

Peel, J. S. (2015). Failed predation, commensalism and parasitism on lower Cambrian linguliformean brachiopods. *Alcheringa*, 39(2), 149-163.

Rudkin, D. M. (1979). Healed injuries in *Ogygopsis klotzi* (Trilobita) from the middle Cambrian of British Columbia. *Royal Ontario Museum Life Sciences Occasional Paper*, 32, 1-8.

Slatkin, M., & Maynard Smith, J. (1979). Models of coevolution. *The Quarterly Review of Biology*, 54(3), 233-263.

Smith, M. P., & Harper, D. A. (2013). Causes of the Cambrian explosion. *Science*, 341(6152), 1355-1356.

Sperling, E. A., Frieder, C. A., Raman, A. V., Girguis, P. R., Levin, L. A., & Knoll, A. H. (2013). Oxygen, ecology, and the Cambrian radiation of animals. *Proceedings of the National Academy of Sciences,* 110(33), 13446-13451.

Van Roy, P., Daley, A. C., & Briggs, D. E. (2015). Anomalocaridid trunk limb homology revealed by a giant filter-feeder with paired flaps. *Nature*, 522(7554), 77.

Vendrasco, M. J., Kouchinsky, A. V., Porter, S. M., & Fernandez, C. Z. (2011). Phylogeny and escalation in Mellopegma and other Cambrian molluscs. *Palaeontologia Electronica*, 14(2), 1-44.

Vermeij, G. J. (1987) Evolution and Escalation. Princeton University, Princeton. 527 pp.

Vermeij, G. J. (1989). The origin of skeletons. *PALAIOS*, 585-589.

Vermeij, G. J. (1994). The evolutionary interaction among species: selection, escalation, and coevolution. *Annual review of ecology and systematics*, 25(1), 219-236.

Vinn, O. (2018). Traces of predation in the Cambrian. *Historical Biology*, 30(8), 1043-1049.

Vinther, J., Stein, M., Longrich, N. R., & Harper, D. A. (2014). A suspension-feeding anomalocarid from the Early Cambrian. *Nature*, 507(7493), 496.

Webster, M. (2007). A Cambrian peak in morphological variation within trilobite species. *Science*, 317(5837), 499-502.

Whittington, H. B., & Briggs, D. E. G. (1985). The largest Cambrian animal, *Anomalocaris*, Burgess Shale, British-Columbia. *Philosophical Transactions of the Royal Society of London B,* 309(1141), 569-609.

Wood, R., & Zhuravlev, A. Y. (2012). Escalation and ecological selectively of mineralogy in the Cambrian Radiation of skeletons. *Earth-Science Reviews*, 115(4), 249-261.

Zamora, S., Mayoral, E., Esteve, J., Gámez-Vintaned, J. A., & Santos, A. (2011). Exoskeletal abnormalities in paradoxidid trilobites from the Cambrian of Spain, and a new type of bite trace. *Bulletin of Geosciences*, 86(3), 665-673.

Zhang, Z., Holmer, L. E., Robson, S. P., Hu, S., Wang, X., & Wang, H. (2011). First record of repaired durophagous shell damages in Early Cambrian lingulate brachiopods with preserved pedicles. *Palaeogeography, Palaeoclimatology, Palaeoecology*, 302(3-4), 206-212.

Zhang, X., Shu, D., Han, J., Zhang, Z., Liu, J., & Fu, D. (2014). Triggers for the Cambrian explosion: hypotheses and problems. *Gondwana Research*, 25(3), 896-909.

Chapter 2

Radiodonta: a primer on the history of research, identification of taxa, and opportunities presented by a redescription of USA specimens

Radiodonta: primer on the history of research, identification of taxa, and opportunities presented by a redescription of USA specimens

Abstract

Radiodonts, stem-euarthropods whose modern relatives include arachnids, crustaceans, and insects, are a group of Palaeozoic nektonic animals including the largest predators in the Cambrian. Fossils are rarely preserved as complete, articulated specimens, but are instead found as isolated parts of the body plan: paired arthropodised frontal appendages, mouthparts made of plates, compound eyes, dorsal cephalic sclerites and lateral carapace elements, metameric body, dorsal and ventral flaps, tail fan, and furcae. It is this disarticulated nature of the radiodont fossil record that is responsible for the lag between the first descriptions of material in the late 1800s and early 1900s and the recognition that the frontal appendages, mouthparts, and bodies belonged to a single animal based on the preparation and description of rare articulated material in the 1980s. This heralded the discovery of new sites bearing radiodont material, including a number of localities in the USA. The subsequent recognition of a high diversity and disparity of radiodont taxa, primarily from isolated frontal appendages, has focussed predominantly on material from the Chengjiang biota and Burgess Shale. The majority of these discoveries were from 2009 onwards; however, material from USA sites had not yet been redescribed and placed into this updated taxonomic context. Material from the Chengjiang and Burgess Shale has allowed the identification of four

families, Amplectobeluidae, Anomalocarididae, Hurdiidae, and Tamisiocarididae, which can be differentiated based on the morphology of mouthparts, frontal appendages, and other body parts. However the geographic and temporal distance between these famous *Lagerstätten* gives an incomplete view of the group. Radiodonts were first described from USA *Lagerstätten* in the 1920s and are known from *Lagerstätten* in the Great Basin (California, Nevada, Utah) and Pennsylvania. These USA *Lagerstätten* provide a high temporal resolution sampling for the group. Thus, the redescription of this material is timely, and required for studies of the diversity, disparity, geographic and temporal ranges of Radiodonta, and a better understanding of the dynamics of the evolution of radiodonts at this early time in animal history (around 520-480 million years ago).

Introduction

Radiodonts, nektonic Palaeozoic stem-euarthropods that ranged in size from under ten centimetres to over two meters, are now known to have occupied a variety of niches, from apex raptorial predators, to sediment sifters, to filter feeders (e.g. Whittington & Briggs 1985; Daley et al. 2009, 2013a, b; Daley & Edgecombe 2014; Cong et al. 2014; Vinther et al. 2014; Van Roy et al. 2015; Lerosey-Aubril & Pates 2018; Liu et al. 2018). These animals can be identified from their metameric body with paired flaps bearing transverse lines, arthropodised frontal appendages with endites on the ventral surface, frontal carapace material, and radial mouthparts comprised of large and small plates. The history of radiodont research can be separated into three waves: the first discoveries of partial material from the late 1800s until mid 1900s; the first descriptions of complete material from the 1970s to early 2000s; and the rapid expansion in the

knowledge of the diversity of the group and feeding strategies employed, from 2009 onwards (dates of description of radiodonts from *Lagerstätten* shown in Fig. 1). Although many species are currently only known from frontal appendages, our knowledge of the group is such that taxa can be identified to the family, genus, or even species level by frontal appendages alone. However our understanding of the group is inherently linked to the history of research, and, as such, material described from before 2009 is in need of re-examination, since so many new taxa and important characters have been described over the last ten years. A better understanding of this older material, analysed with new technologies and improved imaging techniques, will provide new anatomical information on these fossils, and the framework and raw data for studies of the phylogeny, diversity, and disparity, of this group during the Cambrian period.

Three major periods in radiodont research

The history of description of radiodonts can be broadly separated out into three main periods: pre-1960; 1975-2008; and 2009 onwards (Fig. 1). The first period included the first descriptions of the frontal appendages of *Anomalocaris canadensis* from material collected from the Mount Stephen Trilobite Beds (as the body of a phyllocarid – Whiteaves 1892), and the mouthparts and body of *Peytoia nathorsti* (as a jellyfish and sea cucumber, respectively – Walcott 1911), as well as large numbers of *Anomalocaris* specimens, from the first quarrying of the Burgess Shale by Walcott. Subsequent reconstructions and reinterpretations attempted to place the 'body' of *Anomalocaris* with suitable heads (summarized by Collins 1996), and Resser (Walcott's successor at the USNM) identified a new species from the Kinzers Formation, Pennsylvania

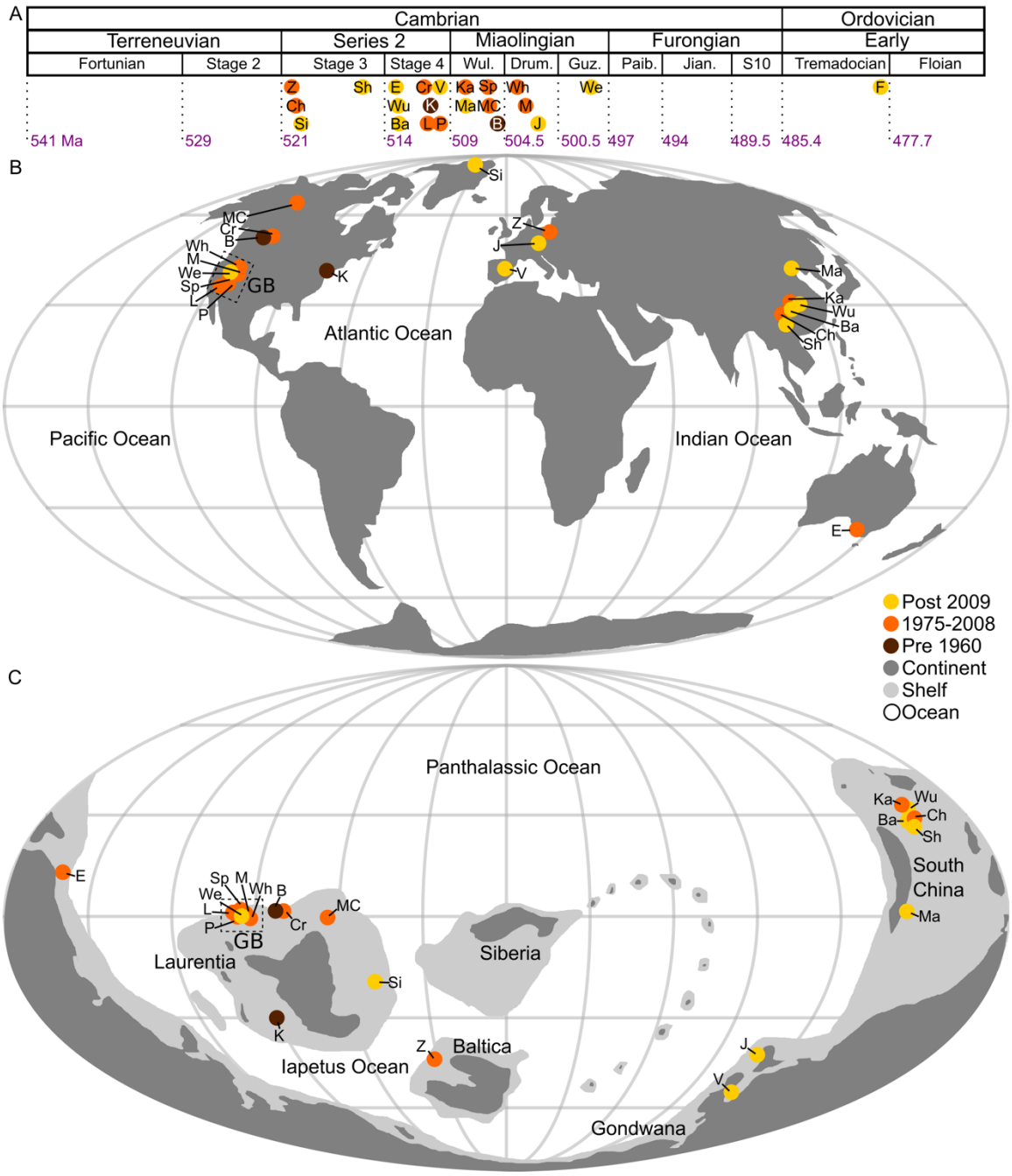

Fig. 1. Location of radiodont-bearing BSTs in time and space. Colour of dot indicates age of first radiodont discovery for that BST. **A.** BSTs placed on Cambrian and Early Ordovician timescale, purple numbers indicate ages of boundaries. **B.** BTS localities on a Present day geographic map. **C.** BTS localities on a palaeogeographic map reconstructed to 510 Ma using GPlates (Scotese 2016). Abbreviations on next page.

Abbreviations within timescale: Drum., Drumian; Guz., Guzhangian; Jian., Jiangshanian; Paib., Paibian; S 10, Stage 10; Wul., Wuliuan.

Abbreviations for radiodont-bearing BSTs: B, Burgess Shale; Ba, Balang Formation; Ch, Chengjiang biota; Cr, Cranbrook Shale; E, Emu Bay Shale; F, Fezouata biota; GB, Great Basin; J, Jince Formation; K, Kinzers Formation; Ka, Kaili biota; L, Latham Shale; M, Marjum Formation; Ma, Mantou Formation; MC, Mount Cap Formation; P, Pioche Formation; Sh, Shuijingtuo Formation; Si, Sirius Passet; Sp, Spence Shale; V, Valdemiedes Formation; We, Weeks Formation; Wh, Wheeler Formation; Wu, Wulongqing Formation; Z, Zawiszyn Formation.

(*Anomalocaris pennsylvanica* – Resser 1929), but radiodonts remained largely misunderstood during this time period.

The redescription of Walcott's material and further excavations of and near Walcott's quarry led to the first descriptions of complete radiodonts, with grasping appendages (*Anomalocaris canadensis*), mouthparts (*Peytoia nathorsti*), and a metameric body (Whittington & Briggs 1985). Previous to this Briggs (1979) hypothesized that *Anomalocaris* was the ambulatory appendage of a large arthropod (Simonetta & Delle Cave had raised this possibility in 1975, but preferred the interpretation that it was a body). This period also saw the identification of radiodonts, in the form of isolated frontal appendages, mouthparts, and complete bodies, from new sites worldwide (orange dots in Fig. 1B, C). These include a number of sites in the Great Basin (California, Nevada, Utah, USA; GB in Fig. 1) (Briggs & Mount 1982; Conway Morris & Robison 1982, 1988; Briggs & Robison 1984; Lieberman 2003; Briggs et al. 2008), and the Chengjiang biota (Chen et al. 1994; Hou et al. 1995) and Kaili biota in China (Zhao et al. 2005). Isolated appendages were reported from the Mount Cap biota, Canada (Butterfield & Nicholas 1996), Zawiszyn Formation, Poland (Dzik & Lendzion 1988, see also Daley & Legg 2015), and the Emu Bay Shale, Australia (McHenry & Yates 1993; Nedin 1995). Debate during this period centred around the affinities of radiodonts (Radiodonta was erected by Collins, 1996, referring to the radiating teeth of circular mouthparts, which at the time was a major distinguishing factor of all members of the order). Briggs (1979) originally suggested *Anomalocaris* was a large arthropod, though after the description of complete body specimens, Whittington & Briggs (1985) preferred a 'hitherto unknown phylum'. Hou et al. (1995) hypothesised an affinity with cycloneuralian worms, with later studies suggesting that radiodonts belonged to the

stem-group (Budd 2002), crown-group of (Chen et al. 2004), or sister to (Hou et al. 2006), euarthropods.

A phylogenetic analysis following the description of the fourth radiodont genus known from complete specimens, *Hurdia* (after *Anomalocaris, Amplectobelua,* and *Peytoia*), from material originally belonging to eight different taxa, established radiodonts as stem-euarthropods (Daley et al. 2009). This study also marks the beginning of the description of abundant new radiodont taxa, alongside detailed redescriptions, from the Burgess Shale (Daley & Budd 2010; Daley et al. 2013a; Daley & Edgecombe 2014) and nearby Stanley Glacier (Caron et al. 2010), as well as the Chengjiang biota (Cong et al. 2014, 2016, 2017, 2018; Guo et al. 2018). In total 14 new radiodont taxa were formally described after 2009, and an additional five were recognised as radiodonts for the first time (Table 1). Before 2009, only seven known radiodonts had been formally described (Table 1). This period also saw the first recognition and description of radiodonts from a number of new sites worldwide (yellow dots in Fig. 1): Greenland (Sirius Passet biota) from which a new genus *Tamisiocaris borealis* was described (Daley & Peel 2010); Czech Republic (Jince Formation – Daley et al. 2013a), USA (Weeks Formation – Lerosey-Aubril et al. 2014); and Morocco (Fezouata biota – Van Roy & Briggs 2011; Van Roy et al. 2015), from where the first Ordovician radiodonts, including the giant filter feeder *Aegirocassis benmoulai*, were described. New sites in China revealed additional radiodont material in the Shuijingtuo Formation, Mantou Formation, Balang Formation, and Wulongqing Formation (Huang et al. 2012; Liu 2013; Wang et al. 2013; Daley et al. 2013a). These new discoveries furthered our understanding of the evolution of euarthropods, including the origin of the compound eye and biramous limb (Paterson et al. 2011; Van

Table 1. List of named radiodont taxa, organised by family

	First description	Recognised as radiodont
Amplectobeluidae		
Amplectobelua stephensis	Daley & Budd 2010	Daley & Budd 2010
Amplectobelua symbrachiata	Hou et al. 1995	Hou et al. 1995
Lyrarapax trilobus	Cong et al. 2016	Cong et al. 2016
Lyrarapax unguispinus	Cong et al. 2014	Cong et al. 2014
Ramskoeldia consimilis	Cong et al. 2018	Cong et al. 2018
Ramskoeldia platyacantha	Cong et al. 2018	Cong et al. 2018
Anomalocarididae		
Anomalocaris canadensis	Whiteaves 1892	Briggs 1979; Whittington & Briggs 1985
Anomalocaris kunmingensis	Wang et al. 2013	Wang et al. 2013
Anomalocaris pennsylvanica	Resser 1929	Briggs 1979
Anomalocaris saron	Hou et al. 1995	Hou et al. 1995
Paranomalocaris multisegmentalis	Wang et al. 2013	Wang et al. 2013
Hurdiidae		
Aegirocassis benmoulai	Van Roy et al. 2015	Van Roy et al. 2015
Hurdia triangulata	Walcott 1912	Daley et al. 2009
Hurdia victoria	Walcott 1912	Daley et al. 2009
Pahvantia hastata	Robison & Richards 1981	Lerosey-Aubril & Pates 2018
Peytoia infercambriensis	Lendzion 1975	Dzik & Lendzion 1988; Daley & Legg 2015
Peytoia nathorsti	Walcott 1911	Whittington & Briggs 1985
Schinderhannes bartelsi	Kühl et al. 2009	Cong et al. 2014
Stanleycaris hirpex	Caron et al. 2010	Caron et al. 2010
Tamisiocarididae		
Anomalocaris briggsi	McHenry & Yates 1993	McHenry & Yates 1993
Tamisiocaris borealis	Daley & Peel 2010	Daley & Peel 2010
Unassigned		
Caryosyntrips serratus	Daley & Budd 2010	Daley & Budd 2010
Laminacaris chimera	Guo et al. 2018	Guo et al 2018
Uncertain		
Cucumericrus decoratus	Hou et al. 1995	Hou et al. 1995

Reference for date of first description and date of first recognition as a radiodont.

Roy et al. 2015), and also revealed that radiodonts employed a number of different ecological strategies, from raptorial predation (e.g. *Anomalocaris canadensis* and *Lyrarapax*– Daley & Edgecombe 2014; Cong et al. 2014, 2016; Liu et al. 2018), to sediment sifting (e.g. *Anomalocaris briggsi* and *Hurdia*– Daley et al. 2009, 2013a, b), to filter feeding (e.g. *Aegirocassis benmoulai* and *Tamisiocaris borealis* – Vinther et al. 2014; Van Roy et al. 2015), and slicing with paired appendages (*Caryosyntrips* – Daley & Budd 2010) (Tables 1, 2).

At the time I started this thesis, in October 2015, 19 named radiodont species were known, belonging to 13 genera. Although radiodonts were known from a number of sites in the USA (Fig. 1; Table 2), the only genera reported were *Anomalocaris* and *Peyotoia*, and many of these specimens were in open nomenclature (see Matthews 1973), indicating uncertainties relating to the identification of the material (Briggs 1979; Briggs & Mount 1982; Briggs & Robison 1984; Conway Morris & Robison 1982, 1988; Lieberman 2003; Briggs et al. 2008).

The radiodont body plan and family level identification

The complete radiodont bodyplan includes a head region with paired frontal appendages adjacent to a ventral mouth (and gnathobase-like-structures in some taxa), compound eyes, a carapace of one or three elements, a metameric body region with setal blades, ventral flaps (and additional dorsal flaps in some taxa), and sometimes a tail fan and/or furcae. Radiodont taxa are not equally well understood. The best known and most complete species are from the Chengjiang biota, Burgess Shale, and Fezouata biota, with many species and genera only known from frontal appendages, and perhaps additional carapace elements or mouthparts (Fig. 2).

Table 2. List of radiodont-bearing *Lagerstätten*, with Cambrian Stage, constituent families, and number of taxa known

	Age	Families	# taxa	References
Baltica				
Zawiszyn Formation	Stage 3	H	1	Lendzion 1975; Dzik & Lendzion 1988; Daley & Legg 2015
Gondwana				
Emu Bay Shale	Stage 4	An, T	2	McHenry & Yates 1993; Nedin 1995; Daley et al. 2013a
Jince Formation	Drumian	H	1	Daley et al. 2013b
Laurentia				
Sirius Passet	Stage 3	T	1	Daley & Peel 2010
Cranbrook Shale	Stage 4	An	1	Briggs 1979
Latham Shale	**Stage 4**	**An**	**1**	**Briggs & Mount 1982**
Kinzers Formation	**Stage 4**	**An, ?**	**2**	**Briggs 1979**
Pioche Formation	**Stage 4**	**An**	**2**	**Lieberman 2003**
Spence Shale	**Wuliuan**	**H**	**1**	**Briggs et al. 2008**
Mount Cap Formation	Wuliuan	?	1	Butterfield & Nicholas 1996
Burgess Shale	Wuliuan	Am, An, Ca, H	8	Daley & Budd 2010; Daley et al. 2013b; Pates & Daley 2017
Stanley Glacier	Wuliuan	An, H	3	Caron et al. 2010
Wheeler Formation	**Drumian**	**H**	**3**	**Briggs et al. 2008; Lerosey-Aubril & Pates 2018**
Marjum Formation	**Drumian**	**H**	**1**	**Briggs & Robison 1984; Conway Morris & Robison 1988**
Weeks Formation	**Guzhangian**	**An**	**2**	**Lerosey-Aubril et al. 2014**
South China				
Chengjiang	Stage 3	Am, An, Cu, ?	9	Chen et al. 1994; Hou et al. 1995; Cong et al. 2014, 2016, 2018; Guo et al. 2018
Shuijingtuo Formation	Stage 3	H	1	Daley et al. 2013b
Balang Formation	Stage 4	An, H	2	Liu 2013
Wulongqing Formation	Stage 4	An	2	Wang et al. 2013
Mantou Formation	Wuliuan	An(?)	1	Huang et al. 2012
Kaili biota	Wuliuan	An(?)	1	Zhao et al. 2005

USA sites in bold. Abbreviations: Am, amplectobeluid; An, anomalocaridid; Ca, *Caryosyntrips*; Cu, *Cucumericrus*; H, hurdiid; T, tamisiocaridid; ?, uncertain.

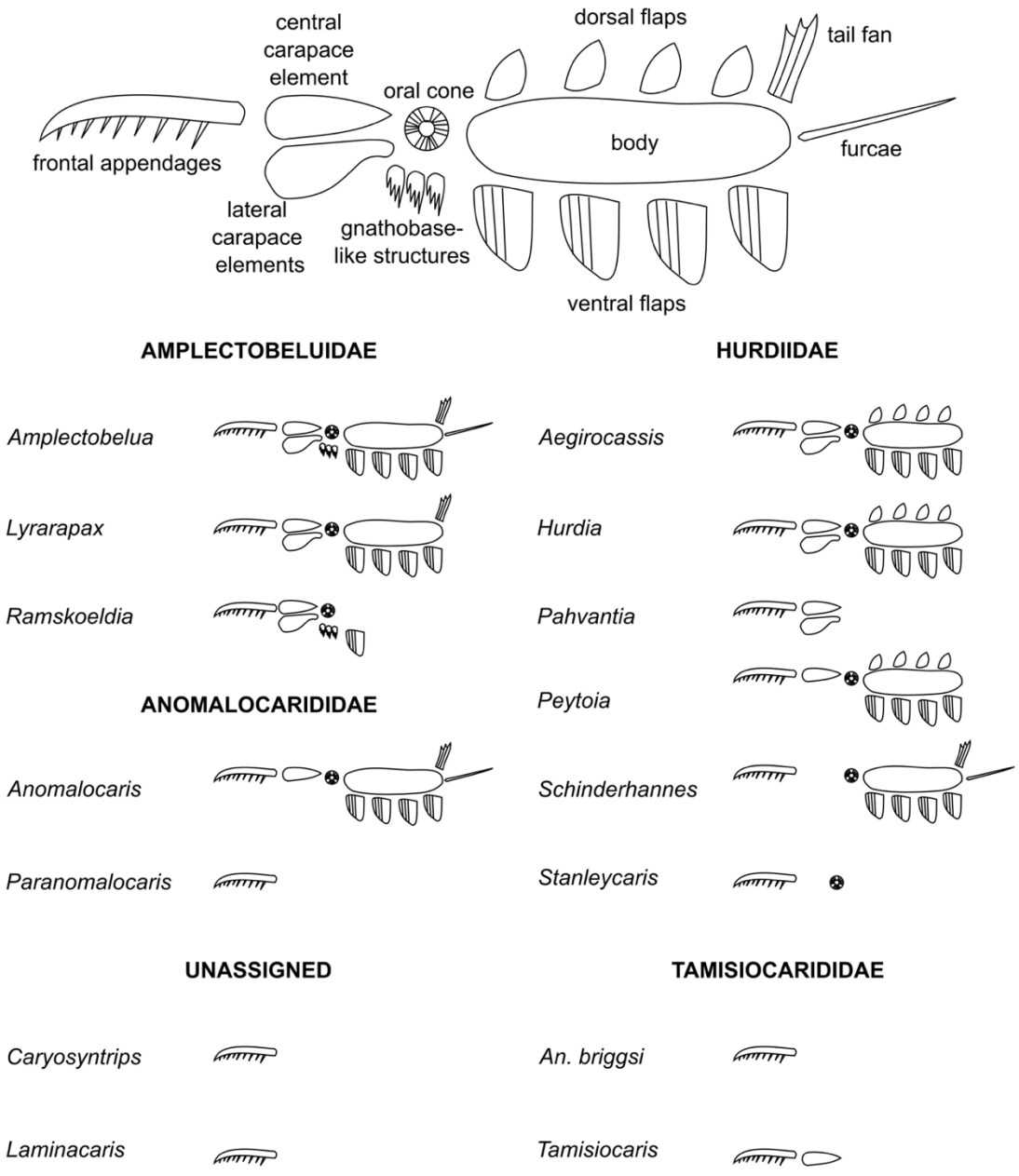

Fig. 2. Schematic showing all radiodont body parts at top. Body parts known in different radiodont genera, arranged by family, below. If a body part is known for a genus, this is indicated by its presence next to the genus name. If a body part is not known, this indicated by its absence next to the genus name. *Anomalocaris briggsi* is here considered separately to the other *Anomalocaris* species and as a member of the family Tamisiocarididae.

Since the first phylogenetic analyses examining internal radiodont relationships, four main families of radiodonts have been recognised (Amplectobeluidae, Anomalocarididae, Hurdiidae, and Tamisiocarididae). The genera *Caryosyntrips* and *Cucumericrus* have not resolved within any of these families (e.g. Vinther et al. 2014; Cong et al. 2014; Van Roy et al. 2015; Liu et al. 2018; Lerosey-Aubril & Pates 2018). With only a few exceptions relating to the overall similarities between some amplectobeluid and anomalocaridid frontal appendages, broad differences between the frontal appendages and mouthparts allow identification to the family level (Fig. 3), even from incomplete specimens, and distinctive features in other body parts are also recognisable and sometimes allow identification.

Organisation of Frontal appendages

Frontal appendages are the most commonly preserved body part, and broad organisational differences between the four families and *Caryosyntrips* allow identification to this taxonomic rank (Fig. 3; Table 3). Within families, finer differences between frontal appendage morphology allows identification to the species level (discussed below).

The frontal appendage (Fig. 3) can be separated into two regions. The ‘shaft’, which is not always preserved, is made of podomeres with generally weakly-visible boundaries between them. The ‘distal articulated region’ is more-often preserved. Podomere boundaries are more visible in this region, endites attach to the ventral surface of podomeres, either one or two per podomere, and on some podomeres spines also attach to the distal dorsal surface. The presence or absence, morphology, and arrangement of endites and dorsal spines, as well as number of podomeres in the

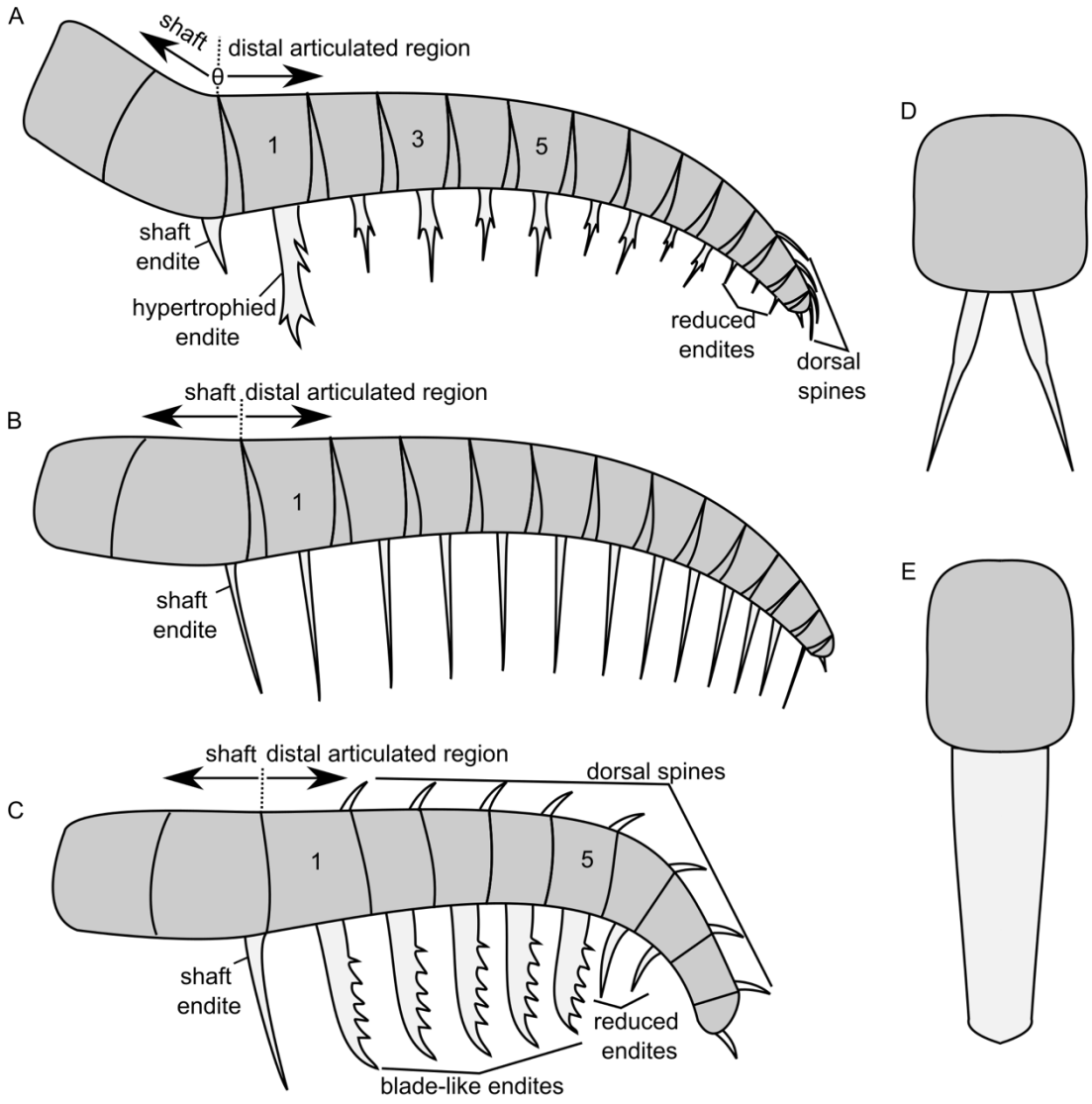

Fig. 3. Organisation of the radiodont frontal appendages of different families, showing key features. **A.** Amplectobeluidae and Anomalocarididae, 1 marks podomere bearing hypertrophied endite, 5 marks podomere where endite is longer that endite on 3 in amplectobeluids, but not anomalocaridids. θ marks angle between dorsal margin of shaft and distal articulated region. **B.** Tamisiocarididae. 1 marks first podomere in distal articulated region which can bear a hypterophied endite in *Anomalocaris briggsi*. **C.** Hurdiidae, 1 and 5 mark first and last podomere bearing a blade-like endite. **D.** Frontal view of endite-bearing podomere in Amplectobeluidae, Anomalocarididae, and Tamisiocarididae. **E.** Frontal view of endite bearing podomere in Hurdiidae.

Table 3. Major diagnostic features of the four radiodont families and *Caryosyntrips*

	Frontal appendages	Mouthparts	Other
Amplectobeluidae	- Enlarged or hypertrophied endite on first podomere in distal articulated region - Endites paired and broadly reduce in length along the appendage, alternating long/short on subsequent podomeres - Endite on fifth podomere in distal articulated region longer than that of the third - Thickened dorsal spines on distalmost podomeres	- Oral cone made of smooth and bumpy plates	- Gnathobase-like-structures on anterior three body metameres
Anomalocarididae	- Endite on first podomere in distal articulated region slightly enlarged - Endites paired and reduce in length along the appendage, alternating long/short on subsequent podomeres - Auxiliary spines on both distal and proximal margins of endites	- Triradial arrangement of three large plates arranged at 120°, with intermediate and small plates between each pair	
Caryosyntrips	- Triangular outline to frontal appendages - Small and simple spines paired on ventral surface of each podomere		
Hurdiidae	- Elongate endites on first five podomeres in distal articulated region only - Endites unpaired and blade-like - Auxiliary spines or setae on distal margin of endites only - Dorsal spines on every podomere in distal articulated region	- Tetraradial arrangement of four large plates arranged at 90°, with seven small plates between each pair (32 plates total)	- Two pairs of flaps present along the body (dorsal and ventral) unlike all other families where only ventral flaps are known
Tamisiocarididae	- Elongate endites on every podomere in distal articulated region except for the distalmost - Endites paired and reduce in length along the appendage without long/short alteration as seen in Amplectobeluidae and Anomalocarididae -Auxiliary spines on both distal and proximal margins of endites		

shaft and distal articulated region, provide the characters for taxonomic and phylogenetic studies, and broadly allow members of the four families to be distinguished (Fig. 3; Table 3).

Amplectobeluidae

Cong et al. (2018) considered *Amplectobelua* and *Ramskoeldia* to be the only currently-known amplectobeluids, with the presence of gnathobase-like structures a key character in identifying members of the group. A secondary character of the frontal appendages, the endite on the fifth podomere in the distal articulated region being longer than the third (5 in Fig. 3A), also unites *Amplectobelua* and *Ramskoeldia* (Cong et al. 2018). Liu et al. (2018) considered *Lyrarapax* to also be a member of this family (as originally proposed by Cong et al. 2014, but later reconsidered in Cong et al. 2018), with the morphology of the frontal appendage of key importance. All three genera bear a large or hypertrophied endite on the first podomere in the distal articulated region, and the shaft attaches to the distal articulated region at an angle lower than 180° (ϑ in Fig. 3A). Phylogenetic analyses (Cong et al. 2014; Van Roy et al. 2015; Liu et al. 2018; Lerosey-Aubril & Pates 2018) have all resolved *Lyrarapax* as a member of Amplectobeluidae (Table 1).

The frontal appendages of these three genera, and the species within them, can be distinguished based on the number of podomeres in the shaft and distal articulated region, the morphology of the large endite on the first podomere in the distal articulated region, and the number and morphology of dorsal spines (Fig. 4). *Ramskoeldia consimilis* and *R. platyacantha* both have 13 podomeres in the distal articulated region, *Amplectobelua stephenensis* and *A. symbrachiata* have 12, as does

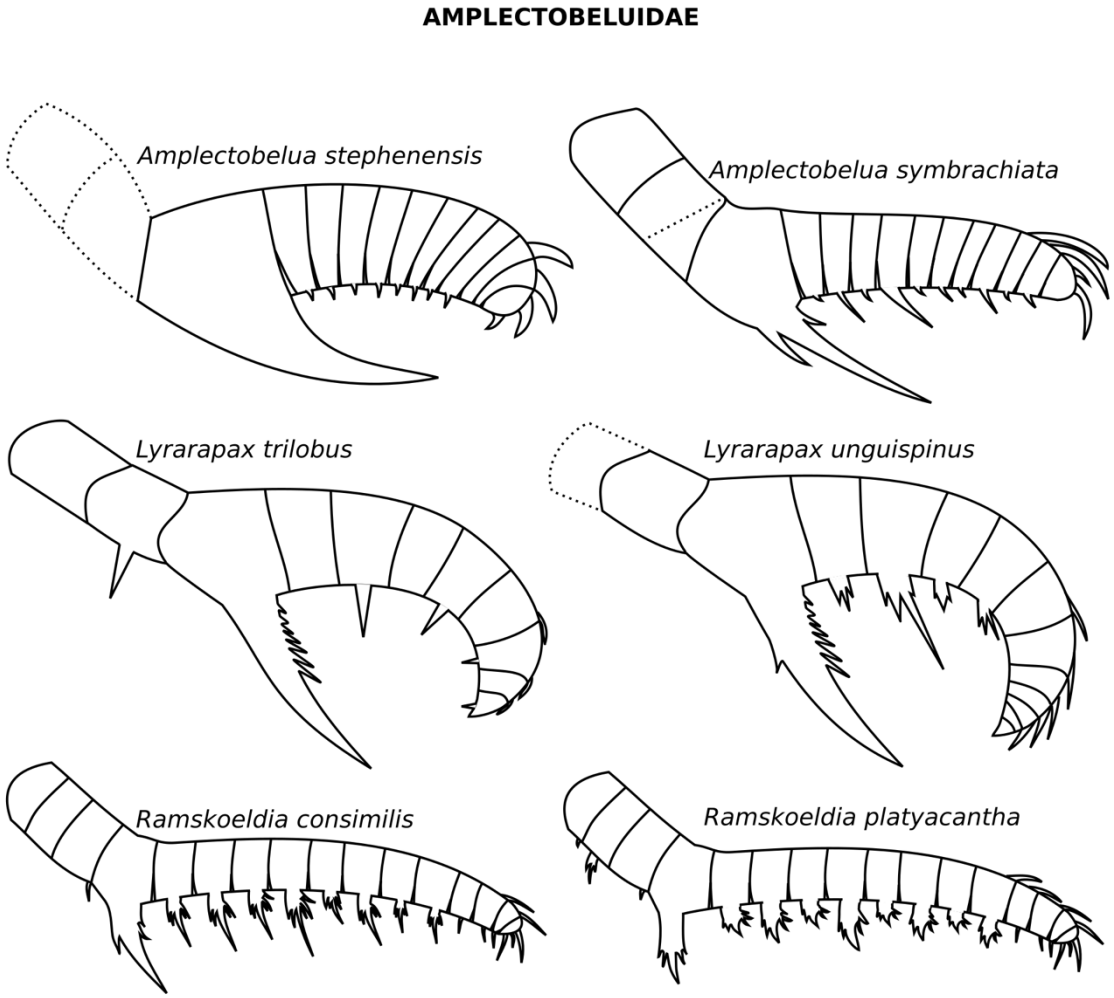

Fig. 4. Schematic frontal appendages of taxa belonging to Amplectobeluidae.

Lyrarapax unguispinus, whereas *L. trilobus* has at least nine (Daley & Budd 2010; Cong et al. 2014, 2016, 2017, 2018; Liu et al. 2018). The hypertrophied endite in *Amplectobelua* and *Lyrarapax* extends much further as a percentage of the total appendage length than in *Ramskoeldia*. In *Lyrarapax*, a number of smaller serrations line the distal margin, unlike in *Amplectobelua* and *Ramskoeldia,* where the endite on the first podomere in the distal articulated region bears a similar morphology to the endites along the rest of the appendage, but is curved distally and enlarged.

Anomalocarididae

Anomalocaris has repeatedly been resolved as polyphyletic by phylogenetic analyses (Table 1), with *Anomalocaris briggsi* as sister to *Tamisiocaris borealis*, in the family Tamisiocarididae (discussed below), and *Anomalocaris kunmingensis* within the amplectobeluids (Vinther et al. 2014; Cong et al. 2014; Van Roy et al. 2015; Liu et al. 2018; Lerosey-Aubril & Pates 2018). *Paranomalocaris* has been resolved within Anomalocarididae (Vinther et al. 2014) and also within a polytomy with a number of *Anomalocaris* species (Cong et al. 2014; Van Roy et al. 2015; Liu et al. 2018; Lerosey-Aubril & Pates 2018). All *A. briggsi* specimens likely belong to a new genus, and are tamisiocaridids. *Anomalocaris kunmingensis* possesses thirteen podomeres in the distal articulated region, and endites that alternate long/short on subsequent podomeres. A hypertrophied endite on the first podomere in the distal articulated region possesses a number of distally facing auxiliary spines, and a single proximal facing spine. In some specimens the endite on the fifth podomere in the distal articulated region is longer than that of the third (Wang et al. 2013, fig. 1g, h), which is a diagnostic feature of Amplectobeluidae (in this case, with 13 podomeres in the distal articulated region, like

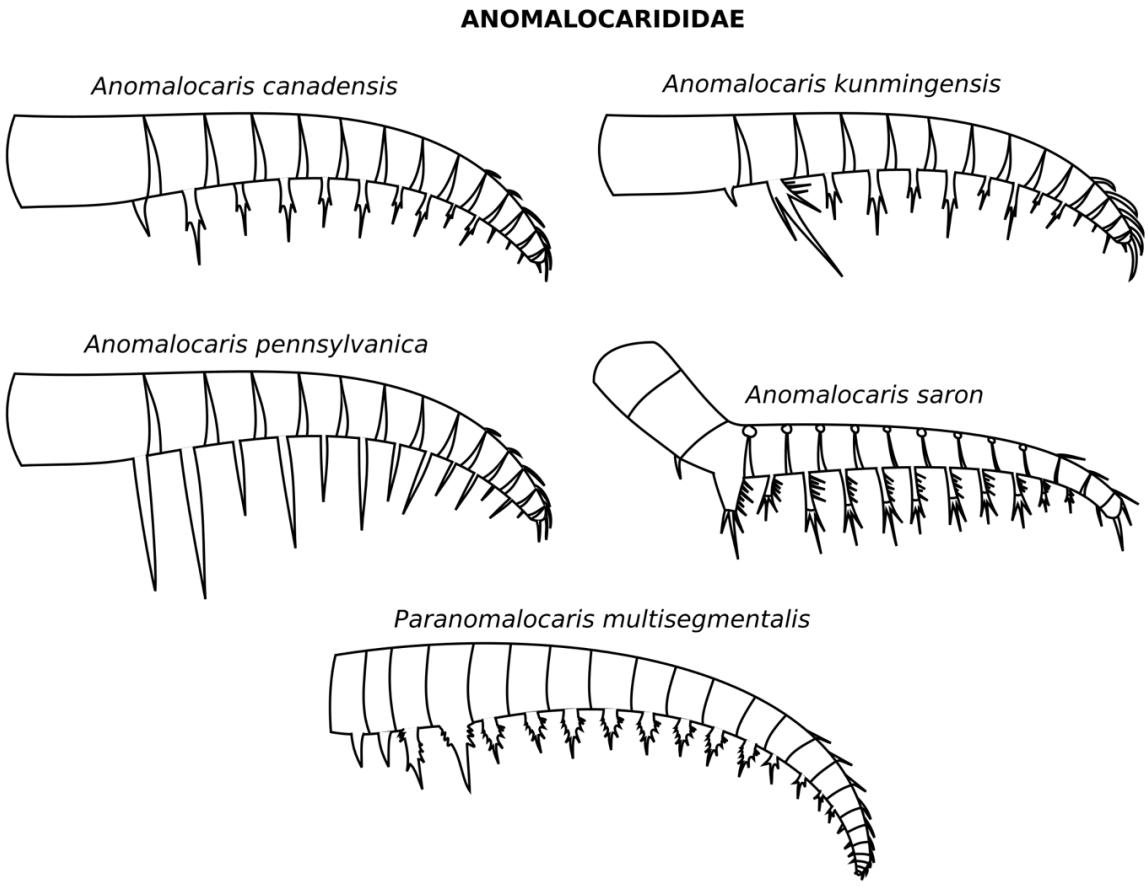

Fig. 5. Schematic frontal appendages of taxa belonging to Anomalocarididae.

Ramskoeldia) (Cong et al. 2018). However this is not visible in all specimens, so it is likely that some are true *Anomalocaris* specimens, with redescription of this material required to reveal if it represents a composite taxon. It is included in Anomalocarididae in this study, reflecting its current taxonomic position.

Anomalocaridid taxa share a similar frontal appendage organisation, with a hypertrophied endite on the first podomere in the distal articulated region, and endites alternating long/short and reducing in length along the appendage (Fig. 3A). Taxa within the family can be distinguished based on the number of podomeres, and morphology of endites, as well as number and morphology of dorsal spines (Fig. 5). *Paranomalocaris* has many more podomeres in the distal articulated region (20) than *Anomalocaris* (13). All anomalocaridids have endites that reduce in length along the appendage and alternate long/short on subsequent podomeres, as well as dorsal spines at the distal end. *Anomalocaris* species can be distinguished based on the morphology of the endites on the distalmost shaft podomere and in the distal articulated region. *A. canadensis*, *A. kunmingensis*, and *A. saron* all have endites with an elongate central blade and two flanking auxiliary spines. *A. saron* additionally bears fine distally-pointing spinules on their endite bases in the distal articulated region. *Anomalocaris canadensis* and *A. kunmingensis* bear very small and simple endites on the distalmost four podomeres (similar to *Paranomalocaris*), unlike the other taxa which bear smaller endites of the same morphology as the rest of the appendage.

Hurdiidae

Hurdiid frontal appendages have the same overall construction, very different to the other radiodont families, with the proximal most five podomeres in the distal

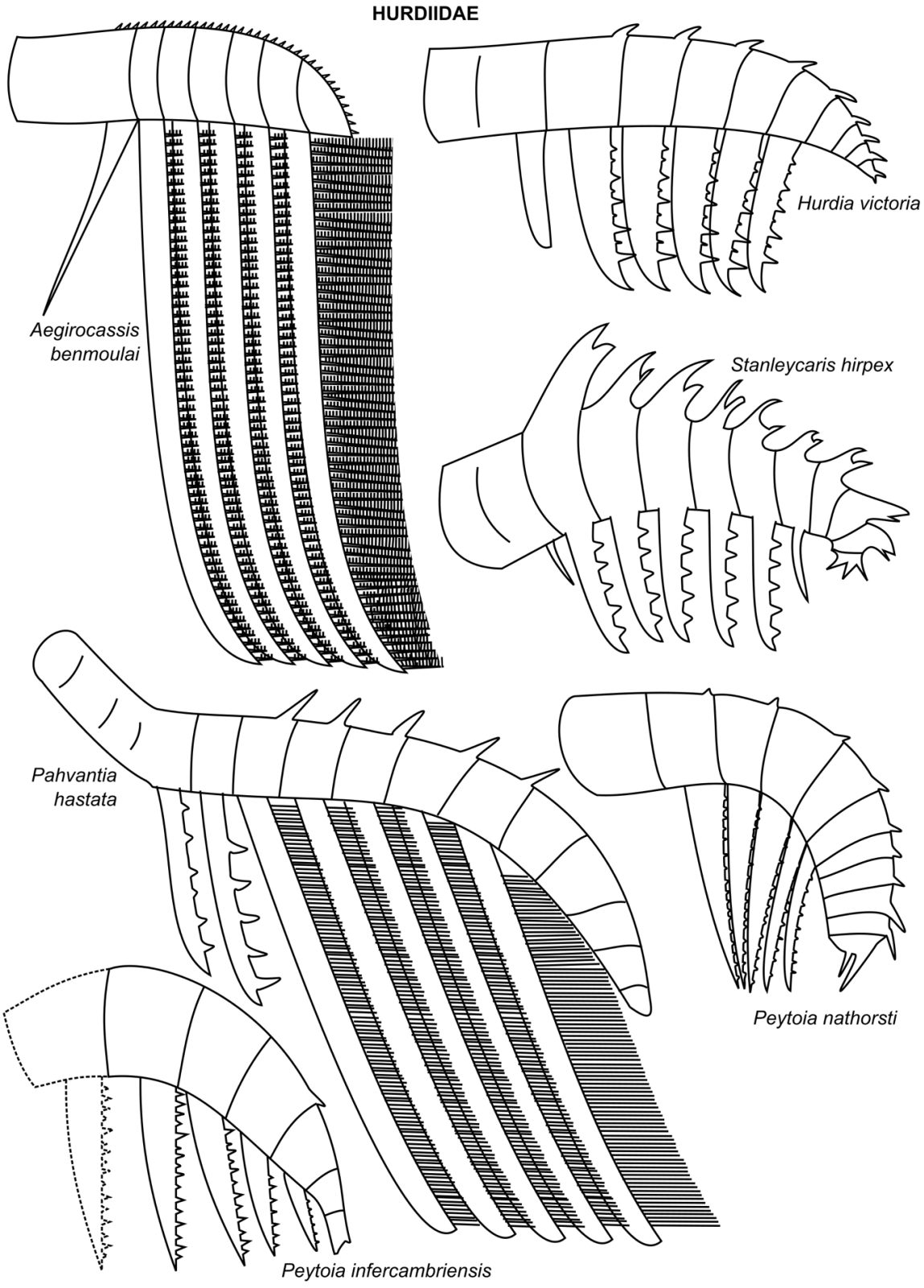

Fig. 6. Schematic frontal appendages of taxa belonging to Hurdiidae.

articulated region bearing subequal elongate blade-like endites with distally pointing spines or setae (Fig. 3C). Crucially, endites are unpaired (Fig. 3E), and one or two reduced endites can be present in some taxa more distally. Some taxa also bear an endite at the distalmost point of the shaft.

Most hurdiid taxa (Table 1), for example *Hurdia, Peytoia, Schinderhannes,* and *Stanleycaris*, bear blade-like endites with auxiliary spines lining the distal margin (Fig. 6; Daley et al. 2009, 2013a; Kühl et al. 2009; Caron et al. 2010). *Schinderhannes* bears an elongate endite on the distalmost shaft podomere, with reduced endites at this point also visible in some *Hurdia* and *Stanleycaris* specimens. The dorsal spines, podomere shape, and arrangement of the appendage distinguish *Stanleycaris, Peytoia,* and *Hurdia*. *Stanleycaris* possesses large double-pointed dorsal spines, and podomeres reduce in height dramatically distally, to less than half the height of more proximal podomeres. *Hurdia* has single-pointed dorsal spines, and *Peytoia,* the only taxon except *Schinderhannes* to possess lateral spines, also has podomeres of a more equal height from proximal to distal extremeties (Daley et al. 2009, 2013; Caron et al. 2010). The dorsal surface of *Schinderhannes* is not known to bear spines, however, the orientation of preservation of the single specimen is not conducive to their recognition. Lateral spines, which join the left and right appendages, have been recognised (Kühl et al. 2009). Two taxa, *Aegirocassis* and *Pahvantia* bear setae along the distal margin of endites, rather than spines. *Aegirocassis* bears a single row of setae per endite, with an additional two rows of densely spaced spinules present on each seta (Van Roy et al. 2015). *Pahvantia* bears two rows of setae per endite, with no additional spinules known (Lerosey-Aubril & Pates 2018).

Tamisiocarididae

Tamisiocaris borealis and *Anomalocaris briggsi* have repeatedly resolved as sister taxa in phylogenetic analyses (Vinther et al. 2014; Cong et al. 2014; Van Roy et al. 2015; Liu et al. 2018; Lerosey-Aubril & Pates 2018). This family (known by the invalid name 'Cetiocaridae' erected by Vinther et al. 2014 and also used in further studies by Cong et al. 2014, Van Roy et al. 2015, and Liu et al. 2018) is united by having elongate and paired endites (greater than the height of the podomere to which they attach) bearing spines which point distally and proximally (Fig. 3B). *Tamisiocaris* has more podomeres in the distal articulated region (17) than *Anomalocaris briggsi* (13), and also has finer and more elongate auxiliary spines (Fig. 7; Daley et al. 2013b; Vinther et al. 2014). *Anomalocaris briggsi* has dorsal spines on the distalmost three podomeres, whereas *Tamisiocaris* only has a single terminal spine (Daley & Peel 2010; Daley et al. 2013b).

Unassigned and uncertain taxa

Laminacaris, Caryosyntrips and *Cucumericrus* are all currently unassigned to families (Table 1). *Laminacaris* (Fig. 8) has an elongate endite on the first podomere in the distal articulated region very similar to hurdiid endites, but the remainder of the appendage has the same organisation as amplectobeluid and anomalocaridid appendages (Fig. 3A; short endites alternating long/short on subsequent podomeres, and auxiliary spines and spinules) (Guo et al. 2018). In a phylogenetic analysis, *Laminacaris* resolved as an amplectobeluid, however this analysis also resolved *Anomalocaris saron* and *Anomalocaris* cf. *canadensis* from the Emu Bay Shale as amplectobeluids (Lerosey-Aubril & Pates 2018). Arguments can therefore be made for including *Laminacaris* as a hurdiid, anomalocaridid, or amplectobeluid.

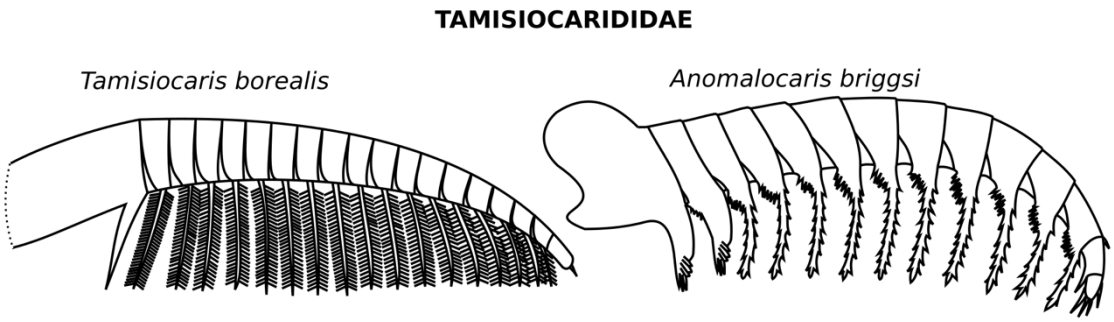

Fig. 7. Schematic frontal appendages of taxa belonging to Tamisiocarididae.

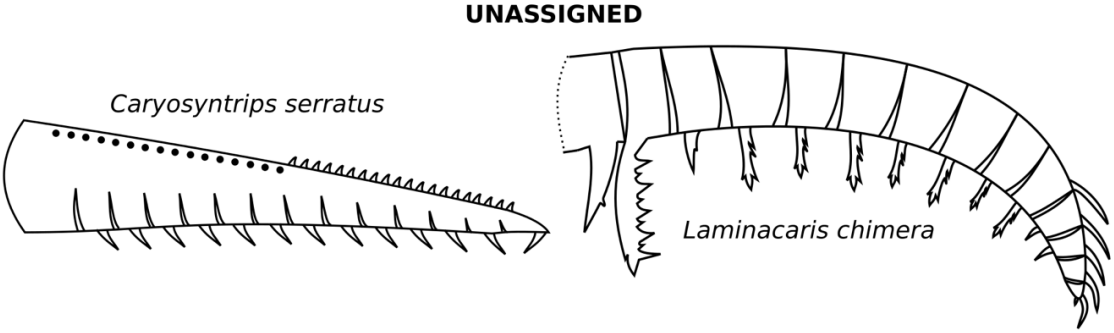

Fig. 8. Schematic frontal appendages of radiodont taxa currently unassigned at the family level.

Caryosyntrips (Fig. 8) has frontal appendages with a triangular outline, unlike any other radiodonts (Daley & Budd 2010). They bear small triangular endites along the ventral surface, and a row of small spines on the dorsal surface (Daley & Budd 2010). If *Caryosyntrips* is a true radiodont, it likely belongs in its own family. In all phylogenetic analyses, *Caryosyntrips* has resolved in a polytomy with Radiodonta, deuteropods, and *Cucumericrus* (e.g. Liu et al. 2018; Lerosey-Aubril & Pates 2018).

Cucumericrus decoratus is a very unusual animal, whose identity as a true radiodont, or relationship to radiodonts, is currently unclear. The frontal appendages of *Cucumericrus* are not known (Hou et al. 1995), but this taxon does possess ventral appendages along the rest of the body. These appendages are clearly biramous, with a leglike ramipod extending from a propod bearing at least five gnathobases. This itself is fused to a flap bearing strong similarities to other radiodont flaps (discussed below), with transverse lines along the anterior half only (Hou et al. 1995).

Morphology of feeding structures

Radiodont feeding structures (Fig. 9; oral cones and gnathobase-like structures) provide additional characters to distinguish families and genera, although they are not known in *Caryosyntrips* or Tamisiocarididae. Oral cones are made of radially arranged plates, with a central opening. These structures have plates of at least two sizes (large and small), with anomalocaridids also having plates of an intermediate size. The number and arrangement of the large plates distinguishes members of Anomalocarididae from Hurdiidae and Amplectobeluidae. In anomalocaridids, three large plates in a triradial arrangement are separated by small and intermediate-sized plates between them, the larger of which bear raised nodes angled towards the central opening (Fig. 9C; Daley &

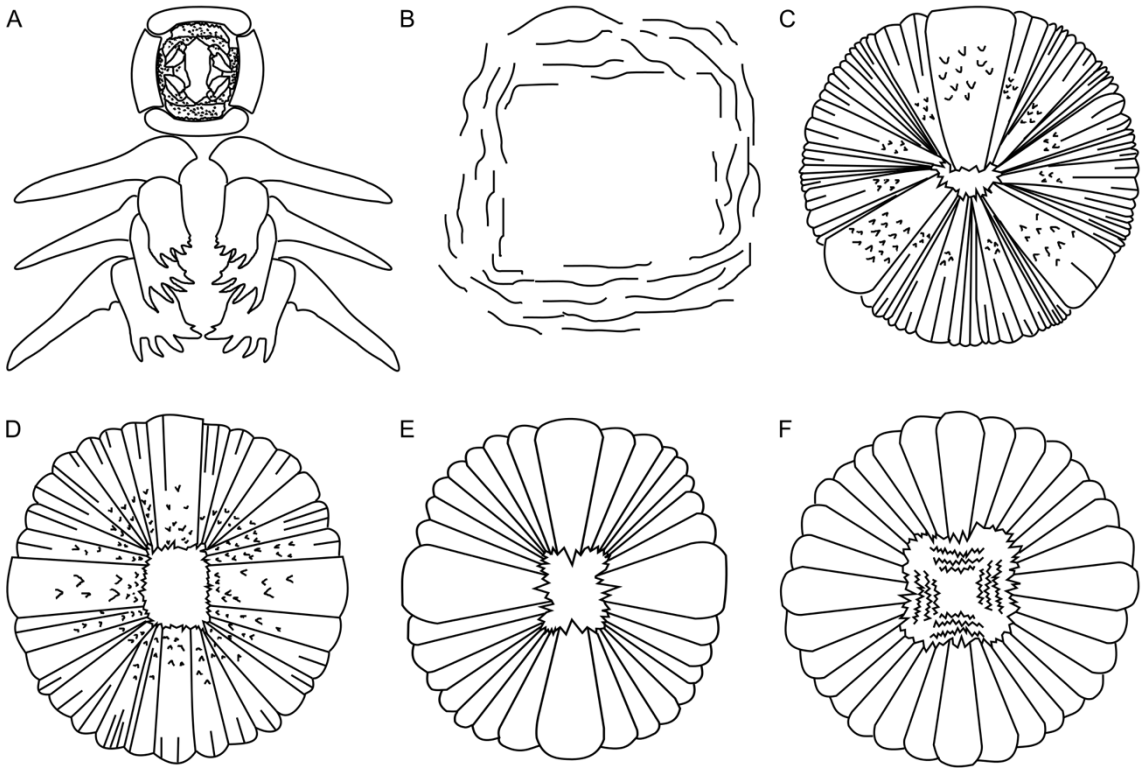

Fig. 9. Mouthparts of different radiodonts. **A.** Amplectobeluid arrangement, with oral cone of bumpy and smooth plates anterior to three pairs of gnathobase-like structures. Known in *Amplectobelua* and *Ramskoeldia*. **B.** Square opening surrounded by folds. Known in adult *Lyrarapax*. **C.** Triradial oral cone with plates of three sizes and raised nodes, known in *Anomalocaris*. **D.** Tetraradial arrangement with plates of three sizes and raised nodes. Known in isolation from the Guanshan biota, suggested to belong to *Anomalocaris kunmingensis*. **E.** Tetraradial arrangement with plates of two sizes. Known in *Peytoia,* and suggested arrangement for juvenile *Lyrarapax*. **F.** Tetraradial arrangement with plates of two sizes and additional teeth rows in the central opening. Known in *Hurdia*.

Bergström 2012). In hurdiids four large plates are arranged in a tetraradial fashion, and *Hurdia* can be distinguished from *Peytoia* based on the presence of additional rows of teeth in the central opening (Fig. 9E, F; Daley & Bergström 2012). *Amplectobelua* and *Ramskoeldia* have an as-yet unresolved arrangement of bumpy and smooth plates making up the oral cone, with three paired gnathobase-like structures present on the anteriormost three body segments (Fig. 9A; Cong et al. 2018). Adult *Lyrarapax* specimens have been preserved only with an opening surrounded by square folds (Fig. 9B; Cong et al. 2014, 2016), however a recent juvenile was shown to have a tetraradial arrangement (Liu et al. 2018). A tetraradial oral cone bearing raised nodes has also been suggested for *Anomalocaris kunmingensis* (Fig. 9D), and a triradial oral cone for *Anomalocaris briggsi*, based on disarticulated material, and the abundance of appendages belonging to these taxa from the Guanshan biota and Emu Bay Shale respectively (Daley et al. 2013b; Zeng et al. 2018).

Bodies, flaps, tail fans and furcae

These features are generally not well known enough or consistent enough within families or genera to allow identification above the species level (Table 4). The number of metameres in individual genera is not always constant (e.g. *Hurdia*) and neither is the presence of a tail fan, furcae, or strengthening rays on the flaps (e.g. *Anomalocaris*). The presence of dorsal flaps is the exception, as this is a character found in all hurdiids where the body is known (Van Roy et al. 2015).

Table 4. Comparison of known body parts in complete radiodonts

	Lateral Carapace Elements	Number of trunk segments bearing flaps	Tail fan/ furcae	Number of sets of flaps	Transverse lines on flaps	References
Amplectobeluidae						
Amplectobelua	Present	9?*	Furcae	1	Anterior half only	Chen et al. 1994; Cong et al. 2017
Lyrarapax	Absent?	10	None	1	Anterior half only	Cong et al. 2016
Anomalocarididae						
Anomalocaris canadensis	Absent	13	Tail fan	1	Absent	Daley & Edgecombe 2014
Anomalocaris saron	Absent	11	Both	1	Anterior half only	Chen et al. 1994
Hurdiidae						
Aegirocassis	Present	11	Unknown	2	Anterior half only	Van Roy et al. 2015
Hurdia	Present	7-9	None	2	Across entire flap	Daley et al. 2013; Van Roy et al. 2015
Peytoia	Absent?	11	Furcae	2	Anterior half only	Whittington & Briggs 1985; Van Roy et al. 2015
Schinderhannes	Absent?	10	Furcae	1?	?	Kühl et al. 2009

*9 flaps are labelled in Chen et al. 1994, fig. 3, but Cong et al. 2017 note that a redescription of all *Amplectobelua* material is required before information from the trunk region can be confidently known, and included in a diagnosis

Opportunities from restudy of USA radiodonts

Studies since 2009 of the Chengjiang biota and Burgess Shale have greatly improved our knowledge of radiodont diversity. However, the two faunas are very different. The Chengjiang biota is dominated by amplectobeluids and anomalocaridids, with the Burgess Shale dominated by hurdiids. Although the two sites share the genera *Amplectobelua* and *Anomalocaris*, there are no shared species. Thus, we have two highly detailed but geographically and temporally limited windows into Cambrian radiodont evolution, with the reasons for the differences in the two faunas remaining unclear (e.g. temporal, geographical). In addition, although phylogenetic analyses of Radiodonta have recovered four families with some consistency, the internal relationships of Anomalocarididae and Hurdiidae are not clear, and the nature of the evolution of the radiodont frontal appendage and the ecology of the 'basal' radiodont are not well known. This is in part resulting from the poor sampling of hurdiids, and old descriptions of anomalocaridids, as well as the large differences between hurdiids and other radiodonts. One particular problem relates to the difference in the number of endites per podomere between hurdiids (one, blade-like endite – Fig. 3E) and other radiodonts (two, slender and paired endites – Fig. 3D), and a lack of information identifying which of these is the plesiomorphic condition for radiodonts.

Burgess Shale-type *Lagerstätten* from the USA provide the perfect case-study to examine the evolution of radiodonts at a high temporal resolution, in a geographically constrained area. Radiodonts are known from eight BSTs in the Great Basin (California, Nevada, and Utah), ranging in age from the middle of Stage 4, to the Guzhangian (511 – 499 Ma, approximately), with four older and four younger than the Burgess Shale (Table 2). Additionally, the Kinzers Formation (Pennsylvania), is known, from a distinct

geographic location on the east cost of the USA. This was the first *Anomalocaris* bearing BST discovered in the USA (Resser 1929). However, with the exception of the Weeks Formation (Guzhangian), the most recent descriptions of radiodonts from these BSTs predates the rapid increase in knowledge of this order since 2009 (the descriptions were either done in the first or second period of radiodont discoveries; orange in Fig. 1B, C), and so the material is in need of redescription and placement in an up-to-date taxonomic context.

BSTs from the USA offer the opportunity to examine the evolution of radiodonts at a high temporal resolution, to better understand the geographic and temporal signals relating to the evolution of this group, as well to understand the diversity and disparity of the group through the Cambrian (bold in Table 2). Restudy of USA material will also provide more detailed information on anomalocaridids from these sites, and reveal new information on hurdiids, which will elucidate the more plesiomorphic conditions for the group and better resolve inter-radiodont relationships.

Geological setting of USA *Lagerstätten*

The majority of material from the USA studied in this thesis section comes from the Great Basin (Arizona, California, Idaho, Nevada, Utah), which occupied an equatorial position during the Cambrian Period (Fig. 1B, C), with additional material studied from a geographically distinct unit, the Kinzers Formation (Pennsylvania). Radiodont material from both the Great Basin and Kinzers Formation was preserved through a similar mechanism as for the famous Burgess Shale fauna (Gaines 2014).

The Great Basin formed on what is now the west coast of North America (GB in Fig. 1B, C), with the oldest deposits late Ediacaran to early Cambrian in age (Webster

2011). This basin provides a number of deposits preserving non-biomineralised material in a geographically constrained area and closely packed ages from the Cambrian Stage 4 to the Guzhangian (Fig. 1). By the upper Dyeran, the age of oldest radiodonts from this basin, the shelf was flooded and contained heterogeneous environments (Stewart & Poole 1974; Webster 2011). The oldest Great Basin radiodonts are known from deposits in the southern part of the basin (modern day California and Nevada), from deep-water quiet environments in the Latham Shale and Pioche Formation (Fig. 1). Although the Latham Shale is cratonic, and the Pioche Formation mid-shelf, the depositional and preservational conditions are considered similar as the Latham material was preserved during a period of high sea level (Webster 2011; discussed in more detail in Chapter 7). Younger deposits from the Great Basin are known from further north: the Spence Shale, Langston Formation; Wheeler Formation; Marjum Formation; and Weeks Formation (in order of ascending age; Fig. 1A). The Spence Shale, outcrops in the Wellsville Mountains (Utah) and comprises a series of parasequences of shales and limestones (Liddell et al. 1997), which correlate through trilobite biostratigraphy to levels slightly older than the Burgess Shale, Canada (Robison et al. 2015). The Wheeler, Marjum, and Weeks formations are all located in the House Range (Utah), and form a continuous sedimentary record from the Drumian to late Guzhangian (Lerosey-Aubril et al. 2018). A second, distinct, Wheeler Formation fauna is known from the Drum Mountains (Utah) (Lerosey-Aubril & Skabelund 2018). The House Range Wheeler Formation comprises mudstones and limestones, with the non-biomineralised material collected from carbonaceous shale units (Gaines et al. 2005). The Drum Mountain Wheeler Formation also comprises mudstones and limestones, however it is at least twice as thick as its House Range counterpart, indicating a more proximal and shallower depositional

environment (Lerosey-Aubril & Skabelund 2018). The Marjum Formation broadly resembles the House Range Wheeler Formation in terms of its stratigraphy and preservation, although it records a time when the Great Basin had undergone more infilling (Gaines & Droser 2010). Lastly the Weeks Formation, whose radiodonts are not discussed in this thesis due to their recent description (Lerosey-Aubril et al. 2014), has a geographic extent substantially lower than these older units, as it represents the final filling of the basin (Lerosey-Aubril et al. 2018). The Weeks Formation, which includes sand and silt-sized quartz, stromatolites, and fauna indicating a shallow water environment such as aglaspadids, was initially thought to represent a shallower environment than the other Utah Cambrian Lagerstätten (e.g. Lerosey-Aubril et al. 2014). A recent comprehensive analysis of a number of field exposures has contradicted this, and shown that the Weeks fauna occupied a deep-water facies near-identical to those of the Wheeler and Marjum Formations (Lerosey-Aubril et al. 2018).

The Kinzers Formation (Pennsylvania) occupies a unique position for a Cambrian *Lagerstätten* in space and time. It is one of the older units preserving non-biomineralised taxa in Laurentia, and the only one known to preserve radiodonts from the east coast of the USA (Fig. 1; Muscente et al. 2017). Unlike the Great Basin, which has received a substantial number palaeontological, geochemical, and stratigraphic studies over the last ten years, little progress has been made for the Kinzers despite the fact that it has been known as a *Konservat-Lagerstätten* for nearly 100 years (Dunbar 1925; discussed in more detail in Chapter 3). The soft-bodied fauna is known from a number of different faunules (Campbell & Kauffman 1969), which all belong to the Fine Pelitic Facies of the Emigsville Member, the oldest part of the Kinzers Formation which

corresponds to the '*Olenellus'* zone (recently subdivided by Webster 2011) (Skinner 2005).

Aims for this thesis section

In this thesis I place material from the USA into an up-to-date taxonomic and ecological context, and delineate the taphonomic histories of these specimens. I redescribe old material, and in addition describe new specimens donated by private collectors. This provides the raw data for studies of the phylogeny, diversity, and disparity of the group.

Chapter 3 focusses on an unexpectedly diverse assemblage of radiodonts from the Kinzers Formation, with the remaining descriptive chapters looking in detail at the Great Basin. Chapter 4 reports the first *Caryosyntrips* from outside of the Burgess Shale, and describes two new species in a review of this genus. Chapter 5 summarizes our knowledge of hurdiids from the Wuliuan and Drumian of Utah, Chapter 6 reports the first occurrence of *Stanleycaris* from outside of Canada, based on the reinterpretation of material first described in the 1980s. The focus then shifts to the oldest BSTs in the Great Basin, with Chapter 7 examining the changing diversity of radiodonts within this basin, reporting the oldest hurdiid from Laurentia, the youngest *Ramskoeldia* worldwide, and placing anomalocaridid material into the modern taxonomic framework. The final descriptive chapter (Chapter 8) provides the first radiodont from the Pyramid Shale Member, Carrara Formation, with the first formal description of radiodonts from the Canadian Lagerstätte, the Mount Cap Formation. I describe a new genus of radiodont, unusual in that it has a frontal appendage organization very similar to hurdiids, but paired and slender endites.

I then use the new data from these findings to provide a more comprehensive group of taxa for a phylogenetic analysis, and shed light on plesiomorphic characters of the radiodont frontal appendage (Chapter 9). This provides a novel arrangement for the relationships between radiodont families, and resolves *Caryosyntrips* within Radiodonta for the first time. Finally, I provide the first analysis of the diversity and disparity of the group through the Cambrian, to assess the patterns of evolution within Radiodonta, within individual families, and consider these patterns in light of preservational, extrinsic, and intrinsic factors (Chapter 10). Ultimately, this work has greatly improved our knowledge of USA radiodonts, and this group as a whole. Eleven genera are now known from USA BSTs, and these deposits provide crucial data for phylogenetic, diversity, and disparity analyses.

References

Briggs, D. E. (1979). *Anomalocaris*, the largest known Cambrian arthropod. *Palaeontology*, 22(3), 631-664.

Briggs, D. E., & Mount, J. D. (1982). The occurrence of the giant arthropod *Anomalocaris* in the Lower Cambrian of southern California, and the overall distribution of the genus. *Journal of Paleontology*, 56(5), 1112-1118.

Briggs, D. E., & Robison, R. A. (1984). Exceptionally preserved nontrilobite arthropods and *Anomalocaris* from the Middle Cambrian of Utah. *University of Kansas Paleontological Contributions*, 111, 1-23.

Briggs, D. E., Lieberman, B. S., Hendricks, J. R., Halgedahl, S. L., & Jarrard, R. D. (2008). Middle Cambrian arthropods from Utah. *Journal of Paleontology*, 82(2), 238-254.

Budd, G. E. (2002). A palaeontological solution to the arthropod head problem. *Nature*, 417(6886), 271.

Butterfield, N. J., & Nicholas, C. J. (1996). Burgess Shale-type preservation of both non-mineralizing and 'shelly' Cambrian organisms from the Mackenzie Mountains, northwestern Canada. *Journal of Paleontology*, 70(6), 893-899.

Campbell, L., & Kauffman, M. E. (1969). Olenellus fauna of the Kinzers Formation, southeastern Pennsylvania. *Proceedings of the Pennsylvania Academy of Science*, 172-176.

Caron, J. B., Gaines, R. R., Mángano, M. G., Streng, M., & Daley, A. C. (2010). A new Burgess Shale–type assemblage from the "thin" Stephen Formation of the southern Canadian Rockies. *Geology*, 38(9), 811-814.

Chen, J. Y., Ramsköld, L., & Zhou, G. Q. (1994). Evidence for monophyly and arthropod affinity of Cambrian giant predators. *Science*, 264(5163), 1304-1308.

Chen, J., Waloszek, D., & Maas, A. (2004). A new 'great-appendage'arthropod from the Lower Cambrian of China and homology of chelicerate chelicerae and raptorial antero-ventral appendages. *Lethaia*, 37(1), 3-20.

Collins, D. (1996). The "evolution" of *Anomalocaris* and its classification in the arthropod class Dinocarida (nov.) and order Radiodonta (nov.). *Journal of Paleontology*, 70(2), 280-293.

Cong, P., Ma, X., Hou, X., Edgecombe, G. D., & Strausfeld, N. J. (2014). Brain structure resolves the segmental affinity of anomalocaridid appendages. *Nature*, 513(7519), 538.

Cong, P., Daley, A. C., Edgecombe, G. D., Hou, X., & Chen, A. (2016). Morphology of the radiodontan *Lyrarapax* from the early Cambrian Chengjiang biota. *Journal of Paleontology*, 90(4), 663-671.

Cong, P., Daley, A. C., Edgecombe, G. D., & Hou, X. (2017). The functional head of the Cambrian radiodontan (stem-group Euarthropoda) *Amplectobelua symbrachiata*. *BMC Evolutionary Biology*, 17(1), 208.

Cong, P. Y., Edgecombe, G. D., Daley, A. C., Guo, J., Pates, S., & Hou, X. G. (2018). New radiodonts with gnathobase-like structures from the Cambrian Chengjiang biota and implications for the systematics of Radiodonta. *Papers in Palaeontology*, 4(4), 605-621.

Conway Morris, S., & Robison, R. A. (1982). The enigmatic medusoid *Peytoia* and a comparison of some Cambrian biotas. *Journal of Paleontology*, 56(1), 116-122.

Conway Morris, S., & Robison, R. A. (1988). More soft-bodied animals and algae from the Middle Cambrian of Utah and British Columbia. *University of Kansas Paleontological Contributions*, 122, 1-48.

Daley, A. C., Budd, G. E., Caron, J. B., Edgecombe, G. D., & Collins, D. (2009). The Burgess Shale anomalocaridid *Hurdia* and its significance for early euarthropod evolution. *Science*, 323(5921), 1597-1600.

Daley, A. C., & Budd, G. E. (2010). New anomalocaridid appendages from the Burgess Shale, Canada. *Palaeontology*, 53(4), 721-738.

Daley, A. C., & Peel, J. S. (2010). A possible anomalocaridid from the Cambrian Sirius Passet Lagerstätte, north Greenland. *Journal of Paleontology*, 84(2), 352-355.

Daley, A. C., & Bergström, J. (2012). The oral cone of *Anomalocaris* is not a classic ‘‘peytoia’’. *Naturwissenschaften*, 99(6), 501-504.

Daley, A. C., Paterson, J. R., Edgecombe, G. D., García-Bellido, D. C., & Jago, J. B. (2013a). New anatomical information on *Anomalocaris* from the Cambrian Emu Bay Shale of South Australia and a reassessment of its inferred predatory habits. *Palaeontology*, 56(5), 971-990.

Daley, A. C., Budd, G. E., & Caron, J. B. (2013b). Morphology and systematics of the anomalocaridid arthropod *Hurdia* from the Middle Cambrian of British Columbia and Utah. *Journal of Systematic Palaeontology*, 11(7), 743-787.

Daley, A. C., & Edgecombe, G. D. (2014). Morphology of *Anomalocaris canadensis* from the Burgess Shale. *Journal of Paleontology*, 88(1), 68-91.

Daley, A. C., & Legg, D. A. (2015). A morphological and taxonomic appraisal of the oldest anomalocaridid from the Lower Cambrian of Poland. *Geological Magazine*, 152(5), 949-955.

Dunbar, C. O. (1925). Antennae in Olenellus getzi n. sp. *American Journal of Science*, 52, 303-308.

Dzik, J., & Lendzion, K. (1988). The oldest arthropods of the East European Platform. *Lethaia*, 21(1), 29-38.

Gaines, R. R. (2014). Burgess Shale-type preservation and its distribution in space and time. *The Paleontological Society Papers*, 20, 123-146.

Gaines, R. R., & Droser, M. L. (2010). The paleoredox setting of Burgess Shale-type deposits. *Palaeogeography, Palaeoclimatology, Palaeoecology*, 297(3-4), 649-661.

Gaines, R. R., Kennedy, M. J., & Droser, M. L. (2005). A new hypothesis for organic preservation of Burgess Shale taxa in the middle Cambrian Wheeler Formation,

House Range, Utah. *Palaeogeography, Palaeoclimatology, Palaeoecology*, 220(1-2), 193-205.

Guo, J., Pates, S., Cong, P., Daley, A. C., Edgecombe, G. D., Chen, T., & Hou, X. (2018). A new radiodont (stem Euarthropoda) frontal appendage with a mosaic of characters from the Cambrian (Series 2 Stage 3) Chengjiang biota. *Papers in Palaeontology*. Online early view, doi: 10.1002/spp2.1231

Hou, X-G., Bergström, J., & Ahlberg, P. (1995). *Anomalocaris* and other large animals in the Lower Cambrian Chengjiang fauna of southwest China. *GFF*, 117(3), 163-183.

Hou, X-G., Bergström, J., & Yang, J. (2006). Distinguishing anomalocaridids from arthropods and priapulids. *Geological Journal*, 41(3-4), 259-269.

Huang, D., Wang, Y., Gao, J., & Wang, Y. (2012). A new anomalocaridid frontal appendage from the Middle Cambrian Mantou Formation of the Tangshan Area. *Acta Palaeontologica Sinica*, 51, 411-415.

Kühl, G., Briggs, D. E., & Rust, J. (2009). A great-appendage arthropod with a radial mouth from the Lower Devonian Hunsrück Slate, Germany. *Science*, 323(5915), 771-773.

Lendzion, K. (1975). Fauna of the Mobergella zone in the Polish Lower Cambrian. *Geological Quarterly*, 19(2), 237-242.

Lerosey-Aubril, R., Hegna, T. A., Babcock, L. E., Bonino, E., & Kier, C. (2014). Arthropod appendages from the Weeks Formation Konservat-Lagerstätte: new occurrences of anomalocaridids in the Cambrian of Utah, USA. *Bulletin of Geosciences*, 89(2), 269-282.

Lerosey-Aubril, R., Gaines, R. R., Hegna, T. A., Ortega-Hernández, J., Van Roy, P., Kier, C., & Bonino, E. (2018). The Weeks Formation *Konservat-Lagerstätte* and the

evolutionary transition of Cambrian marine life. *Journal of the Geological Society*, 175, 705-715.

Lerosey-Aubril, R., & Pates, S. (2018). New suspension-feeding radiodont suggests evolution of microplanktivory in Cambrian macronekton. *Nature Communications*, 9(1), 3774.

Lerosey-Aubril, R., & Skabelund, J. (2018). *Messorocaris*, a new sanctacaridid-like arthropod from the middle Cambrian Wheeler Formation (Utah, USA). *Geological Magazine*, 155(1), 181-186.

Lieberman, B. S. (2003). A new soft-bodied fauna: the Pioche Formation of Nevada. *Journal of Paleontology*, 77(4), 674-690.

Liddell, W. D., Wright, S. W., & Brett, C. E. (1997). Sequence stratigraphy and paleoecology of the Middle Cambrian Spence Shale in northern Utah and southern Idaho*. Brigham Young Geology Studies*, 42, 59-78.

Liu, J., Lerosey-Aubril, R., Steiner, M., Dunlop, J. A., Shu, D., & Paterson, J. R. (2018). Origin of raptorial feeding in juvenile euarthropods revealed by a Cambrian radiodontan. *National Science Review*, nwy057. doi.org/10.1093/nsr/new057.

Liu, Q. (2013). The first discovery of anomalocaridid appendages from the Balang Formation (Cambrian Series 2) in Hunan, China. *Alcheringa*, 37(3), 338-343.

Matthews, S. C. (1973). Notes on open nomenclature and on synonymy lists. *Palaeontology,* 16(4), 713-719.

McHenry, B., & Yates, A. (1993). First report of the enigmatic metazoan *Anomalocaris* from the southern hemisphere and a trilobite with preserved appendages from the Early Cambrian of Kangaroo Island, South Australia. *Records of the South Australian Museum*, 26, 77-86.

Muscente, A. D., Schiffbauer, J. D., Broce, J., Laflamme, M., O'Donnell, K., Boag, T. H., ... & MacKenzie, L. A. (2017). Exceptionally preserved fossil assemblages through geologic time and space. *Gondwana Research*, 48, 164-188.

Nedin, C. (1995). The Emu Bay Shale, a Lower Cambrian fossil Lagerstätten, Kangaroo Island, South Australia. *Memoirs of the Association of Australasian Palaeontologists*, 18, 31-40.

Paterson, J. R., García-Bellido, D. C., Lee, M. S., Brock, G. A., Jago, J. B., & Edgecombe, G. D. (2011). Acute vision in the giant Cambrian predator *Anomalocaris* and the origin of compound eyes. *Nature*, 480(7376), 237.

Robison, R. A., Babcock, L. E., & Gunther, V. G. (2015). Exceptional Cambrian fossils from Utah: a window into the age of trilobites. *Utah Geological Survey*.

Resser, C. E. (1929). New lower and middle Cambrian Crustacea. *Proceedings of the United States National Museum*, 76(9), 1-18.

Scotese, C. R. (2016). PALEOMAP PaleoAtlas for GPlates and the PaleoData Plotter Program, PALEOMAP Project, http://www.earthbyte.org/paleomap-paleoatlas-for-gplates

Simonetta, A. M., & Delle Cave, L. (1975). The Cambrian non-trilobite arthropods from the Burgess Shale of British Columbia. A study of their comparative morphology, taxinomy [sic] and evolutionary significance. *Palaeontographica Italica*, 69(39), 1-37.

Skinner, E. S. (2005). Taphonomy and depositional circumstances of exceptionally preserved fossils from the Kinzers Formation (Cambrian), southeastern Pennsylvania. *Palaeogeography, Palaeoclimatology, Palaeoecology*, 220(1-2), 167-192.

Stewart, J. H., & Poole, F. G. (1974). Lower Paleozoic and uppermost Precambrian Cordilleran miogeocline, Great Basin, western United States. *In* Dickinson, W. R. ed. Tectonics and sedimentation: Society of Economic Paleontologists and Mineralogists Special Publication, 22, 28-57.

Van Roy, P., & Briggs, D. E. (2011). A giant Ordovician anomalocaridid. Nature, 473(7348), 510.

Van Roy, P., Daley, A. C., & Briggs, D. E. (2015). Anomalocaridid trunk limb homology revealed by a giant filter-feeder with paired flaps. *Nature*, 522(7554), 77.

Vinther, J., Stein, M., Longrich, N. R., & Harper, D. A. (2014). A suspension-feeding anomalocarid from the Early Cambrian. *Nature*, 507(7493), 496.

Walcott, C. D. (1911). Middle Cambrian Holothurians and Medusae. Cambrian geology and paleontology II. *Smithsonian Miscellaneous Collections,* 57, 41-68.

Wang, Y., Huang, D., & Hu, S. (2013). New anomalocardid frontal appendages from the Guanshan biota, eastern Yunnan. *Chinese Science Bulletin*, 58(32), 3937-3942.

Webster, M. 2011. Trilobite biostratigraphy and sequence stratigraphy of the upper Dyeran (traditional Laurentian 'Lower Cambrian') in the southern Great Basin, USA. *In* Hollingsworth, J. S., Sundberg, F. A., & Foster, J. R. eds. Cambrian Stratigraphy and Paleontology of Northern Arizona and Southern Nevada: Museum of Northern Arizona Bulletin, 67, 121-154.

Whiteaves, J. F. (1892). Description of a new genus and species of Phyllocarid Crustacea from the Middle Cambrian of Mount Stephen, B. C. *Canadian Record of Science,* 5, 205-208.

Whittington, H. B., & Briggs, D. E. G. (1985). The largest Cambrian animal, *Anomalocaris*, Burgess Shale, British-Columbia. *Philosophical Transactions of the Royal Society of London B,* 309(1141), 569-609.

Zeng, H., Zhao, F., Yin, Z., & Zhu, M. (2018). A new radiodontan oral cone with a unique combination of anatomical features from the early Cambrian Guanshan Lagerstätte, eastern Yunnan, South China. *Journal of Paleontology*, 92(1), 40-48.

Zhao, Y., Zhu, M., Babcock, L. E., Yuan, J., Parsley, R. L., Peng, J., Yang, X., and Wang, Y. (2005). Kaili Biota: a taphonomic window on diversification of metazoans from the basal Middle Cambrian: Guizhou, China. *Acta Geologica Sinica-English Edition*, 79(6), 751-765.

Chapter 3

The Kinzers Formation (Pennsylvania, USA): the most diverse assemblage of Cambrian Stage 4 radiodonts

Author contributions

SP and ACD conceived the project; SP performed the biogeographic reconstruction; SP wrote the manuscript and prepared the figures, with input from ACD.

Publication information

This Chapter has been peer reviewed and published by *Geological Magazine*:

Pates, S. & Daley, A. C. (2018). The Kinzers Formation (Pennsylvania, USA): the most diverse assemblage of Cambrian Stage 4 radiodonts. *Geological Magazine*, Early online view, 1-14. Doi.org/10.1017/S0016756818000547

The Kinzers Formation (Pennsylvania, USA): the most diverse assemblage of Cambrian Stage 4 radiodonts

Stephen Pates[1,2] and Allison C. Daley[2]

[1]Department of Zoology, University of Oxford, South Parks Road, Oxford, OX1 3PS, UK.

[2]Institute of Earth Sciences, University of Lausanne, Lausanne CH-1015, Switzerland

Category: Original article

Short title: Kinzers Formation Radiodonta

Keywords: Cambrian, Kinzers Formation, *Anomalocaris, Amplectobelua, Laminacaris, Tamisiocaris,* Radiodonta

Email for corresponding author: stephen.pates@zoo.ox.ac.uk

Abstract

Radiodonta, apex Cambrian predators such as *Anomalocaris,* have been known from the Kinzers Formation (Cambrian Series 2, Stage 4 - Pennsylvania, USA) for nearly 100 years. Work over the last 10 years mainly on radiodont material from the Chengjiang (Cambrian Series 2, Stage 3 – Yunnan, China) and Burgess Shale (Cambrian Series 3, Stage 5 – British Columbia, Canada), has greatly improved our knowledge of the diversity and disparity of radiodonts and their frontal appendages, including the description of new species, genera and families. Previous work identified two species of radiodonts from the Kinzers Formation: *Anomalocaris pennsylvanica* Resser 1929 and *Anomalocaris*? cf. *pennsylvanica* based on isolated frontal appendage material (Briggs 1979). A restudy of Kinzers Formation material shows that only some of the specimens can be confirmed as *Anomalocaris pennsylvanica*, and a number of specimens previously attributed to *Anomalocaris* belong to other, more recently discovered, radiodont genera *Amplectobelua* and *Tamisiocaris*. This reinterpretation makes the Kinzers Formation the most diverse Cambrian Stage 4 Burgess Shale Type Lagerstätten in terms of number of radiodont species. This assemblage includes the youngest known *Tamisiocaris* and the first from outside Greenland, the only *Amplectobelua* from Stage 4 and the oldest from Laurentia, two specimens tentatively assigned to the recently described Chengjiang genus *Laminacaris*, and the endemic *Anomalocaris pennsylvanica*. The identification of these new radiodont taxa increases the total known diversity of the Kinzers Formation to more than 10 species, and so it should now be considered a Tier 2 Lagerstätten.

1. Introduction

Soft-bodied fossil biota (Konservat-Lagerstätten), such as the famous Chengjiang (Cambrian Series 2, Stage 3) and Burgess Shale (Cambrian Series 3, Stage 5), offer an unrivalled opportunity to study assemblages of animals at snapshots in time. Konservat-Lagerstätten are not distributed evenly through time, but instead are most common in the Cambrian Series 2 and Series 3 (Allison and Briggs 1993; Gaines 2014). The Kinzers Formation (Pennsylvania, USA), has been recognized as a Konservat-Lagerstätten for nearly 100 years, since the discovery of antennae in *Olenellus getzi* (Dunbar 1925) and the subsequent description of soft-bodied animals (e.g. Resser 1929; Resser and Howell 1938). The exceptionally preserved fauna is confined to the Dyeran (Cambrian Series 2, Stage 4) Fine Pelitic Facies of the Emigsville Member (Skinner 2005). Preservation at different localities varies in iron content, which sometimes overlays and obscures parts of the fossils, owing to differences in the concentration of algae and cyanobacteria of the original sediment (Skinner 2005). The currently known soft-bodied fauna of the Kinzers Formation includes the worms *Selkirkia* (Conway Morris 1977)*, Kinzeria crinita* and *Atalotaenia adela* (Garcia-Bellido and Conway Morris 1999), the sponge *Hazelia walcotti* (Rigby 1987), arthropods such as *Serracaris lineata* (Briggs 1978), *Isoxys* (Campbell and Kauffman 1969), *Sidneyia* (Campbell and Kauffman 1969)*, Protocaris* (Campbell and Kauffman 1969)*,* and *Tuzoia* (Resser 1929; Campbell and Kauffman 1969; Vannier et al. 2007), and stem-group euarthropod radiodonts (Resser 1929; Briggs 1979), which are the focus of this study.

Since the original description of radiodont material from the Kinzers Formation, including *Anomalocaris pennsylvanica* (Resser 1929), and subsequent redescription of material following the recognition that *Anomalocaris* was the appendage of a

euarthropod and not the body of a shrimp (Briggs 1979), the number of known species, genera and families of Radiodonta described from other localities has increased substantially. Complete *Anomalocaris* body fossils were discovered and described (Whittington & Briggs 1985), Radiodonta were shown to be stem-group euarthropods (Daley et al. 2009) and what began three species described from isolated appendages (*Anomalocaris canadensis*, *A. pennsylvanica* and 'appendage F' – Briggs 1979) has exploded into a diverse group of apex-predators, many known from complete specimens (Whittington & Briggs 1985; Chen et al. 1994; Hou et al. 1995; Collins 1996; Daley et al. 2009), with diverse feeding strategies representing over 10 genera (Daley et al. 2009; Daley & Budd 2010; Cong et al. 2014, 2016, 2017, 2018; Vinther et al. 2014; Pates et al. 2017; 2018a; Pates & Daley 2017). Radiodonta fossils have been identified worldwide, from the Great Basin, USA (e.g. Briggs and Mount 1982; Lieberman 2003; Briggs et al. 2008; Lerosey-Aubril et al. 2014; Pates et al. 2018b); Iberian Chains, Spain (Pates & Daley 2017); Holy Cross Mountains, Poland (Daley & Legg 2015); Bohemia, Czech Republic (Chlupáč & Kordule 2002; Daley et al. 2013a); Hunsruck, Germany (Kühl et al. 2009); as well as more famous sites such as the Burgess Shale, Canada (e.g. Whittington & Briggs 1985; Collins 1996; Daley and Budd 2010), Chengjiang and Haiku biotas, China (e.g. Chen et al. 1994; Hou et al. 1995; Cong et al. 2014, 2016, 2017, 2018; Guo et al. 2018) and Emu Bay Shale, Australia (Nedin 1995; Daley et al. 2013b).

In this study, the known Radiodonta material from the Kinzers Formation is reassessed in light of the substantial increase in knowledge of these iconic Cambrian animals. Significantly for this study, two genera, *Tamisiocaris* Daley & Peel 2010 and *Amplectobelua* Hou et al. 1995, with frontal appendages superficially similar to *Anomalocaris*, were described since the last review of the Kinzers Radiodonta by Briggs

(1979). Our restudy of the material ascribed to *Anomalocaris pennsylvanica* and *Anomalocaris?* cf. *pennsylvanica* shows that it in fact belongs to at least four different taxa, and confirms that *A. pennsylvanica* is a distinct species from *A. canadensis*.

2. Identifying Radiodonta using frontal appendages

Although rare complete body fossils are known, Radiodonta are most commonly found as isolated elements of the body plan: frontal appendages, mouthparts, carapace elements, or flaps. Of these, isolated frontal appendages are the most common radiodont body element found outside of Tier 1 BSTs, deposits with greater than 100 taxa known, preserved in high fidelity and high abundance (Gaines 2014), and a number of species are known only from frontal appendages, especially from Tier 2 (from 10 to 100 taxa, intermediate fidelity and abundance) and Tier 3 (less than 10 taxa, low fidelity and abundance) BST deposits. Frontal appendages are taxonomically informative, and even partial specimens often provide enough evidence to recognise families, genera or species of radiodonts.

Radiodont frontal appendages consist of a series of podomeres bearing a diverse morphology of spines and/or endites along their length. Radiodont frontal appendages can be separated into the 'shaft' (*sensu* Hou et al. 1995, sometimes referred to as the 'peduncle') and the 'distal articulated region' (*sensu* Cong et al. 2018). The shaft normally has more weakly defined boundaries between podomeres and is less sclerotized than the rest of the appendage, and accordingly it is not always preserved or is only incompletely preserved. It joins the appendage to the body and is joined to the distal articulated region at an angle between 100-180° on the dorsal surface (Fig. 1a, ϑ). The shaft often bears an endite at the distalmost point of the ventral surface (Fig. 1a,

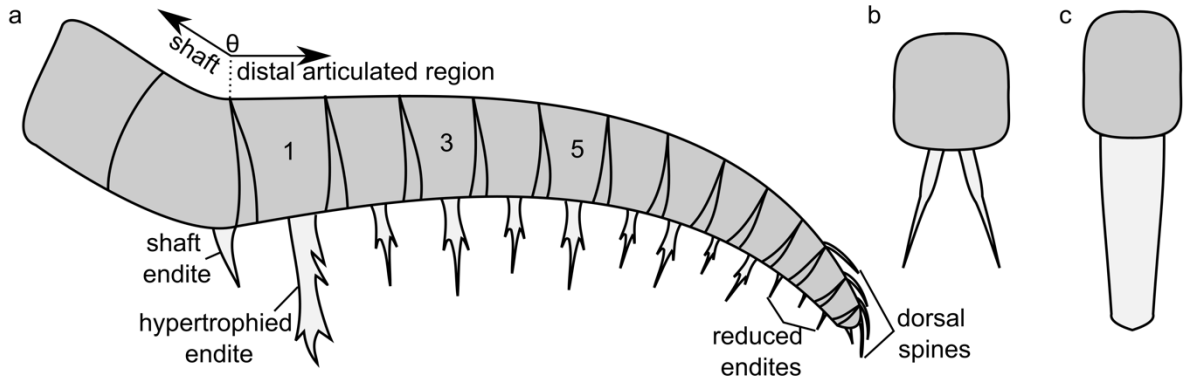

Figure 1. Schematic radiodont frontal appendage showing terminology used. Podomeres in dark grey, ventral endites in light grey. (a) sagittal view. Abbreviations: ϑ, angle between shaft and distal articulated region on dorsal surface; 1, post-shaft podomere; 3 and 5, third and fifth podomere in the distal articulated region. For anomalocaridids, the ventral endites on 3 are longer than those on 5, for amplectobeluids the ventral endites on 5 are longer than those on 3. In hurdiids all podomeres from 1 to 5 will have enlarged endites of the same morphology and equal length. (b) frontal view of non-hurdiid podomere, showing relative width and separate attachment of two ventral endites to one podomere. (c) frontal view of hurdiid podomere showing relative width and attachment of one ventral endite to one podomere.

shaft endite), and rarely other ventral endites are present on the shaft (e.g. *Ramskoeldia platycantha*, Cong et al. 2018). The boundary between the shaft and the distal articulated region can be further identified by the presence, in most taxa, of an enlarged or morphologically differentiated ventral endite on the most proximal podomere of the distal articulated region (e.g. *Amplectobelua*, *Lyrarapax*) (Fig. 1a, hypertrophied endite). The distal articulated region can itself often be separated into two parts. The proximal part bears ventral endites of the same morphology, differentiating it from the distal part, which often bears either no ventral endites, or reduced and simplified endites, together with dorsal spines (Fig. 1a, dorsal spines, reduced endites).

The morphology and pattern of ventral endites in particular have been used to identify isolated appendages (Table 1). In Hurdiidae, blade-like ventral endites are the same width (frontal view) as the podomere, and only one ventral endite projects from each podomere (Fig. 1c). Hurdiids always have five of these large identical blade-like ventral endites in the distal articulated region (Fig. 1a, from 1-5). For all other families, the ventral endites are paired on each podomere, and are less than half the width (frontal view) of the podomere to which they attach (Fig. 1b). Families can be differentiated using the relative lengths of ventral endites, the presence of enlarged ventral endites on the post-shaft podomere, and/or the morphology of dorsal spines in the distal articulated region. Anomalocarididae (a clade that includes all species of *Anomalocaris* except for *Anomalocaris briggsi*) and Amplectobeluidae both have enlarged spine-like ventral endites in the distal articulated region, which alternate in length long/short on odd/even podomeres, with a general reduction in the length of ventral endites over the length of the appendage. Amplectobleuidae differ from

Table 1: Frontal appendage characters used to distinguish radiodont families

	Podomeres and numbers of ventral endites						Morphology of large ventral endite(s)			
	# pd. in shaft	# pd. in distal articulated region	Triangular membrane between pd.	# rows en.	# of longest en.	en. in d.a.r. alternate long/short	as. paired	as. increase in size from base to tip	# Large as.	Small as. between large as.
Amplectobeluidae	3	12/13	Yes	2	1	Yes	Yes	No	0/2	No
Anomalocarididae	1-3	13	Yes	2	1	Yes	Yes	No	0/2	No
Hurdiidae	1/2	8-10	No	1	5	No	No	Yes	0-5	*Hurdia* only
Laminacaris	2	13	Yes	1?	1	Yes	No	Yes	5	Yes
Tamisiocarididae	?1	13/17	Yes	2	0/1*	No	Yes*	?Yes*	?*	No*

**A. briggsi* bears an enlarged post-shaft endite, and *Tamisiocaris* does not. Hence all characters referring to the morphology of the large ventral endite for this family refer to *A. briggsi* only. Abbreviations: as, auxiliary spine; d.a.r., distal articulated region; en, ventral endite; pd, podomere

Anomalocarididae as the ventral endite on the fifth podomere in the distal articulated region is longer than that on the third, and the distal region often bears thickened dorsal spines, in contrast to Anomalocarididae, where they are thinner.

Tamisiocarididae ('Cetiocaridae' of Vinther et al. 2014), a clade comprising *Tamisiocaris borealis* and *Anomalocaris briggsi* (Vinther et al. 2014; Cong et al. 2014; Van Roy et al. 2015) have a pair of elongated and slender ventral endites that have a length at least 1.5x the height (sag) of the podomere to which are attached. The appendage is simple, with the same morphology of ventral endite along the distal articulated region. There is no differentiated post-shaft podomere in *Tamisiocaris* appendages, although *Anomalocaris briggsi* does have an enlarged post-shaft ventral endite and an additional endite of similar morphology on the distalmost position of the shaft. There is no alternation of long/short ventral endites in these taxa, with the overall length of ventral endites decreasing along the length of the appendage. *Caryosyntrips, Laminacaris,* and *Lyrarapax* have an uncertain placement at family level, but can be distinguished based on features of the frontal appendages. *Caryosyntrips* appendages taper distally with an approximately triangular outline. Similar to tamisiocaridids, the appendages are simple, with no alternation of long/short ventral endites, and no enlarged endite distal to the shaft. *Laminacaris,* a recently described monospecific genus from the Chengjiang biota, bears a ventral endite on the most proximal podomere in the distal articulated region similar in morphology to *Hurdia* ventral endites, but the remainder of the distal articulated region is similar to Anomalocarididae and Amplectobeluidae. *Lyrarapax* appendages superficially resemble those of Amplectobeluids, as appendages have an enlarged ventral endite on the post-shaft podomere, and simple ventral endites alternating long/short or present/absent in the distal articulated region. Appendages

differ in podomere shape (near square in *Lyrarapax* and rectangular in *Amplectobelua*) but the major differences are in the oral cone morphology (tetraradial arrangement of large plates with smaller plates between in *Lyrarapax*, an association of tuberculate and smooth plates in Amplectobluidae) and gnathobase-like structures present in Amplectobeluidae but not *Lyrarapax* (Cong et al. 2018; Liu et al. 2018).

3. Materials and Methods

Eight specimens of Radiodonta from the Kinzers Formation are known. Material is held at the National Museum of Natural History, Washington D.C., USA (USNM), North Museum, Franklin and Marshall College, Lancaster, Pennsylvania, USA (PA), and Yale Peabody Musem, New Haven, Connecticut, USA (YPM).

For historical reasons, the part and counterpart of most of the specimens are held at two institutions, the USNM and PA. Some material was not available for study by Briggs (1979), namely the part of the Holotype of *Anomalocaris pennsylvanica*, and USNM 90827 (Resser and Howell 1938, pl. 13, fig. 5). As another specimen was also labelled USNM 90827 that was available for study by Briggs (1979), there is confusion in the literature about the specimens labelled with this number. The USNM 90827 specimen figured in Resser and Howell (1938, pl. 13, fig. 5) is different to that figured by Briggs (1979, pl. 81, fig. 11, text-fig. 34), and Briggs (1979) noted that the specimen figured by Resser and Howell (1938) was different to those in the collection. Both specimens labelled USNM 90827 were available for this study, but are not part and counterpart. The specimen figured first, by Resser and Howell (1938) retained the number USNM 90827, and the specimen figured second, by Briggs (1979) has been

given the altered number USNM 90827A. Both specimens are radiodonts, described herein.

Specimens were photographed wet and dry under polarized and non-polarized light using a Canon EOS 500D digital SLR Camera with a Canon EF-S 60 mm Macro Lens, controlled for remote shooting using EOS Utility 2. Digital measurements were made using Image J (Schneider et al. 2012). Modern longitude and latitude coordinates were reconstructed to 510Ma using GPlates (Scotese 2016). Coordinates were obtained from the literature. Where it was not possible to obtain the exact coordinates of the fossil locality, the nearest town was used in its place.

4. Systematic Palaeontology

Total-group EUARTHROPODA Lankester 1904

Order RADIODONTA Collins 1996

Laminacaris? sp.

Figure 2

v. 1979 *Anomalocaris*? cf. *pennsylvanica;* Briggs, pl. 81, figs 9-11, text-figs 33, 34

Material: Two partial isolated frontal appendages collected from the Kinzers Formation, Pennsylvania, USA, are known from part and counterpart: USNM 213993, PA 394 (counterpart), locality 22L; USNM 90827A, PA 393 (counterpart), locality 12x.

Description. USNM 213993/PA 394 (Fig. 2a,b) is a partial appendage, with one shaft podomere (Fig. 2b, pd1) and six podomeres in the distal articulated region preserved

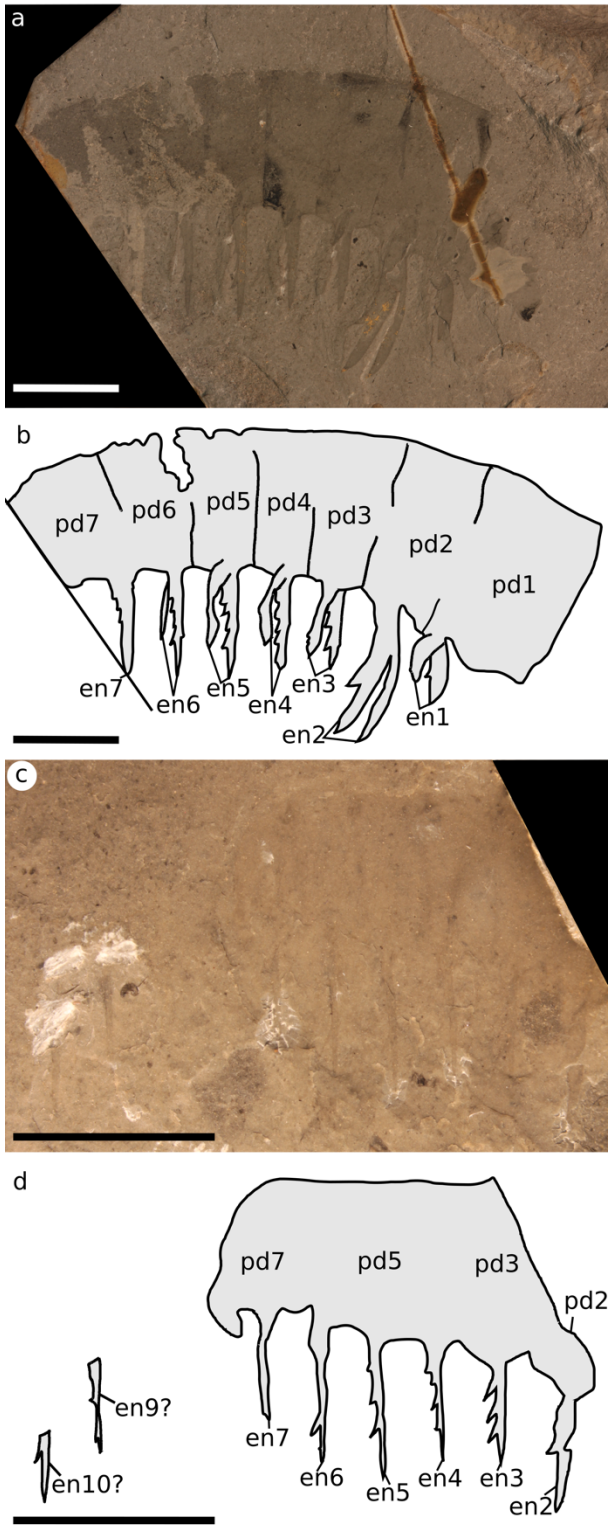

Figure 2. *Laminacaris?* sp. from the Kinzers Formation. (a,b) USNM 213693; (c,d) USNM 90827A. Scale bars 10 mm. Abbreviations: enX, ventral endite X; pdX, podomere X.

(Fig. 2b, pd2-7). A pair of thickened recurved ventral endites with distally pointing auxiliary spines is present on the shaft podomere, at the distalmost ventral point (Fig. 2b, pd1). Ventral endites attach to the midpoint of the other podomeres. The ventral endite on the podomere immediately distal to the shaft is curved distally, and approximately the same length and the height (sag) of the podomere, and bears a distally pointing auxiliary spine 2/3 of the way down the spine (Fig. 2b, en2). The other ventral endites in the distal articulated region are paired and approximately the height (sag) of the podomere to which they are attached. Distally pointing auxiliary spines are present along the length, and rarely a proximally pointing spine is visible (Fig. 2b, en6). Auxiliary spines point slightly ventrally. Podomeres are tall (sag) rectangles, approximately twice as tall as wide, decreasing in size distally. No dorsal spines are visible.

USNM 90827A (Fig. 2c,d) preserves 6 rectangular podomeres approximately twice as high (sag) as wide (trans) with ventral endites attached, and traces of two ventral endites that have been prepared out the matrix (Fig. 2d, en9? & en10?). Just as for USNM213993/PA394, USNM 90827A ventral endites are straight and approximately the same height as the podomere (e.g. Fig. 2d, en5), and an enlarged endite is present with a single auxiliary spine 2/3 of the way along its length at the proximal end, inferred to be pd2 (Fig. 2d, en2). One endite (Fig. 2d, en5) is longer than the others. Auxiliary spines project both distally and proximally, with a slight ventral tilt.

Remarks: This taxon is similar to *Lamincaris chimera* from the Chengjiang biota (Guo et al. 2018). This animal, known only from frontal appendages, has straight ventral endites in the distal articulated region with distally pointing auxiliary spines, and enlarged

ventral endites on the distalmost point of the shaft and proximal-most post-shaft podomere. The distally pointing auxiliary spines along the length of the endite in *Laminacaris chimera* from Chengjiang is similar to the arrangement of auxiliary spines in the Kinzers material. The ventral endites are shorter than the height of the podomere to which they attach in both the Chengjiang and Kinzers material, but the alternating long and short endites of *Laminacaris chimera* is not present in the incompletely preserved Kinzers specimens which are approximately the same length. The enlarged ventral endite in the Kinzers material does not have the distinctive blade-like morphology with a strong similarity to *Hurdia* ventral endites that is seen in *Laminacaris chimera*, however it is enlarged relative to the other endites and recurved. This enlarge endite in the Kinzers material bears more similarity to the post-shaft ventral endite of *Lyrarapax trilobus* or *Amplectobelua stephenensis*, although it is not as thickened as these two taxa. The endite on the shaft is similar in *Laminacaris* and this Kinzers taxon, as it bears a single distally facing auxiliary spine approximately two thirds of the distance from the base to the tip. The Kinzers *Laminacaris* sp. material could also be compared to *Anomalocaris briggsi* from the Emu Bay Shale, particularly the shape of the podomeres and the possible lack of alternating long/short ventral spines. However, the auxiliary spines point both distally and proximally in *A. briggsi*, in contrast to the distally pointing spines of the Kinzers specimens, the ventral endites are shorter relative to podomere height in the Kinzers material than in *A. briggsi*, and the enlarged ventral endites on the shaft and proximal podomere in the distal articulated region are of a different morphology.

Family ANOMALOCARIDIDAE Raymond 1935

Genus ANOMALOCARIS Whiteaves 1892

Type species. Anomalocaris canadensis Whiteaves 1892 from the Stephen Formation (Cambrian Series 3, Stage 5) of British Columbia, Canada.

Anomalocaris pennsylvanica Resser 1929

Figure 3

v. 1929 *Anomalocaris pennsylvanica;* Resser, pl. 5, fig. 5, pl. 79, fig. 5

v. 1938 *Anomalocaris pennsylvanica;* Resser and Howell, pl. 10, fig. 4

v. 1979 *Anomalocaris pennsylvanica;* Briggs, pl. 79, fig. 5, text-fig. 18, pp. 641

Holotype. Isolated appendage, Kinzers Formation, Pennsylvania, USA, USNM 80487 (part and counterpart), locality 12x.

Paratype. Isolated appendage, Kinzers Formation, Pennsylvania, USA, YPM 10425 (part only), locality 12x.

Other material. Partial isolated appendage, Kinzers Formation, Pennsylvania, USA, USNM 255611, locality 22L.

Diagnosis. *Anomalocaris* appendage composed of 14 podomeres; one podomere in the shaft wider than tall; 13 podomeres in the distal articulated region taller than wide; all podomeres in the shaft and the distal articulated region bear a pair of ventral endites projecting from the midpoint of the ventral surface; ventral endites are present on pd1-13, lack auxiliary spines, and alternate long/short on even/odd numbered podomeres; ventral endites on proximal podomeres at least as long as the height of the podomere

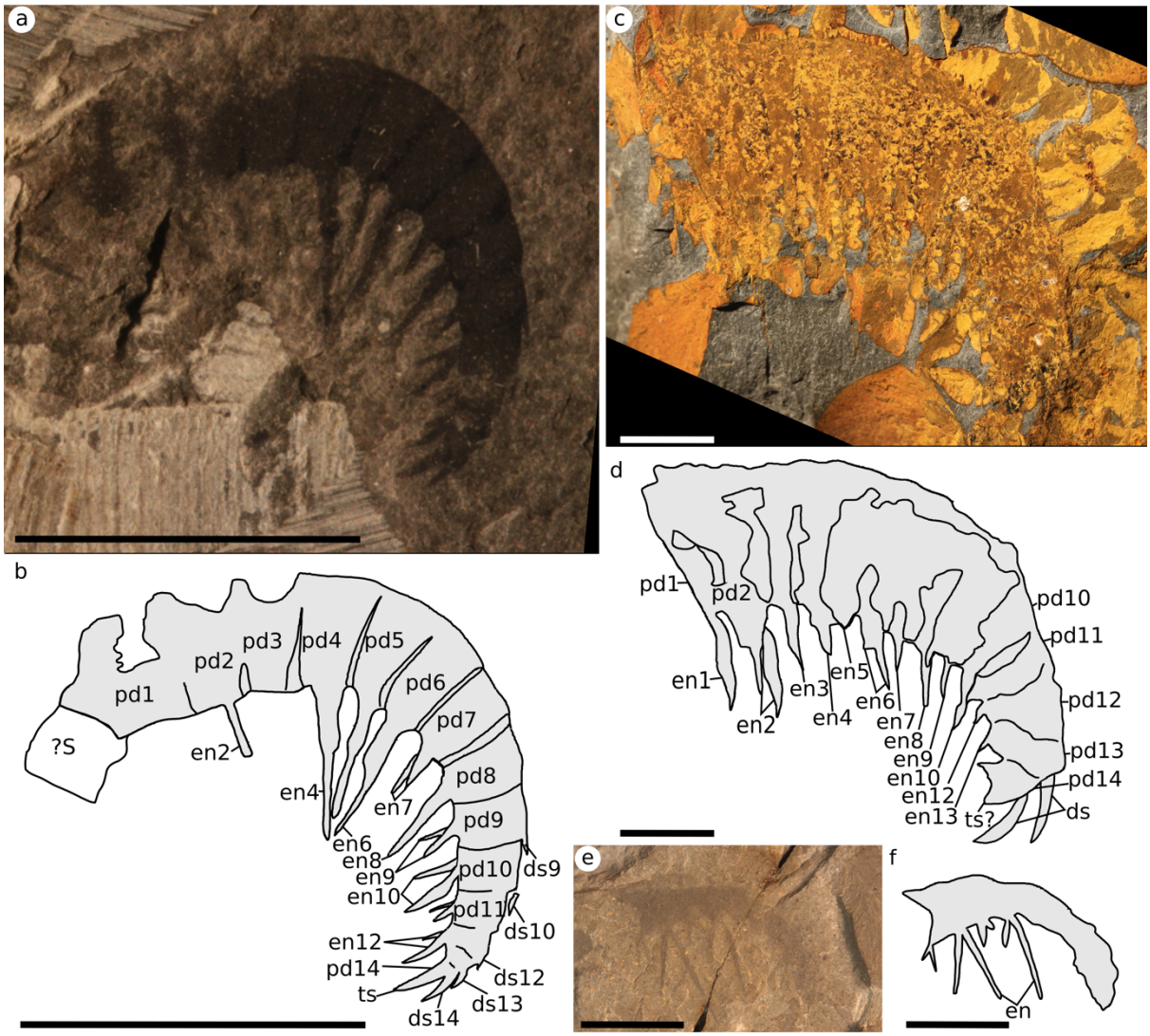

Figure 3. *Anomalocaris pennsylvanica* from the Kinzers Formation. (a,b) Holotype USNM 80487; (c,d) YPM 10425; (e,f) USNM 255611. Scale bars 10 mm. Abbreviations: dsX, dorsal spine X; enX, ventral endite X; pdX, podomere X; ?S, putative shaft podomere; ts, terminal spine.

they attach to, and decrease in length relative to podomere height distally; ventral endite of the shaft is not distinct from the ventral endites of the distal articulated region; thin straight dorsal spines project forward from distal dorsal margin of pd9-14; single robust terminal spine.

Description: *Anomalocaris pennsylvanica* is known from three specimens: the holotype (part and counterpart) measuring 23 mm (Fig. 3a,b); a partial small appendage (USNM 255611) (Fig. 3e,f); and a large complete appendage (YPM 10425) measuring 75 mm (Fig. 3c,d). Complete specimens have 14 podomeres, one in the shaft and 13 in the post-shaft region. The presence of a podomere boundary between pd13 and pd14 is confirmed in the holotype by counting the dorsal spines in the distal region, where the podomere boundaries are not well preserved (see Fig. 3b: ds13, ds14). The holotype also potentially shows a second shaft podomere, an approximately square feature preserved as a faint outline, however it joins at an oblique angle to the ventral surface, not the dorsal surface like shaft podomeres in other species (Fig. 3b: ?S). YPM 10425 shows that the shaft bears a large ventral endite at the distal margin (Fig. 3d: en1). YPM 10425 also appears to have a longer ventral endite on pd6 than pd4 (compare Fig. 3d en4 and en6), however the overprint of iron minerals in the rock means that this cannot be confirmed. This is similar to what is seen in Amplectobleuidae, however the number of podomeres (14) is consistent with *Anomalocaris*.

Although the material is limited, the three specimens of different size suggest that the podomeres grew taller relative to the width of podomeres and length of ventral endites through ontogeny, and so larger appendages have smaller ventral endites relative to podomere height. The smallest of the specimens (USNM 255611) has the

longest endite to podomere height ratio, at 2:1 at the proximal end. The largest specimen (YPM 10425) has the lowest ratio, at close to 1:1 with the ratio in the holotype approximately 1.5:1. Similarly the podomere height:width ratio is higher (2.5:1) in YPM 10425 than the holotype (1.5:1). Podomere boundaries are not preserved in USNM 255611.

Remarks: Much of the material previously assigned to *Anomalocaris pennsylvanica* is here reassigned to other radiodont genera (see below). PA 389, PA 395A, and YPM 63295 are removed from Radiodonta altogether because these likely represent partial bodies and appendages of non-radiodont euarthropods.

The counterpart to the holotype was not available for study by Briggs (1979) however the interpretation of this specimen, and the description of this species has not changed significantly. Briggs (1979) also noted that larger *Anomalocaris pennsylvanica* appendages had shorter ventral endites relative to podomere height than smaller appendages of this species. Although the material with the shortest ventral endites is here reassigned to other genera, this observation still holds.

Anomalocaris pennsylvanica Resser 1929 was the second radiodont species to be described, and is only known from isolated frontal appendages. It can be distinguished from *Anomalocaris canadensis*, the type species, based on the morphology of its ventral endites. In *A. pennsylvanica* these are simple, whereas for *A. canadensis* each ventral endite bears two auxiliary spines, creating a trident shape (Briggs 1979). It has been suggested that the lack of auxiliary spines on ventral endites could be taphonomic, in which case *A. pennsylvanica* could be synonymized with *A. canadensis,* however it was retained as a valid taxon based on the limited material available (Briggs 1979;

Lieberman 2003; Daley and Peel 2010). *Anomalocaris pennsylvanica* is here confirmed as a valid taxon. The ventral endites have smooth margins and show no evidence of taphonomically removed auxiliary spines. Furthermore, the three known specimens of *A. pennsylvanica* show other differences that distinguish it from other *Anomalocaris* species. It can be differentiated from the most similar species, *A. canadensis*, not only by the lack of auxiliary spines on the ventral endites, but also by the ventral endites being longer relative to podomere height towards the proximal end of the appendage, and by the distal end of the appendage not having differentiated shorter and simplified ventral endites, as is seen in *A. canadensis*. *A. canadensis* also has a reduced ventral endite on the distalmost ventral point of the shaft, whereas *A. pennsylvanica* has a long ventral endite similar to those of the distal articulated region.

Anomalocaris pennsylvanica is endemic to the Kinzers Formation, as other specimens attributed to this species from the Pioche Formation (Lieberman 2003) bear auxiliary spines and will be described as a new species of *Anomalocaris* in an upcoming review of Southern Great Basin material (Chapter 7).

Family TAMISIOCARIDIDAE nov.

Type genus. *Tamisiocaris* Daley & Peel 2010

Diagnosis. Radiodont with a frontal appendage bearing slender blade-like ventral endites longer than the podomere to which they are attached; ventral endites do not alternate long/short.

Remarks. The family 'Cetiocaridae' was named by Vinther et al. 2014, however this name is invalid by ICZN conventions (see Van Roy et al. 2015). The family comprises *Tamisiocaris* and *Anomalocaris briggsi*, which were recovered together by a phylogeny of radiodonts (Vinther et al. 2014, fig. 3), and subsequently by Cong et al. (2014) and Van Roy et al. (2015).

Genus TAMISIOCARIS Daley & Peel 2010

Type species. Tamisiocaris borealis Daley & Peel 2010.

Diagnosis. Radiodont with paired frontal appendages adjacent to an oval shaped central carapace element; appendage has at least one podomere in the shaft, with 17 podomeres in the distal articulated region separated by a triangular membrane; shaft podomere is wider (trans) than tall (sag) and bears a straight proximally pointing endite at the distal ventral margin approximately the same length as the height (sag) of the podomere; podomeres in the distal articulated region reduce in height towards the distal end and bear paired slender ventral endites at least twice the length (sag) of the height (sag) of the podomere; length of ventral endites decreases distally forming a straight line between the distal ends of the ventral endites (emended from Daley and Peel, 2010).

Remarks. Fine auxiliary spines were not preserved in the holotype of *Tamisiocaris*, and so not included in the original Diagnosis. They were subsequently recognized in new material described by Vinther et al. (2014), although the diagnosis of genus and species

was not updated in that study. As the specimen from the Kinzers Formation assigned to this genus does not have apparent auxiliary spines (see below) the presence of fine auxiliary spines is not included in the diagnosis of this genus.

Tamisiocaris borealis Daley & Peel, 2010

2010 *Tamisiocaris borealis*; Daley & Peel, fig. 1

2014 *Tamisiocaris borealis*; Vinther et al., figs 1, 2, extended data figs 1-4, 6, 7

Holotype. Isolated frontal appendage, Peary Land, central North Greenland, base of the Buen Formation, MGUH 29154, by original designation.
Paratypes: Isolated frontal appendages, from same locality as holotype. MGUH 30500 (displays articulating triangular membranes); MGUH 30501 (displays fine auxiliary spines), designated herein.
Other material: Three other isolated frontal appendages of this species are known, also from same locality as holotype. MGUH 30502 – 4.

Diagnosis. Tamisiocaris with an appendage that bears fine auxiliary spines along the length of both proximal and distal surfaces of the ventral endites; auxiliary spines are straight, do not change length along the appendage and are separated vertically by less than the width (trans) of the ventral endite (emended from Daley & Peel, 2010).

Remarks. *Tamisiocaris borealis* was originally described as a radiodont frontal appendage by Daley and Peel (2010). A subsequent study by Vinther et al. (2014) with

new material provided new information about the appendage, including the presence of triangular articulating membrane between the podomeres and fine auxiliary spines along the length of the ventral endites. This confirmed the hypothesis that the taxon belongs to Radiodonta, and suggested a sifting/filtering feeding ecology, however Vinther et al. (2014) did not update the Diagnosis of the genus or species, nor designate new paratypes with these new features. This has been done here to allow comparison with the Kinzers Formation material.

Tamisiocaris aff. *borealis*

Figure 4

v. 1938 *Anomalocaris pennsylvanica;* Resser and Howell, pl. 13, fig. 5

v. 1979 *Anomalocaris pennsylvanica;* Briggs pp. 641

Material: Partial isolated frontal appendage, Kinzers Formation, Pennsylvania, USA, USNM 90827, PA 388 (counterpart).

Description. USNM 90827/PA 388 (Fig. 4) shows a partial appendage of 9 podomeres (Fig. 4b, ?pd10-?pd18), each bearing a long and slender ventral endite (Fig. 4b, en). The podomeres are approximately square where boundaries can be discerned (e.g. Fig. 4b, ?pd14) with the ventral endites twice the height (sag) of the podomeres. The podomeres reduce in height towards the distal end, where the shape becomes an elongate rectangle (e.g. Fig. 4b, ?pd18). No auxiliary spines are visible on the ventral endites, and no dorsal spines are visible on the appendage.

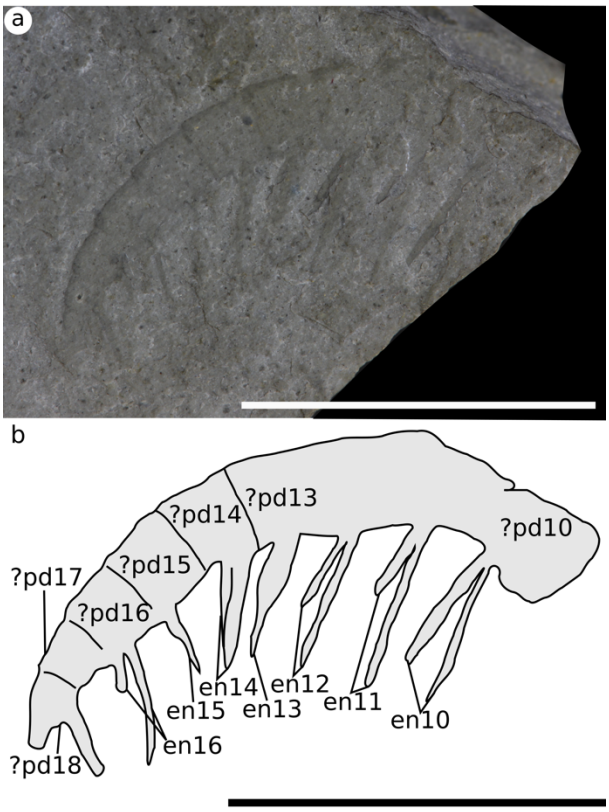

Figure 4. *Tamisiocaris* aff. *borealis* from the Kinzers Formation. (a,b) PA 388. Scale bars 10 mm. Abbreviations: en, ventral endite; ?pdX, podomere X, inferred from complete *T. borealis* appendages.

Remarks: This specimen is no longer considered *Anomalocaris pennsylvanica* as the podomeres are square to elongate rectangular in shape (as opposed to tall rectangles), and the ventral endites, although they lack auxiliary spines, do not alternate long/short on even/odd numbered podomeres and instead reduce in length along the appendage.

This specimen is instead considered to belong to the genus *Tamisiocaris* as it has long, paired, ventral endites which do not alternate long/short, similar to *T. borealis* from Sirius Passet. The approximate square-shape of the podomeres is consistent with the distal end of known *Tamisiocaris* specimens from Sirius Passet. Just as in *Tamisiocaris borealis,* this specimen lacks any dorsal spines, which would instead indicate affinities with *Anomalocaris briggsi*. There is no evidence that this specimen bears auxiliary spines, which are visible in some specimens of *T. borealis* (although not the type specimen), and it is only known as a partial appendage so the number of podomeres cannot be ascertained. Because of this the specimen is left in open nomenclature as *T.* aff. *borealis*.

This is the youngest *Tamisiocaris* known (Cambrian Stage 4) and the first from outside the Sirius Passet Lagerstätte (Cambrian Stage 3, Greenland). *Tamisiocaris* is still only known from Laurentia.

Family AMPLECTOBELUIDAE Vinther et al. 2014

Genus AMPLECTOBELUA Hou et al. 1995

Amplectobelua aff. *symbrachiata*

Figure 5

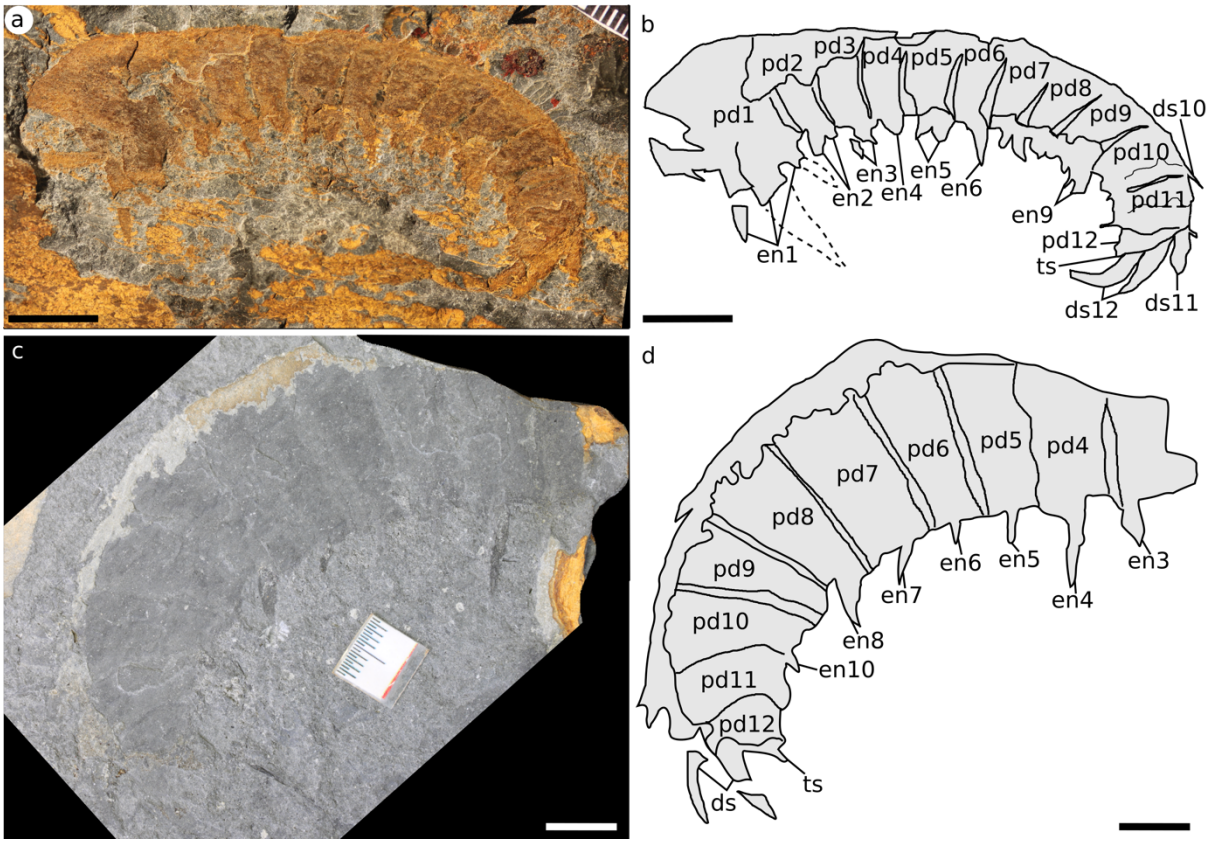

Figure 5. *Amplectobelua* aff. *symbrachiata* from the Kinzers Formation. (a,b) YPM 14388; (c,d) PA 390. Scale bars 10 mm. Abbreviations: ds, dorsal spines; enX, ventral endite X ; pdX, podomere X.

1938 *Anomalocaris pennsylvanica;* Resser and Howell, pl. 13, fig. 6

1953 *Anomalocaris pennsylvanica*; Roger, pl. 2 fig. 4

1979 *Anomalocaris pennsylvanica*; Briggs, pl. 79 figs 4, 6, text-figs 17, 19

Material. Isolated frontal appendages, Kinzers Formation, Pennsylvania, USA, YPM 14388 (part) and PA 387 (counterpart) locality 12x; PA390 (part and counterpart) locality 22L.

Description: Two *Amplectobelua* appendages can be recognized from the Kinzers Formation. YPM 14388 (Fig. 5a, b), with counterpart PA387, is a complete isolated appendage with 12 podomeres. The podomeres are tall and rectangular but become more square towards the distal end (compare pd5 to pd10 in Fig. 5b). A long and stout endite with the base of three spines preserved is present on the most proximal podomere (Fig 5b, pd1, en1). The central spine base is the thickest, with the proximal-most spine preserved in its entirety. Short and paired spinose endites are present on the remaining podomeres, although most are incomplete, and the endite on pd6 shows that they were simple spines shorter than the podomere to which they attached (Fig. 5b, en6). The broken base on pd5 is wider than the broken base of pd3, implying that the ventral endite on this pd5 was more robust than that of pd3 (en3, en5, Fig. 5b). The distalmost two podomeres (pd11-12) bear robust paired dorsal spines which are recurved following the outline of the appendage and combine with a reduced terminal spine to make a claw-like termination (Fig. 5b, ds & ts). PA 390 (Fig. 5c, d) is a partial appendage with the 10 most distal podomeres visible. Podomeres are tall and

rectangular, but become more square at the distal end (compare Fig. 5d, pd4 to pd9 and pd12). All the ventral endites are short (e.g. Fig. 5b, en6-8) and robust recurved dorsal spines are visible at the distal end (Fig. 5d, ds) alongside a reduced terminal spine (Fig. 5d, ts). In both YPM 14388 and PA 390 some smaller and straight dorsal spines are visible proximal to the robust dorsal spines (e.g. Fig. 5b, ds10).

Remarks: These specimens are no longer considered *Anomalocaris pennsylvanica* as the dorsal spines at the distal end are paired and much more robust, the ventral endites along the appendage are short, and the number of podomeres (where they can be counted) is 12 instead of 14. This interpretation differs slightly from the previous descriptions, where both these appendages were interpreted to have 14 podomeres (Briggs 1979, plate 79 figs 4, 6; text-figs 17, 19). The podomere labelled as j6 of PA 390 (Briggs 1979, plate 79 fig 4, text fig 17) is here interpreted as the eighth podomere, j1 and j2 of YPM 14388 (Briggs 1979, plate 79 fig 6, text fig 19) are interpreted as being an enlarged 1st podomere (Fig. 5b, pd1), since no podomere boundary is visible here (none was drawn in Briggs 1979, text fig 19). The structure labelled as j14 is here interpreted as one of a pair of robust dorsal spines (Fig. 5b, ds12).

A number of lines of evidence support the reinterpretation of these two appendages as *Amplectobelua*, including the presence of paired but short ventral endites along the majority of the appendage, the rectangular podomeres, and paired robust dorsal spines at the distal end. In addition, YPM 14388 has an enlarged ventral endite on pd1 (pd1 is not preserved in PA 390), and the base of the endite on pd5 appears more robust than that of pd3. These specimens are most similar to *Amplectobelua symbrachiata*, as they both bear short ventral endites along the

appendage alternating long/short and the morphology of the enlarged ventral endite is constructed of three spines with the thickest in the centre, unlike in *Amplectobelua stephenensis* where there is only one very enlarged and thickened spine on the most proximal podomere*. Amplectobelua symbrachiata* also bears smaller dorsal spines proximally to the enlarged recurved dorsal spines, as is also seen in both the specimens from the Kinzers Formation. The material from the Kinzers however does not have exactly the same morphology as *Amplectobelua symbrachiata*, because it has a reduced terminal spine, not present in the Chengjiang species, and evidence for paired dorsal spines not reported from the Chinese animal, but a feature known from *Amplectobelua stephenensis*. The podomeres become more square shaped towards the distal end in the Kinzers species, a feature not seen in either *Amplectobelua symbrachiata* or *Amplectobelua stephenensis*.

The preservation does not allow all the anatomical features to be recognized. For example the morphology of the enlarged ventral endite is not completely known, specifically the length of the central thickened spine. In addition, there is no evidence of the shaft, which is expected to be of three podomeres in *Amplectobelua*. For these reasons this species is left in open nomenclature.

These are the first *Amplectobelua* from the Cambrian Stage 4, the first from the USA, and the oldest in Laurentia. *Amplectobelua* was previously known from the Stage 3 of China and Stage 5 of Canada. They bear more similarity to the Chinese species, *Amplectobelua symbrachiata,* than the Canadian, *Amplectobelua stephenensis,* perhaps indicating an invasion by the Chinese species at the end of Stage 3 followed by a subsequent radiation in Laurentia.

5. Discussion

5.a. Diverse feeding strategies of Kinzers Formation Radiodonta

The Kinzers Formation contains one species of *Anomalocaris*, *Amplectobelua, Tamisiocaris,* and tentatively *Laminacaris* (Fig. 6; Table 2). The presence of a number of different radiodonts from the same site is not unusual for Cambrian Lagerstätten, and supports previous suggestions that these stem-group euarthropods employed a number of different feeding strategies (Daley & Budd 2010; Vinther et al. 2014; Van Roy et al. 2015). *Anomalocaris pennsylvanica* would have used its flexible appendages to actively grab likely soft-bodied prey and slice it with the simple elongate ventral endites. *Amplectobelua* aff. *symbrachiata* would have used its more robust proximal ventral endite and thickened distal dorsal spines to more tightly hold and slice or potentially crush prey. The presence of reduced ventral endites between the proximal and distal end would have allowed the appendage to coil more tightly, allowing the distal and proximal robust spines to come together more easily in a slicing or crushing motion. *Tamisiocaris* aff. *borealis* may not have been a filter feeder targeting plankton like the Sirius Passet species if the lack of fine auxiliary spines is not an artefact of preservation, and so instead may have sifted or raked through the sediment. It is also possible that it filtered larger particles than the Greenland species, and so did not require auxiliary spines. *Laminacaris?* sp. likely used its straight ventral endites with auxiliary spines to function as a net-like apparatus, potentially similar to some hurdiids, and as suggested for *Anomalocaris briggsi* from the Emu Bay Shale (Daley et al. 2013b). Its longer ventral spines, and lack of clear alternating long/short ventral endites make a raptorial feeding strategy similar to that inferred for *Laminacaris chimera*, less likely.

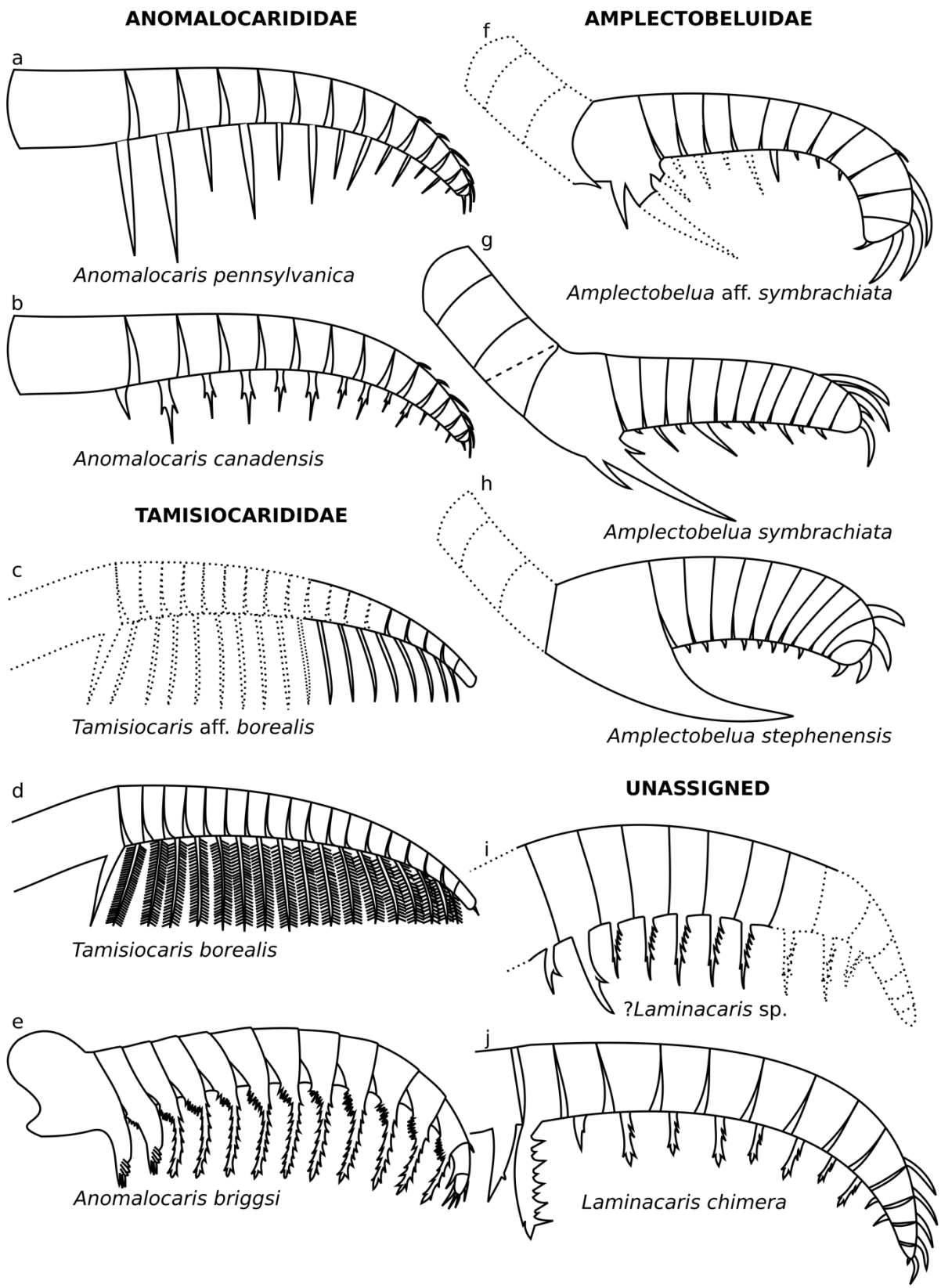

Figure 6. Caption on the next page.

Figure 6. Reconstructions of Radiodonta from the Kinzers Formation, and other frontal appendages with similar morphology. (a) *Anomalocaris pennsylvanica*; (b) *Anomalocaris canadensis*; (c) *Tamisiocaris* aff. *borealis*; (d) *Tamisiocaris borealis*; (e) *Anomalocaris briggsi*; (f) *Amplectobelua* aff. *symbrachiata*; (g) *Amplectobelua symbrachiata*; (h) *Amplectobelua stephenensis*; (i) *Laminacaris?* sp; (j) *Laminacaris chimera*. Dotted lines show parts of appendage that are not preserved. Line drawings (b), (g), and (h) adapted from Daley & Budd (2010, text-fig. 1A, F, G), (d) adapted from Vinther et al. (2014, extended data fig. 6a), (e) adapted from Daley et al. (2013b, fig. 2), and (j) redrawn from Guo et al. (2018, fig. 3A).

Table 2: Current and previous interpretations of Kinzers radiodont appendages.

Catalogue #	Fig.	Site	Previous interpretation	Current interpretation	Reference
USNM 90827A, PA 393 (cpt)	2c,d	22L	*Anomalocaris*? cf. *pennsylvanica*	*Laminacaris?* sp.	Briggs 1979 pl. 81 fig. 11, text-fig. 34.
USNM 213693, PA 394 (cpt)	2a,b	22L	*Anomalocaris?* cf. *pennsylvanica*	*Laminacaris?* sp.	Briggs 1979 pl. 81 figs. 9,10, text-fig. 33.
USNM 80487 (part and cpt)	3a,b	12x	*Anomalocaris pennsylvanica* (holotype)	*Anomalocaris pennsylvanica* (holotype)	Resser 1929, pl. 5, fig. 5; pl. 79, fig. 5; Resser and Howell 1938, pl. 10, fig. 4; Briggs 1979 pl. 79 fig. 5, text-fig. 18.
YPM 10425	3c,d	12x	*Anomalocaris pennsylvanica*	*Anomalocaris pennsylvanica*	Briggs 1979
USNM 255611	3e,f	22L	*Anomalocaris pennsylvanica*	*Anomalocaris pennsylvanica*	Briggs 1979
USNM 90827, PA 388 (cpt)	4	22L	*Anomalocaris pennsylvanica*	*Tamisiocaris* aff. *borealis*	Resser and Howell 1938, pl. 13, fig. 5; Briggs 1979*
YPM 14388, PA 387 (cpt)	5a,b	12x	*Anomalocaris pennsylvanica*	*Amplectobelua* aff. *symbrachiata*	Resser and Howell 1938, pl. 13, fig. 6; Roger 1953, pl. 2 fig. 4; Briggs 1979 pl. 79 fig. 6, text-fig. 19.
PA 390 (part and cpt)	5c,d	22L	*Anomalocaris pennsylvanica*	*Amplectobelua* aff. *symbrachiata*	Briggs 1979, pl. 79 fig. 4, text fig 17
PA 389	-	22L	*Anomalocaris pennsylvanica*	Euarthropoda indet.	Briggs 1979
PA 395a	-	22L	*?Anomalocaris pennsylvanica*	Indet.	Briggs 1979
YPM 63295	-	12x	*Anomalocaris pennsylvanica*	Euarthropoda indet.	Lieberman 2003

Site numbers: 12x, one and three quarter miles north of Rohrerstown, Pennsylvania; 22L, half a mile south of East Petersburg, Pennsylvania (Briggs 1979). References refer to previous interpretation. *Briggs (1979) only had PA 388 available, and was not able to study USNM 90827.

5. b. Importance of the Kinzers Formation

Radiodonta are known from other Cambrian Series 2, Stage 4, Konservat-Lagerstätten, however the Kinzers Formation (30°S palaeolatitude, Laurentia) is uniquely important for understanding the palaeogeographic and palaeolatitudinal distribution of these animals (Fig. 7) because of the high diversity of taxa found there. Radiodonta are known from four other broadly coeval formations in North America from Laurentia (all equatorial): Latham Shale (Briggs and Mount 1982), Comet Shale Member, Pioche Formation (Lieberman 2003), Eagar Formation, Cranbrook Shale (Briggs 1979), and Pyramid Shale Member, Carrara Formation (unpublished material). Radiodonta have also been reported from two formations of this age on the South China palaeocontinent (ca. 30°N palaeolatitude): the Balang Formation (Liu 2013), and Wulongqing Formation (Wang et al. 2013); and from two Gondwanan sites: the Emu Bay Shale in Australia (ca. 15°N palaeolatitude) (Nedin 1995; Daley et al. 2013b) and Valdemiedes Formation in Spain (ca. 60°S palaeolatitude) (Pates & Daley 2017) (Table 3; Fig. 7).

The recognition of four different radiodont taxa, from at least three different families, means that the Kinzers Formation has the most diverse Radiodonta fauna of all the Stage 4 Konservat-Lagerstätten, despite relatively few specimens being known - especially compared to the Emu Bay Shale and Wulongqing Formation (Table 3). The fauna contains links with both the older Sirius Passet (*Tamisiocaris*) and Chengjiang (*Amplectobelua, Anomalocaris* and *Laminacaris*) faunas, as well as the younger Burgess Shale (*Amplectobelua* and *Anomalocaris*). It has a named endemic species with *Anomalocaris pennsylvanica,* with at least two (and potentially all four) of its radiodont species not yet known from other localities. Its unique position at a non-equatorial

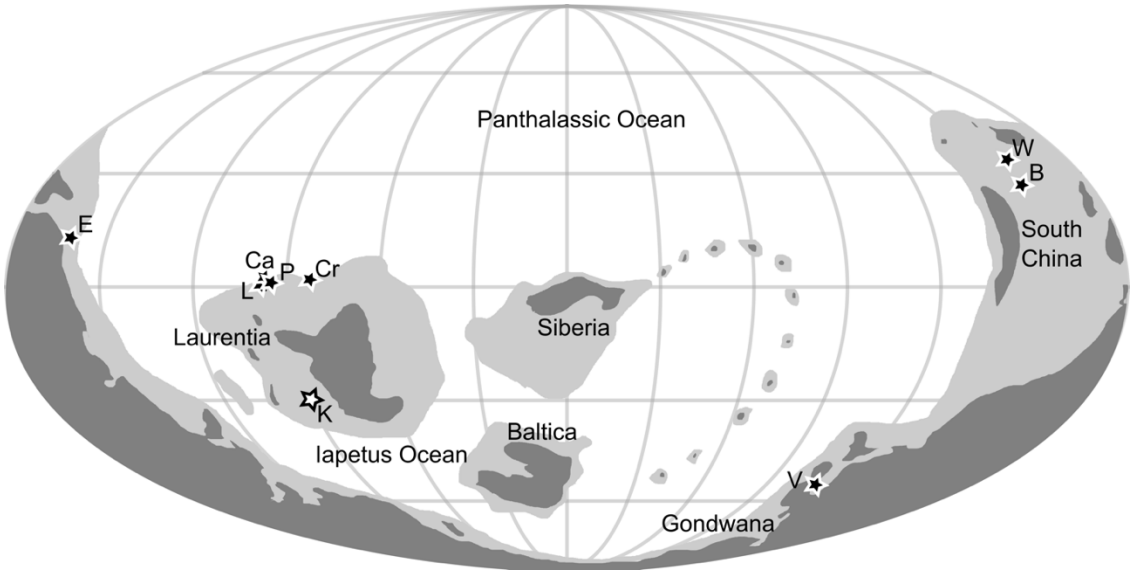

Figure 7. Palaeogeographic reconstruction to 510 Ma from GPlates (Scotese 2016). White star shows Kinzers Formation; black stars show other Stage 4 sites where radiodont fossils have been found. Abbreviations: B, Balang Formation; Ca, Carrara Formation; Cr, Cranbrook Formation; E, Emu Bay Shale; K, Kinzers Formation; L, Latham Shale; P, Pioche Formation; V, Valdemiedes Formation; W, Wulongqing Formation.

Table 3: Cambrian Series 2, Stage 4 Radiodonta bearing Konservat-Lagerstätten.

Formation	Palaeocontinent	Palaeolatitude	# Specimens	# Radiodont taxa	References
Kinzers Formation	**Laurentia**	**30°S**	**8**	**4**	**Resser 1929; Briggs 1979; this study**
Carrara Formation	Laurentia	0° (equator)	(4)	(1)	Unpublished material
Cranbrook Shale	Laurentia	0° (equator)	2	1	Briggs 1979
Latham Shale	Laurentia	0° (equator)	3 (+1)	1	Briggs and Mount 1982
Pioche Formation	Laurentia	0° (equator)	24 (+1)	1 (+1)	Lieberman 2003; unpublished material
Emu Bay Shale	Gondwana	15°N	69	2	Nedin 1995; Daley et al. 2013b
Valdemiedes Formation	Gondwana	60°S	1	1	Pates & Daley 2017
Balang Formation	South China	30°N	2	2	Liu 2013
Wulongqing Formation	South China	30°N	48	2	Wang et al. 2013

Number of known specimens and known taxa, with palaeocontinent and palaeolatitude reconstructed using GPlates (Fig. 7; Scotese 2016). Numbers of unpublished specimens studied by authors in brackets.

latitude in Laurentia, as well as the lack of any Tier 1 Burgess Shale Type deposits (*sensu* Gaines 2014) in the Cambrian Series 2 Stage 4 highlights the importance of the Kinzers Formation. The previous categorization of the Kinzers Formation as a Tier 3 Lagerstätten was because of limited rock exposure, not fossilization conditions (Gaines 2014). The recovery of a highly diverse radiodont fauna from a relatively low number of specimens suggests that further exploration of the Kinzers Formation could yield new taxa rapidly. *Caryosyntrips* and *Hurdia* could also be present in the Kinzers Formation, as the former is present at the higher latitude coeval Valdemiedes Formation (Spain) and equatorial Laurentia in Stage 5 (Pates & Daley 2017), and the latter present at the coeval equatorial Laurentian Pioche Formation (unpublished material) and higher latitude Stage 5 Bohemia (Chlupáč & Kordule 2002; Daley et al. 2013a). Their absence might also be due to similar inferred feeding niches are already occupied in the Kinzers Formation by *Amplectobelua, Tamisiocaris,* and *Laminacaris?*, a result of unfavourable environmental conditions, or reflect the dominance of Amplectobeluidae, Anomalocarididae and Tamisiocarididae in older, Series 2, deposits and later dominance of Hurdiidae in Series 3.

6. Conclusions

The vast progress in our understanding of the diversity of Radiodonta since the previous study of Kinzers Formation radiodonts allowed the identification of *Tamisiocaris* and *Amplectobelua* in the USA for the first time. These reinterpretations mean that the Kinzers Formation can now be considered a Tier 2 BST with more than 10 soft-bodied taxa (*sensu* Gaines 2014), and has the highest known diversity of Radiodonta of any Cambrian Series 2 Stage 4 Konservat-Lagerstätten. The radiodonts found in the Kinzers

Formation are potentially all endemic species, and include the youngest *Tamisiocaris* known, and the oldest *Amplectobelua* in Laurentia. This highlights the importance of the Kinzers Formation in understanding the diversity and evolution of Cambrian Radiodonta, and supports further exploration of this Lagerstätten.

Acknowledgements

We would like to thank the editor, Paul Upchurch, and two anonymous referees for their comments on the manuscript. SP is funded by an Oxford-St Catherine's Brade-Natural Motion Scholarship. A Palaeontological Association Sylvester-Bradley Award (PA-SB201503) allowed travel to Franklin Marshall College, USNM and YPM. For facilitating access to specimens, we thank Susan Butts and Jessica Utrup at YPM, Mark Florence at USNM, and Roger DK Thomas at Franklin Marshall. This manuscript benefitted from discussions with P. Cong, G. Edgecombe, R. R. Gaines, B. S. Lieberman, and R. D. K. Thomas.

Declaration of Interest

None.

References

Allison, P. A. & Briggs, D. E. G. 1993. Exceptional fossil record: Distribution of soft-tissue preservation through the Phanerozoic. *Geology* **21**, 527–530.

Briggs, D. E. G. 1978. A new trilobite-like arthropod from the Lower Cambrian Kinzers Formation, Pennsylvania. *Journal of Paleontology* **52**, 132–140.

Briggs, D. E. G. 1979. *Anomalocaris*, the largest known Cambrian arthropod. *Palaeontology* **22**, 631–664.

Briggs, D. E. G. & Mount, J. D. 1982. The occurrence of the giant arthropod *Anomalocaris* in the Lower Cambrian of southern California, and the overall distribution of the genus. *Journal of Paleontology* **56**, 1112–1118.

Briggs, D. E. G., Lieberman, B.S., Hendricks, J.R., Halgedahl, S.L. & Jarrard, R.D., 2008, Middle Cambrian arthropods from Utah. *Journal of Paleontology* **82,** 238–254.

Campbell, L. & Kauffman, M. E. 1969. *Olenellus* fauna of the Kinzers Formation, southeastern Pennsylvania. *Proceedings of the Pennsylvania Academy of Science* **43**, 172–176.

Chen, J., Ramsköld, L. & Zhou, G. 1994. Evidence for monophyly and arthropod affinity of Cambrian giant predators. *Science* **264**, 1304–1308.

Chlupáč, I. & Kordule, V. 2002. Arthropods of Burgess Shale type from the Middle Cambrian of Bohemia (Czech Republic). *Bulletin of the Czech Geological Survey* **77**, 167–182.

Collins, D. 1996. The “evolution” of *Anomalocaris* and its classification in the arthropod class Dinocarida (nov.) and order Radiodonta (nov.). *Journal of Paleontology* **70**, 280–293.

Cong, P., Ma, X., Hou, X., Edgecombe, G. D. & Strausfield, N. J. 2014. Brain structure resolves the segmental affinity of anomalocaridid appendages. *Nature* **513**, 538–542.

Cong, P., Daley, A.C., Edgecombe, G.D., Hou, X. & Chen, A. 2016. Morphology of the radiodontan Lyrarapax from the early Cambrian Chengjiang biota. *Journal of Paleontology* **90**, 663–671.

Cong, P., Daley, A.C., Edgecombe, G. D. & Hou, X. 2017. The functional head of the Cambrian radiodontan (stem-group Euarthropoda) *Amplectobelua symbrachiata*. *BMC Evolutionary Biology* **17**, 208.

Cong, P., Edgecombe, G. D., Daley, A. C., Guo, J., Pates, S. & Hou, X. G. 2018. New radiodontans with gnathobase-like structures from the Cambrian Chengjiang Biota and implications for the systematics of Radiodonta. *Papers in Palaeontology*, in press. doi: 10.1002/spp2.1219.

Conway Morris, S. 1977. Fossil priapulid worms. *Special Papers in Palaeontology* **20**, 1–155.

Daley, A. C., Budd, G.E., Caron, J.B., Edgecombe, G. D. & Collins, D. 2009. The Burgess Shale anomalocaridid *Hurdia* and its significance for early euarthropod evolution. *Science* **323**, 1597–1600.

Daley, A. C., & Budd, G. E. 2010. New anomalocaridid appendages from the Burgess Shale, Canada. *Palaeontology* **53**, 721–738.

Daley, A. C., & Peel, J. S. 2010. A possible anomalocaridid from the Cambrian Sirius Passet lagerstätte, North Greenland. *Journal of Paleontology* **84**, 352–355.

Daley, A. C., Budd, G. E., & Caron, J. B. 2013a. Morphology and systematics of the anomalocaridid arthropod *Hurdia* from the Middle Cambrian of British Columbia and Utah. *Journal of Systematic Palaeontology* **11**, 743–787.

Daley, A. C., Paterson, J. R., Edgecombe, G. D., García-Bellido, D. C. & Jago, J. B. 2013b. New anatomical information on *Anomalocaris* from the Cambrian Emu Bay Shale of South Australia and a reassessment of its inferred predatory habits. *Palaeontology* **56**, 971–990.

Daley, A. C., & Legg, D. A. 2015. A morphological and taxonomic appraisal of the oldest anomalocaridid from the Lower Cambrian of Poland. *Geological Magazine* **152**, 949–955.

Dunbar, C. O. 1925. Antennae in *Olenellus getzi* n. sp.. *American Journal of Science* **52**, 303–308.

Gaines, R.R. 2014. Burgess Shale-type preservation and its distribution in space and time. Reading and Writing of the Fossil Record: Preservational Pathways to Exceptional Fossilization. *Paleontological Society Papers* **20**, 123–146.

García-Bellido, D. & Conway Morris, S. 1999. New Fossil Worms from the Lower Cambrian of the Kinzers Formation, Pennsylvania, with Some Comments on Burgess Shale-Type Preservation. *Journal of Paleontology* **73,** 394–402.

Guo, J., Pates, S., Cong, P., Daley, A. C., Edgecombe, G. D., Chen, T., & Hou, X. G. 2018. A new radiodont (stem Euarthropoda) frontal appendage with a mosaic of characters from the Cambrian (Series 2 Stage 3) Chengjiang biota. *Papers in Palaeontology*. *In press.*

Hou, X. G., Bergström, J. & Ahlberg, P. 1995. *Anomalocaris* and other large animals in the Lower Cambrian Chengjiang fauna of southwest China. *GFF* **117**, 163–183.

Kühl, G., Briggs, D. E. G. & Rust, J. 2009. A great appendage arthropod with a radial mouth from the Lower Devonian Hunsrück Slate, Germany. *Science* **323**, 771–773.

Lankester E. R. 1904. The structure and classification of Arthropoda. *Quarterly Journal of Microscopical Science* **47**, 523–582.

Lerosey-Aubril, R., Hegna, T. A., Babcock, L. E., Bonino, E. & Kier, C. 2014. Arthropod appendages from the Weeks Formation Konservat-Lagerstätte: new occurrences of anomalocaridids in the Cambrian of Utah, USA. *Bulletin of Geosciences* **89,** 269–282.

Lieberman, B. S. 2003. A new soft-bodied fauna: the Pioche Formation of Nevada. *Journal of Paleontology* **77,** 674–690.

Liu, J., Lerosey-Aubril, R., Steiner, M., Dunlop, J. A., Shu, D. & Paterson, J. R. 2018. Origin of raptorial feeding in juvenile Euarthropods revealed by a Cambrian radiodontan. *National Science Review* **nwy**057. doi: 10.1093/nsr/new057.

Liu, Q. 2013. The first discovery of anomalocaridid appendages from the Balang Formation (Cambrian Series 2) in Hunan, China. *Alcheringa* **37**, 1–6.

Nedin, C. 1995. The Emu Bay Shale, a Lower Cambrian fossil Lagerstätten, Kangaroo Island. *Memoirs of the Association of Australasian Palaeontologists* **18**, 133–141.

Pates, S., Daley, A. C. & Ortega-Hernández, J. 2018. Response to comment "*Aysheaia prolata* from the Wheeler Formation (Drumian, Cambrian) is a frontal appendage of the radiodontan *Stanleycaris*" with the formal description of *Stanleycaris*. *Acta Palaeontologica Polonica* **63,** 105–110.

Pates, S., Daley, A. C. & Lieberman, B.S. 2018b. Hurdiid radiodontans from the middle Cambrian (Series 3) of Utah. *Journal of Paleontology* **92**, 99–113.

Pates, S., Daley, A. C. & Ortega-Hernández, J. 2017. *Aysheaia prolata* from the Wheeler Formation (Drumian, Cambrian) is a frontal appendage of the radiodontan *Stanleycaris*. *Acta Palaeontologica Polonica* **62**, 619–625.

Pates, S. & Daley, A.C. 2017. *Caryosyntrips*: a radiodontan from the Cambrian of Spain, USA and Canada*. Papers in Palaeontology* **3**, 461–470.

Raymond, P.E. 1935. *Leanchoilia* and other mid-Cambrian Arthropoda. *Bulletin of the Museum of Comparative Zoology at Harvard College* **76**, 205–230.

Resser, C. E. 1929. New lower and middle Cambrian Crustacea. *Proceedings of the United States National Museum* **76**, 1–18.

Resser, C. E. & Howell, B. F. 1938. Lower Cambrian *Olenellus* Zone of the Appalachians. *Bulletin of the Geological Society of America* **49**, 195–248.

Rigby, J. K. 1987. Early Cambrian sponges from Vermont and Pennsylvania, the only ones described from North America. *Journal of Paleontology* **61**, 451–461.

Roger, J. 1953. Sous-classe des Malacostracés. In *Traité de Paléontologie* (ed. Piveteau, J.) pp. 309–378. Paris.

Schneider, C. A., Rasband, W. S. & Eliceiri, K. W. 2012. NIH Image to Image J: 25 years of image analysis. *Nature Methods* **9**, 671–675.

Scotese, C. R. 2016. PALEOMAP PaleoAtlas for GPlates and the PaleoData Plotter Program, PALEOMAP Project, http://www.earthbyte.org/paleomap- paleoatlas-for-gplates/

Skinner, E. S. 2005. Taphonomy and depositional circumstances of exceptionally preserved fossils from the Kinzers Formation (Cambrian), southeastern Pennsylvania. *Palaeogeography, Palaeoclimatology, Palaeoecology* **220**, 167–192.

Van Roy, P., Daley, A. C. & Briggs, D. E. G. 2015. Anomalocaridid trunk limb homology revealed by a giant filter-feeder with paired flaps. *Nature* **522**, 77–80.

Vannier, J., Caron, J. B., Yuan, J. L., Briggs, D. E. G., Collins, D., Zhao, Y. L. & Zhu, M. Y. 2007. *Tuzoia*: morphology and lifestyle of a large bivalved arthropod of the Cambrian seas. *Journal of Paleontology*, **81**, 445–471.

Vinther, J., Stein, M., Longrich, N. R. & Harper, D. A. 2014. A suspension-feeding anomalocarid from the Early Cambrian. *Nature* **507**, 496–499.

Wang, Y., Huang, D. & Hu, S. 2013. New anomalocardid frontal appendages from the Guanshan biota, eastern Yunnan. *Chinese Science Bulletin* **58**, 3937–3942.

Whiteaves, J.F. 1892. Description of a new genus and species of phyllocarid crustacean from the Middle Cambrian of Mount Stephen, British Columbia. *Canadian Record of Science* **5**, 205–208.

Whittington, H. B. & Briggs, D. E. G. 1985. The largest Cambrian animal, *Anomalocaris*, Burgess Shale, British Columbia. *Philosophical Transactions of the Royal Society of London. Series B, Biological Sciences* **309**, 569–609.

Chapter 4

Caryosyntrips: a radiodontan from the Cambrian of Spain, USA and Canada

Author contributions

SP conceived the project; SP wrote the manuscript and prepared the figures, with input from ACD.

Publication information

This Chapter has been peer reviewed and published by *Papers in Palaeontology*:

Pates, S. & Daley, A. C. (2017). *Caryosyntrips*: a radiodontan from the Cambrian of Spain, USA and Canada, *Papers in Palaeontology*, 3(3), 461-470.

Caryosyntrips: a radiodontan from the Cambrian of Spain, USA and Canada

by Stephen Pates[1] *and* Allison C. Daley[1,2,3]

[1]Department of Zoology, University of Oxford, Oxford, UK; e-mail: stephen.pates@zoo.ox.ac.uk

[2]Oxford University Museum of Natural History, Oxford, UK

[3] *Current address*: Institute of Earth Sciences, University of Lausanne, Géopolis, CH-1015, Lausanne, Switzerland: e-mail: allison.daley@unil.ch

ABSTRACT

Caryosyntrips appendages have previously been reported from the Burgess Shale (Cambrian, Stage 5), British Columbia, Canada. New specimens of the genus are here reported from the Wheeler Formation (Cambrian, Drumian) and Langston Formation, Spence Shale Member (Cambrian, Stage 5), Utah, USA. The original Burgess Shale specimens are re-examined alongside the new specimens. *Caryosyntrips* is shown to have paired ventral spines on each podomere. Three species of *Caryosyntrips* are recognised: *C. serratus* Daley and Budd, *C. camurus* nov. sp. and *C. durus* nov. sp., differentiated by the overall shape of their appendages and arrangement of dorsal and ventral spines. These differences have potential implications for the feeding methods employed by different species of *Caryosyntrips*. A specimen collected from the upper Valdemiedes Formation of Spain (Cambrian, Stage 4), previously described as the lobopodian *Mureropodia apae* Gámez Vintaned et al., is reinterpreted as a *Caryosyntrips* appendage. This identification is supported by the overall shape of the

fossil, and the presence, orientation, and height:width ratio, of ventral spines. However the dorsal surface of the appendage is not well preserved, and the appendage and its ventral spines are larger than other known *Caryosyntrips*. Therefore it is left in open nomenclature as *C*. cf. *camurus*. These new finds increase the temporal range of *Caryosyntrips* (Cambrian Series 2, Stage 4 to Series 3, Drumian) and the geographic range to a new continent, Gondwana.

Key words: *Caryosyntrips*, Radiodonta, Cambrian, Burgess Shale, Murero, Great Basin.

INTRODUCTION

The study of radiodontans, soft-bodied nektonic apex predators known mostly from the Cambrian, is crucial for understanding the evolution of arthropods. Recent studies have shed light on the origin of the biramous limb (Van Roy et al. 2015), compound eyes (Paterson et al. 2011) and the evolution of head structures (Cong et al. 2014). The evolution of radiodontans and their phylogenetic relationships has been the focus of much recent work increasing our knowledge of the diversity, feeding modes and ecology of these animals (e.g. Daley et al. 2009; Daley & Budd 2010; Daley & Bergström 2012; Daley et al. 2013*a*, *b*; Daley and Edgecombe 2014; Vinther et al. 2014; Van Roy et al. 2015).

The morphology of radiodontans consists of a body region of repeated segments with lateral flaps, a head region consisting of radially arranged mouthparts (oral cone), two large stalked eyes, and a pair of frontal appendages (Whittington & Briggs 1985). The paired appendages are robust, and often preserved isolated or as exuviae, and rarely attached to the rest of the body. Indeed many radiodontan taxa are known from frontal appendages only, for example *Anomalocaris pennsylvanica* (Briggs 1979;

Lieberman 2003), *Caryosyntrips serratus* (Daley & Budd 2010), and *Tamisiocaris borealis* (Daley & Peel 2010; Vinther et al. 2014). Isolated *Caryosyntrips* appendages have been known for over a decade (Caron 2005) and were first described by Daley & Budd (2010) alongside other new appendages from the Burgess Shale.

In this paper we present new specimens of *Caryosyntrips* from the Spence Shale (Cambrian Series 3, Stage 5) and Wheeler Formation (Cambrian Series 3, Drumian) of the Great Basin, USA. We also reinterpret the putative lobopodian *Mureropodia apae* Gámez Vintaned et al., 2011, from the upper Valdemiedes Formation (Cambrian Series 2, Stage 4) of Spain as a *Caryosyntrips* appendage, and, in light of these new findings, identify new features from the original *Caryosyntrips* material from the Burgess Shale (Cambrian Series 3, Stage 5), Canada. Information about the anatomical characters of *Caryosyntrips* allows for separation of *Caryosyntrips* into three distinct species (Fig. 1), and comparison of their functional morphology.

MATERIALS AND METHODS

The Langston Formation (Spence Shale Member) and Wheeler Formation specimens are held at the University of Kansas Natural History Museum, Lawrence, Kansas, USA (KUMIP). The Gunther Family collected KUMIP 314070 and 314071 from the Drum Mountains, Utah, and KUMIP 314275 Miners Hollow, Wellsville Mountains, Utah. An additional Wheeler Formation specimen, KUMIP 415223, was donated by Daniel Windhofer for this study. All Burgess Shale specimens are held at the Royal Ontario Museum, Toronto, Ontario, Canada (ROM). The single specimen from the Valdemiedes Formation (MPZ 2009/1241) is held at the Museo de Ciencias Naturales de la Universidad de Zaragoza, Spain (MPZ).

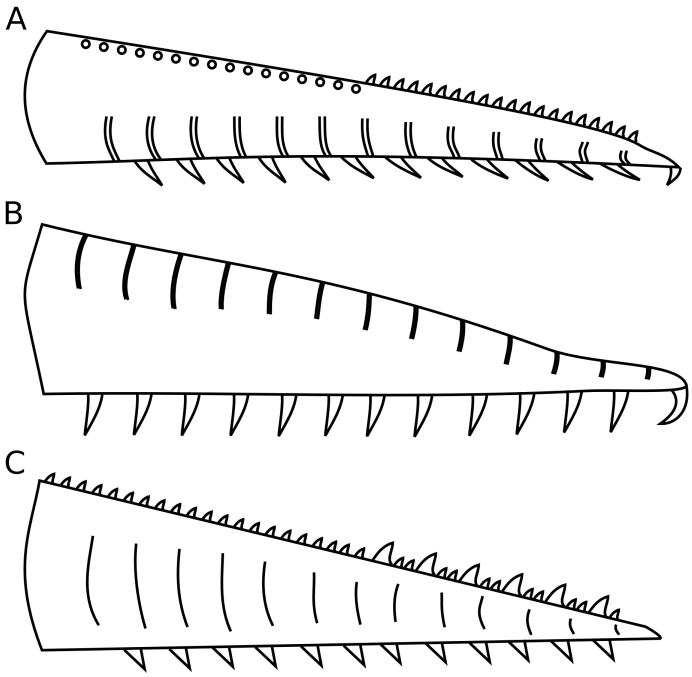

FIG 1. Idealised sketch of each *Caryosyntrips* species. A. *C. serratus* Daley and Budd, 2010, small spines along outer edge preserved as either circular attachment points or as spines; B. *C. camurus* nov. sp., proximal boundary inferred as it is not preserved in any specimen; C. *C. durus* nov. sp., proximal five podomeres inferred as these are not preserved in either specimen.

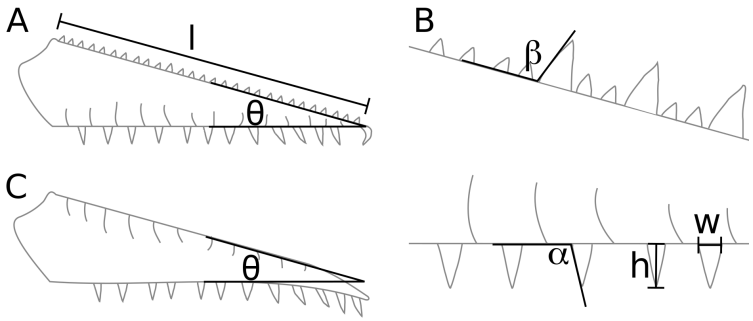

FIG 2. Explanation of measurements. A. length (l) and angle between edges (theta); B. angle between large spine and inner edge (alpha), angle between large spine and outer edge (beta), length of large spine (h) and width of large spine (w); C. how angle between edges (theta) is measured for specimens with a bent end.

Photographs were taken using a Canon EOS 500D camera with Canon EF-S 60 mm macro lens, controlled with EOS Utility 2 remote shooting software. Measurements were taken of all known *Caryosyntrips* specimens from photographs using ImageJ 2 software. The angles between the two edges of the appendage and from the podomere edge to the proximal edge of each ventral spine were measured for each appendage and each ventral spine. The mean angle from the podomere edge to ventral spine was calculated for each specimen and this was plotted against the angle between the two edges of the appendage (see Fig. 2). Photoshop was used to remove white paper arrows from photographs of MPZ 2009/1241. The plot of length of appendage vs. length of longest spine was constructed using R Studio. Lengths of incomplete appendages were reconstructed by calculating the mean length per podomere, and extrapolating to 14 podomeres.

INSTITUTIONAL ABBREVIATIONS

KUMIP, University of Kansas Natural History Museum, Lawrence, Kansas, USA; MPZ, Museo de Ciencias Naturales de la Universidad de Zaragoza, Zaragoza, Spain; ROM, Royal Ontario Museum, Toronto, Canada.

SYSTEMATIC PALAEONTOLOGY

This published work and the nomenclatural acts it contains, have been registered in ZooBank: urn:lsid:zoobank.org:pub:3E73022B-A1EB-4DDD-ADFF-A2F3948F383D

(stem group) EUARTHROPODA Lankester, 1904

Order RADIODONTA Collins, 1996

Genus CARYOSYNTRIPS Daley & Budd, 2010

Type species. *Caryosyntrips serratus* Daley & Budd, 2010

Diagnosis. A radiodontan with 14 podomeres per frontal appendage, which are elongated and tapering in outline. A pair of ventral spines extends from the ventral surface of each podomere. Appendages have a convex bell-shaped proximal margin, a terminal spine protrudes from the distal end in some species. (emended from Daley & Budd 2010, p. 727).

Occurrence. Cambrian Valdemiedes Formation, Spain (Cambrian Series 2, Stage 4); Spence Shale Member, Langston Formation, Utah, USA (Cambrian Series 3, Stage 5); Burgess Shale, British Columbia, Canada (Cambrian Series 3, Stage 5); and Wheeler Formation, Utah, USA (Cambrian Series 3, Drumian).

Caryosyntrips serratus Daley & Budd, 2010

Figs. 1A, 3

2005 'Dinocarida A' Caron, App. 2. 3G.

2010 *Caryosyntrips serratus* Daley & Budd, p. 730-1, text-figs. 5A-I, 6H (non text-figs. 6A-G, I)

Holotype. ROM 57161

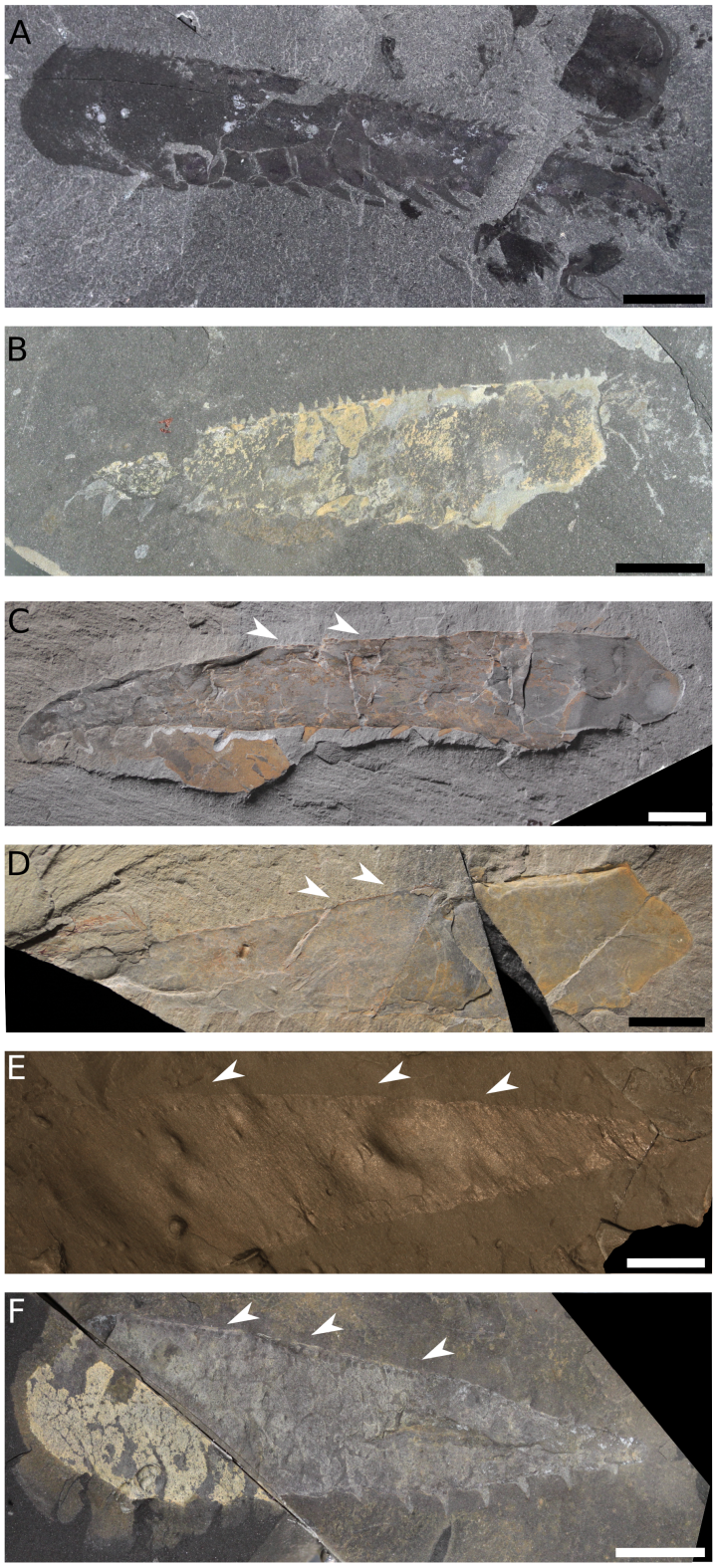

FIG 3. *Caryosyntrips serratus* specimens. A. ROM 57161 (holotype); B. ROM 59499; C. ROM 59502; D. ROM 59498; E. KUMIP 415223; F. ROM 59497. White arrows indicate circular small spine attachment points. All scale bars 10 mm.

Paratypes. ROM 59497, ROM 59498, ROM 59499, ROM 59502

Additional material. KUMIP 415223

Diagnosis. *Caryosyntrips* with one pair of distally pointing ventral spines on each podomere. Ventral spines are less broad than for other *Caryosyntrips* species. A single row of small curved dorsal spines, spaced 1 mm apart, point distally. Distal most podomere ends in recurved terminal spine.

Description. The length of complete appendages (l in Fig. 2A) varies from 64.86 mm to 108.37 mm (mean = 83.57 mm, sd = 16.18 mm, n = 5). The angle between the dorsal and ventral surface (θ in Fig. 2) varies from 11° to 18° (mean = 14.3°, sd = 3.4°, n = 6). Podomere boundaries can usually be clearly seen on the inner edge of the specimens, separated by arthrodial membrane. Appendages have a row of small dorsal spines (approximately 1 mm tall) spaced 1 mm apart, visible either as simple triangles (ROM 59499) (Fig 3B), curved spines pointing distally (ROM 57161) (Fig 3A) or as small circles interpreted as attachment points (ROM 59497, ROM 59502, ROM 59458 and KUMIP 415223) (white arrows in Fig. 3C-F). One pair of ventral spines is present on each podomere, although in most cases only one of the pair can be seen. ROM 59497 (Fig. 3F; Daley & Budd 2010, text-fig. 5C) displays three spines that appear to be on the dorsal surface of the appendage at the distal end. These are interpreted as being one of a pair ventral spines which during compression of the fossil have been preserved apparently on the dorsal surface. They are shorter and face at a different angle to the

ventral spines preserved on the ventral surface, supporting this interpretation. The number of ventral spine pairs preserved per specimen for this species varies from nine in the holotype (ROM 57161) to two in KUMIP 415223 and ROM 59499 (Daley & Budd 2010, text-fig. 5G). Two specimens (ROM 57161 and 59502) display recurved terminal spines, slightly longer than the ventral spines, however for many specimens the distal end is incomplete (e.g. ROM 59498, KUMIP 415223).

Occurrence. Burgess Shale, British Columbia, Canada (Cambrian Series 3, Stage 5) and Wheeler Formation, Utah, USA (Cambrian Series 3, Drumian).

Caryosyntrips camurus nov. sp.

Figs. 1B, 4

LSID. urn:lsid:zoobank.org:act:4211F66A-3C77-42CF-9F4D-CBC2E19A37B0

2010 *Caryosyntrips serratus* Daley & Budd, p. 731, text-figs. 6A-G, I

Derivation of name. From Latin *camurus* (=hooked, bent) referring to the shape of the distal end.

Holotype. ROM 59503 (Daley & Budd, 2010, text-fig. 6I)

Paratype. ROM 59501

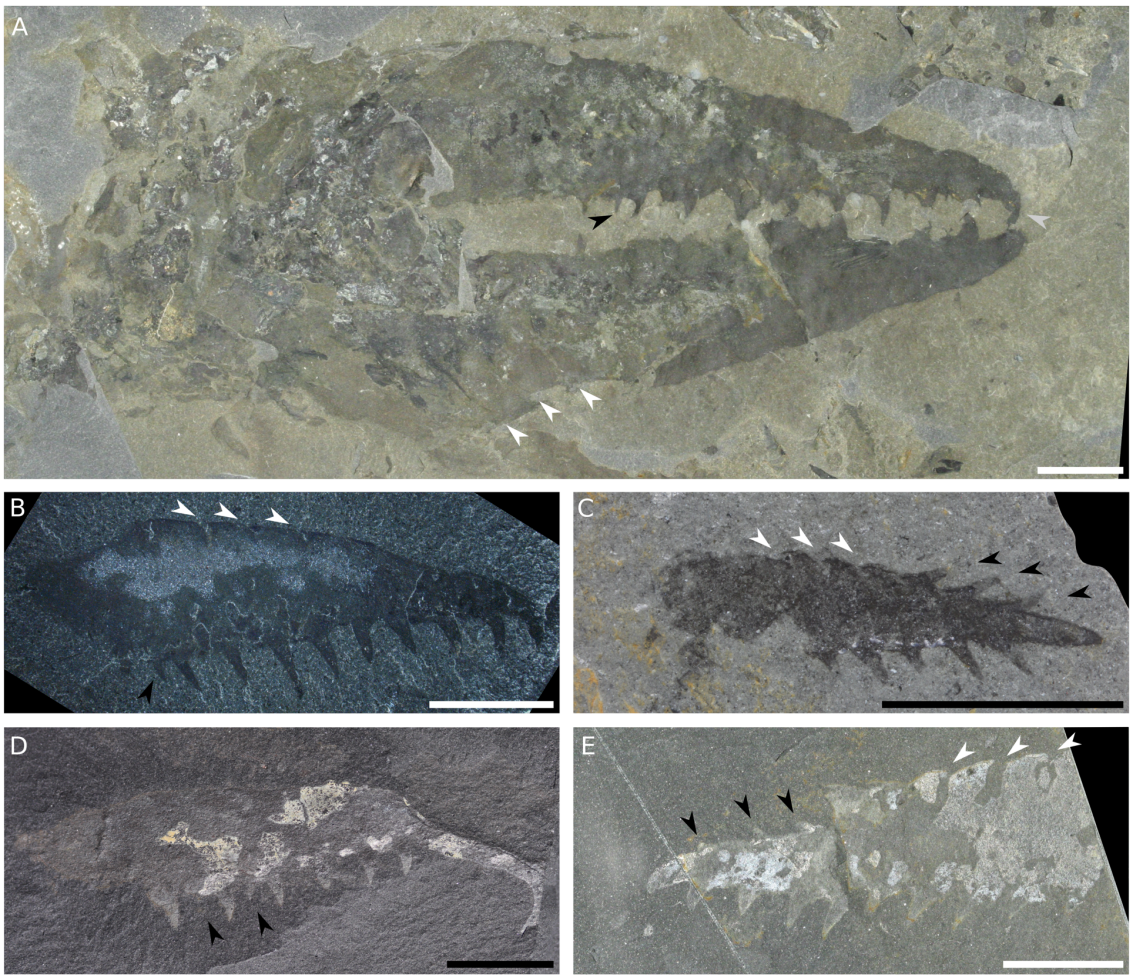

FIG 4. *Caryosyntrips camurus* specimens. A. ROM 59501; B. ROM 59503 (holotype); C. KUMIP 314275; D. ROM 59500; E. ROM 59599. White arrows indicate podomere boundaries, black arrows indicate paired spines mentioned in text, grey arrow indicates terminal spine. All scale bars 10 mm.

Other material. ROM 59500, 59598, 59599, KUMIP 314275

Diagnosis. *Caryosyntrips* with one pair of ventral spines on each podomere, and no dorsal spines. Distal most three podomeres are less tall than the others. Distal most podomere ends in a recurved terminal spine.

Description. This species has 14 podomeres (shown by the only complete appendages for this species, the paired appendages of ROM 59501, Fig. 4A). The measured lengths of the two complete appendages (l in Fig. 2A) are 71.74 mm and 70.69 mm. The angle between the outer and inner edge of the appendages (θ in Fig. 2) varies from 13° to 17° (mean = 14.3°, sd = 1.6°, n = 6).

Podomere boundaries are usually most visible on the dorsal surface and at the proximal end of the appendage. ROM 59501, ROM 59503, ROM 59599 and KUMIP 314275 show clear boundaries on the dorsal surface, but not on the ventral surface (white arrows in Fig. 4A-C, E). There are no dorsal spines of any size preserved, or circular spine attachment points, on any of the specimens of this species.

Ventral spines are simple triangular shapes. One pair of ventral spines is present on each podomere, although usually only one of the pair is visible. Three specimens (ROM 59500, ROM 59501, and ROM 59503) show clear evidence for paired ventral spines. ROM 59500 has two sets of paired spines visible (black arrows in Fig. 4D). ROM 59501 has two paired spines at the proximal end of the podomere on the left side (black arrow in Fig. 4A), and ROM 59503 has two spines on one podomere at the proximal end of the appendage (black arrow in Fig. 4B). ROM 59599, and KUMIP 314275 (black arrows in Fig. 4C, E) display ventral spines at the distal end on both sides of the

appendage. This is interpreted as being a pair of ventral spines, one of which, during compression of the fossil, has been preserved on the dorsal surface. They are shorter and face at a different angle to the spines on the inner edge, supporting this interpretation. The terminal spine, visible on ROM 59501, is recurved (grey arrow in Fig. 4A).

The distal three podomeres of *C*. *camurus* are thinner than would be expected for an appendage with a simple triangular shape when flattened, and is sometimes preserved distorted. This is most visible in ROM 59500 (Fig. 4D), and less pronounced in KUMIP 314275 and ROM 59503 (Fig. 4B, C) where the distal end curves slightly ventrally.

Remarks. *C. camurus* can be differentiated from the other two species as it lacks dorsal spines completely. It has paired ventral spines, and podomere boundaries tend to be clearest on the outer edge. The distalmost three podomeres are less tall than for the other species, and is sometimes preserved distorted, giving it a hooked appearance.

Daley & Budd (2010) mention that *Caryosyntrips* appendages should not be confused with distal ends of anterior appendages of *Sidneyia* (Bruton 1981; Stein 2013; Zacaï et al. 2016) based on segmentation, angle of inner spines and presence of dorsal spines. Although this species of *Caryosyntrips* does not have dorsal spines, it is still possible to distinguish them from *Sidneyia* on account of the segmentation of appendages and angle of ventral spines.

Occurrence. Spence Shale Member, Langston Formation, Utah, USA (Cambrian Series 3, Stage 5); Burgess Shale, British Columbia, Canada (Cambrian Series 3, Stage 5).

Caryosyntrips durus nov. sp.

Figs. 1C, 5

LSID. urn:lsid:zoobank.org:act:5C0ECFBB-3D1C-4269-BB27-E6D706CE51BB

Derivation of name. From Latin *durus* (=hard, inflexible).

Holotype. KUMIP 314071

Paratype. KUMIP 314070

Diagnosis. *Caryosyntrips* with dorsal and ventral surfaces straight, a rounded distal end and no terminal spine. Paired ventral spines on each podomere are simple triangles that end in a sharp point. A single row of small (1 mm tall), curved, distally pointing, dorsal spines spaced 1 mm apart runs along the length of the appendage. A single large dorsal spine, the same size and shape as the ventral spines, is present on each of the distal most seven podomeres.

Description. The two specimens are partial *Caryosyntrips* appendages, with 9 podomeres preserved for each (lengths: KUMIP 314070 = 41.09 mm, KUMIP 314071 = 29.05 mm). Podomere boundaries are preserved as faint, simple curved lines. The proximal shape of the appendages cannot be ascertained, as it is missing in both. The angle between the ventral and dorsal surfaces (θ in Fig. 2) is 17° for KUMIP 314070 and

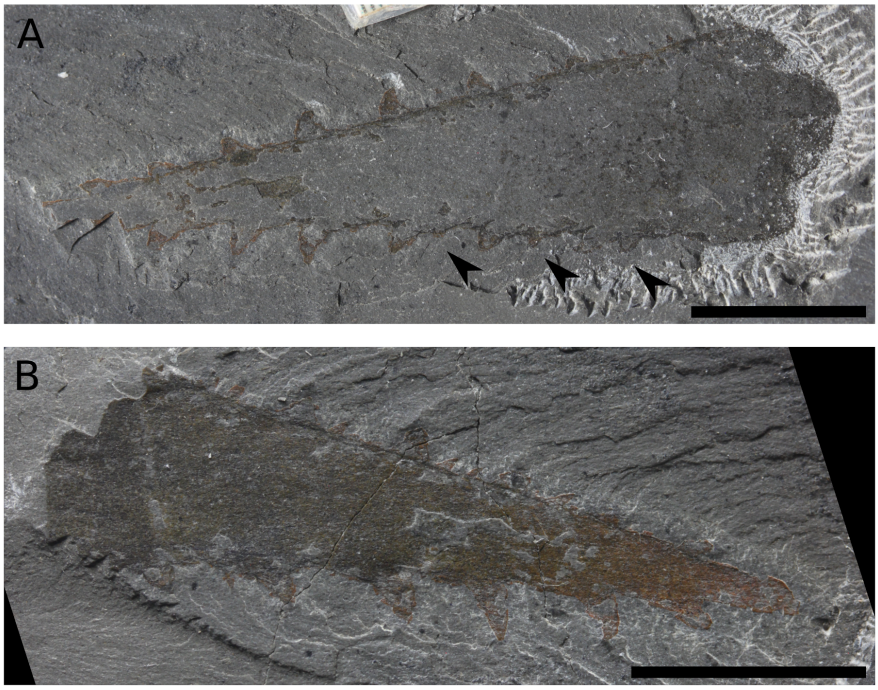

FIG 5. *Caryosyntrips durus* specimens. A. KUMIP 314070 (paratype), black arrows indicate paired spine on lower level of rock; B. KUMIP 314071 (holotype). All scale bars 10 mm.

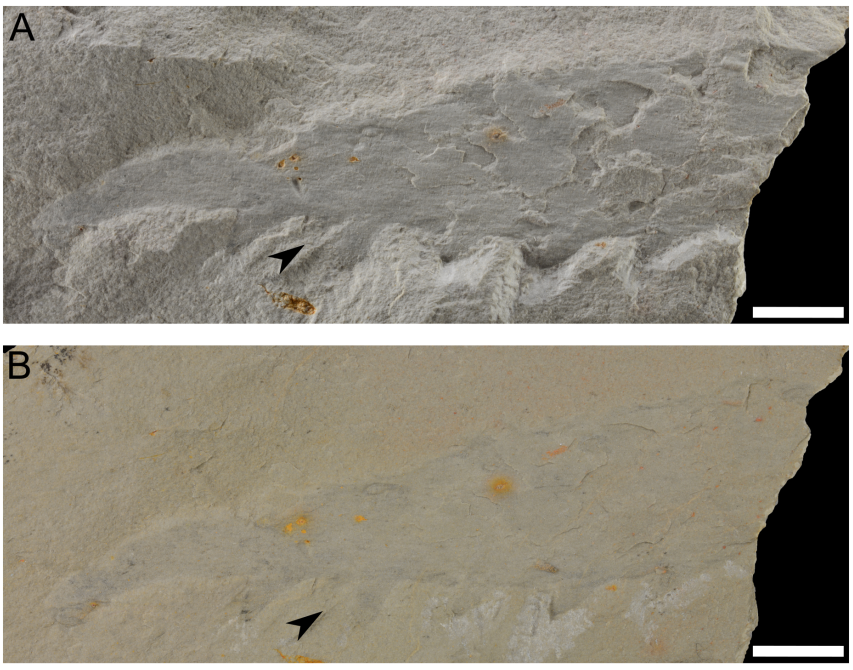

FIG 6. *Caryosyntrips* cf. *camurus*, MPZ 2009/1241. A. dry; B. underwater. Scale bars 10 mm.

15° for KUMIP 314071. The inner edge has a stepped appearance and the outer edge is straight. A row of small spines (1 mm tall, spaced 1 mm apart) run along the dorsal surface, preserved as simple triangles in KUMIP 314070 (Fig. 5A) and curved pointing distally in KUMIP 314071 (Fig. 5B).

Large spines (h in Fig. 2B: 1.1—3.0mm, w in Fig. 2B: 1.2—2.0 mm) are present on both the dorsal and ventral surfaces of the appendage. The large dorsal spines are spaced evenly (3 mm apart in KUMIP 314070), with one spine on each podomere. The angle between the dorsal surface of the appendage and the large dorsal spine (β in Fig. 2B) varies from 115-160°. There is a gap of 8 mm between the proximal-most dorsal spine in KUMIP 314070 (Fig. 5A) to the sediment covered margin, indicating that large dorsal spines are present only on the distal most seven podomeres. Large ventral spines are paired, just as in other species of *Caryosyntrips*. This is most visible on the 6^{th}—8^{th} most distal podomeres of KUMIP 314070 (black arrows in Fig. 5A). The angle from the ventral surface of the appendage to the proximal edge of the ventral spines (α in Fig. 2B) varies from 128-152°.

There are no ventral spines on the distalmost podomere, and no terminal spine. The appendage tapers to a rounded point, with the inner edge extending slightly beyond the outer edge. The distal region of KUMIP 314070 is not preserved, and so no comparison can be made between the two.

Remarks. Although only known from two partial appendages, *C*. *durus* is significantly different from the other species to warrant a formal description. It can be differentiated as it has paired large ventral spines on each podomere, and a single dorsal spine on the

distal most seven podomeres, in addition to a row of small dorsal spines. *C. camurus* and *C.* c.f. *C. camurus* have no dorsal spines, and *C. serratus* has only a row of small dorsal spines.

Occurrence. Wheeler Formation, Utah, USA (Cambrian Series 3, Drumian).

Caryosyntrips cf. *camurus*

Fig. 6

2011 *Mureropodia apae* Gámez Vintaned et al. figs. 12.3, 12.4, 12.5 and 12.9

Material: MPZ 2009/1241

Description: MPZ 2009/1241 is a partial appendage of six podomeres, which measures 82.82 mm in length (giving an extrapolated length for 14 podomeres of 193 mm). The appendage ('body' of Gámez Vintaned et al. 2011 fig. 12.4**)** tapers in outline towards the distal end, which is distorted ('proboscis' of Gámez Vintaned et al. 2011, fig. 12.4). The angle between the dorsal and ventral surfaces (θ in Fig. 2) is 14°. The number of podomeres is indicated by the number of ventral spines ('left lobopods' of Gámez Vintaned et al. 2011 fig. 12.4) and faint boundaries on the dorsal surface, which are visible under low angle light. The ventral spines measure 5.1—6.9 mm in length (h in Fig. 2B). Evidence for paired ventral spines is visible on the third most distal podomere (black arrows in Fig. 6A, B). There is no evidence for dorsal spines, however the dorsal surface is not well preserved.

Remarks. MPZ 2009/1241 was originally described as a lobopodian, *Mureropodia apae*, and to date is the only member of the genus. *Mureropodia* is significantly different to the most similar lobopodian morphologically, *Paucipodia* Hou et al. (2004), as it has a different overall shape, lacks annulation, has a distinct putative 'proboscis' and its putative 'legs' have a length/trunk width ratio far lower than legs in *Paucipodia*. The overall shape of the specimen is very similar to other *Caryoysntrips* appendages, and the 14° angle between the dorsal and ventral surfaces (θ in Fig. 2) is similar to other *Caryosyntrips* appendages (11-18°). Radiodontan appendages do not have annulation, and faint podomere boundaries are visible under low angle light. The 'proboscis' is here interpreted as a distorted distal end of the appendage, similar to some *C. camurus* specimens (e.g. Fig. 4D) and the 'legs' are reinterpreted as paired ventral spines, whose height:width ratio (h and w in Fig. 2B) fits within the measurements of other *Caryosyntrips* ventral spines. These features support the reinterpretation of MPZ 2009/1241 as a partial isolated *Caryosyntrips* appendage, most similar to *C. camurus.* However both the ventral spines and appendage are longer than for other *C. camurus* specimens (Fig. 7), the dorsal surface of the appendage is not well preserved and this specimen would greatly increase the known geographic and stratigraphic range for the species. For these reasons we leave the identification in open nomenclature as *C*. cf. *camurus*.

Occurrence. Valdemiedes Formation, Spain (Cambrian Series 2, Stage 4).

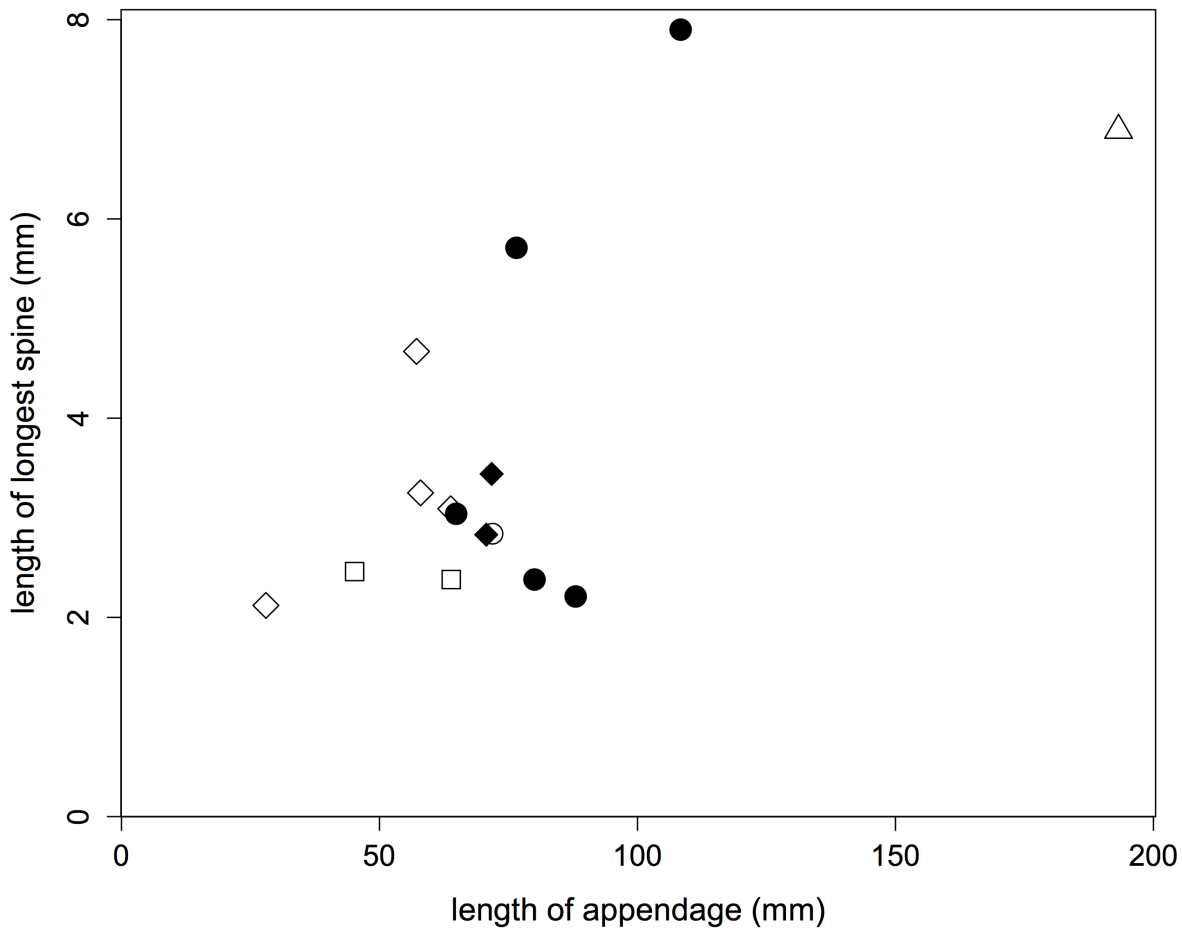

FIG 7. Plot of length of appendages against length of longest spine. Circles = *Caryosyntrips serratus*, diamonds = *C. camurus*, triangles = *C.* cf. *camurus*, squares = *C. durus*. Complete appendage length measurements in black, extrapolated lengths from incomplete appendages in grey. Raw data in Table 2.

DISCUSSION

Appendages described herein show that the morphological variability of *Caryosyntrips*, its geographic and temporal ranges, and the number of species, is higher than previously known. In the original description (Daley & Budd 2010), all *Caryosyntrips* specimens were assigned to *C. serratus*. This study has formally described three species, differentiated by the presence and size of the ventral and dorsal spines, and overall shape of the appendage (Table 1).

Taphonomic, interspecific and intraspecific variation

Some taphonomic effects can distinguished from true morphological variability in *Caryosyntrips*. The angle between the two edges (θ in Fig. 2) varies slightly for all species of *Caryosyntrips* (Table 1). In the *C. camurus* specimen ROM 59501 (Fig 4A; Daley & Budd 2010, text-fig. 6C-G), two appendages from the same animal have slightly different θ values (15° and 17°). The θ range for the whole species (13° to 17°) or genus (11° to 18°) is not significantly broader, suggesting that the variation in θ is related to angle of the appendage relative to the sediment surface during preservation. *C. camurus* specimen ROM 59501 also highlights a different type of taphonomic artefact. Only one of the appendages has a terminal spine, while the other appendage from the same animal ends in a rounded point. This indicates that all appendages of this species have terminal spines, and the rounded tip is a taphonomic artefact. The appearance of podomere boundaries also varies between and within species. *C. serratus* tends to preserve the podomere boundaries on the ventral surface, whereas for *C. camurus* the podomere boundaries tend to be more visible on the dorsal surface. The two specimens of *C. durus* preserve podomere boundaries as a faint line. However within *C. serratus*

Table 1. Comparison of *Caryosyntrips* species

	Caryosyntrips serratus	*Caryosyntrips camurus*	*Caryosyntrips durus*	*Caryosyntrips* cf. *camurus*
Number of specimens	6 isolated appendages	5 isolated appendages, 1 pair of appendages	2 isolated appendages	1 isolated appendage
Row of dorsal spines	Yes	No	Yes	No
Other dorsal spines	No	No	Yes: same size as ventral spines. One on podomeres 8-14.	No
Ventral spines	One pair per podomere	One pair per podomere	One pair per podomere	One pair per podomere
α range	11-18°	13-17°	15-17°	14°
l range	65-108 mm	28-72 mm	45-64 mm	193 mm
Stratigraphic occurrence	Burgess Shale; Wheeler Fm.	Spence Shale; Burgess Shale	Wheeler Fm.	Valdemiedes Fm.
Age range	Stage 5 - Drumian	Stage 5	Drumian	Stage 4
Continent	Laurentia	Laurentia	Laurentia	Gondwana
References	**This study**; Daley & Budd 2010	**This study**; Daley & Budd 2010	**This study**	**This study**; Gámez Vintaned et al. 2011

Measurements for individual specimens in Table 2.

not all specimens clearly show podomere boundaries (Fig. 3B, E) suggesting that the differences in preservation of podomere boundaries is also affected by taphonomy. The distal end *of C. camurus* and *C*. cf. *camurus* is often preserved distorted (e.g. Figs. 4D; 6). This is interpreted as a taphonomic artefact, however it may be more common in *C. camurus* and *C*. cf. *camurus* because the distalmost three podomeres are less tall compared to *C. durus* and *C. serratus*, and so more susceptible to taphonomic stretching and deformation. Ventral spine length (h in Fig. 2B) also varies within all species of *Caryosyntrips* (Fig. 7). It does not correlate clearly with appendage length, although the limited number of appendages longer than 100 mm means that this is difficult to test. The variation of longest ventral spine lengths for appendages of similar lengths suggests that the range of ventral spine lengths is not solely due to the size of the animal. Ventral spines are not always preserved on every podomere of appendages, particularly *C. serratus* (see Fig. 3). *C. serratus* may be more affected than the other species as ventral spines tend to be proximally pointing, and so require a smaller rotation of the appendage to be concealed after compression.

Geographic and temporal range

Caryosyntrips, previously only known from the Burgess Shale (Cambrian Series 3, Stage 5), is here reported from the older Valdemiedes Formation (Cambrian Series 2, Stage 4) and Spence Shale Member, Langston Formation (Cambrian Series 3, Stage 5), as well as the younger Wheeler Formation (Cambrian Series 3, Drumian). *Caryosyntrips* cf. *camurus* from the Valdemiedes Formation is the oldest *Caryosyntrips* known, the first radiodontan reported from this Lagerstätten, and the first *Caryosyntrips* from outside Laurentia. All three species of *Caryosyntrips* are now known from Utah Lagerstätten

(Spence Shale and Wheeler Formation), increasing the faunal overlap in radiodontans between the Burgess Shale and Utah. *Anomalocaris* (Briggs et al. 2008; Lerosey-Aubril et al. 2014), *Hurdia victoria, Peytoia nathorsti* (Conway Morris & Robison 1982; Pates et al. *in press*), and *Stanleycaris* (Pates et al. *submitted*) are all known from both the Burgess Shale and Utah Lagerstätten.

Caryosyntrips cf. *camurus* is added to the other Gondwanan Radiodonta: *Anomalocaris* cf. *canadensis* and *A*. *briggsi* from the Emu Bay Shale (Cambrian Series 2, Stage 4), Australia (Nedin 1999; Daley et al. 2013*b*; Paterson et al. 2016); and *Hurdia* from the Jince Formation (Cambrian Series 3, Drumian), Czech Republic (Chlupáč & Kordule 2002; Daley et al. 2013*a*). The discovery of *Caryosyntrips* in the Cambrian Series 2, Stage 4 of Gondwana shows that its global distribution is much wider than initially thought. *Caryosyntrips* is only known from the high latitude Valdemiedes Formation, not the equatorial Emu Bay Shale. This suggests that *Caryosyntrips* originated at a high latitude in Gondwana during the Cambrian Series 2, and expanded its range to more equatorial Laurentia, where it is known from the Cambrian Series 3. Appendages of *Caryosyntrips* are found in much lower abundance in the Burgess Shale (12) than *Anomalocaris* (385), *Peytoia* (229) and *Hurdia* (290) (Daley & Budd 2010; Daley et al. 2013*a*). This suggests that *Caryosyntrips* may have been a part of Laurentian communities older than the Series 3, Stage 5 Spence, such as the Series 2, Stage 4, Eager, Kinzers, Latham and Pioche Formations (Briggs 1979; Briggs & Mount 1982; Lieberman 2003), but it has not yet been discovered either because of low numbers in the original population, or because it may have a lower fossil preservation potential than other radiodontan appendages.

Ecological interpretation

The large appendages of radidontans were located at the front of the head adjacent to the mouthparts, as indicated by taxa known from full body specimens such as *Anomalocaris*, *Peytoia,* and *Hurdia* (Whittington & Briggs 1985; Collins 1996; Daley et al. 2009; Daley & Edgecombe 2014), and were involved in feeding. In other radiodontan taxa, the functional morphology of frontal appendages has been used to distinguish between the dextrous grasping motion of the actively durophagous *Anomalocaris* (Briggs 1979; Collins 1996; Nedin 1999) and the less specialised prey trapping or sediment sifting motion of taxa with longer ventral spines, such as *Hurdia* and *Peytoia* (Daley & Budd 2010). Filter feeding has been suggested for the giant Ordovician radiodontan *Aegirocassis* because of the presence of dense setae on its frontal appendage (Van Roy et al. 2015). *Caryosyntrips* was previously interpreted as an actively durophagous predator similar to *Anomalocaris*, based on the elongated nature of the frontal appendage and its relatively short ventral spines, however the movement differs between the two taxa. *Caryosyntrips* is thought to have moved its stiffer frontal appendage by pivoting at the bell-shaped basal attachment joint (see Fig. 3A, C-F) to create as scissor-like grasping or slicing motion between the opposing appendage pair (Daley & Budd 2010). *Anomalocaris* displays greater flexibility along the appendage as indicated by its more prominent arthrodial membranes and preservation exhibiting 180° of motion, but appears to have had an immobile basal attachment joint (Whittington & Briggs 1985; Daley & Edgecombe 2014). Both *Caryosyntrips* and *Anomalocaris* may have relied on suction created by the mouthparts to bring prey items towards the mouth, after crushing and slicing by the appendages. While the mouthparts of *Caryosyntrips* are unknown, the flexible oral cone of *Anomalocaris* has been suggested to provide suction

rather than a chewing or crushing motion (Hagadorn et al. 2010; Daley & Bergström 2012). The newly discovered material of *Caryosyntrips* allows for further elaboration of the ecological interpretation of this taxon, supporting a durophagous predatory nature and suggesting that morphological differences between taxa indicate different feeding behaviours and access to different prey items.

While all *Caryosyntrips* taxa are considered to be durophagous predators, the differences in frontal appendage morphology between the species (Fig. 1; Table 1) indicate that the behaviour and prey choice may have differed. The ventral spines in *C. serratus* are the most slender, and generally point distally. Ventral spines in *C. camurus* and *C. durus* tend to point more proximally, and *C. durus* has the most robust ventral spines. This suggests that *C. durus* sought out the most robust prey items. Although the preservation of arthrodial membrane is likely to have been affected by taphonomy, the current evidence suggests that flexibility along the appendage may have varied between taxa. *C. durus* had the most rigid frontal appendage, as indicated by its overall shape and membranes preserved as simple lines, whereas *C. serratus* and *C. camurus* have visible arthrodial membrane between all podomeres along the length of the appendage and so appear more flexible. The thin distalmost three podomeres in *C. camurus* may also have provided additional flexibility. The unique presence of large dorsal spines in *C. durus* (in addition to the smaller dorsal spines present in *C. serratus* and *C. durus*) may have provided additional strength and protection to the frontal appendages of this taxon as its sought out more robust prey items than the other two *Caryosyntrips* species, which would have been more able to manipulate prey items, and so would have sought out less robust, but more difficult to catch, prey.

The study of *Caryosyntrips* has implications for understanding Cambrian ecosystems and ecology. Its putative durophagous predatory lifestyle makes it a potential culprit for Cambrian trilobite repaired injuries that have previously been attributed to *Anomalocaris* (e.g. Rudkin 1979; Babcock 1993). While these damages were thought to have been inflicted by *Anomalocaris* using the dextrous nature of the claw to create fracture lines by repeated bending and twisting (Nedin 1999), the robust ventral spines and strong crushing motion implied for *Caryosyntrips* could provide another way to break mineralized trilobite exoskeletons and cause these injuries. The variation seen between the morphology of the three *Caryosyntrips* species and their corresponding ecological interpretations suggests that this taxon may have been an important factor driving community composition in the Cambrian.

Acknowledgements. B. Lieberman provided access to specimens at the KUMIP. S. Zamora provided access to and photographs of specimen MPZ 2009/1241. J-B. Caron provided original access to Burgess Shale material at the ROM. Daniel Windhofer donated specimen KUMIP 415223. We thank P. Selden for use of photographic equipment at the KUMIP. We acknowledge Parks Canada for permission to collect Burgess Shale material through research permits granted to D. Collins. Funding was provided by a Palaeontological Association Sylvester-Bradley Award (PA-SB201503), a Santander Travel Award and an Oxford-St Catherine's Brade-Natural Motion Scholarship to SP, and by the OUMNH to ACD. We thank the editor X-G. Zhang, and the reviewers J. Ortega-Hernández and G. Edgecombe for their positive, thorough and helpful reviews, which greatly improved the manuscript.

Table 2. Measurements of individual *Caryosyntrips* specimens

	l	h (ls)	h (ss)	θ	n. pods	Length (14 pods)
Caryosyntrips serratus						
ROM 57161	76.55	5.71	2.74	11	14	76.55
ROM 59499	61.64	2.84	5.78	16	12	71.91
ROM 59502	108.37	7.90	2.85	11	14	108.37
ROM 59498	80.05	2.38	1.71	12	14	80.05
KUMIP 415223	88.02	2.21		18	14	88.02
ROM 59497	64.86	3.04	2.20	18	14	64.86
Caryosyntrips camurus						
ROM 59501 (A)	71.74	3.44	2.22	15	14	71.74
ROM 59501 (B)	70.69	2.83	2.53	17	14	70.69
ROM 59503	40.84	4.67	3.05	13	10	57.18
KUMIP 314275	17.99	2.12	1.88	15	9	27.98
ROM 59500	27.35	3.09	2.33	13	6	63.82
ROM 59599	37.26	3.25	2.27	13	9	57.96
Caryosyntrips durus						
KUMIP 314070	41.09	2.38	1.50	17	9	63.92
KUMIP 324071	29.05	2.46	1.86	15	9	45.19
Caryosyntrips cf. *camurus*						
MPZ 2009/1241	82.82	6.90	4.29	14	6	193.25

Abbreviations: h, height (Fig.2); l, length (Fig. 2); ls, longest spine; n. pods, number of podomeres; ss, shortest spine.

REFERENCES

BABCOCK, L. E. 1993. Trilobite malformations and the fossil record of behavioral asymmetry. *Journal of Paleontology*, **67**, 217–229.

BRIGGS, D. E. G. 1979. *Anomalocaris*, the largest known Cambrian arthropod. *Palaeontology*, **22**, 631–664.

--- and MOUNT, J.D. 1982. The occurrence of the giant arthropod *Anomalocaris* in the Lower Cambrian of southern California, and the overall distribution of the genus. *Journal of Paleontology,* **56**, 1112-1118.

--- LIEBERMAN, B.S., HENDRICKS, J.R., HALGEDAHL, S.L. and JARRARD, R.D. 2008. Middle Cambrian arthropods from Utah. *Journal of Paleontology*, **82**(2), 238—254.

BRUTON, D.L. 1981. The arthropod *Sidneyia inexpectans*, Middle Cambrian, Burgess Shale, British Columbia. *Philosophical Transactions of the Royal Society of London. Series B, Biological Sciences*, **18**, 619—653.

CARON, J. B. 2005. Taphonomy and community analysis of the Middle Cambrian Greater Phyllopod Bed, Burgess Shale. Unpublished Ph.D. Thesis, University of Toronto, Toronto, 316 pp.

CHLUPÁČ, I., and KORDULE, V. 2002. Arthropods of Burgess Shale type from the Middle Cambrian of Bohemia (Czech Republic). *Bulletin of the Czech Geological Survey*, **77**, 167–182.

COLLINS, D. 1996. The “evolution” of *Anomalocaris* and its classification in the arthropod class Dinocarida (nov.) and order Radiodonta (nov.). *Journal of Paleontology*, **70**, 280–293.

CONG, P., MA, X., HOU, X., EDGECOMBE, G. D. and STRAUSFIELD, N. J. 2014. Brain structure resolves the segmental affinity of anomalocaridid appendages. *Nature*, **513**, 538–542.

CONWAY MORRIS, S., and ROBISON, R. A. 1982. The enigmatic medusoid *Peytoia* and a comparison of some Cambrian biotas. *Journal of Paleontology*, **56**, 116—122.

DALEY, A. C., and BUDD, G. E. 2010. New anomalocaridid appendages from the Burgess Shale, Canada. *Palaeontology*, **53**, 721–738.

--- and PEEL, J. S. 2010. A possible anomalocaridid from the Cambrian Sirius Passet lagerstätte, North Greenland. *Journal of Paleontology*, **84**, 352–355.

--- and BERGSTRÖM, J. 2012. The oral cone of *Anomalocaris* is not a classic ‘‘*Peytoia*’’. *Naturwissenschaften*, **99**, 501–504.

--- and EDGECOMBE, G. D. 2014. Morphology of *Anomalocaris canadensis* from the Burgess Shale. *Journal of Paleontology*, **88**, 68-91.

--- BUDD, G. E., CARON, J. B., EDGECOMBE, G. D., and COLLINS, D. 2009. The Burgess Shale anomalocaridid *Hurdia* and its significance for early euarthropod evolution. *Science*, **323**, 1597–1600.

--- --- and --- 2013*a*. Morphology and systematics of the anomalocaridid arthropod *Hurdia* from the Middle Cambrian of British Columbia and Utah. *Journal of Systematic Palaeontology*, **11**, 743–787.

--- PATERSON, J. R., EDGECOMBE, G. D., GARCÍA-BELLIDO, D. C., and JAGO, J. B. 2013*b*. New anatomical information on *Anomalocaris* from the Cambrian Emu Bay Shale of South Australia and a reassessment of its inferred predatory habits. *Palaeontology*, **56**, 971–990.

GÁMEZ VINTANED, J. A., LIÑÁN, E., and ZHURALEV, A. Y. 2011. A new Early Cambrian lobopod-bearing animal (Murero, Spain) and the problem of the ecdysozoan early diversification. *In* Editors: PONTAROTTI, P. (ed). *Evolutionary Biology–Concepts, Biodiversity, Macroevolution and Genome Evolution.* Springer Berlin Heidelberg, 193–219 pp.

LEROSEY-AUBRIL, R., HEGNA, T.A., BABCOCK, L.E., BONINO, E. and KIER, C. 2014. Arthropod appendages from the Weeks Formation Konservat-Lagerstätte: new occurrences of anomalocaridids in the Cambrian of Utah, USA. *Bulletin of Geosciences*, **89**(2), 269—282.

LIEBERMAN, B.S., 2003. A new soft-bodied fauna: the Pioche Formation of Nevada. *Journal of Paleontology*, **77**, 674—690.

HAGADORN, J., SCHOTTENFELD, M. T. and McGOWAN, D. 2010. Putting *Anomalocaris* on a soft-food diet? *Geological Society of America, Abstracts with Programs*, **42**, 320.

HOU, X.G., MA, X.Y., ZHAO, J. and BERGSTRÖM, J. 2004. The lobopodian *Paucipodia inermis* from the lower Cambrian Chengjiang fauna, Yunnan, China. *Lethaia*, **37**(3), 235—244.

LANKESTER, E.R. 1904. The structure and classification of Arthropoda. *Quarterly Journal of Microscopical Science,* **47**, 523—582.

NEDIN, C. 1999. *Anomalocaris* predation on nonmineralized and mineralized trilobites. *Geology*, **27**, 987–990.

PATERSON, J. R., GARCÍA-BELLIDO, D. C., LEE, M. S., BROCK, G. A., JAGO, J. B. and EDGECOMBE, G. D. 2011. Acute vision in the giant Cambrian predator *Anomalocaris* and the origin of compound eyes. *Nature*, **480**, 237–240.

--- --- JAGO, J. B., GEHLING, J. G., LEE, M. S., and EDGECOMBE, G. D. 2016. The Emu Bay Shale Konservat-Lagerstätte: a view of Cambrian life from East Gondwana. *Journal of the Geological Society*, **173**, 1–11.

PATES, S., DALEY, A. C., and LIEBERMAN, B. S. *in press*. Hurdiid radiodontans from the middle Cambrian (Series 3) of Utah. *Journal of Paleontology*.

--- --- and ORTEGA-HERNÁNDEZ, J. *submitted*. *Aysheaia prolata* from the Wheeler Formation (Cambrian, Drumian) is a frontal appendage of the radiodontan *Stanleycaris*. *Acta Palaeontologica Polonica*.

RUDKIN, D. 1979. Healed injuries in Ogygopsis klotzi (Trilobita) from the Middle Cambrian of British Columbia. *Royal Ontario Museum Occasional Paper*, **32**, 1-8.

STEIN, M. 2013. Cephalic and appendage morphology of the Cambrian arthropod *Sidneyia inexpectans*. *Zoologischer Anzeiger-A Journal of Comparative Zoology*, **253**, 164—178.

VAN ROY, P., DALEY, A. C. and BRIGGS, D. E. G. 2015. Anomalocaridid trunk limb homology revealed by a giant filter-feeder with paired flaps. *Nature*, **522**, 77–80.

VINTHER, J., STEIN, M., LONGRICH, N. R., and HARPER, D. A. 2014. A suspension-feeding anomalocarid from the Early Cambrian. *Nature*, **507**, 496–499.

WHITTINGTON, H. B., and BRIGGS, D. E. 1985. The largest Cambrian animal, *Anomalocaris*, Burgess Shale, British Columbia. *Philosophical Transactions of the Royal Society of London. Series B, Biological Sciences*, 569–609.

ZACAÏ, A., VANNIER, J. and LEROSEY-AUBRIL, R. 2016. Reconstructing the diet of a 505-million-year-old arthropod: *Sidneyia inexpectans* from the Burgess Shale fauna. *Arthropod structure and development*, **45**, 200—220.

Chapter 5

Hurdiid radiodontans from the middle Cambrian (Series 3) of Utah

Author contributions

SP and ACD conceived the project; SP created the 3D model; ACD performed the analysis in TNT; SP wrote the manuscript and prepared the figures, with input from ACD and BSL.

Publication information

This Chapter has been peer reviewed and published by *Journal of Paleontology*:

Pates, S., Daley, A. C., & Lieberman, B. S. (2018). Hurdiid radiodontans from the middle Cambrian (Series 3) of Utah. *Journal of Paleontology*, 92(1), 99-113.

Hurdiid radiodontans from the middle Cambrian (Series 3) of Utah

Stephen Pates[1], Allison C. Daley[1,2,3], and Bruce S. Lieberman[4,5]

[1]Department of Zoology, University of Oxford, Oxford, OX1 3PS, UK <stephen.pates@zoo.ox.ac.uk>

[2]Oxford University Museum of Natural History, Oxford, OX1 3PW, UK

[3]Faculty of Geosciences and Environment, University of Lausanne, Sorge Géopolis, CH1015, Lausanne, Switzerland <allison.daley@unil.ch>

[4]Division of Invertebrate Paleontology, Biodiversity Institute, University of Kansas, Lawrence, KS 66045, USA <blieber@ku.edu>

[5]Department of Ecology and Evolutionary Biology, University of Kansas, Lawrence, KS 66045, USA

Running Header: Hurdiids from the middle Cambrian of Utah

Abstract.—Radiodontan body elements, some belonging to *Peytoia* and *Hurdia* and some unassigned, have been reported from the Langston Formation (Spence Shale Member), Wheeler Formation, and Marjum Formation of the middle Cambrian (Series 3) of Utah. These identifications are reassessed in light of recent work on the morphology of the radiodontan *Hurdia*. New specimens of *Hurdia* are identified from the Spence Shale, representing mouthparts (oral cones), cephalic carapace H-elements, frontal appendages and a single isolated swimming flap. The shape of the H-elements allows *H. victoria* to be identified from the Spence Shale for the first time. The flap is

larger and more complete than any reported from the Burgess Shale, and allows for a better understanding of the morphology of *Hurdia* swimming flaps. A 3D model of a *Hurdia* frontal appendage indicates that there is only one morph of *Hurdia* frontal appendage found in both species, and apparent morphological differences between disarticulated appendages reflect a preservational continuum caused by varying oblique angles relative to the seafloor. *Peytoia* should no longer be reported from the Spence Shale, but its presence is confirmed in the Wheeler and Marjum formations. New mouthparts (oral cones) of *Hurdia* from the Spence Shale and *Peytoia* from the Marjum Formation with surface textures of sub-millimeter diameter raised nodes are described. These new features have not been observed in material from the Burgess Shale, and suggest slight differences in preservation.

Introduction

Our understanding of the morphology and systematics of *Hurdia* Walcott, 1912 has greatly expanded in recent years, and it is now recognized as a significant taxon within Radiodonta present in several of the well-known Cambrian soft-bodied biotas including: the Burgess Shale in Canada and the nearby Stanley Glacier, Marble Canyon, Tulip Beds and Mount Stephen sites (Daley et al., 2009; 2013a); the Jince Formation in the Czech Republic (Chlupáč and Kordule, 2002, fig. 7); Wheeler Formation (Robison and Richards, 1981, pl. 4, fig. 1a,b) and the Spence Shale (Daley et al., 2013a) in Utah, USA; the Shuijingtuo Formation in China (Cui and Hou, 1990); and the Fezouata Biota in Morocco (Van Roy and Briggs, 2011, figs. 1d–i, S4a–c; 1l, S3c,d, S4f). Notably, the soft-bodied biotas from the middle Cambrian (Series 3) of Utah have yielded a large number of specimens previously identified as radiodontans in general, and usually *Anomalocaris*

Whiteaves, 1892 or *Peytoia* Walcott, 1911 (Daley and Bergström, 2012) (e.g., Conway Morris and Robison, 1982; Briggs and Robison, 1984; Conway Morris and Robison, 1988; Robison, 1991; Briggs et al., 2008), but the systematic position of most of this material has not yet been re-evaluated in light of the new discoveries on *Hurdia*. By analysis of appendages and mouthparts originally described in Conway Morris and Robison (1988) Daley et al. (2013a) were able to conclude that *Hurdia* was in fact present in the middle Cambrian (Series 3) of Utah alongside *Peytoia*, and described four new specimens from the Spence Shale. Herein, we reconsider the identifications of radiodontan specimens from Utah in detail and confirm that *Hurdia* is well represented there. Further, we identify *H. victoria* in the Spence Shale for the first time. A 3D model of an idealized *Hurdia* appendage potentially allows characters used in previous phylogenetic analyses (e.g., Vinther et al., 2014; Cong et al., 2014; Van Roy et al., 2015) to be visualized and evaluated in the hopes of possibly inferring which characters might be influenced by taphonomic factors.

The middle Cambrian (Series 3) of Utah is well known for its soft-bodied deposits that preserve a diverse array of taxa in several different depositional settings (Robison, 1991; Briggs et al., 2008; Gaines et al., 2008, 2012; Brett et al., 2009; Halgedahl et al., 2009). The Gunther family of Utah, along with Richard Robison (Robison, 1965; Gunther and Gunther, 1981), played a pivotal role in helping this treasure trove of fossils come to light. Many significant finds have been made from these deposits over the years (Resser, 1939; Brooks and Caster, 1956; Briggs and Robison, 1984; Babcock and Robison, 1988; Conway Morris and Robison, 1986, 1988; Robison and Wiley, 1995; Briggs et al., 2005), and new discoveries continue to be made (Robison and Babcock, 2011; Stein et al., 2011; Conway Morris et al., 2015; LoDuca et al., 2015; Robison et al., 2015). Taxa

from these deposits have also provided insights into higher-level arthropod relationships (Hendricks and Lieberman, 2008) while forming a core source of data used to study paleobiogeographic and macroevolutionary patterns during the Cambrian radiation interval (Hendricks et al., 2008).

Non-hurdiid radiodontans reported from the Langston Formation (Spence Shale Member), Wheeler Formation and Marjum Formation are limited to two body fossils of *Anomalocaris*: one from the Spence Shale and one from the Wheeler Formation, both described by Briggs et al. (2008, figs. 1, 3). Neither specimen has well preserved large frontal appendages, and the two specimens seem to represent two different and new species. Isolated appendages of *Anomalocaris* aff. *canadensis* Whiteaves, 1892, and *Anomalocaris*? sp. from the younger (Guzhangian) Weeks Formation in Utah have been described by Lerosey-Aubril et al. (2014). No new *Anomalocaris* appendages or bodies were identified during the course of this study. We emphasize new findings relating to *Hurdia* and *Peytoia*.

As is the case for other radiodontans, *Hurdia* and *Peytoia* are found mostly as isolated elements (carapace elements, mouthparts, appendages, and body flaps) and rarely as whole bodies, which can at times make taxonomic identification challenging. In general, the morphology of *Hurdia* can be divided into a head region with a pair of frontal appendages either side of a circular oral cone. The oral cone made up of four large plates, equally spaced, with seven small plates between each pair of large plates; these surround an opening with multiple inner rows of teeth. A large frontal carapace of three sclerotized elements (two lateral P-elements and one dorsal H-element) and stalked eyes complete the head region. The body is made up of seven to nine segments, with reduced swimming flaps and prominent setal structures (Daley et al.,

2009; 2013a). A morphometric analysis showed that there are two species of *Hurdia*, *H. victoria* and *H. triangulata*, which are differentiated by comparing the length and width of the carapace H-element (Daley et al., 2013a). *Hurdia* and *Peytoia* have recently been recovered within Hurdiidae (e.g. Van Roy et al. 2015), but these genera differ in a number of ways. *Peytoia* and *Hurdia* have a similar overall frontal appendage morphology in that both have elongated ventral spines, but these differ in numerous details including the number and length-width ratio of the podomeres, and the shape, arrangement and number of ventral spines (Daley et al., 2013a). *Hurdia* has a complex frontal carapace composed of three sclerite elements, whereas *Peytoia* has no evidence for such a large frontal carapace, with only traces of possible carapace material immediately surrounding the head in ventrally preserved specimens (Daley et al. 2009). The oral cone has the same arrangement of outer plates in *Hurdia* and *Peytoia*, but the multiple inner rows of teeth present in *Hurdia* are absent in *Peytoia*. The body trunk in *Hurdia* consists of seven to nine segments that are more cylindrical than the dorsoventrally flattened body of *Peytoia*, which has 13 body segments. The swimming flaps of *Hurdia* are much smaller than the wide flaps of *Peytoia*, but setal blades are more prominent in *Hurdia* as compared to *Peytoia* (Whittington and Briggs, 1985, fig. 101).

Materials and methods

One body specimen (USNM 374593) is held at the Smithsonian Museum of Natural History, Washington, D.C., USA. The remainder of the material studied is held at the Division of Invertebrate Paleontology, Biodiversity Institute, University of Kansas, Lawrence, USA (KUMIP). Detailed information for the fossil localities are available in

Table 3 of Hendricks et al. (2008). All specimen numbers, previous publications and new identifications are provided in Table 1.

Photographs were taken with a Canon EOS 500D DSLR Camera with Canon EF-S 60 mm Macro Lens, controlled for remote shooting using the EOS Utility 2 program. Photographs were taken under cross polarized light, non-polarized light, wet and dry, and under high and low angle lighting. Measurements for calculating RI values, and length:width ratios were taken from digital photographs using ImageJ 2.The 3D model was made using Blender 2.76b. A box model was created from a sketch of *Hurdia* adapted from Daley and Budd (2010). This was modified with a subdivision surface, and rendered to a video. A phylogenetic analysis in TNT v. 1.5 (Goloboff & Catalano, 2016) was run using implicit enumeration under equal weighting on a data matrix modified from Van Roy et al. (2015) consisting of 33 taxa and 61 characters. Modifications to the phylogenetic analysis data matrix were made in Mesquite v. 3.2 (Maddison and Maddison, 2017).

Geologic setting

The Spence Shale Member of the Langston Formation, middle Cambrian Series 3, Stage 5, is a diverse soft-bodied biota (Gunther and Gunther, 1981; Robison, 1991; Liddell et al., 1997), and knowledge of the paleontology, sedimentology, geochemistry, and taphonomy of this deposit has increased substantially over the past few years (Briggs et al., 2008; Garson et al., 2012; Gaines et al., 2012; Olcott Marshall et al., 2012; Gaines, 2014; Kloss et al., 2015). The Spence Shale is primarily made up of shale, with some limestone, and it is developed in a series of parasequences (Liddell et al., 1997; Garson et al., 2012). Detailed discussions of the sedimentology, taphonomy, and geochemistry

Table 1. Specimens examined in this study, including original and new taxonomic interpretations.

Catalogue number	Figure	Locality Age	Previous interpretation	Reference	New interpretation	Fragment
KUMIP 153093a/b	5.10, 5.11	Wheeler Formation Cambrian Drumian	*Peytoia* cf. *nathorsti*	Conway Morris & Robison, 1982	*Peytoia nathorsti*	Mouthpart
KUMIP 153094	5.5	Wheeler Formation Cambrian Drumian	*Peytoia* cf. *nathorsti*	Conway Morris & Robison, 1982	*Peytoia nathorsti*	Mouthpart
KUMIP 153901a/b	5.6, 5.7	Wheeler Formation, Cambrian Drumian	*Proboscicaris agnosta* *Hurdia*	Robison & Richards, 1981; Daley et al., 2013a	*Hurdia*	P-element
KUMIP 204777-204780	Conway Morris and Robison, 1988, figs. 26.1a, 26.1b, 26.2	Spence Shale Cambrian Stage 5	*Peytoia* cf. *nathorsti*	Conway Morris & Robison, 1988	*Sidneyia*-like taxon	Appendage
KUMIP 204781a/b	5.3, 5.4	Wheeler Formation Cambrian Drumian	*Peytoia nathorsti* *Hurdia*	Conway Morris & Robison, 1988; Daley et al., 2013a	hurdiid	Appendage
KUMIP 312405a/b	3	Spence Shale Cambrian Stage 5	Anomalocarididae gen. et sp. indet.	Briggs et al., 2008	*Hurdia*	Appendage and mouthpart
KUMIP 314039	4.2	Spence Shale Cambrian Stage 5	-	-	*Hurdia victoria*	H-element
KUMIP 314040a/b	2.3, 2.4	Spence Shale Cambrian Stage 5	-	-	*Hurdia*	Appendage

KUMIP 314042	2.5	Spence Shale Cambrian Stage 5	-	-	*Hurdia*	Appendage
KUMIP 314050	4.1, 4.4	Spence Shale Cambrian Stage 5	-	-	*Hurdia victoria*	H-element
KUMIP 314056	4.3, 4.5	Spence Shale Cambrian Stage 5	-	-	*Hurdia victoria*	H-element
KUMIP 314057a/b	4.6, 4.7	Spence Shale Cambrian Stage 5	-	-	*Hurdia*	Flap
KUMIP 314078	5.8, 5.9	Wheeler Formation Cambrian Drumian	Anomalocarididae gen. et sp. indet.	Briggs et al., 2008	*Peytoia nathorsti*	Mouthpart
KUMIP 314086a/b	5.1, 5.2	Wheeler Formation Cambrian Drumian	Anomalocarididae gen. et sp. indet.	Briggs et al., 2008	*Peytoia nathorsti*	Appendage
KUMIP 314095a/b	6.6, 6.7	Marjum Formation Cambrian Drumian	-	-	*Peytoia nathorsti*	Mouthpart
KUMIP 314127	Not figured	Spence Shale Cambrian Stage 5	-	-	hurdiid	Mouthpart
KUMIP 314145a/b	2.1	Spence Shale Cambrian Stage 5	-	-	*Hurdia*	Appendage
KUMIP 314175a/b	2.6	Spence Shale Cambrian Stage 5	-	-	*Hurdia*	Mouthpart
KUMIP 314178	2.2	Spence Shale Cambrian Stage 5	-	-	*Hurdia*	Appendage
KUMIP 314265a/b	2.7	Spence Shale Cambrian Stage 5	-	-	*Hurdia*	Mouthpart
USNM 374593	6, 7	Marjum Formation Cambrian Drumian	*Peytoia nathorsti*	Briggs & Robison, 1984	*Peytoia nathorsti*	Body

of the Spence Shale are provided by Liddell et al. (1997), Garson et al. (2012), and Kloss et al. (2015), respectively. All of the specimens from the Spence Shale discussed herein come from the Wellsville Mountains of northern Utah (Hendricks et al., 2008; Hendricks, 2013).

The Wheeler Formation, Drumian, Cambrian Series 3, from the House Range of Utah is slightly younger than the Spence from the Wellsville Mountains, and it too contains a diverse soft-bodied biota (Robison, 1964; Gunther and Gunther, 1981; Briggs and Robison, 1984; Rogers, 1984; Rees, 1986; Robison, 1991; Robison et al., 2015). There have been a substantial number of relatively recent sedimentological, taphonomic, and geochemical studies of the soft-bodied biota from this formation and region (e.g., Gaines and Droser, 2003, 2005; Briggs et al., 2008; Brett et al., 2009; Halgedahl et al., 2009; Gaines, 2014). The unit consists of homogeneous mudstones and interbedded mudstones with thin-grained, fine-bedded limestones. The soft-bodied material occurs primarily within carbonaceous shales (Gaines and Droser, 2003, 2005).

The still slightly younger soft-bodied deposits from the Marjum Formation, Drumian, Cambrian Series 3, generally resemble lithologically, stratigraphically and taphonomically those deposits from the Wheeler Formation where it is exposed in the House Range (Elrick and Snider, 2002; Brett et al., 2009; and Gaines and Droser, 2010), although they represent a shallower facies (Briggs and Robison, 1984; Brett et al., 2009).

The relative global chronostratigraphic ages and polymerid trilobite biostratigraphy of Radiodonta-preserving units in Utah and British Columbia can be seen in Figure 1.

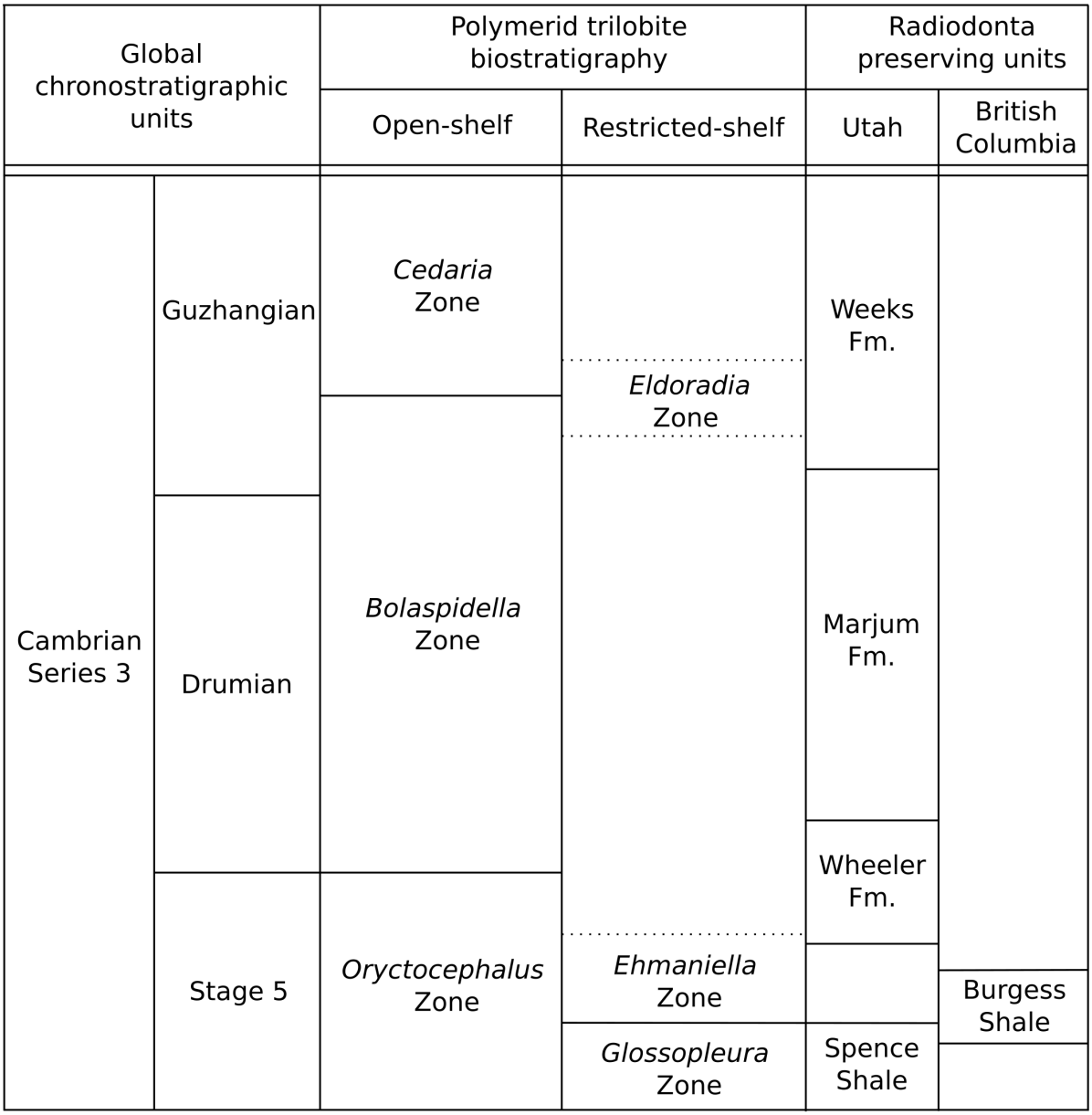

Figure 1. Stratigraphic column showing relative ages of Burgess Shale, Spence Shale, Wheeler Formation, Marjum Formation and Weeks Formation, with reference to global chronostratigraphic units and polymerid trilobite biostratigraphy. Adapted from Robison et al. (2015). Data of this study from Utah Radiodonta preserving units the Spence Shale, Wheeler Fm., and Marjum Fm. Spence Shale radiodont material of *Glossopleura* Zone age (Stage 5), Wheeler Fm. and Marjum Fm. radiodont material of *Bolaspidella* Zone age (Drumian).

Results

Taxonomic identifications of new and previously described material are summarized in Table 1. *Hurdia victoria* Walcott, 1912 is described for the first time from the Spence Shale. *Hurdia* also occurs in the Wheeler Formation. *Peytoia* occurs in the Wheeler and Marjum formations, but should no longer be reported as present in the Spence Shale.

Hurdia from the Spence Shale Member.—Some of the material interpreted as *Hurdia* from the Spence Shale comprise appendages and mouthparts (Figs. 2, 3); these include both previously described specimens (Briggs et al., 2008; Daley et al., 2013a, fig. 24) as well as new material. New carapace material (Fig. 4.1–4.5), which allows identification to the species level, and a large, isolated flap (Fig. 4.6, 4.7) are also discussed here for the first time. In addition, appendages previously interpreted as *Peytoia nathorsti* (Conway Morris and Robison, 1988), are here reinterpreted as belonging to a *Sidneyia*-like taxon.

KUMIP 314145a/b (Fig. 2.1) is a small, single incomplete *Hurdia* appendage with 7 visible podomeres with well-defined boundaries of around 1 mm in thickness. Podomeres at the proximal end of the appendage where the ventral spines attach are not preserved. KUMIP 314178 (Fig. 2.2) is a mostly complete small, single *Hurdia* appendage with ten podomeres separated by clear podomere boundaries of around 1 mm thickness. KUMIP 314040a/b (Fig. 2.3, 2.4) is a small *Hurdia* appendage with nine podomeres. Five large ventral spines, attached to podomeres 2–6, are tightly packed and appear curved forwards, beyond the distal end of the appendage. Auxiliary spines are only visible on the distalmost ventral spine. KUMIP 314042 (Fig. 2.5) is a larger

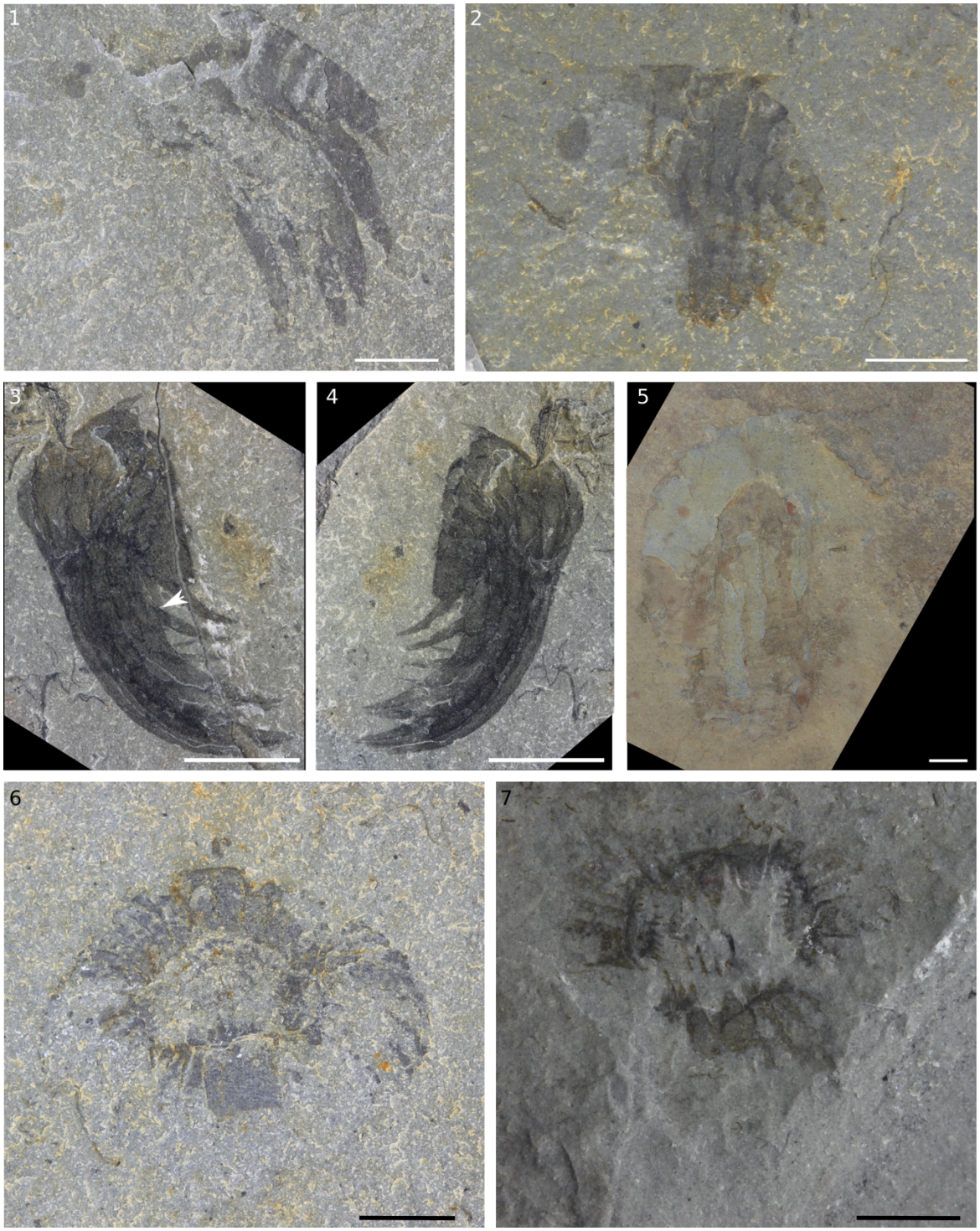

Figure 2. Hurdiid appendages and oral cones from the Spence Shale Member, Langston Formation, Wellsville Mountains, Utah, USA. **(1)** Appendage KUMIP 314145; **(2)** appendage KUMIP 314178; **(3)** appendage KUMIP 314040a with arrow indicating broken ventral spine; **(4)** KUMIP 314040b, counterpart to **3**; **(5)** appendage KUMIP 314042; **(6)** oral cone KUMIP 314175a; **(7)** oral cone KUMIP 314265a; All scale bars represent 5 mm.

Hurdia appendage with ten podomeres with clear podomere boundaries of around 1 mm thickness. The five large, straight ventral spines have slightly curved distal ends.

Briggs et al. (2008) identified KUMIP 312405a/b (Fig. 3 herein) as a pair of radiodontan appendages with mouthparts. The two appendages are preserved with one ('app. 1' in Fig. 3.3) on a higher level of rock than the other ('app. 2' in Fig. 3.3). App. 1 is well preserved and made up of ten podomeres. Large ventral spines are present on podomeres 2–6 and a small ventral spine is visible on podomere 9 ('vs' in Fig. 3.3). A terminal spine is visible on podomere 10 ('ts' in Fig. 3.3). App. 2 is not as clearly visible. The distalmost podomeres are visible. Three large ventral spines are preserved together, with the distal one angled forwards, similar to the overlying appendage. The mouthparts are made up of four large plates ('lp' in Fig. 3.3) arranged at 90° to each other around a rectangular opening. The total number of smaller plates is not clear, as the outer edge of the oral cone is not well preserved, but where it can be counted there are seven smaller plates between the large plates, which extrapolates to a total of 32 plates, four large and 28 small, characteristic of *Hurdia* and *Peytoia*. By contrast, *Anomalocaris* mouthparts have three large plates at 120° (Daley and Bergström, 2012). *Peytoia* mouthparts can be differentiated from *Hurdia* as *Hurdia* has numerous tooth rows in the central opening, whereas in *Peytoia* the central opening lacks tooth rows (Daley and Bergström, 2012). In the central opening of this specimen, additional tooth rows are visible ('tr' in Fig. 3.3), indicating this specimen is a *Hurdia*. The appendages associated with the mouthparts are both consistent with this interpretation, and are likely from the same animal. KUMIP 314175a/b (Fig. 2.6) is a small, oval oral cone of *Hurdia*. It is unusual in that it has small raised nodes (radius 1 mm) visible on one of the large plates and several small plates. KUMIP 314265a/b (Fig. 2.7) is another small

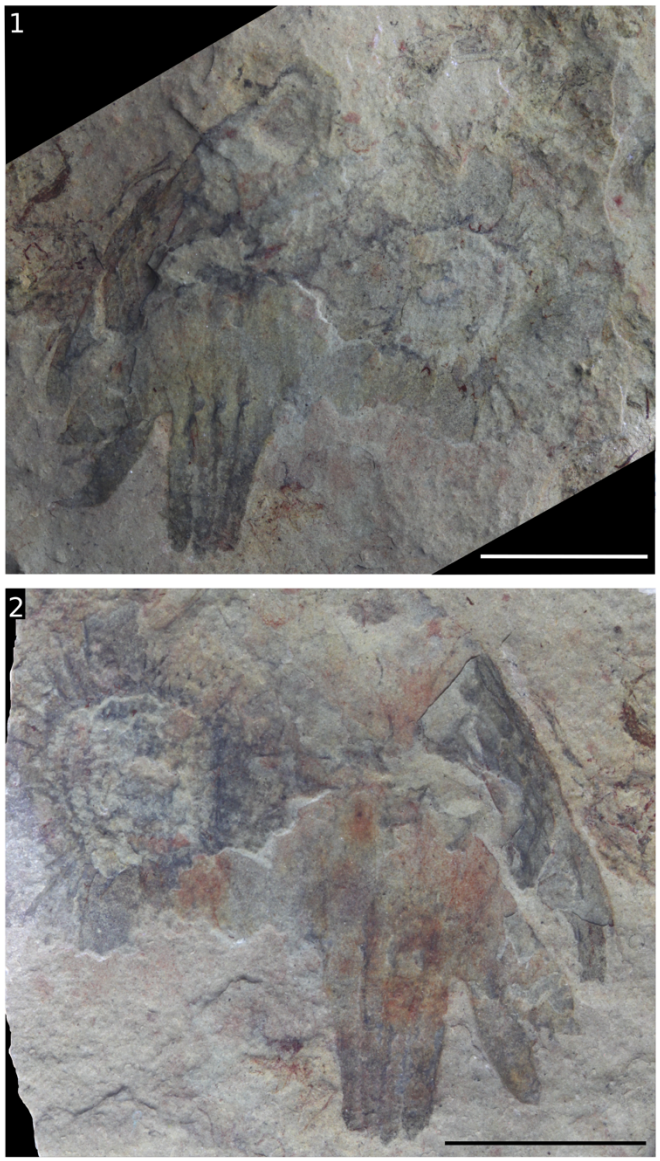

Figure 3. Assemblage of two *Hurdia* appendages with an oral cone **(1)** KUMIP 312405a; **(2)** KUMIP 312405b, counterpart to **1**; **(3)** interpretative drawing of **2**. Abbreviations: app. 1 = appendage 1, app. 2 = appendage 2, as = auxiliary spine, lp = large plate, p1 = podomere 1, p6 = podomere 6, tr = tooth row, ts = terminal spine, vs = ventral spine. All scale bars represent 10 mm.

Hurdia oral cone. The outer margins of the plates are not preserved, but multiple inner rows of teeth in an approximately rectangular central opening are clearly visible. Again, there are some possible small round nodes (radius 1 mm) visible on some plates.

The length:width ratio of H-elements from the carapace of *Hurdia* can be used to distinguish *H. victoria* from *H. triangulata*: *H. victoria* has H-elements with lengths greater than 1.5 times the width (but less than 2.0 times) and *H. triangulata* has H-elements with lengths less than 1.5 the width (Daley et al., 2013a). KUMIP 314039 (Fig. 4.2), KUMIP 314050 (Fig. 4.1, 4.4), and KUMIP 314056 (Fig. 4.3, 4.5), identified by height:width ratios, are the first *H. victoria* specimens identified from the Spence Shale; *H. triangulata* has not yet been identified. Reticulation polygons were observed on parts of the surface of some elements (Fig. 4.4). The specimen illustrated in (Fig. 4.3, 4.5) has ten small brown patches (1–5 mm in radius) and a trilobite with inferred manganese dendrites radiating from it, obscuring parts of the fossil. Similar dendrites with elevated manganese content have been reported from the Pioche Shale (Moore and Lieberman, 2009). Evidence for the two-layered H-element can be seen towards the strengthened tip (Fig. 4.5).

KUMIP 314057a/b (Fig. 4.6, 4.7) is a part and counterpart of an isolated radiodontan swim flap covered with regularly spaced, prominent transverse lines, also referred to as "strengthening rays" (Whittington and Briggs, 1985) or "veins" (Chen et al., 1994; Hou et al., 1995), about 1 mm wide and 2 mm apart. The flap is relatively large compared to Hurdia flaps reported from the Burgess Shale (Daley et al., 2013a), measuring approximately 65 mm in width and 45 mm in height. This specimen is tentatively identified as *Hurdia* because of the presence of transverse lines across the entire surface of the flap, which is not seen in *Peytoia* (where the transverse lines are

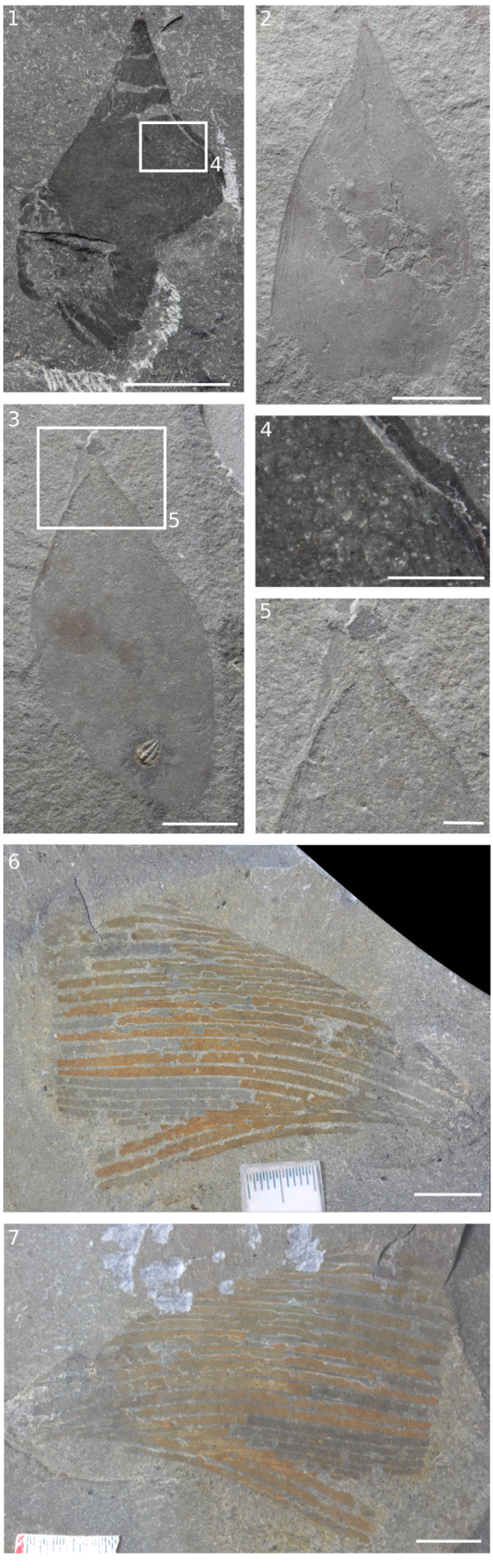

Figure 4. *Hurdia* carapace elements and flap from the Spence Shale Member, Langston Formation, Wellsville Mountains, Utah, USA. **(1)** H-element KUMIP 314050; **(2)** H-element KUMIP 314039; **(3)** H-element 314058; **(4)** Boxed region in **1**; **(5)** Boxed region in **3**; **(6)** flap KUMIP 314057b; **(7)** KUMIP 314057a, part to **6**. Scale bars in **1**–**3**, **6, 7** represent 10 mm, scale bars in **4, 5** represent 2.5 mm.

confined to the anterior half of the flap) or *Anomalocaris* (which lacks transverse lines entirely).

Sidneyia? from the Spence Shale Member.—Conway Morris and Robison (1988, fig. 26.1a, 26.1b, 26.2) identified four specimens (KUMIP 204777–204780) as broken spines of *Peytoia nathorsti* appendages. These are reinterpreted as distal podomeres of endopods (walking appendages) of a *Sidneyia*-like taxon, based on the rounded curvature of the overall structure, the oblique angle of the spines, the characteristic arrangement of repetitive bundles of decreasing spine size, and the presence of podomere boundaries faintly visible on some specimens (compare KUMIP 204777–204780: Conway Morris and Robison, 1988, fig. 26.1a, 26.1b, 26.2 to Bruton, 1981, figs. 48, 53, 55, 58, 60, 88, 92 and Stein, 2013, fig. 7B–D). This therefore indicates *Peytoia* should no longer be reported as present in the Spence Shale. *Sidneyia* was previously reported from the Spence Shale (Briggs et al., 2008).

Hurdiids from the Wheeler Formation.—*Hurdia* is known from the Wheeler Formation by a single P-element. *Peytoia* is known from one appendage and several mouthparts. KUMIP 153901a/b (Fig. 5.6, 5.7) was first described by Robison and Richards (1981, pl., 4, fig. 1a, b) as *Proboscicaris agnosta*, which at the time was thought to be a phyllocarid. *Proboscicaris* is now identified as the P-element of the *Hurdia* carapace (Daley et al., 2009). KUMIP 314086a/b (Fig. 5.1, 5.2) was first described by Briggs et al. (2008, fig. 2.2) as a radiodontan appendage. Owing to the relatively limited preservation, they did not classify it to genus. It is an appendage with 10 podomeres, with elongated ventral spines on podomeres 2–6. Six auxiliary spines are present perpendicular to the ventral

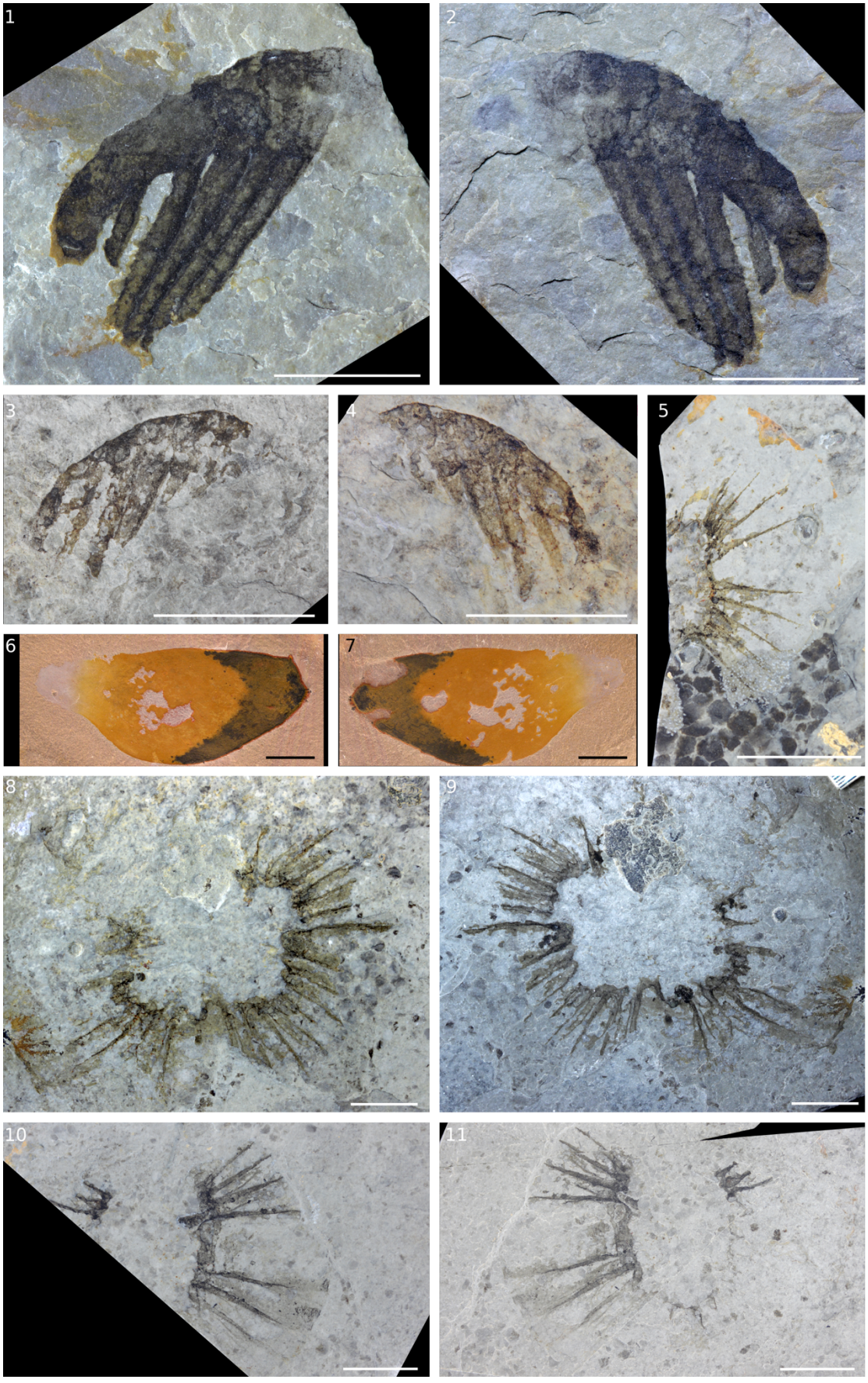

Figure 5. Caption on next page.

Figure 5. Hurdiid appendages, oral cones and carapace element from the Wheeler Formation, House Range, Utah, USA. **(1)** Appendage KUMIP 314086b; **(2)** KUMIP 314086a, part to **1**; **(3)** appendage KUMIP 204781a; **(4)** KUMIP 204781b, counterpart to **3**; **(5)** oral cone KUMIP 314094; **(6)** *Hurdia* P-element 153901a; **(7)** KUMIP 153901b, counterpart to **6**; **(8)** oral cone KUMIP 314078b; **(9)** KUMIP 314078a, part to **8**; **(10)** oral cone KUMIP 153093b; **(11)** KUMIP 153093a, part to **10**. All scale bars represent 10 mm.

spine of podomere 5. There are three small triangular terminal spines on podomere 10. The presence of three terminal spines, the orientation of ventral spines, and the curved distal end indicate it is a *Peytoia* appendage. Conway Morris and Robison (1982, text-fig. 1, pl. 1 figs. 1–5) described two specimens, KUMIP 153093a/b (Fig. 5.10, 5.11) and KUMIP 153094 (Fig. 5.5), of radiodontan oral cones as *Peytoia* cf. *P. nathorsti*, and we support this interpretation based on the overall arrangements of plates, and the lack of tooth rows inside the main opening. The genuine absence of additional rows of teeth can be confirmed by examining the central opening, which well preserved. KUMIP 314078 (Fig. 5.8, 5.9), first described by Briggs et al. (2008, fig. 2.2), is an oral cone with four large plates, and seven smaller plates between each larger plate. Part of the mouth apparatus is not preserved, but it can be inferred that it had 32 plates (four large, 28 small) radially arranged. The central opening of the incomplete mouth apparatus does not have additional tooth rows, so it can be identified as *Peytoia*.

Conway Morris and Robison (1988, fig. 26.3) identified KUMIP 204781a/b (Fig. 5.3, 5.4) from the Wheeler Formation as a *P. nathorsti* appendage. A previous taxonomic analysis (Daley et al., 2013a) suggested that this was potentially a *Hurdia* appendage. As the distal end of the appendage is not preserved and the morphology of the ventral spines is not conclusive, it is identified here as a hurdiid, but no identification to the genus level is made.

Peytoia from the Marjum Formation.—*Hurdia* is not known from the Marjum Formation. Briggs and Robison (1984) identified USNM 374593 (Figs. 6, 7) from the Marjum Formation as a partial body (lacking frontal appendages) of *Peytoia nathorsti*, based on the presence of transverse lines on the flaps. These had only been observed

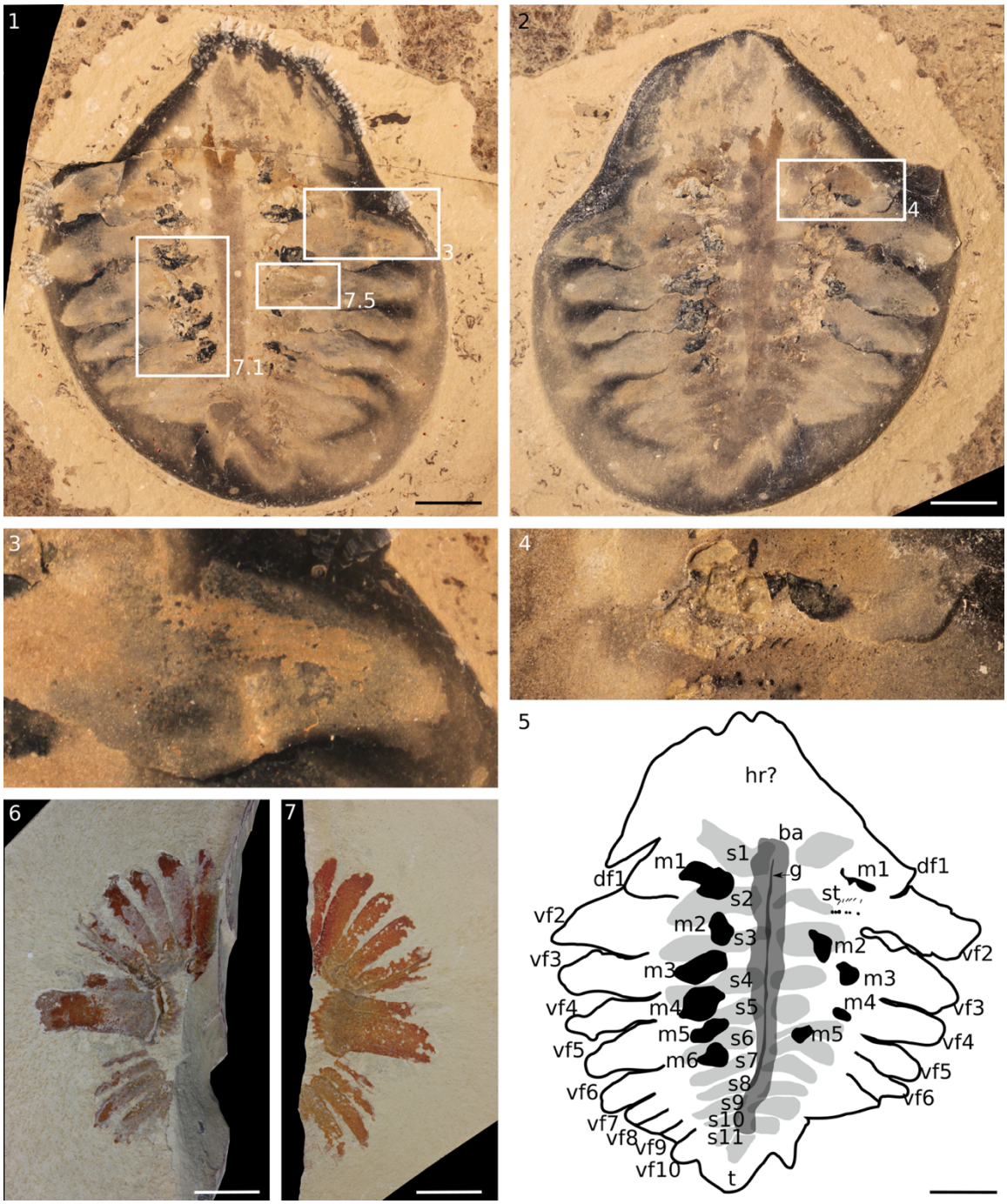

Figure 6. Caption on next page.

Figure 6. *Peytoia* partial body and partial oral cone from the Marjum Formation, House Range, Utah, USA, USNM 374593 **(1)** Counterpart; **(2)** part; **(3)** box from **1**, showing flap and strengthening rays; **(4)** box from **2**, arrow indicates high relief linear structures; **(5)** interpretive sketch of **1**. Abbreviations: ba = body axis, s1–11 = setal blade blocks, labelled anterior to posterior, df = dorsal flap, g = gut, hr? = head region?, m1–6 = muscle blocks, labelled anterior to posterior, st = staples, t = tail, vf = ventral flap; **(6)** partial oral cone KUMIP 314095b; **(7)** part to **6**; All scale bars represent 10 mm.

in *P*. *nathorsti* and not *Anomalocaris canadensis*, which at the time was the only other radiodontan body type known. We support placement in *Peytoia* because of the presence of large posterior-tapering swim flaps (in contrast to the small flaps of *Hurdia*) with transverse lines (which are absent in *Anomalocaris*), and the absence of a tail fan (present in *Hurdia* and *Anomalocaris*). The specimen consists of the 11 most posterior segments and tail of the animal, with flaps and central body structures preserved together. There is slight overlap of the anterior and posterior edges of the flaps, and the presence of some high-relief mineralized structures (Fig. 7, described below). A dark brown-grey linear structure ('ba' in Fig. 6.5) runs down the median axis of the animal, 6–7 mm wide near the anterior, tapering to a point and disappearing as it reaches the pair of body flaps. This region has a very thin (1 mm wide) feature at its midline running along the length of the body, particularly visible in the counterpart ('g' in Fig. 6.5). This is interpreted to be the gut running through the body cavity. It is flanked on both sides by a series of bilaterally symmetrical dark grey features ('s1–s11' in Fig. 6.5). They are larger anteriorly (3 x 25 mm) than posteriorly (1.5 x 10 mm), and are interpreted as setal blade blocks on account of their preservation, position and co-occurrence with body flaps. Lateral to the setal blade structures, and partly overlapping them, there is a series of dark reflective structures with high relief, present in the region where the base of the flaps meets the axial region ('m1–m6' in Fig. 6.5). These structures are interpreted as musculature on account of similarities between them and musculature in *Anomalocaris canadensis* (Daley and Edgecombe, 2014, figs. 15, 17). Both have a fibrous texture (Fig. 7.3–7.5) are similar in size and shape (Fig. 7) and are at the base of body flaps (Fig. 7.1, 7.2). In *A*. *canadensis* these structures are preserved as an orange material, or as a high relief dark grey to black reflective material. In *Peytoia* (USNM 374593) they are similarly

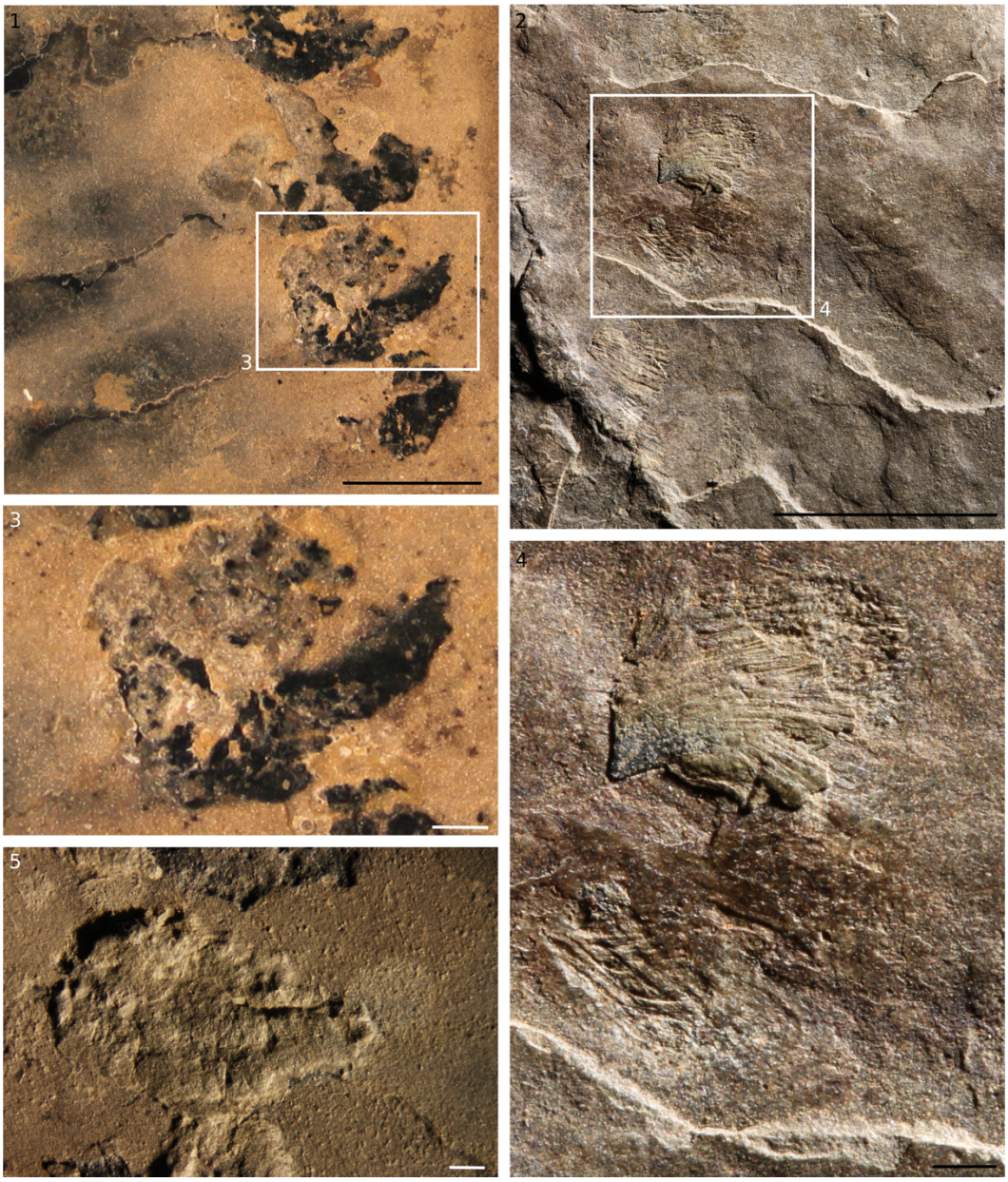

Figure 7. Comparison of musculature in *Peytoia* partial body from the Marjum Formation, House Range, Utah, USA, and *Anomalocaris* from the Burgess Shale, British Columbia, Canada. **(1)** USNM 374593, box **7.1** from Fig. 6.1, showing position of musculature at the base of flaps; **(2)** ROM 62547, showing position of musculature at the base of flaps; **(3)** box from **1**, showing faint linear features in musculature; **(4)** box from **2**, showing clear linear features in musculature **(5)** box **7.5** from Fig. 6.1, showing linear features in matrix where musculature has been removed. Scale bars in **1, 2,** represent 10 mm. Scale bars in **3, 4, 5** represent 1 mm.

preserved as high relief dark reflective material, although the fibrous details are less well preserved than in *A*. *canadensis* (compare Fig. 7.3, 7.5 to Fig. 7.4). They are not interpreted as gut diverticulae, which are often preserved as high relief dark reflective material, as they do not intersect the gut, and are instead associated with the intersection of the body flaps with the cuticularized body, far from the body axis. However it must be noted that euarthropod gut diverticulae are preserved in a variety of ways (Lerosey-Aubril et al., 2012), and the preservation of this musculature is different from musculature reported from some other Burgess-Shale type localities: *Pambdelurion* from Sirius Passet (Budd, 1998); and *Myoscolex* from the Emu Bay Shale (Briggs and Nedin, 1997).

The second most anterior flap on the right side of the counterpart preserves a set of high-relief linear structures near its base, located between the musculature of this flap and the flap in front of it (Fig. 6.4, 'st' in Fig. 6.5). The six parallel, evenly spaced structures are mineralized, and although they are closely packed, they do not touch one another. The longest one, closest to the body axis, is just under 1 mm in length, and the structures become shorter away from the body axis, with the shortest one just under 0.5 mm in length. 2 mm below the linear structures there are a number of circular mineralized structures, around 0.25 to 0.5 mm in diameter. Small spheres 0.5 mm in diameter are present on other phosphatized blocks. Similar structures, which were identified as clusters of pyrite framboids, have been reported from the middle Cambrian (Series 3) Pioche Shale by Moore and Lieberman (2009). Transverse lines only cover the anterior portion of the flap (Fig. 6.3), and no internal structure of the flaps is preserved, similar to *P*. *nathorsti* from the Burgess Shale (Whittington and Briggs, 1985). Ten large

ventral flaps (‘vf1–vf10’ in Fig. 6.5) are preserved on the side that most clearly shows a dorsal flap (‘df1’ in Fig. 6.5), and six large ventral flaps are preserved on the other side (‘vf1–vf6’ in Fig. 6.5), with one dorsal flap preserved there also (‘df1’ in Fig. 6.5). The front pair of flaps is the largest, and they reduce in size sequentially. The flaps associated with body segments 7–11 are overlapping due to the orientation of preservation. There are no flaps associated with the tail (‘t’ in Fig. 6.5). On the part, two dorsal flaps are also preserved at the front of the animal, in addition to the larger ventral flaps (‘df1’ in Fig. 6.5).

A partial mouthpart, KUMIP 314095 (Fig. 6.6, 6.7) is identified as *Peytoia* on account of the visible plate morphology and lack of internal tooth rows. One large plate with large triangular inner spines is preserved, with five smaller plates on one side and seven on the other side of the large plate. These smaller plates are a regular size and overlap each other, with the plate closer to the large plate overlapping the one next closest. The partially preserved central opening shows no evidence of additional rows of teeth. The large plate has 10 small triangular spines pointing inwards, the widest of which, at a central point of the plate, is around 2 mm. The others are smaller, at around 1 mm wide. Some of the smaller plates have a single projection also pointing inwards, around 1 mm wide. Unusually for *Peytoia* this mouthpart has small (diameter approximately 0.3 mm) nodes on the surface of the large plate, and some adjacent plates (visible on both part and counterpart, Fig. 6.6, 6.7).

Discussion

Morphological interpretations on Hurdia appendages can be influenced by specimen orientation.—*Hurdia* appendages are preserved in a variety of orientations (see Daley et

al., 2013a). Ventral spines of *Hurdia* are often preserved curved, both anteriorly (e.g. Fig. 2.3, 2.4) and posteriorly (e.g. Fig. 2.1, 2.2) and straight (e.g. Figs. 2.5, 3), sometimes in the same specimen (e.g. Daley et al., 2009, fig. 2C). The appendages have some element of plasticity, and during preservation they can become deformed. In some specimens the curvature of ventral spines appears to change along the length of the appendage, due to the appendage being preserved at an angle (e.g. Daley et al., 2013a, figs. 12C, E, 24A, where the distalmost ventral spines appear more curved as the appendage is rotated one way, and Daley et al., 2013a, fig. 12G, where the proximalmost ventral spines appear more curved as the appendage is rotated the other way). Appendages not preserved at such angles tend to have the distalmost podomeres more clearly preserved, not overlapping more proximal podomeres (compare the position of the distalmost podomeres in Fig. 3 and Daley et al., 2013a, fig. 12A, to those described as rotated above).

The impact that these preservational factors might have on morphological reconstructions and inferred evolutionary affinities can be observed by considering phylogenetic analyses of Radiodonta. Recent phylogenies (Cong et al., 2014; Van Roy et al., 2015) based on the data matrix and analysis of Vinther et al. (2014) consider four distinct representatives of *Hurdia*: *H. victoria, H.* cf. *victoria* Utah*, H.* sp. B Spence Shale, and *H.* sp. B Burgess Shale (the latter two were coded identically except for missing character states). Other than missing character states, *H. victoria* and H. cf. *victoria* Utah only differ in the condition of character 29: Vinther et al. (2014) coded *H. victoria* as having distally-projecting dorsal spines on the terminal segments; these were coded as absent in *Hurdia* cf. *victoria* Utah. Vinther et al. (2014) coded *Hurdia victoria* (including *Hurdia* cf. *victoria* Utah) and *H.* sp. B as differing in three characters. In character 34,

the ventral spines were coded as broader distally than proximally in *Hurdia victoria*, and subequal or narrower distally in *Hurdia* sp. B. In character 39, the distal tips of the ventral spines are hooked forward in *Hurdia victoria*, but strongly hooked forward and forming a 90° angle with the spine base in *Hurdia* sp. B. The phylogenetic significance of characters 29, 34, and 39 may be called into question by the aforementioned preservational variation. Similarly, character 46 (curvature of ventral spines) may reflect preservational rather than taxonomic variation. *Hurdia* sp. B was coded as having proximal ventral spines that curve posteriorly, whereas *H. victoria* was coded as having ventral spines all straight or anteriorly curved. However, *H. victoria* specimens with straight proximal ventral spines and anteriorly curving distal ends are common (e.g. Daley et al., 2013, fig. 12 A, C, E, G) and this reflects taphonomic variation.

To visualize how the angle of preservation influences morphological interpretations of *Hurdia* appendages, a 3D model was created in Blender based on the morphology of the *Hurdia* appendage in Daley and Budd (2010, text-fig. 1D). This 3D model (Fig. 8) suggests that the apparent broadness of ventral spines on distal podomeres will be influenced by how a specimen is oriented when it is preserved, and so the broadness of ventral spines (Vinther et al., 2014, Character 34) is likely not a good character for distinguishing *Hurdia* species. A small difference in orientation affecting apparent thickness of ventral spines can be seen by comparing KUMIP 314086 (Fig. 5.1, 5.2, with ventral spines of equal thickness) and KUMIP 314042 (Fig. 2.5, where the distalmost ventral spine appears thicker because of its orientation). This is visualized by the 3D model, where Fig. 8.1 (no rotation) shows ventral spines of equal thickness, and Fig. 8.2 (small rotation) shows an apparently thicker distalmost ventral spine. A more extreme example of the variation in the orientation of appendage preservation

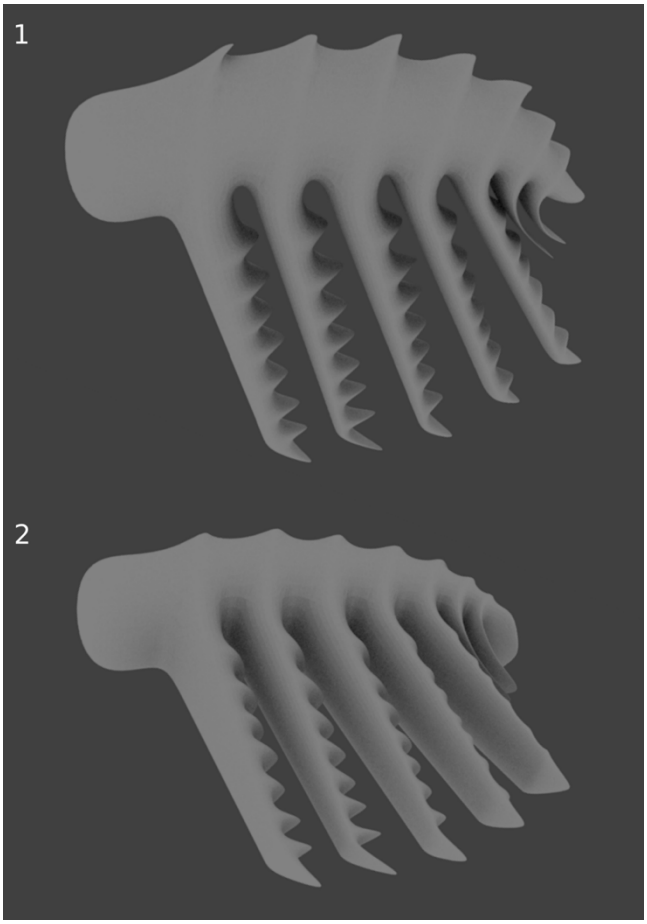

Figure 8. 3D model of *Hurdia* appendage, with ventral spines reconstructed as being of equal thickness. **(1)** Lateral view, showing ventral spines appearing equally thick; **(2)** oblique view, showing distal ventral spines appearing thicker than proximal ones, and differences in 'hooked' appearance at distal tip of ventral spines.

can be seen in the two appendages of KUMIP 312405 (Fig. 3). These appendages are presumably from the same animal but preserved at very different orientations.

In summary Vinther et al.'s (2014) characters 29, 34, 39, and 46, which comprise the evidence to distinguish four different representatives of *Hurdia*, may be influenced by preservational factors. A phylogenetic analysis of the data matrix from Van Roy et al. (2015), which is based on the original data matrix of Vinther et al. (2014), was run in TNT v. 1.5 using implicit enumeration under equal weighting. The data matrix was modified in the following ways: In Character 29, *H.* cf. *victoria* Spence is coded as dorsal spines present, and both *H.* sp. B taxa are coded as unknown; Character 34 was deleted, as is has been shown to reflect preservation and not true morphological difference; Character 39 (now Character 38) was changed to being unordered, and both *H.* sp. B taxa and *Stanleycaris* were coded as having hooked forward ventral spines; and in Character 46 (now Character 45), both *Hurdia* sp. B taxa are coded as having straight or curved anterior ventral spines. An analysis under equal weighting recovers 70 most parsimonious trees of 106 steps, and in strict consensus (CI=0.66, RI=0.85) all four *Hurdia* taxa and *Stanleycaris* are recovered in an unresolved polytomy. This is in contrast to the resolved relationships depicted in Vinther et al. (2014) and Van Roy et al. (2015), where the two *H.* sp. B specimens form a clade that is sister to *Stanleycaris*, rather than to *H. victoria*. Based on current evidence *Hurdia* cannot be identified to the species level by its frontal appendages alone, and appendages from the Spence Shale and the Burgess Shale cannot be distinguished as KUMIP 314040 and 314178, described herein, show that *Hurdia* appendages from Utah do possess dorsal spines (Fig. 2.2–2.4). *Hurdia* can still only be separated into two distinct species by the shape of its H-element (Daley et al., 2013a).

Presence of nodes on mouthparts.— Nodes are present on the plates of *Hurdia* mouthparts from the Spence Shale (KUMIP 314175a/b and 314265a/b, Fig. 2.6, 2.7) and partial *Peytoia* mouthparts from the Marjum Formation (KUMIP 314095, Fig. 6.6, 6.7). Nodes are not often seen in Burgess Shale specimens. The nodes are similar to what is seen in *Anomalocaris* (e.g., Daley and Bergström, 2012, fig. 2a–d; Daley and Edgecombe, 2014, fig. 7.5). However, the plates of these mouthparts lack the subdivisions and furrowing on the outer margins that is often seen in *Anomalocaris* (e.g. Daley and Bergström, 2012, fig. 2g–j). The presence of nodes in the Utah specimens could be due to interspecific variation, however, a more likely cause is preservational differences, which allow more 3D structure to be preserved in Utah than in Burgess Shale specimens. Similar preservational differences are seen in the oral cones of *A. canadensis*, where nodes are preserved in varying degrees of relief in oral cones from the Burgess Shale and the Emu Bay Shale (Daley et al., 2013b, Daley and Bergström, 2012).

Geographical and temporal distribution of hurdiids.—*Hurdia* and *Peytoia* are distributed over a large temporal and geographic range (Table 2). Both are reported from China, the USA, and Canada. *Hurdia* is known additionally from the Czech Republic (Chlupáč and Kordule, 2002), and *Peytoia* from Poland (Daley and Legg, 2015). This study shows that *Peytoia* is not known from the Spence Shale. This does not have any implications for the first or last appearance of *Peytoia*, as its oldest occurrence is from Holy Cross Mountains (Daley and Legg, 2015) and it is reported from the younger Marjum Formation (Briggs and Robison, 1984, this study), however it does change the earliest

Table 2. Locations containing hurdiid specimens.

	HCM	Shui.	Balang	Jince	Spence	Tulip	Burg.	Stan.	Wheel.	Marj.	Fez.
***Hurdia* specimens**											
H. victoria H-elements					Y	Y	Y	Y			Y
H. triangulata H-element						Y	Y	Y			
P-element		Y		Y		Y	Y		Y		Y
Appendage					Y	Y	Y	Y			
Oral cones					Y	Y	Y	Y			
App. + Oral cone assem.							Y	Y			
Body (partial/complete)						Y	Y	Y			
Isolated flap					Y						
***Peytoia* specimens**											
Appendage	Y		Y			Y	Y		Y		
Oral cone						Y	Y		Y	Y	
Body (partial/complete)						Y	Y			Y	
Other hurdiid appendages						Y		Y	Y		Y
Publications	1	2	3	4	5,6	7	7	8	5, 6, 9	10	11

Abbreviations: HCM = Holy Cross Mountains, Poland; Shuj. = Shuijingtuo Formation, China; Balang = Balang Formation, China; Jince = Jince Formation, Czech Republic; Spence = Langston Formation (Spence Shale Member), Utah, USA; Tulip = Tulip Beds, Mount Stephen, Yoho National Park, Canada; Burg. = Fossil Ridge, Burgess Shale, Yoho National Park Canada; Stan. = Stanley Glacier, Kootenay National Park, Canada; Wheel. = Wheeler Formation, Utah, USA; Marj. = Marjum Formation, Utah, USA; Fez. = Fezouata Formation, Morocco. Publications: 1=Daley and Legg (2015); 2=Cui and Hou (1990); 3=Lui (2013); 4= Chlupáč and Kordule (2002); 5=Conway Morris and Robison (1988); 6=Briggs et al. (2008); 7=Daley and Budd (2010); 8=Caron et al. (2010); 9=Robison and Richards (1981); 10=Briggs and Robison (1984); 11=Van Roy and Briggs (2011).

known occurrence of *P. nathorsti* to the Burgess Shale. *Hurdia* is not yet known from the Marjum Formation, however it is reported from the younger Fezouata Lagerstätten (Van Roy and Briggs, 2011). As *Hurdia* and *Peytoia* do not co-occur in the Spence Shale or Marjum Formations, a potential hypothesis is that the similarities of their frontal appendages, and hence similar predation methods, prevented the two genera from co-existing. Indeed, a recent morphospace analysis of the first appendages of 36 euarthropod taxa (Aria and Caron, 2015) supports functional similarities in the feeding appendages of *Peytoia* and *Hurdia*, which plotted close together. However, *Hurdia* and *Peytoia* do co-occur in the Wheeler Formation, Tulip Beds and Burgess Shale (Table 2), suggesting that they were capable of co-existing in the right environment, and the collection of more hurdiids from the Spence Shale and Marjum Formation may in fact show that *Peytoia* and *Hurdia* are present where currently they are not known.

Acknowledgments

M. Florence provided access to the specimen at the USNM. We thank the editor Jisuo Jin, Associate Editor Z. Zhang, an anonymous reviewer and J. Ortega-Hernandez for their valuable comments, and P. Selden (University of Kansas) for use of photographic equipment. The program TNT was made available with the sponsorship of the Willi Hennig Society. Funding was provided by a Palaeontological Association Sylvester-Bradley Award (PA-SB201503) to SP, the OUMNH to ACD and NSF-EAR-0518976 to BSL.

References

Aria, C., and Caron, J.B., 2015, Cephalic and limb anatomy of a new isoxyid from the burgess shale and the role of “stem bivalved arthropods” in the disparity of the frontalmost appendage: PloS one, v. 10, p. e0124979.

Babcock, L.E., and Robison, R.A., 1988, Taxonomy and paleobiology of some Middle Cambrian *Scenella* (Cnidaria) and hyolithids (Mollusca) from western North America: University of Kansas Paleontological Contributions, v. 121, p. 1–22.

Brett, C.E., Allison, P.A., DeSantis, M.K., Liddell, W.D., and Kramer, A., 2009, Sequence stratigraphy, cyclic facies, and lagerstätten in the Middle Cambrian Wheeler and Marjum formations, Great Basin, Utah: Palaeogeography, Palaeoclimatology, Palaeoecology, v. 277, p. 9–33.

Briggs, D.E., and Nedin, C., 1997, The taphonomy and affinities of the problematic fossil *Myoscolex* from the Lower Cambrian Emu Bay Shale of South Australia: Journal of Paleontology, v. 71, p.22–32.

Briggs, D.E., and Robison, R.A., 1984, Exceptionally preserved nontrilobite arthropods and *Anomalocaris* from the Middle Cambrian of Utah: University of Kansas Paleontological Contributions, v. 111, p. 1–23.

Briggs, D.E., Lieberman, B.S., Halgedahl, S.L. and Jarrard, R.D., 2005, A new metazoan from the Middle Cambrian of Utah and the nature of the Vetulicolia: Palaeontology, v. 48, p. 681–686.

Briggs, D.E., Lieberman, B.S., Hendricks, J.R., Halgedahl, S.L. and Jarrard, R.D., 2008, Middle Cambrian arthropods from Utah: Journal of Paleontology, v. 82, p. 238–254.

Brooks, H.K., and Caster, K.E., 1956, *Pseudoarctolepis sharpi*, n. gen., n. sp.(Phyllocarida), from the Wheeler Shale (Middle Cambrian) of Utah: Journal of Paleontology, v. 30, p. 9–14.

Bruton, D.L., 1981, The arthropod *Sidneyia inexpectans*, Middle Cambrian, Burgess Shale, British Columbia: Philosophical Transactions of the Royal Society of London. Series B, Biological Sciences, v. 295, p. 619–653.

Budd, G.E., 1998, Stem group arthropods from the Lower Cambrian Sirius Passet fauna of north Greenland, *in* Fortey, R. A., and Thomas, R. H., ed., Arthropod relationships, p. 125-138. Springer Netherlands.

Caron, J.B., Gaines, R.R., Mángano, M.G., Streng, M., and Daley, A.C., 2010, A new Burgess Shale–type assemblage from the "thin" Stephen Formation of the southern Canadian Rockies: Geology, v. 38, p. 811–814.

Chen, J.Y., Ramsköld, L., and Zhou, G.Q., 1994, Evidence for monophyly and arthropod affinity of Cambrian giant predators: Science, v. 264, p. 1304–1308.

Chlupáč, I., and Kordule, V., 2002, Arthropods of Burgess Shale type from the Middle Cambrian of Bohemia (Czech Republic): Bulletin of the Czech Geological Survey, v. 77, p. 167–182.

Cong, P., Ma, X., Hou, X., Edgecombe, G.D., Strausfeld, N.J., 2014, Brain structure resolves the segmental affinity of anomalocaridid appendages: Nature, v. 513, p. 538-542.

Conway Morris, S., and Robison, R.A., 1982, The enigmatic medusoid *Peytoia* and a comparison of some Cambrian biotas: Journal of Paleontology, v. 56, p. 116–122.

Conway Morris, S., and Robison, R.A., 1986., Middle Cambrian priapulids and other soft-bodied fossils from Utah and Spain: University of Kansas Paleontological Contributions, v. 117, p. 1–22.

Conway Morris, S., and Robison, R.A., 1988, More soft-bodied animals and algae from the Middle Cambrian of Utah and British Columbia: University of Kansas Paleontological Contributions, v. 122, p. 1–48

Conway Morris, S., Selden, P.A., Gunther, G., Jamison, P.G. and Robison, R.A., 2015, New records of Burgess Shale-type taxa from the middle Cambrian of Utah: Journal of Paleontology, v. 89, p. 411–423.

Cui, Z., and Huo, S.,1990, New discoveries of Lower Cambrian crustacean fossils from Western Hubei: Acta Palaeontologica Sinica, v. 29, p. 321–330.

Daley, A.C., and Bergström, J., 2012, The oral cone of *Anomalocaris* is not a classic ‘‘*Peytoia*’’: Naturwissenschaften, v. 99, p. 501–504.

Daley, A.C., and Budd, G.E., 2010, New anomalocaridid appendages from the Burgess Shale, Canada: Palaeontology, v. 53, p. 721–738.

Daley, A.C., and Edgecombe, G.D., 2014, Morphology of *Anomalocaris canadensis* from the Burgess Shale: Journal of Paleontology, v. 88, p. 68–91.

Daley, A.C., and Legg, D.A., 2015, A morphological and taxonomic appraisal of the oldest anomalocaridid from the Lower Cambrian of Poland: Geological Magazine, v. 152, p. 949–955.

Daley, A.C., Budd, G.E., Caron, J.B., Edgecombe, G.D. and Collins, D., 2009, The Burgess Shale anomalocaridid *Hurdia* and its significance for early euarthropod evolution: Science, v. 323, p. 1597–1600.

Daley, A.C., Budd, G.E. and Caron, J.B., 2013a, Morphology and systematics of the anomalocaridid arthropod *Hurdia* from the Middle Cambrian of British Columbia and Utah: Journal of Systematic Palaeontology, v. 11, p. 743–787.

Daley, A.C., Paterson, J.R., Edgecombe, G.D., García-Bellido, D.C. and Jago, J.B., 2013b, New anatomical information on *Anomalocaris* from the Cambrian Emu Bay Shale of South Australia and a reassessment of its inferred predatory habits: Palaeontology, v. 56, p. 971–990.

Elrick, M., and Snider, A.C., 2002, Deep-water stratigraphic cyclicity and carbonate mud mound development in the Middle Cambrian Marjum Formation, House Range, Utah, USA: Sedimentology, v. 49, p. 1021–1047.

Gaines, R.R., 2014, Burgess Shale-type preservation and its distribution in space and time. Reading and Writing of the Fossil Record: Preservational Pathways to Exceptional Fossilization: Paleontological Society Papers, v. 20, p. 123–146.

Gaines, R.R., and Droser, M.L., 2003, Paleoecology of the familiar trilobite *Elrathia kingii*: An early exaerobic zone inhabitant: Geology, v. 31, p. 941–944.

Gaines, R.R., and Droser, M.L., 2005, New approaches to understanding the mechanics of Burgess Shale-type deposits: from the micron scale to the global picture: Sedimentary Record v. 3, p. 4–8.

Gaines, R.R., and Droser, M.L., 2010, The paleoredox setting of Burgess Shale-type deposits: Palaeogeography, Palaeoclimatology, Palaeoecology, v. 297, p. 649–661.

Gaines, R.R., Briggs, D.E., and Yuanlong, Z., 2008, Cambrian Burgess Shale–type deposits share a common mode of fossilization: Geology, v. 36, p. 755–758.

Gaines, R.R., Kennedy, M.J., and Droser, M.L., 2005, A new hypothesis for organic preservation of Burgess Shale taxa in the middle Cambrian Wheeler Formation,

House Range, Utah: Palaeogeography, Palaeoclimatology, Palaeoecology, v. 220, p. 193–205.

Garson, D.E., Gaines, R.R., Droser, M.L., Liddell, W.D. and Sappenfield, A., 2012, Dynamic palaeoredox and exceptional preservation in the Cambrian Spence Shale of Utah: Lethaia, v. 45, p. 164–177.

Goloboff, P., and Catalano, S., 2016, TNT version 1.5, including a full implementation of phylogenetic morphometrics: Cladistics, v. 32, p. 221-238.

Gunther, L. F., and Gunther, V. G., 1981, Some Middle Cambrian fossils of Utah: Brigham Young University Geology Studies, v. 28, p. 1–81.

Halgedahl, S.L., Jarrard, R.D., Brett, C.E., and Allison, P.A., 2009, Geophysical and geological signatures of relative sea level change in the upper Wheeler Formation, Drum Mountains, West-Central Utah: a perspective into exceptional preservation of fossils: Palaeogeography, Palaeoclimatology, Palaeoecology, v. 277, p. 34–56.

Hendricks, J.R., 2013, Global distributional dynamics of Cambrian clades as revealed by Burgess Shale-type deposits: Geological Society, London, Memoirs, v. 38, p. 35–43.

Hendricks, J.R., and Lieberman, B.S., 2008, New phylogenetic insights into the Cambrian radiation of arachnomorph arthropods: Journal of Paleontology, v. 82, p. 585–594.

Hendricks, J.R., Lieberman, B.S. and Stigall, A.L., 2008, Using GIS to study palaeobiogeographic and macroevolutionary patterns in soft-bodied Cambrian arthropods: Palaeogeography, Palaeoclimatology, Palaeoecology, v. 264, p. 163–175.

Hou, X., Bergström, J. and Ahlberg, P., 1995, *Anomalocaris* and other large animals in the Lower Cambrian Chengjiang fauna of southwest China: GFF, v. 117, p. 163–183.

Johnston, P.A., Johnston, K.J., Collom, C.J., Powell, W.G. and Pollock, R.J., 2009, Palaeontology and depositional environments of ancient brine seeps in the Middle Cambrian Burgess Shale at The Monarch, British Columbia, Canada: Palaeogeography, Palaeoclimatology, Palaeoecology, v. 277, p. 86–105.

Kloss, T.J., Dornbos, S.Q., Chen, J.Y., McHenry, L.J., and Marenco, P.J., 2015, High-resolution geochemical evidence for oxic bottom waters in three Cambrian Burgess Shale-type deposits: Palaeogeography, Palaeoclimatology, Palaeoecology, v. 440, p. 90–95.

Lerosey-Aubril, R., Hegna, T.A., Kier, C., Bonino, E., Habersetzer, J., and Carré, M., 2012, Controls on gut phosphatisation: the trilobites from the Weeks Formation Lagerstätte (Cambrian; Utah): PLoS One, v7, p. e32934.

Lerosey-Aubril, R., Hegna, T.A., Babcock, L.E., Bonino, E., and Kier, C., 2014, Arthropod appendages from the Weeks Formation Konservat-Lagerstätte: new occurrences of anomalocaridids in the Cambrian of Utah, USA: Bulletin of Geosciences, v. 89, p. 269–282.

Liddell, W.D., Wright, S.W. and Brett, C.E., 1997, Sequence stratigraphy and paleoecology of the Middle Cambrian Spence Shale in northern Utah and southern Idaho: Brigham Young University Geology Studies, v. 42, p. 59–78.

LoDuca, S.T., Caron, J.B., Schiffbauer, J.D., Xiao, S., and Kramer, A., 2015, A reexamination of Yuknessia from the Cambrian of British Columbia and Utah: Journal of Paleontology, v. 89, p. 82–95.

Liu, Q., 2013, The first discovery of anomalocaridid appendages from the Balang Formation (Cambrian Series 2) in Hunan, China: Alcheringa, v. 37, p. 1–6.

Maddison, W.P., and Maddison, D.R., 2017, Mesquite: a modular system for evolutionary analysis. Version 3.2: http://mesquiteproject.org.

Moore, R.A., Lieberman, B.S., 2009, Preservation of early and Middle Cambrian soft-bodied arthropods from the Pioche Shale, Nevada, USA: Palaeogeography, Palaeoclimatology, Palaeoecology, v. 277, p. 57–62.

Olcott Marshall, A., Wehrbein, R.L., Lieberman, B.S. and Marshall, C.P., 2012, Raman spectroscopic investigations of Burgess Shale–type preservation: a new way forward: Palaios, v. 27, p. 288–292.

Rees, M.N., 1986, A fault-controlled trough through a carbonate platform: The Middle Cambrian House Range embayment: Geological Society of America Bulletin, v. 97, p. 1054–1069.

Resser, C.E., 1939, The Spence shale and its fauna, (with six plates): Smithsonian Institution Miscellaneous Collections, v. 97, p. 1–29.

Robison, R.A., 1964, Late Middle Cambrian faunas from western Utah: Journal of Paleontology, v. 38, p. 510–566.

Robison, R. A. 1965, Middle Cambrian eocrinoids from western North America: Journal of Paleontology, v. 39, p. 355–364.

Robison, R.A., 1991, Middle Cambrian biotic diversity: examples from four Utah Lagerstätten, in Simonetta, A. and Conway Morris, S., ed, The early evolution of metazoa and the significance of problematic taxa: Cambridge University Press, Cambridge, p.77–98.

Robison, R.A. and Babcock, L.E., 2011, Systematics, paleobiology, and taphonomy of some exceptionally preserved trilobites from Cambrian Lagerstätten of Utah: Paleontological contributions, v. 5, p. 1–47.

Robison, R.A. and Richards, B.C., 1981, Larger bivalve arthropods from the Middle Cambrian of Utah: University of Kansas Paleontological Contributions, v. 106, p. 1–28

Robison, R.A. and Wiley, E.O., 1995, A new arthropod, *Meristosoma*: more fallout from the Cambrian explosion: Journal of Paleontology, v. 69, p. 447–459.

Robison, R.A., Babcock, L.E., and Gunther, V.G., 2015, Exceptional Cambrian fossils from Utah: a window into the Age of Trilobites: Utah Geological Survey Miscellaneous Publications, v. 15, p. 1–97.

Rogers, J.C., 1984, Depositional environments and paleoecology of two quarry sites in the Middle Cambrian Marjum and Wheeler Formations, House Range, Utah: Brigham Young University Geology Studies, v. 31, p. 97–115.

Stein, M., 2013, Cephalic and appendage morphology of the Cambrian arthropod *Sidneyia inexpectans*: Zoologischer Anzeiger–A Journal of Comparative Zoology, v. 253, p. 164–178.

Stein, M., Church, S.B., and Robison, R.A., 2011, A new Cambrian arthropod, *Emeraldella brutoni*, from Utah: Paleontological Contributions, v. 3, p.1–9.

Van Roy, P., and Briggs, D.E., 2011, A giant Ordovician anomalocaridid: Nature, v. 473, p.510–513.

Van Roy, P., Daley, A.C., and Briggs, D.E.G., 2015, Anomalocaridid trunk limb homology revealed by a giant filter-feeder with paired flaps. Nature, v. 522, p. 77-80.

Vinther, J., Stein, M., Longrich, N.R., and Harper, D.A., 2014, A suspension-feeding anomalocarid from the Early Cambrian: Nature, v. 507, p. 496–499.

Walcott, C. D., 1911, Middle Cambrian holothurians and medusa: Smithsonian Miscellaneous Collections, v. 57, p. 41-68.

Walcott, C. D., 1912, Middle Cambrian Brachiopoda, Malacostraca, Trilobita and Merostomata: Smithsonian Miscellaneous Collections, v. 57, p. 145–288.

Whiteaves, J. F., 1892, Description of a new genus and species of phyllocarid Crustacea from the Middle Cambrian of Mount Stephen, B.C.: Canadian Record of Science, v. 5, p. 205–208.

Whittington, H.B., and Briggs, D.E., 1985, The largest Cambrian animal, *Anomalocaris*, Burgess Shale, British Columbia: Philosophical Transactions of the Royal Society of London. Series B, Biological Sciences, v. 309, p.569–609.

Chapter 6

Aysheaia prolata from the Wheeler Formation (Cambrian, Drumian) is a frontal appendage of the radiodontan *Stanleycaris*

Author contributions

SP conceived the project; SP wrote the manuscript and prepared the figures, with input from ACD and JOH.

Publication information

This Chapter has been peer reviewed and published by *Acta Palaeontologica Polonica*:

Pates, S., Daley, A. C., & Ortega-Hernández, J. (2017). *Aysheaia prolata* from the Utah Wheeler Formation (Drumian, Cambrian) is a frontal appendage of the radiodontan *Stanleycaris*. *Acta Palaeontologica Polonica*, 62(3), 619-626.

Aysheaia prolata from the Wheeler Formation (Cambrian, Drumian) is a frontal appendage of the radiodontan *Stanleycaris*

STEPHEN PATES, ALLISON C. DALEY and JAVIER ORTEGA-HERNÁNDEZ

Abstract.—*Aysheaia prolata* Robison, 1985, was described as the only lobopodian from the Cambrian (Drumian) Wheeler Formation in Utah, and the sole representative of this genus besides the type species *Aysheaia pedunculata*, from the Cambrian (Stage 5) Stephen Formation, British Columbia. A redescription of *Aysheaia prolata* reveals previously overlooked morphological features, including segmental boundaries between putative lobopods, and curved terminal spines on the putative anterior end. These observations undermine lobopodian affinities of *Aysheaia prolata*, and instead we interpret this specimen as an isolated radiodontan frontal appendage. The presence of 11 podomeres, five of which possess elongate and anteriorly recurved ventral blades with auxiliary spines, together with shorter robust dorsal spines, identify the specimen as *Stanleycaris* Caron et al., 2010. This represents the first report of *Stanleycaris* outside of the Cambrian (Stage 5) thin Stephen Formation in British Columbia, expanding its palaeobiogeographic and stratigraphic range. *Aysheaia* is left as a monotypic genus endemic to the Burgess Shale. The Spence Shale luolishaniid *Acinocrinus stichus* is currently the only lobopodian known from the Cambrian of Utah.

Introduction

Radiodontans, a diverse group of large nektonic predators, are among the most recognizable faunal components in Lower Palaeozoic Burgess Shale-type biotas (e.g.

Daley et al. 2009, 2013a, b; Daley and Edgecombe 2014; Van Roy et al. 2015; Cong et al 2016; Zeng et al. 2017). Despite their fundamentally soft-bodied construction, there is a comprehensive record of radiodontan diversity owing to the preferential preservation of their sclerotized frontal appendages (e.g. Caron et al. 2010; Daley and Budd 2010; Daley and Peel 2010; Wang et al. 2013; Lerosey-Aubril et al. 2014; Vinther et al. 2014). Recent work has expanded the palaeobiogeographic and stratigraphic occurrence of radiodontan taxa previously known only from the Cambrian (Stage 5) Burgess Shale in British Columbia, including new reports from the Cambrian (Series 3) of Utah (Pates et al. 2018; Pates and Daley 2017). Here we demonstrate that *Aysheaia prolata* Robison, 1985, widely regarded for over 30 years as the only lobopodian from the Wheeler Formation (Drumian), is actually a radiodontan frontal appendage, and discuss implications for the known diversity of middle Cambrian radiodontans and lobopodians from Utah.

Institutional abbreviations.—KUMIP, University of Kansas Natural History Museum, Lawrence, Kansas, USA; ROM, Royal Ontario Museum, Toronto, Canada; USNM, Smithsonian Institution National Museum of Natural History, Washington D.C., USA.

Other abbreviations.— Pn, podomere n; sag., sagittal; trans., transverse.

Material and methods

The only known specimen (KUMIP 153923) is housed at the University of Kansas Natural History Museum. A Canon EOS 500D DSLR camera, with Canon EF-S 60 117 mm Macro Lens, controlled for remote shooting with EOSUtility 2 was used for photography.

Photographs were taken wet, dry, under cross-polarized and non-polarized light. Lengths and angles were measured from photographs using ImageJ 2. Photoshop CS6 was used to convert photographs to black and white and manipulate colour channels.

Systematic Palaeontology

Phylum (stem-group) Euarthropoda Lankester, 1904

Order Radiodonta Collins, 1996

Family Hurdiidae Vinther et al., 2014

Genus *Stanleycaris* Caron et al., 2010

Diagnosis.— Frontal appendage with 11 distally tapering podomeres bearing robust, double-pointed spines projecting from the dorsal surface at an oblique angle, as well as five spinous ventral blades that are two to three times the length of the dorsal spines and slightly curved (see Caron et al. 2010).

Remarks.—*Stanleycaris* was originally described from the thin Stephen Formation at Stanley Glacier (Cambrian Stage 5), British Columbia. 37 specimens of the type species, *S. hirpex*, have been described: disarticulated assemblages including frontal appendages, oral cones and carapace material; no post cephalic remains have yet been found.

Occurrence.—Thin Stephen Formation (Cambrian Series 3, Stage 5), British Columbia, Canada (Caron et al. 2010); Wheeler Formation (Cambrian Series 3, Drumian), Utah, USA (this study).

Stanleycaris sp.

Figs. 1A_1—A_4, 2, 3A_1—A_2

1985 *Aysheaia prolata* sp. nov.; Robison 1985: 226—235, text-fig. 3

1989 *Aysheaia*? *prolata* Robison, 1985; Dzik and Krumbiegel 1989: 175

1995 *Aysheaia*? *prolata* Robison, 1985; Hou and Bergström 1995: 13

1998 *Aysheaia prolata* Robison, 1985; Ramsköld and Chen 1998: 108, 134, 138—139, 143—144

2001 *Aysheaia*? *prolata* Robison, 1985; Bergström and Hou 2001: 238, 245

2004 *Aysheaia*? *prolata* Robison, 1985; Hou et al. 2004: 238

2009 *Aysheaia*? *prolata* Robison, 1985; Whittle et al. 2009: 562

2011 *Aysheaia*? *prolata* Robison, 1985; Ou et al. 2011: 587

2011 *Aysheaia*? *prolata* Robison, 1985; Gámez Vintaned et al. 2011: 211

2015 *Aysheaia*? *prolata* Robison, 1985; Robison et al. 2015; 27, fig. 56

2016 *Aysheaia prolata* Robison, 1985; Foster and Gaines 2016: 299, 303, 330, fig. 9H

Material: KUMIP 153923, isolated frontal appendage, preserved flattened in light grey shale.

Locality: Locality 114 of Robison and Richards (1981, p. 3), Utah, USA (Robison 1985).

Horizon: Light brown-grey laminated calcareous mudstone, approximately 100 m below the top of the Wheeler Formation (Robison 1985).

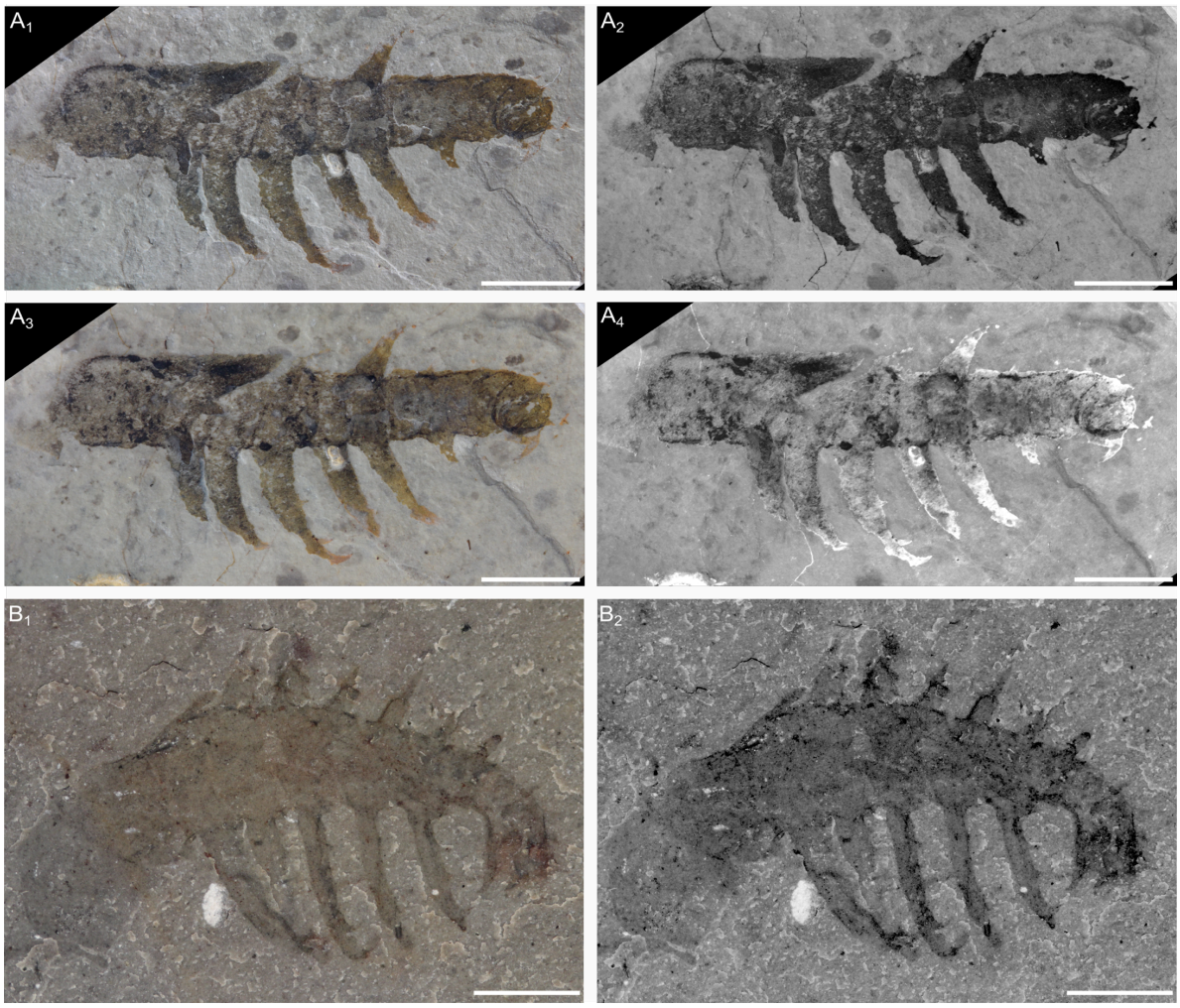

Fig. 1: (**A**) *Stanleycaris* sp. from the Wheeler Formation (Cambrian Series 3, Drumian), Utah, USA. KUMIP 153923: non-polarized light (A_1), cross-polarized light, red and yellow channels reduced (A_2), cross polarized light (A_3), cross-polarized light, red and yellow channels enhanced (A_4). (**B**) *Stanleycaris hirpex* from the Stephen Formation (Cambrian Series 3, Stage 5), British Columbia, Canada. ROM 59944 (holotype): cross-polarized light (B_1), black and white (B_2). Scale bars = 5 mm.

Description.—The appendage measures 26.5 mm in length (sag.), and displays 11 podomeres, indicated by the preservation of serially repeated segmental boundaries. P1 differs from the other podomeres in having a subrectangular outline (length (sag.) ca. 7.0 mm; width (trans.) ca. 4.6 mm). P2 to P11 are shorter (sag.) and wider (trans.). A layer of sediment between P1 and P2 suggests that P1 has shifted forwards to cover the posterior border of P2 (Fig. 2), making the precise dimensions of P2 unclear. P3 to P8 are similar lengths (sag. ca. 2mm). P3 to P6 maintain a stable width (trans. ca. 3.5mm), whereas P7 to P11 taper distally (P7 ca. 3.2 mm; P11 ca. 2.2 mm). P9 to P11 are flexed laterally towards the rock surface, slightly overlapping one another. It is not possible to measure the dimensions of these podomeres owing to their orientation. The armature consists of well-developed spinose ventral blades with auxiliary spines, and short dorsal spines. P1 lacks ornamentation altogether. P2 to P6 possess ventral blades ('lobopods 1 to 5' in Robison 1985, fig. 3.2), which emerge approximately perpendicular to the limb axis. The most complete of the blades, on P4 (Fig. $3A_2$), has a length (sag.) of approximately 8 mm and possesses two distally-pointing auxiliary spines. The tip curves sharply towards the distal end of the appendage, giving the blade a crescent-shape. A ventral blade on P7 is approximately a third of the length (sag.) of the others, with no visible auxiliary spines. Dorsal spines are observed on P4, P6 and P7. The most complete dorsal spine is on P6; it has a subtriangular outline with a robust base ('lobopod 1' in Robison 1985, fig. 3.2), projects at an angle of 71° from the main limb axis, and shows no evidence for more than a single-point. P4 and P7 show poorly preserved dorsal spine bases ('anterior appendage' in Robison 1985, fig. 3.2). Armature is absent from P8 to

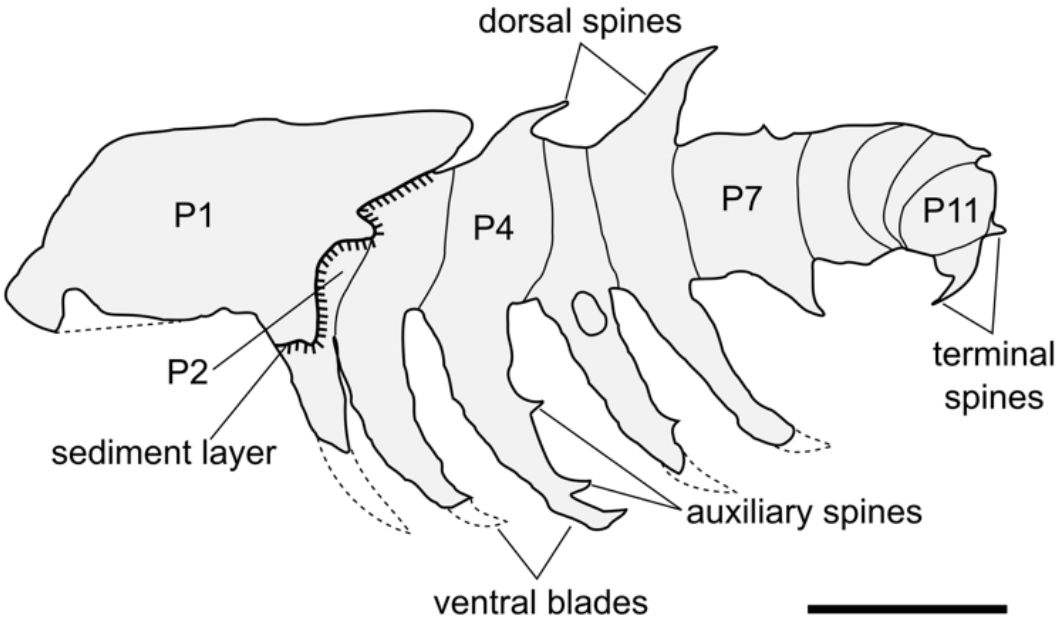

Fig. 2: KUMIP 153923 explanatory drawing. Hachure direction indicates lower sediment level. Dotted lines indicate expected path of incomplete ventral blades. Scale bars = 5 mm.

P10. P11 preserves two recurved terminal spines (Fig. 3A$_1$; 'papillae?' in Robison 1985, fig. 3.2).

Remarks.— The recognition of podomere boundaries, together with the occurrence of ventral, dorsal and terminal spines, support the reinterpretation of KUMIP 153923 as an isolated radiodontan appendage. Robison's (1985) original lobopodian interpretation was largely based on the similar outline of this specimen to *Aysheaia pedunculata* preserved in lateral view (Fig. 4; Whittington 1978). Although *A. pedunculata* frequently displays compaction wrinkles that may resemble segmental boundaries (e.g. Fig. 3D; Ma et al. 2013 fig. 5B), these are generally restricted to the lobopodous limbs. The features identified as podomere boundaries in KUMIP 153923 occur along the main axis of the fossil, rather than on the putative limbs. Furthermore, the podomere boundaries cross the whole width of the specimen, and are more widely spaced than annulations on the trunk of *A. pedunculata* (Fig. 4). The putative lobopods and oral papillae described by Robison (1985) are best regarded as ventral blades and terminal spines respectively. The ventral blades are curved and bear auxiliary spines pointing to the anterior end, as also observed in in *Stanleycaris hirpex* (compare Fig. 3A$_2$ to Fig. 3C). The ventral blades lack compaction wrinkles often preserved on limbs of *A. pedunculata* (Figs. 3D, 4; Ma et al. 2013 fig. 5B). The terminal spines at the anterior end of the specimen are short, recurved, and have a sharp termination. This morphology is similar to that of the spines in *S. hirpex*, and quite unlike the straight and less robust oral papillae of *A. pedunculata* (compare Fig. 3A$_1$ to Fig. 3B). It should be noted that Robison (1985) studied the specimen before the extent of radiodontan frontal appendage morphological diversity

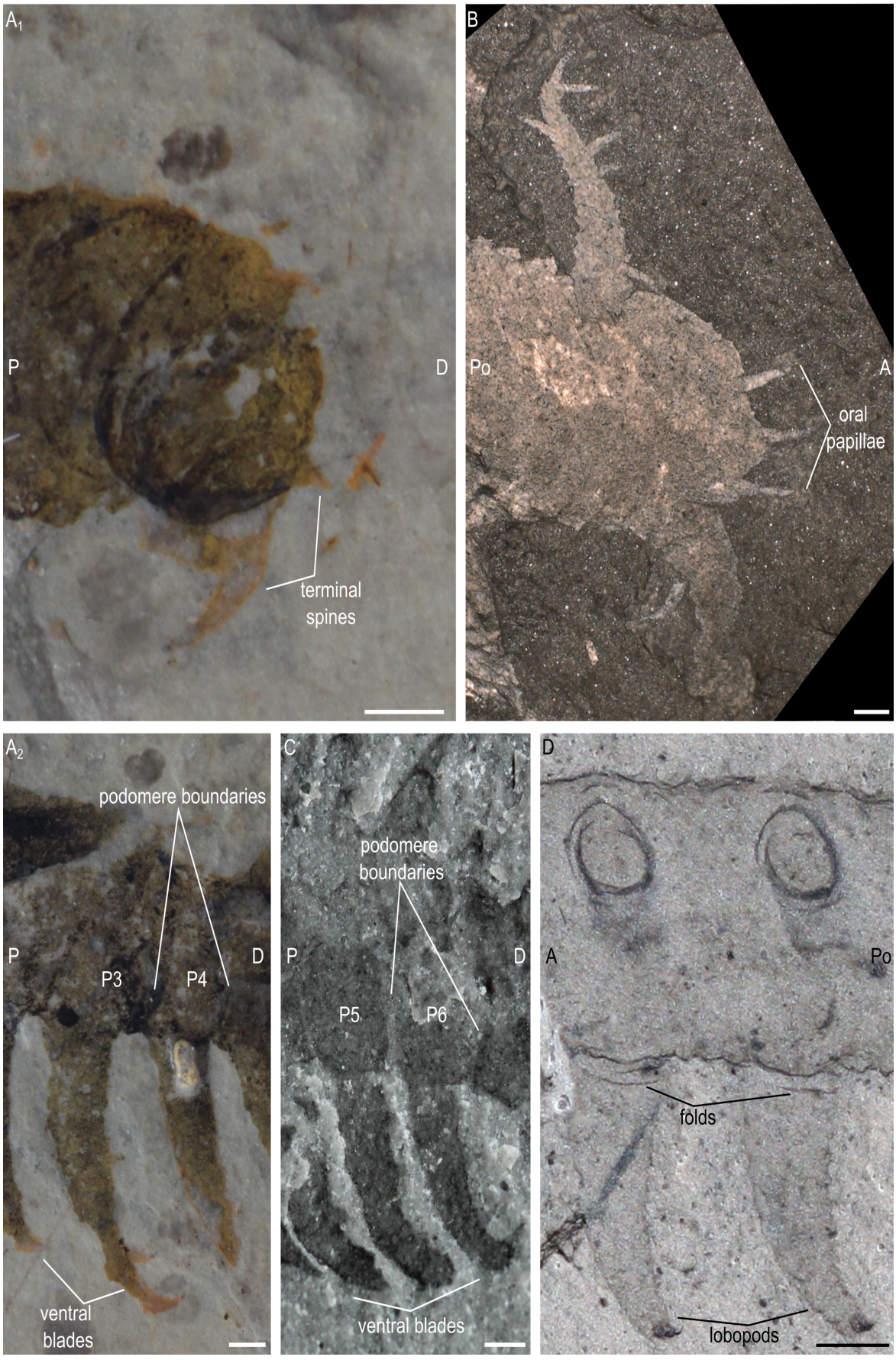

Fig. 3: Caption on next page

Fig. 3: Comparison between terminal spines and vetral blades of *Stanleycaris* and oral papillae and lobopodous limbs of *Aysheaia*. (**A**) *Stanleycaris* sp. from the Wheeler Formation (Cambrian Series 3, Drumian), Utah, USA; (**C, D**) *Stanleycaris hirpex* from the Stephen Formation (Cambrian Series 3, Stage 5), British Columbia, Canada; (**B, E**) *Aysheaia pedunculata* from the Stephen Formation (Cambrian Series 3, Stage 5), British Columbia, Canada. KUMIP 153923: anterior end showing recurved terminal spines (A_1), ventral blade (A_2); USNM 189199: anterior end showing anterior appendages and oral papillae (B); ROM 59975 (paratype): ventral blade (C); USNM 83942: trunk section and lobopods (D). Abbreviations: (**A, C**) P = proximal, D = distal, Pn = podomere n; (**B, D**) Po = posterior, A = anterior. Scale bars = 1 mm.

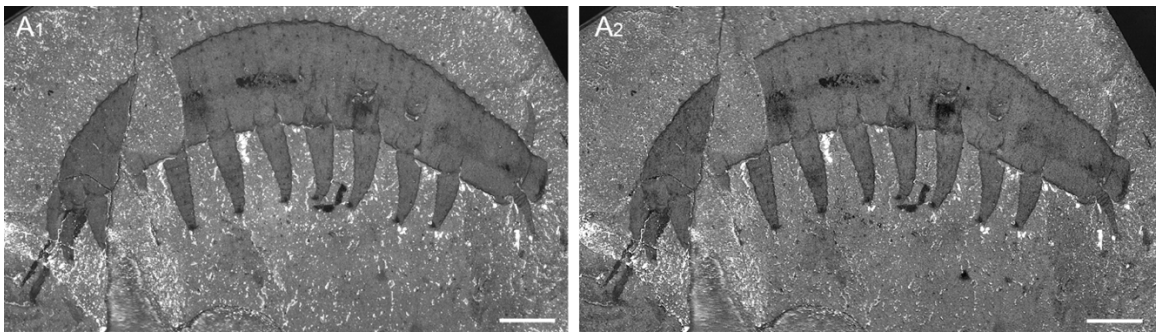

Fig. 4: *Aysheaia pedunculata* from the Stephen Formation (Cambrian Series 3, Stage 5), British Columbia, Canada. (**A**) USNM 365608: cross-polarized light (A_1), cross-polarized light, red and yellow channels reduced (A_2). Scale bars = 5 mm.

was known (e.g. Daley and Budd 2010; Caron et al. 2010), and so lacked the appropriate context for correctly interpreting KUMIP 153923.

Within the known diversity of radiodontan frontal appendages, the presence of five elongated ventral blades with auxiliary spines on P2 to P6, and differentiated distal podomeres, support a more specific classification as a hurdiid (e.g. Daley and Budd 2010; Daley et al. 2013a). Within hurdiids, KUMIP 153923 most closely resembles *Stanleycaris hirpex* (Figs. 1B, 5): both have 11 podomeres, including an elongated P1; long, curved ventral blades with auxiliary spines on P2 to P6; and a distally tapering P7 to P11. The only significant difference is that the dorsal spine preserved on P6 of KUMIP 153923 appears to be single-pointed, whereas dorsal spines of *Stanleycaris* from Stanley Glacier are double-pointed (Figs. 1B, 5; Caron et al. 2010). The lack of a double-point may be the result of incomplete preservation in KUMIP 153923, as the size of the dorsal spine relative to podomere width (trans.), robustness, and angle relative to the dorsal surface of the podomere all conform to the morphology of dorsal spines in *Stanleycaris* from Stanley Glacier (Figs. 1B, 5). Additionally KUMIP 153923 fits within the size-range described for Stanley Glacier specimens (12.5—30.3 mm length, sag.).

KUMIP 153923 differs from *Hurdia* frontal appendages in the possession of 11 podomeres and more than one terminal spine; *Hurdia* usually displays nine podomeres (rarely 10 or 11) and only one terminal spine (Daley et al. 2013a). KUMIP 153923 differs from *Peytoia* frontal appendages in the presence of a small ventral spine on P7; *Peytoia* displays no small ventral spines (Daley et al. 2013a). Furthermore, KUMIP 153923 has a large dorsal spine which projects at a 71° angle to the surface of P6, contrasting with the smaller, more inclined, dorsal spines of both *Hurdia* and *Peytoia* appendages (Daley et al. 2013a).

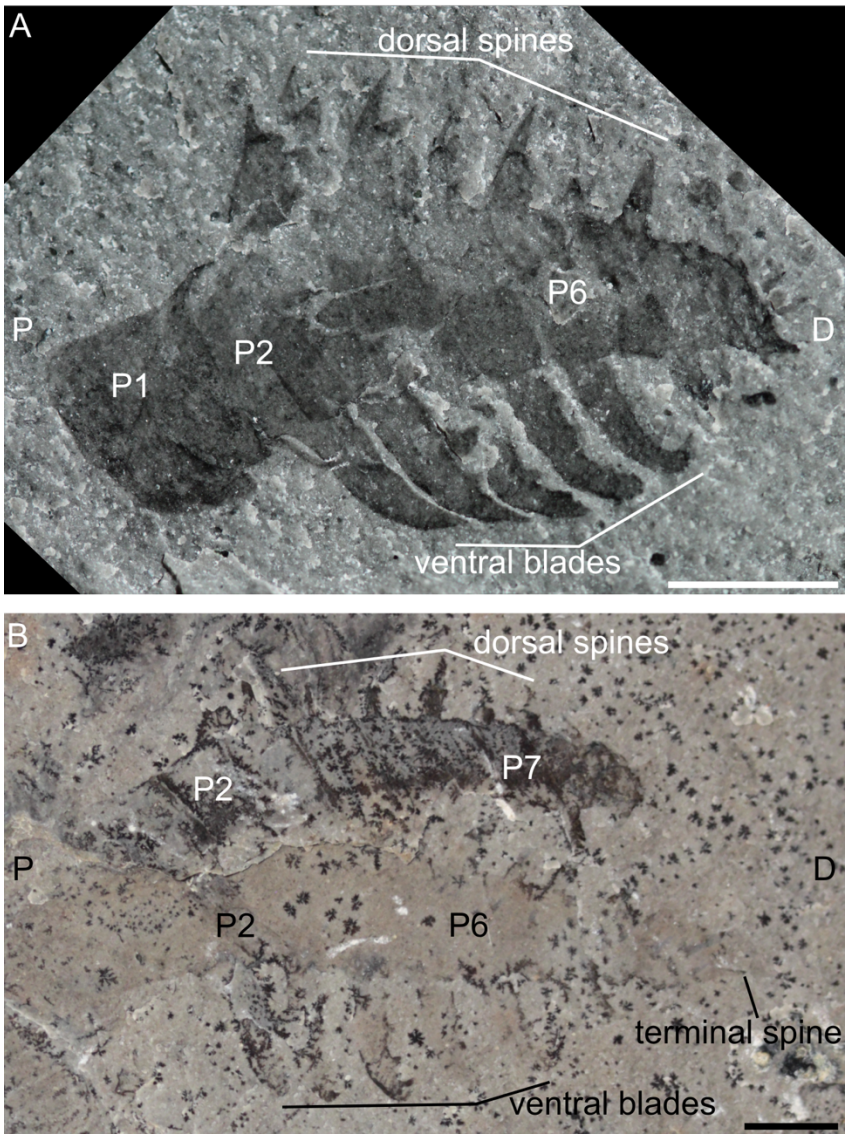

Fig. 5: *Stanleycaris hirpex* from the Stephen Formation (Cambrian Series 3, Stage 5), British Columbia, Canada. (**A**) ROM 59975 (paratype); (**B**) ROM 59976 (paratype). Scale bars = 5 mm.

As the incomplete preservation of KUMIP 153923 precludes a more detailed comparison with the type material of *Stanleycaris hirpex* (Figs. 1B, 5; Caron et al. 2010), we regard KUMIP 153923 as *Stanleycaris* sp. (see Table 1 for comparison between the two species). Additional material from the Wheeler Formation is necessary to determine if the presence of single-pointed dorsal spines in *Stanleycaris* sp. is a legitimate morphological feature or a preservational artefact.

Stratigraphic and geographic range.—Wheeler Formation (Cambrian, Drumian), Utah, USA.

Discussion

The recognition of KUMIP 153923 as a radiodontan frontal appendage directly impacts the known diversity of these extinct organisms for the Lower Palaeozoic of Laurentia. *Stanleycaris* can now be added to the list of radiodontan taxa that have been reported from the Cambrian (Series 3) of Utah and Canada (Table 2). *Peytoia nathorsti* and *Hurdia victoria* (Briggs et al. 2008; Pates et al. 2018) are known in both regions from frontal appendages, mouthparts, and carapace material. Isolated frontal appendages of *Caryosyntrips*, previously only known from the Burgess Shale, have recently been described from the Spence Shale and Wheeler Formation (Pates and Daley 2017). *Anomalocaris* has also been described from post cephalic remains in both the Spence Shale and Wheeler Formation (Briggs et al. 2008), and isolated frontal appendages in the younger (Guzhangian) Weeks Formation (Lerosey-Aubril et al. 2014). The Wheeler Formation specimen is the youngest stratigraphic occurrence of *Stanleycaris*, expanding

Table 1. Comparison between *Stanleycaris* sp. and *Stanleycaris hirpex*

	Stanleycaris sp.	*Stanleycaris hirpex*
Occurrence	Wheeler Formation Cambrian Series 3, Drumian	Stephen Formation Cambrian Series 3, Stage 5
Number of specimens	1	37
Number of podomeres	11	11
Length	26.5 mm	12.5–30.3 mm
Number of large ventral blades	5, on P2—6	5, on P2—6
Morphology of large ventral blades	Elongate, curved, with auxiliary spines	Elongate, curved, with auxiliary spines
Number of short ventral blades	1, on P7	1, on P7
Number of dorsal spines	Evidence for dorsal spines P4, 6, 7, but dorsal surface poorly preserved	9, on P2—10
Morphology of dorsal spines	Robust, single pointed (?)	Robust, double pointed
Angle of projection of dorsal spines	71°, for dorsal spine on P6	45—90°
Morphology of terminal spines	Recurved, pointed	Recurved, pointed
Reference:	**This study**	Caron et al. 2010

Table 2. Diversity of Cambrian radiodontans from Canada and Utah

	Burgess Shale (Stage 5)	Stanley Glacier (Stage 5)	Spence Shale (Stage 5)	Wheeler Formation (Drumian)	Marjum Formation (Drumian)	Weeks Formation (Guzhangian)
Anomalocaris canadensis	A, C, O, P	A				
Anomalocaris sp.			P	P		A
Hurdia victoria	A, C, O, P	A, C	A, C, O			
Hurdia triangulata	A, C, O, P					
Hurdia indet. sp.				C		
Caryosyntrips serratus	A			A		
Caryosyntrips sp.	A, C		A	A		
Peytoia nathorsti	A, O, P			A, O	O, P	
Amplectobelua stephenensis	A					
Stanleycaris hirpex		A, C, O				
***Stanleycaris* sp.**				**A**		
References	Daley et al. 2009; Daley and Budd 2010; Daley et al. 2013a, b; Daley and Edgecombe 2014; Pates and Daley 2017	Caron et al. 2010	Briggs et al. 2008; Pates et al. 2018; Pates and Daley 2017	Briggs et al. 2008; Pates et al.2018; Pates and Daley 2017; **This study**	Pates et al. 2018	Lerosey-Aubril et al. 2014

Abbreviations: A, appendages; carapace element; O, oral cone; P, post cephalic remains.

its temporal range from the *Bathyuriscus-Elrathina* zone to the *Ptychagnostus atavus* zone.

Aysheaia prolata is here shown to be an invalid lobopodian taxon, reducing the known diversity of these organisms for the Cambrian of Laurentia. For over three decades, *A*. *prolata* was regarded as the first lobopodian to be discovered from the numerous Cambrian (Series 3) *Lagerstätten* exposed in Utah (Robison 1985) and was widely referenced as such in subsequent studies (e.g. Dzik and Krumbiegel 1989; Hou and Bergström 1995; Ramsköld and Chen, 1998; Bergström and Hou 2001; Hou et al. 2004; Whittle et al. 2009; Ou et al. 2011; Gámez Vintaned et al. 2011; Robison et al. 2015; Foster and Gaines 2016). Our reappraisal of KUMIP 153923 leaves the luolishaniid *Acinocricus stichus* (Conway Morris and Robison 1988) from the Spence Shale as the only Cambrian lobopodian currently known from the USA (Ramsköld and Chen, 1998; García-Bellido et al. 2013; Yang et al. 2015).

Acknowledgements.—Bruce S. Lieberman and Paul A. Selden (University of Kansas) provided access to the KUMIP and use of photographic equipment, respectively. SP was funded by a Palaeontological Association Sylvester-Bradley Award (PA-SB201503) and is supported by an Oxford—St Catherine's Brade—Natural Motion Scholarship. ACD was funded by the Oxford University Museum of Natural History. JOH is supported by a Herchel Smith Postdoctoral Fellowship in Biological Sciences held at the Department of Zoology, University of Cambridge. We thank G. D. Edgecombe and an anonymous reviewer for their valuable comments and suggested improvements.

References

Bergström, J. and Hou, X.G. 2001. Cambrian Onychophora or xenusians. *Zoologischer Anzeiger-A Journal of Comparative Zoology* 240(3-4):237—245.

Briggs, D.E., Lieberman, B.S., Hendricks, J.R., Halgedahl, S.L. and Jarrard, R.D. 2008. Middle Cambrian arthropods from Utah. *Journal of Paleontology* 82(2):238—254.

Caron, J.B., Gaines, R.R., Mángano, M.G., Streng, M. and Daley, A.C. 2010. A new Burgess Shale–type assemblage from the "thin" Stephen Formation of the southern Canadian Rockies. *Geology* 38(9):811—814.

Collins, D. 1996. The "evolution" of *Anomalocaris* and its classification in the arthropod class Dinocarida (nov.) and order Radiodonta (nov.). *Journal of Paleontology* 70(02):280—293.

Cong, P., Daley, A.C., Edgecombe, G.D., Hou, X. and Chen, A. 2016. Morphology of the radiodontan Lyrarapax from the early Cambrian Chengjiang biota. *Journal of Paleontology* 90(4):663—671.

Conway Morris, S. and Robison, R.A., 1988. More soft-bodied animals and algae from the Middle Cambrian of Utah and British Columbia. *University of Kansas Paleontological Contributions* 122:1—48.

Daley, A.C., Budd, G.E., Caron, J.B., Edgecombe, G.D. and Collins, D. 2009. The Burgess Shale anomalocaridid *Hurdia* and its significance for early euarthropod evolution. *Science* 323(5921):1597—1600.

Daley, A.C. and Budd, G.E. 2010. New anomalocaridid appendages from the Burgess Shale, Canada. *Palaeontology* 53(4):721—738.

Daley, A.C. and Edgecombe, G.D. 2014. Morphology of *Anomalocaris canadensis* from the Burgess Shale. *Journal of Paleontology* 88(1):68—91.

Daley, A.C. and Peel, J.S. 2010. A possible anomalocaridid from the Cambrian Sirius Passet Lagerstätte, north Greenland. *Journal of Paleontology* 84(2):352—355.

Daley, A.C., Budd, G.E. and Caron, J.B. 2013a. Morphology and systematics of the anomalocaridid arthropod *Hurdia* from the Middle Cambrian of British Columbia and Utah. *Journal of Systematic Palaeontology* 11(7):743—787.

Daley, A.C., Paterson, J.R., Edgecombe, G.D., García-Bellido, D.C. and Jago, J.B. 2013b. New anatomical information on *Anomalocaris* from the Cambrian Emu Bay Shale of South Australia and a reassessment of its inferred predatory habits. *Palaeontology* 56(5):971—990.

Dzik, J. and Krumbiegel, G. 1989. The oldest 'onychophoran' *Xenusion*: a link connecting phyla? *Lethaia* 22(2):169—181.

Foster, J.R. and Gaines, R.R. 2016. Taphonomy and Paleoecology of the "Middle" Cambrian (Series 3) Formations in Utah's West Desert: Recent Finds and New Data, *In*: J.B. Comer, P.C. Inkenbrandt, K.A. Krahulec and M.L. Pinnell (eds.), Resources and Geology of Utah's West Desert. *Utah Geological Association Publication* 45: 291—336.

Gámez Vintaned, J.A., Liñán, E. and Zhuravlev, A.Y. 2011. A new Early Cambrian lobopod-bearing animal (Murero, Spain) and the problem of the ecdysozoan early diversification. *In*: P. Pontarottia (ed.) *Evolutionary Biology–Concepts, Biodiversity, Macroevolution and Genome Evolution*, 193—219. Springer Berlin Heidelberg, Heidelberg.

García-Bellido, D.C., Edgecombe, G.D., Paterson, J.R., and Ma. X.Y. 2013. A "Collins's monster" – type lobopodian from the Emu Bay Shale Konservat-Lagerstätte (Cambrian), South Australia. *Alcheringa* 37: 474-478.

Hou, X. and Bergström, J. 1995. Cambrian lobopodians–ancestors of extant onychophorans? *Zoological Journal of the Linnean Society* 114(1):3—19.

Hou, X.G., Ma, X.Y., Zhao, J. and Bergström, J. 2004. The lobopodian *Paucipodia inermis* from the lower Cambrian Chengjiang fauna, Yunnan, China. *Lethaia* 37(3):235—244.

Lankester, E.R. 1904. The structure and classification of Arthropoda. *Quarterly Journal of Microscopical Science* 47:523—582.

Lerosey-Aubril, R., Hegna, T.A., Babcock, L.E., Bonino, E. and Kier, C. 2014. Arthropod appendages from the Weeks Formation Konservat-Lagerstätte: new occurrences of anomalocaridids in the Cambrian of Utah, USA. *Bulletin of Geosciences* 89(2):269—282.

Ma, X., Edgecombe, G.D., Legg, D.A., and Hou, X. 2014. The morphology and phylogenetic position of the Cambrian lobopodian *Diania cactiformis*. *Journal of Systematic Palaeontology* 12(4):445—457.

Ou, Q., Liu, J., Shu, D., Han, J., Zhang, Z., Wan, X. and Lei, Q. 2011. A rare onychophoran-like lobopodian from the Lower Cambrian Chengjiang Lagerstätte, Southwestern China, and its phylogenetic implications. *Journal of Paleontology* 85(3):587—594.

Pates, S., Daley, A.C. and Lieberman, B.S. 2018. Hurdiid radiodontans from the middle Cambrian (Series 3) of Utah. *Journal of Paleontology* 92:99—113.

Pates, S. and Daley, A.C. 2017. *Caryosyntrips*: a radiodontan from the Cambrian of Spain, USA and Canada. *Papers in Palaeontology* 3:461—470.

Ramsköld and Chen, 1998. Cambrian lobopodians: morphology and phylogeny. *In*: G. Edgecombe (ed.), *Arthropod Fossils and Phylogeny*, 107—150. Columbia University Press, New York.

Robison, R.A. 1985. Affinities of *Aysheaia* (Onychophora), with description of a new Cambrian species. *Journal of Paleontology* 59:226—235.

Robison, R.A. and Richards, B.C. 1981. Larger bivalved arthropods from the Middle Cambrian of Utah. *University of Kansas Paleontological Contributions* 106:1—28.

Robison, R.A., Babcock, L.E. and Gunther, V.G. 2015. Exceptional Cambrian fossils from Utah – A window into the age of trilobites. *Utah Geological Survey Miscellaneous Publication* 15(1):1—97.

Van Roy, P., Daley, A.C. and Briggs, D.E. 2015. Anomalocaridid trunk limb homology revealed by a giant filter-feeder with paired flaps. *Nature* 522(7554):77—80.

Vinther, J., Stein, M., Longrich, N.R. and Harper, D.A. 2014. A suspension-feeding anomalocarid from the Early Cambrian. *Nature* 507(7493):496—499.

Wang, Y.Y., Huang, D.Y. and Hu, S.X. 2013. New anomalocardid frontal appendages from the Guanshan biota, eastern Yunnan. *Chinese Scientific Bulletin* 10:1—6.

Whittington, H.B. 1978. The lobopod animal *Aysheaia pedunculata* Walcott, Middle Cambrian, Burgess Shale, British Columbia. *Philosophical Transactions of the Royal Society of London. Series B, Biological Sciences* 16:165—197.

Whittle, R.J., Gabbott, S.E., Aldridge, R.J. and Theron, J. 2009. An Ordovician lobopodian from the Soom Shale Lagerstätte, South Africa. *Palaeontology* 52(3):561—567.

Yang, J., Ortega-Hernández, J., Gerber, S., Butterfield, N.J., Hou, J.B., Lan, T., and Zhang, X.G. 2015. A superarmoured lobopodian from the Cambrian of China and early disparity in the evolution of Onychophora. *Proceedings of the National Academy of Sciences* 112 (28):8678—8683.

Zeng, H., Zhao, F., Yin, Z. and Zhu, M., 2017. Morphology of diverse radiodontan head sclerites from the early Cambrian Chengjiang Lagerstätte, south-west China. *Journal of Systematic Palaeontology*, DOI: 10.1080/14772019.2016.1263685

Stephen Pates [stephen.pates@zoo.ox.ac.uk], Department of Zoology, University of Oxford, Oxford, OX1 3PS, UK

Allison C. Daley [allison.daley@unil.ch], Institute of Earth Sciences, University of Lausanne, Géopolis, CH-1015, Lausanne, Switzerland

Javier Ortega-Hernández [jo314@cam.ac.uk], Department of Zoology, Downing Street, University of Cambridge, Cambridge, CB2 3EJ, UK.

Chapter 7

Systematics, preservation, and biogeography of radiodonts from the southern Great Basin, USA, during the upper Dyeran (Cambrian Series 2, Stage 4)

Author contributions

SP and ACD conceived the project; GDE collected material from the Pioche Formation; SP wrote the manuscript and prepared the figures, with input from ACD, GDE, PC, and BSL.

Publication information

This Chapter has been submitted for publication in *Papers in Palaeontology* (manuscript ID: PALA-10-18-4348-OA.R2) and has been through two rounds of peer review. This is the third, resubmitted, draft.

Systematics, preservation, and biogeography of radiodonts from the southern Great Basin, USA, during the upper Dyeran (Cambrian Series 2, Stage 4)

by STEPHEN PATES[1,2]*, ALLISON C. DALEY[2], GREGORY D. EDGECOMBE[3,4], PEIYUN CONG[3,4,5] *and* BRUCE S. LIEBERMAN[6,7]

[1] Department of Zoology, University of Oxford, South Parks Road, Oxford, OX1 3PS, United Kingdom; e-mail: stephen.pates@zoo.ox.ac.uk

[2] Institute of Earth Sciences, University of Lausanne, Lausanne CH-1015, Switzerland; e-mail: allison.daley@unil.ch

[3] Department of Earth Sciences, The Natural History Museum, Cromwell Road, London SW7 5BD, United Kingdom; e-mails: g.edgecombe@nhm.ac.uk, p.cong@nhm.ac.uk

[4] MEC International Joint Laboratory for Palaeobiology and Palaeoenvironment, Yunnan University, Kunming 650091, China

[5] Yunnan Key Laboratory for Palaeobiology, Yunnan University, Kunming 650091, China

[6] Department of Ecology & Evolutionary Biology, University of Kansas, Lawrence, KS 66045, USA; e-mail: blieber@ku.edu

[7] Biodiversity Institute, University of Kansas, Lawrence, KS 66045, USA

*Corresponding author

Keywords: Radiodonta, *Anomalocaris*, *Ramskoeldia*, *Hurdia*, Great Basin

Abstract

Anomalocaris, the most well-known genus of the diverse stem euarthropod group Radiodonta, was first reported over 100 years ago from the Burgess Shale (Canada). This large Cambrian apex predator was later treated as occurring in the southern Great Basin (California and Nevada, USA). We re-evaluate the systematic affinities of previously described material from the Pioche Formation, Nevada, and the Latham Shale, California, and describe the first radiodonts from the Pyramid Shale Member, Carrara Formation, California. Latham Shale (Cambrian Series 2, Stage 4, upper Dyeran) specimens previously assigned to *Anomalocaris* are reinterpreted as *Ramskoeldia consimilis*?, an amplectobeluid previously known only from the Chengjiang biota (Cambrian Series 2, Stage 3). Younger material from the Pioche and Carrara Formations (Series 2, Stage 4) is described as a new *Anomalocaris* species, *A. magnabasis*. This new species sheds light on the two-part structure of *Anomalocaris* ventral endites, a potentially important character for distinguishing species, and reveals a sequence of five disarticulation stages for frontal appendages. The oldest *Hurdia* from Laurentia is also reported from the Pioche Formation (Cambrian Series 2, Stage 4). A change-over in taxonomic composition of the Radiodonta in the southern Great Basin is recognised: *Anomalocaris* replaces *Ramskoeldia* in the upper Dyeran, but it is not associated with a replacement of local olenelloid trilobites or seen in radiodonts elsewhere in Laurentia. These new data, combined with a summary of known radiodont occurrences, suggest that *Anomalocaris* species did not have large geographic distributions, when compared to other radiodonts such as *Hurdia* and *Caryosyntrips*.

INTRODUCTION

Radiodonts, such as the iconic apex predator from the Burgess Shale *Anomalocaris canadensis* Whiteaves 1892, occur in nearly all *Konservat-Lagerstätten* from the early and middle Cambrian. These nektonic animals were among the largest animals of the Cambrian and Ordovician Periods, and have provided crucial information for understanding the early evolution of arthropods (e.g. Daley et al. 2009; Paterson et al. 2011; Cong et al. 2014; Van Roy et al. 2015). Radiodonta are best known from the famous Burgess Shale, Canada (Miaolingian, Wuliuan), and Chengjiang biota, China (Cambrian Series 2, Stage 3), but had a worldwide distribution in the Cambrian and have been reported from North America, Europe, China and Australia (e.g. Briggs 1979; Whittington and Briggs 1985; Hou et al. 1995; Daley et al. 2013; Nedin 1995; Pates and Daley 2017). Radiodonts are often preserved as disarticulated elements. These include a pair of anterior frontal appendages adjacent to a ventral circular mouth, and a dorsal head sclerite, sometimes flanked by two lateral carapace elements. Extra-oral feeding structures are known in a number of species: either as oral cones made of radial plates in *Anomalocaris, Hurdia* Walcott 1912 and *Peytoia* Walcott 1911; or bumpy and smooth plates together with additional gnathobase-like structures in *Amplectobelua* Hou, Bergström & Ahlberg 1995 and *Ramskoeldia* Cong, Edgecombe, Daley, Guo, Pates & Hou 2018 (Daley and Bergström 2012; Cong et al. 2017, 2018). A segmented body flanked by lateral flaps bearing transverse lines, with a posterior tail fan, and furcae in *Anomalocaris saron* Hou, Bergström & Ahlberg 1995 and *Amplectobelua symbrachiata* Hou, Bergström & Ahlberg 1995, comprises the rest of the body plan (Whittington and Briggs 1985; Chen et al. 1994; Hou et al. 1995; Daley et al. 2009, 2013; Daley and Edgecombe 2014).

Frontal appendages are the most commonly preserved element of radiodonts, and many species are only known from this pair of limbs, for example *Caryosyntrips camurus* Pates & Daley 2017*, C. durus* Pates & Daley 2017*, C. serratus* Daley & Budd 2010*, Anomalocaris pennsylvanica* Resser 1929*, Amplectobelua stephenensis* Daley & Budd 2010*, Laminacaris chimera* Guo, Pates, Cong, Daley, Edgecombe, Chen & Hou 2018, and *Stanleycaris hirpex* Pates, Daley & Ortega-Hernández 2018a (Briggs 1979; Caron et al. 2010; Daley and Budd 2010; Pates and Daley 2017, 2018; Pates et al. 2018a; Guo et al. 2018). Similarly, in most radiodont-bearing *Konservat-Lagerstätten*, and all those that are Cambrian Series 2, Stage 4 in age, such as the Emu Bay Shale (Australia), Kinzers Formation (USA), Valdemiedes Formation (Spain), Balang Formation and Wulonqing Formation (China), radiodonts are only known from isolated elements and frontal appendages (Briggs 1979; Nedin 1995; Liu 2013; Wang et al. 2013; Pates and Daley 2017, 2018).

Frontal appendages (even partial) can often be assigned to family, genus or species level. *Amplectobelua, Anomalocaris, Laminacaris,* and *Ramskoeldia* have superficially similar frontal appendages, but can be distinguished based on finer details (Fig. 1; Table 1). *Anomalocaris, Ramskoeldia* and *Laminacaris* all have 13 podomeres in the distal articulated region, which distinguishes them from *Amplectobelua*, which has 12. *Laminacaris* has a distinctive, large ventral endite on the first podomere in the distal articulated region, which bears a strong similarity to that of *Hurdia* (Guo et al. 2018). *Ramskoeldia* and *Anomalocaris* can be differentiated from each other as the former has a longer ventral endite on the 5th podomere than the 3rd podomere (the endite of pd8 is longer than that of pd6) in the distal articulated region (Table 1).

Anomalocaris has been known from the southern Great Basin, southwestern USA, for over 40 years: from the Latham Shale, California (Mount 1980; Briggs and Mount 1982);

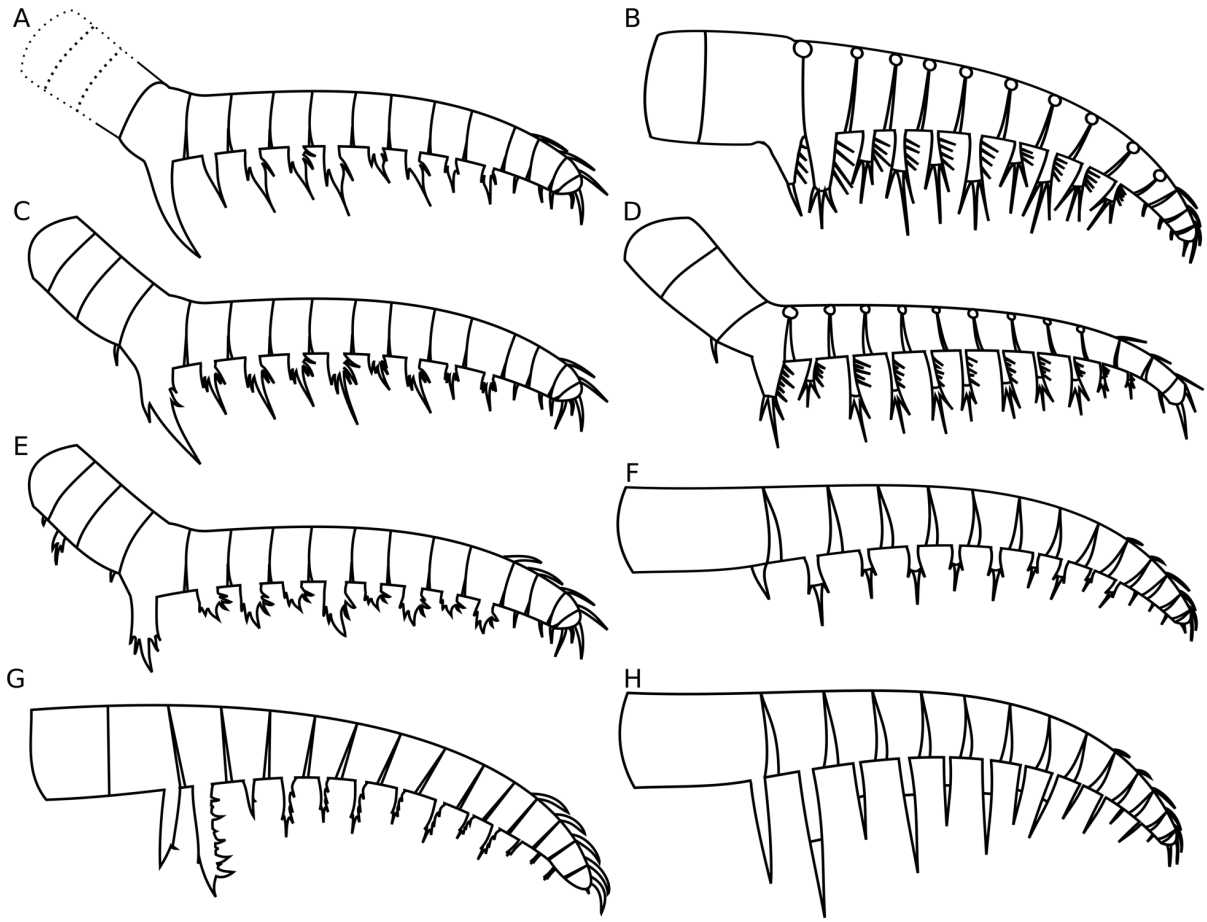

FIG. 1. Reconstructions of *Anomalocaris, Laminacaris* and *Ramskoeldia* frontal appendages. A, *Ramskoeldia* consimilis?. B, *Anomalocaris magnabasis.* C, *Ramskoeldia consimilis*. D, *Anomalocaris saron*. E, *Ramskoeldia platyacantha*. F, *Anomalocaris canadensis*. G, *Laminacaris chimera*. H, *Anomalocaris pennsylvanica*. Dotted lines indicate podomeres not preserved in any specimens. C, D redrawn from Guo et al. 2018, fig. 3; F, G, H redrawn from Pates & Daley 2018, fig. 6.

Table 1. Comparison of frontal appendage characters of select radiodont genera.

	Morphology of frontal appendage						Morphology of largest v.e.			
	#pd shaft	#pd d.a.r.	#rows v.e.	#long v.e.	v.e. in d.a.r. alternate long/short	v.e. on pd8 longer than pd6	Aux on both anterior and posterior	Aux increase distally along v.e.	#Large aux	Small aux between large aux
Amplectobelua	3	12	2	1	Yes	Yes	Yes	No	0/2	No
Ramskoeldia	3	13	2	1	Yes	Yes	Yes	No	2	No
Anomalocaris (excluding *A. briggsi*)	1-2	13	2	1	Yes	No	Yes	No	0/2	No
Laminacaris	2	13	1?	1	Yes	No	No	Yes	5	Yes

Abbreviations: aux, auxiliary spines; d.a.r., distal articulated region; pd, podomere; v.e., ventral endite.

the Combined Metals Member and Comet Shale Member of the Pioche Formation, Nevada (Lieberman 2003), and the Pyramid Shale Member of the Carrara Formation, California (Wilbur 2005). Recent work has focussed on the younger Miaolingian strata from the northern Great Basin (Utah and Idaho), from which predominantly hurdiids are known: *Hurdia* sp. and *Hurdia victoria* Walcott 1912 from the Spence Shale Member, Langston Formation (Wuliuan); *Stanleycaris,* and *Peytoia nathorsti* Walcott 1911 from the Wheeler Formation (Drumian); *Peytoia nathorsti* from the Marjum Formation (Drumian); and two species of *Anomalocaris* from the Weeks Formation (Guzhangian) (Briggs et al. 2008; Daley et al. 2013; Lerosey-Aubril et al. 2014; Pates et al. 2017, 2018a, b). Here we present new radiodont specimens from the Latham Shale and Pioche Formation while re-evaluating previously described material from these units, and formally describing the first radiodonts from the Pyramid Shale Member, Carrara Formation, California. We show that three genera of Radiodonta are present in the Great Basin region, with *Ramskoeldia* in the older Latham Shale and *Anomalocaris* in the younger Pyramid Shale Member, Comet Shale Member, and Combined Metals Member, which also contains *Hurdia*, and discuss the biogeographic implications. In addition we describe a taphonomic pathway for the disarticulation of *Anomalocaris* frontal appendages.

GEOLOGICAL SETTING

The southern Great Basin formed on the margin of Laurentia beginning in the Neoproterozoic and early Cambrian, and by the end of the Dyeran the shelf was well flooded, as far as Utah and Idaho (Stewart and Poole, 1974; Webster 2011). Four depositional sequences have been recognised in the southern Great Basin with recent work on the biostratigraphy of the area subdividing the previously used '*Olenellus* zone' into six

trilobite zones in the upper Dyeran (Webster 2011). The extinction of olenelline trilobites (*sensu* Lieberman 2002) at the end of the Dyeran is followed by the lowermost Delamaran *Eokochaspis nodosa* zone, defined by the first appearance of *E. nodosa* (Sundberg and McCollum 2000). This biostratigraphic framework, combined with a number of horizons with exceptional preservation (Briggs and Mount 1982; Lieberman 2003; Wilbur 2005), allows the study of radiodonts and other soft-bodied animals at a high temporal resolution in a geographically constrained area in the southwestern USA (Figs. 2, 3).

Radiodonts are known from both the Combined Metals Member (Dyeran) and Comet Shale Member (Delamaran) of the Pioche Formation at Ruin Wash, Klondike Gap, and the Highland Range, where Comet Mine and One Wheel Canyon are located (respectively RW, KG and HR, in Fig. 2). They are also known from one site in the Carrara Formation (Dyeran), at Emigrant Pass (EP, Fig. 2), and at least two sites from the Latham Shale (Dyeran), in the Providence and Marble Mountains (PM and MM respectively, Fig. 2). During the Dyeran and Delamaran Stages, when these rocks were deposited, these localities were equatorial (Fig. 2C, D).

The trilobite fauna of the upper Dyeran in the Pioche Formation has been well studied, with olenelloid trilobites being extremely abundant and well preserved at Ruin Wash (Palmer 1998). These trilobites have been used to address palaeobiological, systematic and taphonomic questions (e.g. Webster & Hughes 1999; Webster & Zelditch 2005) and were deposited in a low energy, offshore environment, with subtle changes in energy affecting the abundance of articulated specimens (Webster et al. 2008). The extinction of olenelline trilobites occurs at the top of the *Nephrolenellus multinodus* zone (= the top of the '*Olenellus* zone') (Fig. 3; Palmer 1998; Webster 2011) which marks the Dyeran-Delamaran boundary in this region; ptychopariid trilobites are common after the

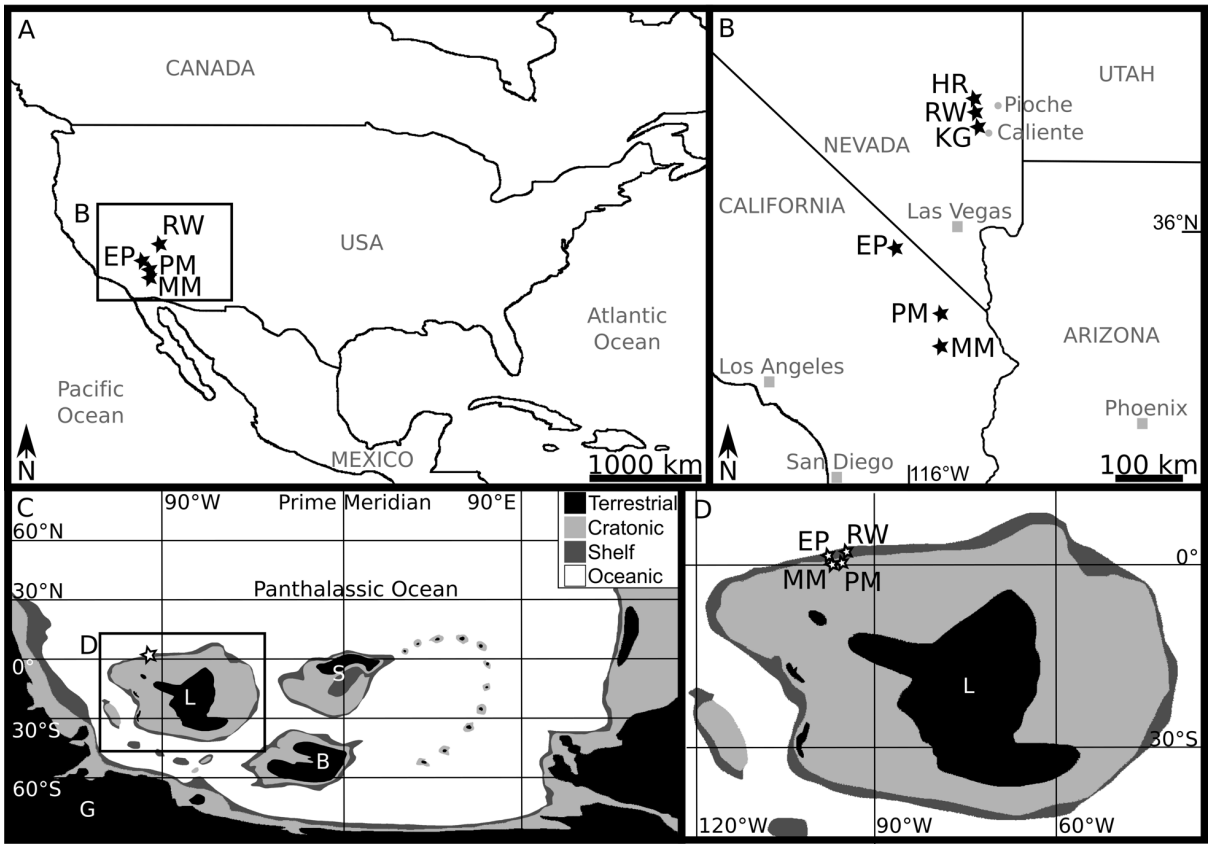

FIG. 2. Geographic position of radiodont sites in the southern Great Basin. Abbreviations: EP: Emigrant Pass; HR = Highland Range (where One Wheel Canyon and Comet Mine are located); KG = Klondike Gap; MM = Marble Mountains; PM = Providence Mountains; RW = Ruin Wash. A, Modern day position of sites in North America. B, box indicated in A, showing in more detail the modern day position of radiodont-bearing sites in the Southwestern USA, modified from Webster 2011, fig. 2. C, Position of sites reconstructed 510 Ma using GPlates (Scotese, 2016). Abbreviations: B, Baltica; G, Gondwana; L, Laurentia; S, Siberia. D, box indicated in C showing Laurentia in more detail.

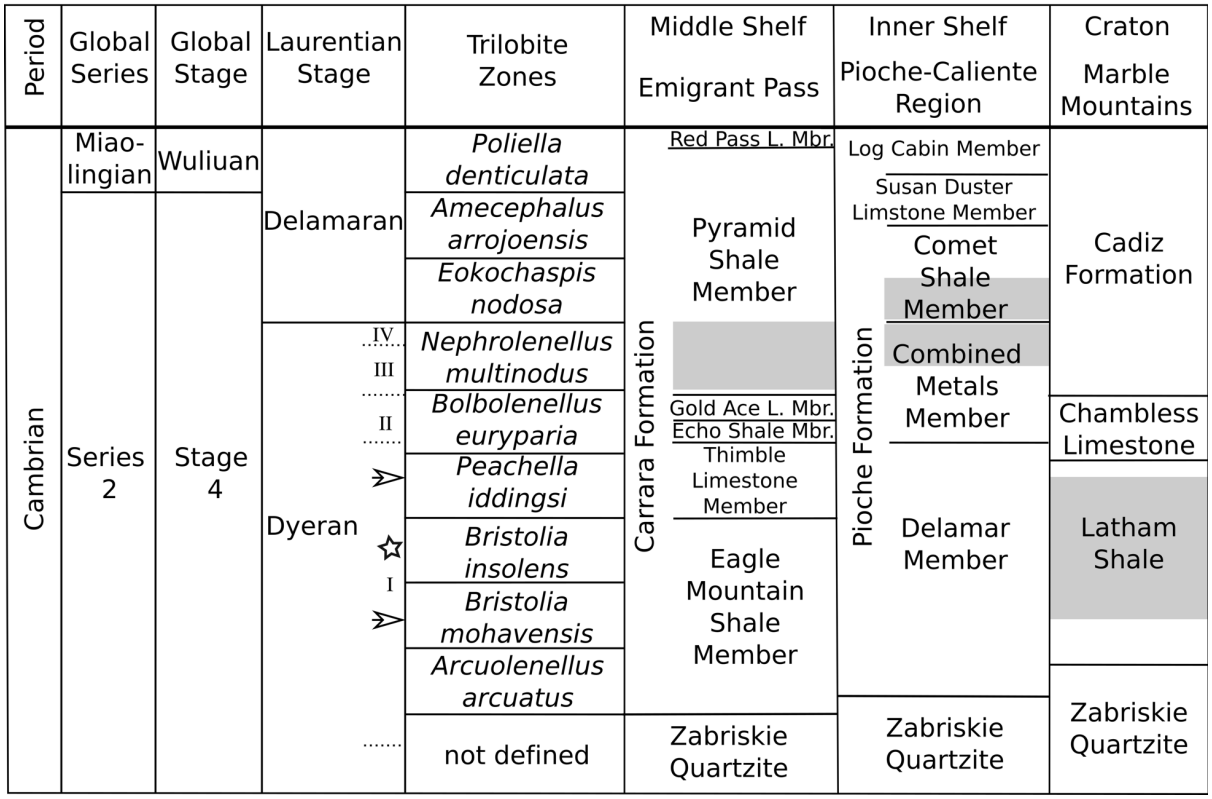

FIG. 3. Stratigraphy of the Middle Shelf, Inner Shelf and Craton, southern Great Basin, with trilobite zones, from upper Dyeran to lower Delamaran. Roman numerals indicate Upper Dyeran Depositional Sequences of Webster 2011. Star indicates approximate position of highstand during Upper Dyeran Depositional Sequence 1. Arrows indicate upper and lower boundary of '*Bristolia* subzone' of '*Olenellus* zone'. Grey areas indicate time ranges for preservation of radiodonts. Modified from Webster 2011, fig. 3.

extinction (Sundberg & McCollum 2000). At least two exceptionally preserved horizons with radiodont frontal appendages are known from the Pioche Formation, either side of this extinction event (Lieberman 2003). The older level is in the upper section of the *Nephrolenellus multinodus* zone (upper Dyeran; Fig. 3), in the Combined Metals Member, and preserves soft-bodied fossils in a reddish botryoidal haematite alongside olenelline trilobites (Moore & Lieberman 2009). The younger level is in the the *Eokochapsis nodosa* zone (Delamaran), in the Comet Shale Member (Lieberman 2003), during the maximum flooding of the shelf (McCollum & Sundberg, 2007). The soft-bodied specimens are preserved as kerogenized carbon films associated with pyrite crystals and framboids alongside ptychopariid trilobites (Moore & Lieberman 2009). Other exceptionally preserved fauna known from the Pioche Formation include the arthropods *Tuzoia* and *Canadaspis*, a cycloneuralian worm originally assigned to *Ottoia* (Lieberman 2003; Smith et al. 2015), coprolites (Kimmig & Strotz 2017), and the enigmatic deuterostome *Herpetogaster* (Kimmig et al., 2018).

The Pyramid Shale Member of the Carrara Formation spans the *Nephrolenellus multinodus* (upper Dyeran) to *Poliella denticulata* zones (Delamaran) (Fig. 3; Webster 2011). The radiodont frontal appendages come from an exceptionally preserved horizon in the *Nephrolenellus multinodus* zone (Fig. 3; Wilbur 2005). The Latham Shale is older than the Pyramid Shale Member, and spans the *Arcuolenellus arcuatus* to *Peachella iddingsi* zones (Fig. 3; Webster 2011). It outcrops in both the Providence and Marble Mountains (Fig. 2; San Bernardino County, California, USA). A shelly fauna of olenelloid and ptychopariid trilobites, brachiopods (Mount 1980), eocrinoids (Durham 1978) and conical fossils (Waggoner & Hagadorn 2005) is known alongside unmineralised fossils such as algae (Waggoner & Hagadorn 2004) and a palaeoscolecid worm (Conway Morris & Peel 2009). The radiodont

appendages were collected from what was originally referred to by Briggs and Mount (1982) as the '*Bristolia* subzone' of the '*Olenellus* zone', which now is treated as ranging from the upper half of the *Bristolia mohavensis* to the *Peachella iddingsi* zones (arrows in Fig. 3). The exceptionally preserved beds originate from the distal, fine grained portions of the unit (Gaines & Droser 2002), likely placing these beds close to the highstand of Upper Dyeran Depositional Sequence I in the *Bristolia insolens* zone (star in Fig. 3; Webster 2011).

MATERIALS AND METHODS

New material described here was collected by Bryan Wilbur (TMM NPL 23925, TMM NPL 64841, KUMIP 492944), Michael Vendrasco (LACMIP 12988), Mark Webster (Latham Shale specimen UCR 9990/1), and Gregory Edgecombe, Tim Ewin, Xiaoya Ma and Mike Smith (Pioche Formation material). The other material has previously been described in Briggs and Mount (1982) and Lieberman (2003), with the exception of the *Hurdia* carapace, which was collected during a field expedition organized by the Yale University Peabody Museum of Natural History, the Museum of Comparative Zoology, Harvard University and the University of Kansas and included participation from scientists and staff at those institutions as well as Lloyd and Val Gunther, Ronald Meyer, Thomas Whitely, Roland Reboul, Christian Gronau, and Marc Behrendt.

Photographs were taken using a Canon EOS 500D camera with Canon EF-S 60 mm macro lens, controlled with EOS Utility 2 remote shooting software. Fossils were photographed both dry and submerged, under high and low angle lighting, using polarized and unpolarized light. Digital measurements were made using ImageJ (Schneider et al. 2012).

Palaeogeographic reconstructions were made with GPlates (Scotese 2016) using modern longitude and latitude coordinates from the localities, including coordinates from Hendricks et al. (2008).

Institutional abbreviations. KUMIP, Division of Invertebrate Paleontology, Biodiversity Institute, University of Kansas, Lawrence, Kansas, USA; LACMIP, Los Angeles County Museum of Invertebrate Palaeontology, California, USA; NHMUK, The Natural History Museum, London, UK; ROM, Royal Ontario Museum, Toronto, Ontario, Canada; TMM NPL, Texas Memorial Museum Non-vertebrate Paleontology Laboratory, Austin, Texas, USA; UCB, University of California, Berkeley, California, USA; UCR, University of California, Riverside, California, USA; YKLP, Yunnan Key Laboratory for Palaeobiology, Yunnan University, Kunming, Yunnan, China; YPM, Yale University Peabody Museum of Natural History, New Haven, Connecticut, USA.

Terminology. The terminology here follows that of Guo et al. (2018), with the addition of the term 'spinule' to describe a thin auxiliary spine projecting from the anterior margin of the base of the ventral endite. This is to distinguish these features from the larger auxiliary spines that flank the large central spine in the 'trident' shape typical of *Anomalocaris canadensis* endites, also present in other radiodonts (e.g. *A. saron*).

Abbreviations. ds, dorsal spine; en, endite; pd, podomere; ts, terminal spine

SYSTEMATIC PALAEONTOLOGY

Superphylum PANARTHROPODA Nielsen, 1995

Order RADIODONTA Collins, 1996

Family AMPLECTOBELUIDAE nov. fam.

Type genus. Amplectobelua Hou et al. 1995.

Included genera. Amplectobelua and *Ramskoeldia*

Diagnosis. Radiodonts with three pairs of gnathobase-like structures associated with reduced transitional segments posterior to the head region; gnathobase-like structures with at least two rows of stout, curved, distal spines set in sockets; distal region of gnathobase-like structures' stem bearing numerous pointed scales; mouth composed of smooth and tuberculate plates, not forming a radial oral circlet; shaft of the frontal appendage consisting of three podomeres; frontal appendage with endites decreasing in size distally except for that of podomere 8, which is larger than that of podomere 6; endite of podomere 4 larger/stouter than others, varying from slightly larger to hypertrophied; smaller endite present on each distal podomere, forming an asymmetric pair with the normal larger one; lateral element small, oval, and of similar size to central element of head (emended from Cong et al. 2018).

Remarks. Vinther et al. (2014) explicitly used a phylogenetic taxonomy (de Queiroz & Gauthier 1990), with families (including Amplectobeluidae) defined using a branch-based approach. These definitions do not provide the required description of characters for the International Code of Zoological Nomenclature (ICZN) article 13.1, and so the new family names are invalid by this system. A formal character-based definition for Amplectobeluidae

was subsequently provided by Cong et al. (2018). This provided diagnostic features for the family, but the family name Amplectobeluidae was not explicitly indicated as intentionally new, and thus this description of the family is also not valid (ICZN article 16.1). The diagnosis provided here, using the work of Cong et al. (2018), formally establishes the family by the ICZN rules. Although retrieved within Amplectobeluidae in recent phylogenetic analyses (e.g. Lerosey-Aubril & Pates 2018; Liu et al. 2018), *Lyrarapax* is not among the included genera here as it lacks gnathobase-like-structures and the endite on podomere 8 is not larger than that of podomere 6 (discussed in more detail in Cong et al. 2018).

Genus RAMSKOELDIA Cong et al. 2018

Type species. Ramskoeldia platyacantha Cong et al. 2018; from the Yu'anshan Member, Chiungchussu Formation (Cambrian Series 2, Stage 3), Yunnan Province, China.

Ramskoeldia consimilis? Cong et al. 2018

Figures 4, 5

1980 *Anomalocaris canadensis* Whiteaves 1892; Mount, 1980, fig. 19

1982 *Anomalocaris canadensis* Whiteaves 1892; Briggs & Mount, 1982, text-fig. 1

Material. UCR 7602.1/2 (part and counterpart); UCR 9990/1; UCR 7002/1; UCB D 7770

Description. Four frontal appendages from the Latham Shale are known, two from the Marble Mountains (Fig. 4) and two from the Providence Mountains (Fig. 5). One appendage

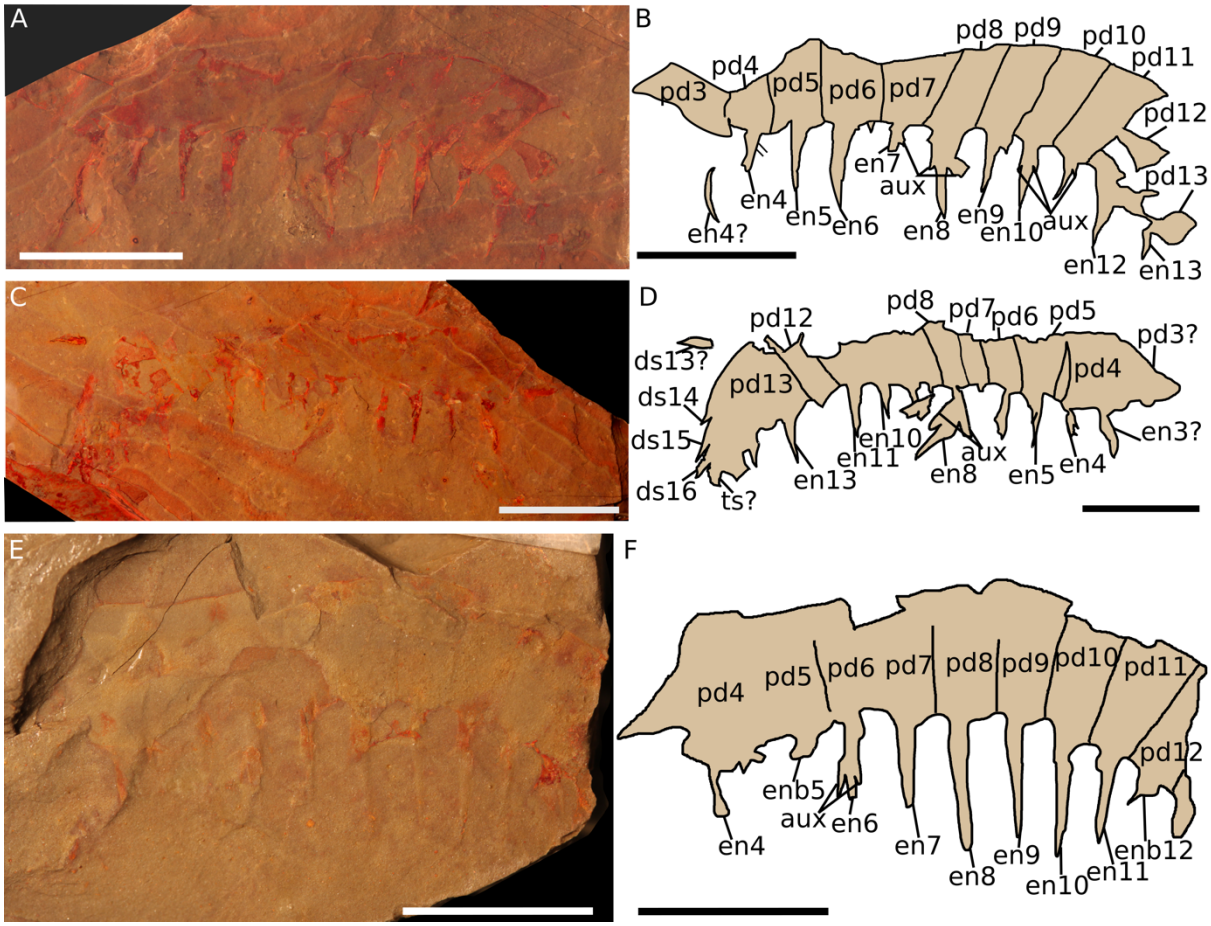

FIG. 4. *Ramskoeldia* consimilis? from the *Bristolia mohavensis* zone – *Peachella iddingsi* zone, Latham Shale, Dyeran, Marble Mountains, California, USA. A, UCR 7602/2. B, interpretative drawing of A. C, UCR 7602/1 (counterpart to specimen shown in A). D, interpretative drawing of C. E, UCR 9990/1. F, interpretative drawing of E. Abbreviations: ds, dorsal spine; en, ventral endite; enb, base of ventral endite; pd, podomere; ts?, terminal spine?. All scale bars = 10 mm.

from each locality shows one podomere (pd3) in the shaft (though the shaft in both specimens is incomplete), which attaches to a distal articulated region of 13 podomeres at an obtuse angle (Figs 4D, 5B, pd4-16; UCR 7602; UCB D 7770). Podomeres are labelled following the standard pattern for species of *Ramskoeldia*: pd1-3 in the shaft; pd4-16 in the distal articulated region (Cong et al. 2018). The first and second podomeres in the shaft (pd1, pd2) are not observed in any of the four specimens from the Latham Shale. The distal articulated region measures 45 mm in UCR 7602 and 41 mm in UCB D 7770. UCR 7002 is the largest specimen, with a distal articulated region of approximately 150 mm (calculated by extrapolating from eight to 13 podomeres).

The morphology of the ventral endite on the first podomere in the distal articulated region is only complete in UCR 7002 (pd4, Fig. 5C, D). It is elongate and curved distally, with no evidence of auxiliary spines (en4, Fig. 4C, D). It is apparently paired, with a layer of sediment between the well preserved endite and its partial pair. The interpretation of this endite being one of a pair instead of an endite on the distalmost podomere of the shaft is preferred because the shaft attaches to the distal articulated region at an obtuse angle, and this endite appears nearly parallel to the endite on pd4. A partial endite could be present on the shaft in UCR 7602 (en3?, Fig. 4C, D). The endites along the rest of the distal articulated region (from pd5 – pd16) alternate long/short on even/odd numbered podomeres, and reduce in size along the length of the appendage, with the exception of the endites on pd8 which are larger than the endites on pd6 (Fig. 4A, B, E, F). Where only the base of the ventral endite is preserved it is thicker on pd8 than pd6, for example in UCB D 7770 (Fig. 5A, B); the base of pd6 is covered with a nevadiid trilobite cephalon in UCR 7002 (t, Fig. 5C, D); the ventral endite on pd6 is incomplete in UCR 9990/1 (en6, Fig. 4E, F). The other ventral endites bear two auxiliary spines (e.g., en6, Fig. 4E, F; en 4-11, Fig. 4A-D) and are

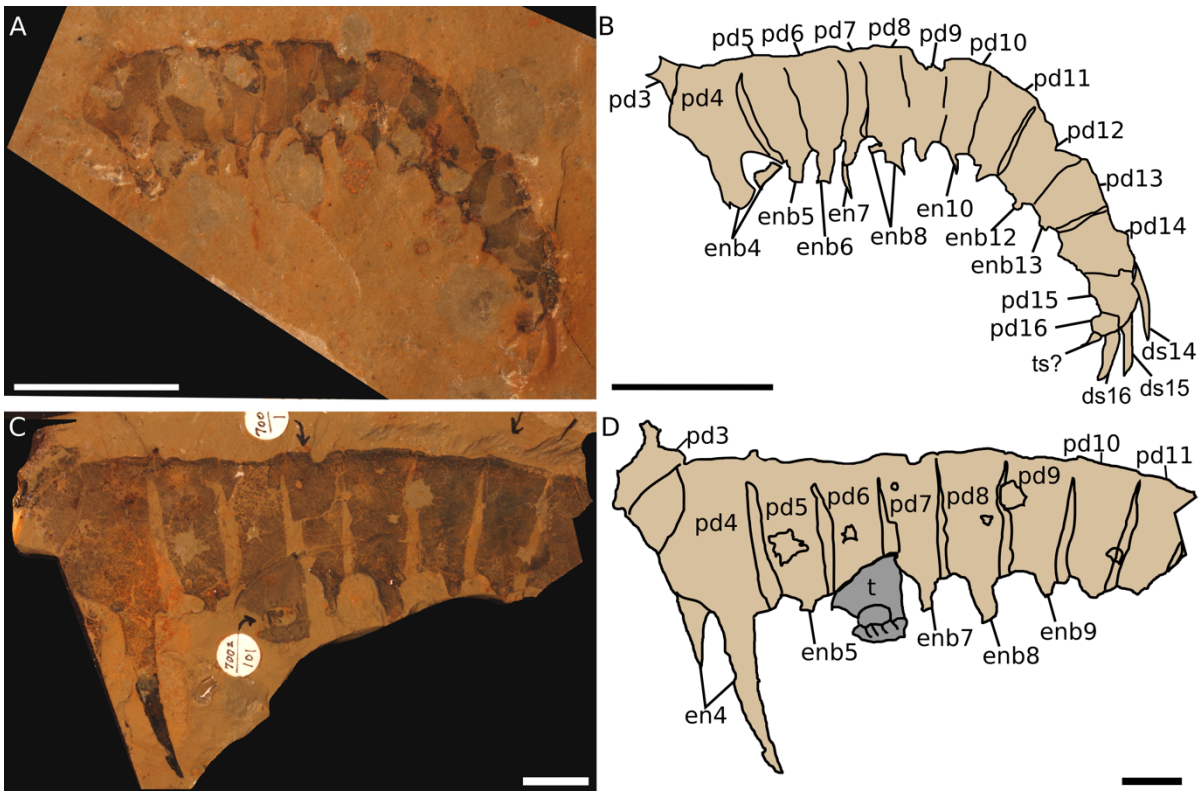

FIG. 5. *Ramskoeldia* consimilis? from the *Bristolia mohavensis* zone – *Peachella iddingsi* zone, Latham Shale, Dyeran, Providence Mountains, California, USA. A, UCB D 7770. B, interpretative drawing of A. C, UCR 7002/1. D, interpretative drawing of C. Abbreviations: aux, auxiliary spine; ds, dorsal spine; en, ventral endite; enb, base of ventral endite; pd, podomere; t, trilobite; ts?, terminal spine?. Scale bars = 10 mm.

approximately the height of the podomere to which they attach. The appendage tapers distally, and podomeres become increasingly square in outline at the distal end. The distalmost four podomeres (pd13-16) bear dorsal spines (ds13-16), and pd16 also appears to bear a terminal spine in UCR 7602 and UCB D 7770 (ts?, Figs. 4C, D, 5 A, B).

Remarks. These specimens (except for UCR 9990/1) were previously identified as *Anomalocaris canadensis* by Briggs and Mount (1982) based on the morphology of the ventral endites and the number of podomeres. Given the state of preservation of the specimens and the knowledge of radiodonts at that time this was a reasonable identification, but recently the presence of a longer ventral endite on pd8 than pd6 has been identified as a character diagnostic of amplectobeluids (Cong et al. 2018) and is not known in anomalocaridids; in the latter the length of the ventral endites decreases along the length of the appendage (e.g. Daley & Edgecombe 2014**)**. Although the evidence for this character is only convincing in one specimen (UCR 7602, Fig. 4A-D), the other material is closely similar to that specimen in those features preserved (there are slight differences in podomere height:width ratio and ventral spine length but these are attributed to overall size differences and ontogeny), so all four specimens are treated as comprising the same species. Notably, these frontal appendages have the same number of podomeres in the distal articulated region as *Ramskoeldia* (13: one more than *Amplectobelua*), and the morphology of the ventral endites (in length and width) is most similar to *Ramskoeldia consimilis* (*R. platycantha*, the type species of the genus, has shorter and wider ventral endites). The distally curved ventral endite on pd4 is also similar to *R. consimilis* (e.g. Cong et al. 2018 figs 3, 4, 5A, B, D, E) but there is no evidence in the Latham specimens of auxiliary spines which are present in the Chinese material. These specimens are thus only

questionably assigned to *R. consimilis*, owing to the incomplete nature of the preservation, which does not allow all diagnostic characters of the species to be determined (such as presence of three podomeres in the shaft and the presence of auxiliary spines on the enlarged endite of pd4). These specimens can be differentiated from the Pioche and Carrara material (described below) by the shaft attaching to the distal articulated region at an obtuse angle, and, where preserved, the endite on pd8 being longer than that of pd6.

Ramskoeldia consmilis? is known from two sites, each with slightly different preservational regimes, providing somewhat complementary information. For instance, the Providence Mountains material (UCB D 7770 and UCR 7002) (Fig. 5) shows the triangular arthrodial membrane between podomeres clearly, but the ventral spines are broken off in the majority of cases. In contrast, the Marble Mountains material (UCR 7602 and UCR 9990/1) (Fig. 4) shows only faint boundaries between the podomeres, but the ventral endites are more often complete. These types of subtle preservational differences within a species are also known in other non-biomineralised animals from more than one distinct BST deposit, for example *Anomalocaris pennsylvanica* from distinct sites in the Kinzers Formation (Pates & Daley 2018). The part and counterpart of UCR 7602 show different details, as 7602/1 has the full complement of podomeres, but preserves the ventral endites with less fidelity. The presence of auxiliary spines is best seen in UCR 7602/2, although the distal end of the appendage is not preserved (compare Fig. 4A, B with 4C, D).

This material represents the first specimens of *Ramskoeldia* identified from outside the Chengjiang region of South China, and also the youngest occurrence for the genus (Cambrian Series 2 Stage 4). The occurrence suggests a possible biogeographic connection between geographically disparate South China and southwestern Laurentia. In addition, even though we have reassigned Briggs and Mount's (1982) material to *R. consmilis?*,

Anomalocaris is still represented in Series 2 of Laurentia. *A. pennsylvanica* occurs in the Kinzers Formation of Pennsylvania, USA (Resser 1929; Resser & Howell 1938; Briggs, 1979; Pates & Daley 2018), *A. canadensis* occurs in the Cranbrook Shale of British Columbia, Canada (Briggs 1979; Daley & Edgecombe 2014), and *A. magnabasis* n. sp. occurs in the Pioche (discussed below).

Occurrence. '*Bristolia* subzone' of the '*Olenellus* zone' (= upper half of the *Bristolia mohavensis* zone to the *Peachella iddingsi* zone), Cambrian Series 2, Stage 4, Latham Shale, San Bernadino County, California: Providence Mountains, 930 m southwest of Summit Spring, 120 m west and 150 m north of the southeast corner of sec. 17, T1N, R14E, Kelso 15' quad, 14 m above base of formation (UCB D-7770; UCR 7002); Marble Mountains, 170 m west, 730 m south of northeast corner of sec. 11, T5N, R14E, Danby 15' quad, 9 m above base of formation (UCR 7602) (Briggs & Mount 1982); undifferentiated float, Marble Mountains (UCR 9990/1).

Family ANOMALOCARIDIDAE Raymond, 1935

Genus ANOMALOCARIS Whiteaves, 1892

Type species. *Anomalocaris canadensis* Whiteaves, 1892; from the Stephen Formation (Miaolingian, Wuliuan) of British Columbia, Canada.

Anomalocaris magnabasis sp. nov.

Figures 6-11

LSID. XXX

Table 2. List of specimens studied showing previous and current taxonomic interpretation.

Catalogue number	Previous interpretation	Stratigraphy	Reference	New interpretation
UCB D 7770 and UCMP 37470 (counterpart)	*Anomalocaris canadensis*	Latham Shale, Providence Mountains	Briggs and Mount 1982, text-fig. 1 C, D	*Ramskoeldia consimilis?*
UCR 7602/1 and UCR 7602/2 (counterpart)	*Anomalocaris canadensis*	Latham Shale, Marble Mountains	Briggs and Mount 1982, text-fig. 1 E, F	*Ramskoeldia consimilis?*
UCR 9990/10	Not previously described.	Latham Shale, Marble Mountains (float)	-	*Ramskoeldia consimilis?*
UCR 7002/1	*Anomalocaris* n. sp.*;* *Anomalocaris canadensis*	Latham Shale, Providence Mountains	Mount 1976, fig. 19; Briggs and Mount 1982, text-fig. 1 A, B	*Ramskoeldia consimilis?*
YPM 163103	*Anomalocaris pennsylvanica*	*Nephrolenellus multinodus* zone, Combined Metals Member, Pioche Formation	Lieberman 2003, p.684	*Anomalocaris magnabasis*
KUMIP 293571	*Anomalocaris pennsylvanica*	*Nephrolenellus multinodus* zone, Combined Metals Member, Pioche Formation	Lieberman 2003, fig. 8.4	*Anomalocaris magnabasis*
KUMIP 293572	*Anomalocaris pennsylvanica*	*Nephrolenellus multinodus* zone, Combined Metals Member, Pioche Formation	Lieberman 2003, fig. 7.3	*Anomalocaris magnabasis*?
KUMIP 293605	*Anomalocaris pennsylvanica*	*Nephrolenellus multinodus* zone, Combined Metals Member, Pioche Formation	Lieberman 2003, fig. 7.2	*Anomalocaris magnabasis*
KUMIP 293609	*Anomalocaris pennsylvanica*	*Nephrolenellus multinodus* zone, Combined Metals Member, Pioche Formation	Lieberman 2003, p.684	*Anomalocaris magnabasis*
KUMIP 298500	*Anomalocaris pennsylvanica*	*Nephrolenellus multinodus* zone, Combined Metals Member, Pioche Formation	Lieberman 2003, fig. 7.1	*Anomalocaris magnabasis*?

KUMIP 298501	*Anomalocaris pennsylvanica*	*Nephrolenellus multinodus* zone, Combined Metals Member, Pioche Formation	Lieberman 2003, p.684	*Anomalocaris magnabasis*?
KUMIP 298502	*Anomalocaris pennsylvanica*	*Nephrolenellus multinodus* zone, Combined Metals Member, Pioche Formation	Lieberman 2003, p.684	*Anomalocaris magnabasis*?
KUMIP 298503	*Anomalocaris pennsylvanica*	*Nephrolenellus multinodus* zone, Combined Metals Member, Pioche Formation	Lieberman 2003, fig. 7.4	*Anomalocaris magnabasis*?
KUMIP 293573 (counterpart KUMIP 293632)	*Anomalocaris pennsylvanica?*	*Nephrolenellus multinodus* zone, Combined Metals Member, Pioche Formation	Lieberman 2003, p.684	*Anomalocaris magnabasis*?
KUMIP 293574	*Anomalocaris pennsylvanica?*	*Nephrolenellus multinodus* zone, Combined Metals Member, Pioche Formation	Lieberman 2003, p.684	*Anomalocaris magnabasis*?
KUMIP 293575	*Anomalocaris pennsylvanica?*	*Nephrolenellus multinodus* zone, Combined Metals Member, Pioche Formation	Lieberman 2003, p.684	*Anomalocaris magnabasis*?
KUMIP 293576	*Anomalocaris pennsylvanica?*	*Nephrolenellus multinodus* zone, Combined Metals Member, Pioche Formation	Lieberman 2003, p.684	*Anomalocaris magnabasis*?
KUMIP 298512	*Anomalocaris pennsylvanica?*	*Nephrolenellus multinodus* zone, Combined Metals Member, Pioche Formation	Lieberman 2003, p.684	*Anomalocaris magnabasis*
KUMIP 298513	*Anomalocaris pennsylvanica?*	*Nephrolenellus multinodus* zone, Combined Metals Member, Pioche Formation	Lieberman 2003, p.684	*Anomalocaris magnabasis*
KUMIP 298515	*Anomalocaris pennsylvanica?*	*Nephrolenellus multinodus* zone, Combined Metals Member, Pioche Formation	Lieberman 2003, p.684	*Anomalocaris magnabasis*?

KUMIP 298516	*Anomalocaris pennsylvanica?*	*Nephrolenellus multinodus* zone, Combined Metals Member, Pioche Formation	Lieberman 2003, p.684	*Anomalocaris magnabasis*?
KUMIP 298532	*Anomalocaris pennsylvanica?*	*Nephrolenellus multinodus* zone, Combined Metals Member, Pioche Formation	Lieberman 2003, p.684	*Anomalocaris magnabasis*?
KUMIP 293578 (counterpart KUMIP 293587)	*Anomalocaris*	Pioche Formation	Lieberman 2003, p.684, 686	*Anomalocaris magnabasis*
KUMIP 293583	*Anomalocaris* cf. *saron*	*Eokochaspis nodosa* zone, Comet Shale Member, Pioche Formation	Lieberman 2003, p.686	*Anomalocaris magnabasis*
KUMIP 293586	*Anomalocaris* cf. *saron*	*Eokochaspis nodosa* zone, Comet Shale Member, Pioche Formation	Lieberman 2003, p.686	*Anomalocaris magnabasis*
KUMIP 293584	*Anomalocaris* cf. *saron*	*Eokochaspis nodosa* zone, Comet Shale Member, Pioche Formation	Lieberman 2003, figs. 8.1, 9	*Anomalocaris magnabasis*
KUMIP 293585	*Anomalocaris* cf. *saron*	*Eokochaspis nodosa* zone, Comet Shale Member, Pioche Formation	Lieberman 2003, p.686	*Anomalocaris magnabasis*
KUMIP 298520 (2 specimens)	*Anomalocaris* cf. *saron*	*Eokochaspis nodosa* zone, Comet Shale Member, Pioche Formation	Lieberman 2003, p.686	*Anomalocaris magnabasis*?
KUMIP 298521	*Anomalocaris* cf. *saron*	*Eokochaspis nodosa* zone, Comet Shale Member, Pioche Formation	Lieberman 2003, p.686	*Anomalocaris magnabasis*
KUMIP 298522	*Anomalocaris* cf. *saron*	*Eokochaspis nodosa* zone, Comet Shale Member, Pioche Formation	Lieberman 2003, p.686	*Anomalocaris magnabasis*
KUMIP 298529	*Anomalocaris* cf. *saron*	*Eokochaspis nodosa* zone, Comet Shale Member, Pioche Formation	Lieberman 2003, fig. 8.2	*Anomalocaris magnabasis*
KUMIP 298530	*Anomalocaris* cf. *saron*	*Eokochaspis nodosa* zone, Comet Shale Member, Pioche Formation	Lieberman 2003, p.686	*Anomalocaris magnabasis*
KUMIP 298543	*Anomalocaris* cf. *saron*	*Eokochaspis nodosa* zone, Comet Shale Member, Pioche Formation	Lieberman 2003, fig. 8.3	*Anomalocaris magnabasis*
KUMIP 293578	*Anomalocaris* cf. *saron?*	*Eokochaspis nodosa* zone, Comet Shale Member, Pioche Formation	Lieberman 2003, p.686	*Anomalocaris magnabasis*

KUMIP 293857	*Anomalocaris* cf. *saron?*	*Eokochaspis nodosa* zone, Comet Shale Member, Pioche Formation	Lieberman 2003, p.686	*Anomalocaris magnabasis*
KUMIP 294226	*Anomalocaris* cf. *saron?*	*Eokochaspis nodosa* zone, Comet Shale Member, Pioche Formation	Lieberman 2003, p.686	*Anomalocaris magnabasis*
KUMIP 294227	*Anomalocaris* cf. *saron?*	*Eokochaspis nodosa* zone, Comet Shale Member, Pioche Formation	Lieberman 2003, p.686	*Anomalocaris magnabasis*
KUMIP 307022 (2 specimens)	*Anomalocaris* cf. *saron?*	*Eokochaspis nodosa* zone, Comet Shale Member, Pioche Formation	Lieberman 2003, p.686	*Anomalocaris magnabasis*?
NHMUK IC 1330a, b	Not previously described.	*Eockochaspis nodosa* zone, Comet Shale Member, Pioche Formation, One Wheel Canyon, Nevada	-	*Anomalocaris magnabasis*?
NHMUK IC 1331 a, b	Not previously described.	*Eockochaspis nodosa* zone, Comet Shale Member, Pioche Formation, One Wheel Canyon, Nevada	-	*Anomalocaris magnabasis*
KUMIP 378539	Not previously described.	*Nephrolenellus multinodus* zone, Combined Metals Member, Pioche Formation	-	*Hurdia* sp.
TMM NPL 23925 (part and counterpart)	*Anomalocaris*	*Nephrolenellus multinodus* zone, Pyramid Shale Member, Carrara Formation	Wilbur 2005, p. 11	*Anomalocaris magnabasis?*
TMM NPL 64841 (part and counterpart)	Not previously described.	*Nephrolenellus multinodus* zone, Pyramid Shale Member, Carrara Formation	-	*Anomalocaris magnabasis?*
KUMIP 492944	Not previously described.	*Nephrolenellus multinodus* zone, Pyramid Shale Member, Carrara Formation	-	*Anomalocaris magnabasis?*
LACMIP 12988	Not previously described.	*Nephrolenellus multinodus* zone, Pyramid Shale Member, Carrara Formation	-	*Anomalocaris magnabasis?*

2003 *Anomalocaris pennsylvanica* Resser 1929; Lieberman 2003, p. 684, fig. 7

2003 *Anomalocaris* cf. *saron* Hou, Bergström, and Ahlberg, 1995; Lieberman 2003, p. 686, figs. 8, 9

Derivation of name. From the latin *magna* (= large) and *basis* (= bases), recognising the large bases on the distalmost shaft podomere and first podomere in the distal articulated region.

Holotype. KUMIP 293584, an isolated appendage associated with a partial oral cone, from the Comet Shale Member, Pioche Formation, *Eokochaspis nodosa* zone. Comet Mine, Highland Range, Lincoln County, Nevada (Coordinates: 37.88974, -114.61394).

Paratype. NHMUK IC 1330a, b, part and counterpart, a disarticulated assemblage of paired frontal appendages, flaps and an oral cone, from the Comet Shale Member, Pioche Formation, *Eockochaspis nodosa* zone. Slope above road at mouth of One Wheel Canyon, Highland Range, Lincoln County, Nevada (Coordinates: 37.915833, -114.605278).

Material. 37 additional specimens, paired, isolated, partial, or complete frontal appendages. A complete list is given in Table 2.

Diagnosis. Anomalocaris with frontal appendages consisting of two podomeres in the shaft and 13 podomeres in the distal articulated region; distalmost shaft podomere rectangular and elongate, possessing an enlarged base to the endite with three ventral spines and

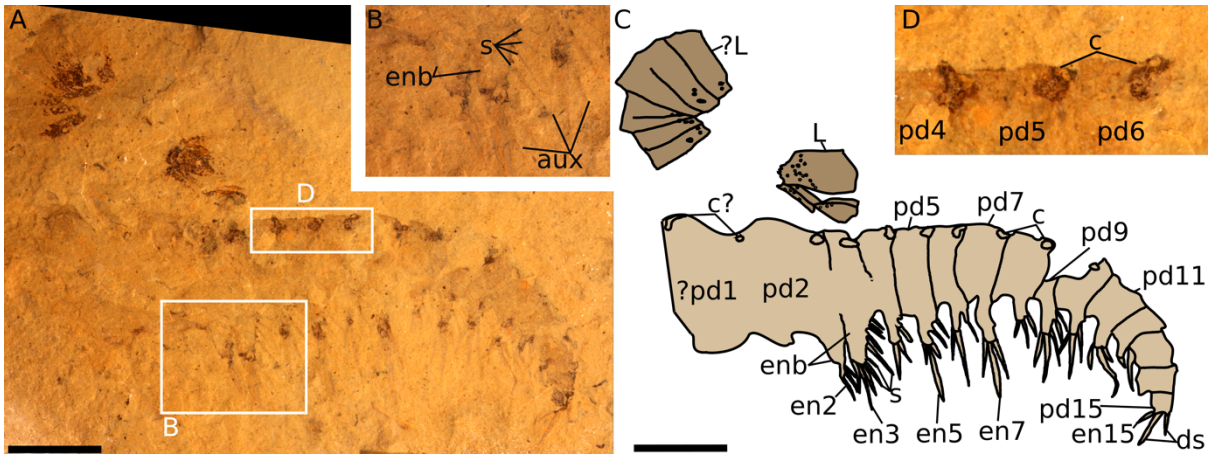

FIG. 6. *Anomalocaris magnabasis* from the *Eokochaspis nodosa* zone, Comet Shale Member, Pioche Formation, Nevada. KUMIP 293584 (holotype). A, Complete appendage with associated partial oral cone. B, close up of ventral endites on podomeres 2 and 3, showing triangular bases, spinules and auxiliary spines. C, interpretative drawing of A. D, close up of circular structures along dorsal side of appendage, interpreted as bases for dorsal spines. Abbreviations: c, circular base; ds, dorsal spine; en, ventral endite; enb, base of the ventral endite; L, large plate of the oral cone; pd, podomere; s, spinule. Scale bars = 10 mm.

multiple distally pointing spinules; second enlarged base to the endite on first podomere in distal articulated region, also with three ventral spines and distally pointing spinules; podomeres in the distal articulated region are separated by triangular flexible arthrodial membrane; proximal nine podomeres in distal articulated region bear pairs of elongate endite bases alternating long/short on odd/even numbered podomeres, each of which has distally directed spinules; one large ventral spine attaches to the base of the ventral endite flanked by two smaller ventral spines; small distally pointing ventral spines attach to the distal ventral margin of pd12-15, which lack enlarged bases; small spines project anteriorly from the distal dorsal margin of pd13-15. Subtriangular flaps bear transverse lines on anterior half. Oral cone consisting of large, intermediate, and small plates.

Description. Lengths of frontal appendages ranging from 22 mm to more than 150 mm. The largest estimated size represented is approximately 175 mm (KUMIP 298500, extrapolated from a partial appendage of 12 podomeres). The appendage has 15 podomeres, including two in the shaft (pd1, 2), which attaches to a distal articulated region of 13 podomeres (pd3-15) at an angle of 180° along the dorsal margin (Fig. 6 - 8), except in KUMIP 294226 in which the angle is 155°. The paratype NHMUK IC 1330 (Fig. 7) shows the elongate (sag.) shaft attaching laterally to the oral cone (described below). Traces of the elongate shaft podomere (pd2) are also present in the holotype KUMIP 293584 (Fig. 6), new specimens from the Carrara Formation (Fig. 8), and KUMIP 293583,294226, 298517, 298522, and 298529 (Fig. 9B, E, F). The holotype, KUMIP 293584, shows the distalmost shaft podomere and the proximal portion of the distal articulated region with ventral endites (pd2-11) most clearly. Podomeres 2 and 3 have a large triangular base of the ventral endites on the ventral surface (enb, Fig. 6) with a large central ventral spine flanked by two auxiliary spines,

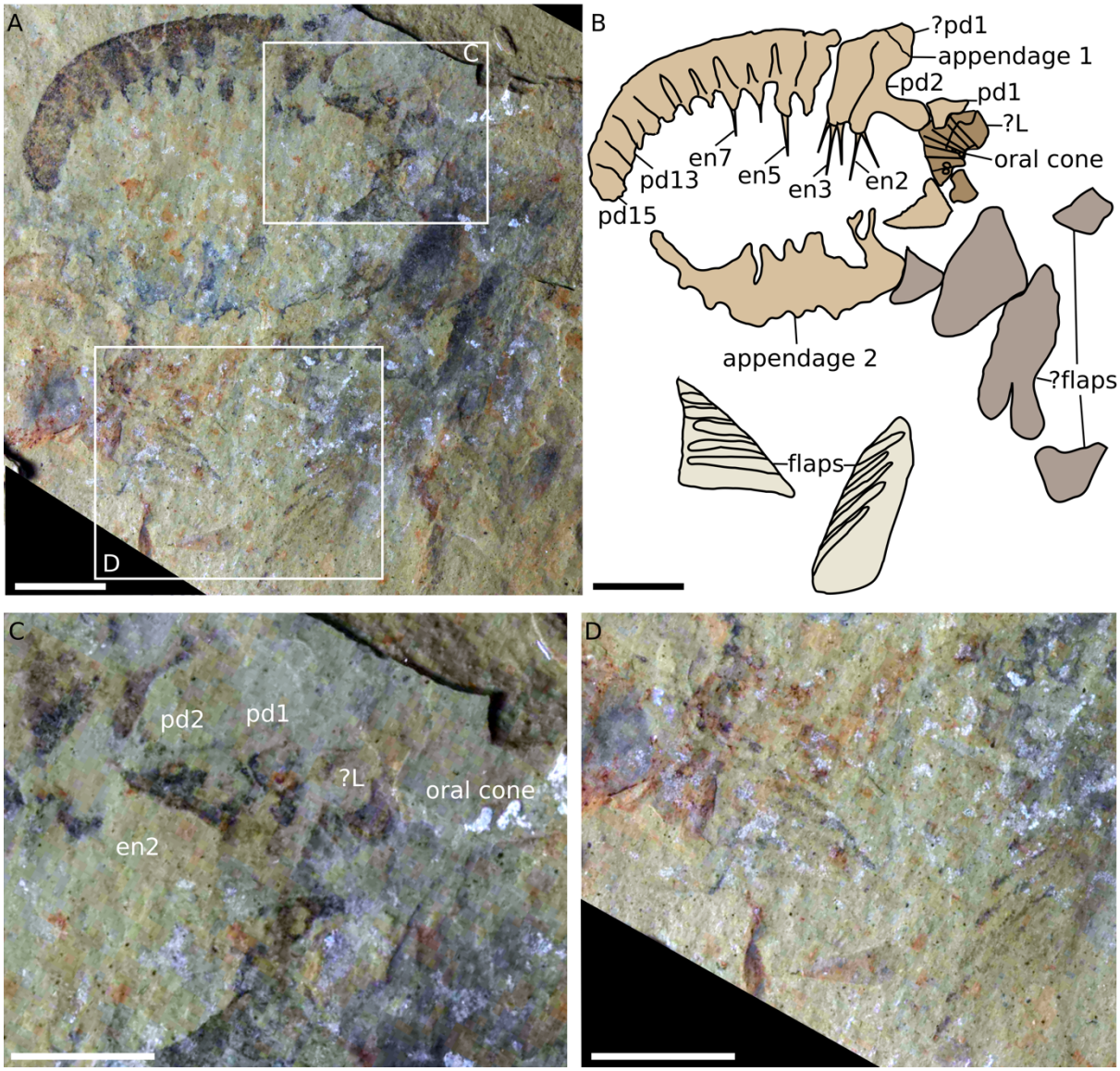

FIG. 7. *Anomalocaris magnabasis* from the *Eokochaspis nodosa* zone, Comet Shale Member, Pioche Formation, Nevada. NHMUK 1330a, b (paratype). A, Disarticulated elements including two frontal appendages, partial oral cone and flaps. B, interpretative sketch of A. C, close up of base of the frontal appendages associated with oral cone. D, close up of well-preserved flaps, showing strengthening rays. Abbreviations: en, ventral endite; ?L, putative large plate of the oral cone; pd, podomere. Scale bars in A, B, D = 10 mm, C = 5 mm.

projecting from its ventral surface. Spinules line the anterior margin (s, Fig. 6). Endite bases are wider (sag.) and taller (trans.) on pd3 than pd2.The base of the ventral endite on pd4-11 is rectangular, and the size of the base of the ventral endite and associated ventral spines reduces distally from pd4-11, alternating long/short on odd/even numbered podomeres (Fig.6, 7, 9B). Seven spinules, thin needle-like projections on the anterior surface of the endite, are present on pd3, with one to two visible on other endite bases. Spinules are oriented ventrally, at an angle approximately 120° from the anterior surface of the endite, and are only preserved in the holotype. Three spines protrude from the base of the ventral endite, a large central spine flanked by two smaller spines, visible in both Dyeran and Delamaran material (aux, Figs. 6B, 10A, B, E, F; Dyeran: KUMIP 293605 and 293609; Delamaran: KUMIP 293522 and 293584 and NHMUK IC 1330). Other material preserves only one central spine and no auxiliary spines (Fig. 11; Combined Metals Member: KUMIP 293572, 293576, 298500 and 298503; Comet Shale Member: KUMIP 298520, 298529 and 307022 and NHMUK IC 1331). In other cases only the base of the ventral endite is preserved (and thus no spines are present), but this base also alternates long/short on odd/even numbered podomeres (e.g. Figs. 6, 8, 9A, E, F). The endites attach to the ventral surface of the podomeres separately, one on the right and one on the left with no evidence for asymmetry in size, as shown by KUMIP 293605 which gives a ventral view (enR, enL, Fig. 10A, B). In most specimens the ventral extensions and spines are approximately perpendicular to the ventral edge of the podomere (e.g. Figs. 6, 7, 8). In some specimens the bases and spines of different podomeres point either distally (white arrows Fig. 9A) or perpendicularly (black arrows, Fig. 9A), in others they all point distally (e.g. Fig. 10A, B, E, F), except in one specimen in which they point both proximally and distally (Fig. 10 C, D). Circular features are present at the distal dorsal surface of each podomere, likely

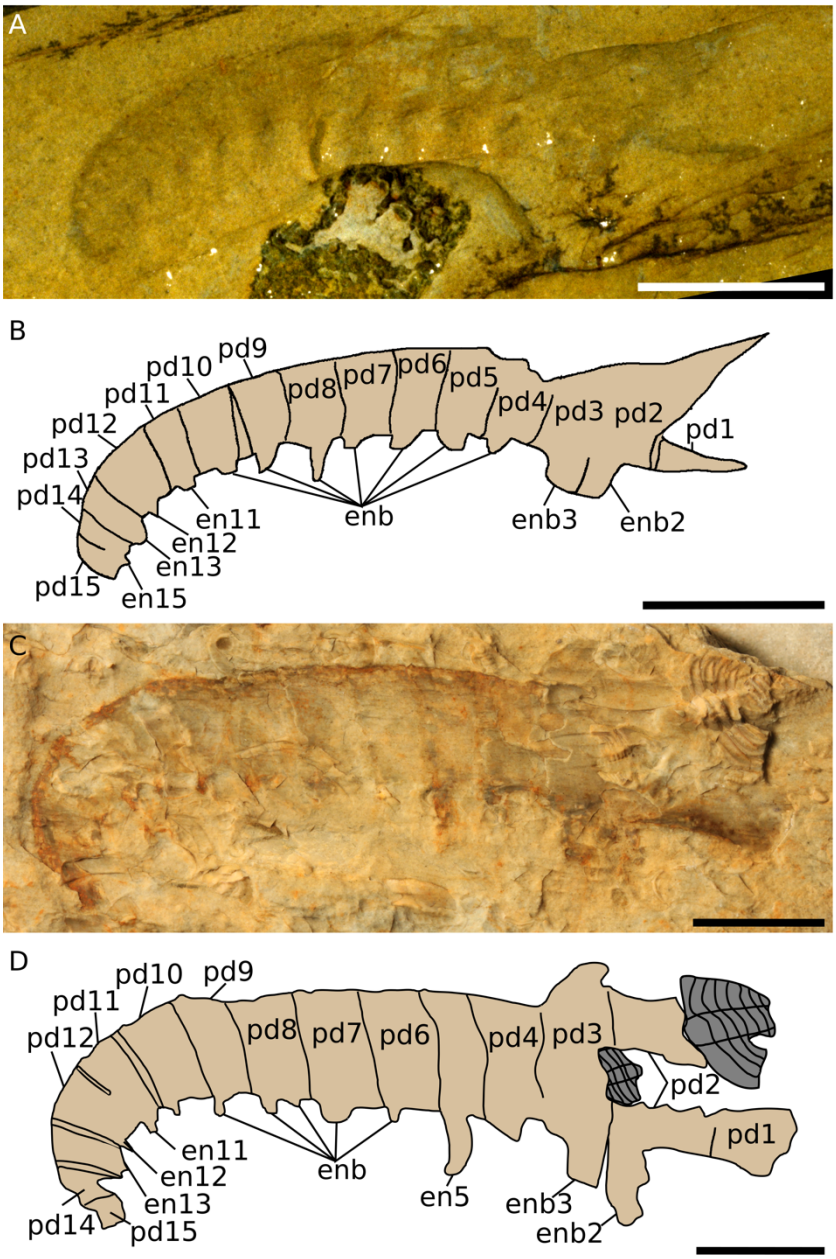

FIG 8. *Anomalocaris magnabasis* from the *Nephrolenellus multinodus* zone, Emigrant Pass, Pyramid Shale Member, Carrara Formation, California. A, TMM NPL 23925, complete appendage (image credit: B. Wilbur). B, interpretative drawing of a. C, LACMIP 12988, complete appendage associated with trilobite. D, interpretative drawing of C. Abbreviations: en, ventral endite; enb, base of the ventral endite; pd, podomere. Scale bars = 10 mm.

attachment points for dorsal spines (c, Fig. 6). The distal-most region (pd12-15) of the appendage does not have the complex ventral endites present on the rest of the appendage. Instead, small ventral spines project from the distal ventral surface of podomeres 12, 13 and 15 (white arrows Fig. 9B-D, en15 Fig. 6), and long and curved dorsal spines which follow the outline of the appendage project from the distal surface of pd13-15 (black arrows Fig. 9B-E, ds Fig. 10C, D).

In smaller specimens the endites are proportionally longer when compared to podomere height than in larger specimens (compare Figs. 10 C and 11 A to Fig. 11 D; this has also been reported in *A. pennsylvanica* - Pates & Daley 2018), and the shape of the enlarged bases on pd2 and pd3 is subrectangular in the smallest specimens (e.g. Fig. 9E, F) but subtriangular in the larger specimens (e.g. Fig. 6).

The oral cone and flaps are preserved in the holotype and paratype. The oral cone is incomplete in both specimens, and is made of plates with nodes present towards the centre. The outer edge of the mouthparts is associated with pd1 of the frontal appendage (Fig. 5C). Larger plates (L and tentatively ?L, Figs. 6, 7) are associated with smaller and intermediate sized plates. Only one large plate is preserved articulated in both the holotype and paratype, and so the angle between two adjacent large plates cannot be measured (Figs. 6, 7). Two disarticulated subtriangular flaps with transverse lines on the anterior half are preserved in the paratype (Fig. 7D). Other material, also flap-shaped, is preserved, although in a different way to the flaps (compare flaps to ?flaps, Fig. 7A, B). In this specimen it seems that the preservation of flaps is analogous to that of the appendages, as there is also differential preservation of the two frontal appendages (compare appendage 1 to appendage 2, Fig. 7A, B).

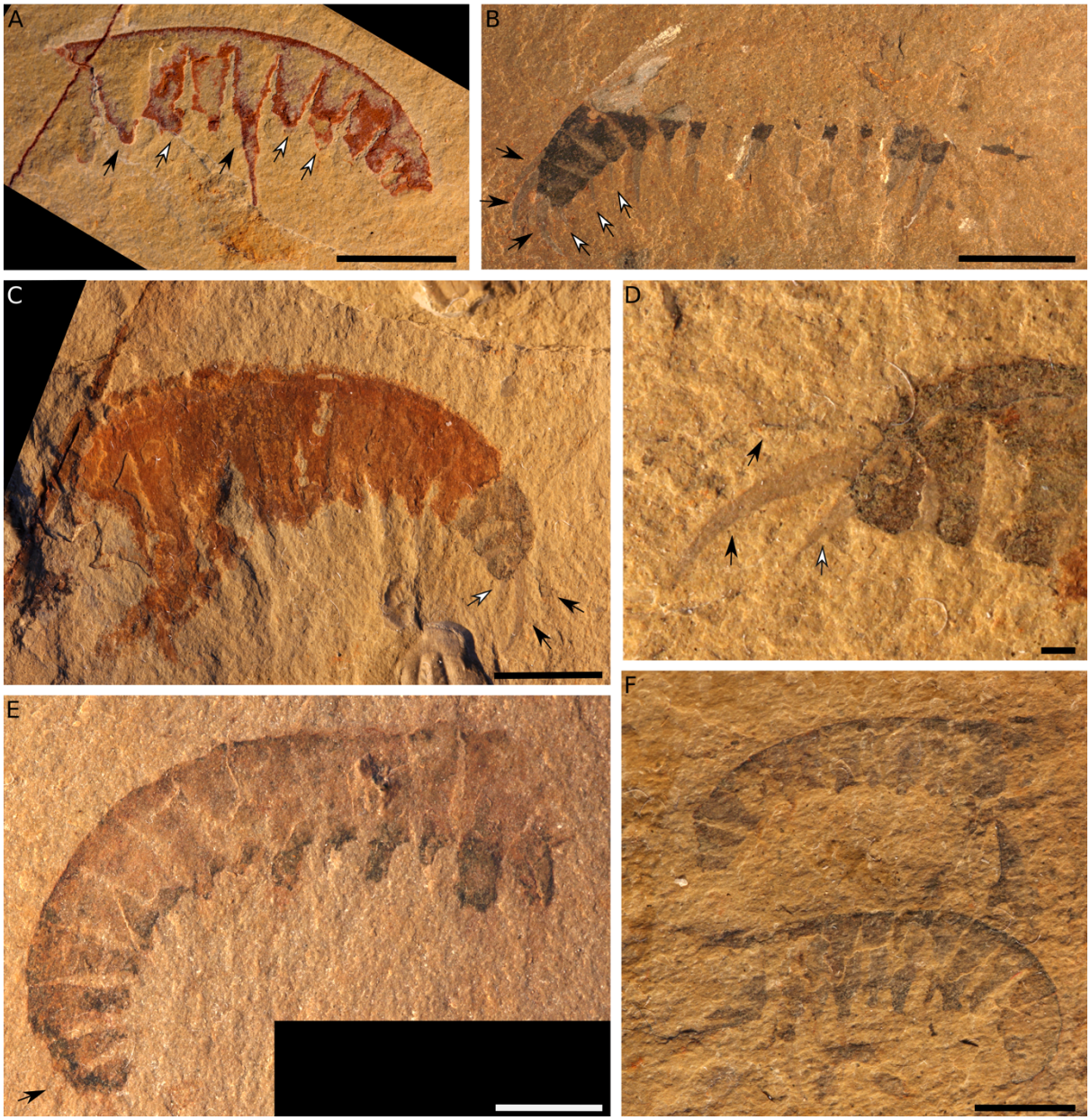

FIG. 9. Caption on next page.

FIG. 9. *Anomalocaris magnabasis* from the Pioche Formation, Nevada, showing a variety of stages of disarticulation. A, KUMIP 293576 from the *Nephrolenellus multinodus* zone, Combined Metals Member, a partial frontal appendage between stages 3 and 4. White arrows indicate distally pointing ventral endite bases, black arrows indicate bases perpendicular to the ventral surface of the frontal appendage. B, KUMIP 298522 from the *Eokochaspis nodosa* zone, Comet Shale Member, a complete appendage in stage 2, white arrows indicate small ventral spines on podomeres 12, 13 and 15, black arrows indicate dorsal spines on podomeres 13, 14 and 15. C, KUMIP 298543, from the *Eokochaspis nodosa* zone, Comet Shale Member, a complete appendage showing poor preservation for majority of proximal region, but well preserved dorsal spines at distal tip, stage 3. White arrow indicates ventral spine on podomere 15, black arrows indicate dorsal spines on podomeres 14 and 15. D, Counterpart to C, close up on distal podomeres of frontal appendage, arrows indicate same as for C. E, KUMIP 293571, from the *Nephrolenellus multinodus* zone, Combined Metals Member, a complete frontal appendage in stage 3, black arrow indicates dorsal spine on podomere 14. F, KUMIP 293583, from the *Eokochaspis nodosa* zone, Comet Shale Member, a pair of complete frontal appendages in stage 4. Scale bars in A, B, C = 10 mm, D = 1 mm, E, F = 5 mm.

Remarks. Here we treat all the specimens from the Pioche as a new *Anomalocaris* species, with similarities to *A. saron*, *A. pennsylvanica* and *A. canadensis* (Table 3; Figs. 1, 12). The presence of enlarged endite bases on the distalmost shaft podomere and first podomere in the distal articulated region (pd2 and pd3) distinguishes this species from all other *Anomalocaris* taxa. This feature can be seen even in poorly preserved specimens (e.g. Fig. 9E, F; see taphonomy and disarticulation section below). Some Dyeran specimens are only tentatively assigned to this new species (Fig. 11B-E; KUMIP 293572, 293576, 298500, 298501 and 298503; Table 2) as they do not preserve auxiliary spines, the shaft, the prominent endite, spinules on the endite, or pd2 and pd3, and so cannot confidently be differentiated from *Anomalocaris pennsylvanica*, to which they were originally assigned (Lieberman 2003). The assignment of all the material to one species, however, is preferred as some Delamaran specimens do not preserve auxiliary spines, yet do preserve a single ventral spine (e.g. Fig. 10C, D; KUMIP 307022) and KUMIP 298529 also preserves the two enlarged bases on pd2 and pd3, but only a single ventral spine (Fig. 11A). Thus, we hypothesize that a taphonomic series or gradient accounts for all the variation among specimens (see taphonomy and disarticulation section below). Irrespective of this hypothesis and the possibility that a few specimens might still be treated as *A. pennsylvanica*, it is clear that *A. magnabasis* represents a new and distinct species. It is also worth noting that in general across many Cambrian deposits the preservation of auxiliary spines is highly variable, likely because of taphonomic factors. The condition or even presence of auxiliary spines may not be the best characters to use for identifying and defining anomalocaridid species. For instance, in Dyeran material auxiliary spines are small and not preserved on every podomere (aux, Fig. 10A, B, E, F). This is similar to the condition of auxiliary spines on some specimens of *A. canadensis* (e.g. Daley & Edgecombe 2014 fig.

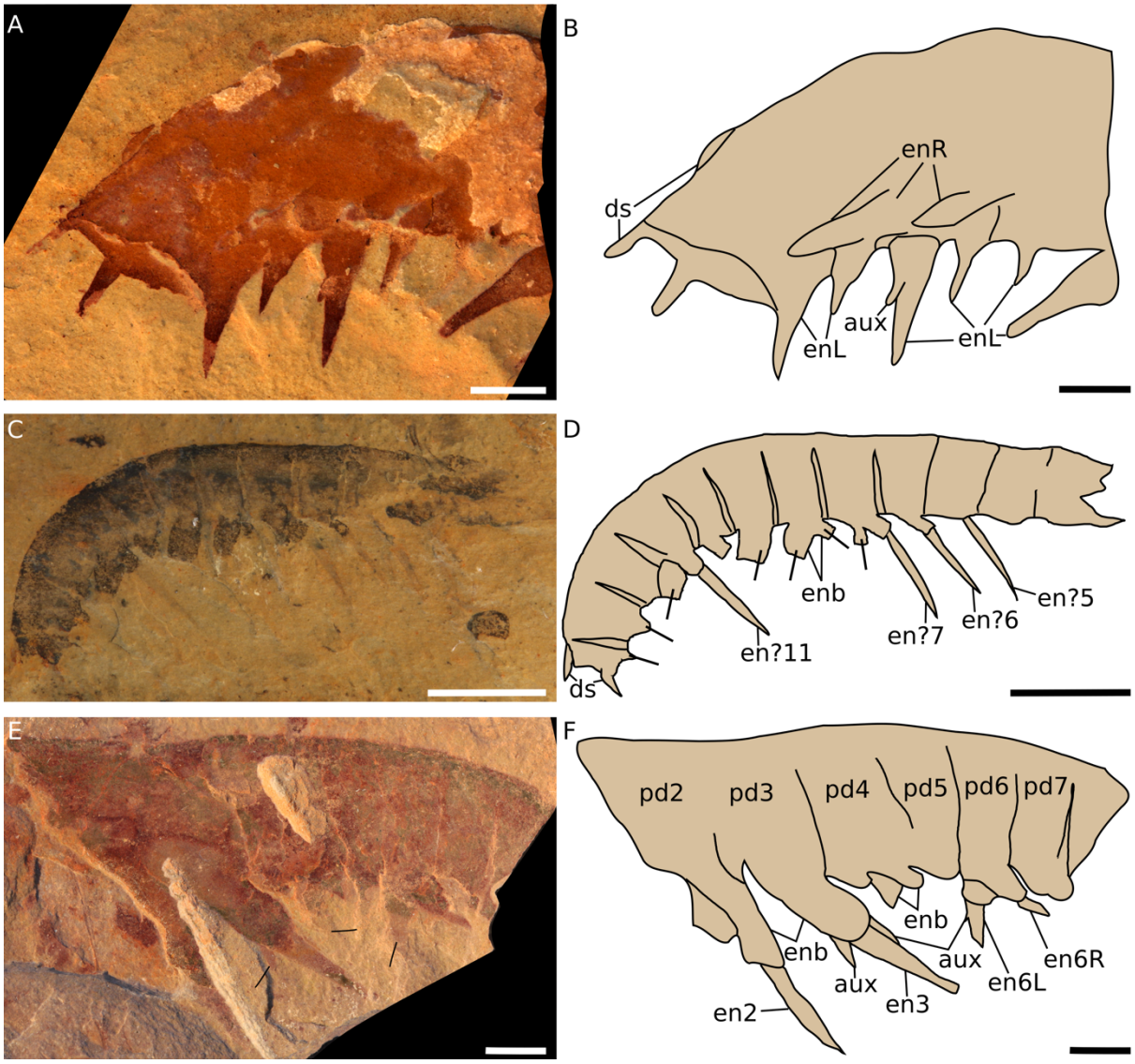

FIG. 10. Caption on next page.

FIG. 10. *Anomalocaris magnabasis* from the Pioche Formation, Nevada, showing bases of the ventral endite at a variety of angles. A KUMIP 293605, from the *Nephrolenellus multinodus* zone, Combined Metals Member, a partial frontal appendage preserved in ventro-lateral view. Arrow indicates auxiliary spine on left ventral endite. B, interpretative drawing of A. C, KUMIP 307022, from the *Eokochaspis nodosa* zone, Comet Shale Member. A partial frontal appendage. D, interpretative drawing of C, arrows indicate direction that ventral endite bases are pointing. E, KUMIP 293609, from the *Nephrolenellus multinodus* zone, Combined Metals Member, a partial frontal appendage. F, interpretative drawing of E. Abbreviations: aux, auxiliary spine; ds, dorsal spine; en, endite; enb, base of the ventral endite; enL, left ventral endite; enR, right ventral endite; pd, podomere. Scale bars = 5 mm.

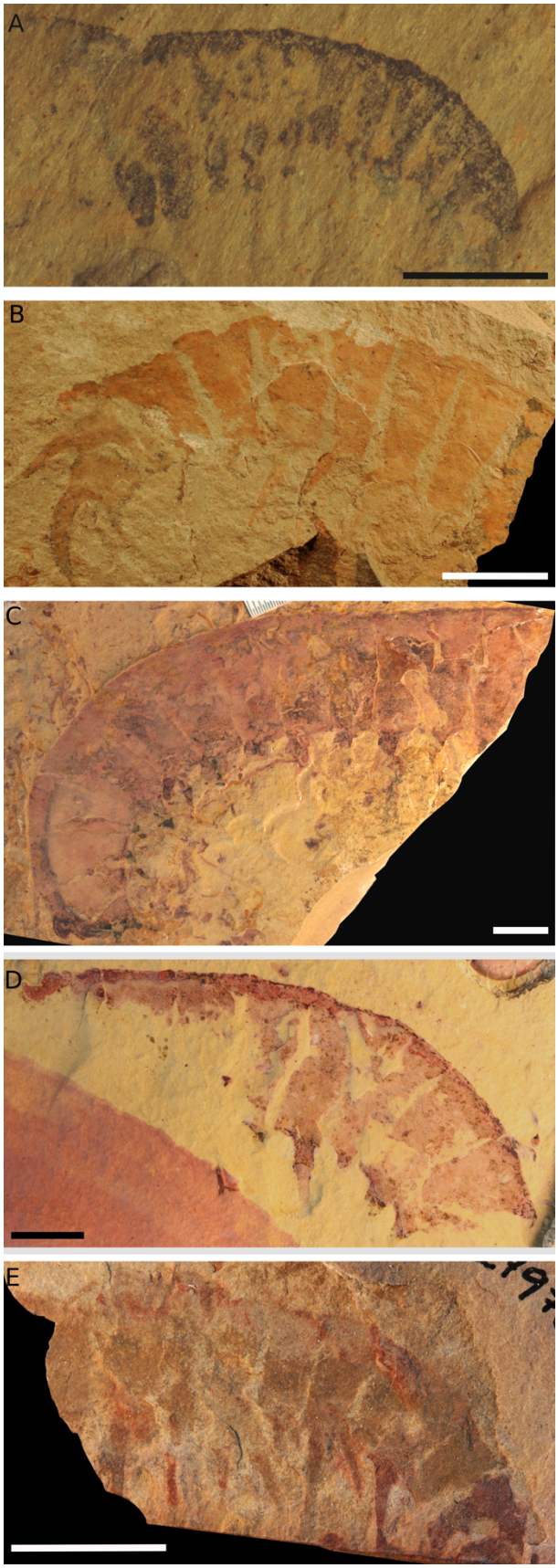

FIG. 11. *Anomalocaris magnabasis* from the Pioche Formation, Nevada, preserved at stage 3 (no auxiliary spines). A, KUMIP 298529, from the *Eokochaspis nodosa* zone, Comet Shale Member, a complete frontal appendage. B, KUMIP 293572, from the *Nephrolenellus multinodus* zone, Combined Metals Member, a partial frontal appendage. C, KUMIP 298500, from the *Nephrolenellus multinodus* zone, Combined Metals Member, a partial frontal appendage. D, KUMIP 298501, from the *Nephrolenellus multinodus* zone, Combined Metals Member, a partial frontal appendage. E, KUMIP 298503, from the *Nephrolenellus multinodus* zone, Combined Metals Member, a partial frontal appendage. Scale bars in A = 5 mm, B, C, D, E = 10 mm.

Table 3. Differences between the frontal appendages of select *Anomalocaris* taxa.

	Anomalocaris saron	*Anomalocaris magnabasis*	*Anomalocaris canadensis*	*Anomalocaris pennsylvanica*
v.e. on distal shaft pd	Simple spine only	Triangular base, three ventral spines, spinules present	Simple spine only	Elongate spine only
Base of v.e. on 1st pd in d.a.r.	Triangular	Triangular	Rectangular	Rectangular
#ventral spines on 1st pd in d.a.r.	3	3	3	1
Spinules on pd3	Yes	Yes	No	No
Length of v.e. bases in d.a.r.	Long	Intermediate	Short	Intermediate
Spinules on v.e. bases	Yes	Yes	No	No
v.e. morphology on pd12-15	Same as rest of d.a.r. but shorter	Simple spine, at distal margin	Simple spine, at distal margin	Same as rest of d.a.r. but shorter

Abbreviations: d.a.r., distal articulated region; pd, podomere; v.e., ventral endite.

12.3). Ultimately, the apparent difference in the presence and condition of the auxiliary spines, the endite and the spinules could represent a true (rather than taphonomic) difference between the material only tentatively assigned to *A. magnabasis*, but at this time we treat these as taphonomic variants of the same form, a single new species, as specimens from both the Dyeran and Delamaran have the unique character of the enlarged bases on the pd2 and pd3, and since no other anomalocaridids (including *bona fide A. pennsylvanica*) bear this character.

A valuable aspect of the material from the southern Great Basin is that it shows that the ventral endite base is distinct from the three spines that project from it. When present, the point at which the three spines converge is preserved in specimens with only one ventral spine (e.g. Fig. 9A), but for the most part the ventral spines are preserved in a different colouration (e.g. Figs. 6, 7, 9B, 10C, E). When it is not preserved this is because only the base of the ventral endite is visible (e.g. Figs. 8, 9 E, F). This merits consideration relative to the ventral spines on the ventral endites of *A. canadensis* and *A. saron*, which clearly branch at a point. Further, in rare cases a difference in preservation can be seen between the base and the spines (e.g. Daley & Edgecombe 2014, fig. 13; Cong et al. 2018, fig. 5E, F). This suggests that a ventral endite base is common across *Anomalocaris* species, with the longest bases present in *A. saron* and the shortest in *A. canadensis* (Table 3).

The large central spine and two auxiliary spines are distinct from the spinules, which are present on the distally facing edge of the base of the endites. This is common across *Anomalocaris* species that possess spinules (*A. saron*, *Anomalocaris* sp. from the Balang Formation, *A. magnabasis*) as well as other genera of radiodonts, such as *Laminacaris* (Liu 2013; Guo et al. 2018).

All *Anomalocaris* species have 13 podomeres in the distal articulated region, with an enlarged ventral endite on the first podomere in the distal articulated region and alternating long/short endites on odd/even numbered podomeres thereafter. The ventral endite on pd2 in the new species is similar to the ventral endite on pd3, but smaller. This distinguishes *A. magnabasis* from all other *Anomalocaris* species (e.g. *A. saron*, *A. canadensis*, and *A. pennsylvanica* bear a simple spine on the distalmost shaft podomere –black arrows, Fig. 12; Table 3). The ventral endite on pd3 in *A. saron* is very similar to that of this new species (with its triangular shape, distally pointing spinules and three ventral spines - one large central spine flanked by two smaller auxiliary spines). There are quite a few similarities between *A. saron* and *A. magnabasis* (Lieberman 2003) as each has long rectangular projections with distally pointing spinules bearing three ventral spines, as well as circular features at the dorsal distal edge of each of the podomeres (these are interpreted as attachment points for dorsal spines). The Great Basin taxon, however, differs from *A. saron* in the distalmost four podomeres, on which it has simple ventral spines (on pd12, 13 and 15). By contrast, in *A. saron* the ventral endites maintain the same morphology in the distal articulated region of the appendage (Figs. 1D, 12A; Table 3). The differences between *A. magnabasis* and *A. canadensis* (Figs. 1F, 12B) are more numerous. While each has reduced ventral spines on the distal four podomeres, *A. canadensis* differs in the condition of the rest of the distal articulated region, as there are no spinules on the base of the ventral endite, and no enlarged triangular ventral endite base on the proximalmost podomere of the distal articulated region (Table 3).

A partial appendage of *Anomalocaris* sp. from the Balang Formation (Cambrian Series 2, Stage 4), Hunan Province, China (Liu 2013, fig. 2) also bears similarity to *A. magnabasis*. The Balang specimen preserves two shaft podomeres with enlarged bases, and

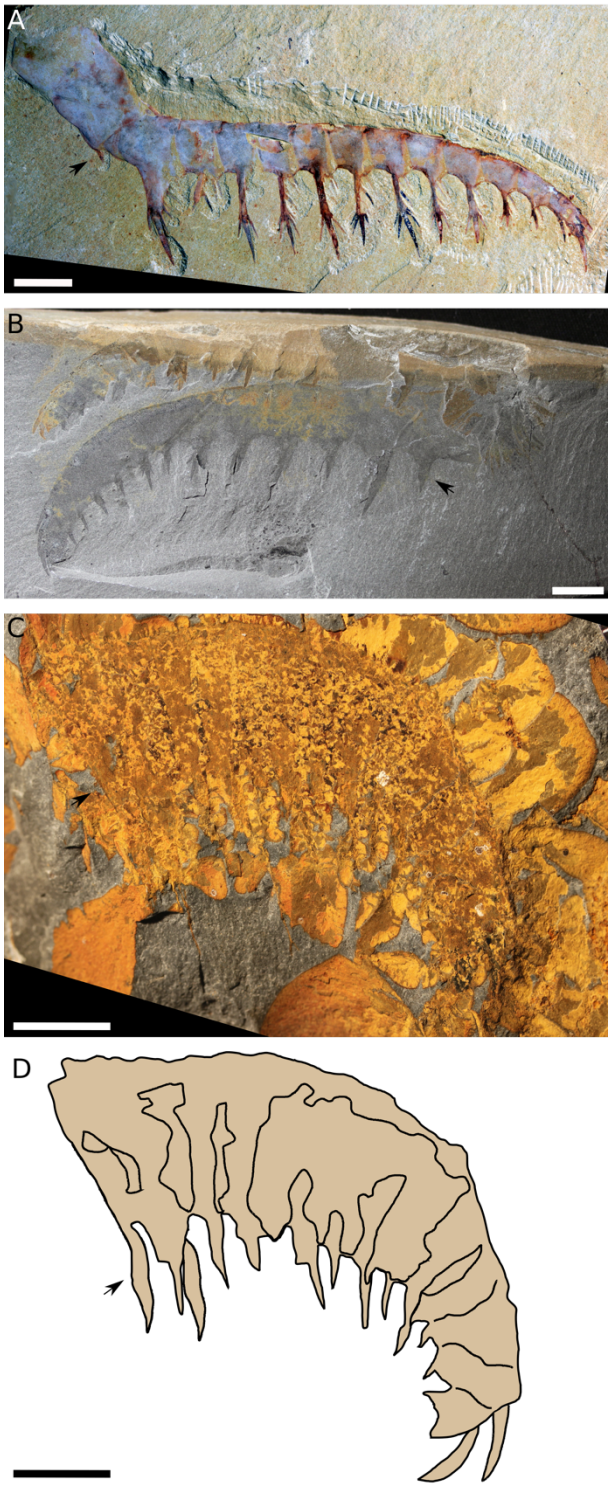

FIG. 12. *Anomalocaris* species with shaft endite indicated with black arrow. A, YKLP 13459, *Anomalocaris saron*. B, ROM 62543, *Anomalocaris canadensis*. C, YPM 10425, *Anomalocaris pennsylvanica*. D, line drawing of C redrawn from Pates & Daley, 2018 fig 3d. Scale bars = 10 mm.

six podomeres in the distal articulated region. The ventral endites in the distal articulated region of the specimen from the Balang Formation bear numerous spinules alongside a central large spine and a pair of auxiliary spines, similar to the condition in *A. saron* and *A. magnabasis*, but the bases to the endites on the distalmost shaft podomere and first podomere in the distal articulated region are not as robust as in *A. magnabasis*. In the partial appendage from the Balang Formation each endite bears two auxiliary spines and a number of distally pointing spinules, and each endite extends from the midpoint of the podomere except in the distalmost shaft podomere. The Balang Formation specimen also differs in the shape of the shaft podomeres (these are taller and thinner than those in *A. magnabasis*), the size of the bases to the endites, and the presence of a reduced spine on the ventral surface of the first shaft podomere. In addition, a small, simple ventral endite is preserved on the proximal shaft podomere in this taxon, and this is not found in *A. magnabasis*, although this part of the appendage is rarely well preserved

The presence of transverse lines on the anterior half of the well preserved flaps further distinguishes this species from *Anomalocaris canadensis*, which does not have transverse lines (Daley & Edgecombe 2014). Transverse lines are also present on the anterior half of the flap in *Peytoia, Amplectobelua, Anomalocaris saron*, and likely *Anomalocaris briggsi* (Hou et al. 1995; Daley et al. 2013a, b; Cong et al. 2017), and along the whole width of the flap in *Hurdia* (Daley et al. 2009; 2013a). No flaps are known in *A. pennsylvanica*.

The oral cone has large, intermediate, and small plates, but the arrangement (triradial, tetraradial, or another organisation) cannot be confirmed owing to the disarticulated nature of the material. This is consistent with *Anomalocaris* (many sizes of plates), and dissimilar to hurdiids (large and small plates only), amplectobeluids (uncertain

arrangement of smooth and tuberculate plates, gnathobase-like-structures) or other radiodonts such as *Lyrarapax* Cong et al. 2014 (tetraradial or wrinkled opening) (Daley & Bergström 2012; Cong et al. 2014, 2017, 2018; Liu et al. 2018).

Anomalocaris magnabasis can be differentiated from *Ramskoeldia* from the Latham Shale based on the condition of the base of the ventral endites on pd2 and pd3 as in the latter the ventral endite on the equivalent distalmost shaft podomere is a reduced spine or absent. Further, in *A. magnabasis* the ventral endites decrease in length along the appendage (alternating long/short on odd/even numbered podomeres), in contrast to *Ramskoeldia*, in which the endite on pd8 is longer than pd6. We refer the material from the Carrara Formation to *A. magnabasis* as all specimens preserve a large base to the ventral endite on pd2 and pd3, all have the same number of podomeres (where the full appendage is preserved) and all bear small ventral spines on podomeres 12, 13 and 15 (en12, en13, en15, Fig. 8). Potential comparisons of *A. magnabasis* from the Carrara Formation could be made with *Laminacaris chimera* (Fig. 1G) from the Chengjiang biota, which also preserves 13 podomeres in the distal articulated region, with two podomeres in the shaft, and enlarged ventral endites on both the distalmost point of the shaft and the first podomere in the distal articulated region. *Laminacaris* however differs from *A. magnabasis* in that it has five dorsal spines, a different morphology of the ventral endites, and an enlarged ventral endite on the first podomere in the distal articulated region that is blade-like and curves distally. Further, *Laminacaris* lacks the enlarged base on the ventral endite that is found in *A. magnabasis* and the ventral endite on the shaft is not a smaller version of that on pd3, but is instead a simple blade-like endite with one distally pointing small auxiliary spine, again without a large base.

Occurrence. Nephrolenellus multinodus zone, Cambrian Series 2, Stage 4: Nopah Range, on the north side of Emigrant Pass, SE 1/4 of NW 1/4 of Section 25, T21N, R8E, Pyramid Shale Member, Carrara Formation, Inyo County, California (LACMIP locality 17162) and nearby locality (53.64'N, 4.62'W); Ruin Wash, 17 km west of Panaca, west side of Chief Range, NW 1/4, SW 1/4, Sec 15, T 2S, R65E, Combined Metals Member, Pioche Formation, Nevada; 0.5 miles east of the Ruin Wash locality (YPM locality D4330), Combined Metals Member, Pioche Formation, Nevada; Klondike Gap NW1/4 SW1/4 sec. 15 R65E T2S, Panaca, west side of Chief Range, Combined Metals Member, Pioche Formation, Nevada. *Eokochaspis nodosa* zone, Cambrian Series 2, Stage 4: Comet Mine, Highland Range, 28 km NW of Panaca, Highland Peak 7.5 Quad, Center W line NW1/4 Section 5 R66E T1S, Comet Shale Member, Pioche Formation, Nevada; Mouth of One Wheel Canyon, Highland Range, east edge of NW 1/4, SW 1/4, Sec 29, T1N, R66E, elevation 2100 m, Comet Shale Member, Pioche Formation, Nevada; 0.3 kms south of Peaslee Canyon, Highland Range, SW1/4, SW 1/4 Sec 32, T1N, R66E road cut, elevation 2130 m, Comet Shale Member, Pioche Formation, Nevada.

Family HURDIIDAE Lerosey-Aubril & Pates 2018

Genus HURDIA Walcott, 1912

Type species. Hurdia victoria Walcott, 1912

Hurdia sp.

Fig. 13

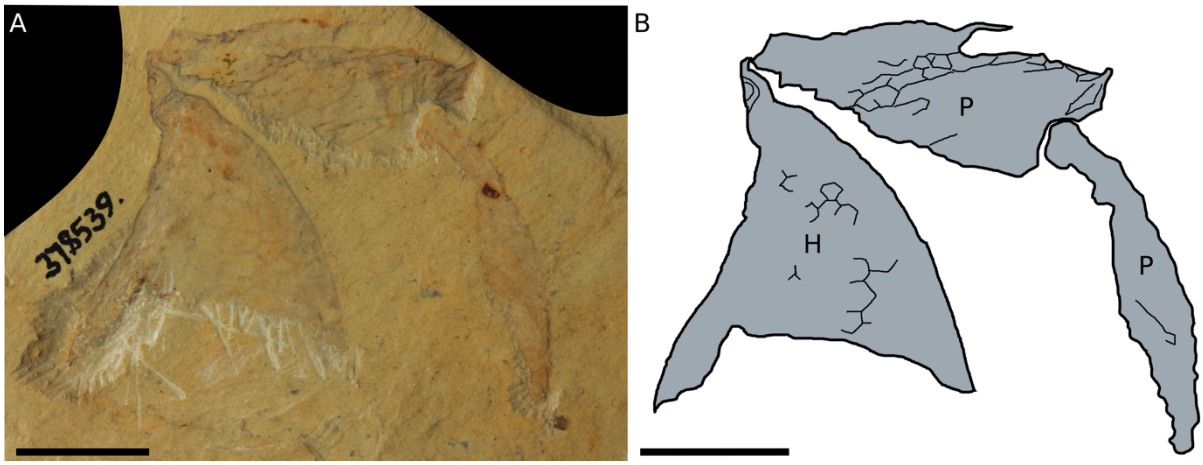

FIG. 13. *Hurdia* carapace from the *Nephrolenellus multinodus* zone, Combined Metals Member Shale Member, Pioche Formation, Nevada. A, KUMIP 378539. B, interpretative drawing of A. Abbreviations: H, H-element; P, P-element. Scale bars = 10 mm.

Material. KUMIP 378539, a partial tripartite frontal carapace.

Description. The single *Hurdia* specimen from the Pioche Formation comprises a partial central dorsal carapace element (H-element) in dorsal view and two lateral carapace elements (P-elements) preserved oblique to the sediment. The central element (H, Fig. 13) measures 28 mm from the strengthened tip to the incomplete edge at its furthest point, and 22 mm wide at its widest point. The lateral elements (P, Fig. 13) are both 24 mm in length. The central element articulates with one of the lateral elements, with the strengthened pointed tip of the H-element adjacent to the beak of the P-element. The other P-element is disarticulated and positioned slightly behind the other two elements, overlying the posterior region of the articulated P-element. A reticulation pattern of poorly defined polygons preserved in a darkened colouration is present on both H and P-elements. The area of the largest reticulation of the H-element is 4.8 mm^2 and the largest for the less-oblique P-element is 2.9 mm^2.

Remarks. Although other members of Radiodonta have lateral and central carapace elements (e.g. *Amplectobelua*, *Aegirocassis* Van Roy et al. 2015, *Pahvantia* Robison & Richards 1981), the presence of a reticulation pattern is currently unique to *Hurdia* (Daley et al. 2013a). The area of the largest polygon in the reticulation pattern is comparable to those measured in *Hurdia* from the Burgess Shale and Great Basin (Daley et al. 2013a; Pates et al. 2018b). The articulation of the H-element and P-elements at the anterior margin, as well as the strengthened tip (H-element) and beak (P-element) are also indicative of *Hurdia* carapace elements. This is the oldest *Hurdia* yet identified from Laurentia, with the oldest worldwide known from the Cambrian Series 2 Stage 3, a single putative P-element from the

Shuijingtuo Formation in China (Cui & Huo 1990; Daley et al. 2013a). This new specimen cannot be identified to the species level as the H-element is incomplete and so the height:width ratio (which is used to distinguish *H. victoria* from *H. triangulata* Walcott 1912) cannot be calculated.

Occurrence. Ruin Wash, 17 km west of Panaca, west side of Chief Range, Locality 4 (Palmer 1998, fig. 1). *Nephrolenellus multinodus* zone, Combined Metals Member, Pioche Formation, Nevada, USA.

RESULTS

Taphonomy and disarticulation

Anomalocaris magnabasis material from the Pioche and Carrara Formations is preserved in a number of stages of disarticulation (e.g. Fig. 9). Indeed, the large number of frontal appendages shows a clear sequence of disarticulation that can be separated into five stages, numbered 1-5 from less to more disarticulated (Table 4; Fig. 14). Note that breaks between podomeres, resulting in partial appendages, can occur at any stage. Crucially for the identification of this species, the enlarged bases on the distalmost shaft podomere and first podomere in the distal articulated region can be seen in any specimens that preserve these two podomeres. This has utility when identifying poorly preserved material. Furthermore, these taphonomic stages are not restricted to this species, and could also be applied to *A. canadensis* and *A. saron*. As these taxa are known from deposits that yield more abundant radiodont material than the localities in the Southern Great Basin the sheer abundance of specimens means that the majority of figured specimens are preserved in what we refer to in Table 4 as stage 1 or 2, although one *A. canadensis* in our stage 4 has previously been

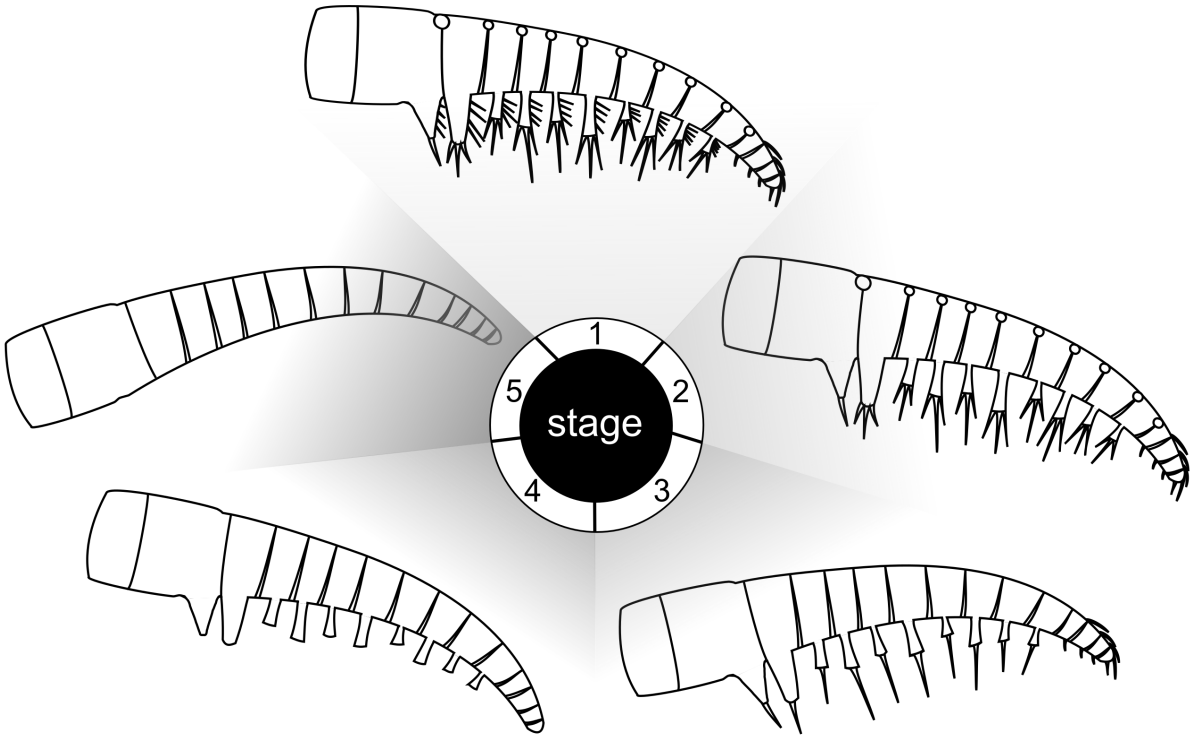

FIG. 14. Preservation stages of Table 4 illustrated diagrammatically for *Anomalocaris magnabasis*.

Table 4. Stages of disarticulation of Pioche Formation *Anomalocaris* specimens from this study

	Spinules	Auxiliary spines	Long ventral blade	Dorsal and terminal spines	Base of ventral endites	Podomeres	Dyeran specimens	Delamaran specimens
Stage 1	X	X	X	X	X	X	None	KUMIP 293584 (Fig. 6)
Stage 2		X	X	X	X	X	KUMIP 293605 (Fig. 10A), 293509 (Fig. 10E)	NHMUK IC 1330 (Fig. 7); KUMIP 298522 (Fig. 9B)
Stage 3			X	?	X	X	KUMIP 293572 (Fig. 11B), 293576 (Fig. 9A), 298500 (Fig. 11C), 298501 (Fig. 11D), 298503 (Fig. 11E)	NHMUK IC 1331; KUMIP 298520, 298529 (Fig. 11A), 298530, 298543 (Fig. 9C ,D), 307022 (Fig. 10 C)
Stage 4					X	X	KUMIP 293571 (Fig. 9E), 293575, 298512, 298514, 298532; YPM 163103	KUMIP 293583 (Fig. 9F), 293585, 293586, 294226/7
Stage 5						X	KUMIP 293574, 293632/573, 298502, 298515, 298516	None

X indicates the presence of a feature in the specimen. Dyeran and Delamaran specimens listed from Pioche Formation only.

figured (Daley & Edgecombe 2014, fig. 10.5). A lack of spines in some specimens was recognised by Briggs (1979) in *A. canadensis* material, and was one factor which led to the synonymy of *A. gigantea* (which lacked spines in the part of the holotype) with *A. canadensis*.

The majority of frontal appendage specimens from the Pioche Formation are between stages 3 and 4, in which features such as the spinules, the small ventral spines in the distal region, and all the dorsal spines and ventral spines are rarely preserved. The only stage 1 appendage is Delamaran in age, and no Delamaran appendages are referred to stage 5. By contrast, all stage 5 appendages are Dyeran (Table 4).

NHMUK IC 1330 and KUMIP 298543 show that very localised factors can also affect the fidelity of preservation of frontal appendages and other body parts, even within a single specimen. For instance, one appendage of NHMUK IC 1330 (appendage 1, Fig. 7) shows podomere boundaries with ventral endites whereas the other can only be recognised as a frontal appendage based on the outline, size, and proximal shaft attaching to oral cone (appendage 2, Fig. 7). The flaps of this specimen show concordant patterns to the appendage, where one set are well preserved and the others are only putatively recognisable (Fig. 7). Another specimen showing this is KUMIP 298543 (Fig. 9C, D) where the distal portion of the appendage is well preserved, with terminal and dorsal spines visible alongside podomere boundaries, but the proximal portion of the appendage is poorly preserved with little or no details visible. This suggests that important aspects of differential preservation of these anomalocaridid specimens relate to the initial burial and redox conditions surrounding carcasses.

DISCUSSION

Taphonomy and Disarticulation

In general, the younger material, from the Pioche Formation in the *Eokochaspis nodosa* zone, is preserved better (represents a lower-numbered taphonomic stage) than the older material from the *Nephrolenellus* zone (Table 4). An alternate hypothesis is that these differences instead represent taxonomic differences between the elements present in these time intervals. In particular, the features preserved at stage 1 for *Anomalocaris* from the *Eokochaspis nodosa* zone are never present in *Anomalocaris* from the *Nephrolenellus multinodus* zone. Partial specimens of *A. magnabasis* which do not preserve pd2 or pd3 (and hence the large bases to the endites on these podomeres), and in stage 3 or below (and so do not preserve auxiliary spines or spinules) are therefore not distinguishable from *A. pennsylvanica* (compare Fig. 1H to Fig. 14), since spinules and auxiliary spines have not been described from this species (Briggs 1979; Pates & Daley 2018).

It has previously been suggested that what has been called *Anomalocaris pennsylvanica* might actually represent a slightly disarticulated or decayed *A. canadensis* (e.g. Briggs 1979; Lieberman 2003; Daley & Peel 2010), and such specimens would be in stage 3 or lower in this new scheme. Other morphological differences in the shaft ventral endite and the lack of reduced ventral endites at the distal end of the appendage differentiate these two taxa (Table 3; Figs. 1H, 12 C, D; Pates & Daley 2018). In this study, the specimens with only one spine (no auxiliary spines) are assigned to *Anomalocaris magnabasis* rather than *Anomalocaris pennsylvanica*. This was done on the basis of the identification of the large proximal bases on the shaft podomere and first podomere in the distal articulated region in certain specimens plus the identification of a clear taphonomic sequence for appendage specimens from the Pioche. We note that for partial specimens not preserving pd2 or pd3 and in stage 3 or lower no characters remain to distinguish these

specimens confidently from *A. pennsylvanica*. However, these are tentatively treated as *A. magnabasis* owing to the geographic and temporal co-occurrence with known *A. magnabasis,* and as KUMIP 298529 (Fig. 11A) preserves both large bases but no auxiliary spines (stage 3). This highlights the problems associated with identifying *Anomalocaris* appendages to the species level where preservation is poor and does not allow the presence/absence of auxiliary spines to be confidently assessed. In these situations, without other diagnostic characters (such as the enlarged bases in this case) it may not be possible to identify such material confidently beyond the genus level, in the absence of co-occurring better preserved material.

The fidelity of fossilisation in BSTs is affected by the decay, transport, burial history and chemistry of the process (Allison 1986; Gaines 2014; Bath Enright et al. 2018). In the small number of Pioche Formation specimens preserved at stages 1 or 2 all the endites are approximately parallel. It is only in specimens at stages 3 and 4 that the endites and their bases point in a variety of orientations. This type of preservation, with the endites preserved at a number of angles relative to each other, is not known in published *Anomalocaris* material from other sites. This could indicate that the poorer preservation of specimens (those classified at higher numbered stages) is related to the amount of decay and transport before fossilisation. Ultimately, it appears that the Pioche Formation specimens collected from the *Eokochaspis nodosa* zone have undergone less decay and/or transport than those from the *Nephrolenellus multinodus* zone. The preservation of specimens may also be influenced by the angle of preservation in the sediment. If specimens were preserved at a high angle relative to bedding, only the podomeres and perhaps bases of the endites would be visible after splitting the rock, and thus specimens would be at taphonomic stage 4 or 5.

When considering all sites, not just the Pioche Formation levels, the number of variables that might influence preservation fidelity greatly increases. The position in the basin is not constant, with the Latham Shale more proximal than the Pioche Formation, itself more proximal than the Carrara Formation (Fig. 3.). This in turn may have influenced the depositional regime and burial times, although it should be noted that the soft-bodied material from the Latham Shale was deposited in a distal fine-grained part of the unit (Gaines & Droser 2002), and the relative rapidity of burial at these three sites is not yet known.

Anomalocaris endites and spinules

Frontal appendages were used in feeding, and the differing morphology of radiodont appendages has been used to show the variety of feeding modes present in this group of large Cambrian predators. Appendages with fine spines or setae may indicate a filter-feeding habit, represented by *Tamisiocaris borealis* Daley & Peel 2010, *Pahvantia hastata* Robison & Richards 1981 and *Aegirocassis benmoulae* Van Roy, Daley & Briggs 2015 (Vinther et al. 2014; Van Roy et al. 2015; Lerosey-Aubril & Pates 2018). Robust appendages with thick spines and less prominent arthrodial membrane, as found in *Hurdia* and *Peytoia*, have been interpreted to indicate a sediment-sifting mode, (Daley et al. 2009; 2013a). Other taxa, such as *Amplectobelua* and *Lyrarapax*, with a hypertrophied endite on the proximal podomere in the distal articulated region and often thickened dorsal spines, have been interpreted as grasping and crushing predators. *Anomalocaris*, with its triangular arthrodial membranes, high number of podomeres and endites that alternate long/short, has been interpreted as a grasping raptorial predator, which could have used the spines at the end of its endites to slice prey.

There are differences in the frontal appendages of *Anomalocaris* species that may indicate slight differences in feeding mode. The presence of spinules suggests that *Anomalocaris saron* and *A. magnabasis* could primarily have fed only on soft prey, as the fine nature of these structures would have likely broken when dealing with hard exoskeletons. It raises the possibility that these *Anomalocaris* species were able to filter fine food particles from the water column, in addition to grabbing larger prey items with flexible appendages. The base of the ventral endite is shorter in *A. canadensis* than in *A. saron* and *A. magnabasis,* and *A. canadensis* also lacks spinules. As shorter endites can be coiled more tightly, and are less liable to break at the tip; this suggests that the Canadian *Anomalocaris* was able to manipulate more robust prey items than the United States and Chinese species.

Regional replacement of radiodonts

The radiodonts described from the Latham Shale are distinct from those in the Combined Metals and Comet Shale Members of the Pioche Formation and Pyramid Shale Member of the Carrara Formation. Given the proximity of the sites in the southern Great Basin, the similarity in depositional setting, and the biostratigraphic information, this change in fauna likely reflects the older age of the Latham radiodonts (*Bristolia mohavensis – Peachella iddingsi* zones, most likely *Bristolia insolens* zone) compared to the Carrara (*Nephrolenellus multinodus* zone) and Pioche (*Nephrolenellus multinodus* and *Eokochaspis nodosa* zones). As the age of the Latham radiodonts cannot be placed exactly (only as precise as '*Bristolia* subzone'), the replacement of *Ramskoeldia* by *Anomalocaris* in the southern Great Basin can only be confidently constrained to have occurred between the *Bristolia insolens* and *Bolbolenellus euryparia* zones. *Ramskoeldia* and *Anomalocaris* are both present together in the Chengjiang Biota (and so the two taxa could coexist), but only *Anomalocaris* (and not

Ramskoeldia) is known from the Stage 4 Chinese localities (Table 5; Liu 2013; Wang et al. 2013) suggesting that replacement occurred in the USA and also in South China. Notably, there is no major extinction of hard skeletal fauna associated with the change in the radiodont fauna, and similarly no noticeable change in the radiodonts after the extinction of Olenellina at the Dyeran-Delamaran boundary (Fig. 3); this shows the disconnect between the extinction of non-biomineralised and shelly fauna.

In northwestern Laurentia *Anomalocaris canadensis* is known from both above and below the Dyeran-Delamaran boundary, from the Cambrian Series 2, Stage 4 Eager Formation, Cranbrook Shale, and Miaolingian, Wuliuan Burgess Shale (Briggs 1979). The presence of *Wanneria* in the Eager Formation indicates that it is slightly older than the Latham Shale, which contains *Bristolia* (Briggs & Mount 1982; Palmer & Repina 1993). This shows that *Anomalocaris* appeared first in northwestern Laurentia and later in southwestern Laurentia. The different species present (*Anomalocaris canadensis* in northwestern Laurentia, *Anomalocaris magnabasis* in southwestern Laurentia, *Anomalocaris pennsylvanica* in eastern Laurentia) also demonstrate local factors, perhaps including smaller scale geographic barriers, controlling the distribution and morphology of this genus. Older *Konservat-Lagerstätten* in Laurentia need to be studied (e.g. the Indian Springs – English & Babcock 2010) to offer additional temporal resolution and range.

Hurdia is reported for the first time in the southern Great Basin. This specimen represents the oldest hurdiid from Laurentia (Cambrian Series 2, Stage 4, upper Dyeran, *Nephrolenellus multinodus* zone). The genus is otherwise known from the Miaolingian, Wuliuan of the Great Basin (Pates et al. 2018b) and Burgess Shale (Daley et al. 2013a). *Hurdia* is not known from the Cambrian Series 2, Stage 4 sites in Canada. This raises the possibility that *Hurdia* spread from southwest to northwest in Laurentia (the opposite of

Table 5. Comparison of common radiodont taxa across Chinese and Laurentian localities.

	Amplectobelua	*Anomalocaris*	*Caryosyntrips*	*Hurdia*	*Peytoia*	*Ramskoeldia*	References
Stage 3							
Chengjiang	*symbrachiata*	*saron*				*consimilis, platyacantha*	Hou et al. 1995; Cong et al. 2018
Shuijingtuo Fm.				sp			Cui and Huo 1990; Daley et al. 2013a
Stage 4							
Balang Fm		sp			sp		Liu 2013
Wulongqing Fm.		*kunmingensis*					Wang et al. 2013
Kinzers Fm.	sp	*pennsylvanica*					Briggs 1979; Pates & Daley in review
Cranbrook Shale		*canadensis*					Briggs 1979
Latham Shale						sp	**This study**
Pyramid Shale		n. sp.					Wilbur 2005; **This study**
Pioche Fm.		n. sp.		sp			Lieberman 2003; **this study**
Wuliuan							
Spence Shale			*camurus*	*victoria*			Pates & Daley 2017; Pates et al. 2018b
Burgess Shale	*stephenensis*	*canadensis*	*camurus, serratus*	*triangulata, victoria*	*nathorsti*		Daley & Budd 2010; Daley et al. 2013a; Pates & Daley 2017
Drumian							
Wheeler Fm.			*serratus*				Pates & Daley 2017;
Drum Mountains							Lerosey-Aubril pers. com.
Wheeler Fm.			*durus*		*nathorsti*		Briggs et al. 2008; Pates &
House Range							Daley 2017; Pates et al. 2018b
Marjum Fm.					*nathorsti*		Briggs & Robison 1984; Pates et al. 2018b

Unnamed taxa referred to as 'sp'. Note the specimens of *Anomalocaris* sp. from the Spence Shale and Wheeler Formation described in Briggs et al. 2008 are not included, as a redescription is required to positively identify these as *Anomalocaris* in the wake of the vast increase in radiodont descriptions over the last decade.

Anomalocaris) although the rarity of *Hurdia* specimens means that the range data may not be as reliable, and thus this conclusion is only tentative. Unlike for *Anomalocaris*, there are no noted differences between *Hurdia* frontal appendages or carapace elements from the Great Basin and Burgess Shale (Daley et al. 2013a; Pates et al. 2018b), potentially suggesting that *Anomalocaris* was more prone to geographic differentiation.

Limited geographic ranges of Anomalocaris species

Some previous discussion has focused on the geographic distribution of soft-bodied taxa (e.g., Hendricks et al. 2008; Hendricks 2013), and the work herein adds to the distributional data on *Anomalocaris* and other radiodonts. Here we emphasize what seem to be patterns of endemism, and apparent geographic isolation of individual species in *Anomalocaris*. *Anomalocaris saron* is limited to the Cambrian Series 2, Stage 3 Chengjiang biota (China) and there are different species present in both the Balang and Wulonquing Formations (China) (Hou et al. 1995; Liu 2013; Wang et al. 2013; Daley et al. 2013b; Table 5). The Emu Bay Shale (Australia, Stage 4) also possesses a distinct species, *Anomalocaris* cf. *canadensis*. Within Laurentia, *A. canadensis, A. pennsylvanica* and *A. magnabasis* are each restricted to northwestern, eastern and southwestern Laurentia respectively, although they overlap temporally (Briggs 1979; Daley & Edgecombe 2014; Pates & Daley 2018). The *Anomalocaris* species from the Miaolingian/Guzhangian Weeks Formation (Lerosey-Aubril et al. 2014) may also be very narrowly distributed, although there is a lack of coeval *Konservat-Lagerstätten* for comparison. By the same token, even in the face of this endemism, clearly at times organisms within the genus *Anomalocaris* must have had greater mobility as closely related species are present across continental blocks as far apart as South China and Laurentia (Table 5; Meert and Lieberman 2008). Further, we can posit that these range expansions

were a product of traditional dispersal, not geodispersal (*sensu* Lieberman 2000), as they do not seem to have occurred in other taxa, nor were these continental blocks interacting at this time (Meert and Lieberman 2008).

This limited geographic range and endemism of *Anomalocaris* species is in direct contrast to what is found in other Laurentian radiodonts such as *Hurdia, Peytoia* and *Caryosyntrips*; these were widespread in Laurentia from the Wuliuan onwards. For instance, *H. victoria* and *C. camurus* are both present in the Spence Shale and Burgess Shale, and *P. nathorsti* and *C. serratus* are found in the Burgess Shale and Wheeler Formation (in both the House Range and Drum Mountains). *Peytoia* is also known from the Marjum Formation (Table 5; Daley et al. 2013a; Pates & Daley 2017; Pates et al. 2018b). There is also a temporal component to these biogeographic patterns as *Anomalocaris* is a widely distributed genus in older Cambrian sites, from Stage 3 to the Wuliuan, whereas *Caryosyntrips, Hurdia* and *Peytoia* became widespread later, from the Wuliuan to the Drumian. This pattern could reflect increased global spread of arthropod taxa through the Cambrian period coincident with the decline in abundance of *Anomalocaris*, and relative increased abundance of these other three genera. We note that the biogeographic situation in *Ramskoeldia*, known from the Latham Shale, seems to be more in line with *Anomalocaris*, though that could change with future discoveries.

The contrast in geographic spread between *Anomalocaris* on the one hand and *Caryosyntrips, Hurdia* and *Peytoia* on the other is only found at the species level: all of these at the generic level were widespread and distributed over at least two palaeocontinents (three in the case of *Anomalocaris*). This points out the importance of considering biogeographic patterns at the species level whenever possible, as without this patterns of

geographic differentiation and isolation reflecting speciation events would have been missed (Hendricks et al., 2014).

This pattern of geographic differentiation by taxon also seems to possibly be reflected in patterns of ecological specialisation. In particular, *Anomalocaris* appendages appear more flexible and seem specialised for grasping, at least compared to the other three genera in which they appear less flexible and were possibly specialised for sediment sifting or slicing prey (Daley & Budd 2010; Daley et al. 2013a, b; Daley & Edgecombe 2014; Pates & Daley 2017). The restricted ranges of individual *Anomalocaris* species and their subtly different frontal appendage morphologies could reflect subtle adaptations to prey in these different basins. The feeding styles of the other three genera which did not grasp individual prey items but instead sifted or sliced them, may not have required such subtle variation in the morphology of frontal appendages, although it should be noted that two species of *Caryosyntrips* with distinct frontal appendages are known from different depths in the Wheeler Formation: *C. durus*, occurs in the House Range, a deeper and more distal environment than *C. serratus*, which occurs in the Drum Mountains (Pates & Daley 2017; Lerosey-Aubril & Skabelund 2018; Lerosey-Aubril pers. com.).

CONCLUSIONS

Material previously identified as *Anomalocaris canadensis* from the Latham Shale, although poorly preserved, likely belongs instead to the recently described amplectobeluid genus *Ramskoeldia*, and is most similar to *Ramskoeldia consimilis* from the Chengjiang biota. This is the youngest known *Ramskoeldia* and the first record of this genus from Laurentia. The oldest *Hurdia* is also recognised from the *Nephrolenellus multinodus* zone of the Combined Metals Member, Pioche Formation.

All other *Anomalocaris* material from the southern Great Basin, including material previously referred to *A.* cf. *saron* and *A. pennsylvanica* in Lieberman (2003), likely belongs to a new species, *Anomalocaris magnabasis*. This species can be identified by the presence of enlarged bases to the endites on the distalmost point of the shaft and first podomere in the distal articulated region. Part of our taxonomic re-assignments are based on the identification of a taphonomic pathway that consistently removes morphology in a predictable way. Differences between the decay, transport and burial history of the Delamaran and Dyeran levels of the Pioche Formation likely result in the observed differences in the material, including, for example the presence or absence of auxiliary spines. We also suggest that all *Anomalocaris* species have two-part ventral endites. The base of the ventral endite is softer and sometimes has spinules projecting from the distal surface and ventral spines attach at the ventralmost point of the base.

Our results also have implications for biogeographic patterns. Hendricks et al. (2008) suggested that in general non-biomineralised taxa were more widely distributed than their skeletal kin and this may indeed be the case, however even among relatively closely related soft-bodied taxa, for instance radiodonts, there does seem to be significant variance in the geographic range of species. In particular, we posit that individual *Anomalocaris* species are not widely distributed even within Laurentia, and this is unlike the situation for other radiodonts such as *Hurdia, Peytoia* and *Caryosyntrips*, which have species shared across the Burgess Shale and Great Basin (discovered subsequent to Hendricks et al. 2008). The difference among radiodonts may relate to the fact that different species were ecologically distinct, with some perhaps more generalised and some perhaps more specialised.

Finally, there is a taxonomic turnover in radiodonts in the southern Great Basin between the *Bristolia insolens* zone and the *Nephrolenellus multinodus* zone, from earlier

Ramskoeldia to later *Anomalocaris* and *Hurdia*. *Anomalocaris* was already present in northwestern Laurentia (Canada) before this turnover, whereas *Hurdia* was not. This reflects a broader change in radiodont fauna, from common Chengjiang taxa such as *Anomalocaris* and *Ramskoeldia* to common Burgess Shale taxa such as *Anomalocaris, Hurdia, Peytoia* and *Caryosyntrips*.

Acknowledgements. We thank Peter Van Roy, John Paterson, an anonymous reviewer, the editor Xi-Guang Zhang, and technical editor Sally Thomas, for their comments and suggestions which improved the manuscript greatly. SP is supported by an Oxford-St Catherine's Brade-Natural Motion Scholarship, and visits to museums were funded by a Palaeontological Association Sylvester-Bradley Award (PA-SB201503). Research by GDE and PC was funded by Leverhulme Trust Research Project Grant RPG-2015-441. ACD was funded by the Oxford University Museum of Natural History, and the Institute of Earth Sciences at the University of Lausanne. Bryan Wilbur donated specimens TMM NPL 64841, TMM NPL 23925, and KUMIP 492944 for study, and provided photographs of TMM NPL specimens. Curatorial assistance was provided by Julien Kimmig (KUMIP), Austin Hendry (LACMIP), Kathryn Estes-Smargiassi (LACMIP), Claire Mellish (NHMUK), Liath Appleton (TMM NPL), Erica Clites (UCB), Nigel Hughes (UCR), Jessica Miller-Camp (UCR), Shelly Wernette (UCR), Susan Butts (YPM), and Jessica Utrup (YPM). GDE thanks the Bureau of Land Management office in Caliente for permission to collect, Tim Ewin, Xiaoya Ma and Mike Smith for joint fieldwork, and Markus Martin for guidance to One Wheel Canyon. Kirsten Jensen and Michael Engel (University of Kansas) provided guidance on ICZN articles, Robert R Gaines provided discussions on the Latham Shale, Rudy Lerosey-Aubril traced the *Caryosyntrips*

serratus specimen KUMIP 415223 to the New Dig locality in the House Range (Wheeler Formation), and Russell DC Bicknell read and offered comments on the paper.

DATA ARCHIVING STATEMENT

This published work and the nomenclatural acts it contains have been registered in ZooBank. XXX.

REFERENCES

ALLISON, P. A. 1986. Soft-bodied animals in the fossil record: the role of decay in fragmentation during transport. *Geology,* **14**, 979-981.

BATH ENRIGHT, O. G., MINTER, N. J. and SUMNER, E. J. 2018. Palaeoecological implications of the preservation potential of soft-bodied organisms in sediment-density flows: testing turbulent waters. *Royal Society Open Science,* **4**, 170212. doi.org/10.1098/rsos.170212.

BRIGGS, D. E. G. 1979. *Anomalocaris*, the largest known Cambrian arthropod. *Palaeontology*, **22**, 631-663.

BRIGGS, D. E. G. and MOUNT, J. D. 1982. The occurrence of the giant arthropod *Anomalocaris* in the Lower Cambrian of southern California, and the overall distribution of the genus. *Journal of Paleontology,* **56**, 1112-1118.

BRIGGS, D. E. G., LIEBERMAN, B. S., HENDRICKS, J. R., HALGEDAHL, S. L. and JARRARD, R. D. 2008. Middle Cambrian arthropods from Utah. *Journal of Paleontology,* **82**, 238–54.

CARON, J. B., GAINES, R. R., MANGANO, M. G., STRENG, M. and DALEY, A. C. 2010. A new Burgess-Shale-type assemblage from the 'thin' Stephen Formation of the southern Canadian Rockies. *Geology*, **38**, 811-814.

COLLINS, D. 1996. The “evolution” of Anomalocaris and its classification in the arthropod class Dinocarida (nov.) and order Radiodonta (nov.) Journal of Paleontology, 70, 280–293.

CONG, P., MA, X., HOU, X., EDGECOMBE, G. D. and STRAUSFELD, N. J. 2014. Brain structure resolves the segmental affinity of anomalocaridid appendages. *Nature*, **513**, 538–542.

--- DALEY, A. C., EDGECOMBE, G. D. and HOU, X. 2017. The functional head of the Cambrian radiodontan (stem-group Euarthropoda) *Amplectobelua symbrachiata*. *BMC Evolutionary Biology*, **17**, 208.

--- EDGECOMBE, G. D., DALEY, A. C., GUO, J., PATES, S. and HOU, X. 2018. New radiodonts with gnathobase-like structures from the Cambrian Chengjiang biota and implications for the systematics of Radiodonta. *Papers in Palaeontology*. 1-17. doi.org/10.1002/spp2.1219

CONWAY MORRIS, S. and PEEL, J. S. 2009. New Palaeoscolecidan Worms from the Lower Cambrian: Sirius Passet, Latham Shale and Kinzers Shale. *Acta Palaeontologica Polonica*, **55**, 141-156.

CUI, Z. L. and HUO, S. C. 1990. New discoveries of Lower Cambrian crustacean fossils from Western Hubei. *Acta Palaeontologica Sinica*, **29**, 321–330.

DALEY, A. C. and BERGSTRÖM, J. 2012. The oral cone of *Anomalocaris* is not a classic ‘‘*Peytoia*’’. *Naturwissenschaften*, **99**, 501–504.

--- and BUDD, G. E. 2010. New anomalocaridid appendages from the Burgess Shale, Canada. *Palaeontology*, **53**, 721–738.

--- and EDGECOMBE, G. D. 2014. Morphology of *Anomalocaris canadensis* from the Burgess Shale. *Journal of Paleontology*, **88**, 68–91.

--- and PEEL, J. S. 2010. A possible anomalocaridid from the Cambrian Sirius Passet Lagerstätte, North Greenland. *Journal of Paleontology*, **84**, 352–355.

--- BUDD, G. E., CARON, J. B., EDGECOMBE, G. D. and COLLINS, D. 2009. The Burgess Shale anomalocaridid *Hurdia* and its significance for early euarthropod evolution. *Science*, **323**, 1597–1600.

--- --- --- 2013a. Morphology and systematics of the anomalocaridid arthropod *Hurdia* from the Middle Cambrian of British Columbia and Utah*. Journal of Systematic Palaeontology,* **11**, 743–787.

--- PATERSON, J. R., EDGECOMBE, G. D., GARCIA-BELLIDO, D. C. and JAGO, J. B. 2013b. New anatomical information on *Anomalocaris* from the Cambrian Emu Bay Shale of South Australia and a reassessment of its inferred predatory habits. *Palaeontology*, **56**, 971–990.

DURHAM, J. W. 1978. A lower Cambrian eocrinoid. *Journal of Paleontology*, **52**, 195-199.

ENGLISH, A. M. and BABCOCK, L. E. 2010. Census of the Indian Springs Lagerstätte, Poleta Formation (Cambrian), western Nevada, USA. *Palaeogeography, Palaeoclimatology, Palaeoecology*, **295,** 216-244.

GAINES, R. R. 2014. Burgess Shale-Type preservation and its distribution in space and time*. The Palaeontological Society Papers*, **20,** 123-146.

--- and DROSER, M. L. 2002. Depositional environments, ichnology, and rare soft-bodied preservation in the Lower Cambrian Latham Shale, East Mojave. 153-164. *In* CORSETTI, F. A. (ed.) *SEPM Pacific Section Book 93: Proterozoic-Cambrian of the Great Basin and Beyond*, 186 pp.

GUO, J., PATES, S., CONG, P., DALEY, A. C., EDGECOMBE, G. D., CHEN, T. and HOU, X. 2018. A new radiodont (stem Euarthropoda) frontal appendage with a mosaic of characters from the Cambrian (Series 2 Stage 3) Chengjiang biota. *Papers in Palaeontology*. 1-12. doi.org/10.1002/spp2.1231.

HENDRICKS, J. R. 2013. Global distributional dynamics of Cambrian clades as revealed by Burgess Shale-type deposits. *Geological Society London Memoirs,* **38**, 35-43.

--- LIEBERMAN, B. S. and STIGALL, A. L. 2008. Using GIS to study palaeobiogeographic and macroevolutionary patterns in soft-bodied Cambrian arthropods. *Palaeogeography, Palaeoclimatology Palaeoecology*, **264**, 163-175.

--- SAUPE, E. E., MYERS, C. E., HERMSEN, E. J. and ALLMON, W. D. 2014. The generification of the fossil record. *Paleobiology* **40**, 511-528.

HOU, X. G., BERGSTRÖM, J. and AHLBERG, P. 1995. *Anomalocaris* and other large animals in the Lower Cambrian Chengjiang fauna of southwest China. *GFF*, **117**, 163–183.

KIMMIG, J. and STROTZ, L. C. 2017. Coprolites in middle Cambrian (Series 2–3) Burgess Shale-type deposits of Nevada and Utah and their ecological implications. *Bulletin of Geosciences,* **92**, 297–309.

--- MEYER, R. C., and B. S. LIEBERMAN. 2018. *Herpetogaster* from the early Cambrian (Series 2: Stage 4) of Nevada and its implications for the early evolution of deuterostomes. *Geological Magazine,* 1-7, doi.org/10.1017/S0016756818000389.

LEROSEY-AUBRIL, R. and PATES, S. 2018. New suspension-feeding radiodont suggests evolution of microplanktivory in Cambrian macronekton. *Nature Communications,* **9,** 3774.

--- and SKABELUND, J. 2018. *Messorocaris*, a new sanctacaridid-like arthropod from the middle Cambrian Wheeler Formation (Utah, USA). *Geological Magazine*, **155**, 181-186.

--- HEGNA, T. A., BABCOCK, L. E., BONINO, E., and KIER, C. 2014. Arthropod appendages from the Weeks Formation Konservat-Lagerstätte: new occurrences of anomalocaridids in the Cambrian of Utah, USA. *Bulletin of Geosciences*, **89**, 269-282.

LIEBERMAN, B. S. 2000. *Paleobiogeography: Using Fossils to Study Global Change, Plate Tectonics, and Evolution*. Plenum Press/Kluwer Academic Publishers, New York, 208 pp.

--- 2002. Phylogenetic analysis of some basal Early Cambrian trilobites, the biogeographic origins of the eutrilobita, and the timing of the Cambrian radiation. *Journal of Paleontology,* **76**, 672-688.

--- 2003. A new soft-bodied fauna: the Pioche Formation of Nevada. *Journal of Paleontology*, **77**, 674-690.

LIU, J., LEROSEY-AUBRIL, R., STEINER, M., DUNLOP, J. A., SHU, D. and PATERSON, J. R. 2018. Origin of raptorial feeding in juvenile Euarthropods revealed by a Cambrian radiodontan. *National Science Review*, **nwy**057. doi.org/10.1093/nsr/new057.

LIU, Q. 2013. The first discovery of anomalocaridid appendages from the Balang Formation (Cambrian Series 2) in Hunan, China. *Alcheringa*, **37**, 1–6.

MCCOLLUM, L. B. and SUNDBERG, F. A. 2007. Cambrian trilobite biozonation of the Laurentian Delamaran Stage in the southern Great Basin, USA: Implications for global correlations and defining a Series 3 global boundary stratotype. *Memoirs of the Association of Australasian Palaeontologists,* **34**, 147-156.

MEERT, J. G. and LIEBERMAN, B. S. 2008. The Neoproterozoic assembly of Gondwana and its relationship to the Ediacaran-Cambrian Radiation. *Gondwana Research* **14**, 5-21

MOORE, R. A. and LIEBERMAN, B. S. 2009. Preservation of early and Middle Cambrian soft-bodied arthropods from the Pioche Shale, Nevada, USA. *Palaeogeography, Palaeoclimatology, Palaeoecology*, **277**, 57-62.

MOUNT, J. D. 1980. Characteristics of Early Cambrian faunas from Eastern San Bernardino County, California. *Southern California Paleontological Society Special Publication*, **2**, 19-29.

NEDIN, C. 1995. The Emu Bay Shale, a Lower Cambrian fossil Lagerstätten, Kangaroo Island. *Memoirs of the Association of Australasian Palaeontologists,* **18**, 133– 41.

NIELSEN, C. 1995. *Animal evolution: Interrelationships of the living phyla.* Oxford University Press.

PALMER, A. R. 1998. Terminal Early Cambrian extinction of the Olenellina: documentation from the Pioche Formation, Nevada. *Journal of Paleontology*, **72,** 650-672.

--- and REPINA, L. N. 1993. Through a glass darkly: taxonomy, phylogeny, and biostratigraphy of the Olenellina. *The University of Kansas Paleontological Contributions*, **3,** 1-35.

PATERSON, J. R., GARCIA-BELLIDO, D. C., LEE, M. S. Y., BROCK, G. A., JAGO, J. B. and EDGECOMBE, G. D. 2011. Acute vision in the giant Cambrian predator *Anomalocaris* and the origin of compound eyes. *Nature*, **480**, 237-240.

PATES, S. and DALEY, A. C. 2017. *Caryosyntrips*: a radiodontan from the Cambrian of Spain, USA and Canada. Papers in Palaeontology, **3**, 461–470.

--- --- 2018. The Kinzers Formation (Pennsylvania, USA): the most diverse assemblage of Cambrian Stage 4 radiodonts. *Geological Magazine*, 1-14, doi.org/10.1017/S0016756818000547.

--- --- and ORTEGA-HERNANDEZ, J. 2017. *Aysheaia prolata* from the Wheeler Formation (Drumian, Cambrian) is a frontal appendage of the radiodontan *Stanleycaris*. *Acta Palaeontologica Polonica*, **62**, 619-625.

--- --- --- 2018a. Response to comment "*Aysheaia prolata* from the Wheeler Formation (Drumian Cambrian) is a frontal appendage of the radiodontan *Stanleycaris*" with the formal description of *Stanleycaris*. *Acta Palaeontologica Polonica*, **63**, 105–110.

--- --- and LIEBERMAN, B. S. 2018b. Hurdiid radiodontans from the middle Cambrian (Series 3) of Utah. *Journal of Paleontology,* **92**, 99-113.

de QUEIROZ, K. and GAUTHIER, J. 1990. Phylogeny as a Central Principle in Taxonomy: Phylogenetic Definitions of Taxon Names. *Systematic Biology* **39**, 307–322. https://doi.org/10.2307/2992353

RAYMOND, P. E. 1935. *Leanchoilia* and other mid-Cambrian Arthropoda. *Bulletin of the Museum of Comparative Zoology at Harvard College,* **76**, 205–230.

ROBISON, R. A., and RICHARDS, B. C. 1981. Larger bivalve arthropods from the Middle Cambrian of Utah. *The University of Kansas Paleontological Contributions,* **106**, 1-28.

SCHNEIDER, C. A., RASBAND, W. S. and ELICEIRI, K. W. 2012. NIH Image to ImageJ: 25 years of image analysis. *Nature Methods* **9**, 671–675.

SCOTESE, C. R. 2016. PALEOMAP PaleoAtlas for GPlates and the PaleoData Plotter Program, PALEOMAP Project. www.earthbyte.org/ paleomap- paleoatlas- for- gplates/.

SMITH, M. R., HARVEY, T. H. P. and BUTTERFIELD, N. J. 2015. The macro- and microfossil record of the Cambrian priapulid *Ottoia*. *Palaeontology,* **58**, 705-721.

STEWART, J. H. 1970. Upper Precambrian and Lower Cambrian Strata in the Southern Great Basin California and Nevada. *Geological Survey Professional Paper*, **620**, 1-206.

--- and POOLE, F. G. 1974. Lower Paleozoic and uppermost Precambrian Cordilleran miogeocline, Great Basin, western United States. *Special Publications of the Society of Economic Paleontologists and Mineralogists*, **22**, 28-57.

SUNDBERG, F. A. and MCCOLLUM, L. B. 2000. Ptychopariid trilobites of the Lower-Middle Cambrian boundary interval, Pioche Shale, southeastern Nevada. *Journal of Paleontology*, **74**, 604-630.

VAN ROY, P., DALEY, A. C. and BRIGGS, D. E. G. 2015. Anomalocaridid trunk limb homology

revealed by a giant filter-feeder with paired flaps. *Nature,* **522**, 77– 80.

VINTHER, J., STEIN, M., LONGRICH, N. R. and HARPER, D. A. 2014. A suspension-feeding anomalocarid from the Early Cambrian. *Nature* **507**, 496–499.

WAGGONER, B. and HAGADORN, J. W. 2004. An unmineralized alga from the Lower Cambrian of California, USA. *Neues Jahrbuch füh Geologie und Paläontologie-Abhandlungen,* **2***,* 67-83.

--- --- 2005. Conical fossils from the Lower Cambrian of Eastern California. *PaleoBios*, **25**, 1-10.

WALCOTT, C. D. 1911. Cambrian geology and paleontology. II. Middle Cambrian holothurians and medusae. *Smithsonian Miscellaneous Collections*, **57**, 41–68.

--- 1912. Middle Cambrian Branchiopoda, Malacostraca, Trilobita and Merostomata. *Smithsonian Miscellaneous Collections*, **57**, 145–228.

WANG, Y., HUANG, D. and HU, S. 2013. New anomalocardid frontal appendages from the Guanshan biota, eastern Yunnan. *Chinese Science Bulletin,* **58**, 3937– 3942.

WEBSTER, M. 2011. Trilobite biostratigraphy and sequence stratigraphy of the upper Dyeran (traditional Laurentian 'Lower Cambrian') in the southern Great Basin, USA. 121-154. *In* HOLLINGSWORTH, J. S., SUNDBERG, F. A. and FOSTER, J. R. (eds.) *Cambrian Stratigraphy and Paleontology of Northern Arizona and Southern Nevada*. Museum of Northern Arizona Bulletin, **67**, 321 pp.

--- and HUGHES, N. C. Compaction-related deformation in Cambrian olenelloid trilobites and its implications for fossil morphometry. *Journal of Paleontology,* **73**, 355-371.

--- and ZELDITCH, M. L. 2005. Evolutionary modifications of ontogeny: heterochrony and beyond. *Paleobiology*, **31**, 354-372.

--- GAINES, R. R. and HUGHES, N. C. 2008. Microstratigraphy, trilobite biostratinomy, and depositional environment of the 'Lower Cambrian' Ruin Wash Lagerstätte, Pioche Formation, Nevada. *Palaeogeography, Palaeoclimatology, Palaeoecology*, **264**, 100-122.

WHITEAVES, J. F. 1892. Description of a new genus and species of phyllocarid crustacean from the Middle Cambrian of Mount Stephen, British Columbia. *Canadian Record of Science,* **5**, 205–208.

WHITTINGTON, H. B. and BRIGGS, D. E. G. 1985. The largest Cambrian animal, *Anomalocaris*, Burgess Shale, British Columbia. *Philosophical Transactions of the Royal Society of London. Series B, Biological Sciences,* **309**, 569–609.

WILBUR, B. C. 2005. A revision of helicoplacoids and other early Cambrian echinoderms of North America. Unpublished PhD thesis, The University of Texas at Austin, 365 pp.

Chapter 8

The hurdiid *Ursulinacaris* nov. identifies two ancestral characters of radiodont frontal appendages

Author contributions

SP and ACD conceived the project; NJB collected material from the Mount Cap Formation; SP wrote the manuscript and prepared the figures, with input from ACD and NJB.

Publication information

This Chapter has been submitted for publication in *Zoological Letters* (manuscript ID: ZLET-D-18-00069) and is currently in review. This version has not been peer-reviewed.

The hurdiid *Ursulinacaris* nov. identifies two ancestral characters of radiodont frontal appendages

Stephen Pates[1,2*], Allison C. Daley[2] and Nicholas J. Butterfield[3]

[1] Department of Zoology, University of Oxford, South Parks Road, Oxford, OX1 3PS, UK; email: stephen.pates@zoo.ox.ac.uk

[2] Institute of Earth Sciences, University of Lausanne, Lausanne, CH-105, Switzerland; email: allison.daley@unil.ch

[3] Department of Earth Sciences, University of Cambridge, Downing Street, Cambridge, CB2 3EQ, UK; email: njb1005@esc.cam.ac.uk

*corresponding author

Abstract

Background: Radiodonta, large Cambro-Ordovician nektonic predators, occupy a pivotal evolutionary position as stem-euarthropods and occupied important ecological niches in Palaeozoic ecosystems. Analyses of the anatomy and phylogenetic affinity of these large Palaeozoic animals has revealed the origin of the arthropod compound eye and biramous limb, and interpretations of their diverse feeding styles have placed various radiodont taxa as primary consumers and apex predators. Critical to our understanding of both radiodont evolution and ecology are the paired frontal appendages. However, the vast differences in frontal appendage morphology between different radiodont families have made it difficult to identify plesiomorphic characters of this body part.

Results: Here we describe a new genus of hurdiid, *Ursulinacaris*, from the middle Cambrian (Miaolingian, Wuliuan) Mount Cap Formation (Northwest Territories, Canada) and Jangle Limestone (Nevada, USA). *Ursulincaris* has the same organisation as other hurdiid frontal appendages, with an endite on the distalmost point in the shaft, and elongate endites on the first five podomeres in the distal articulated region. Unlike all other hurdiid genera, which possess a single row of elongated and broad ventral endites, this taxon uniquely bears paired slender endites.

Conclusion: *Ursulinacaris*, likely the basal-most known hurdiid, demonstrates two plesiomorphic characters for radiodont frontal appendages: paired endites and the presence of an endite at the distal-most point of the shaft. These characters, common across all four radiodont families (Amplectobeluidae, Anomalocarididae, Hurdiidae and Tamisiocarididae), will be useful for determining internal hurdiid and radiodont relationships in future phylogenetic analyses.

Keywords: Radiodonta, Hurdiidae, *Ursulinacaris grallae*, frontal appendages, plesiomorphy, Cambrian, Mount Cap Formation, Carrara Formation.

Background

Radiodonta, as the largest nektonic predators in Palaeozoic oceans, were an important member of marine ecosystems and played a pivotal role in structuring these early animal communities. Since the recognition that the first described member of this group, *Anomalocaris canadensis,* was a large stem euarthropod apex predator with raptorial appendages, and the description of complete specimens from the Burgess Shale [1, 2], radiodonts have subsequently been shown to be a diverse and disparate group with over 25 species and 10 genera named worldwide, from Africa, Australia,

China, Europe and North America [3-10]. Known from the Cambrian Series 2 Stage 3 to at least the Early Ordovician, and possibly the Early Devonian, these animals had body lengths ranging from under 10 cm to around two meters [10-16]. Their body plan consists of paired frontal appendages that attach adjacent to radial mouthparts, with two compound eyes attached to the dorsal surface of the head with stalks. The body itself is segmented, bearing lateral flaps and setal blades [2].

Radiodonts have provided crucial information for understanding euarthropod evolution, for example the origin of the biramous limb (homologous to the ventral and dorsal flaps in hurdiids) and compound eye [10, 17, 18]. The paired frontal appendages have been shown to be homologous to the labrum in crown-group arthropods, based on the neuroanatomical position (protocerebral), and patterns of labrum development [11]. These frontal appendages were composed of two sections, a proximal shaft and distal articulated region with podomeres bearing endites and dorsal spines. As these were used in feeding, the wide variety of morphologies known indicates that radiodonts occupied a number of niches in Cambrian ecosystems, including roles as primary consumers, sediment sifters and raptorial predators [7,15,17,19,20]. Frontal appendages are also critical for understanding radiodont internal relationships because they have the highest preservation potential of all radiodont body parts (numerous taxa are only known from frontal appendages) and are character-rich, making the useful for phylogenetic analyses and taxonomy. Each of the four radiodont families (Amplectobeluidae, Anomalocarididae, Hurdiidae and Tamisiocarididae) having a recognisable and unique frontal appendage morphology (table 1 in [21]).

Hurdiid frontal appendages in particular have a distinctive organisation and arrangement of endites. This family contains the genera *Aegirocassis*, *Hurdia,*

Pahvantia, Peytoia and *Stanleycaris*, as well as questionably the early Devonian animal *Schinderhannes* [2, 10, 14, 15, 17, 20, 23, 24]. Hurdiids possess frontal appendages with five unpaired elongate and blade-like endites on the first five podomeres in the distal articulated region, and auxiliary spines on only the distal-facing margin (Fig. 1). The other three radiodont families have paired endites along the entire length of the appendage, which reduce in length distally, and have auxiliary spines facing both distally and proximally.

The large differences between the frontal appendages of hurdiids and those of other radiodont families mean that the plesiomorphic characters of radiodont appendages are not well known. Here we describe a new genus of hurdiid, *Ursulinacaris*, known only from frontal appendages, possessing paired endites and an elongate shaft endite. These two characters are present in all four radiodont families, and allows us to identify them as plesiomorphies of radiodont frontal appendages, a body part crucial for evolutionary and ecological studies of this highly successful and diverse stem-euarthropod.

Materials and Methods

Isolated radiodont frontal appendages have been known for over twenty years from the Mount Cap Formation, alongside bivalved arthropods and segmented coprolites [25, 26]. Four appendages, preserved as flattened carbon films, were studied from this deposit. Unusually for BST assemblages, the Mount Cap Formation was formed in an intracratonic basin cut off from the ocean by the Mackenzie Arch [26]. Trilobite biostratigraphy identifies a *Glossopleura walcotti* zone age (middle Cambrian, Wuliuan) for this biota [26].

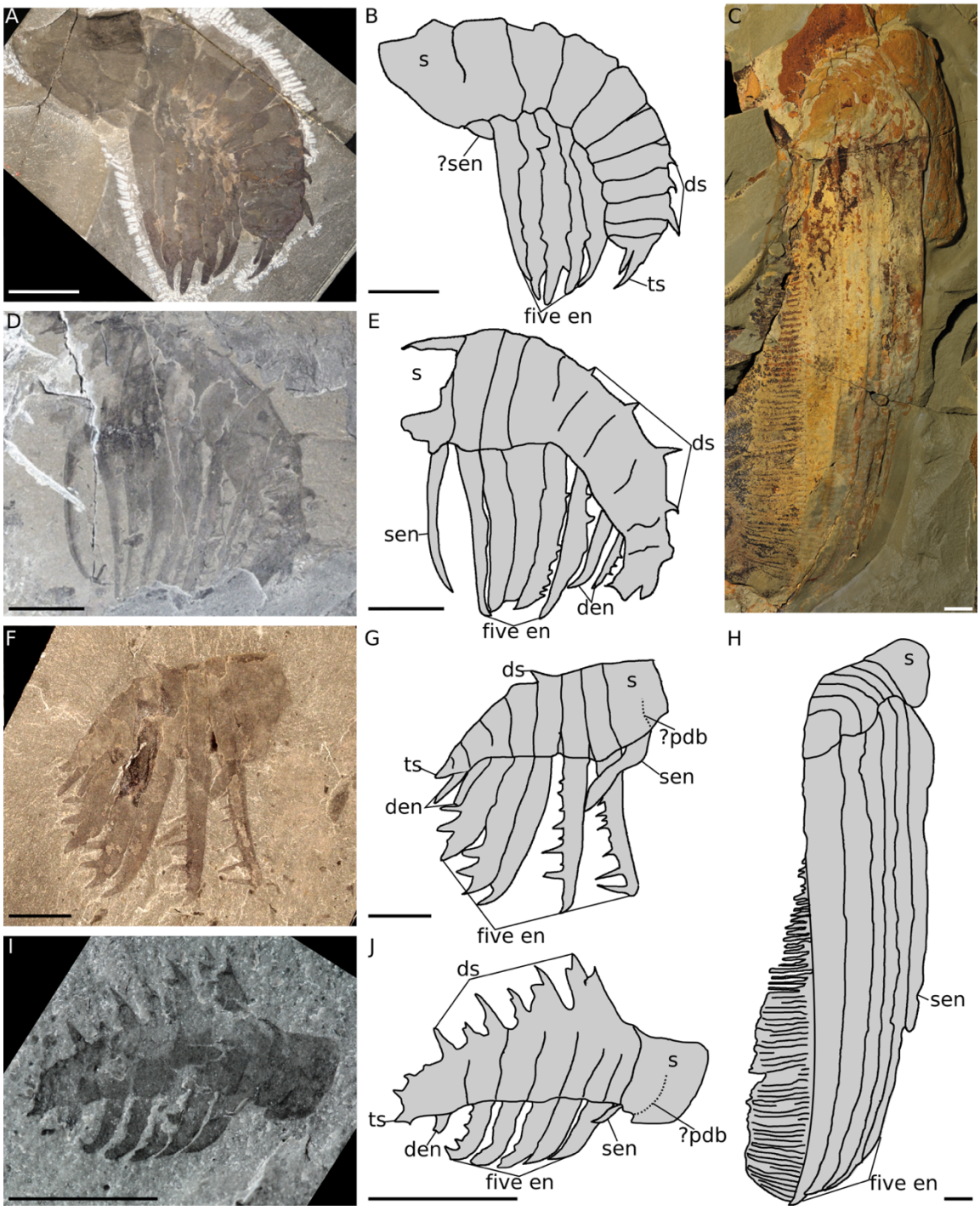

Fig. 1. Caption on next page.

Fig. 1. Hurdiid frontal appendages. A, B. *Peytoia nathorsti* from the Burgess Shale, British Columbia, Canada, USNM 240984. C, H. *Aegirocassis benmoulae* from the Fezouata Formation, Morocco, YPM 527123. D, E. ?*Peytoia* from the Burgess Shale, British Columbia, Canada, ROM 59508. F, G. *Hurdia* from the Burgess Shale, British Columbia, Canada, ROM 60048. I, J. *Stanleycaris hirpex* from Stephen Formation, British Columbia, Canada, ROM 59975. Abbreviations: den, distal endites; ds, dorsal spines; five en, five subequal endites on first five podomeres in distal articulated region; pdb, podomere boundary; s, shaft; sen, shaft endite. Scale bars = 10 mm.

The single radiodont frontal appendage, preserved as a flattened carbon film, reported herein is the first soft-bodied fossil known from the Jangle Limestone Member, Carrara Formation. The Jangle Limestone Member preserves a marine environment with the fauna dominated by trilobites [27]. Trilobite biostratigraphy identifies the level from which the frontal appendage was obtained as *Mexicella mexicana* zone (middle Cambrian, Wuliuan), slightly older than the Mount Cap Formation specimens, which correlate with a level at the very top of the Jangle Limestone Member [27].

Specimens were photographed using a Canon EOS 500D digital SLR camera with Canon EF-S 60 mm Macro Lens, controlled for remote shooting using EOS Utility 2.

Terminology. The term 'shaft' is used (following [28]) to identify the proximal podomeres of the appendage attaching them adjacent to the mouthparts. It is equivalent to 'peduncle' used in other studies (e.g. [15]). The term 'endite' is used (following [29]), and is equivalent to 'ventral spine' and 'ventral blade' used in other studies (e.g. [24, 30]).

List of abbreviations. d.a.r., distal articulated region; en, endite; pd, podomere, sag., sagittal; trans., transverse

List of institutional abbreviations. GSC, Geological Survey of Canada, Ottawa, Ontario, Canada; KUMIP, Division of Invertebrate Paleontology, Biodiversity Institute, University of Kansas, Lawrence, Kansas, USA; ROM, Royal Ontario Museum, Toronto, Ontario, Canada; USNM, National Museum of Natural History, Washington DC, USA; YPM, Yale Peabody Museum, New Haven, Connecticut, USA.

Results

Systematic Palaeontology

(total-group) Euarthropoda Lankester, 1904

Radiodonta Collins, 1996

Hurdiidae Lerosey-Aubril and Pates, 2018

Genera. *Aegirocassis, Hurdia, Pahvantia, Peytoia, Stanleycaris* and *Ursulinacaris.* Questionably *Schinderhannes.*

Key characters. The frontal appendages of all these taxa bear endites of subequal length on the first five podomeres in the distal articulated region (five en ,Fig. 1). Each of these endites is at longer than the height of the podomere to which it attaches, and bears auxiliary spines or setae on the distal margin only. Podomeres distal to the five subequal endites are reduced in height, and in some taxa (*Hurdia, Stanleycaris, Ursulinacaris* and *Peytoia?* from the Burgess Shale) additional shorter endites are present (den, Fig. 1; en8, 9 Fig. 2). An elongate endite is present at the distalmost ventral point of the shaft in *Aegirocassis, Ursulinacaris* and *Peytoia?* from the Burgess Shale, with a reduced endite visible in *Hurdia* and *Stanleycaris*, and potentially *Peytoia* (sen and ?sen, Fig. 1; en2, Fig. 2)

Where mouthparts are known (in *Hurdia, Peytoia* and *Stanleycaris*), these consist of radial plates, with four large plates arranged around a square or rectangular opening, with seven smaller plates between them. Triangular spines line the central opening, and in *Hurdia* additional rows of spines are present within [23, 33].

Where the remainder of the body is known (*Aegirocassis, Hurdia* and *Peytoia*), two sets of flaps (dorsal and ventral) are present, distinguishing hurdiids from all other radiodonts (which only have one set of flaps) [10].

A number of phylogenetic analyses [10, 11, 15, 16, 20] have recovered *Schinderhannes* within a monophyletic Hurdiidae, so it is questionably included here pending a redescription revealing more details of, for example, the mouthparts. The frontal appendage of *Schinderhannes* bears a number of similarities with hurdiids, specifically an elongate shaft endite and five subequal endites in the distal articulated region. The morphology of the mouthparts is not well known (only that they are radial) and flaps are present along the trunk. *Schinderhannes* also possesses a number of characters not associated with other radiodonts such as putative tergites and biramous trunk appendages, which resulted in the first phylogenetic analysis including this taxon resolving it between radiodonts and deuteropods [14].

Ursulinacaris gen. nov.

Etymology. From Latin: 'ursulina', the diminuative adjective of 'ursa', meaning 'from little bear', a reference to the locality of the holotype; and 'caris' meaning 'crab', a commonly used suffix for marine arthropods. Gender feminine.

Type species. *Ursulinacaris grallae* sp. nov.

Diagnosis. Radiodont with frontal appendage consisting of at least 12 podomeres, including two in the shaft, and at least 10 in the distal articulated region; distalmost

shaft podomere bears a single elongate ventral endite orientated distally; five proximal podomeres in distal articulated region bear paired elongate ventral endites with small auxiliary spines along their distal edge; distalmost podomeres recurved ventrally and are reduced in height; two shorter endites present on podomeres 8 and 9; small dorsal spines present at the distal margin of all podomeres in the distal articulated region.

Ursulinacaris grallae sp. nov.

Figs. 2, 3

v. 1996 'anomalocarid claw'; Butterfield & Nicholas, p. 895, fig. 2.2

v. 2011 'Anomalocaridid claw'; Harvey & Butterfield, p.168, fig. 3a

Etymology. From Latin: '*grallae'* meaning 'stilts', referring to the long and slender ventral endite morphology, and pairing of endites.

Referred specimens. 140185 (counterpart GSC 140185a) (holotype); GSC 135494 (counterpart GSC 135494a); GSC 140184, GSC, GSC 140186 (counterpart GSC 140186a) and questionably a partial frontal appendage KUMIP 492945 (part and counterpart).

Locality and horizon. *Glossopleura walcotti* zone, Little Bear biota, Mount Cap Formation, Northwest Territories, Canada; *Mexicella mexicana* zone, Jangle Limestone Member, Carrara Formation, North Face, Mount Montgomery, Last Chance Range, Nye County, Nevada, USA.

Diagnosis. as for genus

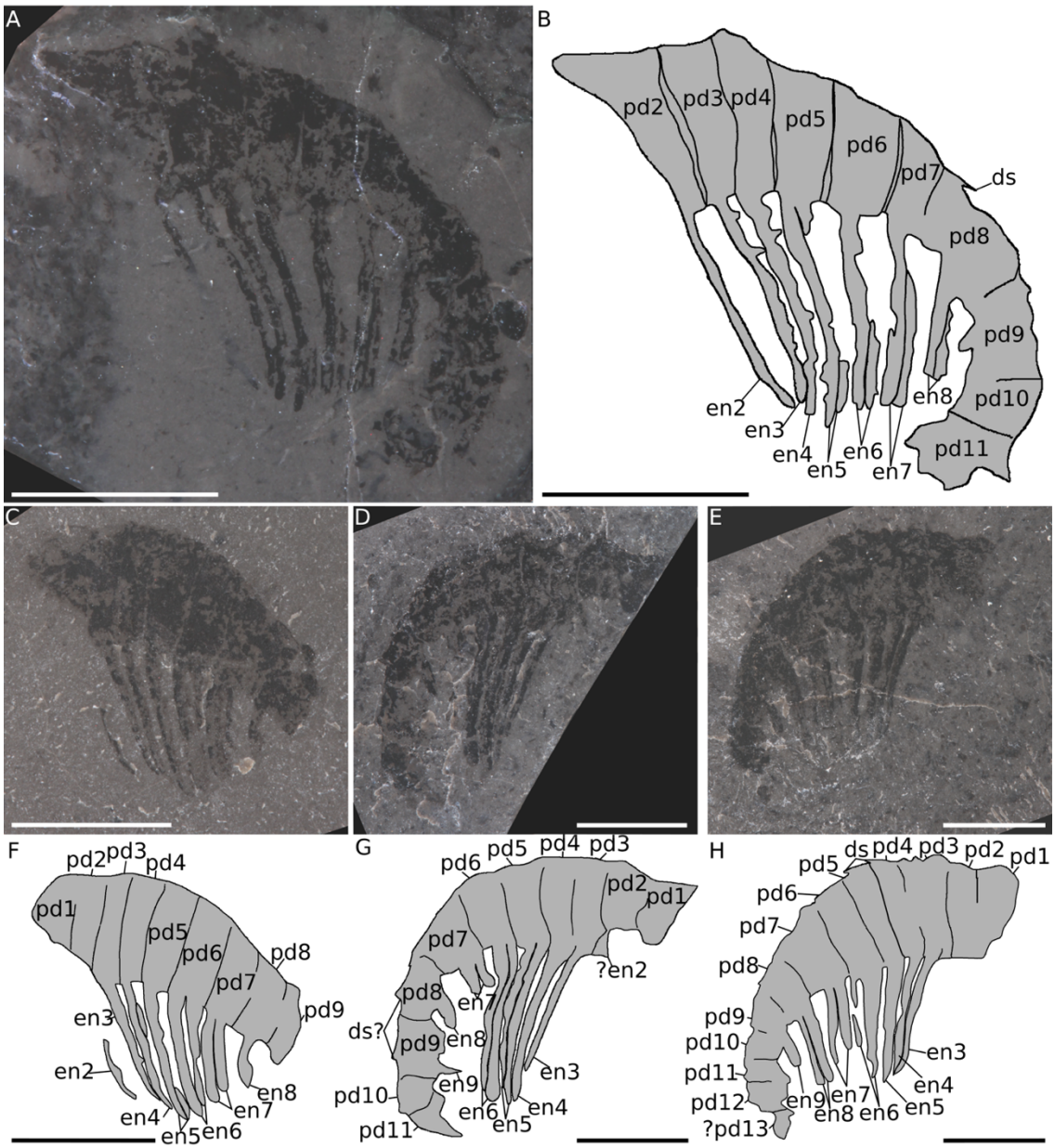

Fig. 2. *Ursulinacaris grallae* appendages from the Little Bear biota, Mount Cap Formation, Northwest Territories, Canada. A, B. GSC 140185. C, F. GSC 135494a. D, G. GSC 140186a. E, H. GSC 140184. Abbreviations: ds, dorsal spine; enX, endite on podomere X; pdX, podomere X. Scale bars = 5 mm.

Description. This taxon is known from four complete or nearly complete frontal appendages (length of dorsal surface between 13 and 24 mm) from the Little Bear biota (Fig. 2), and one questionable partial specimen (length of dorsal surface 14 mm) from the Jangle Limestone Member (Fig. 3). The shaft is composed of two podomeres, approximately twice as tall (sag.) as wide (trans.) (pd1, pd2, Fig. 2C-H), and an elongate curved endite extends from the distalmost portion of the shaft, angled towards the distal end of the appendage (en2, Fig.2). Immediately distal to the shaft are five podomeres (pd3-7) at least twice as tall (sag.) as wide (trans.). Each of these bears a pair of thin, straight, endites, which attach at the midpoint (trans.) of the podomere, and are approximately twice as long (sag.) as the podomere is tall (sag.) (en3-7, Fig. 2). Only four of these podomeres are preserved in the Jangle Limestone specimen, with one long endite visible and the base of its pair (en4-7, Fig. 3). These endites attach separately to the podomeres and run parallel to each other and to the sagittal plane of the appendage, best seen in the obliquely preserved GSC 135494a (en6 ,en7, Fig 2C, F). Small auxiliary spines are present on the distal margin of the endites, most visible on endites 3 and 4 in GSC 140185 (en3, en4, Fig. 2A, B). Podomere 8, and more distal podomeres where they are preserved, are shorter (sag.), and appear wider (trans.) than more proximal podomeres. The endites on podomere 8 are paired shorter than the endites on podomeres 3 to 7 (en8, Figs. 2A, B E, H; 3), it is not clear if the endite on podomere 9 is paired (en9, Fig. 2D, E, G, H). The oblique orientation of preservation prevents the total number of podomeres from being counted with certainty, however at least five (possibly six) podomeres are present in this most distal region (pd8-12, ?pd13, Fig. 2E, H). Small, thin, dorsal spines are rarely preserved, but can be seen at the distal

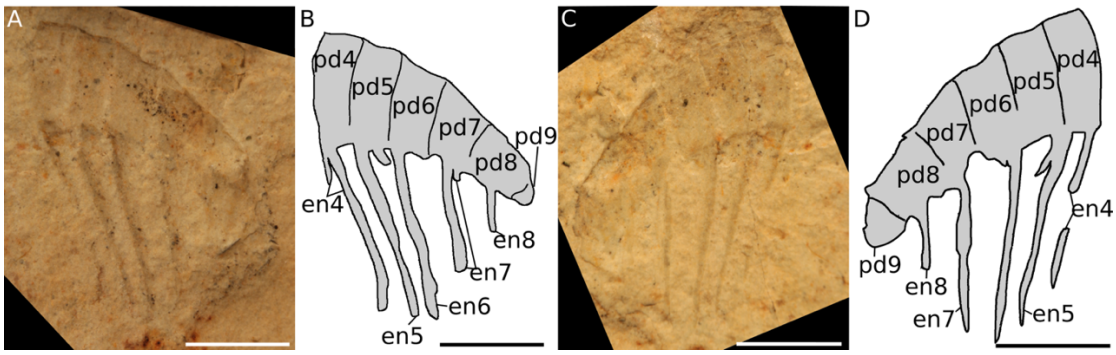

Fig. 3. *Ursulinacaris grallae*? partial appendage from the Jangle Limestone Member, Carrara Formation, Nevada, USA. KUMIP 492945. A, B. part. C, D. counterpart. Abbreviations: enX, endite on podomere X; pdX, podomere X. Scale bars = 5 mm.

margin of some podomeres (ds, Fig. 2A, B, D, E, G, H) The presence of terminal spines cannot be confirmed owing to the poor preservation of the distal region in all specimens.

Remarks. These frontal appendages have an overall organisation very similar to all other hurdiids, with the proximal five podomeres in the distal articulated region separated by straight arthrodial membrane, bearing elongate endites approximately twice as long (sag.) as the podomeres are tall (sag.), and auxiliary spines only on the distal margin. The shaft is composed of two podomeres, with an endite projecting forwards at the distal margin, a feature also seen in *Aegirocassis, Hurdia, Stanleycaris* and *Peytoia?* from the Burgess Shale (Fig. 1C-J). The podomeres in the distalmost region are reduced in height, and curved ventrally (a feature often seen in *Peytoia* appendages from the Burgess Shale – Fig. 1A, B). The ventral endites on pd8 and pd9 are shorter than those on pd3-7, just as the distalmost endites in *Hurdia, Stanleycaris* and *Peytoia?* from the Burgess Shale are shorter than the five elongate subequal endites (Fig. 1D-G, I, J). The number of endites per podomere and morphology of endites differs between *Ursulinacaris* (paired, thin, straight) and other hurdiids (unpaired, thick, recurved blade-like). The endites bear a resemblance to tamisiocaridid endites, as they do not alternate long/short, are longer than the podomere they attach to, and are paired. They differ however as they are not present on every podomere, bear auxiliary spines only on the dorsal surface, and do not diverge symmetrically from the sagittal axis of the appendage (as tamisiocaridids do) instead running parallel to each other. Thus despite the paired and slender morphology of the endites, these frontal appendages have more similarities

to hurdiids (Table 1), warranting the identification of this new taxon as a hurdiid, most similar to *Peytoia?* from the Burgess Shale (Fig. 1D, E).

Discussion

Plesiomorphic characters of radiodont frontal appendages

Ursulinacaris shows that paired endites are present in a hurdiid, and therefore that this character is present in all four radiodont families, as all non-hurdiid radiodonts have paired endites. Similarly *Ursulinacaris*, and a number of other hurdiids (*Aegirocassis, Hurdia, Peytoia?* from the Burgess Shale, and *Stanleycaris*), possess an endite on the shaft podomere. This is also known in all other radiodont families, for example the amplectobeluid *Ramskoeldia* [28], the anomalocaridid *Anomalocaris* (e.g. [21]) and the tamisiocaridids *Tamisiocaris* and *Anomalocaris briggsi* [7, 20]. The presence of these two characters in all radiodont families suggests that they represent plesiomorphies of the frontal appendage, and that the lack of a shaft endite in *Peytoia,* and the broad unpaired endite in all hurdiids except *Ursulinacaris* represent derived states.

Problems with resolving internal hurdiid relationships with phylogenetic methods

Hurdiid appendages have a consistent arrangement, and vary only subtlety, for example in the relative length and thicknesses of endites, morphology and robustness of dorsal spines, the morphology of the shaft endite, and morphology of auxiliary spines (Fig. 1). Two taxa, *Aegirocassis* and *Pahvantia*, possess setae on the distal margin of endites, in place of auxiliary spines present in all other taxa. Only few of these differences in frontal appendage morphology can be coded in phylogenetic analyses.

Table 1. Comparison of frontal appendage characters in select hurdiid and tamisiocaridid genera.

	Endite morphology	Endites paired	Endites diverge	Auxiliary spines	#pd with elongate endites in d.a.r.	Shape of arthrodial membrane
Hurdiidae						
Aegirocassis	Blade-like, curved	N	N/A	Dist	5	Straight
Hurdia	Blade-like, curved	N	N/A	Dist	5	Straight
Peytoia	Blade-like, straight	N	N/A	Dist	5	Straight
Stanleycaris	Blade-like, curved	N	N/A	Dist	5	Straight
Ursulinacaris	Thin, straight	Y	N	Dist	5	Straight
Tamisiocarididae						
Tamisiocaris	Thin, straight	Y	Y	Dist and prox*	17	Triangular
Anomalocaris briggsi	Thin, straight	Y	Y	Dist and prox	12	Triangular

*No auxiliary spines are known in *Tamisiocaris* from the Kinzers Formation, however this could be the result of taphonomic removal [21]. Abbreviations: d.a.r, distal articulated region; dist, distal margin of endite; prox, proximal margin of endite

Hurdiids differ more in the anatomy of other body parts, such as the number of body segments, and morphology of frontal carapaces and lateral flaps, but these are known in under half of hurdiid taxa (Table 2). Because the frontal appendages are the most character-rich body part used in phylogenetic analyses, and because there are very few shared character states between the few genera with known body, flaps and carapaces, the hurdiid clade of radiodont phylogenetic analyses tends to be poorly resolved (e.g. [15, 16]). The identification of plesiomorphies in the frontal appendage of *Ursulinacaris*, a hurdiid, will therefore inform future radiodont phylogenetic analyses, helping to resolve both internal hurdiid relationships and the relationship between hurdiids and other radiodont families.

Conclusion

The description of paired endites and an elongate shaft endite in a new genus of hurdiid, *Ursulinacaris*, show that these characters are present in all families of radiodont. These characters therefore likely represent plesiomorphies of the radiodont frontal appendage, and *Ursulinacaris* is likely the most basal known hurdiid. These characters will be of use in determining internal hurdiid relationships, which are currently not well known.

Table 2. Body parts known in hurdiids.

	Frontal appendages	Mouthparts	Body and flaps	Carapace
Aegirocassis	**X**		**X**	**X**
Fezouata hurdiid	**X**			
Hurdia triangulata	X	X	X	X
Hurdia victoria	**X**	**X**	**X**	**X**
***Hurdia* sp. B (Burgess)**	**X**			
***Hurdia* sp. B (Spence)**	**X**			
***Hurdia* cf. *victoria* (Spence)**	**X**			
Pahvantia	**X**			**X**
Peytoia infercambriensis	X			
Peytoia nathorsti	**X**	**X**	**X**	**X**
***Peytoia* sp. (Balang)**	**X**			
Peytoia? (Burgess)	X			
Schinderhannes	**X**	**X**	**X**	
Stanleycaris	**X**	**X**		
Ursulinacaris	X			

Those analysed in the most recent phylogenetic analysis of radiodonts [15] in bold.

Declarations

Ethics approval and consent to participate

Not applicable

Consent for publication

Not applicable

Availability of data and material

Fossil material used in this study is accessioned at the GSC and KUMIP.

Competing interests

The authors declare that they have no competing interests.

Funding

SP is supported by an Oxford-St Catherines Brade-Natural Motion Scholarship.

Authors' contributions

SP and ACD conceived the project; NJB collected material from the Mount Cap Formation; all authors contributed to the interpretation; SP wrote the manuscript and prepared the figures, with input from ACD and NJB; all authors read and approved the final manuscript.

Acknowledgements

We thank Craig Stevenson for donating a specimen to the KUMIP, Michelle Coyne (GSC) and Julien Kimmig (KUMIP) for curatorial assistance, and Peter Van Roy for providing the image of the *Aegirocassis* frontal appendage in Fig. 1C.

References

[1] Briggs DE. *Anomalocaris*, the largest known Cambrian arthropod. Palaeontology. 1979;22:631-64.

[2] Whittington HB, Briggs DE. The largest Cambrian animal, *Anomalocaris*, Burgess Shale, British-Columbia. Phil. Trans. R. Soc. Lond. B. 1985;309:569-609.

[3] Briggs DE, Mount JD. The occurrence of the giant arthropod *Anomalocaris* in the Lower Cambrian of southern California, and the overall distribution of the genus. Journal of Paleontology. 1982;1:1112-8.

[4] Lieberman BS. A new soft-bodied fauna: the Pioche Formation of Nevada. Journal of Paleontology. 2003;77:674-90.

[5] Nedin C. The palaeontology and palaeoenvironment of the Early Cambrian Emu Bay Shale, Kangaroo Island, South Australia (Doctoral dissertation).

[6] Chen JY, Ramsköld L, Zhou GQ. Evidence for monophyly and arthropod affinity of Cambrian giant predators. Science. 1994;264:1304-8.

[7] Daley AC, Paterson JR, Edgecombe GD, García-Bellido DC, Jago JB. New anatomical information on *Anomalocaris* from the Cambrian Emu Bay Shale of South Australia and a reassessment of its inferred predatory habits. Palaeontology. 2013;56:971-90.

[8] Daley AC, Legg DA. A morphological and taxonomic appraisal of the oldest anomalocaridid from the Lower Cambrian of Poland. Geological Magazine. 2015;152:949-55.

[9] Pates S, Daley AC. *Caryosyntrips*: a radiodontan from the Cambrian of Spain, USA and Canada. Papers in Palaeontology. 2017;3:461-70.

[10] Van Roy P, Daley AC, Briggs DE. Anomalocaridid trunk limb homology revealed by a giant filter-feeder with paired flaps. Nature. 2015;522:77-80.

[11] Cong P, Ma X, Hou X, Edgecombe GD, Strausfeld NJ. Brain structure resolves the segmental affinity of anomalocaridid appendages. Nature. 2014;513:538-42.

[12] Cong P, Daley AC, Edgecombe GD, Hou X, Chen A. Morphology of the radiodontan *Lyrarapax* from the early Cambrian Chengjiang biota. Journal of Paleontology. 2016;90:663-71.

[13] Hou XG, Bergström J, Ahlberg P. *Anomalocaris* and other large animals in the Lower Cambrian Chengjiang fauna of southwest China. GFF. 1995;117:163-83.

[14] Kühl G, Briggs DE, Rust J. A great-appendage arthropod with a radial mouth from the Lower Devonian Hunsrück Slate, Germany. Science. 2009;323:771-3.

[15] Lerosey-Aubril R, Pates S. New suspension-feeding radiodont suggests evolution of microplanktivory in Cambrian macronekton. Nature communications. 2018; doi:10.1038/s41467-018-06229-7

[16] Liu J, Lerosey-Aubril R, Steiner M, Dunlop JA, Shu D, Paterson JR. Origin of raptorial feeding in juvenile euarthropods revealed by a Cambrian radiodontan. National Science Review. 2018; doi:10.1093/nsr/nwy057.

[17] Daley AC, Budd GE, Caron JB, Edgecombe GD, Collins D. The Burgess Shale anomalocaridid *Hurdia* and its significance for early euarthropod evolution. Science. 2009;323:1597-600.

[18] Paterson JR, García-Bellido DC, Lee MS, Brock GA, Jago JB, Edgecombe GD. Acute vision in the giant Cambrian predator *Anomalocaris* and the origin of compound eyes. Nature. 2011;480:237-40.

[19] Daley AC, Budd GE. New anomalocaridid appendages from the Burgess Shale, Canada. Palaeontology. 2010;53:721-38.

[20] Vinther J, Stein M, Longrich NR, Harper DA. A suspension-feeding anomalocarid from the Early Cambrian. Nature. 2014;507:496-500.

[21] Pates S, daley AC. The Kinzers Formation (Pennsylvania, USA): the most diverse assemblage of Cambrian Stage 4 radiodonts. Geological Magazine. 2018; doi: 10.1017/S0016756818000547

[22] Daley AC, Budd GE, Caron JB. Morphology and systematics of the anomalocaridid arthropod *Hurdia* from the Middle Cambrian of British Columbia and Utah. Journal of Systematic Palaeontology. 2013;11:743-87.

[23] Caron JB, Gaines RR, Mángano MG, Streng M, Daley AC. A new Burgess Shale–type assemblage from the "thin" Stephen Formation of the southern Canadian Rockies. Geology. 2010;38:811-4.

[24] Pates S, Daley AC, Ortega-Hernández J. *Aysheaia prolata* from the Utah Wheeler Formation (Drumian, Cambrian) is a frontal appendage of the radiodontan *Stanleycaris*. Acta Palaeontologica Polonica. 2017;62:619-26.

[25] Butterfield NJ, Nicholas CJ. Burgess Shale-type preservation of both non-mineralizing and 'shelly' Cambrian organisms from the Mackenzie Mountains, northwestern Canada. Journal of Paleontology. 1996;70:893-9.

[26] Harvey TH, Butterfield NJ. Great Canadian Lagerstätten 2. Macroand Microfossils of the Mount Cap Formation (Early and Middle Cambrian, Northwest Territories). Geoscience Canada. 2011;38:165-74.

[27] Palmer AR, Halley RB. Physical stratigraphy and trilobite biostratigraphy of the Carrara Formation (Lower and Middle Cambrian) in the southern Great Basin. Geological Survey Professional Paper. 1979;1047.

[28] Cong PY, Edgecombe GD, Daley AC, Guo J, Pates S, Hou XG. New radiodonts with gnathobase-like structures from the Cambrian Chengjiang biota and implications for the systematics of Radiodonta. Papers in Palaeontology. 2018; doi:10.1002/spp2.1219.

[29] Guo J, Pates S, Cong P, Daley AC, Edgecombe GD, Chen T, Hou X. A new radiodont (stem Euarthropoda) frontal appendage with a mosaic of characters from the Cambrian (Series 2 Stage 3) Chengjiang biota. Papers in Palaeontology. 2018; doi:10.1002/spp2.1231.

[30] Pates S, Daley AC, Lieberman BS. Hurdiid radiodontans from the middle Cambrian (Series 3) of Utah. Journal of Paleontology. 2018;92:99-113.

[31] Lankester ER. The structure and classification of Arthropoda. Quarterly journal of microscopical science. 1904;47:523-82.

[32] Collins D. The “evolution” of *Anomalocaris* and its classification in the arthropod class Dinocarida (nov.) and order Radiodonta (nov.). Journal of Paleontology. 1996;70:280-93.

[33] Daley AC, Bergström J. The oral cone of *Anomalocaris* is not a classic ‘‘*Peytoia*’’. Naturwissenschaften. 2012;99:501-4.

Chapter 9

The evolution of the hurdiid frontal appendage, and a novel phylogenetic hypothesis for radiodont families

Author contributions

SP conceived the project; SP performed the phylogenetic analyses; SP wrote the manuscript and prepared the figures, with input from ACD.

Publication information

This Chapter has not been submitted for publication.

Additional information

The supplemental material for this Chapter is in Appendix 2.

The evolution of the hurdiid frontal appendage, and a novel phylogenetic hypothesis for radiodont families

Stephen Pates[1,2]* and Allison C. Daley[2]

[1] Department of Zoology, University of Oxford, South Parks Road, Oxford, OX1 3PS, UK

[2] Institute of Earth Sciences, University of Lausanne, Lausanne Ch-1015, Switzerland

*email: stephen.pates@zoo.ox.ac.uk

Abstract

Radiodonts are large nektonic stem-euarthropods which were iconic members of early animal communities during the Cambrian Explosion. They are often recognised in the fossil record by their lightly sclerotized body parts, in particular their frontal appendages, which provide a wealth of readily-identifiable characters. Radiodonts belonging to the family Hurdiidae have a unique organisation of the frontal appendage, with five elongate blade-like endites on subsequent podomeres. This is very different to radiodonts in the other three families (Amplectobeluidae, Anomalocarididae, and Tamisiocarididae) which bear slender endites along the appendage. This has led to uncertainty about the evolutionary history of this body part both within Hurdiidae and for Radiodonta as a whole. Two recently described taxa, *Laminacaris* and *Ursulinacaris*, provide conflicting information on the sequence of character acquisition for the hurdiid frontal appendage. *Laminacaris* suggests that the blade-like endite predated the organisation of five podomeres bearing elongate endites, whereas *Ursulinacaris* suggests the opposite. Here we describe a new hurdiid body specimen from the Spence

Shale, Utah (Wuliuan) that resolves this conflict. This taxon is identified as a hurdiid because it possesses small frontal appendages conforming to typical hurdiid organisation, a tripartite frontal carapace, and putative dorsal and ventral flaps. A phylogenetic analysis of the most comprehensive sampling of hurdiids to date, including the new hurdiid described herein, *Peytoia*? from the Burgess Shale, *Laminacaris* and *Ursulinacaris*, was undertaken to test between the *Laminacaris* and *Ursulinacaris* frontal appendage character acquisition hypotheses, and to better resolve the position of Hurdiidae within Radiodonta. Our analysis shows that Hurdiidae is sister to a clade containing the three other radiodont families, and that the organisation of the hurdiid frontal appendage predated the blade-like endite. *Caryosyntrips* is resolved within Radiodonta for the first time, and of the three non-hurdiid families, Tamisiocarididae diverges first, followed by Anomalocarididae and Amplectobeluidae. This suggests that the basal radiodont possessed frontal appendages with elongate endites of subequal length, and thus likely sifted sediment. As such the raptorial predatory ecology most traditionally associated with the group in fact represents a derived ecology specific to amplectobeluids and anomalocaridids.

Key words: Radiodonta, Hurdiidae, frontal appendages, phylogenetic analysis

Introduction

Radiodonts, a diverse clade of nektonic animals that originated in the early Cambrian, are known from deposits worldwide as isolated elements of the bodyplan (e.g. frontal appendages, mouthparts, triangular flaps) and complete specimens. The first complete specimens described, Burgess Shale taxa we now know as *Anomalocaris canadensis* and *Peytoia nathorsti,* were considered to belong to a ‘hitherto unknown phylum’

(Whittington & Briggs 1985). Later studies suggested that radiodonts belonged instead to the stem- (Budd 2002) or crown-group of Euarthropoda (Chen et al. 2004), as sister to arthropods (Hou et al. 2006), or within cycloneuralian worms (Hou et al. 1995). The description of the third taxon known from complete specimens, *Hurdia victoria*, conclusively demonstrated that radiodonts are stem-group euarthropods (Daley et al. 2009), and the continued discovery of new taxa from Australia, China, and Morocco revealed insights into the evolution of the compound eye, segmental homology of the labrum, and formation of the biramous appendage respectively (Paterson et al. 2011; Cong et al. 2014; Van Roy et al. 2015).

The first analysis to examine the relationships of taxa within Radiodonta in detail, by Vinther et al. (2014), recognised four distinct families, Amplectobeluidae, Anomalocarididae, Hurdiidae, and Tamisiocarididae ('Cetiocaridae' of Vinther et al. 2014). The taxa chosen by Vinther et al. (2014), and the novel matrix created, were developed in subsequent studies, as new taxa and morphological characters were discovered (Cong et al. 2014; Van Roy et al. 2015; Liu et al. 2018). All of these analyses, including the most recent (Lerosey-Aubril & Pates 2018), resolved the same relationships between these four families, with a clade comprising Hurdiidae and Tamisiocarididae sister to a clade of Amplectobeluidae and Anomalocarididae.

The paired frontal appendages that attach to the radiodont head, adjacent to the radial mouthparts that give the group its name, are made up of podomeres separated by flexible membrane (e.g. Briggs 1979; Whittington & Briggs 1985; Daley and Budd 2010; Pates & Daley 2017, 2018). They are made of two parts, a shaft which attaches to the head, and a distal articulated region with modified endites along the ventral surface, which are specialised for different feeding modes (Cong et al. 2017,

2018; Guo et al. 2018). Further characters, such as dorsal spines, podomere shape, and auxiliary spines add further information, allowing identification of even isolated appendages to the family, genus, or species level. This, in conjunction with the fact that these body parts are the most commonly preserved element, makes frontal appendages vital for taxonomic and phylogenetic studies of the group (e.g. Daley & Budd 2010; Vinther et al. 2014; Lerosey-Aubril & Pates 2018).

Hurdiidae has been poorly resolved in all previous phylogenetic analyses of Radiodonta, partly a result of the similarity between hurdiid frontal appendages, and their vast differences as compared to the appendages of all other radiodonts. Hurdiid frontal appendages have a recognisable organisation, with the first five podomeres in the distal articulated region bearing unpaired elongate endites, with auxiliary spines on the distal margin only (or setae, in the case of *Aegirocassis* and *Pahvantia*). All other radiodonts bear paired endites along most or all of the podomeres, which are slender in morphology and bear auxiliary spines on the proximal and distal margin (if present) (*this thesis Chapter 8*).

Two recently described taxa, with different combinations of both hurdiid and non-hurdiid frontal appendage characters, provide two different and conflicting hypotheses on the relationship of hurdiid frontal appendage organisation to that of other radiodonts. The first of these is *Ursulinacaris grallae*, a putative hurdiid radiodont known only from frontal appendages. These appendages have the same organisation as hurdiids, with endites on the first five podomeres in the distal articulated region, but the endites are paired and slender, as in tamisiocaridids, rather than broad, blade-like, and in a single row, as in hurdiids (*this thesis Chapter 8*). The second taxon, *Laminacaris chimera*, possesses a blade-like endite on the first podomere in the distal articulated

region with strong similarities to the blade-like endites *Hurdia* (Guo et al. 2018), however the rest of the podomeres bear endites that alternate long/short and possess auxiliary spines on both anterior and posterior faces, as in amplectobeluids and anomalocaridids. It is not yet known if endites are paired in *Laminacaris chimera.* Paired endites are known in *Laminacaris?* from the Kinzers Formation, although this taxon is only known from partial appendages with similarities not only to *Laminacaris chimera* but also the tamisiocaridid *Anomalocaris briggsi,* and thus this taxon may belong to its own genus (Pates & Daley 2018). If *Ursulinacaris* represents an early diverging hurdiid, the organisation of hurdiid frontal appendages (specifically, the arrangement of endites on only the first five podomeres of the distal articulated region) occurred before the development of the morphology of these endites as blade-like and unpaired, as seen in most hurdiid taxa (e.g. *Hurdia, Peytoia, Stanleycaris*). If *Laminacaris* represents the earliest known diverging hurdiid, the blade-like unpaired endite morphology developed first, and was later organised into the hurdiid arrangement of five elongate endites.

In this study, the matrix of Lerosey-Aubril & Pates (2018) is used with a novel selection of radiodont taxa representing the broadest selection of hurdiids available. *Ursulinacaris grallae* and *Laminacaris chimera* are both included, alongside *Peytoia*? from the Burgess Shale ('?*Laggania*' described in Daley & Budd 2010) and a body specimen from the Spence Shale, Utah, (*Anomalocaris* sp. of Briggs et al. 2008) redescribed below. This analysis provides a new phylogenetic framework to understand the relationship of Hurdiidae with the other radiodont families, and the sequence of character acquisition within radiodont frontal appendages.

Methods

Institutional abbreviations

KUMIP, Division of Invertebrate Paleontology, Biodiversity Institute, University of Kansas, Lawrence, Kansas, USA.

Fossil description and photography

A single body specimen from the Spence Shale Member of the Langston Formation in Utah, USA was re-examined. KUMIP 314037 was photographed wet and dry using a Canon EOS 500 DSLR with macro lens and polarizing filter. Digital measurements were made using ImageJ (Schneider et al. 2012). Figures were prepared using Inkscape 0.91 and GIMP 2.10.

Parsimony analysis

A parsimony analysis was performed to test how the recent description of new putative early-diverging hurdiids (*Ursulinacaris grallae*, *Laminacaris chimera,* and the specimen redescribed in this study) affects our hypotheses for internal radiodont relationships. New taxa were coded into the matrix of Lerosey-Aubril & Pates (2018), itself modified from the original matrix of Vinther et al. (2014) and also used and modified by Cong et al. (2014), Van Roy et al. (2015), and Liu et al. (2018). A series of parsimony analyses were conducted under implied weighting (concavity constant k values from 1 to 10) using TNT (Goloboff et al. 2008). 1000 trees were retained per analysis, which was conducted using the New Technology search with multiple replications, 25 cycles of ratchet, 25 cycles of drift, and 1000 hits.

Alterations to the matrix

Only one *Hurdia* terminal was included in the analysis. Previous studies (Vinther et al. 2014; Cong et al. 2014; Van Roy et al. 2015; Lerosey-Aubril & Pates 2018; Liu et al. 2018) have used four: *Hurdia victoria*, *Hurdia* cf. *victoria* (Spence), *Hurdia* sp. B (Burgess), and *Hurdia* sp. B (Spence), however these represent taphonomic grades of the same single species, rather than biological variation (Pates et al. 2018). Two species of *Hurdia* are known, *H. triangulata* and *H. victoria*, but these would be coded identically in the matrix, as the only current differences between these two taxa relates to the shape of the central carapace element (Daley et al. 2013a).

A number of putative hurdiids not included in previous phylogenetic analyses of the group were added, including the complete body specimen redescribed here, *Peytoia?* from the Burgess Shale (Daley & Budd 2010), and *Ursulinacaris grallae* (*this thesis Chapter 8*). *Laminacaris chimera* was first included in the analysis of Lerosey-Aubril & Pates (2018).

Anomalocaris magnabasis was included following its redescription (*this thesis Chapter 7*). *Anomalocaris pennsylvanica* (excluded by Lerosey-Aubril & Pates 2018, but included in previous analyses) and *Lyrarapax trilobus* were also included to increase the representation of amplectobeluids and anomalocaridids. *Anomalocaris* sp. from the Balang Formation (Wang et al. 2013) was coded but subsequently removed, as it only contains character states already coded for *A. magnabasis*, alongside a number of unknown or inapplicable characters. Similarly, *Ramskoeldia platyacantha* and *Caryosyntrips camurus* and *C. durus* were not included, as they contain identical codings in this matrix to taxa already present (*R. consimilis* and *C. serratus* respectively).

Individual changes to coded characters, for example resulting from recent descriptive work, are outlined below the description of character states (Supplemental 1) with the complete matrix in Supplemental 2.

Systematic Palaeontology

Superphylum PANARTHROPODA Nielsen 1995

Phylum (total-group) EUARTHROPODA Lankester 1904

Order RADIODONTA Collins 1996

Family HURDIIDAE Lerosey-Aubril & Pates 2018

Hurdiid nov gen et sp.

Figs 1, 2

v. 2008 *Anomalocaris* sp.; Briggs et al., p. 240, figs. 1.1, 1.2

Material. KUMIP 314037, part only, a complete specimen with poorly preserved frontal appendages.

Occurrence. *Glossopleura walcotti* zone, Spence Shale Member, Langston Formation, Miners Hollow, Wellsville Mountains, Box Elder County, Utah, USA.

Description

This complete body specimen is preserved in lateral oblique orientation, with a head region bearing a pair of frontal appendages (Fig. 1, fa) associated with lateral carapace elements (Fig. 1, ce) at the anterior end, a central carapace element, an oral cone (Fig.

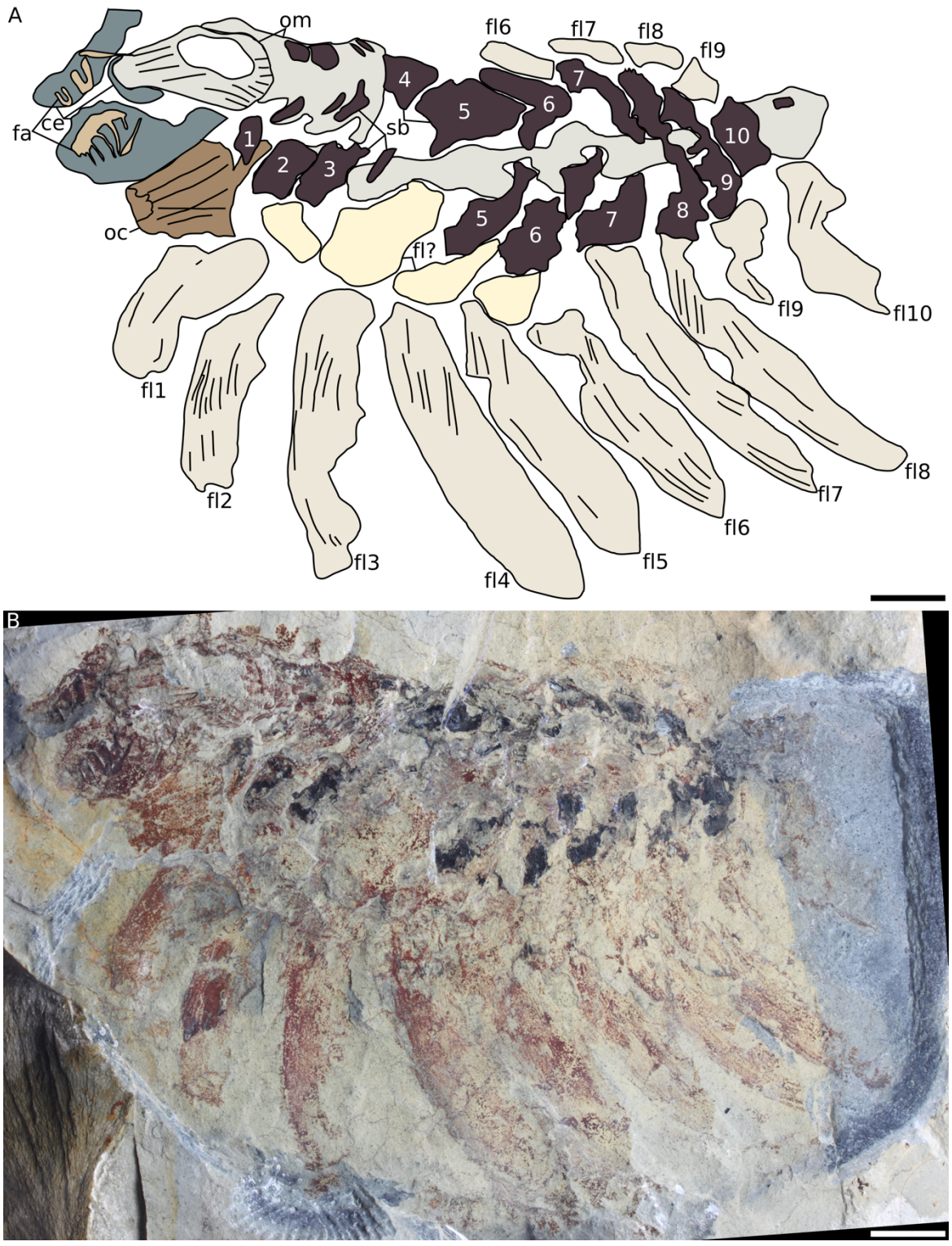

Fig. 1. KUMIP 314037, hurdiid nov gen et sp. Line drawing with key features, and photograph under water using polarized lighting. Abbreviations: ce, carapace element; fa, frontal appendages; flX, ventral flap X; fl?, putative dorsal flap; sb, setal blade; 1, 2,…,10, setal blades associated with body segment. Scale bars = 10 mm.

1, oc), and unidentified organic material (Fig. 1, om) immediately posterior, and ten sets of setal blades (Fig. 1, sb, 1-10) associated with lateral flaps (Fig. 1, fl1 – fl10) making up the rest of the body.

The frontal appendages ('mouth apparatus' of Briggs et al. 2008, fig. 1) are poorly preserved (length of dorsal surface of left appendage is 12 mm). The ventral endites are preserved in a black colour with relief, anterior to a pale region (Fig. 2F, black and white arrows). Podomeres are preserved in the same pale colour, separated by thin red podomere boundaries. The podomeres are preserved close to parallel to sagittal plane of the body, with the tips of the ventral endites pointing towards the lateral margins of this plane. For both left and right appendages, the shaft endite is orientated distally, with horizontal ridges apparent on the shaft endite of the left appendage (?en2, Fig. 2E). Four endites from the distal articulated region of equal length are preserved on the proximalmost four podomeres (Fig 2E, en3-6). It is not clear whether the slightly shorter, more distal, endite attaches to the sixth or seventh podomere (Fig. 2E, en?6). The left frontal appendage shows at least six podomeres, all from the distal articulated region, and additional shorter endites (Fig. 2E, en) on more distal podomeres. Faint straight podomere boundaries can be seen between pd2, pd3 and pd4, with even fainter traces visible more distally (Fig. 2E, pdb?). The distal end of the appendages is not preserved.

Associated with the appendages are two lateral carapace elements (Fig. 2C, lat; 'eye' of Briggs et al. 2008. fig. 1), which are preserved in a textured red coloration. The right lateral element is preserved at an oblique angle, with the left element preserved near-parallel to bedding, so its outline can be more clearly seen. The anterior margin is subcircular, with the dorsal and ventral margins tapering towards a posterior projection,

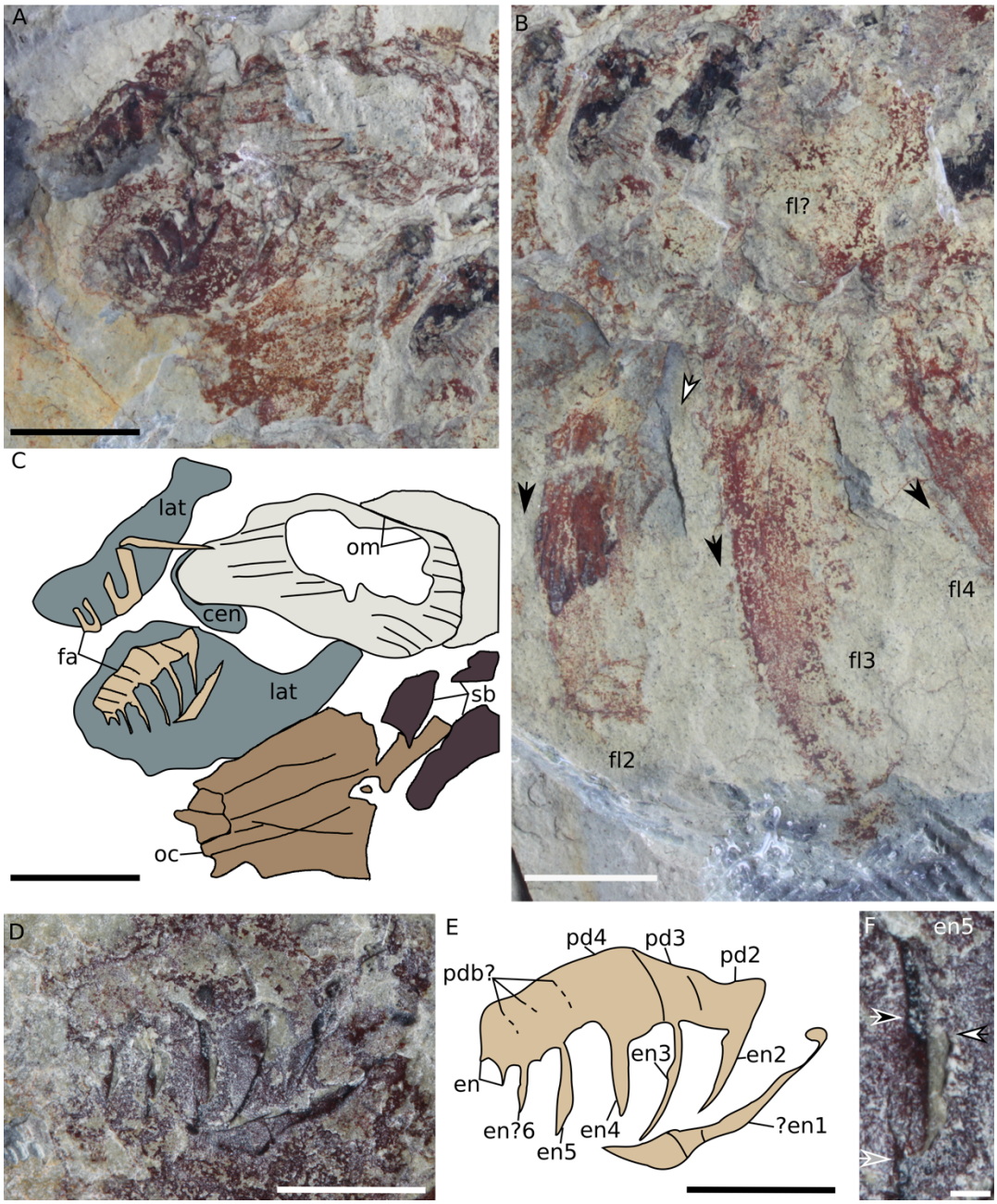

Fig. 2. KUMIP 314037, hurdiid nov gen et sp. cropped close-ups of key features. **A, C.** Anterior region with carapace elements, frontal appendages, and oral cone. **B.** Body region showing ventral flaps and putative dorsal flaps. **D, E.** Left frontal appendage with endites and podomere boundaries. **F.** Endite, arrows indicate differential preservation. Abbrevations: cen, central carapace element; enX, endite X; fa, frontal appendage; flX, ventral flap X; fl?, putative dorsal flap; lat, lateral carapace element; pdX, podomere X; sb, setal blade. Scale bars: A, B, C = 10 mm; D, E = 5 mm; F = 0.5 mm.

which leads under the organic material towards the posterior of the central carapace element. Only the very anterior margin of the central element (Fig. 2C, cen) can be seen under this organic material.

Adjacent to the left lateral carapace element is an oral cone preserved compressed laterally, composed of a number of overlying plates (Fig. 2C, oc). The texture and coloration of the oral cone is different to both the flaps and the carapace elements. A small subcircular opening can be seen at the anterior of the cone. The arrangement of large and small plates, and the presence or absence of any interior rows of teeth, cannot be ascertained owing to the orientation of preservation.

At the posterior of the oral cone, the anteriormost setal blades can be seen, preserved in a blue-grey coloration (Fig. 2C, sb). Ten setal blade blocks ('phosphatic material' of Briggs et al. 2008, fig. 1) are present along the body, although these are overlain by indistinct cuticle material ('?ridges' of Briggs et al. 2008, fig. 1) at the anterior and along part of the sagittal axis (Fig. 1, sb, 1-10). Each of the setal blades is associated with a large lobate flap ('lobate appendages' of Briggs et al. 2008, fig. 1) on the left side of the body, with transverse lines visible. Partial flaps associated with setal blades six to nine can also be seen on the right-hand side of the body. The transverse lines run parallel to the long axis of the flap, and are most visible on the flap associated with the second setal blade (Fig. 2B, fl2). There is weak evidence for smaller flaps dorsal to the larger flaps at the anterior of the body, overlying parts of setal blades 2-6 (Fig. 1A, fl?, 2B fl?). This material is preserved in a similar texture and coloration to the large flaps, and the transverse lines, when visible, point in a different orientation (contrast the white and black arrows in Fig. 2B). The putative second pair of flaps are not preserved along the length of the animal, and do not have a clear outline.

Other organic material (Fig. 2C, om), overlying the central carapace element, also preserves strong lineations, although the texture is very different to that of the flaps and the lineations diverge. There is evidence for compaction wrinkling at the posterior of this unidentified organic material.

Remarks

The presence of dorsal and ventral flaps, as well as lateral carapace elements of similar size and associated with frontal appendages confirms the identity of this body as a hurdiid. The poorly preserved appendages bear most similarity to the frontal appendages of *Ursulinacaris grallae* (*this thesis Chapter 8*) and *Peytoia?* from the Burgess Shale (Daley & Budd 2010), owing to the five slender endites in the distal articulated region, and elongate endite on the distalmost point of the shaft.

This specimen has a longer body relative to frontal appendages and carapaces than other radiodonts. The ratio of the length of frontal appendage to body length (approximately 1:8) is lower than for other hurdiids (e.g. *Peytoia*, approximately 1:4) and other radiodonts as a whole (*Amplectobelua* has the lowest ratio of any other radiodont, approximately 1:5). Similarly, the ratio of the carapace length to body length, here measured from the lateral carapace element, is much lower (approximately 4.5:1) than in *Hurdia* (2.5:1) (Lerosey-Aubril & Pates 2018).

The lobate appearance of the flaps may be a taphonomic artefact. Similar preservation of *Lyrarapax* flaps was reported in the holotype, but other specimens show a flap morphology much more similar to other radiodonts such as *Anomalocaris* and *Hurdia* (Cong et al. 2014; 2016; Daley et al. 2009; Daley & Edgecombe 2014). The possible presence of two pairs of flaps adds further support for its inclusion within

Hurdiidae, as the presence of two pairs of body flaps has only been reported from radiodonts within this family, in *Aegirocassis, Hurdia,* and *Peytoia* (Van Roy et al. 2015).

Results

Parsimony analysis

Two different tree topologies were obtained (Fig. 3), one for k values from 1 to 4 (Fig 3A), the other for k values of 5 to 10 (Fig. 3B). Analyses using the lower k values produced 36 trees (CI 0.581, RI 0.779), and the higher k values produced 6 trees (CI 0.595, RI 0.791) (results produced by all analyses are provided in Supplemental Document 3). A number of results are consistent across all the analyses: Hurdiidae is resolved as sister to all other radiodonts, Anomalocarididae is polyphyletic and sister to Amplectobeluidae, and Tamisiocarididae is sister to a clade containing Amplectobeluidae and Anomalocarididae. The topology of taxa within Hurdiidae and Amplectobeluidae is mostly consistent, with the exception of a few taxa. In addition, in both topologies, Amplectobeluidae forms a clade nested within a paraphyletic Anomalocarididae (k = 5-10) or as part of an unresolved node with several members of Anomalocarididae (k =1-4).

The positions of *Caryosyntrips, Ursulinacaris grallae, Peytoia?, Anomalocaris kunmingensis,* and *Laminacaris chimera* represent the major differences between the two tree topologies, alongside differences in the internal relationships of Anomalocarididae. *Caryosyntrips* is resolved as the earliest diverging member of the non-hurdiid clade for lower k values, but diverges later than tamisiocaridids at higher k values (compare C in Fig. 4A to 4B). *Ursulinacaris* resolves as the earliest diverging hurdiid at lower k values, but as the earliest diverging member of the non-hurdiid

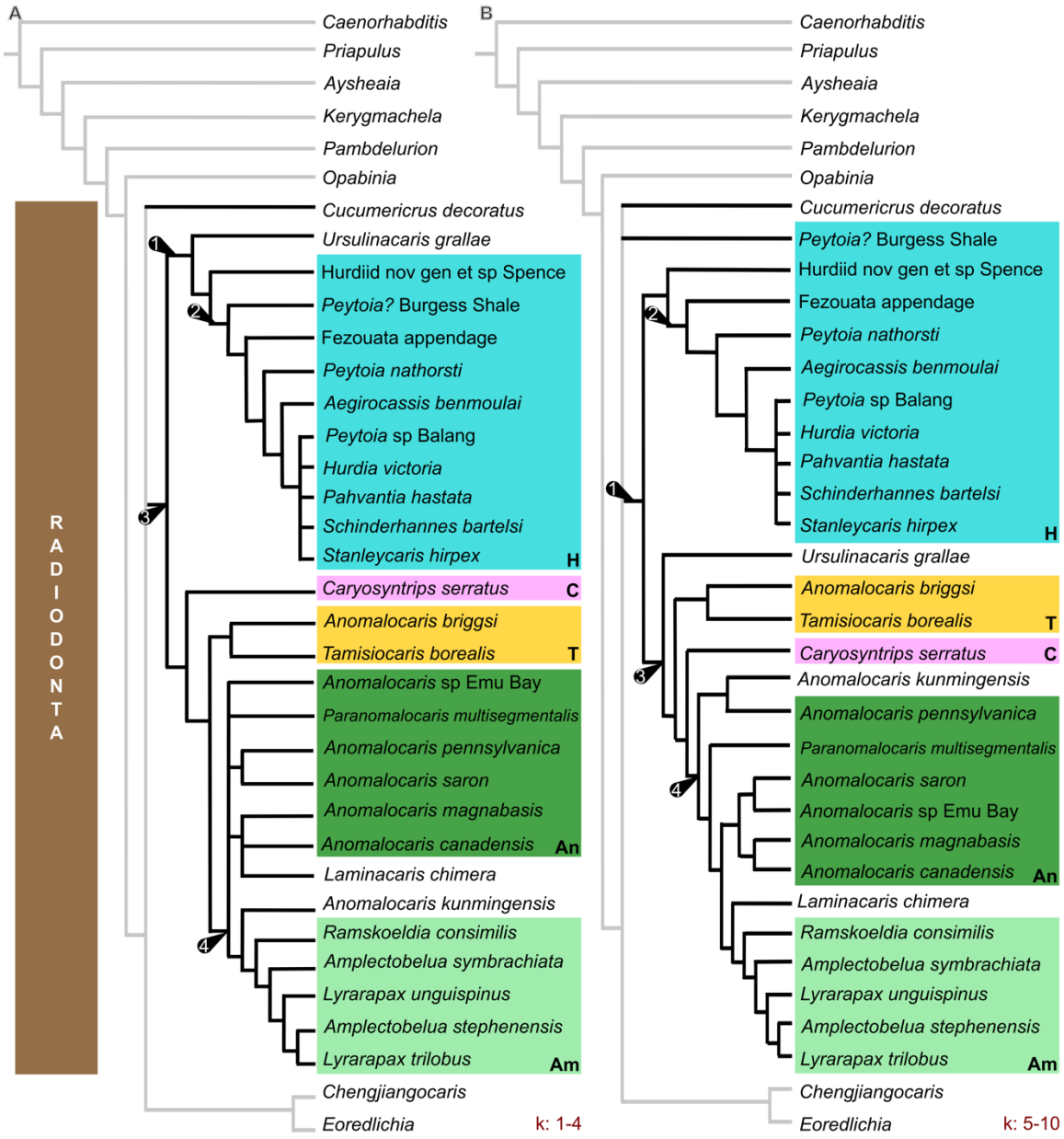

Fig. 3. Majority consensus of the most parsimonious trees (mpts) obtained under different values of the concavity constant k. **A.** k: 1-4, 36 mpts, CI = 0.581, RI = 0.779. **B.** k: 5-10, 6 mpts, CI = 0.595, RI = 0.791. Numbered arrows: 1, hurdiid endite organisation; 2, unpaired blade-like endites; 3, paired slender endites; 4, endites alternating long/short on subsequent podomeres. Abbreviations: Am, Amplectobeluidae; An, Anomalocarididae; C, *Caryosyntrips*; H, Hurdiidae; T, Tamisiocarididae.

branch at higher k values. *Anomalocaris kunmingensis* and *Laminacaris chimera* switch places between resolving as the earliest diverging amplectobeluids, or as anomalocaridids, depending on the concavity constant employed.

Sequence of character acquisition in frontal appendages

The sequence of character acquisition in both phylogenetic hypotheses is slightly different. For the low k tree, the hurdiid organisation of the proximal five podomeres in the distal articulated region bearing endites is basal to hurdiids, but this is plesiomorphic for all radiodonts in the high k value tree (Fig. 3, arrow 1). The acquisition of blade-like endites in hurdiids occurs very early in the group in both hypotheses (Fig. 3, arrow 2). The presence of paired slender endites is plesiomorphic to all radiodonts by the low k hypothesis, but only to all non-hurdiid radiodonts by the high k hypothesis (Fig. 3, arrow 3), with the presence of endites which alternate long/short on subsequent podomeres a derived trait unique to amplectobeluids and anomalocaridids in both hypotheses (Fig. 3, arrow 4).

Discussion

Radiodont family relationships

Regardless of the concavity constant employed, the relationships of the radiodont families to one another is different compared to all previous analyses, as a result of the introduction of a number of previously uncoded taxa, and the removal of the taphonomic *Hurdia* terminals (*Hurdia* cf. *victoria* Spence, *Hurdia* sp. B, and *Hurdia* sp. B Spence) used in previous analyses. In addition, although its exact position is not consistent between the two topologies, *Caryosyntrips* is resolved within Radiodonta,

rather than in a polytomy with other radiodonts (compare the position of C in Fig. 4A, B to Fig. 4C), *Cucumericrus*, and deuteropods, as in previous studies, but *Cucumericrus* is still in this polytomy and outside of Radiodonta. *Caryosyntrips* has a unique and very different frontal appendage morphology compared to all other radiodonts, and no other body parts, with the exception of the very anterior of a central carapace element, are known (Daley & Budd 2010; Pates & Daley 2017). This is the reason it does not resolve in one of the four described families (and previously resolved outside of Radiodonta), and indeed *Caryosyntrips* likely belongs in its own, discrete, family. The frontal appendages of *Caryosyntrips* are so unique that its position (either as the earliest diverging member of the non-hurdiid branch, or between Tamisiocarididae and Anomalocarididae) should be treated with scepticism until other body parts are known.

Polyphyletic anomalocaridids and problematic taxa

Anomalocaridids are resolved as polyphyletic, likely a result of the poorly known nature of these taxa. Only two of eight potential members of this family, *Anomalocaris canadensis* and *A. saron,* are known from complete body fossils (Hou et al. 1995; Daley & Edgecombe 2014), and there are differences between these bodies, although mouthparts and flaps are known in *A. magnabasis* (*this thesis Chapter 7*). This is in contrast to hurdiids (five of 11) and amplectobeluids (three of six). This polyphyly is likely augmented by the history of research into radiodonts. *Anomalocaris* was the first taxon described, and as such, some taxa that are now in need of redescription or reassignment (e.g. *Anomalocaris kunmingensis*) are currently treated as belonging to this genus, because at the time of their original description (Wang et al. 2013), fewer radiodont taxa were known and the genus *Anomalocaris* was the best fit.

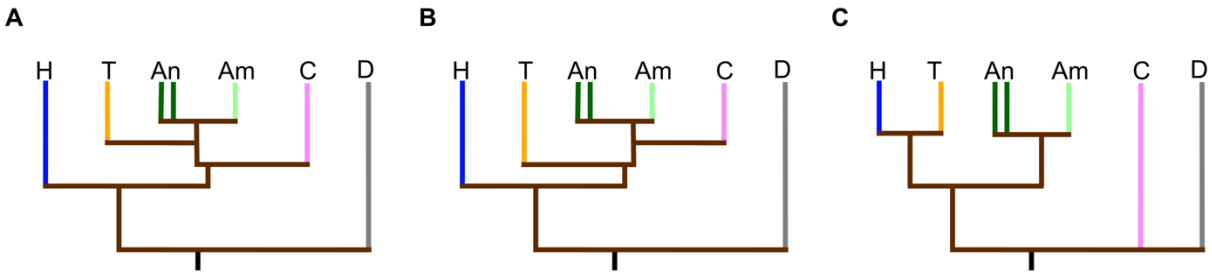

Fig. 4. A comparison of different phylogenetic hypotheses for radiodont families presented in this study, and all previous phylogenetic analyses of radiodonts. **A.** This study, low k hypothesis (Fig. 3A). **B.** This study, high k hypothesis (Fig. 3B). **C.** All phylogenetic analyses from Vinther et al. (2014) to Lerosey-Aubril & Pates (2018). Abbreviations: Am, Amplectobeluidae; An, Anomalocarididae; C, *Caryosyntrips*; D, Deuteropoda; H, Hurdiidae; T, Tamisiocarididae.

Laminacaris chimera (and *Anomalocaris kunmingensis*) resolves as either an amplectobeluid or anomalocaridid, and as such the similarity in the hypertrophied blade-like endite to *Hurdia* endites represents a convergence rather than evidence for this character, predating the organisation of hurdiid frontal appendages. The presence of a small spine on the proximal edge of the hypertrophied endite represents a slight difference between these two forms, which adds support to this result, and indeed the presence of proximal auxiliary spines is a character that separates the non-hurdiid branch from hurdiids in the low k hypothesis, and is derived later in the high k hypothesis (at arrow 3 in Fig. 3B). Placing *Laminacaris* more exactly is currently problematic, as this taxon is known only from frontal appendages, and amplectobeluid and anomalocaridid frontal appendages can be very similar. This is highlighted by the frontal appendages of *Ramskoeldia*, which are superficially very similar to *Anomalocaris* but have a slightly longer endite on the fifth podomere in the distal articulated region than the third (Cong et al. 2018). Amplectobeluid frontal appendages tend to have larger hypertrophied endites on the first podomere in the distal articulated region, although this is not the case in *Ramskoeldia*. The presence of gnathobase-like-structures is diagnostic for amplectobeluids, (though not present in *Lyrarapax*) and a triradial oral cone would be diagnostic for Anomalocarididae. As *A. kunmingensis* and *L. chimera* lack information on these feeding structures, and other body parts in general, their current position between these two families cannot be resolved.

Character acquisition in radiodont frontal appendages and the ecology of ancestral radiodonts

Both low and high k value trees (Fig. 3A, B) support the hypothesis that the organisation of the hurdiid frontal appendage has a deep root in hurdiid evolution, that predated the origin of the blade-like endite in this group (arrow 1 predates arrow 2 in both Fig. 3A and Fig. 3B). If *Ursulinacaris* is an early-diverging hurdiid (Fig. 3A, low k value tree), this would mean that paired endites represents the plesiomorphic condition for radiodont frontal appendages (arrow 3 in Fig. 3A), with the blade-like endite representing a derived state for this family (arrow 2 in Fig. 3A). If instead *Ursulinacaris* is an early-diverging member of non-hurdiid branch (Fig. 3B, high k value tree), this would mean that the arrangement of endites visible in all hurdiids (elongate endites on the first five podomeres in the distal articulated region) represents the plesiomorphic condition for all radiodonts (arrow 1 in Fig. 3B), but that the plesiomorphic number of endites per podomere (paired or unpaired) is not known. The earliest diverging hurdiid in the high k topology is the new hurdiid described in this contribution (Figs. 1, 2), which bears thin endites, not the broad blades known in most hurdiid taxa. The identification of other body parts belonging to *Ursulinacaris*, such as oral cones, dorsal flaps, or lateral carapace elements, would provide the evidence required to confidently place this taxon in one of these two positions, and reveal more plesiomorphic characters of radiodont frontal appendages.

There is overlap between the feeding modes proposed for Hurdiidae and Tamisiocarididae, with both sediment sifting and suspension feeding hypothesised for members of both families. Suspension feeding evolved at least twice in Radiodonta, once in Tamisiocarididae (*Tamisiocaris borealis*) and twice within Hurdiidae, as

Aegirocassis and *Pahvantia* do not form a clade and have different arrangements of setae on their endites (Vinther et al. 2014; Van Roy et al. 2015; Lerosey-Aubril & Pates 2018). Sediment sifting, using long endites without a fine mesh (which would imply suspension feeding) is the inferred habit for most hurdiids (all except *Aegirocassis* and *Pahvantia*), as well as the tamisiocaridid *Anomalocaris briggsi* (Daley et al. 2013b), and putative hurdiid *Ursulinacaris* (*this thesis Chapter 8*). Assuming that the character states in Caryosyntrips represent a derived form, a sifting or filtering ecology can be inferred as basal to radiodonts, with the characters required for raptorial predation being derived. The character endites of sub equal length is a plesiomorphic character of radiodont frontal appendages under both phylogenetic hypotheses, as shown by the positions of Hurdiidae and Tamisiocarididae as the earliest diverging members of both branches of the radiodont trees obtained here (excluding the derived *Caryosyntrips;* Fig. 3).

The characters crucial for the raptorial predatory feeding mode inferred for members of Amplectobeluidae and Anomalocarididae, a large or hypertrophied endite on the first podomere in the distal articulated region and endites which alternate long/short on subsequent podomeres, are derived and only found in these two late-diverging families (arrow 4 in Fig. 3). Thus the raptorial predatory style traditionally associated with these large Cambrian animals (e.g. Whittington & Briggs 1985; Nedin 1999) in fact represents a derived ecology found only in two of four currently diagnosed radiodont families, and one of two branches of the radiodont tree proposed here.

Conclusions

Including recently (re)described hurdiid taxa, alongside removing putative *Hurdia* species that in fact represent taphonomic grades of the same taxon, resulted in a novel phylogenetic hypothesis for the relationships of radiodont families. Hurdiidae is suggested to be sister to a clade containing other radiodont families, with Tamisiocarididae in a sister group position to Anomalocarididae and Amplectobeluidae. *Caryosyntrips* is hypothesized to belong to the non-hurdiid branch (and resolved within Radiodonta for the first time), however, its position, either as the earliest diverging taxon, or diverging after Tamisiocarididae and before Anomalocarididae, should be treated with scepticism as this genus is known only from frontal appendages that have a very different morphology to all other radiodont genera.

The new phylogenetic hypothesis put forward here suggests that raptorial predation, as demonstrated by amplectobeluids and anomalocaridids, represents a derived ecological style among radiodonts, with sediment sifting in Hurdiidae and Tamisiocarididae representing the ecology of early diverging members of the group. The ancestral radiodont appendage likely had elongate slender endites of sub equal length, either paired and/or in the hurdiid arrangement.

Anomalocarididae was resolved as polyphyletic, likely a result of poorly known taxa (those only known from frontal appendages), taxa in need of redescription, and the confounding influences of the unstable position (between anomalocaridids and amplectobeluids) of *Anomalocaris kunmingensis* and *Laminacaris chimera* depending on analysis parameters. The similarities between the hypertrophied endite of *Laminacaris* and *Hurdia* endites are suggested to be convergent.

Ursulinacaris grallae represents either the earliest (known) diverging hurdiid, or the earliest known diverging member of the non-hurdiid clade. Either placement demonstrates that the organisation of the hurdiid frontal appendage has a deep root in the group, and raises the potential that this organisation is plesiomorphic for radiodonts as a whole. The alternate explanation shows that paired elongate endites are plesiomorphic for radiodonts as a whole, as previously suggested (*this thesis, Chapter 8*).

Acknowledgements

SP is funded by an Oxford-St Catherines Brade-Natural Motion Scholarship, and the visit to the KUMIP was funded by a Palaeontological Association Sylvester-Bradley Award (PA-SB201503). We thank P Cong, GD Edgecombe, and BS Lieberman for discussions. The program TNT was made available with the sponsorship of the Willi Hennig Society.

References

Briggs, D. E., Lieberman, B. S., Hendricks, J. R., Halgedahl, S. L., & Jarrard, R. D. (2008). Middle Cambrian arthropods from Utah. *Journal of Paleontology*, 82(2), 238-254.

Budd, G. E. (2002). A palaeontological solution to the arthropod head problem. *Nature*, 417(6886), 271.

Chen, J., Waloszek, D., & Maas, A. (2004). A new 'great-appendage'arthropod from the Lower Cambrian of China and homology of chelicerate chelicerae and raptorial antero-ventral appendages. *Lethaia*, 37(1), 3-20.

Cong, P., Ma, X., Hou, X., Edgecombe, G. D., & Strausfeld, N. J. (2014). Brain structure resolves the segmental affinity of anomalocaridid appendages. *Nature*, 513(7519), 538.

Cong, P., Daley, A. C., Edgecombe, G. D., Hou, X., & Chen, A. (2016). Morphology of the radiodontan *Lyrarapax* from the early Cambrian Chengjiang biota. *Journal of Paleontology*, 90(4), 663-671.

Cong, P., Daley, A. C., Edgecombe, G. D., & Hou, X. (2017). The functional head of the Cambrian radiodontan (stem-group Euarthropoda) *Amplectobelua symbrachiata*. *BMC Evolutionary Biology*, 17(1), 208.

Cong, P. Y., Edgecombe, G. D., Daley, A. C., Guo, J., Pates, S., & Hou, X. G. (2018). New radiodonts with gnathobase-like structures from the Cambrian Chengjiang biota and implications for the systematics of Radiodonta. *Papers in Palaeontology*, 4(4), 605-621.

Daley, A. C., Budd, G. E., Caron, J. B., Edgecombe, G. D., & Collins, D. (2009). The Burgess Shale anomalocaridid *Hurdia* and its significance for early euarthropod evolution. *Science*, 323(5921), 1597-1600.

Daley, A. C., & Budd, G. E. (2010). New anomalocaridid appendages from the Burgess Shale, Canada. *Palaeontology*, 53(4), 721-738.

Daley, A. C., Budd, G. E., & Caron, J. B. (2013a). Morphology and systematics of the anomalocaridid arthropod *Hurdia* from the Middle Cambrian of British Columbia and Utah. *Journal of Systematic Palaeontology*, 11(7), 743-787.

Daley, A. C., Paterson, J. R., Edgecombe, G. D., García-Bellido, D. C., & Jago, J. B. (2013b). New anatomical information on *Anomalocaris* from the Cambrian Emu Bay Shale of South Australia and a reassessment of its inferred predatory habits. *Palaeontology*, 56(5), 971-990.

Daley, A. C., & Edgecombe, G. D. (2014). Morphology of *Anomalocaris canadensis* from the Burgess Shale. *Journal of Paleontology*, 88(1), 68-91.

Goloboff, P. A., Farris, J. S., & Nixon, K. C. (2008). TNT, a free program for phylogenetic analysis. *Cladistics*, 24(5), 774-786.

Guo, J., Pates, S., Cong, P., Daley, A. C., Edgecombe, G. D., Chen, T., & Hou, X. (2018). A new radiodont (stem Euarthropoda) frontal appendage with a mosaic of characters from the Cambrian (Series 2 Stage 3) Chengjiang biota. *Papers in Palaeontology*. Online early view, doi: 10.1002/spp2.1231

Hou, X-G., Bergström, J., & Ahlberg, P. (1995). *Anomalocaris* and other large animals in the Lower Cambrian Chengjiang fauna of southwest China. *GFF*, 117(3), 163-183.

Hou, X-G., Bergström, J., & Yang, J. (2006). Distinguishing anomalocaridids from arthropods and priapulids. *Geological Journal*, 41(3-4), 259-269.

Lankester, E.R. (1904). The structure and classification of Arthropoda. Quarterly journal of microscopical science. 47, 523-582.

Lerosey-Aubril, R., Hegna, T. A., Babcock, L. E., Bonino, E., & Kier, C. (2014). Arthropod appendages from the Weeks Formation Konservat-Lagerstätte: new occurrences of anomalocaridids in the Cambrian of Utah, USA. *Bulletin of Geosciences*, 89(2), 269-282.

Lerosey-Aubril, R., & Pates, S. (2018). New suspension-feeding radiodont suggests evolution of microplanktivory in Cambrian macronekton. *Nature Communications*, 9(1), 3774.

Liu, J., Lerosey-Aubril, R., Steiner, M., Dunlop, J. A., Shu, D., & Paterson, J. R. (2018). Origin of raptorial feeding in juvenile euarthropods revealed by a Cambrian radiodontan. *National Science Review*.

Nedin, C. (1999). *Anomalocaris* predation on nonmineralized and mineralized trilobites. *Geology*, 27(11), 987-990.

Nielsen, C. (1995). Animal evolution: interrelationships of living phyla. Oxford University Press.

Paterson, J. R., García-Bellido, D. C., Lee, M. S., Brock, G. A., Jago, J. B., & Edgecombe, G. D. (2011). Acute vision in the giant Cambrian predator *Anomalocaris* and the origin of compound eyes. *Nature*, 480(7376), 237.

Pates, S., & Daley, A. C. (2017). *Caryosyntrips*: a radiodontan from the Cambrian of Spain, USA and Canada. *Papers in Palaeontology*, 3(3), 461-470.

Pates, S., & Daley, A. C. (2018). The Kinzers Formation (Pennsylvania, USA): the most diverse assemblage of Cambrian Stage 4 radiodonts. Geological Magazine, Online early view: doi.org/10/1017/S0016756818000547.

Pates, S., Daley, A. C., & Lieberman, B. S. (2018). Hurdiid radiodontans from the middle Cambrian (Series 3) of Utah. *Journal of Paleontology*, 92(1), 99-113.

Van Roy, P., Daley, A. C., & Briggs, D. E. (2015). Anomalocaridid trunk limb homology revealed by a giant filter-feeder with paired flaps. *Nature*, 522(7554), 77.

Vinther, J., Stein, M., Longrich, N. R., & Harper, D. A. (2014). A suspension-feeding anomalocarid from the Early Cambrian. *Nature*, 507(7493), 496.

Wang, Y., Huang, D., & Hu, S. (2013). New anomalocardid frontal appendages from the Guanshan biota, eastern Yunnan. *Chinese Science Bulletin*, 58(32), 3937-3942.

Whittington, H. B., & Briggs, D. E. G. (1985). The largest Cambrian animal, Anomalocaris, Burgess Shale, British-Columbia. *Philosophical Transactions of the Royal Society of London B,* 309(1141), 569-609.

Chapter 10

Analysis of the diversity and disparity of Radiodonta reveals two phases of evolution within the group

Author contributions

SP conceived the project; SP performed the analyses; SP wrote the manuscript and prepared the figures, with input from ACD.

Publication information

This Chapter has not been submitted for publication.

Additional information

The supplemental material for this Chapter is in Appendix 3.

Analysis of the diversity and disparity of Radiodonta reveals two phases of evolution within the group

Stephen Pates[1,2]* and Allison C. Daley[2]

[1] Department of Zoology, University of Oxford, South Parks Road, Oxford, OX1 3PS, UK

[2] Institute of Earth Sciences, University of Lausanne, Lausanne Ch-1015, Switzerland

*email: stephen.pates@zoo.ox.ac.uk

Key words: Radiodonta, Cambrian, diversity, disparity, Hurdiidae

Abstract

Patterns of morphological change and diversity provide evidence for how clades diversified. Radiodonta, a group of large nektonic animals known from nearly all Cambrian Burgess Shale-type Lagerstätten (BSTs), offer a good model for disparity studies in the early Palaeozoic, as they were diverse and ecologically important raptorial predators, sediment sifters, and filter feeders. The frontal appendages of radiodonts provide a suitable object for studies of disparity as they have a high preservation potential in BSTs, contain a large number of characters, and are the most readily identifiable and informative body part for the ecology of these animals.

Five time bins of 4 to 4.5 million year lengths were defined, from 521 – 500.5 Ma, to assess the changing diversity and disparity of the group through time. A novel character matrix (20 characters) for radiodont frontal appendages was created bespoke for a study of the disparity. This was subjected to a principal coordinate analysis, and

the disparity (sums of ranges and variances) of Radiodonta was assessed at each time bin and at the family level.

Radiodont diversity peaks in the first time bin (521 – 517 Ma) and fourth time bin (509 – 504.5 Ma). Amplectobeluidae (nine), Anomalocarididae (nine), and Hurdiidae (14) have the highest number of taxa overall, with Tamisiocarididae and *Caryosyntrips* offering three each. Amplectobeluidae and Anomalocarididae dominate radiodont diversity in the oldest three time bins (521 – 509 Ma) and Hurdiidae the youngest two (509 – 500.5 Ma), with the differing evolutionary histories of these families responsible for the two peaks in radiodont diversity. Radiodont disparity shows a different pattern, being highest in the first three time bins (521 – 509 Ma) and is lower for the younger two (509 – 500.5 Ma). The disparities of Amplectobeluidae, Anomalocarididae, and Hurdiidae are broadly similar. Amplectobeluids and anomalocaridids slightly overlap in morphospace area occupation in the oldest time bin, with hurdiids occupying a position very far from both. Hurdiids continue to occupy novel areas in morphospace after their peak diversity, whereas amplectobeluids and anomalocaridids do not.

The relative success of hurdiids after 509 Ma, when compared to amplectobeluids and anomalocaridids, could be in part related to the ability of this group to continue to occupy new areas in morphospace (i.e. continue to innovate) and occupy new ecological niches (as shown by the convergent evolution of filter feeding). The lack of hurdiids from older (pre 509 Ma) Lagerstätten represents a true signal, not geographic or sampling bias, but the reasons for this are unclear.

Introduction

Studies of the dynamics of how clades diversified and evolved new bodyplans during the Cambrian provide the opportunity to explore the patterns of morphological change during this crucial period in animal history. The dynamics of disparity within different groups through the Phanerozoic show a convincing pattern for animal clades reaching their maximum morphological variety early in their history (Erwin 2007) with a meta-analysis of 98 metazoan clades revealing a tendency towards this early high disparity (Hughes et al. 2013). Disparity trends have also been compared to taxonomic diversity, and these two features of a clade often peak at different times (e.g. Foote 1993, 1994, 1995, 1999; Wagner 1997; Wills 1998; Deline & Ausich 2011; Hopkins 2013), since they measure different features of a clade's evolution. Taxonomic diversity measures the origination and extinction of species within a clade, whereas disparity measures the differences in bodyplans or individual body parts. It is possible for a clade to have a high number of taxa with very similar morphologies (high diversity, low disparity), and similarly for a clade to be made up of a few taxa with very different bodyplans (low diversity, high disparity). In fact, a constrained body plan may result in an increase in diversity (Rabosky et al. 2012).

There is a tendency for taxa to 'clump' in morphospace (a multidimensional representation of a character matrix), and the apparent large differences between members of the same clade indicate controls on body form (and hence morphospace occupation). These differences can be the result of intrinsic or extrinsic factors. Intrinsic controls include gene regulation and developmental canalisation, with extrinsic factors including ecology and environment (e.g. Myers & Saupe 2013). Studies exploring the disparity of Cambrian animals have shown both intrinsic and extrinsic controls on body

form, which can fluctuate through time (e.g. Hopkins 2014; Aria & Caron 2015; Yang et al. 2015; Caron & Aria 2017).

Radiodonts as study animals for Cambrian disparity

Radiodonts are a good study animal for the exploration of disparity in the early Palaeozoic. Over thirty species belonging to different families with a number of ecologies are known from BSTs worldwide (Table 1). As such this group allows for the study of changes in disparity at a high resolution in the Cambrian period, and its potential interaction with phylogenetic and ecological factors.

Radiodonta are a diverse group of nektonic animals ranging in size from under 10 centimetres to over two meters (Lerosey-Aubril & Pates 2018) originating in the early Cambrian and with representatives in the Ordovician and potentially the Devonian (e.g. Chen et al. 1994; Hou et al. 1995; Kühl et al. 2009; Daley & Legg 2015; Van Roy et al. 2015). After the first complete radiodonts were described, these animals were considered to be apex predators capable of durophagous predation (e.g. Whittington & Briggs 1985; Nedin 1999); however, as the true diversity of the group was revealed over the next thirty years, a variety of ecologies, informed by frontal appendage morphology (e.g. Daley & Budd 2010) and detailed examination of the oral cone (Daley & Bergström 2012) were recognised for the group. Radiodonts are now suggested to occupy a variety of ecological niches, including filter feeders (Vinther et al. 2014; Van Roy et al. 2015; Lerosey-Aubril & Pates 2018), sediment sifters (Daley et al. 2013a, b), raptorial predators (Daley & Edgecombe 2014), and slicing predators (Daley & Budd 2010; Pates & Daley 2017). These ecological niches are not spread evenly throughout the group, but are instead clustered within family groupings. Of the four radiodont families diagnosed

Table 1. List of BSTs with known radiodont taxa.

	Families	Taxa	References
Stage 3			
Zawiszyn Formation	H	*Peytoia infercambriensis*	Daley & Legg 2015
Sirius Passet biota	T	*Tamisiocaris borealis*	Daley & Peel 2010
Chengjiang biota	Am, An, Cu	*Amplectobelua symbrachiata, Anomalocaris saron, Anomalocaris* sp., *Cucumericrus decoratus, Laminacaris chimera, Lyrarapax trilobus, Lyrarapax unguispinus, Ramskoeldia consimilis, Ramskoeldia platyacantha*	Chen et al. 1994; Hou et al. 1995; Cong et al. 2014, 2016, 2018
Shuijingtuo Formation	H	*Hurdia*?	Daley et al. 2013b
Stage 4			
Poleta Formation	?	Anomalocaridid indet.	English & Babcock 2010
Balang Formation	An, H	*Anomalocaris* sp., *Peytoia* sp.	Liu 2013
Wulongqing Formation	An	*Anomalocaris kunmingensis, Paranomalocaris multisegmentalis*	Wang et al. 2013
Emu Bay Shale	An, T	*Anomalocaris briggsi, Anomalocaris* sp.	Daley et al. 2013a
Cranbrook Shale	An	*Anomalocaris canadensis*	Briggs 1979
Kinzers Formation	Am, An, T	*Amplectobelua* sp., *Anomalocaris pennsylvanica*, *Laminacaris*? sp., *Tamisiocaris* sp.	Pates & Daley 2018
Latham Shale	Am	*Ramskoeldia* sp.	*This thesis Chapter 7*
Valdemiedes Formation	Ca	*Caryosyntrips* sp.	Pates & Daley 2017
Jangle Limestone	An	*Anomalocaris magnabasis*?	*This thesis Chapter 7*
Pioche Formation	An, H	*Anomalocaris magnabasis, Hurdia* sp.	*This thesis Chapter 7*
Wuliuan			
Mantou Formation	An(?)	Anomalocaridid indet.	Huang et al. 2012
Kaili biota	An(?)	Anomalocaridid indet.	Zhao et al. 2005
Pyramid Shale	H	*Ursulinacaris grallae*?	*This thesis Chapter 8*
Spence Shale	H	*Caryosyntrips camurus, Hurdia victoria,* Hurdiid gen et sp nov	Pates & Daley 2017; Pates et al.

			2018; *This thesis Chapter 9*
Mount Cap Formation	H	*Ursulinacaris grallae*	*This thesis Chapter 8*
Burgess Shale	Am, An, Ca, H	*Amplectobelua stephenensis, Anomalocaris canadensis, Caryosyntrips camurus, Caryosyntrips serratus, Hurdia triangulata, Hurdia victoria, Peytoia nathorsti, Peytoia*?	Daley & Budd 2010; Daley et al. 2013b; Pates & Daley 2017
Stanley Glacier	An, H	*Anomalocaris canadensis, Hurdia victoria, Stanleycaris hirpex*	Caron et al. 2010
Drumian			
Wheeler Formation	Ca, H	*Caryosyntrips durus, Caryosyntrips serratus, Pahvantia hastata, Peytoia nathorsti, Stanleycaris* sp.	Lerosey-Aubril & Pates 2018; Pates & Daley 2017; Pates et al. 2017, 2018
Marjum Formation	H	*Peytoia nathorsti*	Pates et al. 2018
Jince Formation	H	*Hurdia*	Daley et al. 2013b
Guzhangian			
Weeks Formation	An	*Anomalocaris* sp. 1, *Anomalocaris* sp. 2	Lerosey-Aubril et al. 2014
Ordovician			
Fezouata biota	H	*Aegirocassis benmoulai,* Hurdiid indet.	Van Roy & Briggs 2011; Van Roy et al. 2015
Devonian			
Hunsrück Slate	H	*Schinderhannes bartelsi*	Kühl et al. 2009; Cong et al. 2014

Abbreviations: Am, Amplectobeluidae; An, Anomalocarididae; Ca, Caryosyntrips; Cu, Cucumericrus; H, Hurdiidae; T, Tamisiocarididae; ?, uncertain or unknown.

to-date, two, Amplectobeluidae and Anomalocarididae, are thought to have utilised raptorial predation (e.g. Daley & Edgecombe 2014; Liu et al. 2018), and the other two, Hurdiidae and Tamisiocarididae, likely sifted sediment and filtered water in search of prey items ranging in size from micro to macroscopic (Daley et al. 2013a, b; Vinther et al. 2014; Van Roy et al. 2015; Lerosey-Aubril et al. 2018). Sediment sifting is plesiomorphic in hurdiids. Filter feeding likely evolved twice convergently, once in *Pahvantia hastata* and once in *Aegirocassis benmoulai,* as indicated by the differing morphology and arrangement of setae in these groups, and as they do not form a single clade in phylogenetic analyses (Van Roy et al. 2015; Lerosey-Aubril & Pates 2018). *Caryosyntrips*, a radiodont genus that likely belongs to its own family, is the only radiodont taxon thought to have used its frontal appendages as a pair to slice prey (Daley & Budd 2010; Pates & Daley 2017). Its unusual frontal appendage morphology means that its phylogenetic position is uncertain (*this thesis Chapter 9*), and this group has not always resolved within Radiodonta (e.g. Cong et al. 2014; Van Roy et al. 2015; Lerosey-Aubril & Pates 2018).

The frontal appendages of radiodonts provide a large number of characters for phylogenetic analyses and taxonomy, and allow identification of sometimes even partial material to the family, genus, or species level (Fig 1). The frontal appendage consists of a shaft that attaches adjacent to the mouthparts, and a distal articulated region that bears endites and dorsal spines. The number of podomeres, their shape, and morphology of endites and spines vary between and within families. Typically, amplectobeluids have a kink in the dorsal surface between the shaft and distal articulated region (Fig. 1A), and bear a hypertrophied endite on the first podomere in the distal articulated region (Fig. 1A, B). Endites along the remainder of the appendage

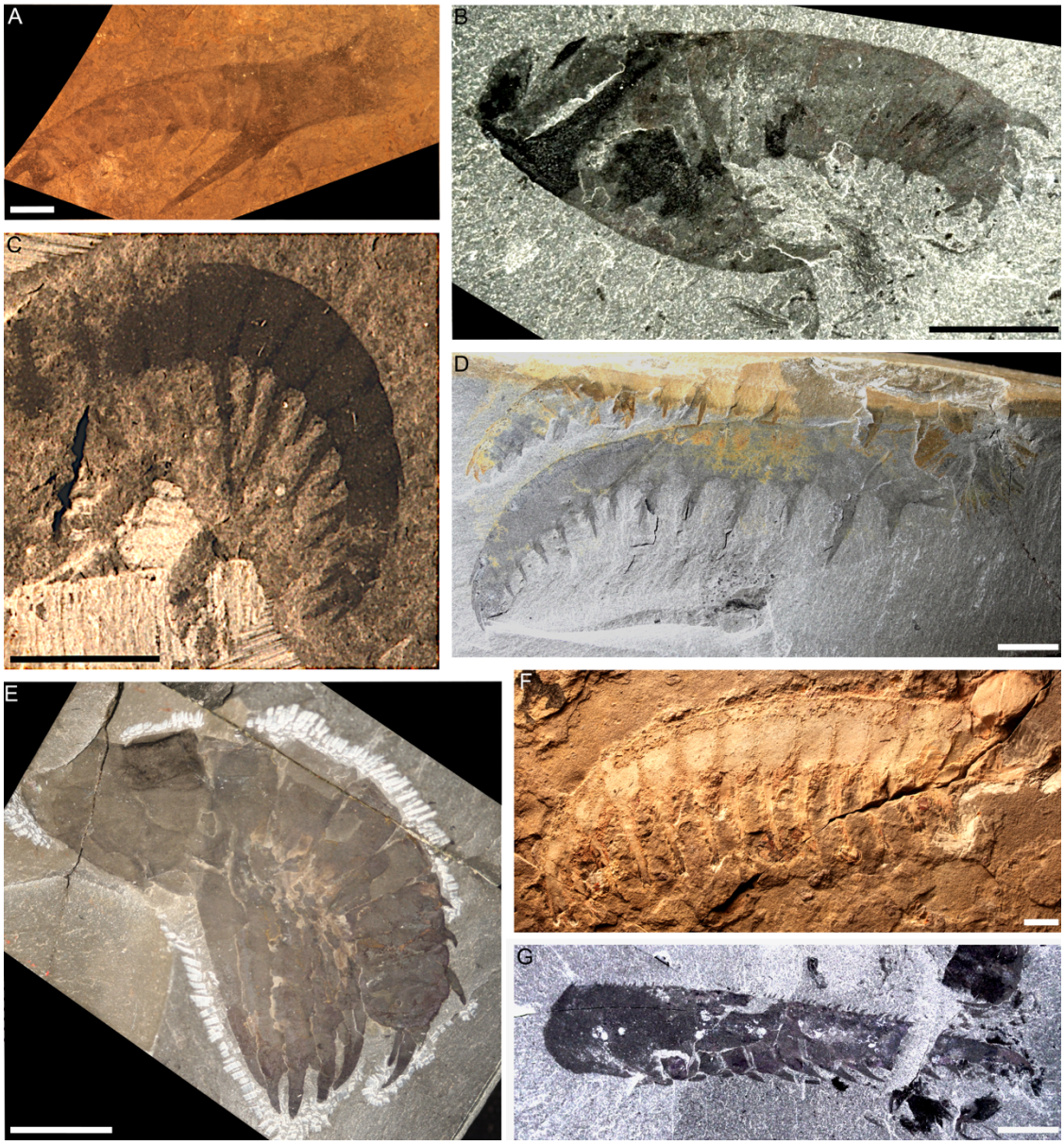

Fig. 1. Radiodont frontal appendages. **A.** *Amplectobelua symbrachiata* (Amplectobeluidae), Chengjiang biota, China, JS0600. **B.** *Amplectobelua stephensis* (Amplectobeluidae), Burgess Shale, Canada, ROM 59493. **C.** *Anomalocaris pennsylvanica* (Anomalocarididae), Kinzers Formation, USA, USNM 80487. **D.** *Anomalocaris canadensis* (Anomalocarididae), Burgess Shale, Canada, RQ 93-1106A (accessioned at the ROM). **E.** *Peytoia nathorsti* (Hurdiidae), Burgess Shale, Canada, USNM 240984. **F.** *Anomalocaris briggsi* (Tamisiocarididae), Emu Bay Shale, Australia, SAM 40180. **G.** *Caryosyntrips serratus,* Burgess Shale, Canada, ROM 57161, Photo credit: A, D. Fu; B, D – G, A. C. Daley. Scale bars: A, B, D – G = 10 mm; C = 5 mm.

in this family are reduced or absent, and paired and fairly simple when present. When they are present along the appendage, the endite on the fifth podomere is longer than that of the third (Fig. 1A, B). In addition, robust dorsal spines are often present at the distalmost end (Fig. 1B). Anomalocaridids tend to have an enlarged (but not hypertrophied) endite on the first podomere in the distal articulated region (Fig. 1D), and paired endites (Fig. 1C, D) which can be fairly complex and sometimes bear auxiliary spines (Fig. 1D), alternate long/short on subsequent podomeres, and reduce in length along the appendage (Fig. 1C, D). The distalmost four podomeres often bear very reduced endites (Fig. 1D). *Caryosyntrips* appendages bear only paired simple small triangular endites, on every podomere, and the appendages themselves have a subtriangular outline, very different to all other radiodonts (Fig .1G). Tamisiocaridids bear paired and elongate endites on every podomere in the distal articulated region with fine auxiliary spines on both distal and proximal faces (Fig. 1F). Hurdiids are the only family to bear unpaired endites, which are present on the first five podomeres in the distal articulated region (Fig. 1E). Endites on these podomeres are elongate, and bear auxiliary spines on the distal margin only (Fig. 1E). Additional reduced endites are sometimes present on one or two more distal podomeres, and also sometimes on the distalmost podomere in the shaft.

A few taxa are more problematic to assign (Fig 2), as they possess characters from a number of these families, and amplectobeluids and anomalocaridids in particular have sometimes proved difficult to distinguish based on frontal appendages alone. *Anomalocaris kunmingensis* (Wang et al. 2013) bears a hypertrophied endite on the first podomere in the distal articulated region, but otherwise the appendages appear more similar to anomalocaridids. *Laminacaris chimera* (Fig. 2C) similarly bears a

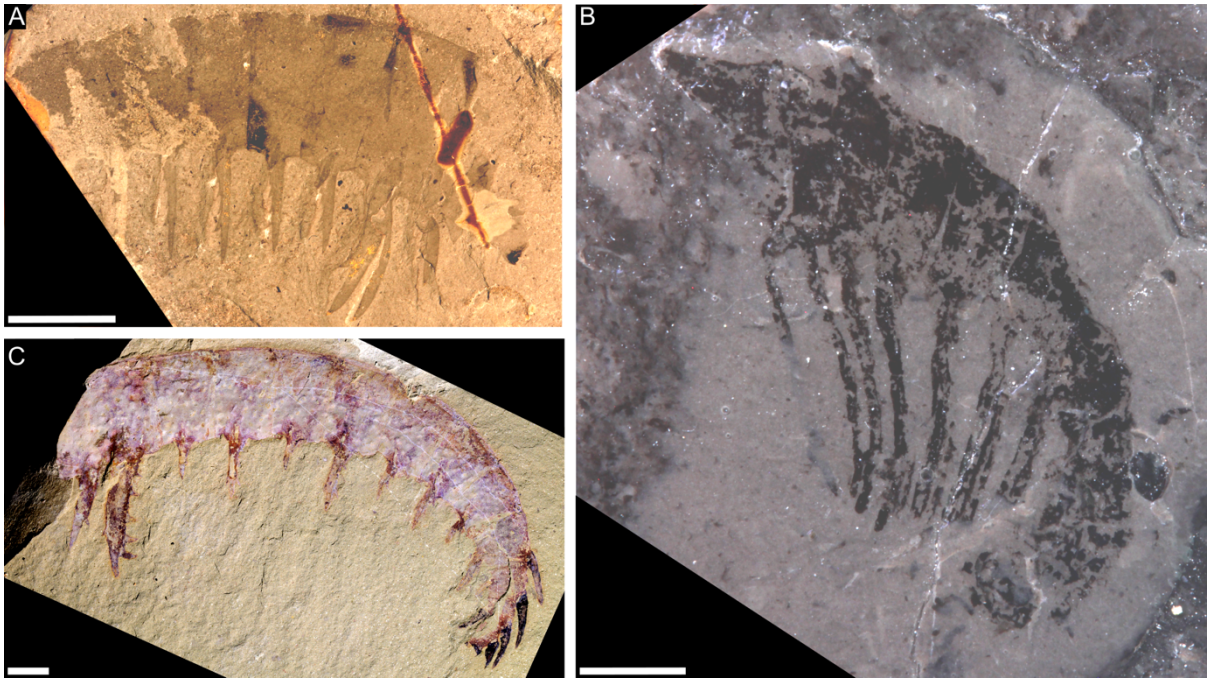

Fig. 2. Radiodont frontal appendages of uncertain family. **A.** *Laminacaris*? sp., Kinzers Formation, USA, USNM 213993. **B.** *Ursulinacaris grallae*, Mount Cap Formation, Canada, GSC 140185. **C.** *Laminacaris chimera*, Chengjiang biota, China, CJHMD 00003. Photo credit: C, P. Cong. Scale bars: A, C = 10 mm; B = 2 mm.

hypertrophied endite on the first podomere in the distal articulated region (which bears a strong resemblance to the endites of *Hurdia*), but otherwise again appears more similar to anomalocaridids *(*Guo et al. 2018*)*. Both of these taxa have been resolved with amplectobeluids and anomalocaridids in recent analyses, with an uncertain position that depends on the concavity constant (previous chapter). *Ursulinacaris grallae* (Fig. 2B) has an overall organisation identical to hurdiids, but bears slender and paired endites (*this thesis Chapter 8)*. It was originally assigned as a hurdiid (*this thesis Chapter 8)*, but has resolved both as the earliest diverging hurdiid, and earliest diverging member of a clade containing all non-hurdiid radiodonts, again depending on the concavity constant (*this thesis Chapter 9*). A final problematic taxon, *Laminacaris?* from the Kinzers Formation (Fig. 2A; Pates & Daley 2018), is only known from partial frontal appendages, and has not been included in phylogenetic analyses to date. What is known from its appendages makes assigning a genus and family problematic, as it has two hypertrophied endites towards the proximal portion (one shaft, one in the distal articulated region), and paired endites of subequal length along the rest of the known appendage, with similar morphology to *Laminacaris* endites. As such it has similarities with tamisiocaridids, anomalocaridids, and amplectobeluids.

Aims

In this study we use radiodonts as a study animal to understand the dynamics of morphological change from the Cambrian Stage 3 to Drumian. Specifically, we use the disparity of ecologically and taxonomically informative radiodont frontal appendages to assess whether the limits of diversity and disparity were established early in the evolution of the group, and whether diversity tracks disparity. We do this both at the

level of Radiodonta, and also individual families, and consider intrinsic and extrinsic controls on the evolutionary history of the group.

Methods

Radiodonta through time

All known radiodont taxa from the literature were compiled, with their geographic, temporal, and stratigraphic locations (Table 1; Supplemental 1). The analysis here focusses on changing diversity and disparity from the beginning of Stage 3 (the oldest known radiodonts) to the end of the Drumian (after which BST preservation is rarer). Five time bins of 4 to 4.5 million year lengths were assigned. The oldest (Div1) corresponds to the first four million years of Stage 3 (521 – 517 Ma). The second (Div2) to the final three million years of Stage 3 and first one million years of Stage 4 (517-513 Ma). The third (Div3) to the remaining four million years of Stage 4 (513-509 Ma). Div4 and Div5 correspond to the Wuliuan and Drumian respectively (509-504.5 Ma, and 504.5-500.5 Ma). Lagerstätten were assigned to one of these five time bins, based on their biozone, local correlations, and the global correlations of Landing et al. (2013) (Fig 3; Supplemental 1, 2). Radiodonts from younger Lagerstätten, the Guzhangian Weeks Formation, Ordovician Fezouata Formation, and Devonian Hunsrück Slate, were also noted (Table 1).

Taxa were identified to the family level, under two phylogenetic hypotheses (the result of low k and high k values for the concavity constant in *this thesis Chapter 9*).

To assess for uneven sampling of radiodonts for each time bin (i.e. to assess whether number of BSTs is a good indicator of number of radiodont taxa), raw counts of the number of radiodont taxa belonging to each family were compared to raw counts of

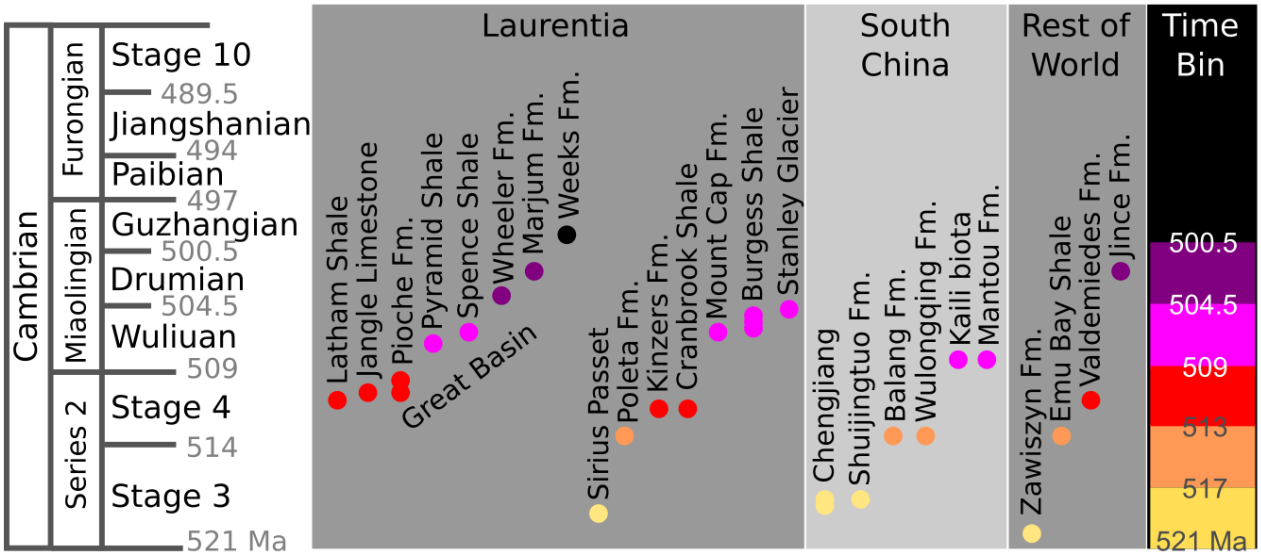

Fig. 3. Radiodont bearing BSTs placed in their respective time bins. Yellow: Div1; Orange: Div2; Red: Div3; Pink: Div4; Purple: Div5.

BSTs. A list of BSTs of Stage 3 to Drumian in age was taken from Muscente et al. (2017), and updated to add missing *Lagerstätten*, and place them in the correct Cambrian Stages and equal-length time bins, following the same method as for radiodont-bearing Lagerstätten above (Supplemental 1, 2). To assess the impact of the changing number of potential sites where radiodonts can be found on the raw counts of radiodont taxa, raw counts of BSTs were compared to raw counts of radiodont taxa for each of the Cambrian Stages and time bins from Stage 3 to Drumian using a chi-squared test (MASS package, R Studio; Venables & Ripley 2002).

Construction of character matrix

A novel character matrix, of twenty characters (9 ordered, 9 unordered, and 2 binary) was constructed to describe the disparity of radiodont frontal appendages (Supplemental 3, 4). As the matrix is designed for comparisons of disparity, and is non-phylogenetic in nature, there was no requirement that characters were homologous, but instead they were required to describe areas of the appendage that were functionally similar. For example, the separation of the appendage into three regions, the shaft, medial region, and distal region: these areas are unlikely to be homologous across taxa as they are composed of different numbers of podomeres in different taxa, however they do describe both the arrangement of endites across the appendage, and the relative shape of appendages, and as such these areas are functionally important to distinguish. A further difference between the disparity analysis in this study and the phylogenetic analysis which provided the family groupings, is that the phylogenetic analysis used characters from the whole radiodont bodyplan, whereas the disparity analysis focusses solely on the morphology of frontal appendages.

Analysis of character matrix

The method used broadly follows that of Aria & Caron (2015) and Hopkins & Smith (2015). Dissimilarities between taxa in the character matrix were calculated using the daisy function (cluster package, R Studio), which in turn were ordinated using a principal coordinate analysis, generated with the cmdscale function (stats package, R Studio; R Core Team 2017). Principal coordinates were then visualised using the plot function (R Studio; R Core Team 2017).

Daisy is able to handle different data types in the same dataset (binary, ordinal, nominal etc.) and uses the Gower coefficient to do so (Gower 1971) (but the dissimilarity is 1-similarity defined by Gower). The Gower coefficient rescales each character based on the amount of information available. If two taxa share a character state for a given character, the dissimilarity for that character is 0, otherwise it is 1. The number of mismatched characters is then divided by the total number of non-missing characters. As such, a large number of missing characters for a given taxon will increase its dissimilarity.

Cmdscale (multidimensional scaling) presents the dissimilarities between taxa as distances, using the fewest number of principal coordinates as possible. The contribution of each principal coordinate to the total variation was estimated by dividing the eigenvalue by the sum of all positive eigenvalues.

Taxon sampling and removal

All radiodont taxa were coded into the matrix. Taxa were then removed if they contained only states coded in other taxa and uncertain values. For example

Anomalocaris sp. from the Balang Formation was removed as it consisted only of uncertain characters and states already known in *Anomalocaris magnabasis*. The Balang taxon would have an artificially large dissimilarity as a result of the unknown values, but adds no new information on the disparity of radiodont frontal appendages.

In studies of disparity through time or within families, the location in morphospace of removed taxa was represented by the taxon which they shared all known character states with. For example *Anomalocaris* sp. from the Balang Formation was represented by the location in morphospace of *Anomalocaris magnabasis*, and *Ramskoeldia* cf. *consimilis* from the Latham Shale was represented by *Ramskoeldia consimilis*. This means that the disparity is not overestimated as a result of the inclusion of too many uncertain characters, and also that all taxa are represented in the morphospace.

Measures of disparity

Two measures of disparity were used: sums of ranges and sums of variances. These quantify different aspects of disparity. Sums of ranges is a measure of the total multidimensional volume occupied by taxa. As such it is sensitive to sample size (e.g. Foth et al. 2012). Sums of variances measure the spread of taxa within a group, and is more robust to differences in sample size (e.g. Foth et al. 2012). These were calculated by summing the ranges (diff function and the range function; R Core Team 2017) and variances (var function; R Core Team 2017) across the first 19 principal coordinates. To give an estimate of error, these were subjected to a one sample jackknife (jackknife function in the resample package; Hesterberg 2014), with the mean of the replicates used as the sum of ranges or variances, and the standard error used to give estimates of

error. These measures were calculated for radiodont families (under both phylogenetic hypotheses), and for all radiodonts in different time bins. In addition, to test whether the longer known temporal range of hurdiids (Cambrian to Devonian) than other families (Cambrian only) may have affected these values, they were calculated for Cambrian hurdiids only (i.e. excluding *Aegirocassis,* the unnamed hurdiid from Fezouata, and *Schinderhannes*).

In addition to raw scores of disparity, such as the sums of ranges or variances, the relative location of taxa in morphospace and the direction of evolution in morphospace are also important (e.g. Hopkins 2016). The mean position of radiodont taxa at each time bin was calculated using the colMeans function (R Core Team 2017) on each principal coordinate, for each radiodont present in the time bin. Distances between mean positions at each time bin were calculated using the dist function (stats package, R Core Team 2017). The same method was also used to calculate pairwise distances between all taxa and all mean family members.

Results

Principal coordinate analysis

The principal coordinate analysis returned 20 positive eigenvalues (37 total). The first principal coordinate accounts for 40% of the total variation, with the second accounting for 14% (Supplemental 5). The first 19 principal coordinates account for ~99% of variation (Supplemental 5).

Radiodont taxa through time

From Stage 3 to the Wuliuan, greater than 10 radiodont taxa are known from each Stage, with the number of taxa dropping off in the Drumian (five), Guzhangian (two), Ordovician (two) and Devonian (one) (Table 2). This is similar to the number of BSTs in each of these time bins (Supplemental 2) and these two raw counts (number of BSTs and number of radiodont taxa) could not be separated in a chi-squared test of bins from Stage 3 to Drumian (chi-squared = 0.46588, df = 3, p-value = 0.9263). Within time bins of equal size, Div1 (521 – 517 Ma) and Div 4 (509 – 504.5 Ma) both contain more than 10 radiodont taxa, with Div 3 next highest (nine taxa, 513 – 509 Ma), Div 2 (seven taxa, 517 – 513 Ma) and finally Div5 (five taxa, 504.5 – 500.5 Ma). This pattern through time could again not be separated from the pattern of number of BSTs in each time bin (chi-squared = 0.81773, df = 4, p-value = 0.9361).

The number of taxa belonging to each radiodont family in each time bin is not consistent. Amplectobeluids and anomalocaridids are the most diverse in Stage 3 and Stage 4 respectively, with very few taxa known from the Wuliuan onwards. Tamisiocaridids are only known from Stage 3 and 4, but do not account for a large proportion of radiodont diversity at any stage. In contrast, hurdiids are rare in the early Cambrian (two taxa in Stage 3 and Stage 4 each) but account for more than half of total radiodont diversity from the Wuliuan onwards (seven taxa in the Wuliuan, three in the Drumian) and only hurdiid taxa are known in post-Cambrian deposits. *Caryosyntrips* is similarly rare in the early Cambrian, but accounts for two of five taxa known from the Drumian. (Table 2).

Table 2. Number of radiodont taxa known from each Cambrian Stage and Time Bin

Cambrian Stage	# Taxa	# Am	# An	# C	# H	# T	# Unknown
Stage 3	12	5	3		2	1	1
Stage 4	16	3	6	1	2	2	2
Wuliuan	13	1	1	2	7		2
Drumian	5			2	3		
Guzhangian	2		2				
Ordovician	2				2		
Devonian	1				1		
Time bin							
Div1	12	5	3		2	1	1
Div2	7	1	3		1	1	1
Div3	9	2	3	1	1	1	1
Div4	13	1	1	2	7		2
Div5	5			2	3		

Taxa assigned to families following low k value phylogenetic hypothesis of *this thesis Chapter 9*. *Anomalocaris kunmingensis* is counted as an amplectobeluid, *Laminacaris chimera* is counted as an anomalocaridid, *Ursulinacaris grallae* and *Peytoia*? are counted as hurdiids. *Cucumericrus decoratus, Laminacaris*?, and Anomalocaridid indet (Poleta Formation, Kaili biota, and Mantou Formation) are counted as Unknown. By the high k value phylogenetic hypothesis, there would be one more amplectobeluid in Stage 3 and one fewer in Stage 4 (*Laminacaris chimera* and *Anomalocaris kunmingensis* respectively) with one fewer anomalocaridid in Stage 3 and one more in Stage 4. In addition there would be two fewer hurdiids in the Wuliuan (*Ursulinacaris grallae* and *Peytoia*?) with these taxa counting as unknown instead.
Age of the top of each time bin: Div1 = 517Ma (lower part of Stage 3); Div2 = 513 Ma (1Myr above base of Stage 4); Div3 = 509 (base of Wuliuan); Div4 = 504.5 (base of Drumian); Div5 = 500.5 (base of Guzhangian). Abbreviations: Am, amplectobeluid; An, anomalocaridid; C, *Caryosyntrips*; H, hurdiid; T, tamisiocaridid.

Within the time bins, the signal is more nuanced. Amplectobeluids still dominate in the earliest time bin (Div1, 521 - 517 Ma), with five of 12 taxa, however in Div2 (517 – 513 Ma) only one amplectobeluid (*Anomalocaris kunmingensis* – which is only considered an amplectobeluid under one of the two phylogenetic hypotheses used here) is known, with anomalocaridids making up three of seven taxa. Div3 (513 – 509 Ma) contains the most even spread of taxa, with three of nine being anomalocaridids. From Div4 (509 – 504.5 Ma) hurdiids dominate, with seven of 13 taxa in this time bin, and three of five in Div5 (504.5 – 500.5 Ma) (Table 2).

Disparity of Radiodonta: families

Sums of ranges and sums of variances are used as proxies for overall disparity, with higher values meaning higher disparity. The results for both measures are presented in table form in Supplemental 6.

Sums of Ranges

Under both phylogenetic hypotheses, *Caryosyntrips* has the lowest jackknifed sum of ranges (0.50, standard error = 0.08), and Tamisiocarididae has the second lowest (1.10, standard error = 0.24). Anomalocarididae has the third highest sum of ranges, which is much closer to that of Amplectobeluidae and Hurdiidae than *Caryosyntrips* and Tamisiocarididae (Fig 4 A, C; low k: 2.83, standard error = 0.24, high k: 2.58, standard error = 0.20). The family with the highest sum of ranges depends on whether non-Cambrian hurdiids are considered, and the choice of low or high k phylogenetic hypothesis. Under the low k hypothesis, Hurdiidae has the highest mean sum of ranges (3.21, standard error = 0.36), with Amplectobeluidae having the second highest (3.06,

standard error = 0.13). When hurdiids are restricted to Cambrian-only (3.07, standard error = 0.43) they cannot be separated from amplectobeluids. Under the high k hypothesis, Amplectobeluidae has the highest sum of ranges (3.26, standard error = 0.21), regardless of whether non-Cambrian hurdiids are considered (3.01, standard error = 0.38) or not (2.83, standard error = 0.47). Under this phylogenetic hypothesis, the sum of ranges for Amplectobeluidae also decreases (2.58, standard error = 0.20), but *Caryosyntrips* and Tamisiocarididae are unchanged, as their constituent taxa are the same.

Sums of variances

Under both phylogenetic hypotheses, and regardless of whether non-Cambrian hurdiids are considered, Amplectobeluidae has the highest sum of variances (low k: 0.10, standard error = 0.009; high k: 0.11, standard error = 0.008). Anomalocarididae, Hurdiidae, and Tamisiocarididae have comparable sums of variances under both phylogenetic hypotheses, both including and excluding non-Cambrian hurdiids. Anomalocarididae has the second highest under the low k hypothesis and third highest under the high k hypothesis (low k: 0.072, standard error = 0.016; high k: 0.060, standard error = 0.011) with Tamisiocarididae (0.062, standard error = 0.031) second highest under the low k and third highest under the high k hypothesis (Fig. 4 B, D). Hurdiidae has a slightly lower sum of variances (low k: 0.058, standard error = 0.013; high k: 0.056, standard error = 0.015) than these other two families, and this measure is slightly raised when non-Cambrian hurdiids are excluded (low k: 0.060, standard error = 0.016; high k: 0.059, standard error = 0.018). *Caryosyntrips* has the lowest sum of variances by some distance (0.010, standard error = 0.003) (Fig. 4 B, D).

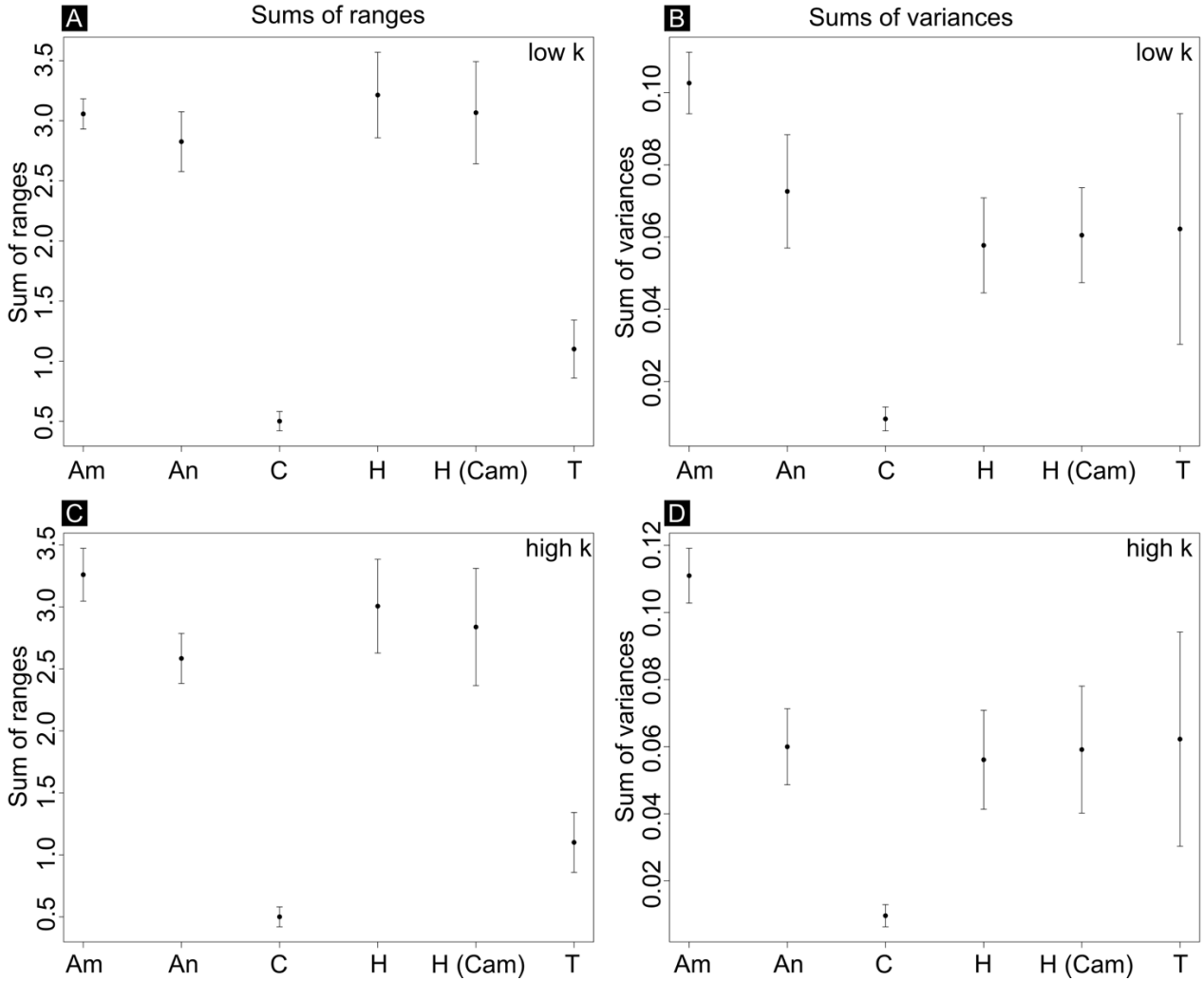

Fig. 4. Jackknifed sums of ranges and sums of variances for families under the two phylogenetic hypotheses considered here. **A.** Sums of ranges under low k phylogenetic hypothesis. **B.** Sums of variances under low k phylogenetic hypothesis. **C.** Sums of ranges under high k phylogenetic hypothesis. **D.** Sums of variances under high k phylogenetic hypothesis. Error bars indicate range of jackknifed standard error. Abbreviations: Am, Amplectobeluidae; An, Anomalocarididae; C, Caryosyntrips; H, Hurdiidae; H(Cam), Cambrian Hurdiidae; T, Tamisiocarididae.

Distributions in morphospace

Caryosyntrips, Hurdiidae, and Tamisiocarididae all occupy distinct regions in morphospace. Under the high k hypothesis Amplectobeluidae and Anomalocarididae also occupy distinct regions, however under the low k hypothesis there is overlap between these two families, as *Laminacaris chimera* (an anomalocaridid under this hypothesis) occupies a position very close to the mean amplectobeluid (compare Fig. 5 and Fig. 6).

The mean amplectobeluid and mean anomalocaridid occupy positions much closer to each other than to other families (Table 3). Hurdiidae and Tamisiocarididae occupy positions very far from each other, and also to all other families (Table 3). *Caryosyntrips* occupies a position close to the centre of the morphospace plot (the origin; Fig. 5) but still occupies distances far from all of the named radiodont families (Table 3).

Of the problematic taxa, *Ursulinacaris* occupies a position much closer to Hurdiidae (distance measured using dist function = 0.27) than any other family (Amplectobeluidae: 0.51; Anomalocarididae: 0.52; Tamisiocarididae: 0.48; *Caryosyntrips*: 0.39) but is also closer to Amplectobeluidae, Anomalocarididae, and Tamisiocarididae than the mean hurdiid (Table 3). *Anomalocaris kunmingensis* is slightly closer to the mean anomalocaridid than mean amplectobeluid, but is closer to both than *Laminacaris*, which represents the most distant member of either family (from the family centroid) if included.

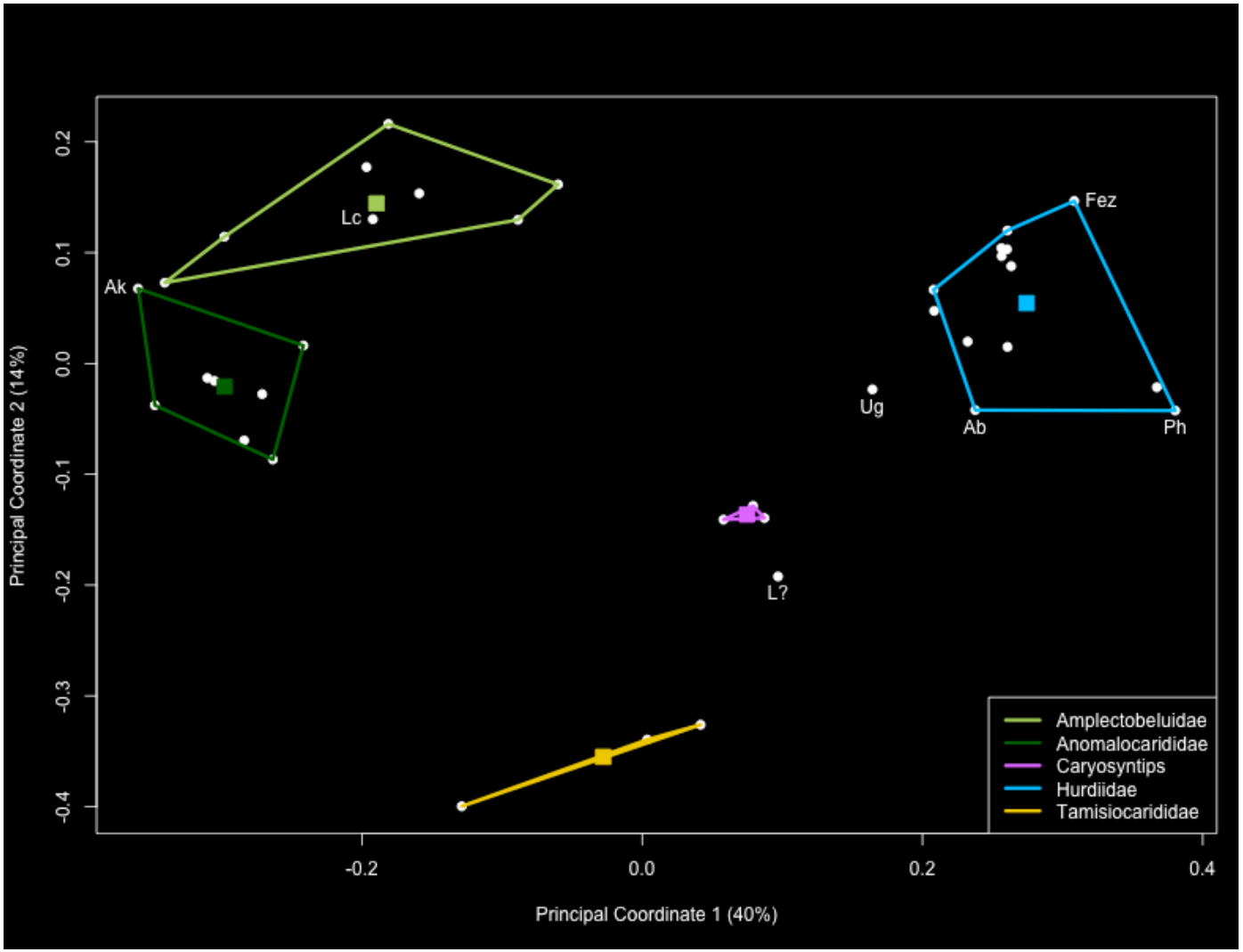

Fig. 5. Position of radiodont frontal appendages in the morphospace visualising principal coordinates 1 and 2. Each taxon represented by white circle. Centroids for families (high k phylogenetic hypothesis) shown as coloured squares, with extremities of area occupied by families indicated by coloured outlines. Abbreviations: Ab, *Aegirocassis benmoulai*; Ak, *Anomalocaris kunmingensis*; Fez, Fezouata hurdiid; Lc, *Laminacaris chimera*; L?, *Laminacaris*?; Ph, *Pahvantia hastata*; Ug, *Ursulinacaris grallae*.

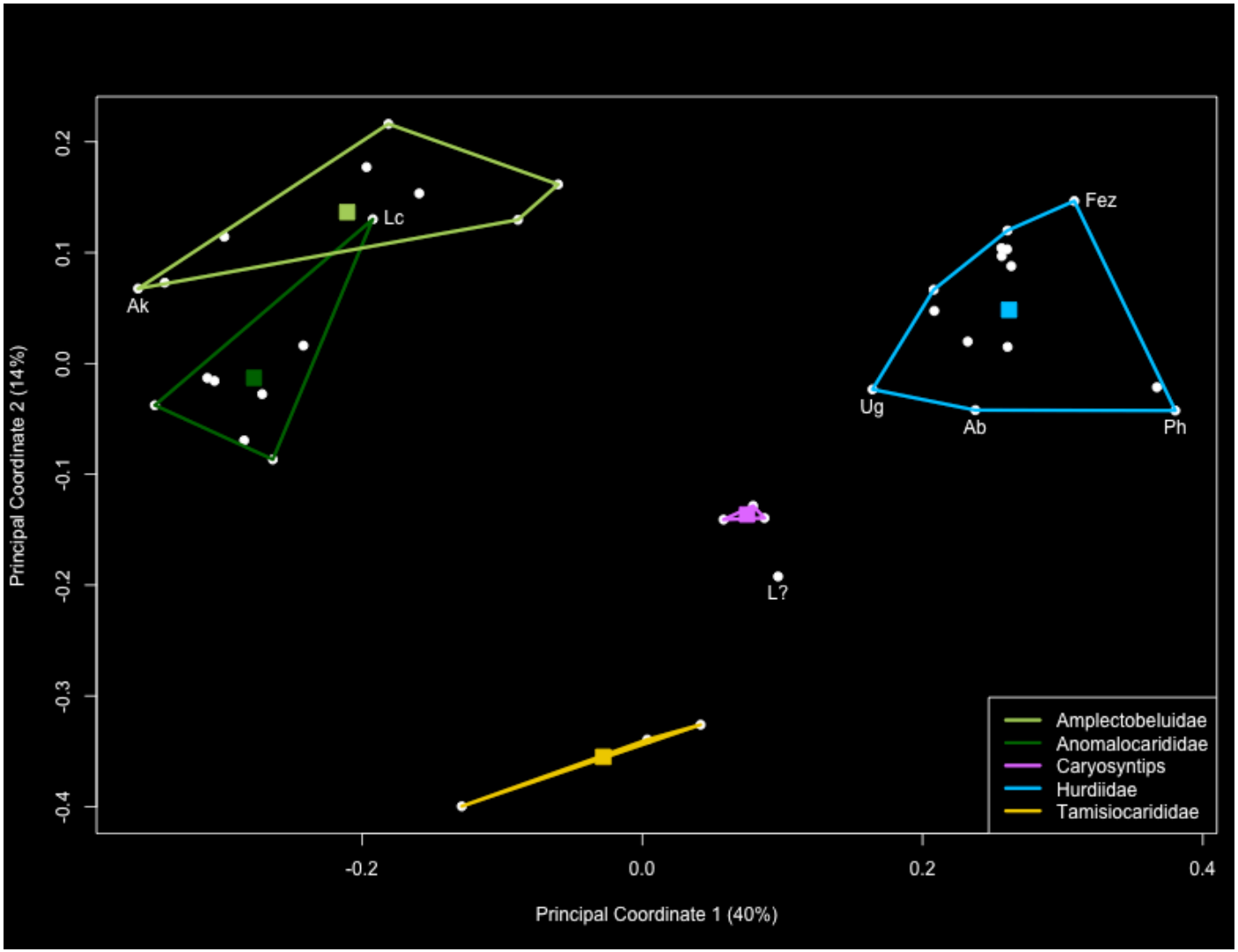

Fig. 6. Position of radiodont frontal appendages in the morphospace visualising principal coordinates 1 and 2. Each taxon represented by white circle. Centroids for families (low k phylogenetic hypothesis) shown as coloured squares, with extremities of area occupied by families indicated by coloured outlines. Abbreviations: Ab, *Aegirocassis benmoulai*; Ak, *Anomalocaris kunmingensis*; Fez, Fezouata hurdiid; Lc, *Laminacaris chimera*; L?, *Laminacaris*?; Ph, *Pahvantia hastata*; Ug, *Ursulinacaris grallae*.

Table 3. Pairwise distances between the centroids of every radiodont familiy, and *Caryosyntrips*

	Amplectobeluidae	Anomalocarididae	*Caryosyntrips*	Hurdiidae	Tamisiocarididae
Amplectobeluidae	-				
Anomalocarididae	0.2638352	-			
Caryosyntrips	0.4334948	0.4743263	-		
Hurdiidae	0.5008810	0.5504287	0.3674081	-	
Tamisiocarididae	0.5338415	0.4721059	0.3186634	0.5142972	-

Calculated using the dist function.

Excluding potentially problematic taxa, *Lyrarapax unguispinus* is the most distant amplectobeluid, and *Paranomalocaris multisegmentalis* the most distant anomalocaridid. *Pahvantia hastata* is the most distant hurdiid from the mean hurdiid.

Hurdiids with convergently derived filter feeding morphologies were still closer in morphospace to the morphology of the mean hurdiid than all other families (Table 4). In addition, *Aegirocassis benmoulai* and *Pahvantia hastata* are further from the means of all other families than the mean hurdiid is from the mean of all other families, with the exception of *Aegirocassis* and the mean tamisiocaridid (Table 4). *Pahvantia* is further from the mean hurdiid (0.40) than the mean hurdiid is to the mean *Caryosyntrips* (0.37; Table 3). *Aegirocassis benmoulai* is further from the coeval and co-occurring undescribed Fezouata appendage (0.38) than the mean amplectobeluid is from the mean anomalocaridid (0.26).

Disparity of Radiodonta: through time

Sums of ranges

The highest sum of ranges of the four Cambrian stages calculated (Stage 3 to the Drumian) was for Stage 4 (4.32, standard error = 0.31) with Stage 3 within its standard error (4.02, standard error = 0.28). The Wuliuan had the third highest sum of ranges (3.32, standard error = 0.40), higher than the Drumian (2.47, standard error = 0.65) (Fig. 7 A).

Within the equal length time bins, a similar pattern of decreasing sums of ranges through this part of the Cambrian can be seen, with the exception of Div2 (517 – 513 Ma) which also shows a low sum of ranges (2.85, standard error = 0.33). A steady decrease in the sum of ranges is present from Div1 (4.02, standard error = 0.28) to Div 3

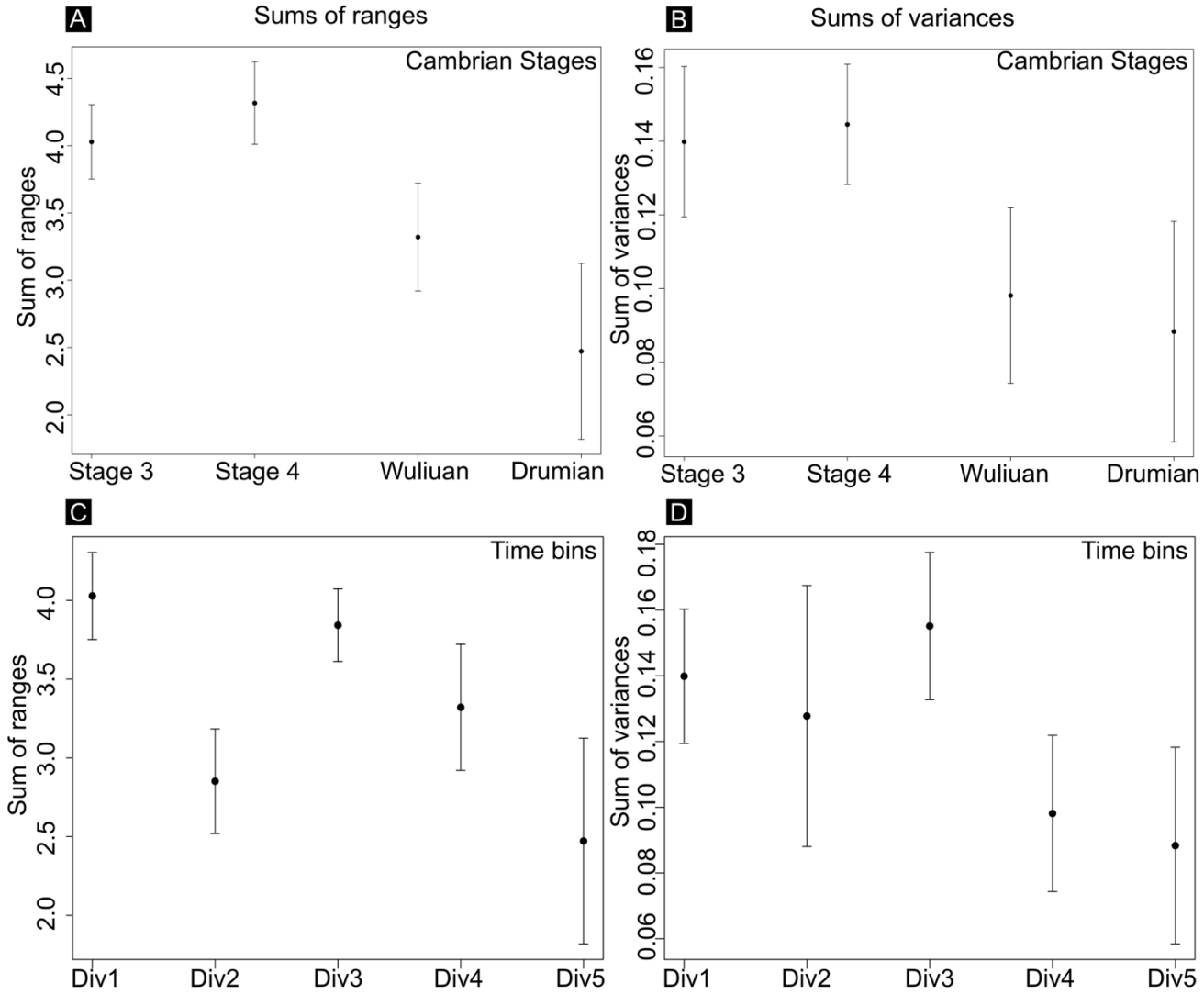

Fig. 7. Jackknifed sums of ranges and sums of variances for Cambrian Stages and time bins. **A.** Sums of ranges for Cambrian Stages. **B.** Sums of variances for Cambrian Stages. **C.** Sums of ranges for time bins. **D.** Sums of variances for time bins. Error bars indicate range of jackknifed standard error. Time bins: Div1, 521 – 517 Ma; Div2, 517 – 513 Ma; Div3, 513-509 Ma; Div4; 509 – 504.5 Ma; Div5, 504.5 – 500.5 Ma

Table 4. Pairwise distances between select radiodont taxa and families

	Aegirocassis	*Pahvantia*	*Ursulinacaris*
Amplectobeluidae	0.5397910	0. 7258628	0.5075973
Anomalocarididae	0.5681828	0. 7562901	0.5173093
Caryosyntrips	0.3753422	0. 5793264	0.3904768
Hurdiidae	**0.2266707**	**0. 4022390**	**0.2659635**
Tamisiocarididae	0.4835137	0. 6781100	0.4846924

Pairwise distances between *Aegirocassis benmoulai, Pahvantia hastata,* and *Ursulinacaris grallae*, and the means of the four radiodont families and *Caryosyntrips*. Calculated using the dist function.

Table 5. Pairwise distances between mean values of taxa at each Cambrian Stage

	Stage 3	Stage 4	Wuliuan	Drumian
Stage 3	-			
Stage 4	0.1103474	-		
Wuliuan	0.3052082	0.2821067	-	
Drumian	0.3857646	0.3633938	0.1290314	-

Distances between mean values of taxa (centroids) at each Cambrian Stage, calculated using the dist function.

Table 6. Pairwise distances between mean values of taxa at each Time Bin

	Div1	Div2	Div3	Div4	Div5
Div1	-				
Div2	0.1583695	-			
Div3	0.1171296	0.1643804	-		
Div4	0.3052082	0.3638703	0.2623703	-	
Div5	0.3857646	0.4475240	0.3414913	0.1290314	-

Distances between mean values of taxa (centroids) at each Time Bin, calculated using the dist function.

(3.84, standard error = 0.23), to Div 4 (3.32, standard error = 0.40), to Div 5 (2.47, standard error = 0.65) (Fig. 7 C).

Sums of variances

For the Cambrian stages, Stage 4 also had the highest sum of variances calculated (0.144, standard error = 0.016) slightly higher than Stage 3 (0.140, standard error = 0.020) and much higher than the Wuliuan (0.098, standard error = 0.024) and Drumian (0.088, standard error = 0.030) (Fig. 7 B).

Within the equal length time bins, a similar pattern can be seen. The highest sum of variances is in Div3 (0.156, standard error = 0.022) followed by Div1 (0.140, standard error = 0.020) and Div2 (0.128, standard error = 0.040). Div4 (0.098, standard error = 0.024) and Div5 (0.088, standard error = 0.030) have the lowest sums of variances (Fig. 7 D).

Distributions in morphospace

All four Cambrian Stages considered in this study overlap to some extent in the multidimensional morphospace (Fig. 8). Stage 3 and Stage 4 broadly occupy the same areas of morphospace, and similarly the area occupied by the Drumian is nearly all completely occupied by the Wuliuan. The Wuliuan however also occupies areas of amplectobeluid and anomalocaridid morphospace, not occupied by the Drumian (as only hurdiid and *Caryosyntrips* taxa are known from this Stage). The Wuliuan and Drumian occupy areas of the morphospace not occupied by Stage 3 and Stage 4 – an area occupied by hurdiids. A single point (the unnamed Fezouata hurdiid – Van Roy et

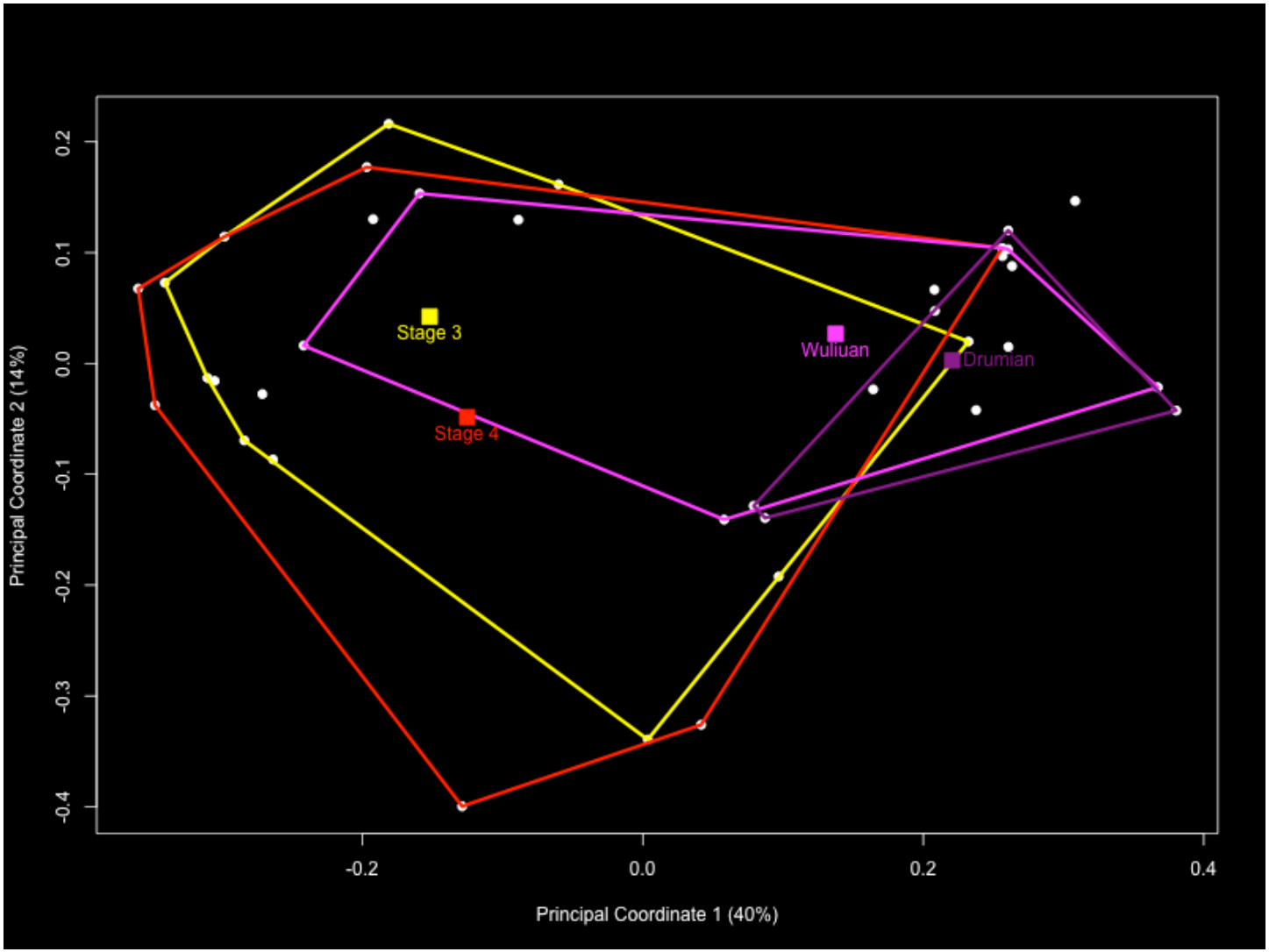

Fig. 8. Position of radiodont frontal appendages in the morphospace visualising principal coordinates 1 and 2. Each taxon represented by white circle. Centroids for Cambrian Stages shown as coloured squares, with extremities of area occupied at each Stage indicated by coloured outlines. Yellow: Stage 3; Red: Stage 4; Pink: Wuliuan; Purple: Drumian.

al. 2011) does not fall within the areas occupied by any of the four Cambrian Stages considered here (Fig. 8).

The mean positions (centroids) for taxa at each Cambrian Stage are visualised as squares in Fig. 8. The mean position of Stage 3 is closest to the mean amplectobeluid, the mean position of Stage 4 is closest to the mean anomalocaridid, with the mean position of the Wuliuan and Drumian closest to the mean hurdiid. The mean position of Drumian taxa falls within the hurdiid polygon (Fig. 8). The distance between the Stage 4 and Wuliuan centroids (0.28, Table 5) is more than double any other distance between adjacent time bins. Stage 3 and Stage 4 have the closest centroids (0.11, Table 5) followed by the Wuliuan and Drumian centroids (0.12, Table 5).

Similarly the time bins all overlap to some extent in the multidimensional morphospace (Fig. 9). Div1, Div2, and Div3 broadly occupy the same area, except Div2 lacks occupation of most of the amplectobeluid area. Div4 and Div5 correspond exactly to the Wuliuan and Drumian, described above. The centroids for Div1, Div2, and Div3 also cluster together, with Div1 closest to the mean amplectobeluid, Div2 closest to the mean anomalocaridid, and Div3 slightly closer to the right hand side, where the hurdiids cluster. The shortest distance between centroids of adjacent age is Div4 - Div5 (0.13), with both centroids close to the centroid of Hurdiidae. The distances Div1-Div2 (0.16) and Div2-Div3 (0.16) are much shorter than the longest distance: Div3 - Div4 (0.26) (Table 6).

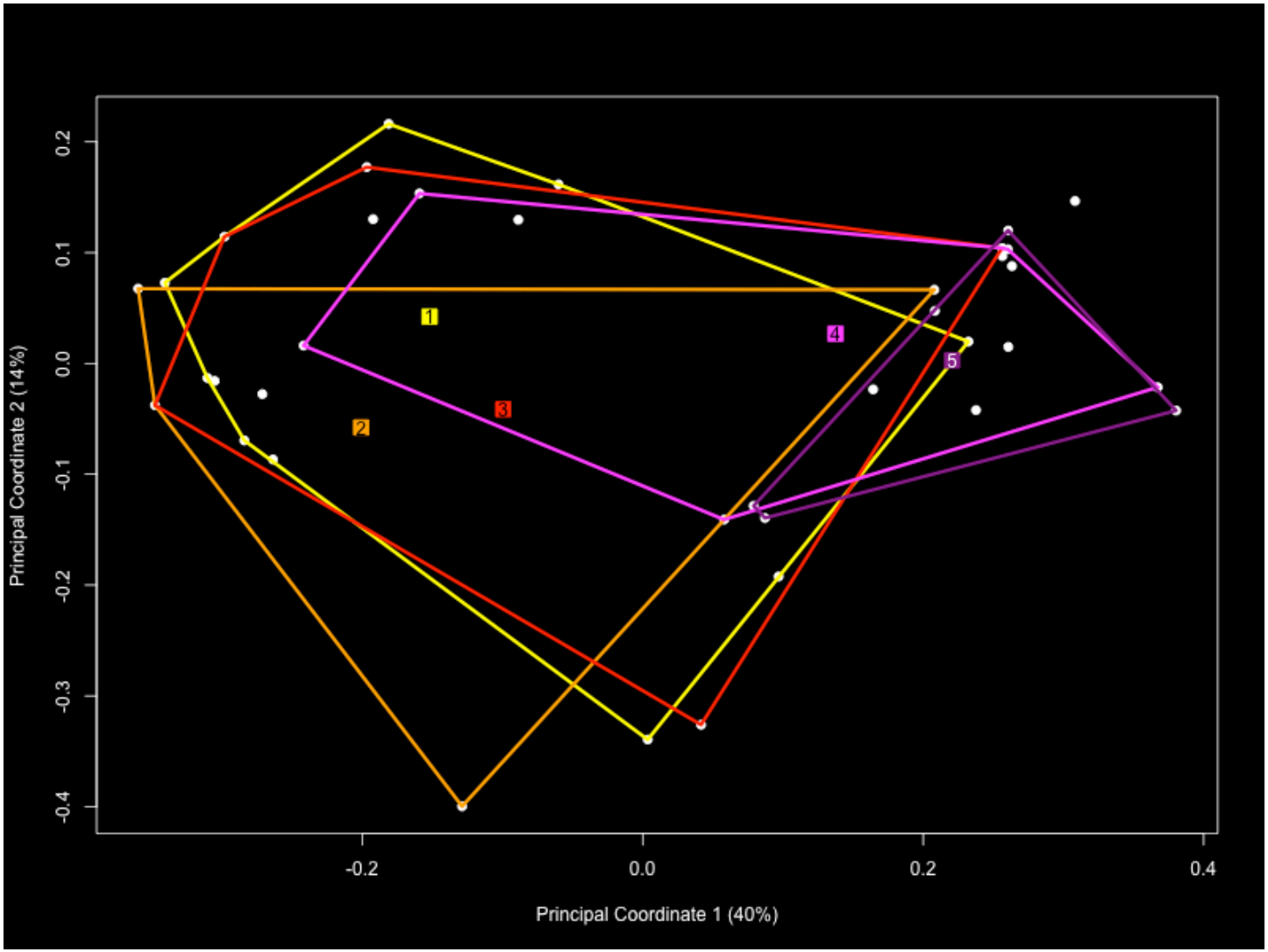

Fig. 9. Position of radiodont frontal appendages in the morphospace visualising principal coordinates 1 and 2. Each taxon represented by white circle. Centroids for each Time bin shown as coloured squares, with extremities of area occupied at each Time bin indicated by coloured outlines. Yellow: Div1 (521-517 Ma); Orange: Div2 (517-513 Ma); Red: Div3 (513-509 Ma); Div4 (509-504.5 Ma); Div5 (504.5-500.5 Ma)

Discussion

Cambrian BSTs – an uneven view of radiodonts

Deposits with soft-bodied fossils are not spread evenly throughout the Palaeozoic, or even within the Cambrian (Fig. 3; Gaines 2014; Muscente et al. 2017), and so our view of radiodont evolution is open to potential temporal or geographic bias. The oldest Cambrian BSTs are predominantly from South China (Fig. 3) with the youngest predominantly from North America (Fig. 3) and a limited overlap is present. As our knowledge of radiodont diversity is linked to the number of BSTs in each time bin (as shown by the insignificant chi-squared test results between them), the apparent drop in radiodont diversity after the Drumian is likely an artefact of the limited BSTs available to sample. The absence of Cambrian BSTs older than 521 Ma limits our ability to study the first radiodonts (and earliest euarthropods in general - Daley et al. 2018), and the relative rarity of BSTs from the Drumian onwards makes it difficult to study in detail the diversity and disparity before their extinction (or even pinpoint when the group went extinct). The diversity and disparity analyses here do not provide any evidence to suggest that radiodonts as a whole were in decline at the end of the Drumian.

Diversity and disparity of Radiodonta

The diversity and disparity of radiodont frontal appendages are not coupled. The diversity shows a double peak, once in the oldest time bin (Div1, 521 – 517 Ma) and again in Div4 (509 – 504.5 Ma), whereas the disparity remains close to its highest point in the oldest three time bins (Div1 – Div3, 521 – 509 Ma) and drops off subsequently in the Wuliuan and Drumian (Div4 and Div5, 509 Ma and younger). The second peak in diversity is coincident with the decline in radiodont disparity, a signal particularly

striking in the sums of variances, which are less affected by sample size (Fig. 7; Foth et al. 2012). Diversity and disparity are often not coupled, and the pattern seen here, with an early high disparity that subsequently declines uncoupled from diversity, is common in metazoan clades that do not terminate at mass extinctions (Hughes et al. 2013).

The limits of radiodont disparity are not set at the moment of highest diversity, instead radiodonts continue to innovate, as shown by the shifting position of the centroid (Figs. 8, 9). The largest shift in the centroid between time bins considered here occurs at the drop in disparity, and second diversity peak (Div3 to Div4, 509 Ma), with the centroid position broadly shifting to the right of the morphospace plot, from a negative value for principal coordinate one, to a positive. This feature of morphospace occupation, with younger taxa occupying a different volume when compared to older taxa, is also seen in other groups. For example in onychophorans and priapulids, where Cambrian taxa occupy a distinct area of morphospace compared to extant taxa (e.g. Wills 1998; Yang et al. 2015).

Diversity and disparity of families within Radiodonta

In the case for Radiodonta, the shift in morphospace occupation and centroid position through time (from left to right in the morphospace plots - Figs. 8, 9) is directly related to the changing relative diversities of individual families, from amplectobeluids and anomalocaridids in the older three time bins, to hurdiids in the younger two. In fact, hurdiids show a very different evolutionary history to amplectobeluids and anomalocaridids. There are too few taxa to confidently assess the history for tamisiocaridids and *Caryosyntrips*. From the limited data available tamisiocaridids are more common in the older three time bins and *Caryosyntrips* in the younger two.

The diversity and disparity of amplectobeluids and anomalocaridids dominates the early signal for radiodonts, with very few hurdiid taxa known, while the reverse is true from the Wuliuan (509 Ma) onwards, where the increase in hurdiid diversity provides the second peak in radiodont diversity. As Amplectobeluidae, Anomalocarididae, and Hurdiidae all have similar disparities, this does not adequately explain the drop in disparity in the fourth time bin (509 – 504.5 Ma). Amplectobeluids and anomalocaridids peak in disparity early in the history of these families, at the point of highest diversity for the families (Div1 for amplectobeluids, a more spread out Div1 – Div3 for anomalocaridids). In contrast, the disparity of Hurdiidae continues to increase throughout the Cambrian, and hurdiids continue to occupy novel areas in morphospace, to the right hand side of the PCO plot (more positive values for principal coordinate 1), as shown by the Drumian taxa *Pahvantia hastata* and *Stanleycaris* sp (Wheeler Formation), and the two Ordovician taxa from the Fezouata biota. In addition, the disparity for radiodonts drops off even more in the Drumian (fifth time bin, 504.5 – 500.5 Ma) as no amplectobeluids or anomalocaridids (or tamisiocaridids) are known from this time period, and so radiodont disparity is only sampling hurdiids (and *Caryosyntrips*).

This difference in the evolutionary history of hurdiids, compared to amplectobeluids and anomalocaridids, requires explanation. The morphological differences between hurdiids and these other two families has a deeper root than the differences between amplectobeluids and anomalocaridids. This is shown by the distance between the centroids of the families (the mean hurdiid is around twice the distance from the mean amplectobeluid and anomalocaridid than they are to each other) and also by the relative divergences of these families predicted by phylogenetic

analyses (hurdiids are the earliest diverging family, with amplectobeluids and anomalocaridids diverging last – *this thesis Chapter 9*). The later divergence of amplectobeluids and anomalocaridids (when compared to any other combination of two radiodont families) can also be seen by comparing the occupation of morphospace of amplectobeluids and anomalocaridids in different time bins. In the earliest time bin, there is overlap between the morphologies of the two families, and in the oldest three time bins phylogenetically problematic taxa such as *Anomalocaris kunmingensis* and *Laminacaris chimera* occupy positions nearly midway between the centroid of amplectobeluids and centroid of anomalocaridids. However later in radiodont history, for example the Wuliuan (Div4, 8-12 million years later) the Burgess Shale taxa *Amplectobelua stephenensis* and *Anomalocaris canadensis* occupy clearly distinct positions in morphospace, with clear amplectobeluid and anomalocaridid morphologies respectively. The best candidates for 'intermediate' frontal appendage morphologies linking known family morphologies are *Laminacaris*? (Kinzers Formation – Pates & Daley 2018) and *Ursulinacaris grallae* (Mount Cap Formation and Carrara Formation – *this thesis Chapter 8*). Both occupy positions outside of family groupings (except in the phylogenetic hypothesis where *Ursulinacaris* is considered as a hurdiid) (Figs. 5, 6) with unusual frontal appendage morphologies perhaps showing a remnant of radiodont frontal appendage disparity from the currently un-samplable 20 million years without Cambrian BSTs when the first radiodonts likely evolved (Daley et al. 2018).

This still leaves an apparent discord in the evolutionary history of hurdiids and amplectobeluids and anomalocaridids, as there is a long time gap between the initial divergence of hurdiids from the other radiodont families, and the large increase in hurdiid diversity in the fourth time bin. Why was the major hurdiid radiation delayed so

long after the initial appearance of the family? This could be the result of uneven sampling, extrinsic (environmental factors, competition), or intrinsic factors (developmental constraints, adaptability).

An uneven sampling explanation is built around the over-representation of Chinese Lagerstätten in the oldest Cambrian BST record. Nine radiodont taxa are known from the Chengjiang biota (South China – e.g. Chen et al. 1994; Hou et al. 1995; Cong et al. 2014, 2016, 2017, 2018), yet none of these are hurdiids, with amplectobeluids dominating. A single hurdiid appendage (*Peytoia infercambriensis*) is known from the older Zawiszyn Formation (Poland, Baltica – Daley & Legg 2015) and indeed no tamisiocaridids are known from Chengjiang either, but the filter feeding *Tamisiocaris borealis* is known from Sirius Passet (Greenland, Laurentia – Daley & Peel 2010; Vinther et al. 2014). From the second and third time bin onwards support for a geographic cause for the lack of hurdiids becomes less convincing. Firstly the oldest hurdiid appendage from China, *Peytoia* cf. *nathorsti* from the Balang Formation is known from this time bin (Wang et al. 2013) and secondly, the oldest Laurentian sites (as well as the Emu Bay Shale in Gondwana) show a predominance of amplectobeluid and anomalocaridid taxa (e.g. Lieberman 2003; Daley et al. 2013a; Pates & Daley 2018; *this thesis Chapter 7*). The oldest *Hurdia* from the Great Basin of Laurentia (the *Nephrolenellus multinodus* Zone of the Pioche Formation – *this thesis Chapter 7*) is known only from one specimen, in a deposit containing tens of *Anomalocaris* appendages, with Wuliuan and Drumian deposits in the same basin preserving hurdiids and *Caryosyntrips*, but no known amplectobeluids or anomalocaridids (Pates & Daley 2017; Pates et al. 2017, 2018). This suggests that the rarity of hurdiids before 509 Ma,

and the rarity of amplectobeluids and anomalocaridids after this date, reflects a real signal, rather than geographic bias.

Extrinsic explanations include environmental and ecological factors. The timing of this changeover between hurdiids and other radiodonts is coincident with an increased global homogenization of BST biotas in the Wuliuan onwards – when there were more shared taxa (measured at the genus level) from distant localities (Holmes et al. 2018) and the transition from an unstable 'Proterozoic style' ocean with frequent large carbon isotope excursions to a more stable 'Phanerozoic style' ocean (Babcock et al. 2015). A change in ocean stability does not offer a clear reason why hurdiid diversity should suddenly increase, as radiodonts either side of the olenelloid extinction at the end of the Dyeran (just before the start of the Wuliuan) which can be pinpointed to the centimetre level in the Pioche Formation and coincides with a carbon isotope excursion (Palmer 1998), are unchanged, with *Anomalocaris magnabasis* present above and below (*this thesis Chapter 7*). Invoking the apparently larger geographic range of hurdiids compared to anomalocaridids (*this thesis Chapter 7*) is also problematic, as it could be a result of the increased mixing of BSTs from the Wuliuan onwards (when hurdiids are common), rather than a root cause of hurdiid success. In addition a recent study on lophotrochozoa showed a turnover in this group at 513 Ma (Zhuravlev & Wood 2018), one time bin earlier than for radiodonts (this study), and for the extrinsic causes described above. Thus it may be that one extrinsic factor cannot explain the extinctions and radiations within different groups at this time, similar to what is known about the later Great Ordovician Biodiversification Event, where such turnovers within different groups are known from the late Cambrian to late Ordovician (e.g. Harper 2006; Servais et al. 2010; Servais & Harper 2018).

An ecological cause, linked to the increased mixing of faunas, could provide a possible explanation. Hurdiids are hypothesised to have fed through sediment sifting or filter feeding (e.g. Daley et al. 2009, 2013b; Van Roy et al. 2015; Lerosey-Aubril & Pates 2018) and thus their frontal appendages are specialised for particular mediums (sediment or water) rather than prey items. Amplectobeluids and anomalocaridids, hypothesised to have used raptorial predation, would have had frontal appendages more closely specialised for individual prey animals, and thus may have not been able to adapt as easily to a rapid change in available prey animals. However this explanation by itself is not sufficient, as tamisiocaridids are thought to have occupied the same ecological niches as hurdiids, and do not reach the same levels of disparity and diversity.

Intrinsic factors considering the adaptability of frontal appendages of the groups, as shown by the morphospace analysis in this study, could offer additional explanation for the continued success of hurdiids as other groups fell away. Hurdiids continued to occupy novel areas in morphospace from the middle Cambrian (Div4 onwards) to at least the early Ordovician, and thus were able to continue to innovate (also shown by the convergent adaptation to filter feeding in the hurdiids *Aegirocassis* and *Pahvantia*– Van Roy et al. 2015; Lerosey-Aubril & Pates 2018) whereas amplectobeluids and anomalocaridids were apparently not. This continued innovation by hurdiids may have allowed them to better compete with the globalised fauna in the Wuliuan onwards, whereas amplectobeluids and anomalocaridids may have been outcompeted by more successful raptorial predators.

None of these explanations adequately explain the lack of hurdiids from older deposits, or the apparently long fuse to hurdiid diversification. It is plausible that this reflects internal radiodont competition, between tamisiocaridids and hurdiids.

Tamisiocaridids are hypothesised to have fed also by sediment sifting and filter feeding (Daley et al. 2013a; Vinther et al. 2014), with the youngest tamisiocaridid known (from the Kinzers Formation – Pates & Daley 2018) older than the oldest *Hurdia* from Laurentia (from the Pioche Formation – *this thesis Chapter 7*). Thus it is plausible that the radiation of hurdiids was facilitated by the removal of tamisiocaridids from niches into which hurdiids were able to diversify (relatively large nektonic sediment sifters and filter feeders).

The resolution of this study (four million year time bins) necessary to guarantee even sampling and a modicum of sample size, limits our ability to examine finer scale variation in radiodont disparity or diversity. The Burgess Shale contains a number of levels of slightly different age, and so offers a window into the finer scale variation. The abundance of individual taxa, as well as raw radiodont diversity, are variable, but with an overall trend for reducing diversity in younger deposits (Daley & Budd 2010). It is notable that hurdiids are the most common family at nearly all levels, and *Amplectobelua* is only in the very oldest level, and makes up only two percent of the total number of specimens (Daley & Budd 2010). Thus the broader scale shift to a hurdiid-dominated radiodont world, and removal of amplectobeluids, during the Wuliuan is picked up even at this fine resolution.

Conclusions

When treated as a single entity, radiodonts appear to show the same pattern of early high disparity as many other groups, with two peaks in diversity. However at a family level the pattern is more complex with Hurdiidae showing a very different history to Amplectobeluidae, Anomalocarididae, and Tamisiocarididae. Amplectobeluids and

anomalocaridids, which dominate the early Cambrian radiodont record, have a high early disparity, which subsequently reduces in the middle Cambrian, whereas hurdiid disparity increases into the Wuliuan as the other three families become much rarer. The apparent rarity of hurdiids before the Wuliuan is likely a real signal. It is not clear why hurdiids have a delayed diversification when compared to other families, though it could be the result of internal radiodont competition between tamisiocaridids and hurdiids.

The large differences between radiodont families represent deep evolutionary rooted differences in the organisation of the frontal appendage. Morphological intermediates of frontal appendages between the latest diverging families, amplectobeluids and anomalocaridids, can be seen in Stages 3 and 4, however by the Wuliuan the remaining members of these families are clearly distinct. *Laminacaris?* (Kinzers Formation) and *Ursulinacaris* offer potential 'intermediate' frontal appendage morphologies.

The turnover in radiodont families, from amplectobeluids and anomalocaridids to hurdiids, coincides with a global homogenisation of BST faunas, although a direct link between these two events is problematic. It is possible that the ability of hurdiids to occupy novel areas of morphospace resulted in their success and ability to compete in a more homogenised world, with amplectobeluids and anomalocaridids becoming outcompeted.

Acknowledgements

SP is funded by an Oxford-St Catherines Brade-Natural Motion Scholarship. C Aria provided discussions of character-based morphospace visualisation, and assisted with

recreating the results from Aria & Caron (2015). N Brocklehurst provided discussion of disparity metrics.

References

Aria, C., & Caron, J. B. (2015). Cephalic and limb anatomy of a new isoxyid from the Burgess Shale and the role of "stem bivalved arthropods" in the disparity of the frontalmost appendage. *PloS one*, 10(6), e0124979.

Babcock, L. E., Peng, S. C., Brett, C. E., Zhu, M. Y., Ahlberg, P., Bevis, M., & Robison, R. A. (2015). Global climate, sea level cycles, and biotic events in the Cambrian Period. *Palaeoworld*, 24(1-2), 5-15.

Briggs, D. E. (1979). *Anomalocaris*, the largest known Cambrian arthropod. *Palaeontology*, 22(3), 631-664.

Caron, J. B., Gaines, R. R., Mángano, M. G., Streng, M., & Daley, A. C. (2010). A new Burgess Shale–type assemblage from the "thin" Stephen Formation of the southern Canadian Rockies. *Geology*, 38(9), 811-814.

Caron, J. B., & Aria, C. (2017). Cambrian suspension-feeding lobopodians and the early radiation of panarthropods. *BMC Evolutionary Biology*, 17(1), 29.

Chen, J. Y., Ramsköld, L., & Zhou, G. Q. (1994). Evidence for monophyly and arthropod affinity of Cambrian giant predators. *Science*, 264(5163), 1304-1308.

Cong, P., Ma, X., Hou, X., Edgecombe, G. D., & Strausfeld, N. J. (2014). Brain structure resolves the segmental affinity of anomalocaridid appendages. *Nature*, 513(7519), 538.

Cong, P., Daley, A. C., Edgecombe, G. D., Hou, X., & Chen, A. (2016). Morphology of the radiodontan *Lyrarapax* from the early Cambrian Chengjiang biota. *Journal of Paleontology*, 90(4), 663-671.

Cong, P., Daley, A. C., Edgecombe, G. D., & Hou, X. (2017). The functional head of the Cambrian radiodontan (stem-group Euarthropoda) *Amplectobelua symbrachiata*. *BMC Evolutionary Biology*, 17(1), 208.

Cong, P. Y., Edgecombe, G. D., Daley, A. C., Guo, J., Pates, S., & Hou, X. G. (2018). New radiodonts with gnathobase-like structures from the Cambrian Chengjiang biota and implications for the systematics of Radiodonta. *Papers in Palaeontology*, 4(4), 605-621.

Daley, A. C., Budd, G. E., Caron, J. B., Edgecombe, G. D., & Collins, D. (2009). The Burgess Shale anomalocaridid *Hurdia* and its significance for early euarthropod evolution. *Science*, 323(5921), 1597-1600.

Daley, A. C., & Budd, G. E. (2010). New anomalocaridid appendages from the Burgess Shale, Canada. *Palaeontology*, 53(4), 721-738.

Daley, A. C., & Peel, J. S. (2010). A possible anomalocaridid from the Cambrian Sirius Passet Lagerstätte, north Greenland. *Journal of Paleontology*, 84(2), 352-355.

Daley, A. C., & Bergström, J. (2012). The oral cone of *Anomalocaris* is not a classic ‘‘peytoia’’. *Naturwissenschaften*, 99(6), 501-504.

Daley, A. C., Paterson, J. R., Edgecombe, G. D., García-Bellido, D. C., & Jago, J. B. (2013a). New anatomical information on *Anomalocaris* from the Cambrian Emu Bay Shale of South Australia and a reassessment of its inferred predatory habits. *Palaeontology*, 56(5), 971-990.

Daley, A. C., Budd, G. E., & Caron, J. B. (2013b). Morphology and systematics of the anomalocaridid arthropod *Hurdia* from the Middle Cambrian of British Columbia and Utah. *Journal of Systematic Palaeontology*, 11(7), 743-787.

Daley, A. C., & Edgecombe, G. D. (2014). Morphology of *Anomalocaris canadensis* from the Burgess Shale. *Journal of Paleontology*, 88(1), 68-91.

Daley, A. C., Antcliffe, J. B., Drage, H. B., & Pates, S. (2018). Early fossil record of Euarthropoda and the Cambrian Explosion. *Proceedings of the National Academy of Sciences*, 115(21), 5323-5331.

Deline, B., & Ausich, W. I. (2011). Testing the plateau: a reexamination of disparity and morphologic constraints in early Paleozoic crinoids. *Paleobiology*, 37(2), 214-236.

English, A. M., & Babcock, L. E. (2010). Census of the Indian Springs Lagerstätte, Poleta Formation (Cambrian), western Nevada, USA. *Palaeogeography, Palaeoclimatology, Palaeoecology*, 295(1-2), 236-244.

Erwin, D. H. (2007). Disparity: morphological pattern and developmental context. *Palaeontology*, 50(1), 57-73.

Foote, M. (1993). Contributions of individual taxa to overall morphological disparity. *Paleobiology*, 19(4), 403-419.

Foote, M. (1994). Morphological disparity in Ordovician-Devonian crinoids and the early saturation of morphological space. *Paleobiology*, 20(3), 320-344.

Foote, M. (1995). Morphological diversification of Paleozoic crinoids. *Paleobiology*, 21(3), 273-299.

Foote, M. (1999). Morphological diversity in the evolutionary radiation of Paleozoic and post-Paleozoic crinoids. *Paleobiology*, 25(S2), 1-115.

Foth, C., Brusatte, S. L., & Butler, R. J. (2012). Do different disparity proxies converge on a common signal? Insights from the cranial morphometrics and evolutionary history of Pterosauria (Diapsida: Archosauria). *Journal of Evolutionary Biology*, 25(5), 904-915.

Gaines, R. R. (2014). Burgess Shale-type preservation and its distribution in space and time. *The Paleontological Society Papers*, 20, 123-146.

Gower, J. C. (1971). A general coefficient of similarity and some of its properties. *Biometrics*, 857-871.

Guo, J., Pates, S., Cong, P., Daley, A. C., Edgecombe, G. D., Chen, T., & Hou, X. (2018). A new radiodont (stem Euarthropoda) frontal appendage with a mosaic of characters from the Cambrian (Series 2 Stage 3) Chengjiang biota. *Papers in Palaeontology*. Online early view, doi: 10.1002/spp2.1231

Harper, D. A. (2006). The Ordovician biodiversification: Setting an agenda for marine life. *Palaeogeography, Palaeoclimatology, Palaeoecology*, 232(2-4), 148-166.

Hesterberg, Tim (2014), What Teachers Should Know about the Bootstrap: Resampling in the Undergraduate Statistics Curriculum. *Arxiv.* arxiv.org/abs/1411.5279.

Holmes, J. D., García-Bellido, D. C., & Lee, M. S. (2018). Comparisons between Cambrian Lagerstätten assemblages using multivariate, parsimony and Bayesian methods. *Gondwana Research*, 55, 30-41.

Hopkins, M. J. (2013). Decoupling of taxonomic diversity and morphological disparity during decline of the Cambrian trilobite family Pterocephaliidae. *Journal of Evolutionary Biology*, 26(8), 1665-1676.

Hopkins, M. J. (2014). The environmental structure of trilobite morphological disparity. *Paleobiology*, 40(3), 352-373.

Hopkins, M. J., & Smith, A. B. (2015). Dynamic evolutionary change in post-Paleozoic echinoids and the importance of scale when interpreting changes in rates of evolution. *Proceedings of the National Academy of Sciences*, 112(12), 3758-3763.

Hopkins, M. J. (2016). Magnitude versus direction of change and the contribution of macroevolutionary trends to morphological disparity. *Biological Journal of the Linnean Society*, 118(1), 116-130.

Hou, X-G., Bergström, J., & Ahlberg, P. (1995). *Anomalocaris* and other large animals in the Lower Cambrian Chengjiang fauna of southwest China. *GFF*, 117(3), 163-183.

Huang, D., Wang, Y., Gao, J., & Wang, Y. (2012). A new anomalocaridid frontal appendage from the Middle Cambrian Mantou Formation of the Tangshan Area. *Acta Palaeontologica Sinica*, 51, 411-415.

Hughes, M., Gerber, S., & Wills, M. A. (2013). Clades reach highest morphological disparity early in their evolution. *Proceedings of the National Academy of Sciences*, 110(34), 13875-13879.

Kühl, G., Briggs, D. E., & Rust, J. (2009). A great-appendage arthropod with a radial mouth from the Lower Devonian Hunsrück Slate, Germany. *Science*, 323(5915), 771-773.

Landing, E., Geyer, G., Brasier, M. D., & Bowring, S. A. (2013). Cambrian evolutionary radiation: context, correlation, and chronostratigraphy—overcoming deficiencies of the first appearance datum (FAD) concept. *Earth-Science Reviews*, 123, 133-172.

Lerosey-Aubril, R., Hegna, T. A., Babcock, L. E., Bonino, E., & Kier, C. (2014). Arthropod appendages from the Weeks Formation Konservat-Lagerstätte: new occurrences

of anomalocaridids in the Cambrian of Utah, USA. *Bulletin of Geosciences*, 89(2), 269-282.

Lerosey-Aubril, R., & Pates, S. (2018). New suspension-feeding radiodont suggests evolution of microplanktivory in Cambrian macronekton. *Nature Communications*, 9(1), 3774.

Lieberman, B. S. (2003). A new soft-bodied fauna: the Pioche Formation of Nevada. *Journal of Paleontology*, 77(4), 674-690.

Liu, J., Lerosey-Aubril, R., Steiner, M., Dunlop, J. A., Shu, D., & Paterson, J. R. (2018). Origin of raptorial feeding in juvenile euarthropods revealed by a Cambrian radiodontan. *National Science Review*.

Liu, Q. (2013). The first discovery of anomalocaridid appendages from the Balang Formation (Cambrian Series 2) in Hunan, China. *Alcheringa*, 37(3), 338-343.

Muscente, A. D., Schiffbauer, J. D., Broce, J., Laflamme, M., O'Donnell, K., Boag, T. H., Meyer, M., Hawkins, A. D., Huntley, J. W., McNamara, M., MacKenzie, L. A., Stanley Jr., G. D., Hunman, N. W., Hofmann, M. H., & Xiao, S. (2017). Exceptionally preserved fossil assemblages through geologic time and space. *Gondwana Research*, 48, 164-188.

Myers, C. E., & Saupe, E. E. 2013. A macroevolutionary expansion of the modern synthesis and the importance of extrinsic abiotic factors. *Palaeontology,* 56(6), 1179-1198.

Nedin, C. (1999). *Anomalocaris* predation on nonmineralized and mineralized trilobites. *Geology*, 27(11), 987-990.

Palmer, A. R. (1998). Terminal early Cambrian extinction of the Olenellina: documentation from the Pioche Formation, Nevada. *Journal of Paleontology*, 72(4), 650-672.

Pates, S., & Daley, A. C. (2017). *Caryosyntrips*: a radiodontan from the Cambrian of Spain, USA and Canada. *Papers in Palaeontology*, 3(3), 461-470.

Pates, S., Daley, A. C., & Ortega-Hernández, J. (2017). *Aysheaia prolata* from the Utah Wheeler Formation (Drumian, Cambrian) is a frontal appendage of the radiodontan *Stanleycaris*. *Acta Palaeontologica Polonica*, 62(3), 619-626.

Pates, S., & Daley, A. C. (2018). The Kinzers Formation (Pennsylvania, USA): the most diverse assemblage of Cambrian Stage 4 radiodonts. *Geological Magazine*, Online early view: doi.org/10.1017/S0016756818000547.

Pates, S., Daley, A. C., & Lieberman, B. S. (2018). Hurdiid radiodontans from the middle Cambrian (Series 3) of Utah. *Journal of Paleontology*, 92(1), 99-113.

Rabosky, D. L., Slater, G. J., & Alfaro, M. E. (2012). Clade age and species richness are decoupled across the eukaryotic tree of life. *PLoS biology*, 10(8), e1001381.

R Core Team. (2017). R: A language and environment for statistical computing. *Vienna, Austria: R Foundation for Statistical Computing*; 2016.

Servais, T., Owen, A. W., Harper, D. A., Kröger, B., & Munnecke, A. (2010). The great ordovician biodiversification event (GOBE): the palaeoecological dimension. *Palaeogeography, Palaeoclimatology, Palaeoecology*, 294(3-4), 99-119.

Servais, T., & Harper, D. A. (2018). The Great Ordovician Biodiversification Event (GOBE): definition, concept and duration. *Lethaia*, 51(2), 151-164.

Van Roy, P., & Briggs, D. E. (2011). A giant Ordovician anomalocaridid. Nature, 473(7348), 510.

Van Roy, P., Daley, A. C., & Briggs, D. E. (2015). Anomalocaridid trunk limb homology revealed by a giant filter-feeder with paired flaps. *Nature*, 522(7554), 77.

Venables, B., & Ripley, B. (2002). Modern Applied Statistics with S, 4th Edition. Springer, New York.

Vinther, J., Stein, M., Longrich, N. R., & Harper, D. A. (2014). A suspension-feeding anomalocarid from the Early Cambrian. *Nature*, 507(7493), 496.

Wagner, P. J. (1997). Patterns of morphologic diversification among the Rostroconchia. *Paleobiology*, 23(1), 115-150.

Wang, Y., Huang, D., & Hu, S. (2013). New anomalocardid frontal appendages from the Guanshan biota, eastern Yunnan. *Chinese Science Bulletin*, 58(32), 3937-3942.

Whittington, H. B., & Briggs, D. E. G. (1985). The largest Cambrian animal, Anomalocaris, Burgess Shale, British-Columbia. *Philosophical Transactions of the Royal Society of London B,* 309(1141), 569-609.

Wills, M. A. (1998). Cambrian and recent disparity: the picture from priapulids. *Paleobiology*, 24(2), 177-199.

Yang, J., Ortega-Hernández, J., Gerber, S., Butterfield, N. J., Hou, J. B., Lan, T., & Zhang, X. G. (2015). A superarmored lobopodian from the Cambrian of China and early disparity in the evolution of Onychophora. *Proceedings of the National Academy of Sciences*, 112(28), 8678-8683.

Zhao, Y., Zhu, M., Babcock, L. E., Yuan, J., Parsley, R. L., Peng, J., Yang, X., and Wang, Y. (2005). Kaili Biota: a taphonomic window on diversification of metazoans from the basal Middle Cambrian: Guizhou, China. *Acta Geologica Sinica-English Edition*, 79(6), 751-765.

Zhuravlev, A. Y., & Wood, R. A. (2018). The two phases of the Cambrian Explosion. *Scientific Reports,* 8(1), 16656.

Chapter 11

Trilobite abnormalities: their history, causes,

and potential

Trilobite abnormalities: their history, causes, and potential

Abstract

Abnormal trilobites were first reported over 100 years ago, and since then abnormalities have been attributed to predation, accidental injuries from ecdysis, parasites, and genetic malfunction. Records of abnormalities are based mainly on reports of individual occurrences, and the cause is often unknown. One of the rare quantitative studies conducted on trilobite abnormalities showed that Cambrian trilobites have an injury pattern bias: injuries are located more commonly on the rear, right-hand side of the thorax. This was attributed either to behavioural asymmetry in trilobites or to their predators. The identity of trilobite consumers (predators and/or scavengers) is confirmed by the rare occurrence of trilobite sclerites in gut contents. Other evidence, such as coprolites, broken sclerites, and repaired injuries, cannot be used to identify the consumer. Other ways of identifying trilobite predators include functional morphology and finite element analysis. Radiodonts have often been implicated as consumers, on account of their presumed large size. However, recent work highlighted that radiodont mouthparts were unsuitable for breaking trilobite exoskeletons, thus their importance as trilobite predators may have been overstated. Euarthropods such as sanctacaridids and other artiopdans with gnathobasic spines were more probable predators of trilobites. Regardless, trilobites are very suitable animals for quantitative studies of predation pressure in the Cambrian as they are an abundant and well preserved ecologically, morphologically, and taxonomically diverse group. Furthermore, the effects of geography, time, and morphology can be assessed.

History of research

The earliest papers figuring an abnormality on a trilobite are over 100 years old (Matthews 1887; Burling 1916) and anecdotal identifications of trilobite abnormalities either as stand-alone reports or part of larger studies are common and semi-regular in the literature (Cambrian examples include: Lochman 1936, 1941; Resser & Howell 1938; Palmer 1958; Pocock 1974; Alpert & Moore 1975; Bergström & Levi-Setti 1978; Snajdr 1978, Rudkin 1979; Briggs & Mount 1982; Vorwald 1984; Conway Morris & Jenkins 1985; Zhang 1989; Nedin 1999; Jago & Haines 2002; Hu et al. 2004; Skinner 2004; Fatka et al. 2009, 2015; Robison & Babcock 2011; Zamora et al. 2011). Radiodonts, such as the large putative apex-predator *Anomalocaris*, have often been suggested as potential culprits for repaired injuries in trilobites, especially 'V' and 'W' shaped scars (e.g. Whittington & Briggs 1985; Babcock 1993; Nedin 1999; Bicknell & Paterson 2018, table 1). This is on account of the shape of the radiodont oral cone, the large size of known complete radiodont specimens compared to other Cambrian predators, and the preservation of radiodont material alongside injured trilobites (Whittington & Briggs 1985; Babcock 1993; Chen et al. 1994; Nedin 1999). However, more recent studies have suggested that the radiodont oral cone was not suitable for breaking mineralised trilobite exoskeletons (Hagadorn 2009; Hagadorn et al. 2010; Daley & Bergström 2012).

Abnormal trilobites are not limited to the Cambrian, and examples are also known from the Ordovician to the Carboniferous (e.g. Sinclair 1947; Whittington 1956; Ludvigsen 1977; Snajdr 1979, 1981; Owen 1980; Owen & Harper 1982; Rudkin 1985; Owen & Tisley 1996; Budil et al. 2010; Kandemir & Lerosey-Aubril 2011; Nielsen & Nielsen 2017; Schoenemann et al. 2017), though currently no abnormal Permian examples are known (Owen 1985). Although radiodonts are known in deposits younger

than the Cambrian (e.g. Van Roy et al. 2015), they have not been suggested as culprits for Ordovician-and-younger repaired injuries and broken sclerites, with other groups such as nautiloids preferred (e.g. Sá & Gutiérrez-Marco 2015).

Periodic reviews have synthesized these anecdotal reports, providing insight into trilobite palaeobiology, their predators, and predation in the Cambrian in general (e.g. Owen 1985; Babcock 1993; Babcock 2003; Bicknell & Paterson 2018; Vinn 2018). The first substantial review of abnormalities in trilobites outlined potential causes of abnormalities and separated them into injuries, teratologies, and pathologies (Owen 1985). Injuries, which have either a predatory cause or accidental cause such as moulting, can be recognised by a thickening of the exoskeleton during the intermoult period when the injury was sustained, or by partial regeneration of the injured area over a series of moults (Ludvigsen 1977; Owen 1985). Teratologies, the result of genetic or embryological malfunctions, can be seen as missing or reduced body parts, but cannot always be differentiated from healed injuries when examples are considered in isolation (Owen 1985). Pathologies, caused by disease or parasitic infection, can be recognised as swellings, borings, or local atrophy (Owen 1985), although it is not always possible in the case of borings to assess whether this is the result of a parasitic infection or developed post-mortem or in exuviae (Owen 1985).

Babcock (1993), building on an earlier study (Babcock & Robison 1989), focused on the location of trilobite injuries, using data from the literature and museum specimens. These studies demonstrated that, when injuries on Cambrian trilobites were treated as one sample, there was a location bias for injuries to the right-side and posterior of the thorax. This contrasts with post-Cambrian trilobite injuries, where no such location specificity (stereotypy) was found (Babcock 1993). Behavioural asymmetry

in trilobites and/or their predators was offered as an explanation for this stereotypy, with Cambrian predators considered to have made first contact with trilobite prey on the right-hand side of the body and/or the majority of trilobites turning the same way when attacked, consistently exposing one side of the body to predatory damage (Babcock & Robison 1989; Babcock 1993). This lumping of taxa together did produce a large enough sample size for statistical analysis of injuries, but may have obscured finer scale variation in injury location in Cambrian trilobites. It may therefore be premature to suggest that all Cambrian trilobites, or all Cambrian predators of trilobites, shared the same behavioural asymmetry.

Radiodonts: predators of trilobites?

Babcock (1993) also briefly considered potential trilobite predators, noting the co-occurrence of *Anomalocaris* in beds containing injured trilobites, building on previous connections between their iconic status as the largest Cambrian predators and trilobite injuries (e.g. Whittington & Briggs 1985; Chen et al. 1994). Indeed, a recent review (Bicknell & Paterson 2018, table 1) that collated all possible durophagous injuries in Cambrian trilobites noted in the literature and their suggested predators showed that where a predator had been suggested (24 of 83 reports), *Anomalocaris* (12 of 24), or more generally radiodonts (18 of 24), were by far the most commonly suggested predators. Other suggestions included sea anemones (Alpert & Moore 1975), *Sidneyia inexpectans* (Rudkin 1979), *Redlichia* or other trilobites (Conway Morris & Jenkins 1985; Jell 1989), or *Tuzoia* (twice; Fatka et al. 2009, 2015).

Direct evidence where both predator (or scavenger) and its prey can be identified comes in two forms in the fossil record: caught-in-the-act fossilization events,

and gut contents (cololites). Direct evidence for predation where only prey can be recognised (and not the predator) comes in a further three forms: coprolites, repaired injuries, and sclerites with lethal damage (Kowalewski 2002). When trilobites are considered as prey items, there are no occurrences of caught-in-the-act fossilization events, and no radiodont with mineralised sclerites in the gut of any form has yet been reported (e.g. Daley & Edgecombe 2014; Bicknell & Paterson 2018).

Indirect forms of evidence for predators feeding on trilobites come from functional morphology inferences, and comparisons between the shape of injuries and feeding structures. These form the basis of the hypothesis that radiodonts fed on trilobites and produced many repaired injuries. The radial mouthparts of radiodonts may have caused the 'V' or 'W' shaped trilobite repair scars, if such scars were shallow (Whittington & Briggs 1985). However, Whittington & Briggs (1985) did not consider trilobites to be preferred prey for radiodonts, instead suggesting other arthropods that lacked mineralised exoskeletons would be more ideal prey items. Nedin (1999) proposed a complex prey-handling motion for radiodonts that involved the bending of trilobite exoskeletons between the mouthparts and frontal appendages to break sclerites. Both of these hypothesised trilobite-breaking methods require radiodont mouthparts to be able to undergo a significant amount of stress – enough so that the trilobite exoskeleton fails before the mouth plates. An assessment of the crushing ability of radiodont mouthparts, using Finite Element Analysis (FEA), suggested that radiodonts were unable to crush mineralised exoskeletons (Hagadorn 2009; Hagadorn et al. 2010). Furthermore, the discovery that *Anomalocaris* possessed a triradial oral cone with a small and irregularly shaped opening, unsuitable for biting motions (Daley & Bergström 2012), refuted the idea that specifically *Anomalocaris* mouthparts made 'V'

or ‘W’ shaped injuries in mineralised trilobites. These studies were complemented by the discoveries that radiodonts were in fact a highly diverse group with frontal appendages specialised to a variety of feeding modes including raptorial predation, slicing predation, sediment sifting, and filter feeding (e.g. Daley et al. 2009, 2013a, b; Daley & Budd 2010; Vinther et al. 2014; Van Roy et al. 2015). In summary, the previous concept that *Anomalocaris* was an apex predator specialised to break and consume trilobites was incorrect (Daley & Bergström 2012). This does not preclude the possibility that radiodonts fed on trilobites, but suggests that attacks were limited to trilobites in the soft-shell stage immediately after ecdysis or that trilobite were ingested whole, and that trilobites were not the preferred food item for radiodonts, as originally suggested by Whittington & Briggs (1985).

Repaired injuries on trilobite exoskeletons, the presence of trilobite sclerites in coprolites (e.g. Daley et al. 2013b) and the gut contents of the stem- and crown-euarthropods *Sidneyia* (Bruton 1981; Briggs & Whittington 1985), *Wisangocaris* (Jago et al. 2016), a *Fuxianhuia*-like arthropod (Zhu et al. 2004), and the priapulid worm *Ottoia* (Vannier 2012) are testament to the fact that some animals were capable of breaking and consuming mineralised trilobites. A recent FEA study of the gnathobase-bearing *Sidneyia* showed that it would have been capable of breaking mineralized exoskeletons (Bicknell et al. 2018), and Cambrian sanctacaridids, such as *Sanctacaris, Utahcaris,* and *Wisangocaris,* all likely bore chelicerae (Legg & Pates 2016) and thus would also have been capable of breaking trilobite exoskeletons.

Opportunities for trilobite repaired injury studies

Regardless of whether the direct culprit for a particular injury can be identified or not, studies of repaired injury frequency on prey remains offer an excellent way to study predation pressure in the fossil record. This is because data of sufficient quality and quantity can be gathered to test hypotheses (Harper 2016). However, studies of predation pressure from the Cambrian are lacking (Leighton 2011). To this end, trilobites are a perfect study animal to provide raw data on predation levels in the aftermath of the Cambrian Explosion, and subsequently assess the importance of predation as a shaper of evolution at this time.

Trilobites were a diverse, morphologically disparate, widespread group in the early Palaeozoic (e.g. Foote 1991; Webster 2007) and, as noted above, exoskeletal injuries are well known. Given that Cambrian aged deposits with abundant, autochthonous, near-articulated trilobite exoskeletons are known, there is excellent potential to use this material to assess the changing predation pressure throughout the early Palaeozoic. Furthermore, the effectiveness of putative anti-predatory morphologies can be tested in cases where multiple trilobite species showing prominent morphological differences are known from a single deposit. Unlike studies of gastropods, bivalves, and brachiopods, where methodology is well established (e.g. Vermeij et al. 1981; Alexander 1986; Dietl et al. 2000; Harper & Peck 2016), no study on trilobites has yet been undertaken. Pilot studies are necessary to create a workable and reproducible methodology that can be used test macroevolutionary hypotheses and understand predation pressure on trilobites throughout the Palaeozoic.

Aims for this thesis section

I conduct two pilot studies, the first quantitative studies of predation pressure on trilobites, to test hypotheses relating to how geographic and temporal (Chapter 12) or morphological (Chapter 13) differences between trilobite communities and bodyplans influences the repair frequency (and thus predation pressure) experienced by these animals. These pilot studies, one using a field sample (Chapter 12) and the other an indirect bulk sample from museum collections (*sensu* Kowalewski 2002; Chapter 13), offer a methodology for the quantitative study of injuries to trilobites. This methodology has the potential for future studies of predation pressure through the Palaeozoic, and testing the anti-predatory effectiveness of different morphological features.

References

Alexander, R. R. (1986). Resistance to and repair of shell breakage induced by durophages in Late Ordovician brachiopods. *Journal of Paleontology*, 60(2), 273-285.

Alpert, S. P., & Moore, J. N. (1975). Lower Cambrian trace fossil evidence for predation on trilobites. *Lethaia*, 8(3), 223-230.

Babcock, L. E., & Robison, R. A. (1989). Preferences of Palaeozoic predators. *Nature*, 337, 695-696.

Babcock, L. E. (1993). Trilobite malformations and the fossil record of behavioral asymmetry. *Journal of Paleontology*, 67(2), 217-229.

Babcock, L. E. (2003). Trilobites in Paleozoic predator-prey systems, and their role in reorganization of early Paleozoic ecosystems. *In* Predator—prey interactions in the fossil record (pp. 55-92). Springer, Boston, MA.

Bergström, J., & Levi-Setti, R. (1978). Phenotypic variation in the Middle Cambrian trilobite *Paradoxides davidis* Salter at Manuels, SE Newfoundland. *Geologica et Palaeontologica*, 12, 1-40.

Bicknell, R. D., & Paterson, J. R. (2018). Reappraising the early evidence of durophagy and drilling predation in the fossil record: implications for escalation and the Cambrian Explosion. *Biological Reviews*, 93(2), 754-784.

Bicknell R. D. C., Ledogar J. A. , Wroe S., Gutzler B. C., Watson III W. H., Paterson, J. R. (2018). Computational biomechanical analyses demonstrate similar shell-crushing abilities in modern and ancient arthropods. Proceedings of the Royal Society B, 19-35. doi: 10.1098/rspb.2018.1935

Briggs, D. E., & Mount, J. D. (1982). The occurrence of the giant arthropod *Anomalocaris* in the Lower Cambrian of southern California, and the overall distribution of the genus. *Journal of Paleontology*, 56(5), 1112-1118.

Briggs, D. E. G., & Whittington, H. B. (1985). Modes of life of arthropods from the Burgess Shale, British Columbia. *Earth and Environmental Science Transactions of The Royal Society of Edinburgh*, 76(2-3), 149-160.

Bruton, D. L. (1981). The arthropod *Sidneyia inexpectans*, middle Cambrian, Burgess Shale, British Columbia. *Philosophical Transactions of the Royal Society of London, Series B: Biological Sciences*, 295, 619–656.

Budil, P., Fatka, O., Zwanzig, M., & Rak, Š. (2010). Two unique Middle Ordovician trilobites from the Prague Basin, Czech Republic. *Journal of the National Museum (Prague), Natural History Series*, 179(8), 95-104.

Burling, L. (1916). *Paedeumias* and the Mesonacidae, with description of a new species, having at least 44 segments, from the lower Cambrian of British Columbia. *The Ottawa Naturalist,* 30, 53–58.

Chen, J. Y., Ramsköld, L., & Zhou, G. Q. (1994). Evidence for monophyly and arthropod affinity of Cambrian giant predators. *Science*, 264(5163), 1304-1308.

Conway Morris, S., & Jenkins, R. J. F. (1985). Healed injuries in early Cambrian trilobites from South Australia. *Alcheringa*, 9(3), 167-177.

Daley, A. C., Budd, G. E., Caron, J. B., Edgecombe, G. D., & Collins, D. (2009). The Burgess Shale anomalocaridid *Hurdia* and its significance for early euarthropod evolution. *Science*, 323(5921), 1597-1600.

Daley, A. C., & Budd, G. E. (2010). New anomalocaridid appendages from the Burgess Shale, Canada. *Palaeontology*, 53(4), 721-738.

Daley, A. C., & Bergström, J. (2012). The oral cone of *Anomalocaris* is not a classic ‘‘peytoia’’. *Naturwissenschaften*, 99(6), 501-504.

Daley, A. C., Paterson, J. R., Edgecombe, G. D., García-Bellido, D. C., & Jago, J. B. (2013a). New anatomical information on *Anomalocaris* from the Cambrian Emu Bay Shale of South Australia and a reassessment of its inferred predatory habits. *Palaeontology*, 56(5), 971-990.

Daley, A. C., Budd, G. E., & Caron, J. B. (2013b). Morphology and systematics of the anomalocaridid arthropod *Hurdia* from the Middle Cambrian of British Columbia and Utah. *Journal of Systematic Palaeontology*, 11(7), 743-787.

Daley, A. C., & Edgecombe, G. D. (2014). Morphology of *Anomalocaris canadensis* from the Burgess Shale. *Journal of Paleontology*, 88(1), 68-91.

Dietl, G. P., Alexander, R. R., & Bien, W. F. (2000). Escalation in Late Cretaceous-early Paleocene oysters (Gryphaeidae) from the Atlantic Coastal Plain. *Paleobiology*, 26(2), 215-237.

Fatka, O., Szabad, M., & Budil, P. (2009). Malformed agnostids from the Middle Cambrian Jince Formation of the Příbram-Jince Basin, Czech Republic. *Bulletin of Geosciences*, 83(1), 121-126.

Fatka, O., Budil, P., & Grigar, L. (2015). A unique case of healed injury in a Cambrian trilobite. *Annales de Paléontologie,* 101(4), 295-299.

Foote, M. (1991). Morphologic patterns of diversification: examples from trilobites. *Palaeontology*, 34(2), 461-485.

Hagadorn, J.W. (2009). Taking a bite out of *Anomalocaris*. *Walcott 2009: International Conference on the Cambrian Explosion, abstract volume*, 33–34.

Hagadorn, J. W., Schottenfeld, M. T. & McGowan, D. (2010). Putting *Anomalocaris* on a soft-food diet? *Geological Society of America Abstracts,* 42, 320.

Harper, E. M. (2016). Uncovering the holes and cracks: from anecdote to testable hypotheses in predation studies. *Palaeontology*, 59(5), 597-609.

Harper, E. M., & Peck, L. S. (2016). Latitudinal and depth gradients in marine predation pressure. *Global Ecology and Biogeography*, 25(6), 670-678.

Hu, S., Zhu, M., Luo, H., Steiner, M., Zhao, F., Li, G., Liu, Q. & Zhang, Z. (2004). *The Guanshan Biota*. Yunnan Publishing Group Co. Ltd., Yunnan Science and Technology Press, Kunming.

Jago, J. B., García-Bellido, D. C. & Gehling, J. G. (2016). An early Cambrian chelicerate from the Emu Bay Shale, South Australia. *Palaeontology,* 59, 549–562.

Jago, J. B. & Haines, P. W. (2002). Repairs to an injured early middle Cambrian trilobite, Elkedra area, Northern Territory. *Alcheringa,* 26, 19–21.

Jell, P. A. (1989). Some aberrant exoskeletons from fossil and living arthropods. *Memoirs of the Queensland Museum,* 27, 491–498.

Kandemir, R., & Lerosey-Aubril, R. (2011). First report of a trilobite in the Carboniferous of Eastern Pontides, NE Turkey. *Turkish Journal of Earth Sciences,* 20, 179-183.

Kowalewski, M. (2002). The fossil record of predation: an overview of analytical methods. *The Paleontological Society Papers*, 8, 3-42.

Legg, D. A., & Pates, S. (2016). A restudy of *Utahcaris orion* (Euarthropoda) from the Spence Shale (middle Cambrian, Utah, USA). *Geological Magazine*, 154(1), 181-186.

Leighton, L. R. (2011). Analyzing predation from the dawn of the Phanerozoic. *In* Quantifying the Evolution of Early Life (pp. 73-109). Springer, Dordrecht.

Lochman, C. (1936). New trilobite genera from the Bonneterre dolomite (Upper Cambrian) of Missouri. *Journal of Paleontology*, 10, 35-43.

Lochman, C. (1941). A pathologic pygidium from the Upper Cambrian of Missouri. *Journal of Paleontology*, 15(3), 324-325.

Ludvigsen, R. (1977). Rapid repair of traumatic injury by an Ordovician trilobite. *Lethaia,* 10, 205–207.

Matthew, G. (1887). Illustrations of the fauna of the St. John Group, number 4, Pt. 2, the smaller trilobites with eyes (Ptychoparidae and Ellipsocephalidae). *Transactions and Proceedings of the Royal Society of Canada*, 2, 39–66.

Nedin, C. (1999). *Anomalocaris* predation on nonmineralized and mineralized trilobites. *Geology*, 27(11), 987-990.

Owen, A. W. (1980). An abnormal cranidium of the trilobite *Calyptaulax norvegicus*. *Norsk Geologisk Tidsskrift*, 60, 87-88.

Owen, A. W., & Harper, D. A. (1982). The Middle Ordovician of the Oslo Region, Norway, 31. The upper Caradoc trilobites and brachiopods from Vestbråten, Ringerike. *Norsk Geologisk Tidsskrift*, 62, 95-120.

Owen, A. W. (1985). Trilobite abnormalities. *Earth and Environmental Science Transactions of The Royal Society of Edinburgh*, 76(2-3), 255-272.

Owen, A. W., & J. W. Tilsley. (1996). An abnormal pygidium of the trilobite *Brachymetopus ornatus* Woodward from the Lower Carboniferous of Derbyshire. *Geological Journal*, 31(4), 389-392.

Nielsen, M. L., & Nielsen, A. T. (2017). Two abnormal pygidia of the trilobite Toxochasmops from the Upper Ordovician of the Oslo Region, Norway. Bulletin of the Geological Society of Denmark, 65, 171-175.

Palmer, A. R. (1958). Morphology and ontogeny of a lower Cambrian ptychoparioid trilobite from Nevada. *Journal of Paleontology,* 32, 154–170.

Pocock, K. J. (1974). A unique case of teratology in trilobite segmentation. *Lethaia* 7, 63-66.

Resser, C. E. & Howell, B. F. (1938). Lower Cambrian Olenellus Zone of the Appalachians. *Geological Society of America Bulletin,* 49, 195–248.

Robison, R. A. & Babcock, L. E. (2011). Systematics, paleobiology, and taphonomy of some exceptionally preserved trilobites from Cambrian *Lagerstätten* of Utah. *Paleontological Contributions,* 5, 1–47.

Rudkin, D. M. (1979). Healed injuries in *Ogygopsis klotzi* (Trilobita) from the middle Cambrian of British Columbia. *Royal Ontario Museum Life Sciences Occasional Paper*, 32, 1-8.

Rudkin, D. M. (1985). Exoskeletal abnormalities in four trilobites. *Canadian Journal of Earth Sciences,* 22, 479-483.

Sá, A. A., & Gutiérrez-Marco, J. C. (2015). *Aroucaichnus* igen. nov. y otros icnofósiles singulares del Ordovícico del Geoparque Arouca (Portugal). *Boletín de la Sociedad Geológica del Perú*, 110, 8-23.

Schoenemann, B., Clarkson, E. N. K., & Høyberget, M. (2017). Traces of an ancient immune system – how an injured arthropod survived 465 million years ago. *Scientific Reports*, 7, 40330.

Sinclair, G. W. (1947). Two examples of injury in Ordovician trilobites. *American Journal of Science,* 4, 250-257.

Skinner, E. S. (2004). Taphonomy of exceptionally preserved fossils from the Kinzers Formation (Cambrian), southeastern Pennsylvania. *PhD Thesis: Ohio State University*.

Snajdr, M. (1978). Anomalous carapaces of Bohemian paradoxid trilobites. *Sborník Geologickych Ved Paleontologie*, 20, 7–31.

Snajdr, M. (1979). Two trinucleuid trilobites with repair of traumatic injury. *Vestnik Ustredniho ustavu geologickeho*, 54(1), 49-51.

Snajdr, M. (1981). Bohemian Proetidae with malformed exoskeletons (Trilobita). *Sborník Geologickych Ved Paleontologie*, 24, 37-60.

Van Roy, P., Daley, A. C., & Briggs, D. E. (2015). Anomalocaridid trunk limb homology revealed by a giant filter-feeder with paired flaps. *Nature*, 522(7554), 77.

Vannier, J. (2012). Gut contents as direct indicators for trophic relationships in the Cambrian marine ecosystem. *PloS one*, 7(12), e52200.

Vermeij, G. J., Schindel, D. E., & Zipser, E. (1981). Predation through geological time: evidence from gastropod shell repair. *Science*, 214(4524), 1024-1026.

Vinn, O. (2018). Traces of predation in the Cambrian. *Historical Biology*, 30(8), 1043-1049.

Vinther, J., Stein, M., Longrich, N. R., & Harper, D. A. (2014). A suspension-feeding anomalocarid from the Early Cambrian. *Nature*, 507(7493), 496.

Vorwald, G. R. (1984). Paleontology and paleoecology of the upper Wheeler Formation (late middle Cambrian), Drum Mountains, West-central Utah. *PhD Thesis: University of Kansas.*

Webster, M. (2007). A Cambrian peak in morphological variation within trilobite species. *Science*, 317(5837), 499-502.

Whittington, H. B. 1956. Silicified Middle Ordovician trilobites: the Odontopleuridae. *Bulletin of the Museum of Comparative Zoology, Harvard,* 114, 155-288.

Whittington, H. B., & Briggs, D. E. G. (1985). The largest Cambrian animal, Anomalocaris, Burgess Shale, British-Columbia. *Philosophical Transactions of the Royal Society of London B,* 309(1141), 569-609.

Zamora, S., Mayoral, E., Esteve, J., Gámez-Vintaned, J. A., & Santos, A. (2011). Exoskeletal abnormalities in paradoxidid trilobites from the Cambrian of Spain, and a new type of bite trace. *Bulletin of Geosciences*, 86(3), 665-673.

Zhang, X. G. (1989). Ontogeny of an early Cambrian eodiscoid trilobite from Henan, China. *Lethaia,* 22, 13–29.

Zhu, M. Y., Vannier, J., Iten, H. & Zhao, Y. L. (2004). Direct evidence for predation on trilobites in the Cambrian. *Proceedings of the Royal Society of London B: Biological Sciences*, 271, S277–S280.

Chapter 12

Quantitative analysis of repaired and unrepaired damage to trilobites from the Cambrian (Stage 4 – Drumian) Iberian Chains, NE Spain

Author contributions

SP conceived the project; SZ led the fieldwork and prepared figures 1 and 2; RDCB performed the semi-landmark analyses and prepared figures 8 and 9; SP performed the remainder of statistical analyses, wrote the manuscript, and prepared the remaining figures, with input from RDCB, ACD, and SZ.

Publication information

This Chapter has been peer reviewed and published by *PALAIOS*:

Pates, S., Bicknell, R. D. C., Daley, A. C., & Zamora, S. (2017). Quantitative analysis of repaired and unrepaired damage to trilobites from the Cambrian (Stage 4, Drumian) Iberian Chains, NE Spain. *PALAIOS*, 32(12), 750-761.

Additional information

The supplemental material for this Chapter is in Appendix 4.

QUANTITATIVE ANALYSIS OF REPAIRED AND UNREPAIRED DAMAGE TO TRILOBITES FROM THE CAMBRIAN (STAGE 4 - DRUMIAN) IBERIAN CHAINS, NE SPAIN

STEPHEN PATES,[1,2] RUSSELL D. C. BICKNELL,[3] ALLISON C. DALEY,[2] and SAMUEL ZAMORA[4,5]

[1]Department of Zoology, University of Oxford, Oxford, OX1 3PS, United Kingdom

[2]Institute of Earth Sciences, University of Lausanne, Lausanne, CH-1015, Switzerland

[3]Paleoscience Research Centre School of Environmental and Rural Science, University of New England, Armidale, New South Wales, 2351, Australia

[4]Instituto Geológico y Minero de España, C/Manuel Lasala, 44, 9ºB, 50006, Zaragoza, Spain

[5]Unidad Asociada en Ciencias de la Tierra, Universidad de Zaragoza-IGME, Zaragoza, Spain

email: stephen.pates@zoo.ox.ac.uk

ABSTRACT: Repaired fossil skeletons provide the opportunity to study predation rates, repair mechanisms, and ecological interactions in deep time. Trilobites allow the study of repaired damage over long time periods and large geographic areas due to their longevity as a group, global distribution, and well-preserved mineralized exoskeletons. Repair frequencies on trilobites from three sites representing offshore marine environments in the Iberian Chains (Spain) show no injuries on 45 complete redlichiid thoraces from Minas Tierga (Huérmeda Formation, Cambrian Series 2, Stage 4), or 23 complete *Eccaparadoxides pradoanus* thoraces from Mesones de Isuela (Murero

Formation, Cambrian Series 3, Drumian). Ten injuries on 69 *E. pradoanus* thoraces from Purujosa (Murero Formation, Cambrian Series 3, Drumian) were noted. There is no evidence for laterally asymmetric predation or size selection on the trilobites in this study. Weak evidence for selection for the rear of the thorax is documented. A series of injured trilobites illustrates four stages of the healing process. Analysis of injury locations and frequency suggests that injuries to these trilobites are predatory in origin. Semilandmark analysis of previously described exoskeletons with unrepaired damage assigned to the ichnotaxon *Bicrescomanducator serratus* alongside newly collected damaged exoskeletons from Purujosa (Mansilla and Murero Formations, Stage 5, Drumian), Mesones de Isuela (Murero Formation, Drumian), and Minas Tierga (Huérmeda Formation, Stage 4) found that shapes of biotic and abiotic breaks could not be distinguished.

INTRODUCTION

Predator-prey interactions, including sub-lethal and lethal damage, have been studied using repaired exoskeletons, shells, drillholes, and broken sclerites, exemplifying the importance of predation as a potential evolutionary driver (e.g., Vermeij 1987; Kowalewski et al. 1998; Kowalewski 2002; Kelley et al. 2003). Repaired injuries preserved in different depositional environments and on skeletons of a wide variety of prey offer direct evidence of biotic interaction between predators and prey (e.g., Kowalewski 2002; Babcock 2003). Studies on repaired injuries have shown that the morphology of prey affects the frequency of repaired damages (e.g., Alexander 1986; Dietl et al. 2000; Alexander and Dietl 2001; Dietl 2003a, 2003b; Dietl and Hendricks

2006; Harper et al. 2009), and morphological characters such as spiny shells and reduced aperture sizes are adaptations in response to predation pressure (Vermeij 1977, 1987; Kelley 1989; Klompmaker and Kelley 2015). Potential physical defensive adaptations in trilobites include growth to large size (e.g., *Paradoxides davidis*, Bergström and Levi-Setti 1978), development of additional spines and lengthening existing spines (e.g., *Psychopyge elegans*, Morzadec 1988), and thickening of the exoskeleton. Behavioral defensive adaptations include enrolment (e.g., *Eccaparadoxides pradoanus*, Esteve et al. 2011, 2013), burrowing (e.g., *Symphysurus angustatus*, Fortey 1986), or infaunal habit (e.g., *Paciphacops*, Rustán et al. 2011). Finally, some trilobites occupied low oxygen environments, potentially as refugia from predation (e.g., *Elrathia kingii*, Gaines and Droser 2003). Many of these adaptations (enrolment, occupation of low oxygen environments, growth of elongated pleural spines) originated in the Cambrian, perhaps driven by predatory pressure. The sophistication of predatory behavior also increased over time, showing the importance of predator-prey escalation as an evolutionary driver (Kowalewski et al. 1998; Brett and Walker 2002; Aberhan et al. 2006).

Trilobites were preyed upon since the Cambrian, and have been reported in the gut contents of *Ottoia prolifica* Walcott 1911, *Sidneyia inexpectans* Walcott 1911, *Wisangocaris barbarahardyae* Jago et al. 2016*,* and a *Fuxianhuia*-like arthropod (Conway Morris 1977; Bruton 1981; Zhu et al. 2004; Vannier 2012; Zacaï et al. 2015; Jago et al. 2016) as well as in coprolites (Sprinkle 1973; Conway Morris and Robison 1988; Nedin 1999; Babcock 2003, Skinner 2005; Vannier and Chen 2005; English and Babcock 2010; Daley et al. 2013; Kimmig and Strotz 2017). Such examples are only recorded in exceptional preservation fossilization events, whereas damage and repair of

mineralized trilobite exoskeletons are more easily preserved (Lochman 1941; Sinclair 1947; Šnajdr 1978; Rudkin 1979; Owen 1985; Babcock 1993). Trilobite abnormalities and repair have been attributed to predation, problematic molting, genetic malfunction, parasites, and accidental damage. The predation or scavenging trace fossil taxon *Bicrescomanducator serratus* (Zamora et al. 2011) describes unrepaired damage on trilobite sclerites that consists of asymmetric V- or W-shaped serrated breakage of variable length, with a first-order path that is straight, or sometimes slightly arcuate (Zamora et al. 2011; Buatois et al. 2017). This trace can be seen on trilobite exoskeletons and fragments from the Cambrian Series 3 (Drumian) Purujosa 3 section of the Murero Formation, NE Spain (Zamora et al. 2011, fig. 2), Cambrian Drumian (Marjuman) section of the Rabbitkettle Formation, SW Canada (Pratt 1998, figs. 8–10), and the Ordovician Valongo Formation in Portugal (Sá and Gutiérrez-Marco 2015, fig. 12), and is attributed to *Anomalocaris* in the Cambrian and orthoceratids in the Ordovician (Zamora et al. 2011; Sá and Gutiérrez-Marco 2015). Sá and Guitiérrez-Marco (2015) synonymized *Mandibulichnus* Zamora et al. 2011 with *Bicrescomanducator* Donovan et al. in Andrew et al. 2010, as both describe irregular asymmetric breaks which occur singularly, with the difference between the type species *Bicrescomanducator rolli* Donovan et al. in Andrew et al. 2010 and *B. serratus* being the shape of the breaks: *B. rolli* is sub-crescentic and *B. serratus* is serrated. Although subsequent authors have continued to use *Mandibulichnus* (e.g., Neto de Carvalho et al. 2016; Buatois et al. 2017), here we treat the differences between these bioerosion traces at the species level, and so use *Bicrescomanducator serratus*. Not all broken trilobite sclerites are caused by the action of predators or scavengers and abiotic

damage in trilobites has been recognized (e.g., Webster and Hughes 1999; Webster et al. 2008).

Injuries and abnormalities in trilobites are used to understand the repair mechanisms of exoskeletons, as reviewed in the landmark publication by Owen (1985) and subsequently by Bicknell and Paterson (2017). Trilobite abnormalities can result from injuries, teratologies, and pathologies (Owen 1985). Injuries can be caused by predation, accidental damage, intraspecific competition, or damage during molting (Owen 1985; Babcock 1993). Trilobites healed over a number of molt cycles (e.g., Šnajdr 1978; Owen 1985) that followed an initial callousing and regrowth over the injury (e.g., Schoenemann et al. 2017). When attacked during the soft post-ecdysial stage, trilobite spines could wrinkle or distort (Conway Morris and Jenkins 1985), and rarely additional pleural spines grew from injured areas (Babcock 1993). Regeneration of spines is controlled by segment polarity genes (McNamara and Tuura 2011), and begins during ecdysis after the damage was sustained (Lochman 1941). Regrown spines remain shorter than original spines for a variable number of molts, likely dependent on the severity of the injury. This process is comparable to the regeneration of tail spines in *Daphnia* and crinoid arms (Murtaugh 1981; Baumiller and Gahn 2012).

Examining repaired injuries and drillholes on exoskeletons at various locations and in different formations is important for understanding the variability of predation pressure across space and time (Harper 2016). Such data can also be used to identify stereotypy of predators targeting specific locations on prey exoskeletons or specific prey sizes (e.g., Conway Morris and Bengtson 1994; Leighton 2001, 2011; Robson and Pratt 2007). Previous quantitative studies on repaired trilobites showed non-random distribution of repaired injuries as evidence for predator site selection (Babcock and

Robison 1989; Babcock 1993, 2003). When data from Cambrian trilobites was treated statistically it was shown that most scars on trilobites were incurred on the posterior right-hand side of the thorax (Babcock 1993).

Using exoskeletons and broken sclerites of trilobites from three sites (Purujosa, Mesones de Isuela, and Minas Tierga) from two formations (Murero Formation and Huérmeda Formation) in the Iberian Chain, NE Spain, evidence of sub-lethal predation and broken sclerites was recorded. Repaired injuries demonstrate unequivocally damage during the life of the animal. The proportion of injured trilobites at each site, and position of repaired injuries on the exoskeletons are analyzed to provide information about causes, selection pressures, and predation intensity. The location of repaired injuries is statistically tested for lateral asymmetry and anteroposterior selection. Breaks on isolated sclerites from these sites and additional specimens from the Mansilla Formation (Cambrian Series 3, Stage 5) and *Bicrescomanducator serratus* breaks from the literature are assessed using a semilandmark morphometric analysis to quantify the variance of abiotic and *B. serratus* breaks.

GEOGRAPHIC AND GEOLOGICAL SETTING

All trilobites were collected from the Iberian Chain (NE Spain), near Zaragoza (Fig. 1A). Specimens from the Murero Formation (Cambrian Series 3, Drumian) were collected at two localities, the first near the village of Mesones de Isuela (Fig. 1C) and the second near Purujosa (Fig. 1D), specifically the Purujosa 3 section (2 km south of Purujosa village, Zaragoza province) inside the limits of the Moncayo Natural Park (Fig. 1D). The trilobite taxon examined for predation traces at this site, *Eccaparadoxides*

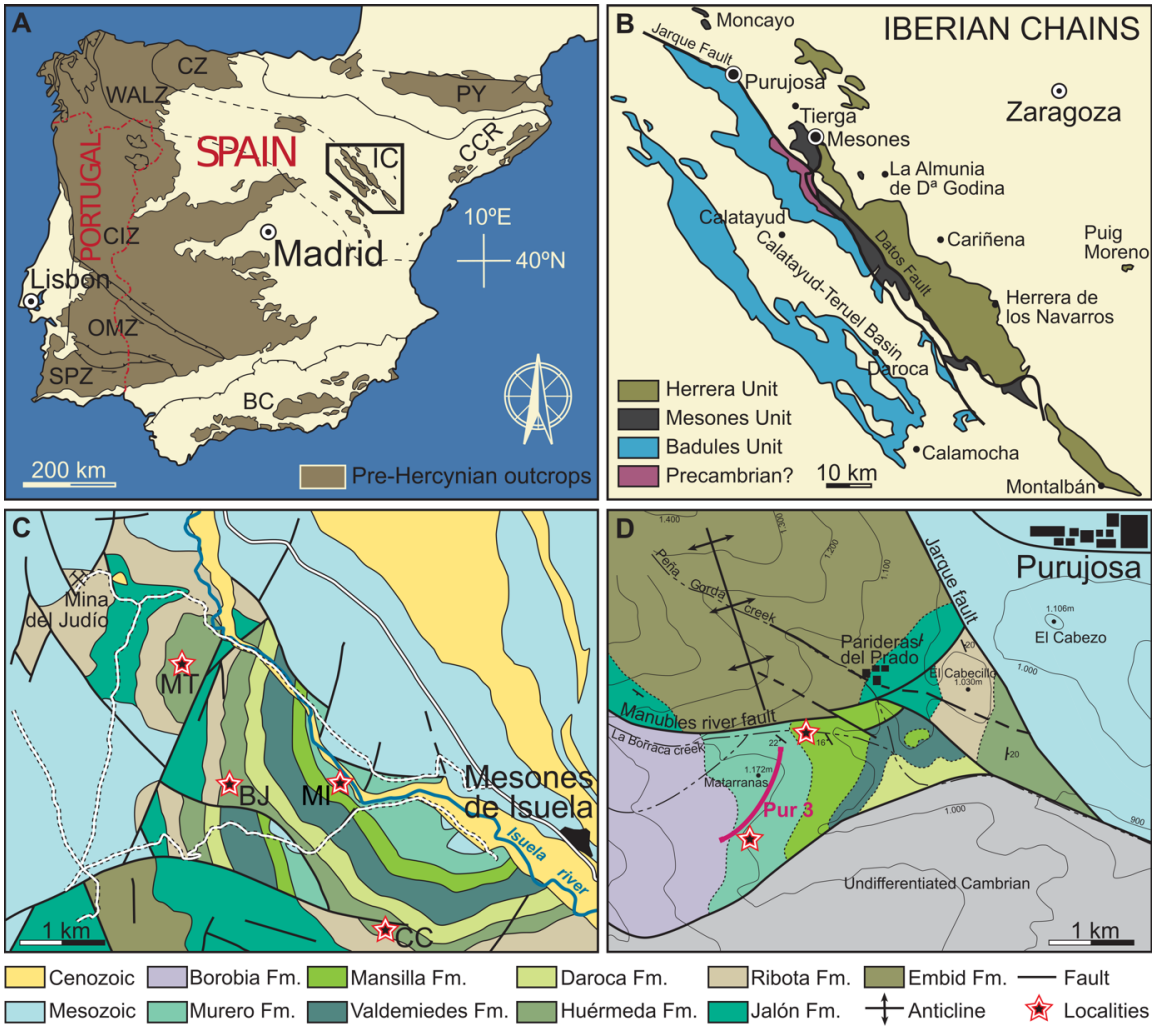

FIG. 1.—Map of study area. **A**) Iberian Chains box shown in B. Abbreviations: IC: Iberian Chains; BC: Betic Cordillera; CCR: Catalan Coastal Ranges; CIZ: Central Iberian Zone; CZ: Cantabrian Zone; OMZ: Ossa-Morena Zone; PY: Pyrenees; SPZ: South Portuguese Zone; WALZ: West Asturian-Leonese Zone. **B**) Box from A with Purujosa, Tierga, and Mesones de Isuela marked. **C**) Stars indicate field sites. MI: Mesones de Iseula; MT: Minas Tierga; BJ: Barranco del Judio; CC: Las Cuevas/ Las Coronadas. **D**) Town of Purujosa with Purujosa 3 series marked; stars indicate field sites in Murero and Mansilla Formations. Key: Units increase in age from left to right, top older than bottom (see Figure 2). (Jalón Formation is older than Ribota Formation, and Embid Formation is older than Jalón Formation.)

pradoanus (Verneuil and Barrande in Prado et al. 1860) is found as abundant broken sclerites, together with ptychopariids in the uppermost red shales of the upper Murero Formation (Fig. 2, star). The Murero Formation at both Mesones de Isuela and Purujosa represents an offshore marine environment (Álvaro and Vennin 1997; Gámez Vintaned et al. 2009). Other biomineralized groups within the faunal assemblage include protorthacean and lingulid brachiopods, sponges, echinoderms, and agnostids (Zamora 2010; Mergl and Zamora 2012). *Eccaparadoxides* is also known from lower levels in the Purujosa 3 section, and both repaired injuries and broken sclerites have been reported (Zamora et al. 2011, fig. 1C). The Mesones de Isuela locality is an outcrop 500 m east of the M3 section (Valenzuela et al. 1990) (Fig. 1C). At the Mesones de Isuela locality, the Murero Formation has been subdivided into two parts: a lower part with green shales alternating with sandy units, and an upper part with red shales. Articulated *E. pradoanus* were collected from upper section of the green shale, just below the appearance of the first sandy unit, alongside numerous isolated broken sclerites of the same taxon (Fig. 2).

The Huérmeda Formation, Cambrian Series 2, Stage 4 (Gozalo et al. 2008) was also deposited in open marine offshore conditions (Gámez Vintaned et al. 2009). It is a monotonous succession of green-gray shales with subsidiary dolostone interbeds (Figs. 1C, 2). Trilobites, mostly redlichiid taxa, are present at the base of the Huérmeda Formation (e.g., Sdzuy 1961; Schmitz 1971; Schmidt-Thomé 1973). Beds consisting of large accumulations of isolated sclerites are found between the beds containing complete trilobites.

MATERIALS AND METHODS

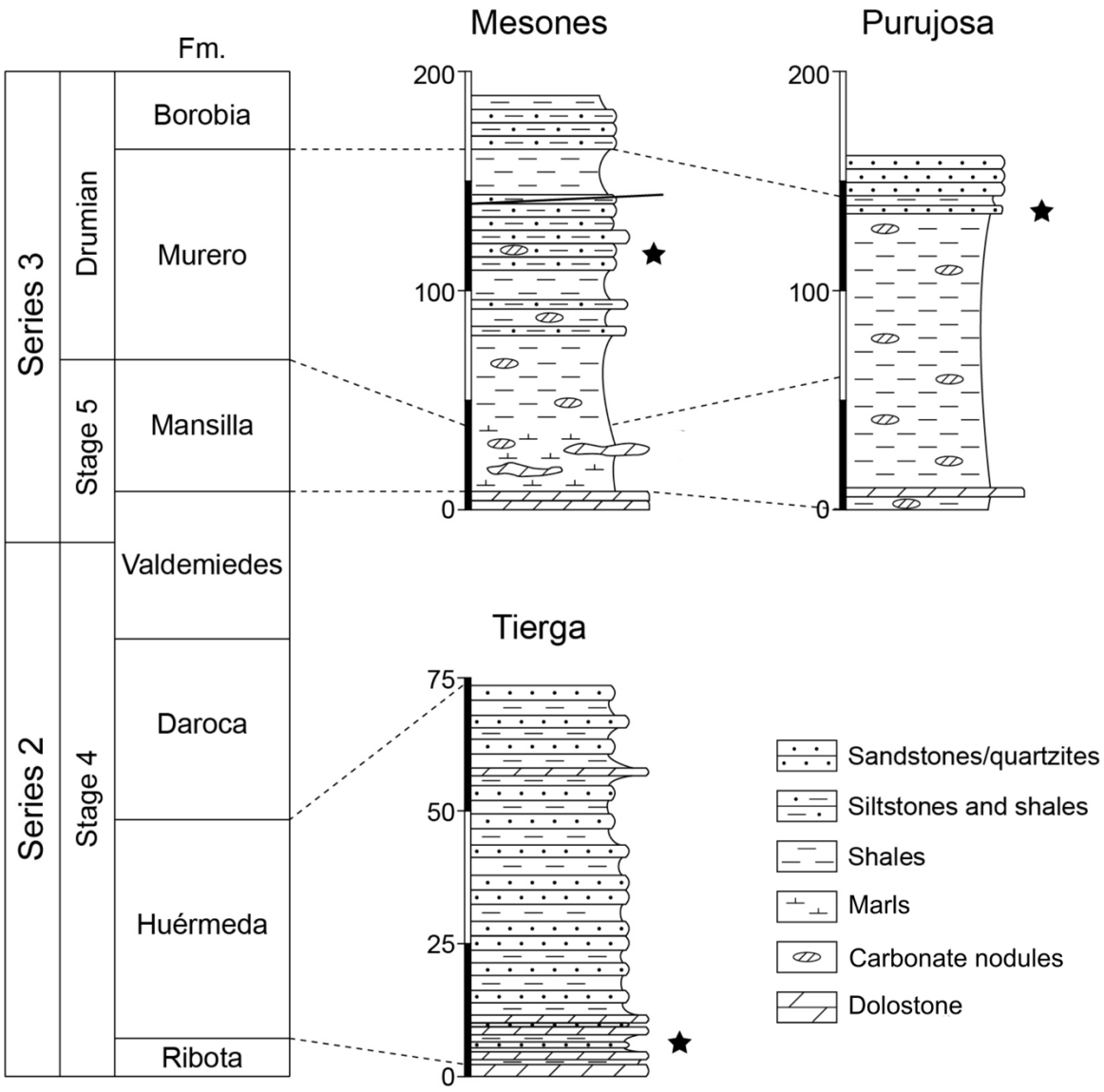

FIG. 2.—Stratigraphy of the studied sections. Unit thicknesses and local lithologies at each of the three field sites are depicted. Stars mark levels where articulated trilobites were collected. Adapted from Gozalo et al. (2008), Gámez Vintaned et al. (2009), and Zamora et al. (2011).

Collection of Trilobites

Bulk samples of trilobites were collected from all sites, and broken trilobite sclerites were collected from the Mansilla Formation (Cambrian Series 3, Stage 5) near Purujosa (Figs. 1C, 2), allowing the analysis of broken sclerites to be extended through the Cambrian Stage 4, Stage 5, and Drumian. Specimens collected from the field, studied and illustrated herein, are housed at the Museo de Ciencias Naturales de la Universidad de Zaragoza (MPZ). Additional specimens, collected from the nearby Barranco del Judio and Las Cuevas/Las Coronadas localities (Fig. 1C) and other levels at the Minas Tierga locality (Fig. 2), were examined from private collections (Online Supplemental File) and the MPZ collections. The data from private specimens were recorded separately from field specimens in case of collection bias in private collections, however as these collectors assisted in the field for this study, collection bias in the private collection is unlikely. Measurements of trilobites and abnormalities were made using digital calipers. Specimens in private collections were measured using photographs and ImageJ.

Measurement Collection and Observations

Specimens with an equal number of thoracic spines visible on each side were used to calculate potential asymmetry in repair location, and only specimens with complete thoraces were used to calculate repair frequencies and multiple repair frequencies. Other incomplete specimens were not used for any analysis. The pygidium and cephalon were not studied for injuries as they were not always preserved. Comparative data on repaired injuries from the Wheeler Formation was obtained from

Babcock (1993). Repaired injuries were identified as shortened spines with recognizable healing, either in the form of rounded edges or partially regrown distal spine tips.

Specimens from the northern part of the Iberian Chains are preserved slightly flattened, but still show some three-dimensional features as fragile regional deformation and carbonate interbeds prevented strong deformation. This is different from specimens from the classic Murero locality, which are more flattened. Other studies on trilobites from the northern Iberian Chains (and the same locality as specimens in this study) have shown three dimensional behaviors, such as enrolment (Esteve et al. 2011, 2013).

Statistics and Calculations for Repaired Injuries

Frequency of Repairs.—Repair frequency was calculated using the following metrics to allow direct comparison between sites:

$$\mathrm{F} = \frac{\text{Number of repairs}}{\text{Number of animals}}$$

$$\mathrm{MF} = \frac{\text{Number of animals with} > 1 \text{ repaired injury}}{\text{Number of animals with 1 repaired injury}}$$

$$\mathrm{R} = \frac{\text{Number of animals with} \geq 1 \text{ repaired injury}}{\text{Number of animals}}$$

Metric F gives an inflated representation of the percentage of individuals damaged and subsequently repaired (Dietl et al. 2000), and metric R gives an underestimated frequency of individuals repaired (Alexander and Dietl 2003). Following

Alexander and Dietl (2003), both are presented to mitigate the limitations of both methods. For the Huérmeda Formation, the repair frequency was calculated using all redlichiid trilobites, and for the Murero Formation the repair frequency was calculated using *Eccaparadoxides pradoanus*. Although repair frequencies for the Wheeler Formation could not be calculated from the literature, a multiple repair frequency value, MF, was derived using data from Babcock (1993, p. 222).

Collecting very large sample sizes of complete or near-complete trilobites is not always possible, and this affects the uncertainty of calculated repair frequencies. We use a Bayesian inference method to estimate the effect of sample size on repair frequencies, calculating 5th and 95th percentile confidence values. This analysis was run in R Studio (R Core Team 2017; see Online Supplemental File for code).

Origin and Location of Repaired Injuries.—Distinguishing between accidental damage, damage due to problems during molting, or predatory damage is a complicated task when considering the cause of repaired injuries. We propose a statistical method to estimate the likelihood of damage having occurred during molting. For trilobites that have thoracic spines of approximately equal length and similar morphology, the likelihood that a given spine is injured due to molting complications is expected be the same as all other spines. This would result in randomly distributed injuries on trilobite exoskeletons, assuming that injuries occurred during the holaspis phase. As segments are added at the posterior of the thorax throughout meraspid stages, individual injuries due to molting could be more common at the anterior than at the posterior, as these segments undergo more molt stages. For species with particularly long, thin, or intricate spines, this expectation changes as such spines are more susceptible to molting damage than others. Accidental injuries from copulation,

interspecific combat, or unsuccessful predatory attacks would be more likely to injure multiple adjacent spines, and so injured spines would not be randomly distributed across the thorax (Babcock 1993). The 'stats' package (R Core Team 2017) in R Studio was employed to conduct a binomial test, comparing the observed number of adjacent injured spines to the expected distribution of randomly arranged injured spines (see Online Supplemental File for code). A random distribution of injured spines would suggest that molting was a major cause, whereas a significant number of short spines adjacent to each other supports a predatory or accidental origin of the injuries.

Repair frequencies at Purujosa and Mesones de Isuela were calculated, as the same species (*Eccaparadoxides pradoanus*) was recovered at both sites and both deposits occurred in similar environments of the same age (Cambrian Series 3, Drumian). Repair frequencies were also calculated on trilobites from Minas Tierga (Cambrian Series 2, Stage 4) as they are morphologically similar to *E. pradoanus*, from a similar environment, and geographically close to Mesones de Isuela.

We tested both lateral and anteroposterior selection of injury location. Lateral asymmetry was tested using a two-tailed binomial test, so that selection for either the left or right could be detected. Our null hypothesis was that there is no lateral asymmetry in injury location, so an equal distribution of injuries on the left and right sides is expected. A rejection of this hypothesis supports the existence of lateral asymmetry in injury location. A two-tailed binomial test facilitates the detection of laterally asymmetric selection for the left and right sides of the thorax. A one-sided binomial, as used in other studies (e.g., Babcock and Robison 1989; Babcock 1993, 2003) allows only detection for either the right side or the left side (which must be determined before the analysis is undertaken).

Anteroposterior selection for the most posterior three thoracic segments of the trilobite was also tested using a two-tailed binomial test. These three thoracic segments have posterior-pointing thoracic spines, and would have covered the anterior of the cephalon during enrolment. The null hypothesis was that there was no selectivity in injury location: the probability of injuring each spine is equal. This gives an expected percentage of 18.75% of injuries occurring on the rear three thoracic segments in a thorax of 16 segments. Rejecting this null hypothesis in favor of the alternative would illustrate selection either for the front 13 or rear three thoracic segments.

Size Distribution and Selection.—To test if the size distribution of trilobites was similar between the three sites and to assess whether size impacted the frequency of repaired injury frequency, a Mann-Whitney U test was undertaken using the 'stats' package in R Studio. The Mann-Whitney U test is a non-parametric test that determines whether the means of two independent samples are equal. In this case, if the mean lengths of injured trilobites are distinguished from the mean lengths of uninjured trilobites using a Mann-Whitney U test, a size preference for attacks can be demonstrated.

Statistics and Calculations for Broken Sclerites

A morphometric analysis was used to quantitatively assess broken sclerites. A semilandmark analysis of sclerites collected from the Murero Formation (Drumian) the Mansilla Formation (Stage 5), the Huérmeda Formation (Stage 4), *B. serratus* from the Rabbitkettle Formation (Pratt 1998), and Middle Darriwilian Valongo Formation (Sá and Gutiérrez-Marco 2015). Semilandmarking was conducted using the Thin-Plate Spline (tps) suite (http://life.bio.sunysb.edu/morph/index.html). A tps file was constructed using tpsUtil64 (v.1.7). The tps file was imported into tspDig2 (v.2.26), which was used

to place the 80 semi-landmarks along the breaks in a counter clockwise direction. As these outlines are not closed curves, a consistent placement of semilandmark direction was needed. These points were used to populate the tps file with the semilandmark data. The tps file was imported into an R environment. The 'geomorph' package (Adams and Otarola-Castillo 2013) was used to conduct the Procrustes Superposition and Principal Components Analysis (PCA) of the superimposed data. The Procrustes Superposition was standardized for size and orientation, and so the analysis was performed solely on the variation of the outline shapes. Note that as these breaks do not have a biologically homologous landmark, no landmarked points were produced.

RESULTS OF ANALYSES ON REPAIRED INJURIES

Description of Repaired Injuries

Injuries at a number of stages of regeneration were recognized in this study (Figs. 3, 4; Zamora et al. 2011, fig. 4). These injuries healed over multiple molt stages: after callousing and initial repair (Fig. 3A, 3E) the end of the spine became rounded (Fig. 3B, 3F). This stage was followed by a thin growth with a pointed end during the subsequent molt(s) (Fig. 3C, 3G; Zamora et al. 2011, fig. 4D, 4E). Complete, but comparably shorter spines arose in the following molts (Fig. 3D, 3H; Zamora et al. 2011, fig. 4A–4C, 4F–4K). In one case (Fig. 4) multiple spines grew from an injured area.

Frequency of Repairs

In the Murero Formation, a record of predation is only reported from the Purujosa locality (Table 1). No evidence for sublethal predation is reported from

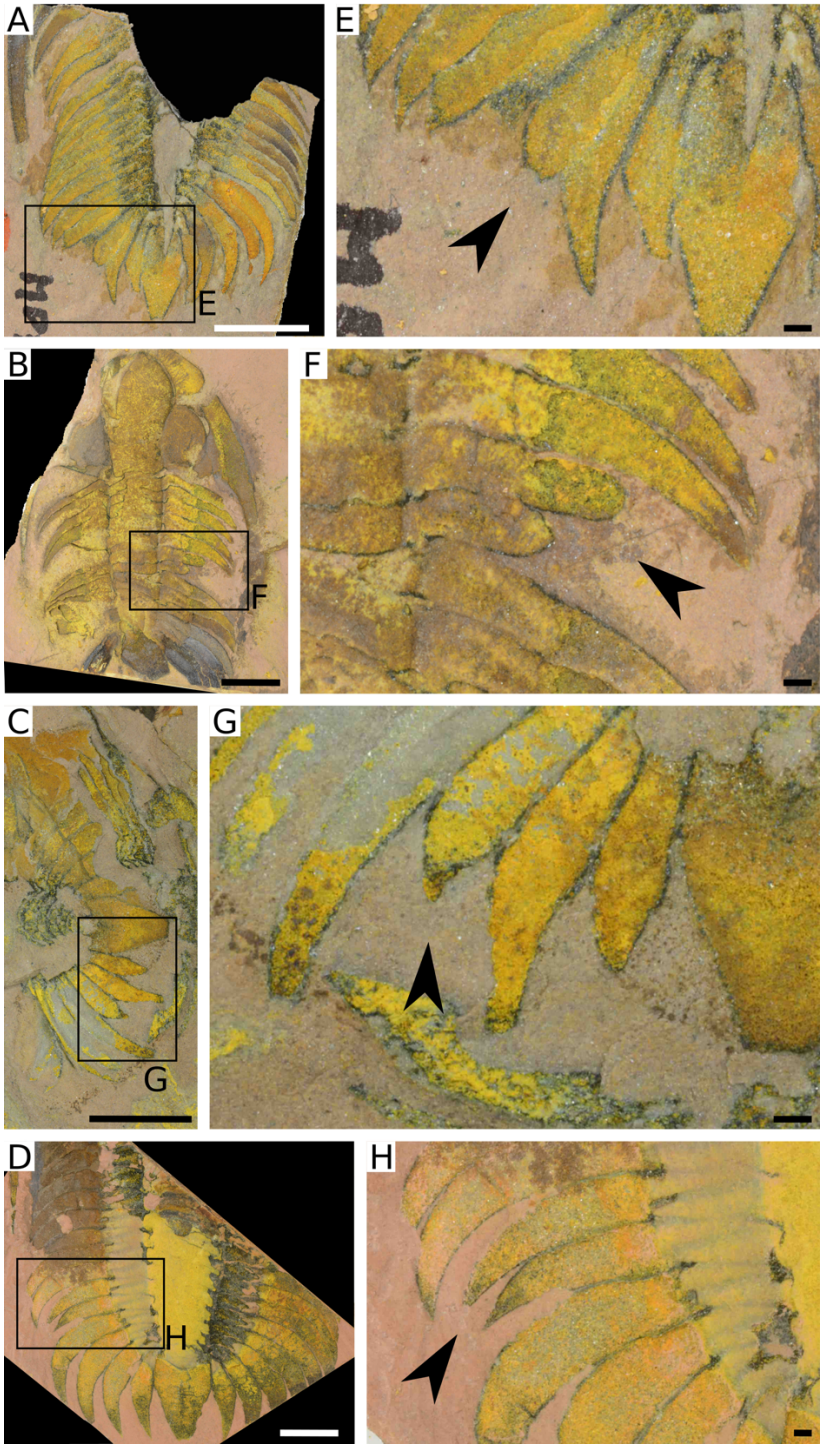

FIG. 3.—*Eccaparadoxides pradoanus* (Verneuil and Barrande in Prado et al. 1860) from the Purujosa Red Beds, Murero Formation (Cambrian Series 3, Drumian), Iberian Chains, Spain, at a number of stages of repair. **A**) MPZ 2011/6: nearly complete thorax with crescent shaped recent injury on a thoracic spine. **B**) MPZ 2012/844: slightly disarticulated specimen with two shortened thoracic spines. **C**) MPZ 2012/1009: rear of a thorax showing thoracic spine with slight regrowth of the tip. **D**) MPZ 2012/7808: near complete thorax with two shortened thoracic spines. **E**) Box from A, arrow indicates injured spine. **F**) Box from B, arrow indicates shortened spines. **G**) Box from C, arrow indicates spine beginning regrowth. **H**) Box from D, arrow indicates two nearly fully repaired spines. Scale bars: **A**–**D**) 10 mm, **E**–**H**) 1 mm.

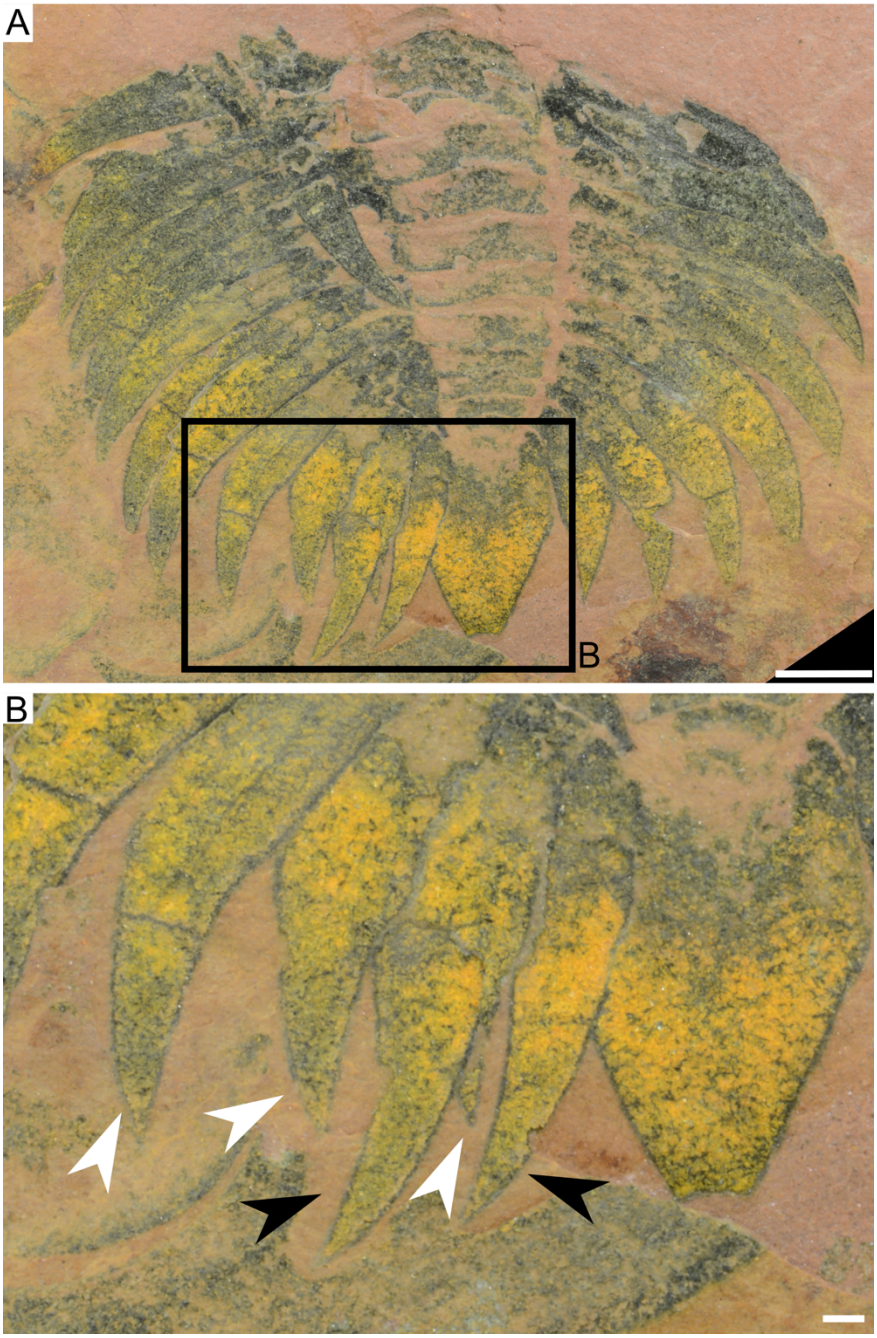

FIG. 4.—*Eccaparadoxides pradoanus* (Verneuil and Barrande in Prado et al. 1860) nearly complete thorax from the Purujosa Red Beds, Murero Formation (Cambrian Series 3, Drumian), Iberian Chains, Spain, with additional spines growing from a previously injured area. **A**) MPZ 2017/1088, scale bar = 5 mm. **B**) Box from A, white arrows indicate spines fully repaired, black arrows indicate additional spines grown from previously injured area, scale bar = 1 mm.

Table 1. Frequency of repairs in Cambrian trilobites.

Formation/ Site	Age	# trilobites	# injured trilobites	# injuries	F	R	MF	F 5th Percentile	F 95th Percentile	R 5th Percentile	R 95th Percentile
Huérmeda Formation	Stage 4	45	0	0	0	0	0	0.00	0.06	0.00	0.06
Murero Formation	Drumian	97	10	12	0.11	0.09	0.20	0.08	0.19	0.06	0.17
Wheeler Formation	Drumian	N/A	27	28	N/A	N/A	0.04	N/A	N/A	N/A	N/A
Minas Tierga (Huérmeda Fm)	Stage 4	30	0	0	0	0	0	0.00	0.09	0.00	0.09
Barranco del Judio (Huérmeda Fm)	Stage 4	1	0	0	0	0	0	0.02	0.78	0.02	0.78
Private collection, (Huérmeda Formation)	Stage 4	14	0	0	0	0	0	0.00	0.18	0.00	0.18
Mesones de Isuela (Murero Fm)	Drumian	23	0	0	0	0	0	0.00	0.12	0.00	0.12
Purujosa Red Beds (Murero Fm)	Drumian	69	9	10	0.14	0.13	0.11	0.09	0.23	0.08	0.21
Purujosa (other levels, from MPZ) (Murero Fm)	Drumian	5	1	2	0.4	0.2	1	0.15	0.73	0.06	0.58

Formation and locality information for trilobite repair frequencies and Bayesian Inference 5th and 95th percentile values. F and R are repair frequency metrics and MF is the multiple repair frequency metric (defined in methods). Wheeler Formation data from Babcock (1993).

Mesones de Isuela (Murero Formation), from any locality, or private collection of material from the Huérmeda Formation. The 5th and 95th confidence intervals suggest that even though different population sizes were considered, the repair frequencies (both R and F) are significantly different (Table 1). The multiple repair frequency in the Murero Formation (0.22) is an order of magnitude higher than the Wheeler Formation (0.04) (Table 1).

Origin and Location of Injuries

Injured spines are not randomly distributed on trilobite exoskeletons, instead they are found adjacent to each other (Binomial text, n = 15, p-value < 0.001, Table 2). Injuries on *E. pradoanus* are found at Purujosa (F = 0.14, R = 0.13) but not Mesones de Isuela (F = 0, R = 0) (Table 1).

Spines are not significantly more likely to be injured on the left or right sides (two-tailed binomial test, n = 16, p-value = 1) and spines on the rear three thoracic segments were more likely to be injured than other segments (two-tailed binomial test, n = 10, p-value = 0.0045) (Table 3).

Size Distribution and Selection in the Murero Formation

No significant size selection was detected between the injured trilobite sample (mean = 38.98 mm, median = 32.83 mm, sd = 21.81 mm) and the non-injured sample (mean = 32.14 mm, median = 30.91 mm, sd = 13.31 mm) at Purujosa (Mann Whitney U test, W = 224, p = 0.46). This suggests that predators in the Murero Formation did not target smaller or larger trilobites at Purujosa. The size distributions of trilobites collected from the field at Purujosa, Mesones, and Minas Tierga cannot be distinguished according to Mann-Whitney U tests (thoracic means: Purujosa, 33.02 mm, Mesones,

Table 2. Adjacent injuries in complete trilobite thoraxes from Purujosa Red Beds.

Number of short/injured spines	Total number of spines (assuming 32 per animal)	Number of expected injuries adjacent to another injury	Number of injured spines adjacent to injured spines	p-value
15	2208	0.013	10	2.2×10^{-16}

P-values calculated using a binomial test with 10 successes from 14 attempts. The random probability of a success (a short spine adjacent to another short spine) is 2/2207 (2 available adjacent spines, with 2207 available spines in total).

Table 3. Location of injuries and size analysis for trilobites from Purujosa locality.

Measured location of injuries		Expected location of injuries		Measured location of injuries		Expected location of injuries		2-tailed binomial p-value	
Anterior 13 thoracic segments	Posterior 3 thoracic segments	Anterior 13 thoracic segments	Posterior 3 thoracic segments	Left side of thorax	Right side of thorax	Left side of thorax	Right side of thorax	Posterior 3 thoracic segments	Left/Right side of thorax
4	6	7.3	1.7	8	8	7.5	7.5	0.0045	1

Expected values calculated using a binomial analysis. Measured values are from observations. P-values calculated as described in methods.

32.42 mm, Minas Tierga, 41.45 mm; Mann Whitney U tests: Purujosa and Mesones, W = 816.5, p = 0.86; Purujosa and Minas Tierga, W = 786, p = 0.058; Mesones and Minas Tierga, W = 439, p = 0.094; lengths of specimens plotted in Online Supplemental File), suggesting that size differences are not the cause of differences in calculated repair frequencies.

RESULTS OF ANALYSES ON BROKEN SCLERITES

A biotic origin for trace fossils can be inferred if they have a distinct geometric shape, a narrow size range, and/or a non-random distribution of traces across taxa, size of prey, or location on the skeletons (Kowalewski 2002). Some broken sclerites found here are putatively of biotic origin (Figs. 5A, 6 [white arrows], 7), some abiotic (Figs. 5C, 6 [black arrows]), and some breaks are of indeterminate origin (Fig. 5B). Semilandmark analyses describe the shape variation of the broken sclerites very effectively, as the two illustrated Principal Components explain 46.3% of the shape variation (Fig. 8). PC1 shows a change from a deep to shallow break, and PC2 shows a change from a break indented on the left side to one on the right side. Fossils that are referred to *Bicrescomanducator serratus* do not have a restricted shape variation in the Principal Coordinate (PC) space: there is a large spread of *B. serratus* specimens (red squares) across both PC1 and PC2 (Fig. 8). As specimens assigned to *B. serratus* overlap in morphospace with previously described *B. serratus* specimens (Fig. 9, red shapes: compare the points with black dots to those without), the assignment of *B. serratus* is acceptable. However, the new specimens also overlap with putative abiotic shapes (Fig.

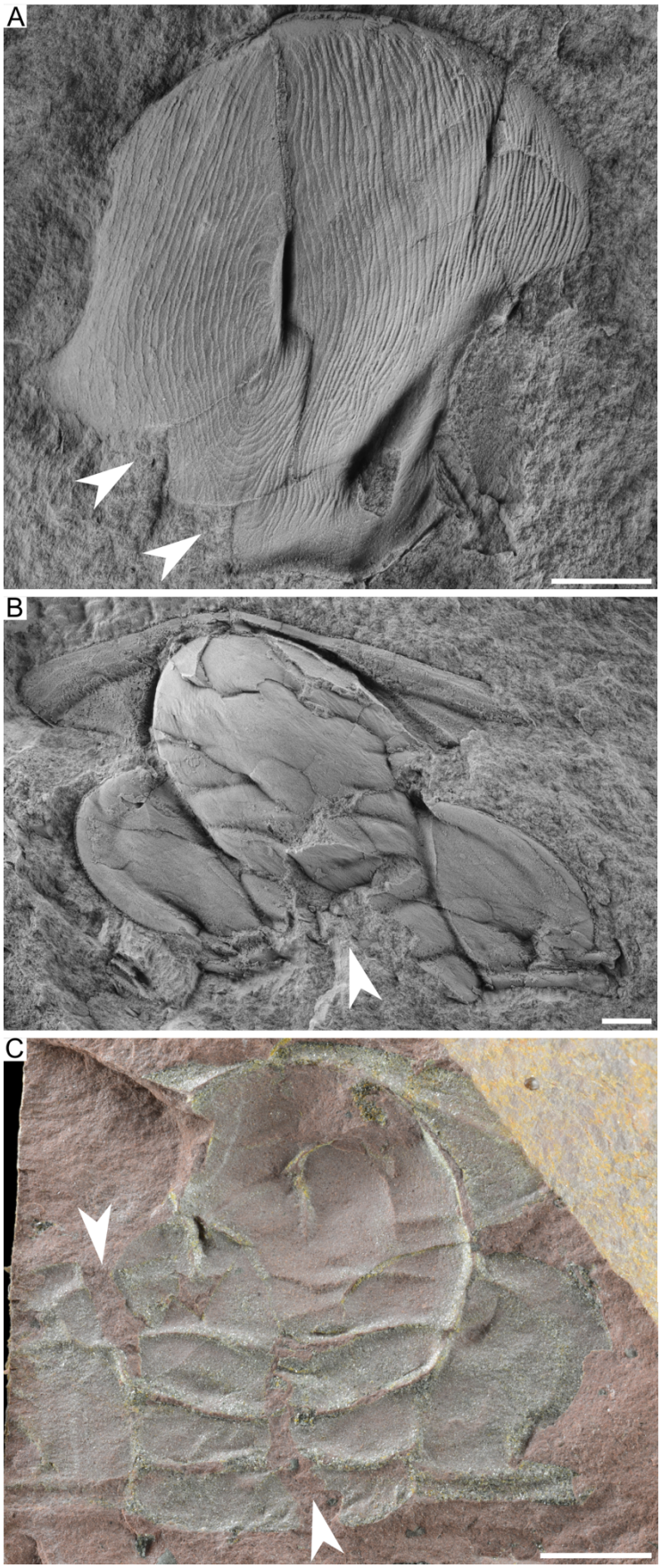

FIG. 5.—Broken sclerites of *Eccaparadoxides pradoanus* (Verneuil and Barrande in Prado et al. 1860) from the Purujosa Red Beds and near Mesones de Isuela, Murero Formation (Cambrian Series 3, Drumian), Iberian Chains, Spain. **A**) MPZ 2017/398: hypostome with *Bicrescomanducator serratus* (Zamora et al. 2011) trace. **B**) MPZ 2017/398 curved break on posterior of cranidium. **C**) MPZ 2017/358 abiotic fracture at rear of cranidium. Arrows point to breaks. Scale bars = 5 mm.

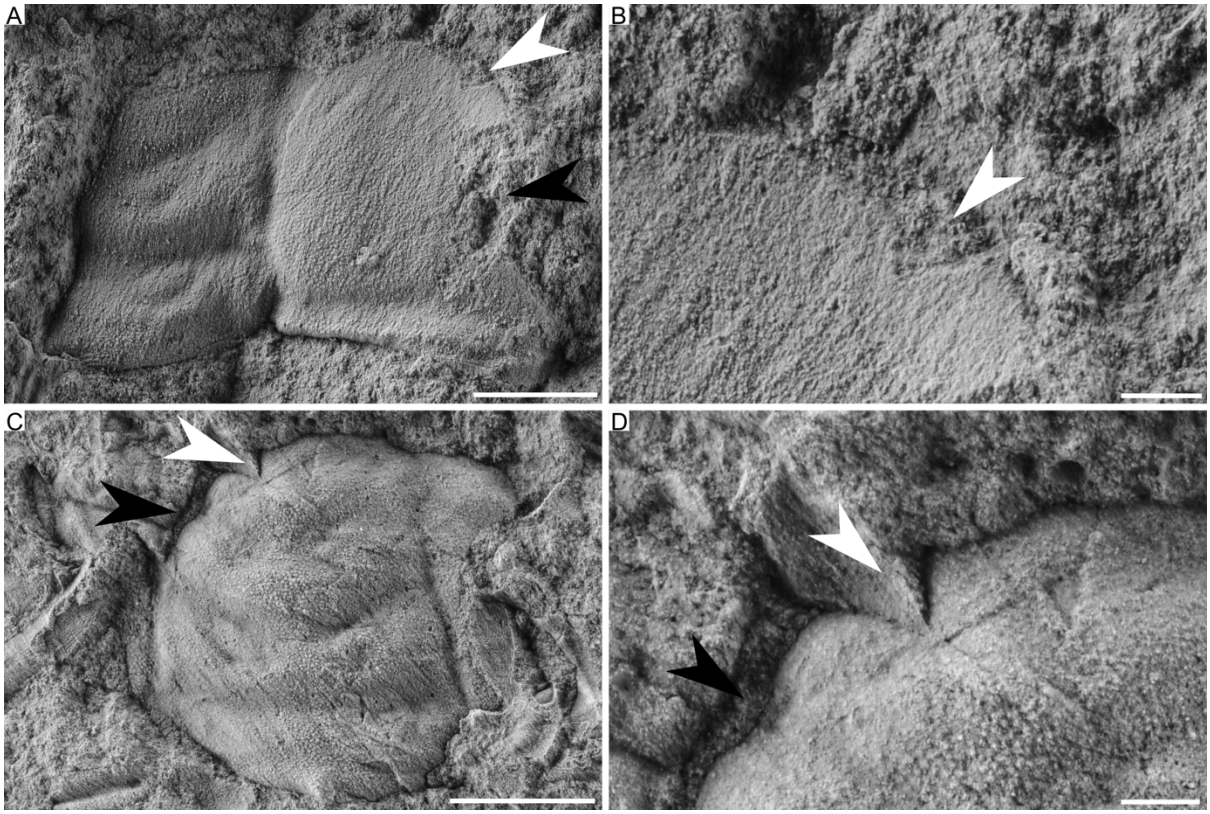

FIG. 6.—Broken sclerites of redlichiid trilobites with *Bicrescomanducator* serratus (Zamora et al. 2011) traces and abiotic breaks from the Huérmeda Formation near Minas Tierga (Cambrian Series 2, Stage 4), Iberian Chains, Spain. **A**) MPZ 2017/338: partial cranidium showing biotic (white arrow) and abiotic (black arrow) breaks. **B**) Close up of biotic break in A. **C)** MPZ 2017/349: partial cranidium showing biotic and abiotic breaks. **D**) Close up of C. *B. serratus* indicated by white arrow, abiotic break indicated by black arrow. Scale bars: A, C = 5 mm; B, D = 1 mm.

FIG. 7.—Broken sclerites with *Bicrescomanducator serratus* (Zamora et al. 2011) traces from the Mansilla Formation near Purujosa (Cambrian Series 3, Stage 5), Iberian Chains, Spain. **A**) MPZ 2017/427: cranidium. **B**) MPZ 2017/431: fragmentary trilobite sclerite. **C**) MPZ 2017/428: cranidium. **D**) MPZ 2017/430: fragmentary trilobite sclerite, *B. serratus* indicated by white arrows. Scale bars = 5 mm.

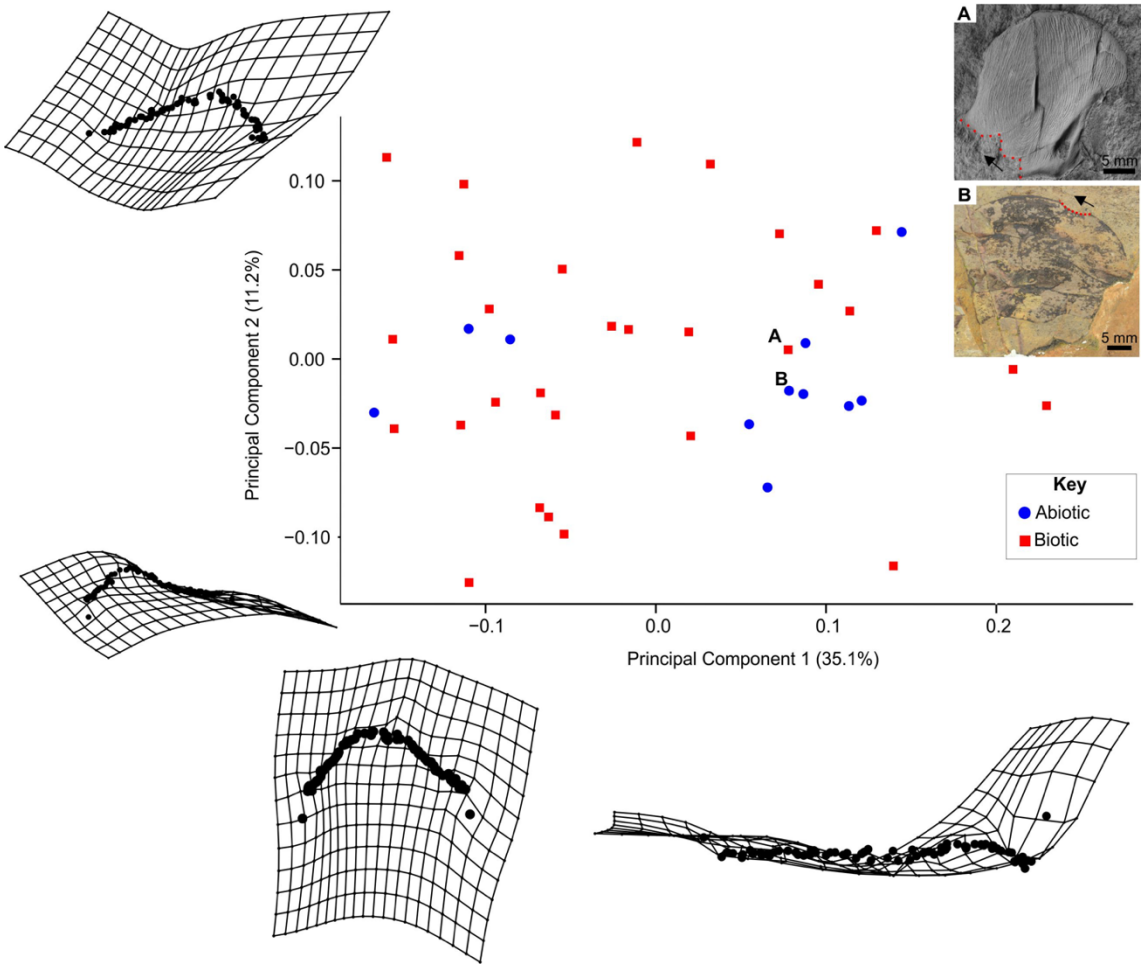

FIG 8.—Principal Component Analysis of *Bicrescomanducator serratus* (Zamora et al. 2011) and abiotic breaks. Outline of the shapes of the breaks semilandmarked, as shown by dotted red line in A and B. Black arrows indicate the direction of semilandmark placement. Scale bars = 5 mm.

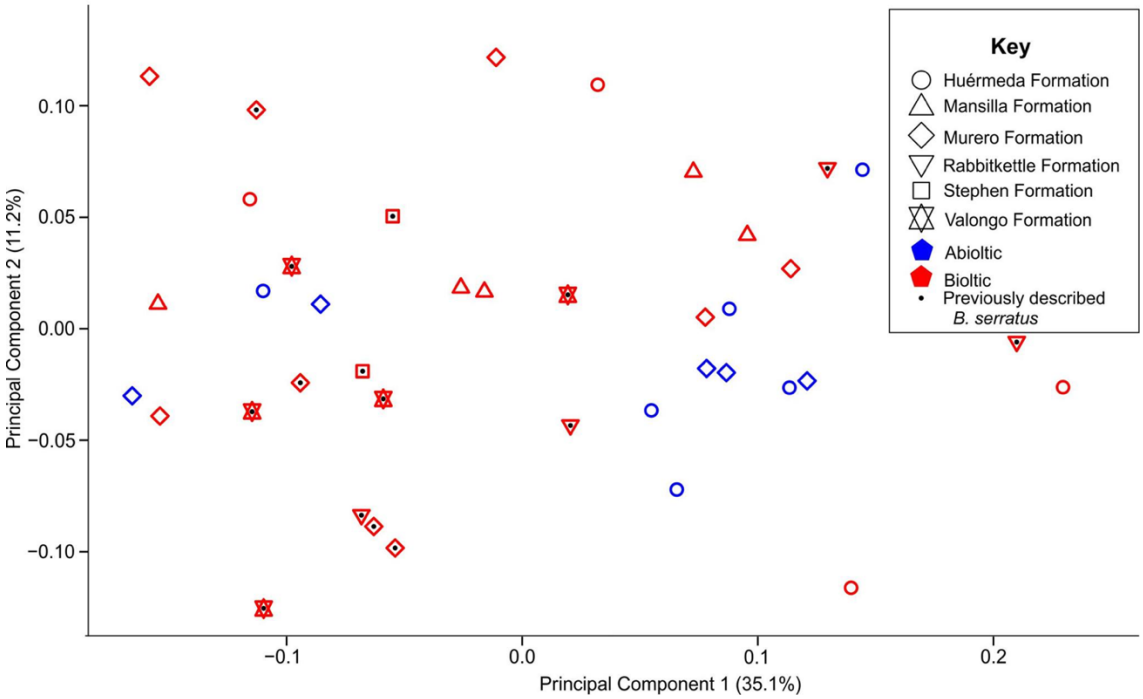

FIG. 9.—Principal Component Analysis plot of the semilandmarked breaks (same as Fig. 8), separating specimens by formation and by origin of the breaks. The overlap of previously described examples of *Bicrescomanducator serratus* (Zamora et al. 2011) (points with black dots) with new examples (points without black dots), shows the positive assignment of new material to the ichnotaxon. Key: circles = Huérmeda Formation (Spain, Cambrian Stage 4); triangles with point upwards: Mansilla Formation (Spain, Cambrian Stage 5); diamonds: Murero Formation (Spain, Cambrian Drumian); triangles with point downwards: Rabbitkettle Formation (Canada, Cambrian Drumian); squares: Stephen Formation (Canada, Cambrian, Stage 5); stars: Valongo Formation (Portugal, Ordovician Darriwilian); blue: abiotic; red: biotic.

9, blue shapes) and so a biotic origin of the new specimens cannot unambiguously be assigned.

DISCUSSION

Repaired Injuries

Complete Repair of Trilobite Injuries?—Trilobite injuries at a number of stages of repair are reported in this study (Figs. 3, 4). Trilobites are thought to have had indeterminate growth, and so continued to molt after reaching adult morphology (Daley and Drage 2016). Therefore, it is likely that given enough time, a trilobite with an injury would heal completely, removing all evidence that an injury occurred. Each molt stage is a stage of healing (Fig. 10A–10D) and after a number of molts, dependent on the location and severity of the injury, all evidence of the injury would be removed (Fig. 10E). This has a direct implication for the comparison of repair frequencies of trilobites (and other ecdysozoans) with other groups which do not molt. The calculated repair frequency for ecdysozoans is likely an underestimate of the true frequency of injuries in the population. Larger injuries, which would require more molt stages to heal, therefore have a greater impact on the repair frequency than small injuries which would heal more quickly.

Origin of Injuries.—The low statistical likelihood of adjacent spines being injured by chance illustrates that injuries on *Eccaparadoxides pradoanus* likely result from predatory attacks, rather than from accidents and/or problematic molting (Table 2). This is corroborated by the lower frequency of injuries on *E. pradoanus* from Mesones: if injuries were the result of molting problems or another consistent behavior of the

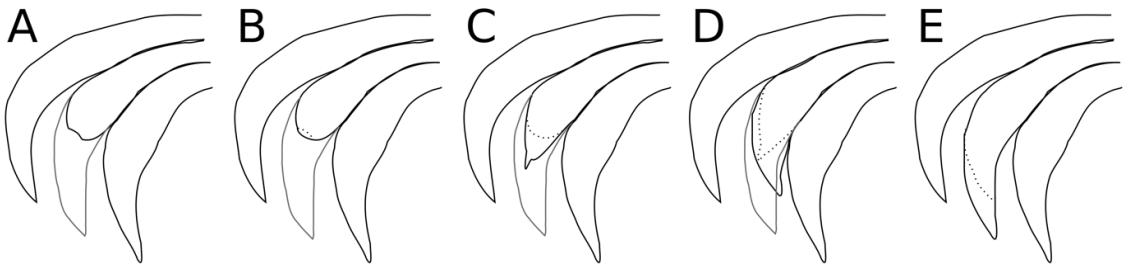

FIG 10.—Idealized repair sequence of trilobite pleural spines, based on Figure 3. Gray lines show uninjured shape of middle spine, dotted black line shows previous stage of healing. Healing stages: **A**) Immediately after injury. **B**) Rounded spine after initial healing. **C**) Regrowth begins, with thin tip of pleural spine. **D**) Short spine. **E**) Healing complete, spine same length as uninjured spines.

trilobites, the injury value would not vary markedly between sites. As the 95th percentile repair frequency value at Mesones is lower than the measured repair frequency at Purujosa, the smaller sample size at Mesones does not account for the difference in injury frequency between these two sites. Consequently, when using the frequency of repaired trilobite injuries as a proxy for predation on *E. pradoanus*, the 'noise' from non-predatory damage is likely to be minimal. This may not be the case for all trilobite injuries. Indeed Šnajdr (1978) considered molting damage the most significant cause of injury in Bohemian paradoxidids.

Comparison between Sites.—A difference in repair frequency between two sites of the same age, environment, and species of trilobite suggests a difference in predator pressure at those two sites. This may not follow when the energy of the depositional environment is significantly different (as this may affect the likelihood of accidental injuries), or where the sizes of trilobites vary significantly (as predators may preferentially attack smaller or larger animals). At all three field sites, complete trilobites have similar body plans with similar sized pleural spines on relatively large thoraces. Furthermore both the Huérmeda and Murero Formations are considered to represent offshore environmental conditions, sporadically affected by storms. These similarities facilitate comparison between all three sites.

The repair frequency metrics (R, F, and MF) in the Huérmeda Formation (Cambrian Stage 4) are lower than the Murero Formation (Drumian); however trilobites at neither Minas Tierga (Huérmeda Formation) or Mesones de Isuela (Murero Formation) show evidence for repaired injuries. These two sites are geographically closer to each other than to Purujosa, where there is evidence for repaired injuries in the Drumian (see Figs. 1, 2; Table 1) and from other levels of the Purujosa 3 section

(Table 1; Zamora et al. 2011). This suggests a geographic rather than temporal cause for the difference in predation, although the absolute distances between these sites in the Cambrian would have been different than at present as the Iberian Chains have been subjected to substantial tectonic activity. A lack of injured individuals suggests that either predation intensity on the trilobites studied was very low, or that predators were 100% efficient (Schoener 1979; Alexander 1981). Three lines of evidence support an interpretation of low predation intensity in this case: failure by predators is common; trilobites could repair even extensive damage; and trilobites of the same species at a different site show repaired injuries (Vermeij 1982; McNamara and Tuura 2011; Schoenemann et al. 2017).

Selectivity in Repaired Damage Location.—*Eccaparadoxides pradoanus* likely enrolled as a defensive measure (Esteve et al. 2013). During enrolment, the posterior part of the thorax was located over the cephalon, an area where damage would have been more likely to be fatal (Babcock 1993). The high occurrence of damage to the posterior three segments may be the result of damage incurred during defensive enrolment. Alternatively, posterior injuries may indicate that predators attacked from the rear (Babcock 1993). The lack of anterior injuries supports the observation that posterior injuries are less lethal than anterior attacks (Babcock 1993), especially as the anterior segments were created before the posterior, although the small sample size and p-value (0.0045), means this result is only tentative.

Comparison between the Wheeler Formation and the Murero Formation.—There is a higher multiple repair frequency in the Murero than the Wheeler Formation (Table 1). Assuming that the data collected are directly comparable, this indicates that injured

specimens from the Murero Formation were more likely to be attacked a second time than those recovered from the Wheeler Formation.

The data from the Murero Formation show no lateral asymmetry of injuries on Cambrian trilobites, differing from the results of previous studies where site selectivity was reported for the right side of the body (Babcock and Robison 1989; Babcock 1993, 2003), specifically in the Wheeler Formation (Babcock 1993). Differences between the Wheeler and Murero Formations including environment, paleolatitude, and taxa studied, are factors that may impact on the differences observed for site selectivity of injuries and multiple repair frequency. More studies of trilobites using large datasets and similar taxa are needed to understand variation in repair frequencies and injury location selectivity.

Broken Sclerites

It is often not possible to distinguish between predation and scavenging (e.g., Babcock 1993). Similar complications occur when differentiating between abiotic and biotic breakages, as fragmentation of shapes can arise from abiotic and biotic factors (Kowalewski 2002; Webster et al. 2008). While taphonomic alteration of cuticle is thought to be uncommon, trilobite cephala often fractured sagittally along the axis of highest vertical relief (Pratt 1998; Webster and Hughes 1999; Fig. 5C). Both biotic and abiotic damage to sclerites are presented and described morphometrically here.

V- and W-shaped traces on broken sclerites from the Huérmeda, Mansilla and Murero Formations fit the current definition of *Bicrescomanducator serratus* and overlap in PC space, but show a wide variety of shapes, sizes, and angles. The large morphological variation in *B. serratus* is problematic because the semilandmark analyses did not clearly distinguish between abiotic and biotic damage, suggesting that

the species definition requires refining and that caution must be applied when assigning biotic origin. Circumstantial evidence, such as co-occurring predators or repaired predatory damage, could be used to strengthen future assignments. If a biotic origin is confirmed, breaks from the Huérmeda Formation would be the oldest known representatives of *B. serratus*.

CONCLUSIONS

Based on the relative frequencies of damage in trilobites from multiple localities, repaired injuries on *Eccaparadoxides pradoanus* appear to be predatory in nature. Variation in repair frequencies between the Murero, Huérmeda, and Wheeler Formations show that predation intensity can vary even on the same species of trilobite at different sites, and between different trilobite species worldwide. Evidence for predation is present at numerous levels at Purujosa, but absent in localities of the same age that are geographically more distant, suggesting that geography may be one factor affecting predation pressure. This does not mean that predation is absent at Minas Tierga or Mesones de Isuela. The location of injuries on trilobites from Purujosa showed no significant lateral asymmetry, differing from previous reports on Cambrian trilobites (Babcock and Robison 1989; Babcock 1993, 2003). The posterior three thoracic segments were targeted more often than expected from random attacks, perhaps due to *E. pradoanus* enrolling as a defensive measure.

A novel approach was employed using morphometric analyses to assess and compare the shape of unrepaired damage on trilobite sclerites. While the shape variation of serrated breaks on isolated sclerites was well described using this

technique, *Bicrescomanducator serratus* traces could not be distinguished from abiotically broken sclerites, suggesting that a revision to the definition of this trace fossil taxon is needed.

ACKNOWLEDGMENTS

We thank the Coeditor Thomas Olszewski, Associate Editor Brian Pratt, and the two reviewers Oldřich Fatka and Alan Owen, for their thoughtful comments and editorial notes that greatly improved the manuscript. We also thank Brian Pratt and Artur Sá for providing images of *Bicrescomanducator serratus* from previous studies. We appreciate the invaluable help of Fernando Gracia and Jesus García (Zaragoza, Spain) who assisted in the field; Supratik Paul for discussions of statistics; and Luis Buatois, Gabriela Mangano, and Mark Wilson for discussions of inchotaxonomy. SP was funded by a Santander Travel Award and Oxford-St Catherine's Brade-Natural Motion Scholarship; RDCB was funded by an Australian Postgraduate Award; and SZ was funded by a Ramón y Cajal Grant (RYC-2012-10576) and project CGL2013-48877-P from the Spanish Ministry of Economy and Competitiveness.

SUPPLEMENTAL MATERIAL

Data are available from the PALAIOS Data Archive:

http://www.sepm.org/pages.aspx?pageid=332.

REFERENCES

ABERHAN, M., KIESSLING, W., AND FÜRSICH, F.T., 2006, Testing the role of biological interactions in the evolution of mid-Mesozoic marine benthic ecosystems: Paleobiology, v. 32, p. 259–277.

ADAMS, D.C. AND E. OTAROLA-CASTILLO, 2013, Geomorph: an R package for the collection and analysis of geometric morphometric shape data: Methods in Ecology and Evolution, v. 4, p. 393–399.

ALEXANDER, R.R., 1981, Predation scars preserved in Chesterian brachiopods: probable culprits and evolutionary consequences for the articulates: Journal of Paleontology, v. 55, p. 192–203.

ALEXANDER, R.R., 1986, Resistance to and repair of shell breakage induced by durophages in Late Ordovician brachiopods: Journal of Paleontology, v. 60, p. 273–285.

ALEXANDER, R.R. AND DIETL, G.P., 2001, Latitudinal trends in naticid predation on *Anadara ovalis* (Bruguiere, 1789) and *Divalinga quadrisulcata* (Orbigny, 1842) from New Jersey to the Florida Keys: American Malacological Bulletin, v. 16, p. 179–194.

ALEXANDER, R.R. AND DIETL, G.P., 2003, The fossil record of shell-breaking predation on marine bivalves and gastropods, *in* P. Kelly, M. Kowalewski, and T.A. Hansen (eds.), Predator-Prey Interactions in the Fossil Record: Kluwer Academic, New York, p. 141–176.

ÁLVARO, J.J. AND VENNIN, E., 1997, Episodic development of Cambrian eocrinoid-sponge meadows in the Iberian Chains (NE Spain): Facies, v. 37, p. 49–63.

ANDREW, C., HOWE, P., PAUL, C.R.C., AND DONOVAN, S.K., 2010, Fatally bitten ammonites from the lower Lias Group (Lower Jurassic) of Lyme Regis, Dorset: Proceedings of the Yorkshire Geological Society, v. 58, p. 81–94.

BABCOCK, L.E., 1993, Trilobite malformations and the fossil record of behavioral asymmetry: Journal of Paleontology, v. 67, p. 217–229.

BABCOCK, L.E., 2003, Trilobites in Paleozoic predator-prey systems, and their role in reorganization of early Paleozoic ecosystems, *in* P. Kelly, M. Kowalewski, and T.A. Hansen (eds.), Predator-Prey Interactions in the Fossil Record: Kluwer Academic, New York, p. 55–92.

BABCOCK, L.E. AND ROBISON, R.A., 1989, Preferences of Palaeozoic predators: Nature, v. 337, p. 695–696.

BAUMILLER, T.K. AND GAHN, F.J., 2012, Reconstructing predation pressure on crinoids: estimating arm-loss rates from regenerating arms: Paleobiology, v. 39, p. 40–51.

BERGSTRÖM, J. AND LEVI-SETTI, R., 1978, Phenotypic variation in the middle Cambrian trilobite *Paradoxides davidis*: Geologica et Palaeontologica, v. 12, p. 1–40.

BICKNELL, R.D.C AND PATERSON J.R., 2017, Reappraising the early evidence of durophagy and drilling predation in the fossil record: implications for escalation and the Cambrian Explosion: Biological Reviews, Online early view. doi: 10.1111/brv.12365.

BRETT, C.E. AND WALKER, S.E., 2002, Predators and predation in Paleozoic marine environments: Paleontological Society Papers, v. 8, p. 93–118.

BRUTON, D.L., 1981, The arthropod *Sidneyia inexpectans*, middle Cambrian, Burgess Shale, British Columbia: Philosophical Transactions of the Royal Society of London, Series B, Biological Sciences, v. 296, p. 619–653.

BUATOIS, L.A., WISSHAK, M., WILSON, M.A. AND MÁNGANO, M.G., 2017, Categories of architectural designs in trace fossils: a measure of ichnodisparity: Earth-Science Reviews, v. 164, p. 102–181.

CONWAY MORRIS, S., 1977, Fossil priapulid worms: Special Papers in Palaeontology, v. 20, p. 1–155.

CONWAY MORRIS, S. AND BENGTSON, S., 1994, Cambrian predators: possible evidence from boreholes: Journal of Paleontology, v. 68, p. 1–23.

CONWAY MORRIS, S. AND JENKINS, R., 1985, Healed injuries in early Cambrian trilobites from South Australia: Alcheringa, v. 9, p. 167–177.

CONWAY MORRIS, S. and ROBISON, R.A., 1988, More soft-bodied animals and algae from the middle Cambrian of Utah and British Columbia: University of Kansas Paleontological Contributions, v. 122, p. 1–48.

DALEY, A.C., AND DRAGE, H.B., 2016, The fossil record of ecdysis, and trends in the moulting behavior of trilobites: Arthropod Structure and Development, v. 45, p. 71–96.

DALEY, A.C., PATERSON, J.R., EDGECOMBE, G.D., GARCIA-BELLIDO, D. C. AND JAGO, J. B., 2013, New anatomical information on *Anomalocaris* from the Cambrian Emu Bay Shale of South Australia and a reassessment of its inferred predatory habits: Palaeontology, v. 56, p. 971–990.

DIETL, G.P., 2003a, Interaction strength between a predator and dangerous prey: *Sinistrofulgur* predation on *Mercenaria*: Journal of Experimental Marine Biology and Ecology, v. 289, p. 287–301.

DIETL, G.P., 2003b, Coevolution of a marine gastropod predator and its dangerous bivalve prey: Biological Journal of the Linnean Society, v. 80, p. 409–436.

DIETL, G.P., ALEXANDER, R.R. AND BIEN, W.F., 2000, Escalation in Late Cretaceous–early Paleocene oysters (Gryphaeidae) from the Atlantic Coastal Plain: Paleobiology, v. 26, p. 215–237.

DIETL, G.P. AND HENDRICKS, J.R., 2006, Crab scars reveal survival advantage of left-handed snails: Biology Letters, v. 2, p. 439–442.

ENGLISH, A.M. AND BABCOCK, L.E., 2010, Census of the Indian Springs Lagerstätte, Poleta Formation (Cambrian), western Nevada, USA: Palaeogeography, Palaeoclimatology, Palaeoecology, v. 295, p. 236–244.

ESTEVE, J., HUGHES, N.C., AND ZAMORA, S., 2011, Purujosa trilobite assemblage and the evolution of trilobite enrolment: Geology, v. 39, p. 575–578.

ESTEVE, J., HUGHES, N.C., AND ZAMORA, S., 2013, Thoracic structure and enrolment style in middle Cambrian *Eccaparadoxides pradoanus* presages caudalization of the derived trilobite trunk: Palaeontology, v. 56, p. 589–601.

FORTEY, R.A., 1986, The type species of the Ordovician trilobite *Symphysurus*: systematics, functional morphology and terrace ridges: Paläontologische Zeitschrift, v. 60, p. 255–275.

GÁMEZ VINTANED, J.A., SCHMITZ, U., AND LIÑÁN, E., 2009, Upper Vendian-lowest Ordovician sequences of the western Gondwana margin, NE Spain: Geological Society, London, Special Publications, v. 326, p. 231–244.

GAINES, R.R. AND DROSER, M.L., 2003, Paleoecology of the familiar trilobite *Elrathia kingii*: an early exaerobic zone inhabitant: Geology, v. 31, p. 941–944.

GOZALO, R., LIÑÁN, E., GÁMEZ VINTANED, J.A., DIES ÁLVAREZ, M.E., CHIRIVELLA MARTORELL, J.B., ZAMORA, S., ESTEVE, J., AND MAYORAL, E., 2008, The Cambrian of the Cadenas Ibéricas (NE Spain) and its trilobites: Cuadernos del Museo Geominero, v. 9, p. 137–151.

HARPER, E.M., 2016. Uncovering the holes and cracks: from anecdote to testable hypotheses in predation studies: Palaeontology, v. 59, p. 597–609.

HARPER, E.M., PECK, L.S. AND HENDRY, K.R., 2009, Patterns of shell repair in articulate brachiopods indicate size constitutes a refuge from predation: Marine Biology, v. 156, p. 1993–2000.

JAGO, J.B., GARCÍA-BELLIDO, D.C, AND GEHLING, J.G., 2016, An early Cambrian chelicerate from the Emu Bay Shale, South Australia: Palaeontology v. 59, p. 549–562.

KELLEY, P.H., 1989. Evolutionary trends within bivalve prey of Chesapeake Group naticid gastropods: Historical Biology, v. 2, p. 139–156.

KELLY, P.H., KOWALEWSKI, M., AND HANSEN, T.A., 2003, Predator-Prey Interactions in the Fossil Record: Kluwer Academic, New York, 455 p.

KIMMIG, J. AND STROTZ, L.C., 2017, Coprolites in mid-Cambrian (Series 2-3) Burgess Shale-type deposits of Nevada and Utah and their ecological implications: Bulletin of Geosciences, v. 92, p. 297–309.

KLOMPMAKER, A.A. AND KELLEY, P.H., 2015, Shell ornamentation as a likely exaptation: evidence from predatory drilling on Cenozoic bivalves: Paleobiology, v. 41, p.187–201.

KOWALEWSKI, M., 2002, The fossil record of predation: an overview of analytical methods: Paleontological Society Papers, v. 8, p. 3–42.

KOWALEWSKI, M., DULAI, A., AND FÜRSICH, F.T., 1998, A fossil record full of holes: the Phanerozoic history of drilling predation: Geology, v. 26, p. 1091–1094.

LEIGHTON, L.R., 2001, New example of Devonian predatory boreholes and the influence of brachiopod spines on predator success: Palaeogeography, Palaeoclimatology, Palaeoecology, v. 165, p. 53–69.

LEIGHTON, L.R., 2011, Analyzing predation from the dawn of the Phanerozoic, *in* M. Laflamme, J.D. Schiffbauer, and S.Q. Dornbos (eds.), Quantifying the Evolution of Early Life: Springer, Netherlands, p. 73–109.

LOCHMAN, C., 1941, A pathologic pygidium from the upper Cambrian of Missouri: Journal of Paleontology, v. 15, p. 324–325.

MCNAMARA, K.J. AND TUURA, M.E., 2011, Evidence for segment polarity during regeneration in the Devonian asteropygine trilobite *Greenops widderensis*: Journal of Paleontology, v. 85, p. 106–110.

MERGL, M. AND ZAMORA, S., 2012, New and revised occurrences of rhynchonelliformean brachiopods from the middle Cambrian of the Iberian Chains, NE Spain: Bulletin of Geosciences, v. 87, p. 571–586.

MORZADEC, P., 1988, Le genre *Psychopyge* (Trilobita) dans le Dévonien inférieur du Nord de l'Afrique et l'Ouest de l'Europe: Palaeontographica Abteilung A, v. 200, p. 153–161.

MURTAUGH, P.A., 1981, Inferring properties of mysid predation from injuries to *Daphnia*: Limnology and Oceanography, v. 26, p. 811–821.

NEDIN, C., 1999, *Anomalocaris* predation on nonmineralized and mineralized trilobites: Geology, v. 27, p. 987–990.

NETO DE CARVALHO, C., COUTO, H., FIGUEIREDO, M. V. AND BAUCON, A., 2016, Estruturas biogénicas com relação microbiana nas ardósias Ordovícico Médio de Canelas (Norte de Portugal): Comunicações Geológicas, v. 103, Especial 1, p. 23–38.

OWEN, A.W., 1985, Trilobite abnormalities: Transactions of the Royal Society of Edinburgh, Earth Sciences, v. 76, p. 255–272.

PRADO, M.C., VERNEUIL, E. AND BARRANDE, J., 1860, Sur l'existence de la faune primordial dans la Chaıˆne Cantabrique: Bulletin de la Société Géologique de France, Series 2, v. 17, p. 516–542.

PRATT, B.R., 1998, Probable predation on upper Cambrian trilobites and its relevance for the extinction of soft-bodied Burgess Shale-type animals: Lethaia, v. 31, p. 73–88.

R CORE TEAM, 2017, R: a language and environment for statistical computing: R Foundation for Statistical Computing, Vienna, Austria, http://www.R-project.org/.

ROBSON, S.P. AND PRATT, B.R., 2007, Predation of late Marjuman (Cambrian) linguliformean brachiopods from the Deadwood Formation of South Dakota, USA: Lethaia, v. 40, p. 19–32.

RUDKIN, D.M., 1979, Healed injuries in *Ogygopsis klotzi* (Trilobita) from the middle Cambrian of British Columbia: Royal Ontario Museum Life Sciences Occasional Papers, v. 32, p. 1–8.

RUSTÁN, J.J., BALSEIRO, D., WAISFELD, B., FOGLIA, R.D., AND VACCARI, N.E., 2011, Infaunal molting in Trilobita and escalatory responses against predation: Geology, v. 39, p. 495–498.

SÁ, A.A. AND GUTIÉRREZ-MARCO, J.C., 2015, *Aroucaichnus* igen. nov. y otros icnofósiles singulares del Ordovícico del Geoparque Arouca (Portugal): Boletín de la Sociedad Geológica del Perú, v. 110, p. 8–23.

SCHMIDT-THOMÉ, M., 1973, Beiträge zur Feinstratigraphie des Unter-Kambriums in den-Iberischen Ketten (Nordost-Spanien): Geologisches Jahrbuch Reihe, Band B7, p. 3–43.

SCHMITZ, U., 1971, Stratigraphie und sedimentologie im Kambrium und Tremadoc der Westlichen Iberischen Ketten nördlich Ateca (Zaragoza), NE-Spanien: Münstersche Forschungen zur Geologie und Paläontologie, v. 22, p. 1–123.

SCHOENEMANN, B., CLARKSON, E.N., AND HØYBERGET, M., 2017, Traces of an ancient immune system—how an injured arthropod survived 465 million years ago: Scientific Reports, v. 7, p. 40330.

SCHOENER, T.W., 1979, Inferring the properties of predation and other injury-producing agents from injury frequencies: Ecology, v. 60, p. 1110–1115.

SDZUY, K., 1961, Das Kambrium Spaniens, Teil II: Trilobiten: Abhandlungen der Akademie der Wissenschaften Lit Mainz Math Nat Kl, v. 7, p. 499–594.

SINCLAIR, G.W., 1947, Two examples of injury in Ordovician trilobites: American Journal of Science, v. 245, p. 250–257.

SKINNER, E.S., 2005, Taphonomy and depositional circumstances of exceptionally preserved fossils from the Kinzers Formation (Cambrian), southeastern Pennsylvania: Palaeogeography, Palaeoclimatology, Palaeoecology, v. 220, p. 167–192.

SPRINKLE, J., 1973, Morphology and evolution of blastozoan echinoderms: Museum of Comparative Zoology Harvard University Special Publications, Boston, p. 283.

ŠNAJDR, M., 1978, Anomalous carapaces of Bohemian paradoxid trilobites: Sborník Geologických Věd Paleontologie, v. 20, p. 7–31.

VALENZUELA, J.I., GÁMEZ, J.A., LIÑÁN, E., AND SDZUY, K., 1990, Estratigrafia del Cámbrico de la región de Brea. Cadena Ibérica oriental: Boletín de la Real Sociedad Española de Historia Natural (Sección Geológica), v. 85, p. 45–54.

VANNIER, J., 2012, Gut contents as direct indicators for trophic relationships in the Cambrian marine ecosystem: PLoS ONE, v. 7, p. 1–20. e52200, https://doi.org/10.1371/journal.pone.0052200.

VANNIER, J. AND CHEN, J., 2005, Early Cambrian food chain: new evidence from fossil aggregates in the Maotianshan Shale biota, SW China: Palaios, v. 20, p. 3–26.

VERMEIJ, G.J., 1977, The Mesozoic marine revolution: evidence from snails, predators and grazers: Paleobiology, v. 3, p. 245–258.

VERMEIJ, G.J., 1982, Unsuccessful predation and evolution: The American Naturalist, v. 120, p. 701–720.

VERMEIJ, G.J., 1987, Evolution and Escalation: An Ecological History of Life: Princeton University Press, New Jersey, 544 p.

WALCOTT, C.D., 1911, Cambrian geology and paleontology, II, middle Cambrian Merostomata: Smithsonian Miscellaneous Collections, v. 57, p. 17–40.

WEBSTER, M., GAINES, R.R., AND HUGHES, N.C., 2008, Microstratigraphy, trilobite biostratinomy, and depositional environment of the “lower Cambrian” Ruin Wash Lagerstätte, Pioche Formation, Nevada: Palaeogeography, Palaeoclimatology, Palaeoecology, v. 264, p. 100–122.

WEBSTER, M. AND HUGHES, N.C., 1999, Compaction-related deformation in Cambrian olenelloid trilobites and its implications for fossil morphometry: Journal of Paleontology, v. 73, p. 355–371.

ZACAÏ, A., VANNIER, J. AND LEROSEY-AUBRIL, R., 2015, Reconstructing the diet of a 505-million-year-old arthropod: *Sidneyia inexpectans* from the Burgess Shale fauna: Arthropod Structure and Development, v. 45, p. 200–220.

ZAMORA, S., 2010, Middle Cambrian echinoderms from North Spain show echinoderms diversified earlier in Gondwana: Geology, v. 38, p. 507–510.

ZAMORA, S., MAYORAL, E., ESTEVE, J., GÁMEZ VINTANED, J. A., AND SANTOS, A., 2011, Exoskeletal abnormalities in paradoxidid trilobites from the Cambrian of Spain, and a new type of bite trace: Bulletin of Geosciences, v. 86, p. 665–673.

ZHU, M.-Y., VANNIER, J., ITEN, H., AND ZHAO, Y.-L., 2004, Direct evidence for predation on trilobites in the Cambrian: Proceedings of the Royal Society of London B, Biological Sciences, v. 271, p. S277–S280.

Received 26 June 2017; accepted 2 November 2017.

Chapter 13

Elongated thoracic spines as potential predatory deterrents in olenelline trilobites from the lower Cambrian of Nevada

Author contributions

SP conceived the project; SP performed the statistical analyses; SP wrote the manuscript and prepared the figures, with input from RDCB.

Publication information

This Chapter has peer reviewed and published by *Palaeogeography, Palaeoclimatology, Palaeoecology*:

Pates, S. & Bicknell, R. D. C. (2019). Elongated thoracic spines as potential predatory deterrents in olenelline trilobites from the lower Cambrian of Nevada. *Palaeogeography, Palaeoclimatology, Palaeoecology*, 516, 295-306.

Additional information

The data for this Chapter can be found online at: osf.io/974yh

Elongated thoracic spines as potential predatory deterrents in olenelline trilobites from the lower Cambrian of Nevada

by Stephen Pates[1,2] and Russell D. C. Bicknell[3]

[1] Department of Zoology, University of Oxford, South Parks Road, Oxford, OX1 3PS, UK. Email: stephen.pates@zoo.ox.ac.uk.

[2] Institute of Earth Sciences, University of Lausanne, Lausanne CH-1015, Switzerland

[3] Palaeoscience Research Centre, School of Environmental and Rural Science, University of New England, Armidale, New South Wales 2351, Australia. Email: rdcbicknell@gmail.com.

Key words: predation pressure; *Olenellus; Nephrolenellus;* repair frequency; Ruin Wash

Abstract

Repaired injuries offer the opportunity to study predation in the fossil record and test hypotheses concerning predation intensity, anti-predatory characters, and predator selectivity. Many studies have used the late Palaeozoic and Mesozoic records but quantitative explorations of early Palaeozoic predation, especially during the Cambrian, are lacking. Trilobites, a group of biomineralised arthropods with a high early Palaeozoic disparity and diversity are an ideal study system for exploring repaired injury frequencies. The Ruin Wash *Lagerstätte* (Nevada, USA; Stage 4, Cambrian Series 2) provides a bulk sample of closely related but morphologically distinct taxa. The five most abundant, *Olenellus chiefensis, O. fowleri, O. gilberti, O. terminatus,* and *Nephrolenellus geniculatus* differ in the spinosity of the cephalon, axial lobe of the thorax, and pleural lobes of the thorax. A total of 26 repaired injuries on 330 articulated

trilobite cephalothoraces reveal that *O. terminatus* has the highest incidence of repaired injuries (repair frequency = 0.18) and *N. geniculatus* has the lowest (repair frequency = 0.043). The role of enlarged spines on the third thoracic segment, which are most elongate in *N. geniculatus,* are suggested as predation deterrents. Predator selection for prey of a larger size may have played a minor role, though we did not find statistical support for this. Three cephala with repaired injuries were noted in a sample of 685 specimens: a much lower repair frequency compared to thoraces. This indicates that cephalic attacks were more often fatal when compared to thoracic attacks. Our study provides the first quantitative support for species specific predation on Cambrian trilobites.

1. Introduction

The dramatic increase in diversity and disparity during the Cambrian period (the Cambrian Explosion) was likely a result of numerous biological, ecological and environmental factors (Smith and Harper 2013; Zhang et al. 2014). Among these, predation was likely an important evolutionary shaper of events and morphologies (e.g. Bengtson 2002; Knoll 2003; Wood and Zhuravlev 2012; Erwin and Valentine 2013; Sperling et al. 2013; Zhang et al. 2014; Bicknell and Paterson 2018). Predation has been the subject of numerous large scale studies through geological time (e.g. Kowalewski et al. 1998; Huntley and Kowalewski 2007; Klompmaker et al. 2017) and has been touted as a major component of the Cambrian Explosion and the development of biomineralised exoskeletons and shells (Vermeij 1989, 2013; Bengston 2002; Babcock 2003; Knoll 2003). However, few studies on Cambrian predation intensity or selection have been conducted (but see Pratt 1998) and quantitative evidence for a Cambrian

'arms race' or escalation event is currently lacking (Leighton 2011; Bicknell and Paterson 2018).

Predation is an important agent of selection when predators and prey encounter each other often, and when predators fail to kill prey (Vermeij 2002). Repaired injuries (on bone, exoskeletons, or shells) are useful indicators of predation, as these fossils are common across depositional environments and present throughout the Phanerozoic (Kowalewski 2002). Furthermore, a repaired injury shows that the attack occurred during the animal's life, unlike unrepaired broken sclerites or shells that can also reflect post-mortem damage (e.g scavengers or taphonomy), complicating quantitative predation studies (Pates et al. 2017). Predation events that result in damage only to the soft-parts, or no damage at all, would not be measured by repaired injuries on hard exoskeletons, and so the predation pressure considered here pertains only to predation damage to a hard exoskeleton.

Repair frequency (a measure of the proportion of injured animals in a sample) is a useful proxy for predation intensity in the fossil record (e.g. Vermeij et al. 1981; Dietl et al. 2010; Harper 2016; Harper and Peck 2016), as supported by studies of modern gastropods (Molinaro et al. 2014; Stafford et al. 2015). Repair frequency is affected by the frequency of attacks (predation intensity), the proportion of failed attacks (predator efficiency) (Alexander 1981), and, as shown by a theoretical analysis of age-structured populations, the frequency of other sources of injury and death (Schoener 1979). These models show that repair frequency for animals damaged or killed only by predation is a result of only predator efficiency (Schoener 1979; Budd and Mann 2018). Schoener (1979) presented three competing hypotheses to explain differences in repaired specimens between samples: i) increased predator efficiency; ii) increased predation

intensity, coupled with other causes of non-fatal injuries; and iii) decreased predation intensity coupled with a significant source of alternative mortality. We explore these three hypotheses to assess a record of differing repair frequencies in five Cambrian trilobite taxa. Our interpretation is complemented by data relating to the relative preservation frequency of near-articulated cephalothoraces (specimens where the length of the cephalothorax could be confidently measured) and isolated cephala.

2. Background

2.1 Trilobites as a study system

Repair frequency in brachiopods and molluscs is affected by prey morphology (e.g. Alexander 1986; Dietl et al. 2000; Alexander and Dietl 2001; Dietl 2003a, b; Dietl and Hendricks 2006; Harper et al. 2009) and defensive adaptations like spiny shells and reduced aperture sizes (Vermeij 1977, 1987; Kelley 1989; Vendrasco et al. 2011; Klompmaker and Kelley 2015). Such records have been extensively studied as shell drilling and crushing spans the Phanerozoic. Conversely, trilobites have been less explored, despite their large disparity and high diversity through the early Palaeozoic (Foote 1991; Adrain et al. 1998; Webster 2007a).

The high preservation potential of Cambrian trilobites, coupled with their diversity and global distribution, makes this group ideal for providing quantitative data and evidence of early Palaeozoic predation. Repaired injuries on Cambrian trilobite exoskeletons are well known (see Owen 1985; Babcock 1993, 2003; Vinn 2018; Bicknell and Paterson 2018 for reviews) and trilobite rich gut contents (Conway Morris 1977; Bruton 1981; Zhu et al. 2004; Vannier 2012; Zacaï et al. 2016; Jago et al. 2016) and coprolites (Sprinkle 1973; Conway Morris and Robison 1988; Nedin 1999; Babcock 2003,

Skinner 2005; Vannier and Chen 2005; English and Babcock 2010; Daley et al. 2013; Kimmig and Strotz 2017) confirm that trilobites were prey items. Additionally, recent biomechanical analyses that built on functional morphological studies have confirmed that at least some Cambrian predators, such as *Sidneyia inexpectans* of the middle Cambrian Burgess Shale, were mechanically capable of injuring trilobites (Bicknell et al 2018a, b). Trilobites likely engaged in anti-predatory behaviors, such as burrowing, hiding, and enrolment (Fortey 1986; Esteve et al. 2011, 2013; Fatka and Budil 2014), and had select exoskeletal characters with anti-predatory roles: elongate spines and thick biomineralised exoskeletons (Fortey and Owens 1999; Clarkson and Ahlberg 2002). However, the anti-predatory effectiveness of these features has not yet been explored.

Studies of repaired injuries in trilobites are complicated by ecdysis, which can cause injuries, death, and discarded moults bearing similarities to carcasses. Different groups of trilobites utilized a vast array of moulting modes, that varied inter- and intra-generically (Daley and Drage 2016). The two genera considered in this study, *Olenellus* and *Nephrolenellus,* used the same two major moulting modes: the Marginal Suture Mode and Salterian Mode (Hennigsmoen 1975; Webster 2015; Drage in review; Drage et al. 2018). Moulting events likely regenerated injured areas, removing evidence for injuries from the fossil record (Pates et al. 2017; Bicknell et al. 2018c). Also problematic moulting is another potential cause for injuries and death (e.g. Owen 1985). Ultimately, the repair frequencies of trilobites should not be compared to non-trilobite groups without considering these factors. To assess potential trilobitic anti-predatory features, a bulk sample (either direct or indirect, *sensu* Kowalewski 2002) containing multiple species with different anti-predatory features are needed from a single site. A bulk sample (the collection of every specimen in a deposit) precludes collection bias for

species, animal sizes, and preferential collection of injured or uninjured specimens. Additionally, the trilobites must be autochthonous (as different sources could have different environments, predators and injury sources), and not be size sorted (size can affect predator preference and therefore repair frequency, see Paine 1976 or Harper et al. 2009). Finally, the collection should be large enough (relative to injury frequency) to allow for statistical comparisons between species.

Extensive work at the Ruin Wash *Lagerstätte*, Nevada, USA (Cambrian Series 2, Stage 4; Fig. 1C) has documented the ontogeny, systematics, and taphonomy of the trilobite fauna (e.g. Palmer 1998; Webster and Hughes 1999; Webster 2007b, 2015; Webster et al. 2008). Here, predator selection is explored by comparing the relative frequency of injuries in the five most common Ruin Wash *Lagerstätte* trilobite taxa. Disparity in prothorax spinosity is used to assess the role of different spines as predatory deterrents and subsequent differences in repair frequencies between these species.

2.2 Ruin Wash

The Ruin Wash *Lagerstätte* (Fig. 1A, B), the top 43 cm of the Combined Metals Member, Pioche Formation (Nevada, USA), is uppermost Dyeran in age (Cambrian Series 2, Stage 4; Fig. 1C). A field study in 1999 (Webster et al. 2008) collected every specimen, providing an indirect bulk sample (*sensu* Kowalewski 2002) for this study. Bottom currents likely removed the smallest (<2 mm length) specimens but no other evidence for size-sorting or faunal transport is present. Trilobites therefore represent an autochthonous assemblage deposited in a low energy environment, buried by tempestite events (Webster et al. 2008). Slight variations in the pre-burial exposure

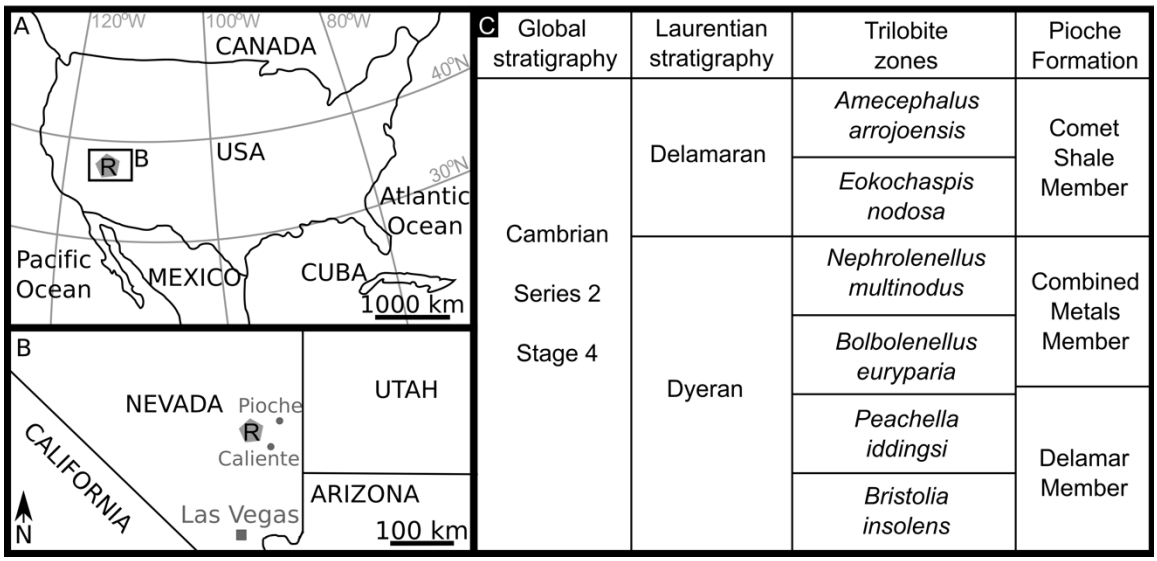

Fig. 1. A. Map showing geographic location of the Ruin Wash *Lagerstätte* (R in grey pentagon). **B.** Inset from A. **C.** Global and local stratigraphy with trilobite zones of Ruin Wash and neighbouring units. The Ruin Wash *Lagerstätte* is found at the top 43 cm of the Combined Metals Member, and is in the *Nephrolenellus multinodus* biozone. A small-scale map showing the detailed position of localities can be found in Webster et al. (2008, fig. 1).

time and current intensity in certain horizons resulted in some beds containing more articulated specimens than others (Webster et al. 2008).

The five most common species, *Olenellus chiefensis, O. fowleri, O. gilberti, O. terminatus,* and *Nephrolenellus geniculatus* can be recognized by morphological differences in the cephalon and prothorax. The opisthothorax is well known in *N. geniculatus* as it is often preserved, but is rarely preserved in *Olenellus* species and unknown for *O. chiefensis* and *O. terminatus* (Fig. 2; Palmer 1998). All five taxa bear genal spines, but the length of these spines relative to the overall cephalic and thoracic lengths varies: *Nephrolenellus geniculatus* and *O. fowleri* have the shortest genal spines, and *O. chiefensis* and *O. gilberti* have the longest. All five taxa bear an enlarged third thoracic segment (T3), with associated elongated pleural spines on the prothorax. T3 is hyperpleural (*sensu* Palmer 1998) in *N. geniculatus*, as it distorts both the thoracic segment immediately anterior (T2) and posterior (T4). The *Olenellus* species are macropleural (*sensu* Palmer 1998), as only T4 is distorted in the genus. *Olenellus* species are varyingly macropleural: weakly (amplipleural *sensu* Palmer 1998) in *O. fowleri*, moderately in *O. terminatus*, and more strongly in *O. chiefensis* and *O. gilberti* (Palmer 1998). The pleural spine on T3 extends significantly beyond the posterior prothorax in *N. geniculatus* (dolichospinous *sensu* Palmer 1998). The T3 pleural spines are larger than adjacent spines, but do not extend beyond the prothorax in the four *Olenellus* species (macrospinous *sensu* Palmer 1998). *Olenellus fowleri* has proportionally longer pleural spines along the entire prothorax, with *O. chiefensis* and *O. gilberti* the taxa with the next most spinous prothoraces. *Nephrolenellus geniculatus* and *O. terminatus* have the proportionally shortest pleural spines on the prothorax. All *Olenellus* species bear an axial spine on T15, which is unknown in *N. geniculatus*.

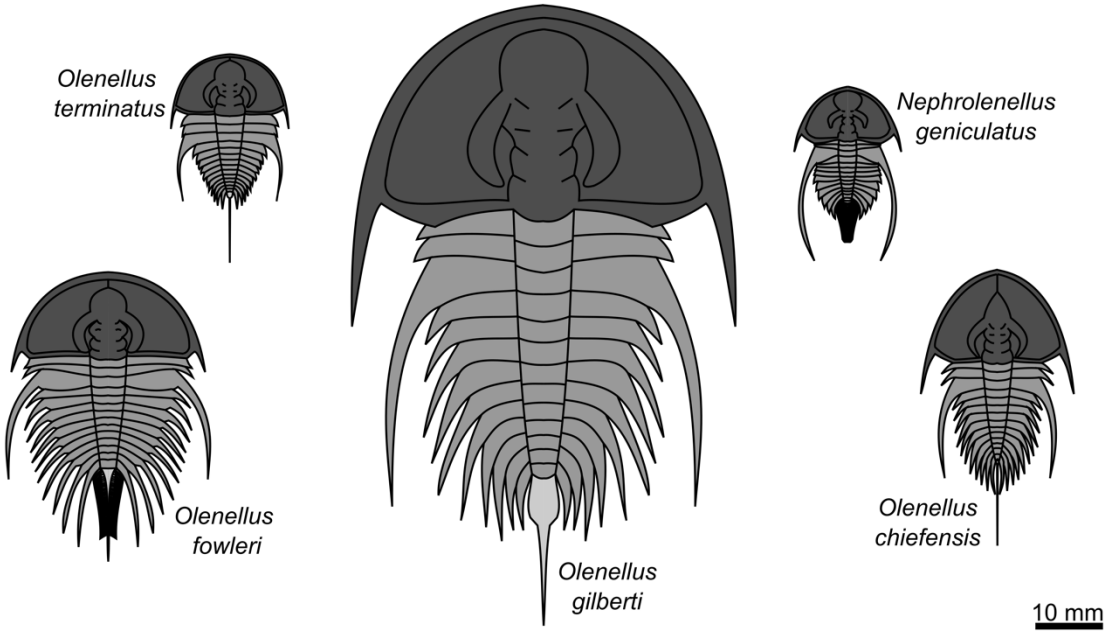

Fig. 2. The five most abundant taxa at Ruin Wash *Lagerstätte*, shown at their maximum measured sizes measured in this study. Cephalon in dark grey, prothorax in medium grey, spine on 15th thoracic segment in light grey. Opisthothorax visible as black shading in *Olenellus fowleri* and *Nephrolenellus geniculatus.* Scale bar = 10 mm.

Individual taxa can therefore be considered the most or least spinous from different perspectives. When only genal spines are considered, *Olenellus chiefensis* and *O.* gilberti are the most spinous. When only T15 is considered, the *Olenellus* taxa are more spinous than *N. geniculatus*. When T3 spines and all other thoracic spines are considered together, *O. fowleri* is the most spinous. When T3 is considered most important and the other thoracic spines have secondary importance, *N. geniculatus* would be considered the most spinous and *O. terminatus* the least spinous. We consider each of these in turn, in relation to the injury frequencies discussed below.

3. Methods

3.1 Institutional abbreviations.

CMCP, CMNH, Cincinnati Museum Center, Cincinnati, Ohio, USA; DMNH, Denver Museum of Natural History, Denver, Colorado, USA; FMNH, Field Museum of Natural History, Chicago, Illinois, USA; ICS, Institute for Cambrian Studies, University of Chicago, Chicago, Illinois, USA; MCZ, Museum of Comparative Zoology, Harvard, Boston, Massachusetts, USA; UCR, University California Riverside, Riverside, California, USA; YPM, Yale Peabody Museum, New Haven, Connecticut, USA.

3.2 Data collection

The bulk sample of Ruin Wash *Lagerstätte* trilobites from a 1999 field study is accessioned across a large number of institutes (see *Institutional abbreviations* above); with the ICS collection also holding latex peels of specimens accessioned at the DMNH. Ruin Wash trilobites at these institutions were examined (latex peels at the ICS were used in place of DMNH specimens). Additional Ruin Wash specimens from earlier, non-

exhaustive, excavations and donations from collectors are present in the ICS. These were also included in the study to increase sample size, introducing a minor sampling bias to the indirect bulk sample. Evidence for repaired injuries on trilobites, as defined and discussed in Bicknell and Paterson (2018) and Bicknell et al. (2018c), was noted, including single spine injuries (SSIs). The length from the anteriormost point of the cephalon to the posteriormost point of the axial lobe of the prothorax was measured for all injured trilobites, and those with at least an articulated or nearly articulated cephalothorax (referred to as cephalothoraces from this point, even if they also had the opisthothorax or additional body parts preserved) and well preserved spines (i.e. where an injury could be identified if present). Measurements were performed using digital calipers. It is worth noting that telescoping of thoracic segments and slight cephalic disarticulations in some specimens will have introduced a small degree of error. Cephalic measurements (e.g. just cephalon width, or sagittal length) would have not introduced such errors, however cephalothoracic length was gathered as the cephalothorax as a whole was assessed for damage.

Injured specimens were photographed with a Canon EOS 500 DSLR camera, and injury location (side, body part, location on that body part) was noted. All isolated cephala in the CMCP, CMNH, DMNH, ICS, YPM and UCR collections were counted and examined for injuries, to provide an additional injury frequency dataset.

3.3 Data analysis

3.3.1. Frequency of preservation.

Isolated cephala can result from the disarticulation of complete skeletons after moulting, predation, or scavenging, and the disruption of carcasses by bottom currents.

Specimens including at least a cephalothorax reflect either Marginal Suture moulting (MSM) mode (Drage in review), or carcasses. If all taxa were attacked and killed without predator selection, and the proportions moulting through the MSM mode were not significantly different, the percentage of each taxon in an assemblage would be the same for both isolated cephala and cephalothoraces. The frequency of isolated cephala and cephalothoraces for taxa from the Webster et al. (2008) field study were compared with our dataset using a Chi-squared test (α=0.05). The test was performed using the 'MASS' package in RStudio (Venables and Ripley, 2002). A higher proportion of isolated cephala from a taxon compared to cephalothoraces thereof could reflect i) higher predation, scavenging, or disarticulation frequency relative to other taxa, or ii) lower frequency of MSM mode and non-predatory death (not resulting in exoskeletal disarticulation). The following hypothesis was tested:

H_0: cephalothoraces and cephala are preserved in the same relative frequency between taxa. There is therefore no predatory selection or difference in moulting mode frequency.

H_1: cephalothoraces and cephala are not preserved in the same relative frequency between taxa. Predatory selection, moulting behavior, and/or propensity to disarticulate prior to burial is significantly different between taxa.

3.3.2 Frequency of repair.

Repair frequencies have been calculated in two ways. The first, dividing the total number of injuries by total number of animals (F-value in Pates et al. 2017) gives an inflated percentage value of injured animals (Dietl et al. 2000). The second, dividing total number of injured animals by total number of animals (R-value in Pates et al.

2017), gives an underestimate for the percentage value of injured animals (Alexander and Dietl 2003). Here, no articulated cephalothorax had multiple injuries: F- and R-values are therefore the same. One example of an *O. gilberti* from Ruin Wash with two injuries (one on T4 and T5, the second on T8) is known in the literature (Palmer 1998, fig. 9.2).

A Bayesian inference method was used to assess the effect of sample size on calculated repair frequencies (following Pates et al. 2017). This method produces a distribution of possible outcomes, therefore accounting for uncertainty induced by low sample sizes by producing a broader distribution. In contrast, a higher sample size will produce a more constrained posterior distribution. Here, an uninformative prior was used, as we had no knowledge of injury abundance before sampling. The total number of specimens and number of injured specimens were input to produce the posterior distribution, from which the 5^{th} and 95^{th} percentile values were taken as confidence limits. This approach is preferred to a Chi-squared test for two reasons: i) Chi-squared tests perform poorly with low expected values and ii) a Bayesian-inference value allows the expected spread of values to be examined for individual taxa. The 5^{th} and 95^{th} percentile Bayesian Inference repair frequencies were calculated for each taxon. The 5^{th} percentile value gives a lower bound where 95% of the inferred distribution of possible repair frequencies is expected to have a higher repair frequency, and the 95^{th} percentile value gives an upper bound where 95% of the inferred distribution is expected to have a lower repair frequency.

3.3.3 Size selection.

The distributions of the cephalothoracic lengths of two groups (injured and not injured trilobites) were compared using a Mann-Whitney U test using the 'stats' package in R Studio (R Core Team 2017). This was done for the bulk sample (all trilobites) and for a subset (*Olenellus* specimens), to assess possible relationship between the cephalothoracic length of trilobites and injury likelihood (i.e. size selection by predators).

3.3.4 Injury location.

Preferential injury location (stereotypy) for either pleural lobe of trilobite specimens was tested using two-tailed binomial tests calculated using the 'stats' package in RStudio (R Core Team 2017). The hypothesis tested was:

H_0: Injuries are equally likely on both trilobite pleural lobes.

H_1: Injuries are more likely on one pleural lobe or the other of the trilobite. This would provide evidence for lateral asymmetry of injuries (Babcock and Robison 1989; Babcock 1993, 2003).

A second test for injury stereotypy explored the role T3 pleural spines in active defense, and the suggestion that elongated spines were more commonly injured during problematic moulting. The T3 segment bears larger pleural spines than other prothoracic segments in all five taxa considered. Tips of the T3 spines were not always visible due to sediment cover, and an injury was only counted if an injury could be confirmed (and differentiated from sediment cover). The hypothesis tested was:

H_0: Enlarged spines on the third thoracic segment are equally likely to be injured as other spines.

H_1: Enlarged spines are more or less likely to be injured than other spines. This provides evidence for use of these spines in defense or evidence for problematic moulting preferentially causing injuries to the longest spines. If used for active defense, these spines would be broken, but the animal would survive and spines subsequently repair. If instead they were used as deterrents, or had no anti-predatory function, these spines would not be more likely broken than other spines, as the predator would not attack the animal.

The axial spine on T15 is only known in *Olenellus*, and due to its orientation outside the plane of the rest of the body, we were not confident in identifying repaired injuries in this structure and distinguishing them from variation in taphonomic compression. No quantitative data was collected for this spine, and so its likelihood of injury during defense or accidental injury was not analyzed. Furthermore, genal spine injuries were not analyzed statistically due to the apparent rarity of cephalic injuries in general (see results below).

4. Results

4.1 Frequency of preservation.

The five taxa were not recovered in equal proportions, and the relative frequency of taxa preserved was not consistent between cephala and cephalothoraces. *Olenellus gilberti* was the most common taxon recovered, with *O. chiefensis* and *Nephrolenellus geniculatus* the next most abundant respectively (Table 1). The Chi-squared test indicates that the taxon-frequency of cephala from Webster et al. (2008) (Table 1, N cephala Webster et al. 2008) differs significantly from the taxon-frequency of cephalothoraces in our results (Table 1, N cephalothoraces this study) (χ^2= 12.35, p-

Table 1. Relative proportions of each taxa in this study compared to field sample

Taxon	N cephalothoraces (this study)	N cephala (Webster et al. 2008)	N cephalothoraces (Webster et al. 2008)
Olenellus chiefensis	60 (20%)	47 (24%)	1 (6%)
Olenellus fowleri	17 (6%)	16 (6%)	1 (6%)
Olenellus gilberti	163 (55%)	131 (52%)	9 (53%)
Olenellus terminatus	11 (3%)	27 (11%)	0 (0%)
Nephrolenellus geniculatus	47 (16%)	28 (11%)	6 (35%)

Number of specimens used in this study, and reported from a field study by Webster et al. (2008). Raw values given for each of the five taxa considered in this study, with the percentage of each group made up by that taxon given in brackets. Cephalothoraces refers to a specimen where at least the cephalothorax is present. Cephala refers to isolated cephala.

Table 2. Repair frequencies for individual taxa

Taxon	N	Inj.	F, R	5%	95%
Olenellus chiefensis	60	5	0.083	0.044	0.12
Olenellus fowleri	17	2	0.12	0.047	0.31
Olenellus gilberti	163	12	0.074	0.048	0.12
Olenellus terminatus	11	2	0.18	0.072	0.44
Olenellus sp.	32	3	0.094	0.042	0.22
Olenellus (total)	283	24	0.088	0.062	0.12
Nephrolenellus geniculatus	47	2	0.043	0.017	0.13

Number of specimens (N), number of injured specimens (Inj.), repair frequency (F, R), and 5th and 95th percentile Bayesian Inference values for each taxon considered in this study.

value = 0.015). The Webster et al. (2008) cephala sample also differs from the cephalothorax frequency in the same study (Table 1, N cephalothoraces Webster et al. 2008) (χ^2 = 10.54, p-value = 0.032). The percentage of animals belonging to each taxon in the two cephalothoraces samples are not significantly different when treated with a Chi-squared test (χ^2= 5.97, p-value = 0.20); however, the result is only tentative as the field sample had a small sample size (n=17) (Webster et al. 2008).

More *Nephrolenellus geniculatus* cephalothoraces were preserved relative to the frequencies of isolated cephala reported by Webster et al. (2008). *Olenellus terminatus* cephalothoraces are preserved in a lower proportion compared to other taxa than isolated cephala. For the other three *Olenellus* taxa, the percentage of each taxon represented as isolated cephala is broadly similar to the percentage of each taxon in the cephalothoraces sample (Table 1, columns 1 and 2).

4.2 Frequency of thoracic repair.

Twenty-three injuries were found across 298 complete specimens of *Olenellus* and *Nephrolenellus*. An additional three injuries were noted on 32 *Olenellus* specimens that could not be identified to species level (Table 2; all the specimen and injury data is available to download through the Open Science Framework - Pates & Bicknell 2018). All *Olenellus* species record higher repair frequencies than *Nephrolenellus geniculatus,* with highest repair frequency calculated for *O. terminatus* (Table 2).

Repair frequencies for all *Olenellus* species were below the 95% Bayesian-inferred value for *Nephrolenellus geniculatus* (0.13) with the exception of *O. terminatus* (0.18). Bayesian-inference values for *N. geniculatus* equaled the measured repair frequencies of *Olenellus gilberti* at 70% (0.74), *O. chiefensis* at 77% (0.83) and *O. fowleri*

at 94% (0.12). The *N. geniculatus* repair frequency (0.043) is similar to the 5% Bayesian-inferred value for *O. chiefensis* (0.044)*, O. fowleri* (0.047)*,* and *O. gilberti* (0.048), and below the 5% Bayesian-inferred value for *Olenellus* as a genus (0.062) and *O. terminatus* (0.072). *Olenellus terminatus* has the highest repair frequency (0.18), with the 5% Bayesian-inferred value lower than the recorded repair frequencies for all other *Olenellus* species (Table 2).

4.3 Description of injuries.

Thoracic injuries are limited to shortened pleural spines, on T3 and other segments. Eleven of 26 injuries are visible as two adjacent short spines, representing a single injury that damaged adjacent thoracic segments (e.g. Figs 3A, B; 4A, B), with the remaining 15 injuries limited to SSIs (e.g. Figs. 3C, D; 4C, D). No thoracic specimens showed signs of cicatrisation, suggesting a recent injury. Injured spines are at various stages of regeneration, but nonetheless are i) shorter than undamaged spines on the opposite side and ii) shorter than expected length relative to adjacent spines. In some cases they are much shorter (e.g. Fig. 3C) or show signs of distortion (e.g. Fig. 4A). Injured spines are distinguished from missing and broken spines (which have jagged or sharp edges) as the spine edge is smooth, indicating that some regeneration has occurred.

Three injured cephala, one *Olenellus fowleri* and two *O. terminatus*, at different stages of repair were identified (Fig. 5). The smallest specimen, *O. fowleri* (Fig. 5A), displays a cicatrised injury with a raised margin immediately interior to the 'U'-shaped indentation, and a missing genal spine. The second smallest specimen (Fig. 5B) has an uncicatrised 'V'-shaped injury to the right cephalon that is approximately as wide as it is

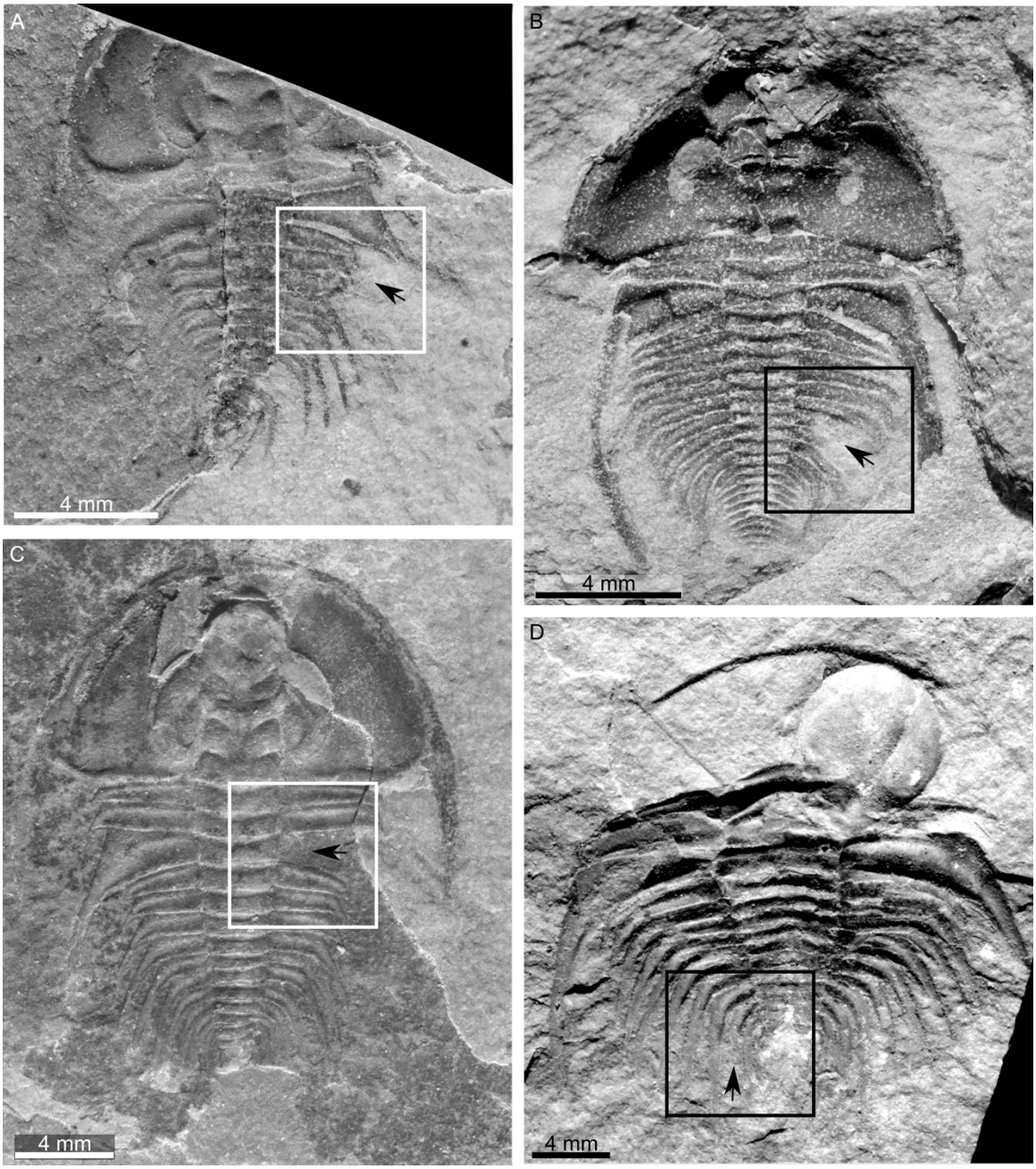

Fig. 3. Examples of repaired injuries on Ruin Wash trilobite cephalothoraces. **A, B.** Injuries to two adjacent thoracic segments. **C. D.** Single spine injuries. **A.** MCZ 188159, *Olenellus gilberti*. **B.** MCZ 188351, *Nephrolenellus geniculatus*. **C.** MCZ 188149, *Olenellus gilberti*. **D.** MCZ 188467, *Olenellus fowleri*. Injuries marked by arrows, boxes show areas inset figured in Fig. 4. Scale bars = 4 mm. Image credit: Museum of Comparative Zoology, Harvard University.

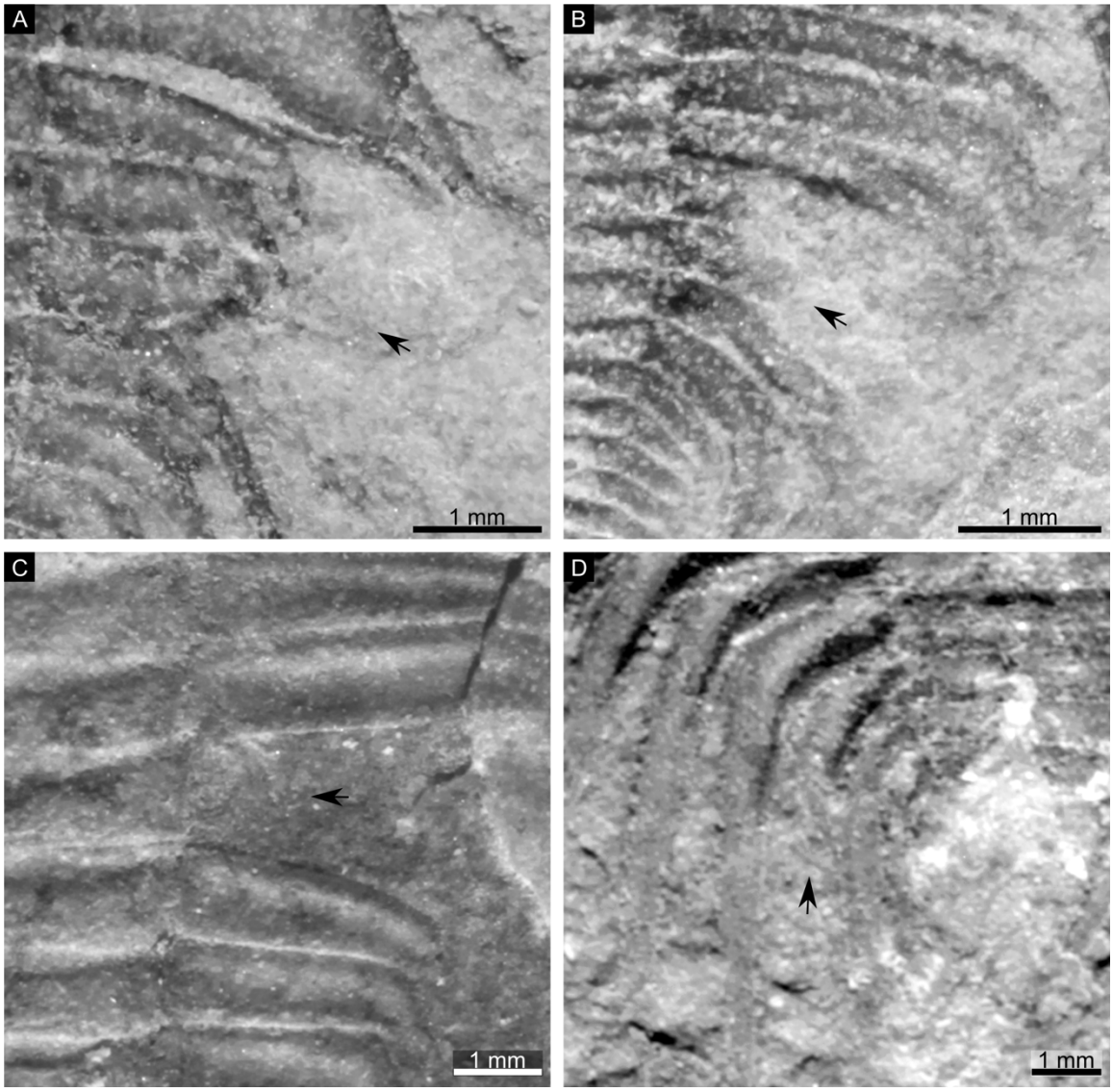

Fig. 4. Enlarged areas showing repaired injuries from Figure 3. **A.** MCZ 188159, *Olenellus gilberti*. **B.** MCZ 188351, *Nephrolenellus geniculatus*. **C.** MCZ 188149, *Olenellus gilberti*. **D.** MCZ 188467, *Olenellus fowleri*. Injuries marked by arrows. Scale bars = 1 mm. Image credit: Museum of Comparative Zoology, Harvard University.

deep. The presence of genal spines cannot be confirmed due to sediment cover. The largest specimen (Fig. 5C) shows damage and repair on both sides of the cephalon. Both genal spines are missing and the lateral borders immediately interior to these indents are slightly distorted.

4.4 Size selection.

Specimens of the largest and smallest trilobites were *Olenellus gilberti,* likely reflecting the large number of specimens (n=163, Table 1). On average (median and mean) *Nephrolenellus geniculatus* were the smallest, *O. fowleri* the largest, and *O. terminatus* second largest (Table 3; Fig. 6A).

The median and mean length of injured specimens (23.90 mm and 25.72 mm) is higher than specimens without injuries (20.50 mm and 22.69 mm), both when all trilobites are treated as a bulk sample (Fig. 6B) and when considering just *Olenellus* taxa (Table 3, Fig. 6C). However, these size distributions of injured and not injured populations are not resolved as statistically different when interrogated with a Mann-Whitney U test (bulk sample: W = 2803.5, p-value = 0.06913; *Olenellus* only: W = 2813.5, p-value = 0.2114).

4.5 Injury location.

Fourteen of 26 thoracic injuries were on the right side of the body, 12 on the left side, and none present on the axial lobe. Three injuries are present on T3, with the remaining 23 on other prothoracic segments. The two-tailed binomial tests failed to reject either null hypothesis: injuries were equally likely to occur on either thoracic side (p-value = 0.845) and T3 was injured as frequently as other thoracic segments (p-value =

Fig. 5. Examples of repaired injuries on Ruin Wash isolated *Olenellus* cephala. **A.** *Olenellus fowleri* cephalon with cicatrized injury on the right hand side. FMNH PE 58503**. B.** *Olenellus terminatus* cephalon with indent to the right hand side. FMNH PE 58505**. C.** *Olenellus terminatus* with bilateral injury and missing genal spines. FMNH PE 58504**.** Injuries marked by arrows. Scale bars = 5 mm.

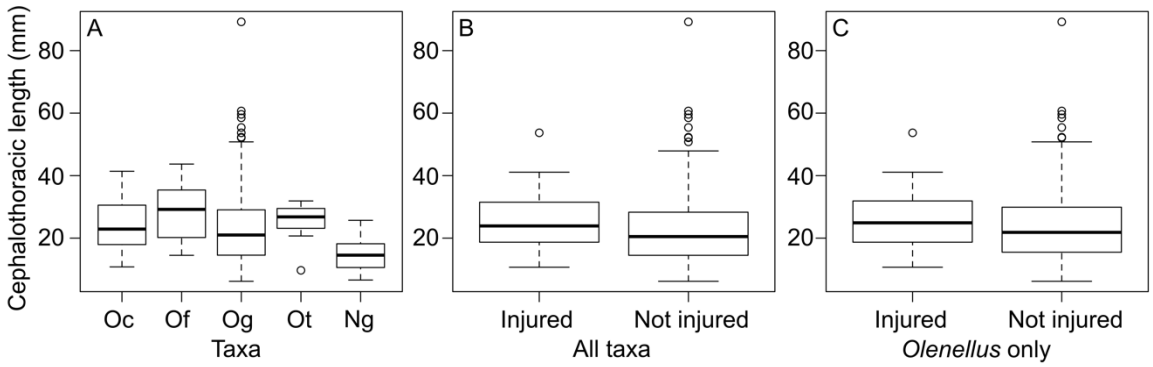

Fig. 6. Boxplots showing relative lengths of trilobite cephalothoraces from Ruin Wash *Lagerstätte* included in this study. **A.** Each of the five taxa studied, Oc = *Olenellus chiefensis,* Of = *Olenellus fowleri*, Og = *Olenellus gilberti*, Ot = *Olenellus terminatus*, Ng = *Nephrolenellus geniculatus*. **B.** Lengths of all injured trilobites and all not injured trilobites. **C.** Lengths of all injured *Olenellus* trilobites and all not injured *Olenellus* trilobites.

Table 3. Length distributions of trilobite taxa in this study

Taxon	Smallest	1st quartile	Median	Mean	3rd quartile	Largest
Olenellus chiefensis	10.80	18.02	22.90	24.78	30.48	41.40
Olenellus fowleri	14.50	20.20	29.20	27.92	35.40	43.70
Olenellus gilberti	6.20	14.55	21.00	23.92	29.05	89.20
Olenellus terminatus	9.70	23.15	26.80	25.40	29.50	31.90
Nephrolenellus geniculatus	6.60	10.60	14.55	14.61	18.20	25.70
Injured (all taxa)	10.70	18.75	23.90	25.72	31.43	53.70
Not injured (all taxa)	6.20	14.50	20.50	22.69	28.30	89.20
Injured (*Olenellus* only)	10.70	18.70	24.90	26.62	31.90	53.70
Not injured (*Olenellus* only)	6.20	15.53	21.85	24.26	29.90	89.20

Length distributions for taxa considered in this study. All lengths in mm.

0.4743). Injured thoraces (repair frequency = 0.079, n=26 out of 330) are more common than injured cephala (repair frequency = 0.004, n= 3 out of 685).

5. Discussion

5.1 Differences in thoracic repair frequency

The three hypotheses that might explain the lower repair frequency of *Nephrolenellus geniculatus* relative to *Olenellus terminates* are considered (Schoener 1979): i) increased predator efficiency; ii) higher predation intensity with a significant alternate cause of non-fatal injury; or iii) a lower predation intensity with a significant alternate cause of mortality. The third cause appears most likely, as it is supported by both injury frequency data (Table 2) and cephalothorax preservation data (Table 1). Fewer potentially injury-inducing encounters for *N. geniculatus* relative to *O. terminatus,* coupled with an alternate explanation for cephalothoraces in the fossil record (e.g., death during ecdysis) would result in more *N. geniculatus* cephalothoraces and a higher injury frequency for *O. terminatus*. The three other *Olenellus* species have repair frequencies higher than *N. geniculatus* and lower than *O. terminatus*, and also preserve more cephalothoraces than *O. terminatus* but fewer than *N. geniculatus*.

Hypotheses i) and ii) inadequately explain the differential preservation frequency of cephalothoraces and isolated cephala. For i) an increased success of predatory attacks to *Nephrolenellus geniculatus* relative to *Olenellus terminatus* predicts that *N*. *geniculatus* cephalothoraces would be rarer than *O. terminatus*. This assumes that successful predation produces fragmentary or disarticulated specimens. A major difference in the relative frequency of moulting modes employed by Ruin Wash trilobites would also be needed to explain why the *N. geniculatus* cephalothoraces are

more abundant than expected and *O. terminatus* are lower than expected. The more frequent preservation of *Nephrolenellus geniculatus* opisthothoraces compared to *O. terminatus* suggests that the *N. geniculatus* thorax was less prone to disarticulation after death or moulting. This may contribute to the higher-than-expected percentage of cephalothoraces for *N. geniculatus* relative to *O. terminatus*. However, this difference does not account for the lower-than-expected percentage of cephalothoraces for *O. terminatus* compared to all other *Olenellus* species (Table 1). Similarly for hypothesis ii) a higher predation pressure on *N. geniculatus* coupled with an alternative injury source and significant differences in the MSM modes between the five species are required to produce the relative proportions of articulated specimens for *N. geniculatus* and *O. terminatus* (Table 1). However, assuming there is no difference in the predator efficiency, a higher predation pressure on *N. geniculatus* compared to *O. terminatus* would result in fewer articulated *N. geniculatus* than expected, with more *O. terminatus* (as successful predation would remove these from the record). This is the opposite of what is observed at Ruin Wash. In addition, exuviae with attached cephalon an thorax may also have been disturbed – a study using models of Mesozoic oysters showed that predators in the modern ocean (specifically crabs) attack suitable-looking prey even when no soft parts or nutrition are available (LaBarbera 1981). Such behavior at Ruin Wash (the action of a different, now long extinct predator) would have removed additional cephalothoraces of taxa experiencing the highest predation pressure. For hypothesis ii) to hold, an additional further mechanism is needed to explain the lower percentage of articulated *O. terminatus* compared to other *Olenellus* species, as under this hypothesis *O. terminatus* experienced the lowest predation pressure. Interspecific differences in the use of the Salterian Moulting mode could provide this.

In summary, hypothesis iii) is considered the most likely explanation for the differences in repair frequency and preservation of articulated material reported here, as it requires no additional explanation beyond predation pressure. Hypotheses i) and ii) cannot be completely ruled out, as we do not know the relative frequencies of the moulting mode used by these taxa. However, these differences in moulting mode would have to align perfectly to exactly counteract the signal from higher predation efficiency or pressure on *Nephrolenellus geniculatus*.

5.2 Moulting – a non-predatory cause of injury frequency differences?

Spine length could potentially influence another, non-predatory, cause of injury: problematic moulting. Longer spines may be damaged more often than shorter specimens during moulting (Babcock 1993). However, in this study the T3 injury frequency (the macro- or dolichospinous segment) is the same as for other pleural spines. Additionally, the incidence of injuries is highest in *Olenellus terminatus*, and lowest in *Nephrolenellus geniculatus,* which have similarly sized prothoracic segments, except for T3. This suggests that either self-inflicted moulting injuries are not the major cause of shortened spines in, or that spine length does not influence the likelihood of moulting injuries for these animals.

A second consideration is whether differences in the relative frequency of the moulting mode (MSM or Salterian), with no differences in predation efficiency or intensity, could produce the observed differences in the frequency of predator-induced injuries. Modelling approaches using data from modern crabs have shown that the expected size-distribution of corpses and exuviae in fossil assemblages are very similar (Hartnoll and Bryant 1990). This is because corpses and exuviae together comprise the

total number of individuals to reach each instar (Hartnoll and Bryant 1990). Assuming that the presence or absence of an injury did not affect moulting mode used by the a given trilobite, the proportion of exuviae preserving a cephalothorax (through the MSM mode) and injured carcasses should be the same. The repair frequency of a species (which is calculated using both carcasses and exuviae) is therefore unaffected by differences in relative frequency of moulting mode, assuming that the presence of an injury does not affects the moulting mode used by a given trilobite.

5.3 Spines as a predation deterrent?

The variation in predation intensity across taxa requires consideration. Differences in spinosity between the taxa provides a possible explanation; however, there are a number of different spine morphologies and locations on these taxa, and we discuss each in turn. As the predation intensity on *Olenellus* was likely higher than on *Nephrolenellus*, there is no evidence that the axial T15 spine acted as a predatory deterrent for attacks to pleural lobes (a T15 spine is present on all *Olenellus* taxa but absent in *Nephrolenellus*). This does not preclude this axial spine from having performed a defensive or deterrent function for attacks to other body parts, such as the axial lobe. Similarly, although genal spines would have overlapped and perhaps offered some defense for the anterior prothorax, the relative length of these spines does not appear to have a relation to the inferred predation intensity. Thus they were unlikely an effective deterrent for attacks on the prothoracic pleural lobes. Genal spines may have played helped defense or deter attacks to the anteriormost segments of the prothorax, or the cephalon. A larger sample size of injuries is required to test these hypotheses (only three injured cephala were identified in this study).

When considering the thorax as a whole, *Olenellus fowleri* is arguably the most well defended taxon, with longer pleural spines on all segments except T3 relative to the other taxa assessed here. Conversely, *O. terminatus* and *Nephrolenellus geniculatus* have the shortest pleural spines. Although *O. terminatus* has the highest incidence of repair, the apparently well-defended *O. fowleri* has the second highest, and *N. geniculatus* the lowest. There is therefore no clear relationship between prothoracic pleurae spinosity and predation intensity, when all thoracic spines are considered together.

There is some support for the elongate T3 pleural spine acting as a deterrent. This spine is longest (dolichospinous) in *Nephrolenellus geniculatus*, the species that experienced the lowest predation intensity. As this spine extends to the posterior of the prothorax in all species considered, a dolichospinous T3 may have offered no more protection than a macrospinous T3. Thus any damage differences would be expected on the opisthothorax, as this area is protected by the dolichospinous condition but not the macrospinous. However the injury frequency on T3 compared to other thoracic segments does not provide evidence supporting a role for these spines in active defense as the frequency of T3 spine injuries is statistically indistinguishable from injuries on other thoracic pleural spines. Instead, we suggest that T3 spines likely acted primarily as a deterrent, dissuading predators from attacking altogether (and thus resulting in a lower predation intensity). Thus a trilobite with a longer spine may have been a less appealing target for a predator than one with shorter spines, resulting in *N. geniculatus* experiencing the lowest predation pressure with its doliichospinous T3, compared to the macrospinous *Olenellus*. As *Olenellus fowleri* has the relatively shortest T3 spines, it is possible that the remaining thoracic pleural spines provided less substantial

deterrent. This would explain why *O. terminatus* has the highest repair frequency with *O. fowleri* second highest. However, as the confidence intervals for *O. terminatus* and *O. fowleri* overlap substantially (Table 2), perhaps no such secondary deterrent explanation is required, and a larger sample size would reveal a higher repair frequency in *O. fowleri* than *O. terminatus*.

5.4 Other explanations

Size is not considered a major factor affecting predation pressure, as the lengths of injured and non-injured trilobite cephalothoraces are not statistically distinguished, however size may have played a minor role. Injured trilobites are on average larger than non-injured trilobites (Fig. 6). Additionally, *Olenellus fowleri* and *O. terminatus,* the taxa with the highest repair incidences and consequently the highest inferred predation pressure, have the largest mean and median sizes (Table 3). This may suggest that larger trilobites (regardless of the species) experienced higher predation pressure than smaller trilobites, perhaps as they offer a more substantial 'reward' for successful predators. The overall smaller size of *Nephrolenellus geniculatus* may therefore partly explain the lower predation pressure experienced by this species.

Other potential explanations for the lower predation pressure on *Nephrolenellus geniculatus* include behavioral adaptations. Predation pressure, as measured here, reflects failed fatal attacks on trilobites which caused some damage. Interactions with predators are more complex than just attacking, as predators must observe, catch, then kill prey. If *N. geniculatus* was more effective at hiding or escaping from predators, the number of injury-causing events would be lower, regardless of the number of interactions, producing the observed signal. Unfortunately, we do not have knowledge

of the relative hiding, escaping, and surviving capabilities of these taxa, and so we are limited to considering morphological features and injury-causing events.

5.5 Location-selectivity of repair

Thoracic injuries are far more common than cephalic examples in this study. Five cephalic injuries are present in the literature (Resser and Howell 1938; Alpert and Moore 1975; Cowie and McNamara 1978; Babcock 1993, 2007; Skinner 2004; Bicknell and Paterson 2018; Bicknell et al. 2018c). Two abnormal *Olenellus gilberti* prothoraces in Ruin Wash trilobites were reported by Palmer (1998, figs 9.2, 9.4), and thoracic injuries are known in other *Olenellus* taxa (Rudkin 1979; Whittington 1989), the closely related nevadiid trilobites (*sensu* Lieberman 1998) *Buenellus higginsi* (Babcock and Peel 2007), and *Nevadia weeksi* (Whittington 1989). No axial injuries are known to any Cambrian trilobite (Owen 1985; Babcock 1993; Bicknell and Paterson 2018), supported by the data in this study. Higher repair frequency of injuries to pleural lobes compared to axial lobes and cephala adds support to previous suggestions that trilobites are more likely to survive damage to pleural lobes than other exoskeletal parts. This is because vital nervous, alimentary and circulatory organ systems were likely housed in the axial lobe and cephalon (Babcock 1993), and likely exacerbated by the difficulties in identifying biologically (rather than taphonomically) damaged axial spines.

No evidence for thoracic injury stereotypy was found. This contrasts with data in Babcock and Robison (1989) and Babcock (1993), where a right-side injury stereotypy for Cambrian trilobites was demonstrated. The absence of stereotypy in this study mirrors the findings of Pates et al. (2017), for injuries to *Eccaparadoxides pradoanus* from the Murero Formation. Evidence for injury lateralization on Cambrian trilobites

presented by Babcock may potentially reflect lumping data from multiple taxa, across different temporal and geographical regions, masking taxon-specific palaeoecological signals. Further work exploring location-specific and taxon-level sampling of injuries on Cambrian trilobites is needed. A useful avenue would be the targeted analysis of taxa in the bulk sample of Babcock and Robison (1989) and Babcock (1993), to determine which individual species were responsible for the right-sided signal.

6. Conclusions

This is the first study to show evidence for predator selectivity on trilobites from the same site and suggests that phenotypic differences resulted in differences in predation intensity. We identified injuries on thoraces and cephala of five trilobite taxa from the Ruin Wash *Lagerstätte: Olenellus chiefensis, O. fowleri, O. gilberti, O. terminatus,* and *Nephrolenellus geniculatus.* Thoracic injuries are far more common than cephalic injuries. The highest injury repair frequency of the five taxa was found for *O. terminatus* and the lowest for *N. geniculatus*. Differences in repair frequencies are likely a result of predation intensity, not predator (in)efficiency. This is suggested as the taxon with the highest percentage of articulated remains experienced the lowest repair frequency. If instead predation on this taxon was the most efficient, *N. geniculatus* would be expected to be the taxon with the lowest percentage with articulated remains.

We propose that elongate spines on T3 spines on these taxa acted as predator-deterrent features for this group. Of the proposed measures of spinosity, the elongate spines on T3 offer the best case for a morphological feature affecting predation intensity. These spines were not used in active defense, and instead it is suggested that T3 pleural spines on olenelline taxa were predation deterrents in the Ruin Wash

Lagerstätte. The role of genal or axial T15 spines as predation deterrents or in defense of the axial lobe or cephalon could not be tested as too few injuries were recorded on these parts. Size may have played an additional minor role in predator selection as injured trilobites were on average larger than trilobites without injuries, but no statistical support for this was found.

7. Acknowledgments

We thank the editor Thomas Algeo (University of Cincinnati), Olev Vinn (University of Tartu), and an anonymous reviewer, for their comments and suggestions, which greatly improved the manuscript and refined our interpretation of these results. SP was funded by a Schuchert and Dunbar Grant-in-Aid from the Yale Peabody Museum, and a Santander Travel Award, for visits to museums for this project, and is supported by an Oxford-St Catherine's Brade-Natural Motion Scholarship. RDCB is supported by an Australian Postgraduate Award. We thank S. Butts (YPM), J. Cundiff (MCZ), P. Mayer (FMNH), J. Utrup (YPM), and M. Webster (ICS) for facilitating access to specimens. We thank S. Zamora (Instituto Geológico y Minero de España) for the suggestion to study the Ruin Wash trilobites, M. Webster (Chicago University) and H. Drage (University of Oxford) for discussions of the Ruin Wash and trilobite moulting respectively, and A. C. Daley (University of Lausanne) for reading an earlier version of the manuscript and offering suggestions.

8. References

Adrain, J. M., Fortey, R. A., & Westrop, S. R. (1998). Post-Cambrian trilobite diversity and evolutionary faunas. Science, 280(5371), 1922-1925.

Alexander, R. R. (1981). Predation scars preserved in Chesterian brachiopods: probable culprits and evolutionary consequences for the articulates. Journal of Paleontology, 55(1) 192-203.

Alexander, R. R. (1986). Resistance to and repair of shell breakage induced by durophages in Late Ordovician brachiopods. Journal of Paleontology, 60(2), 273-285.

Alexander, R. R., & Dietl, G. P. (2001). Shell repair frequencies in New Jersey bivalves: a recent baseline for tests of escalation with Tertiary, Mid-Atlantic congeners. Palaios, 16(4), 354-371.

Alexander, R. R., & Dietl, G. P. (2003). The fossil record of shell-breaking predation on marine bivalves and gastropods. In Predator—Prey Interactions in the Fossil Record (eds. Kelley, P., Kowalewski, M., Hansen, T. A.) (pp. 141-176). Springer, Boston, MA.

Alpert, S. P., & Moore, J. N. (1975). Lower Cambrian trace fossil evidence for predation on trilobites. Lethaia, 8(3), 223-230.

Babcock, L. E. (1993). Trilobite malformations and the fossil record of behavioral asymmetry. Journal of Paleontology, 67(2), 217-229.

Babcock, L. E. (2003). Trilobites in Paleozoic predator-prey systems, and their role in reorganization of early Paleozoic ecosystems. In Predator—prey interactions in the fossil record (eds. Kelley, P., Kowalewski, M., Hansen, T. A.) (pp. 55-92). Springer, Boston, MA.

Babcock, L. E. (2007). Role of malformations in elucidating trilobite paleobiology: a historical synthesis. Fabulous Fossils–300 Years of Worldwide Research on Trilobites, 3-19.

Babcock, L. E., & Robison, R. A. (1989). Preferences of Palaeozoic predators. Nature, 337 (6209), 695-696.

Babcock, L. E., & Peel, J. S. (2007). Palaeobiology, taphonomy and stratigraphic significance of the trilobite Buenellus from the Sirius Passet Biota, Cambrian of North Greenland. Memoirs of the Association of Australasian Palaeontologists, (34), 401.

Bengtson, S. (2002). Origins and early evolution of predation. The Paleontological Society Papers, 8, 289-318.

Bicknell R. D. C. , Ledogar J. A. , Wroe S., Gutzler B. C., Watson III W. H., Paterson, J. R. (2018a). Computational biomechanical analyses demonstrate similar shell-crushing abilities in modern and ancient arthropods. Proceedings of the Royal Society B, 285 (1889), 20181935.

Bicknell, R. D. C., & Paterson, J. R. (2018). Reappraising the early evidence of durophagy and drilling predation in the fossil record: implications for escalation and the Cambrian Explosion. Biological Reviews, 93(2), 754-784.

Bicknell R. D. C, Paterson, J. R., Caron, J.-B., & Skovsted, C., B. (2018b) The gnathobasic spine microstructure of Recent and Silurian chelicerates and the Cambrian artiopodan *Sidneyia*: functional and evolutionary implications. Arthropod Structure & Development, 47 (1), 12–24.

Bicknell, R. D. C., Pates, S., & Botton, M. L. (2018c). Abnormal xiphosurids, with possible application to Cambrian trilobites. Palaeontologia Electronica, 21(2), 1-17.

Bruton, D. L. (1981). The arthropod *Sidneyia inexpectans*, Middle Cambrian, Burgess Shale, British Columbia. Philosophical Transactions of the Royal Society of London. Series B, Biological Sciences, 295(1079), 619-653.

Budd, G., & Mann, R. P. (2018). Modelling predation and mortality rates from the fossil record of gastropods. bioRxiv, 373399.

Conway Morris, S. (1977). A redescription of the Middle Cambrian worm *Amiskwia sagittiformis* Walcott from the Burgess Shale of British Columbia. Paläontologische Zeitschrift, 51(3-4), 271-287.

Cowie, J., & McNamara, K. J. (1978). *Olenellus* (Trilobita) from the Lower Cambrian strata of north-west Scotland. Palaeontology, 21(3), 615-634.

Daley, A. C., & Drage, H. B. (2016). The fossil record of ecdysis, and trends in the moulting behaviour of trilobites. Arthropod Structure & Development, 45(2), 71-96.

Daley, A. C., Paterson, J. R., Edgecombe, G. D., García-Bellido, D. C., & Jago, J. B. (2013). New anatomical information on *Anomalocaris* from the Cambrian Emu Bay Shale of South Australia and a reassessment of its inferred predatory habits. Palaeontology, 56(5), 971-990.

Dietl, G. P. (2003a). Coevolution of a marine gastropod predator and its dangerous bivalve prey. Biological Journal of the Linnean Society, 80(3), 409-436.

Dietl, G. P. (2003b). Interaction strength between a predator and dangerous prey: *Sinistrofulgur* predation on *Mercenaria*. Journal of Experimental Marine Biology and Ecology, 289(2), 287-301.

Dietl, G. P., & Hendricks, J. R. (2006). Crab scars reveal survival advantage of left-handed snails. Biology Letters, 2(3), 439-442.

Dietl, G. P., Alexander, R. R., & Bien, W. F. (2000). Escalation in Late Cretaceous-early Paleocene oysters (Gryphaeidae) from the Atlantic Coastal Plain. Paleobiology, 26(2), 215-237.

Dietl, G. P., Durham, S. R., & Kelley, P. H. (2010). Shell repair as a reliable indicator of bivalve predation by shell-wedging gastropods in the fossil record. Palaeogeography, Palaeoclimatology, Palaeoecology, 296(1-2), 174-184.

Drage, H. submitted. *Quantifying intra- and interspecific variability in trilobite moulting behavior across the Palaeozoic*.

Drage, H. B., Holmes, J. D., García-Bellido, D. C., & Daley, A. C. (2018). An exceptional record of Cambrian trilobite moulting behaviour preserved in the Emu Bay Shale, South Australia. Lethaia, 51(4), 473-492.

English, A. M., & Babcock, L. E. (2010). Census of the Indian Springs Lagerstätte, Poleta Formation (Cambrian), western Nevada, USA. Palaeogeography, Palaeoclimatology, Palaeoecology, 295(1-2), 236-244.

Erwin, D. H., & Valentine, J. W. (2013). The Cambrian explosion. Genwodd Village, Colorado: Roberts and Company.

Esteve, J., Hughes, N. C., & Zamora, S. (2011). Purujosa trilobite assemblage and the evolution of trilobite enrolment. Geology, 39(6), 575-578.

Esteve, J., Hughes, N. C., & Zamora, S. (2013). Thoracic structure and enrolment style in middle Cambrian *Eccaparadoxides pradoanus presages* caudalization of the derived trilobite trunk. Palaeontology, 56(3), 589-601.

Fatka, O., & Budil, P. (2014). Sheltered gregarious behavior of middle Ordovician harpetid trilobite. Palaios, 29(9), 495-500.

Foote, M. (1991). Morphologic patterns of diversification: examples from trilobites. Palaeontology, 34(2), 461-485.

Fortey, R. A. (1986). The type species of the Ordovician trilobite *Symphysurus*: systematics, functional morphology and terrace ridges. Paläontologische Zeitschrift, 60(3-4), 255-275.

Fortey, R. A., Owens, R. M. (1999). The trilobite exoskeleton. Functional morphology of the invertebrate skeleton, 42(3), 537-562.

Harper, E. M. (2016). Uncovering the holes and cracks: from anecdote to testable hypotheses in predation studies. Palaeontology, 59(5), 597-609.

Harper, E. M., & Peck, L. S. (2016). Latitudinal and depth gradients in marine predation pressure. Global Ecology and Biogeography, 25(6), 670-678.

Harper, E. M., Peck, L. S., & Hendry, K. R. (2009). Patterns of shell repair in articulate brachiopods indicate size constitutes a refuge from predation. Marine Biology, 156(10), 1993-2000.

Hartnoll, R. G., & Bryant, A. D. (1990) Size-Frequency Distributions in Decapod Crustacea: The Quick, the Dead, and the Cast-Offs. *Journal of Crustacean Biology*, 10(1), 14-19.

Henningsmoen, G. (1975). Moulting in trilobites. Fossils and Strata, 4, 179-200.

Huntley, J. W., & Kowalewski, M. (2007). Strong coupling of predation intensity and diversity in the Phanerozoic fossil record. Proceedings of the National Academy of Sciences, 104(38), 15006-15010.

Jago, J. B., García-Bellido, D. C., & Gehling, J. G. (2016). An early Cambrian chelicerate from the Emu Bay Shale, South Australia. Palaeontology, 59(4), 549-562.

Kelley, P. H. (1989). Evolutionary trends within bivalve prey of Chesapeake Group naticid gastropods. Historical Biology, 2(2), 139-156.

Kimmig, J., & Strotz, L. C. (2017). Coprolites in mid-Cambrian (Series 2-3) Burgess Shale-type deposits of Nevada and Utah and their ecological implications. Bulletin of Geosciences, 92(3), 297-309.

Klompmaker, A. A., & Kelley, P. H. (2015). Shell ornamentation as a likely exaptation: evidence from predatory drilling on Cenozoic bivalves. Paleobiology, 41(1), 187-201.

Klompmaker, A. A., Kowalewski, M., Huntley, J. W., & Finnegan, S. (2017). Increase in predator-prey size ratios throughout the Phanerozoic history of marine ecosystems. Science, 356(6343), 1178-1180.

Knoll, A. H. (2003). Biomineralization and evolutionary history. Reviews in Mineralogy and Geochemistry, 54(1), 329-356.

Kowalewski, M. (2002). The fossil record of predation: an overview of analytical methods. The Paleontological Society Papers, 8, 3-42.

Kowalewski, M., Dulai, A., & Fursich, F. T. (1998). A fossil record full of holes: the Phanerozoic history of drilling predation. Geology, 26(12), 1091-1094.

LaBarbera, M. (1981). The ecology of Mesozoic *Gryphaea, Exogyra*, and *Ilymatogyra* (Bivalvia: Mollusca) in a modern ocean. Paleobiology, 7(4), 510-526.

Leighton, L. R. (2011). Analyzing predation from the dawn of the Phanerozoic. In Quantifying the Evolution of Early Life (eds. M. Laflamme, J. D. Schiffbauer, S. Q Dornbos) (pp. 73-109). Springer, Dordrecht.

Lieberman, B. S. (1998). Cladistic analysis of the Early Cambrian olenelloid trilobites. Journal of Paleontology, 72(1), 59-78.

Molinaro, D. J., Stafford, E. S., Collins, B. M., Barclay, K. M., Tyler, C. L., & Leighton, L. R. (2014). Peeling out predation intensity in the fossil record: a test of repair scar

frequency as a suitable proxy for predation pressure along a modern predation gradient. Palaeogeography, Palaeoclimatology, Palaeoecology, 412(2014), 141-147.

Owen, A. W. (1985). Trilobite abnormalities. Earth and Environmental Science Transactions of the Royal Society of Edinburgh, 76(2-3), 255-272.

Pates, S., Bicknell, R. D. C., Daley, A. C., & Zamora, S. (2017). Quantitative analysis of repaired and unrepaired damage to trilobites from the Cambrian (Stage 4, Drumian) Iberian Chains, NE Spain. Palaios, 32(12), 750-761.

Pates, S., and Bicknell, R. D. C. (2018). Specimen Data: Elongated Thoracic Spines as Potential Predatory Deterrents in Olenelline Trilobites from the Lower Cambrian of Nevada. OSF. Retrieved from:osf.io/974yh.

Paine, R. T. (1976). Size-limited predation: an observational and experimental approach with the Mytilus-Pisaster interaction. Ecology, 57(5), 858-873.

Palmer, A. R. (1998). Terminal early Cambrian extinction of the Olenellina: documentation from the Pioche Formation, Nevada. Journal of Paleontology, 72(4), 650-672.

Pratt, B. R. (1998). Probable predation on Upper Cambrian trilobites and its relevance for the extinction of soft-bodied Burgess Shale-type animals. Lethaia, 31(1), 73-88.

R Core Team. (2014). R: A language and environment for statistical computing.

Resser, C. E., & Howell, B. F. (1938). Lower Cambrian *Olenellus* Zone of the Appalachians. Bulletin of the Geological Society of America, 49(2), 195-248.

Rudkin, D. M. (1979). Healed injuries in *Ogygopsis klotzi* (Trilobita) from the Middle Cambrian of British Columbia. Royal Ontario Museum, Life Sciences Occasional Paper, 32, 1-8.

Schoener, T. W. (1979). Inferring the properties of predation and other injury-producing agents from injury frequencies. Ecology, 60(6), 1110-1115.

Skinner, E. S. (2004). Taphonomy of exceptionally preserved fossils from the Kinzers Formation (Cambrian), southeastern Pennsylvania (Doctoral dissertation, The Ohio State University).

Smith, M. P., & Harper, D. A. (2013). Causes of the Cambrian explosion. Science, 341(6152), 1355-1356.

Sprinkle, J. (1973). Morphology and evolution of blastozoan echinoderms. Museum of Comparative Zoology, Harvard.

Sperling, E. A., Frieder, C. A., Raman, A. V., Girguis, P. R., Levin, L. A., & Knoll, A. H. (2013). Oxygen, ecology, and the Cambrian radiation of animals. Proceedings of the National Academy of Sciences, 110(33), 13446-13451.

Stafford, E. S., Tyler, C. L., & Leighton, L. R. (2015). Gastropod shell repair tracks predator abundance. Marine Ecology, 36(4), 1176-1184.

Vannier, J. (2012). Gut contents as direct indicators for trophic relationships in the Cambrian marine ecosystem. PLoS ONE, 7(12), e52200.

Vannier, J., & Chen, J. (2005). Early Cambrian food chain: new evidence from fossil aggregates in the Maotianshan Shale biota, SW China. Palaios, 20(1), 3-26.

Venables, W. N. & Ripley, B. D. (2002) Modern Applied Statistics with S. Fourth Edition. Springer, New York. ISBN 0-387-95457-0

Vendrasco, M. J., Kouchinsky, A. V., Porter, S. M., & Fernandez, C. Z. (2011). Phylogeny and escalation in *Mellopegma* and other Cambrian molluscs. Palaeontologia Electronica, 14(2), 1-44.

Vermeij, G. J. (1977). The Mesozoic marine revolution: evidence from snails, predators and grazers. Paleobiology, 3(3), 245-258.

Vermeij, G. J. (1987). Evolution and Escalation. 527 pp. Princeton University Press, Princeton.

Vermeij, G. J. (1989). The origin of skeletons. Palaios 4(6), 585-589.

Vermeij, G. J. (2002). Evolution in the consumer age: predators and the history of life. The Paleontological Society Papers, 8, 375-394.

Vermeij, G. J. (2013). On escalation. Annual Review of Earth and Planetary Sciences, 41, 1-19.

Vermeij, G. J., Schindel, D. E., & Zipser, E. (1981). Predation through geological time: evidence from gastropod shell repair. Science, 214(4524), 1024-1026.

Vinn, O. (2018). Traces of predation in the Cambrian. Historical Biology, 30(8), 1043-1049.

Webster, M. (2007a). A Cambrian peak in morphological variation within trilobite species. Science, 317(5837), 499-502.

Webster, M. (2007b). Ontogeny and Evolution of the Early Cambrian Trilobite Genus *Nephrolenellus* (Olenelloidea). Journal of Paleontology, 81(6), 1168-1193.

Webster, M. (2015). Ontogeny and intraspecific variation of the early Cambrian trilobite *Olenellus gilberti*, with implications for olenelline phylogeny and macroevolutionary trends in phenotypic canalization. Journal of Systematic Palaeontology, 13(1), 1-74.

Webster, M., & Hughes, N. C. (1999). Compaction-related deformation in Cambrian olenelloid trilobites and its implications for fossil morphometry. Journal of Paleontology, 73(2), 355-371.

Webster, M., Gaines, R. R., & Hughes, N. C. (2008). Microstratigraphy, trilobite biostratinomy, and depositional environment of the “lower Cambrian” Ruin Wash Lagerstätte, Pioche Formation, Nevada. Palaeogeography, Palaeoclimatology, Palaeoecology, 264(1-2), 100-122.

Whittington, H. B. (1989). Olenelloid tribolites: type species, functional morphology and higher classification. Philosophical Transactions of the Royal Society of London B, 324(1221), 111-147.

Wood, R., & Zhuravlev, A. Y. (2012). Escalation and ecological selectively of mineralogy in the Cambrian Radiation of skeletons. Earth-Science Reviews, 115(4), 249-261.

Zacaï, A., Vannier, J., & Lerosey-Aubril, R. (2016). Reconstructing the diet of a 505-million-year-old arthropod : *Sidneyia inexpectans* from the Burgess Shale fauna. Arthropod Structure & Development, 45, 200-220.

Zhang, X., Shu, D., Han, J., Zhang, Z., Liu, J., & Fu, D. (2014). Triggers for the Cambrian explosion: hypotheses and problems. Gondwana Research, 25(3), 896-909.

Zhu, M.–Y., Vannier, J., Iten, H. V., & Zhao, Y. L. (2004) Direct evidence for predation on trilobites in the Cambrian. Proceedings of the Royal Society of London B: Biological Sciences, 271(2004), S277-S280.

Competing interests

There are no competing interests to report

Chapter 14

Discussion and Conclusions

Discussion and Conclusions

In order to understand the role of predation in shaping the evolution of Cambrian animals, I have presented a detailed analysis of the diversity and disparity of the largest nektonic animals of the time, the radiodonts, and the first studies of predation pressure on trilobites, a diverse and disparate group of prey animals. These two strands of information, from radiodonts and trilobites, both provide evidence for a complex ecological picture during the early Cambrian, and suggest that evolutionary pressures related to predation, and feeding modes in general, played a role in the evolutionary histories of both radiodonts and trilobites.

Radiodonts: Summary of thesis findings

A re-examination of radiodont material, alongside newly collected specimens, from USA Burgess Shale- type *Lagerstätten* (BSTs) revealed a higher than expected diversity of radiodonts from the USA. Members of all radiodont families, alongside *Caryosyntrips* and two taxa of uncertain affinity (*Laminacaris*? from the Kinzers Formation, and *Ursulinacaris grallae*) were identified. Frontal appendages proved to be highly useful in taxonomic identification, and taphonomic pathways for this body part were identified. Hurdiids appear to have had larger geographic ranges, at least in Laurentia, than anomalocaridids. USA BSTs did not just increase the temporal and geographic ranges for already known radiodont taxa, but substantially increased our knowledge of the number of radiodont taxa and revealed hitherto unknown morphologies of the frontal appendage. Of particular note, the Kinzers Formation provided the most diverse Stage 4

radiodont fauna of any site worldwide, even compared to the much more comprehensively studied and sampled Emu Bay Shale, Australia (e.g. McHenry & Yates 1993; Nedin 1999; Paterson et al. 2011, 2016; Daley et al. 2013a). The importance of USA BSTs is emphasised by the four named radiodont taxa known only from these deposits (*Anomalocaris magnabasis, A. pennsylvanica, Caryosyntrips durus,* and *Pahvantia hastata*), and a further four described specimens left in open nomenclature that likely represent new radiodont species or genera (*Laminacaris*? and *Tamisiocaris* sp. from the Kinzers Formation, *Stanleycaris* sp. from the Wheeler Formation, and the hurdiid body specimen from the Spence Shale).

These additional taxa, and new information and characters from redescribed taxa, allowed me to conduct a phylogenetic analysis with the most comprehensive sampling of hurdiids to date. Two phylogenetic hypotheses were recovered, dependent on the concavity constant used in the parsimony analysis. The first predicts that paired, elongate, slender endites represents the plesiomorphic condition, the second that the hurdiid arrangement of having elongated endites on only the proximalmost five podomeres in the distal articulated region is plesiomorphic, meaning that taxa with endites along the length of the appendage are more derived. Our current knowledge of radiodonts means that we do not have the data to choose between these hypotheses. Although there are slight differences in these two topologies, this analysis showed that hurdiids were sister to a clade containing all other radiodont families, unlike all previous analyses where hurdiids and tamisiocaridids formed one clade, with amplectobeluids and anomalocaridids forming the other (Vinther et al. 2014; Cong et al. 2014; Van Roy et al. 2015; Liu et al. 2018; Lerosey-Aubril & Pates 2018).

USA BSTs provide a high temporal resolution view of radiodont diversity and disparity from Stage 4 to the Drumian, which shows that although the three most diverse families, amplectobeluids, anomalocaridids, and hurdiids, have similar disparities of frontal appendages, their evolutionary histories are different. Amplectobeluids and anomalocaridids peak in diversity and disparity early, and become rare after 509 Ma. In contrast hurdiids are rare before 509 Ma, but expand into new areas of morphospace and continue to diversify after this time through into the Ordovician and perhaps Devonian. No extrinsic factors satisfactorily explain this turnover, and the later success of hurdiids could reflect this ability to continue to innovate ecologically, with the repeated evolution of a filter-feeding habit (Van Roy et al. 2015; Lerosey-Aubril & Pates 2018).

As the largest nektonic animals of the time, radiodonts would have applied top-down predation pressure on ecosystems. As shown by these studies, radiodonts would not have applied this pressure consistently throughout the Cambrian, with the ecology and diversity of radiodonts before and after the beginning of the Wuliuan being very different. As such, the role of radiodonts in shaping Cambrian evolution would have been variable. Conversely, predation on radiodonts by other taxa may have also played a role in shaping the evolution of radiodonts. The raptorial radiodont predators that became much less diverse and disparate, especially in the Wuliuan, may have been outcompeted by other predators more able to quickly subdue prey, and to break hard exoskeletons when required, such as gnathobase-bearing sanctacaridids and other artiopodans. The greater durophagous abilities of these animals is underlined by the presence of gut contents containing mineralised fragments, including trilobites in some cases, in members from the Chengjiang biota (Stage 3), the Emu Bay Shale (Stage 4),

and the Spence Shale (Wuliuan) (Conway Morris & Robison 1988; Zhu et al. 2004; Jago et al. 2016; Legg & Pates 2016), and by a recent Finite Element Analysis study on the gnathobases of *Sidneyia* (Bicknell et al. 2018).

Radiodonts: Future opportunities from deposits of different ages and locations

The USA BSTs have provided a good picture of radiodont diversity and disparity from the middle of Stage 4 up until the Drumian, however the picture from 521 Ma until 513 Ma is less clear. A number of BSTs of suitable age, and younger, are known from China, such as the Shuijingtuo Formation, Wulongqing Formation, Guanshan biota, Balang Formation, Kaili biota, and Mantou Formation (Cui & Huo 1990; Zhao et al. 2005; Daley et al. 2009, 2013b; Huang et al. 2012; Weber et al. 2012; Liu 2013; Wang et al. 2013). A restudy of these sites, and their constituent radiodonts, would provide crucial information on the diversity and disparity of radiodonts at this time, and may result in additional new taxa, as was the case for the USA BSTs. Restudy of these sites would also provide a temporal overlap between Chinese and Laurentian sites, thus allowing more certainty to be placed on the global radiodont diversity signal, through a better understanding of geographical variation. Of critical importance would be discoveries of any hurdiid taxa of Stage 4 and older, to better understand how quickly the diversity of this family increased, and any morphological changes in the frontal appendage that may have led to the apparently rapid increases in diversity of this group in the Wuliuan. Amplectobeluids and anomalocaridids of Wuliuan and younger would also provide vital information on the morphology of these appendages and diversity of these families after their peak diversity and disparity in Stages 3 and 4.

The discovery of Drumian and younger BSTs will improve our understanding of the success of radiodonts from the Miaolingian to the Ordovician, although the apparent beginning of the closing of the taphonomic window for BSTs during the Drumian makes this challenging. Continued discoveries of radiodonts from the Fezouata biota (following Van Roy & Briggs 2011; Van Roy et al. 2015) will show if any of the other radiodont families (or *Caryosyntrips*) persisted beyond the Cambrian. From the data presented in this thesis, it would be expected that *Caryosyntrips* is the most likely non-hurdiid radiodont to be found in deposits of Ordovician age.

Finally, the further study of BSTs outside of Laurentia and China will give a far more accurate picture of the global distribution of radiodonts. This thesis has provided data suggesting that hurdiids have a greater geographic range than amplectobeluids or anomalocaridids, and a larger sample size of BSTs containing radiodont fossils will allow such observations to be quantitatively tested at the species level using biogeographic techniques (for example similar to the work that Hendricks et al. 2008 performed comparing soft-bodied and mineralised taxa). Concerted fieldwork efforts outside of North America and China would be required to identify suitable deposits, and then collect sufficient material to find radiodonts, however the relatively high preservation potential of radiodont frontal appendages when compared to other BST specimens makes such studies feasible.

Radiodonts: Future opportunities from novel methodologies

As modern analogues for radiodont feeding are currently lacking, computational modelling may help to resolve details of their predatory behaviour, and compare feeding abilities between closely related taxa. Pilot studies on the oral cones using Finite

Element Analysis have been conducted, but never published (Hagadorn 2009; Hagadorn et al. 2010), and we now know much more about radiodont oral cones (Daley & Bergström 2012; Liu et al. 2018; Zeng et al. 2018) and other non-frontal appendage feeding structures (e.g. Cong et al. 2017, 2018).

The frontal appendages of radiodonts could also be comparatively analysed using such techniques, and to test hypotheses related to escalation. One study could examine trends within the radiodont families Amplectobeluidae and Anomalocarididae, which are suggestive of increased competition, and a drive towards more specialised raptorial predation. In Cambrian Stage 3 and Stage 4, these families are diverse and occupy neighbouring and slightly overlapping volumes in morphospace. In contrast, the Burgess Shale (Wuliuan) taxa *Amplectobelua stephenensis* and *Anomalocaris canadensis* appear more specialised for tight coiling and potentially crushing/slicing than the closely related taxa *Amplectobelua symbrachiata* and *Anomalocaris saron* from the Chengjiang biota (Stage 3), and the diversity of these families at this time is very low. The specialisation of these appendages towards tighter raptorial grabbing/crushing could be tested through an application of Finite Element Analysis. Without an appreciation of the three-dimensional qualities of these appendages, absolute values for the power of these appendages would have to be treated with caution, however the relative abilities of taxa could still be assessed, and thus a hypothesis of increased specialisation for particular ecologies quantitatively tested.

Trilobite repaired injuries: Summary of thesis findings

The case studies exploring predation pressure on trilobites in this thesis demonstrated that predation pressure was not constant during the Cambrian. Factors affecting

predation pressure on trilobites include geography and morphology, and potentially also time. As such, predation had the potential to shape the evolution of trilobites, for example by driving poorly defended species into quiet refugia or latitudinal bands with low predation, or even reinforcing particular anti-predatory morphologies.

This thesis has provided a stable methodology for studying trilobite repaired injuries to assess predation pressure on these Palaeozoic arthropods. However large sample sizes of autochthonous and articulated trilobites are necessary to perform statistical tests of hypotheses, as repair frequencies are relatively low (compared for example to brachiopods and gastropods, e.g. Vermeij et al. 1981, Alexander 1986, but caution should be used when comparing ecdysozoan repair frequencies to other taxa, e.g. Pates et al. 2017). This low repair frequency suggests that durophagous predators on Cambrian trilobites were relatively successful (i.e. that a large proportion of attacked trilobites were killed). The predominance for injuries to the pleural lobes of the thorax when compared to the cephalon (very rare) or axial lobe (unknown), suggests that attacks to the head or central lobe of the body were particularly lethal (as suggested by Babcock 1993). It is unlikely that it reflects an absence of attacks to these body parts, as trilobite sclerites which have been split through the axial lobe, and through the cephalon, are common at both Ruin Wash, and the Cambrian Spanish sites where the studies of repaired injuries were conducted.

Trilobite repaired injuries: Future directions

The case studies from this thesis have provided evidence that some morphological and geographic factors were important for trilobite predation pressure at particular places and times. A more comprehensive sampling of Cambrian trilobites, and testing of a

number of hypotheses relating to different morphologies, behaviours, and environments, is still required in order to fully explore the impact of these variables on trilobite predation pressure, and hence the potential that predation shaped aspects of trilobite evolution at a larger scale.

Further case studies examining the role of the environment, body size, and morphology on trilobite predation pressure, include: *Elrathia kingii* from the Wheeler Formation, where a fluctuating oxygen level has been demonstrated, and abundant specimens can be easily collected (Gaines & Droser 2003); *Paradoxides davidis* from the Manuels River Formation, where large and articulated trilobites (>30 cm) are known, with repaired injuries (Bergström & Levi-Setti 1978); and the Builth Inlier, where eight genera are known in great abundance (>15,000 specimens) from levels sampled at high temporal resolution (Sheldon 1987, 1988). The examination of particular putative anti-predatory morphologies along evolutionary lineages could be explored, and the predation pressure quantified, to infer the coupling of a putative evolutionary driver (predation) and morphology.

If trilobites are to provide data on predation pressure for the early Palaeozoic (as suggested by Leighton 2011), a large number of data points at each time bin is required, so as to account for the variation (owing to e.g. morphology, geography) in predation pressure identified in this thesis, and also the potential variation owing to the variables identified above. Only then will patterns of predation pressure over longer stretches of time be able to be distinguished from other ecological and environmental noise, allowing us to confidently use trilobite predation pressure to identify and explore the escalation in predation through the Cambrian or Palaeozoic, and its relation to larger

extrinsic factors such as carbon isotope excursions, anoxic events, and global mixing of faunas (e.g. Babcock et al. 2015; Holmes et al. 2018; Zhuravlev & Wood 2018).

Implications for the role of predation in shaping evolution during the Cambrian

Predation pressure was complex and apparently changeable during the Cambrian. Radiodonts, the largest nektonic animals of the time, did not apply a consistent top-down pressure, as the evolutionary history of the group shows a decline in raptorial predators around 509 Ma, with an influx of sediment sifters and filter feeders. Radiodont families and genera appear to have gone through periods of stasis, and periods of rapid change (e.g. between Stage 4 and the Wuliuan- *this thesis Chapter 10*), however whether this is owing to intrinsic developmental innovations, extrinsic factors, or is a reaction to changes in prey animals, is currently not clear. What is known is that the group shows at least two non-conforming evolutionary trajectories that cannot be adequately linked as one to extrinsic factors during the Cambrian. The situation for trilobite anti-predatory behaviours and morphologies is also complex, with trilobites showing variation in their antipredatory strategies even early in their evolution. At this time we do not have enough data points currently to assess how predation pressure was changing through the Cambrian, however many complex anti-predatory behaviours (such as enrolment) and morphological features, such as elongate spines, have been shown to influence or have been influenced by predation pressure in the case studies presented in this thesis. Elongate spines and/or enrolment are known in some of the earliest trilobites, such as *Fallotaspis* (Cambrian Stage 3, Morocco; Geyer 1996) and *Mummaspis* (lower Stage 4, Canada; Ortega-Hernández et al. 2013), respectively. Thus the apparent rapid appearance of this group, with anti-predatory behaviours and

morphologies already in existence, could inform us of the role of predation in the evolutionary dynamics among these oldest trilobites. The variation in successful strategies, and the high disparity of trilobites at this time, may also be linked.

Predation pressure also apparently varied within close geographic areas, and the identity of the large nektonic animals was not constant through this time. As such predation pressure was dependent on a large number of variables even over 509 million years ago, and the optimisation of these variables by predators and prey to increase their chances of success in predator-prey encounters would allow a role for predation in shaping evolution at this time.

Conclusions

Stephen J. Gould observed that 'many of the finest … discoveries are made in museum drawers'. Although I make no claims that the discoveries and data in this thesis belong with 'the finest', this work has once again demonstrated the value of bringing new information, techniques, and questions, to existing museum collections. In particular, this project benefitted from recent rapid increases in our knowledge of radiodonts from the Chengjiang biota and Burgess Shale, and the new imaging and analysis tools that these studies had utilised (e.g. Daley et al. 2009, 2013b; Daley & Budd 2010; Cong et al. 2014, 2016, 2017, 2018), and historical collections of radiodonts from the USA (e.g. Resser 1929; Briggs 1979; Briggs & Mount 1982; Briggs & Robison 1984; Conway Morris & Robison 1988; Lieberman 2003; Briggs et al. 2008). Similarly the extensive collection of trilobites from the Ruin Wash, from fieldwork conducted in 1999 (Webster et al. 2008) provided a large indirect bulk sample for a study of predation that would have taken a substantial amount of time to collect *de novo*.

The availability of large amounts of fossils and data from the restudy of these museum collections allowed the translation of morphology and individual repaired injuries into quantitative datasets which can be used to support or refute hypotheses of ecological and evolutionary studies. For Radiodonta, I conducted the first comprehensive study of the diversity and disparity of this group through the Cambrian, and for trilobites I performed the first quantitative studies of repaired damage frequencies on trilobite exoskeletons.

These studies, datasets, and analyses provide groundwork which has the potential to be expanded into quantitative studies exploring the evolution of ecosystems during the Cambrian. More progress has been made in this thesis on the evolutionary history of radiodonts (though finer details will still emerge from the restudy of Chinese material, and new material from other BSTs) than for trilobites, but both these strands (radiodonts and trilobites) will provide crucial information on the finer-scale dynamics of the radiation of animals during the Cambrian, and the emergence of modern style ecosystems, oceans, and body-plans.

References

Alexander, R. R. (1986). Resistance to and repair of shell breakage induced by durophages in Late Ordovician brachiopods. Journal of Paleontology, 60(2), 273-285.

Babcock, L. E. (1993). Trilobite malformations and the fossil record of behavioral asymmetry. *Journal of Paleontology*, 67(2), 217-229.

Babcock, L. E., Peng, S. C., Brett, C. E., Zhu, M. Y., Ahlberg, P., Bevis, M., & Robison, R. A. (2015). Global climate, sea level cycles, and biotic events in the Cambrian Period. *Palaeoworld*, 24(1-2), 5-15.

Bergström, J., & Levi-Setti, R. (1978). Phenotypic variation in the Middle Cambrian trilobite *Paradoxides davidis* Salter at Manuels, SE Newfoundland. *Geologica et Palaeontologica*, 12, 1-40.

Bicknell R. D. C., Ledogar J. A. , Wroe S., Gutzler B. C., Watson III W. H., Paterson, J. R. (2018). Computational biomechanical analyses demonstrate similar shell-crushing abilities in modern and ancient arthropods. Proceedings of the Royal Society B, 19-35. doi: 10.1098/rspb.2018.1935

Briggs, D. E. (1979). *Anomalocaris*, the largest known Cambrian arthropod. *Palaeontology*, 22(3), 631-664.

Briggs, D. E., & Mount, J. D. (1982). The occurrence of the giant arthropod *Anomalocaris* in the Lower Cambrian of southern California, and the overall distribution of the genus. *Journal of Paleontology*, 56(5), 1112-1118.

Briggs, D. E., & Robison, R. A. (1984). Exceptionally preserved nontrilobite arthropods and *Anomalocaris* from the Middle Cambrian of Utah. *University of Kansas Paleontological Contributions*, 111, 1-23.

Briggs, D. E., Lieberman, B. S., Hendricks, J. R., Halgedahl, S. L., & Jarrard, R. D. (2008). Middle Cambrian arthropods from Utah. *Journal of Paleontology*, 82(2), 238-254.

Cong, P., Ma, X., Hou, X., Edgecombe, G. D., & Strausfeld, N. J. (2014). Brain structure resolves the segmental affinity of anomalocaridid appendages. *Nature*, 513(7519), 538.

Cong, P., Daley, A. C., Edgecombe, G. D., Hou, X., & Chen, A. (2016). Morphology of the radiodontan *Lyrarapax* from the early Cambrian Chengjiang biota. *Journal of Paleontology*, 90(4), 663-671.

Cong, P., Daley, A. C., Edgecombe, G. D., & Hou, X. (2017). The functional head of the Cambrian radiodontan (stem-group Euarthropoda) *Amplectobelua symbrachiata*. *BMC Evolutionary Biology*, 17(1), 208.

Cong, P. Y., Edgecombe, G. D., Daley, A. C., Guo, J., Pates, S., & Hou, X. G. (2018). New radiodonts with gnathobase-like structures from the Cambrian Chengjiang biota and implications for the systematics of Radiodonta. *Papers in Palaeontology*, 4(4), 605-621.

Conway Morris, S., & Robison, R. A. (1988). More soft-bodied animals and algae from the Middle Cambrian of Utah and British Columbia. *University of Kansas Paleontological Contributions*, 122, 1-48.

Cui, Z-L., & Huo, S-C., (1990). New discoveries of lower Cambrian crustacean fossils from western Hubei. *Acta Palaeontologica Sinica*, 3, 007.

Daley, A. C., Budd, G. E., Caron, J. B., Edgecombe, G. D., & Collins, D. (2009). The Burgess Shale anomalocaridid *Hurdia* and its significance for early euarthropod evolution. *Science*, 323(5921), 1597-1600.

Daley, A. C., & Budd, G. E. (2010). New anomalocaridid appendages from the Burgess Shale, Canada. *Palaeontology*, 53(4), 721-738.

Daley, A. C., & Bergström, J. (2012). The oral cone of *Anomalocaris* is not a classic ‘‘peytoia’’. *Naturwissenschaften*, 99(6), 501-504.

Daley, A. C., Paterson, J. R., Edgecombe, G. D., García-Bellido, D. C., & Jago, J. B. (2013a). New anatomical information on *Anomalocaris* from the Cambrian Emu Bay Shale

of South Australia and a reassessment of its inferred predatory habits. *Palaeontology*, 56(5), 971-990.

Daley, A. C., Budd, G. E., & Caron, J. B. (2013b). Morphology and systematics of the anomalocaridid arthropod *Hurdia* from the Middle Cambrian of British Columbia and Utah. *Journal of Systematic Palaeontology*, 11(7), 743-787.

Gaines, R. R., & Droser, M. L. (2003). Paleoecology of the familiar trilobite Elrathia kingii: an early exaerobic zone inhabitant. *Geology*, 31(11), 941-944.

Geyer, G. E. R. D. (1996). The Moroccan fallotaspidid trilobites revisited. *Beringeria*, 18, 89-199.

Hagadorn, J.W. (2009). Taking a bite out of *Anomalocaris*. *Walcott 2009: International Conference on the Cambrian Explosion, abstract volume*, 33–34.

Hagadorn, J. W., Schottenfeld, M. T. & McGowan, D. (2010). Putting *Anomalocaris* on a soft-food diet? *Geological Society of America Abstracts,* 42, 320.

Hendricks, J. R., Lieberman, B. S., & Stigall, A. L. (2008). Using GIS to study palaeobiogeographic and macroevolutionary patterns in soft-bodied Cambrian arthropods. *Palaeogeography, Palaeoclimatology, Palaeoecology*, 264(1-2), 163-175.

Holmes, J. D., García-Bellido, D. C., & Lee, M. S. (2018). Comparisons between Cambrian Lagerstätten assemblages using multivariate, parsimony and Bayesian methods. *Gondwana Research*, 55, 30-41.

Huang, D., Wang, Y., Gao, J., & Wang, Y. (2012). A new anomalocaridid frontal appendage from the Middle Cambrian Mantou Formation of the Tangshan Area. *Acta Palaeontologica Sinica*, 51, 411-415.

Jago, J. B., García-Bellido, D. C. & Gehling, J. G. (2016). An early Cambrian chelicerate from the Emu Bay Shale, South Australia. *Palaeontology,* 59, 549–562.

Legg, D. A., & Pates, S. (2016). A restudy of Utahcaris orion (Euarthropoda) from the Spence Shale (middle Cambrian, Utah, USA). *Geological Magazine*, 154(1), 181-186.

Leighton, L. R. (2011). Analyzing predation from the dawn of the Phanerozoic. *In* Quantifying the Evolution of Early Life (pp. 73-109). Springer, Dordrecht.

Lerosey-Aubril, R., & Pates, S. (2018). New suspension-feeding radiodont suggests evolution of microplanktivory in Cambrian macronekton. *Nature Communications*, 9(1), 3774.

Lieberman, B. S. (2003). A new soft-bodied fauna: the Pioche Formation of Nevada. *Journal of Paleontology*, 77(4), 674-690.

Liu, J., Lerosey-Aubril, R., Steiner, M., Dunlop, J. A., Shu, D., & Paterson, J. R. (2018). Origin of raptorial feeding in juvenile euarthropods revealed by a Cambrian radiodontan. *National Science Review*.

Liu, Q. (2013). The first discovery of anomalocaridid appendages from the Balang Formation (Cambrian Series 2) in Hunan, China. *Alcheringa*, 37(3), 338-343.

McHenry, B., & Yates, A. (1993). First report of the enigmatic metazoan *Anomalocaris* from the southern hemisphere and a trilobite with preserved appendages from the Early Cambrian of Kangaroo Island, South Australia. *Records of the South Australian Museum*, 26, 77-86.

Nedin, C. (1999). *Anomalocaris* predation on nonmineralized and mineralized trilobites. *Geology*, 27(11), 987-990.

Ortega-Hernández, J., Esteve, J., & Butterfield, N. J. (2013). Humble origins for a successful strategy: complete enrolment in early Cambrian olenellid trilobites. *Biology Letters*, 9(5), 20130679.

Paterson, J. R., García-Bellido, D. C., Lee, M. S., Brock, G. A., Jago, J. B., & Edgecombe, G. D. (2011). Acute vision in the giant Cambrian predator *Anomalocaris* and the origin of compound eyes. *Nature*, 480(7376), 237.

Paterson, J. R., García-Bellido, D. C., Jago, J. B., Gehling, J. G., Lee, M. S., & Edgecombe, G. D. (2016). The Emu Bay Shale Konservat-Lagerstätte: a view of Cambrian life from East Gondwana. *Journal of the Geological Society*, 173(1), 1-11.

Pates, S., Bicknell, R. D., Daley, A. C., & Zamora, S. (2017). Quantitative analysis of repaired and unrepaired damage to trilobites from the Cambrian (Stage 4, Drumian) Iberian Chains, NE Spain. *PALAIOS*, 32(12), 750-761.

Resser, C. E. (1929). New lower and middle Cambrian Crustacea. *Proceedings of the United States National Museum*, 76(9), 1-18.

Sheldon, P. R. (1987). Parallel gradualistic evolution of Ordovician trilobites. *Nature*, 330(6148), 561-563.

Sheldon, P. R. (1988). Trilobite size-frequency distributions, recognition of instars, and phyletic size changes. *Lethaia*, 21(4), 293-306.

Van Roy, P., & Briggs, D. E. (2011). A giant Ordovician anomalocaridid. Nature, 473(7348), 510.

Van Roy, P., Daley, A. C., & Briggs, D. E. (2015). Anomalocaridid trunk limb homology revealed by a giant filter-feeder with paired flaps. *Nature*, 522(7554), 77.

Vermeij, G. J., Schindel, D. E., & Zipser, E. (1981). Predation through geological time: evidence from gastropod shell repair. Science, 214(4524), 1024-1026.

Vinther, J., Stein, M., Longrich, N. R., & Harper, D. A. (2014). A suspension-feeding anomalocarid from the Early Cambrian. *Nature*, 507(7493), 496.

Wang, Y., Huang, D., & Hu, S. (2013). New anomalocardid frontal appendages from the Guanshan biota, eastern Yunnan. *Chinese Science Bulletin*, 58(32), 3937-3942.

Weber, B., Hu, S., Steiner, M., & Zhao, F. (2012). A diverse ichnofauna from the Cambrian Stage 4 Wulongqing Formation near Kunming (Yunnan Province, South China). *Bulletin of Geosciences*, 87(1), 71-92 .

Webster, M., Gaines, R. R., & Hughes, N. C. (2008). Microstratigraphy, trilobite biostratinomy, and depositional environment of the “lower Cambrian” Ruin Wash Lagerstätte, Pioche Formation, Nevada. Palaeogeography, Palaeoclimatology, Palaeoecology, 264(1-2), 100-122.

Zeng, H., Zhao, F., Yin, Z., & Zhu, M. (2018). A new radiodontan oral cone with a unique combination of anatomical features from the early Cambrian Guanshan Lagerstätte, eastern Yunnan, South China. *Journal of Paleontology*, 92(1), 40-48.

Zhao, Y., Zhu, M., Babcock, L. E., Yuan, J., Parsley, R. L., Peng, J., Yang, X., and Wang, Y. (2005). Kaili Biota: a taphonomic window on diversification of metazoans from the basal Middle Cambrian: Guizhou, China. *Acta Geologica Sinica-English Edition*, 79(6), 751-765.

Zhu, M. Y., Vannier, J., Iten, H. & Zhao, Y. L. (2004). Direct evidence for predation on trilobites in the Cambrian. *Proceedings of the Royal Society of London B: Biological Sciences*, 271, S277–S280.

Zhuravlev, A. Y., & Wood, R. A. (2018). The two phases of the Cambrian Explosion. *Scientific Reports,* 8(1), 16656.

Appendix 1

List of publications that are not included in the thesis

List of publications that are not included in the thesis

1. Lerosey-Aubril, R. and **Pates, S**. **2018**. New suspension-feeding radiodont suggests evolution of microplanktivory in Cambrian macronekton. *Nature Communications.* 9, 3774. doi.org/10.1038/s41467-018-06229-7.

2. Daley, A. C., Antcliffe, J. B., Drage, H. B. and **Pates, S. 2018**. Early fossil record of Euarthropoda and the Cambrian Explosion. *PNAS,* 115, 5323 – 5331. doi.org/10.1073/pnas.1719962115

3. Bicknell, R. D. C., **Pates, S.** and Botton, M. L. **2018**. Abnormal xiphosurids, with possible application to Cambrian trilobites. *Palaeontologia Electronica*, 21, 1–17. doi.org/10.26879/866

4. Guo, J., **Pates, S.***, Cong, P., Daley, A. C., Edgecombe, G. D., Chen, T. and Hou, X. G. **2018**. A new radiodont (stem Euarthropoda) frontal appendage with a mosaic of characters from the Cambrian (Series 2 Stage 3) Chengjiang biota. *Papers in Palaeontology, Online early view:* doi.org/10.1002/spp2.1231 ***corresponding author***

5. Cong, P., Edgecombe, G. D., Daley, A. C., Guo, J., **Pates, S.,** and Hou, X. G. **2018**. New radiodonts with gnathobase-like structures from the Cambrian Chengjiang Biota and implications for the systematics of Radiodonta. *Papers in Palaeontology,* 4, 605-621. doi.org/10.1002/spp2.1219

6. **Pates, S.,** Daley, A. C., and Ortega-Hernández, J. **2018**. Response to Comment on "*Aysheaia prolata* from the Wheeler Formation (Cambrian, Drumian) is a frontal appendage of the radiodontan *Stanleycaris*" with the formal description of *Stanleycaris*. *Acta Palaeontologica Polonica,* 63, 105-110. doi.org/10.4202/app.00443.2017

7. Bicknell, R. D. C. and **Pates, S.** *accepted***.** Malformed xiphosurids. *Bulletin of the Yale Peabody Museum of Natural History*.

8. Legg, D., and **Pates, S. 2016**. A restudy of *Utahcaris orion* (Euarthropoda) from the Spence Shale (Middle Cambrian, Utah, USA). *Geological Magazine*, 154, 181-186. doi.org/10.1017/S0016756816000789

Appendix 2

Supplemental material for Chapter 9

The evolution of the hurdiid frontal appendage, and a novel phylogenetic hypothesis for radiodont families

Supplemental information 1

Explanation of characters, and coding changes from Lerosey-Aubril & Pates 2018.

GENERAL

1. General: divisions of external body surface
(0) undivided
(1) annuli
(2) segments

Amplectobelua symbrachiata is treated as having segments in this analysis, on account of the 'segmentally arranged structures' described in ELRC 21002a (Chen et al. 1994, fig. 3a).

2. General: digestive glands
(0) absent
(1) present

3. General: paried lateral appendages
(0) absent
(1) present

4. General: number of appendage pairs (refers to limbs including frontal appendages, sclerotized or unsclerotized, and flaps)
(0) 13 or fewer
(1) 13 or more

Hurdia victoria is only known from specimens with up to nine body segments, and no reduced 'neck' segments are known (unlike *Amplectobelua, Lyrarapax* and *Peytoia nathorsti*). As such, *H. victoria* has fewer than 14 appendage pairs.

HEAD

5. Head: Sclerotization
(0) unsclerotized
(1) bearing one or more sclerotized elements (i.e. anterior sclerite, carapace central and lateral elements, cephalic shield; excludes frontal appendages and appendicular derivatives such as the hypostome)

6. Head: Anterior sclerite size
(0) Small antero-dorsal plate

(1) Large plate (forming the central element of a carapace and projecting anteriorly beyond frontal appendages)

7. Head: Anterior sclerite anterolateral margin
(0) rounded
(1) ogival
(2) forming an anteriorly projecting sagittal spine

Peytoia nathorsti is treated as having a rounded anterior sclerite margin.

8. Head: Anterior sclerite postero-lateral constricutions
(0) absent
(1) present

9. Head: Lateral sclerites
(0) absent
(1) small plates associated with proximal parts of frontal appendages
(2) large plates forming a cephalic carapace in conjunction with anterior sclerite

Tamisiocaris borealis is only known from frontal appendages and a partial anterior sclerite. As such the presence or absence of lateral sclerites cannot be confirmed, and this character was coded as uncertain for this animal.

10. Head: lateral sclerites postero-dorsal margin
(0) convex
(1) straight or concave

11. Head: dorsal sclerites belonging to two or more segments fused into a cephalic shield
(0) absent
(1) present

12. Head: number of segments
(0) one
(1) two or more

13. Head: eyes
(0) absent
(1) large compound eyes composed of clustered visual units

14. Head: eye stalks
(0) absent
(1) present

15. Head: mouth direction
(0) anterior
(1) ventral
(2) posterior

16. Head: mouth circumoral plates
(0) absent
(1) radially-arranged and sclerotized

The recent formal description of *Anomalocaris magnabasis* (*This thesis Chapter 7*) including new material, revealed partial oral cones, in the holotype and paratype. This taxon (*Anomalocaris* cf. *saron* Nevada in previous analyses) is therefore regarded as having a mouth made of circumoral plates, with at least two sizes represented (Character 17) and a triradial arrangement (Character 18).

17. Head: mouth circumoral plate size differentiation within main ring
(0) absent
(1) at least two sizes represented

18. Head: mouth circumoral plate distribution of large plates
(0) triradial
(1) tetraradial

19. Head: mouth circumoral plates sculpture of main ring
(0) smooth
(1) bearing rounded or triangular nodes

Both *Anomalocaris magnabasis* and *A. saron* have small nodes on their oral cone plates and lack an inner ring of smaller plates within the primary ring (Character 20). As such the codings of Character 19 and 20 have been updated to reflect this (*This thesis Chapter 7*; Hou et al. 1995).

20. Head: mouth inner ring of smaller plates forming a cohesive structure within the primary ring
(0) absent
(1) present

21. Head: protocerebral appendages sclerotized
(0) absent
(1) present

22. Head: protocerebral appendages
(0) frontal appendages made of annuli
(1) frontal appendages made of segments
(2) appendages fused into a hypostome or labrum

FRONTAL APPENDAGES

23. Frontal appendages: orientation of terminal spine
(0) downwards
(1) upwards

24. Frontal appendages: dorsal spines
(0) absent
(1) present

Dorsal spines are present in *Caryosyntrips serratus* (Daley & Budd 2010; Pates & Daley 2017) and *Lyrarapax unguispinus* (Liu et al. 2018), absent in *Tamisiocaris borealis* (Pates & Daley 2018). This character, and Character 25 are inapplicable for *Chengjiangocaris kunmingensis*.

25. Frontal appendages: endites
(0) absent
(1) present

26. Frontal appendages: endites length
(0) short
(1) at least two exceed in length the height of the podomeres to which they attach

27. Frontal appendages: endite width
(0) spiniform (strongly narrowing distally)
(1) plate-like (remaining wide distally)

28. Frontal appendages: width evolution towards the distal tip of the appendage
(0) remains unchanged or decreases
(1) increases

29. Frontal appendages: orientation of proximal endites
(0) projecting ventrally
(1) projecting anteriorly (at least 45 degrees) forming a claw with the distal end of the appendage

30. Frontal appendages: single hypertrophied endite on first podomere in distal articulated region
(0) absent
(1) present

31. Frontal appendages: individual curvature of endites
(0) straight or slightly curved
(1) curved anteriorly
(2) strongly curved anteriorly making a 90 degree angle between the tip and base

32. Frontal appendages: curvature variability
(0) all are straight or curved anteriorly
(1) all are curved posteriorly

Anomalocaris briggsi and *Tamisiocaris borealis* bear straight endites, which due to preservation sometimes appear to bend posteriorly. These are coded as straight or slightly

curved. The character state '(2) only proximal ones are curved posteriorly' is removed as no taxa in the matrix have this state.

33. Frontal appendages: length of adjacent endites
(0) subequal
(1) alternating long/short on subsequent podomeres

The endites on *Amplectobelua stephenensis* although very short do appear to alternate long/short on subsequent podomeres (Daley & Budd 2010 text-fig. 3).

34. Frontal appendages: length of adaxial and abaxial (relative to body sagittal axis) endites of a given pair
(0) subequal
(1) adaxial endite reduced relative to abaxial one, or absent

The paired endites of *Anomalocaris* sp. Balang, *A.* sp. Emu Bay, *A. magnabasis, A. saron, Paranomalocaris multisegmentalis, Lyrarapax trilobus* and *L. unguispinus* are treated as being subequal in length.

35. Frontal appendages: auxiliary spines on endites
(0) absent
(1) present

36. Frontal appendages: anterior setae
(0) absent
(1) present

37. Frontal appendages: auxiliary spines distribution
(0) auxiliary spines on the endites of several podomeres
(1) auxiliary spines on the endites of a single podomere only

38. Frontal appendages: arrangement of auxiliary spines
(0) radiating
(1) pectinate

39. Frontal appendages: modal number of anterior auxiliary spines
(0) none
(1) one
(2) two
(3) three
(4) four or more

Anomalocaris pennsylvanica does not bear auxiliary spines (Pates & Daley 2018).

40. Frontal appendages: orientation of anterior auxiliary spines
(0) project distally towards the tip of endites
(1) project anteriorly, towards the distal end of the appendage

41. Frontal appendages: posterior auxiliary spines
(0) absent
(1) present on at least one endite

Anomalocaris pennsylvanica does not have auxiliary spines (Pates & Daley 2018).

42. Frontal appendages: number of posterior auxiliary spines
(0) one
(1) two or more

This was coded as inapplicable for *Aysheaia, Kerygmachela, Pambdelurion, Opabinia, Caryosyntrips, Anomalocaris kunmingensis, Amplectobelua stephenensis, Peytoia nathorsti, Schinderhannes bartelsi, Hurdia victoria, Stanleycaris hirpex*, and the Fezouata hurdiid, as these taxa have already been coded as not having posterior auxiliary spines (Character 41). *Anomalocaris magnabasis* and *Lyrarapax unguispinus* have a single posterior facing auxiliary spine (*This thesis Chapter 7*; Liu et al. 2018).

43. Frontal appendages: total number of podomeres
(0) 14 or more
(1) 13 or fewer

Both *Lyrarapax* species have fewer than 14 podomeres in the frontal appendage (Cong et al. 2014, 2016; Liu et al. 2018).

44. Frontal appendages: length of distal podomeres
(0) elongate
(1) short and closely packed relative to proximal podomeres

Both *Lyrarapax* species have shorter podomeres in the distal region than in the proximal region (Cong et al. 2014, 2016; Liu et al. 2018).

45. Frontal appendages: curvature
(0) straight or down curved proximally
(1) with a dorsal kink separating the shaft from the distal articulated region

HEAD/TRUNK

46. Head/trunk: deutocerebral appendages
(0) absent or undifferentiated compared to more posterior appendages
(1) differentiated compared to more posterior appendages, either antenniform or chelate

TRUNK

47. Trunk: shape
(0) cylindrical

(1) broad anteriorly and tapering posteriorly, with the maximum width of the anterior trunk 300% the width of the posteriormost trunk segment

48. Trunk: arthrodisation
(0) absent
(1) present

49. Trunk: relative length of segments
(0) segments subequal along the length of the body
(1) posterior segments reduced, with anterior segments 150% or more the lengths of posterior ones

50. Trunk: sclerotized appendages
(0) absent
(1) present

51. Trunk: ventral element of appendages
(0) lobopodous limb (independent and annulated)
(1) ventral flap

Following the description of new material, *Anomalocaris magnabasis* is now known to possess ventral flaps (*This thesis Chapter 7*).

52. Trunk: dorsal element of appendages
(0) absent
(1) independent dorsal flap
(2) segmented ramus (either independent or attached to a ventral element to form a biramous appendage)

53. Trunk: dorsal element of appendages possesses exites/setal blades
(0) absent
(1) present

54. Trunk: biramous appendage
(0) absent
(1) present

55. Trunk: length of dorsal flaps
(0) subequal along the length of the body
(1) anterior flaps approximately twice as long as posterior flaps

56. Trunk: internal reinforcements on dorsal flaps
(0) absent
(1) present

Following the description of new material, ventral flaps in *Anomalocaris magnabasis* are known to contain internal reinforcements (*This thesis Chapter 7*). *Lyrarapax unguispinus* does not have a dorsal element, and so this character is coded as inapplicable.

57. Trunk: distribution of exites/setal blades
(0) confined to dorsal flaps or exopods (lateral region of the body)
(1) extend to the medial region of the body dorsally

58. Trunk: fusion of exites/setal blades
(0) absent
(1) present

59. Trunk: tailfan
(0) absent
(1) present

60. Trunk: tailfan form
(0) small fluke, a single pair of flaps
(1) large fan, multiple pairs of flaps

61. Trunk: furca
(0) absent
(1) present

References

Chen, J. Y., Ramsköld, L., & Zhou, G. Q. (1994). Evidence for monophyly and arthropod affinity of Cambrian giant predators. *Science*, 264(5163), 1304-1308.

Cong, P., Ma, X., Hou, X., Edgecombe, G. D., & Strausfeld, N. J. (2014). Brain structure resolves the segmental affinity of anomalocaridid appendages. *Nature*, 513(7519), 538.

Cong, P., Daley, A. C., Edgecombe, G. D., Hou, X., & Chen, A. (2016). Morphology of the radiodontan *Lyrarapax* from the early Cambrian Chengjiang biota. *Journal of Paleontology*, 90(4), 663-671.

Daley, A. C., & Budd, G. E. (2010). New anomalocaridid appendages from the Burgess Shale, Canada. *Palaeontology*, 53(4), 721-738.

Hou, X-G., Bergström, J., & Ahlberg, P. (1995). *Anomalocaris* and other large animals in the Lower Cambrian Chengjiang fauna of southwest China. *GFF*, 117(3), 163-183.

Lerosey-Aubril, R., & Pates, S. (2018). New suspension-feeding radiodont suggests evolution of microplanktivory in Cambrian macronekton. *Nature Communications*, 9(1), 3774.

Liu, J., Lerosey-Aubril, R., Steiner, M., Dunlop, J. A., Shu, D., & Paterson, J. R. (2018). Origin of raptorial feeding in juvenile euarthropods revealed by a Cambrian radiodontan. *National Science Review*.

Pates, S., & Daley, A. C. (2017). *Caryosyntrips*: a radiodontan from the Cambrian of Spain, USA and Canada. *Papers in Palaeontology*, 3(3), 461-470.

Pates, S., & Daley, A. C. (2018). The Kinzers Formation (Pennsylvania, USA): the most diverse assemblage of Cambrian Stage 4 radiodonts. Geological Magazine, Online early view: doi.org/10/1017/S0016756818000547.

The evolution of the hurdiid frontal appendage, and a novel phylogenetic hypothesis for radiodont families

Supplemental information 2

```
Caenorhabditis_elegans        000-0------00-00---0-------------------------00---00--------
Priapulus_caudatus            100-0------00-00---0-------------------------00---00--------
Aysheaia_pedunculata          10100------00?00---?00?01000??010-0--???0-----0000000--------
Kerygmachela_kierkegaardi     11100------01000---?00?0100000000-0--???0-----0000011000000-1
Pambdelurion_whittingtoni     11100------0??110???00?01000?0000?0--???0-----0000011000000-?
Opabinia_regalis              21110------01110-???00?0100?????0?0--???0-???-000??1101000110
Caryosyntrips_serratus        ??1????????0?????????1101100000000000--??0-000?????????????????
Anomalocaris_pennsylvanica    ??1????????0?????????1101110000001000--0-0-00?????????????????
Anomalocaris_canadensis       211110000-00111111010110110000000010100-10100010101010-110110
Anomalocaris_saron            2?1110000-00111111010110111000000010100020110010?01010-110111
Anomalocaris_magnabasis       ??1????????0???1101011011000000001010003010001?????1????1?????
Anomalocaris_Balang           ??1????????0?????????11??1000000001010003010??1?????????????????
Paranomalocaris_multiseg      ??1????????0?????????1101100000000101000401100?????????????????
Anomalocaris_Emu_Bay          ??1????????0????1???11?1100000000101000201100?????????????????
Lyrarapax_unguispinus         211110001000111111???11?1100011001010111??10111010101010--1011?
Lyrarapax_trilobus            211110001000111?????11?1100011001010114 00-111010101010--1011?
Anomalocaris_kunmingensis     ??1????????0????1???1101100010001?100?000-00?????????????????
Amplectobelua_stephenensis    ??1????????0?????????1101100011001010110 00-?1?????????????????
Amplectobelua_symbrachiata    2?111000100001?1?????1101100011001010101000110110101010101010-110111
Ramskoeldia_consimilis        ??1?1???10?0????????1101100011001010003011011??0??1??0?1?????
Laminacaris_chimera           ??1????????0?????????1101100001001?1001301001?????????????????
Tamisiocaris_borealis         ??1?1000??00?????????11?011000000000100140110 0?????????????????
Anomalocaris_briggsi          ??1????????0?????????1101110000000001001401100 1?????????????????
Hurdiid_Fezouata              ??1????????0?????????11011110??100?1001400-?0?????????????????
Peytoia_nathorsti             2111100??00111111100110111100010011001410-100010101111011110-0
Schinderhannes_bartelsi       2?1?????0-00111111???11??111000100110014 10-11001?1???1???1?101
Peytoia_Balang                ??1????????0?????????1101111000100??00?????110?????????????????
Hurdia_victoria               2?10112111001111110111111111100100110014 10-110010?011101110100
Stanleycaris_hirpex           ??1????????0?????????1111111000200110014 10-110?????????????????
Aegirocassis_benmoulae        2?1?11111000??1?????110?111000100101--0-111100101011101110-0
Ursulinacaris_grallae         ??1????????0?????????11?111000000001001410-110?????????????????
Pahvantia_hastata             ??1?112121?0????????11?111100010011101410-1?1?????????????????
Hurdiid_Spence                2?10100?100000111?0?11??110000000100--0-0-1?00100011 10?110000
Hurdiid_S7_Burgess            ??1????????0?????????11  000000011001410-100?????????????????
Cucumericrus_decoratus        ??1????????0?????????????????????????????????????????0?00110?1?????
Chengjiangocaris_kunmingensis 201110?0??111120----12--------------------10?111112011--001-0
Eoredlichia_intermedia        201110????111020----12----------------------111012011--000-0
```

The evolution of the hurdiid frontal appendage, and a novel phylogenetic hypothesis for radiodont families

Supplemental information 3

Output from phylogenetic analyses and code used to run them. Results for concavity constants 1-10 presented below.

Code

```
proc thesis_matrix_17oct.txt.tnt ;
hold 1000 ;
xmult:rat25 drift25 hits 1000 level 4 chklevel 5;

log thesismatrixoutputk1.txt ;
piwe=1 ;
xmult ;
majority ;
stats.run ;
taxname= ;
export*thesismatrixoutputk1.nex ;

log thesismatrixoutputk2.txt ;
piwe=2 ;
xmult ;
majority ;
stats.run ;
taxname= ;
export*thesismatrixoutputk2.nex ;

log thesismatrixoutputk3.txt ;
piwe=3 ;
xmult ;
majority ;
stats.run ;
taxname= ;
export*thesismatrixoutputk3.nex ;

log thesismatrixoutputk4.txt ;
piwe=4 ;
xmult ;
majority ;
stats.run ;
taxname= ;
export*thesismatrixoutputk4.nex ;

log thesismatrixoutputk5.txt ;
piwe=5 ;
xmult ;
majority ;
stats.run ;
taxname= ;
export*thesismatrixoutputk5.nex ;

log thesismatrixoutputk6.txt ;
piwe=6 ;
xmult ;
majority ;
stats.run ;
taxname= ;
export*thesismatrixoutputk6.nex ;

log thesismatrixoutputk7.txt ;
piwe=7 ;
xmult ;
majority ;
stats.run ;
taxname= ;
export*thesismatrixoutputk7.nex ;

log thesismatrixoutputk8.txt ;
piwe=8 ;
xmult ;
majority ;
stats.run ;
taxname= ;
export*thesismatrixoutputk8.nex ;

log thesismatrixoutputk9.txt ;
piwe=9 ;
xmult ;
majority ;
stats.run ;
taxname= ;
export*thesismatrixoutputk9.nex ;

log thesismatrixoutputk10.txt ;
piwe=10 ;
xmult ;
majority ;
stats.run ;
taxname= ;
export*thesismatrixoutputk10.nex ;

proc/ ;
```

```
k =1

Implied Weighting is ON
Repl. Algor.    Tree      Score      Best Score  Time      Rearrangs.
999  FUSE       4         ------     ------      0:00:17   416,094,469
Completed search.
Total rearrangements examined: 416,094,469.
No target score defined.  Best score hit 1000 times.
Best score: 15.45714.  36 trees retained.

Majority rule tree (from 36 trees, cut 50)
  ,-- 'Caenorhabditis_elegans'
  |    ,-- 'Priapulus_caudatus'
|--|    |    ,-- 'Aysheaia_pedunculata'
  `--100|    |    ,-- 'Kerygmachela_kierkegaardi'
     `--100|    |    ,-- 'Pambdelurion_whittingtoni'
        `--100|    |    ,-- 'Opabinia_regalis'
           |    |    |    ,-- 'Cucumericrus_decoratus'
           `--100|    |    |    ,-- 'Eoredlichia_intermedia'
              |    |    |--100--- 'Chengjiangocaris_kunmingensis'
              `--100|    |         ,-- 'Ursulinacaris_grallae'
                 |    |         |    ,-- 'Hurdiid_Spence'
                 |    |    ,--100|    |    ,-- 'Hurdiid_S7_Burgess'
                 `--100|    |    `--100|    |    ,-- 'Hurdiid_Fezouata'
                    |    |         `--100|    |    ,-- 'Peytoia_nathorsti'
                    |    |              `--100|    |    ,-- 'Aegirocassis_benmoulae'
                    |    |                   `--100|    |    ,-- 'Pahvantia_hastata'
                    |    |                        `--100|    |-- 'Stanleycaris_hirpex'
                    `--100|                             `--66+-- 'Hurdia_victoria'
                       |                                  |-- 'Peytoia_Balang'
                       |                                  `-- 'Schinderhannes_bartelsi'
                       |    ,-- 'Caryosyntrips_serratus'
                       |    |         ,-- 'Anomalocaris_briggsi'
                       |    |    ,--100--- 'Tamisiocaris_borealis'
                       `--100|    |    ,-- 'Anomalocaris_Emu_Bay'
                          |    |    |-- 'Paranomalocaris_multisegmental
                          `--100|    |    ,-- 'Anomalocaris_saron'
                             |    |--100--- 'Anomalocaris_pennsylvanica'
                             `--100|    ,-- 'Laminacaris_chimera'
                                |--100+-- 'Anomalocaris_magnabasis'
                                |    `-- 'Anomalocaris_canadensis'
                                |    ,-- 'Anomalocaris_kunmingensis'
                                `--100|    ,-- 'Ramskoeldia_consimilis'
                                   `--100|    ,-- 'Amplectobelua_symbrachiata'
                                      `--100|    ,-- 'Lyrarapax_unguispinus'
                                         `--100|    ,-- 'Amplectobelua_stephenensis'
                                                `--100--- 'Lyrarapax_trilobus'
Reading from stats.run
Running stats.run with arguments: .run

Macro language is ON
Macros: 50.5 Kb in use, 51.8 Kb free
Report is ON
Floating point printing uses 3 digits
Consistency index

       0    1    2    3    4    5    6    7    8    9

  0 0.581 0.581 0.581 0.581 0.581 0.581 0.581 0.581 0.581 0.581
 10 0.581 0.581 0.581 0.581 0.581 0.581 0.581 0.581 0.581 0.581
 20 0.581 0.581 0.581 0.581 0.581 0.581 0.581 0.581 0.581 0.581
 30 0.581 0.581 0.581 0.581 0.581 0.581

Retention index

       0    1    2    3    4    5    6    7    8    9

  0 0.779 0.779 0.779 0.779 0.779 0.779 0.779 0.779 0.779 0.779
 10 0.779 0.779 0.779 0.779 0.779 0.779 0.779 0.779 0.779 0.779
 20 0.779 0.779 0.779 0.779 0.779 0.779 0.779 0.779 0.779 0.779
 30 0.779 0.779 0.779 0.779 0.779 0.779

Again reading from thesismatrixscriptk1to10
Taxon names is ON

WARNING:
File "thesismatrixoutputk1.nex" already exists.  It will be overwritten.

Saved data and trees (Nexus format) to file thesismatrixoutputk1.nex
```

k = 2

Repl. Algor. Tree Score Best Score Time Rearrangs.
999 FUSE 4 ------ ------ 0:00:20 407,388,963
Completed search.
Total rearrangements examined: 407,388,963.
No target score defined. Best score hit 1000 times.
Best score: 11.65000. 36 trees retained.

Majority rule tree (from 36 trees, cut 50)

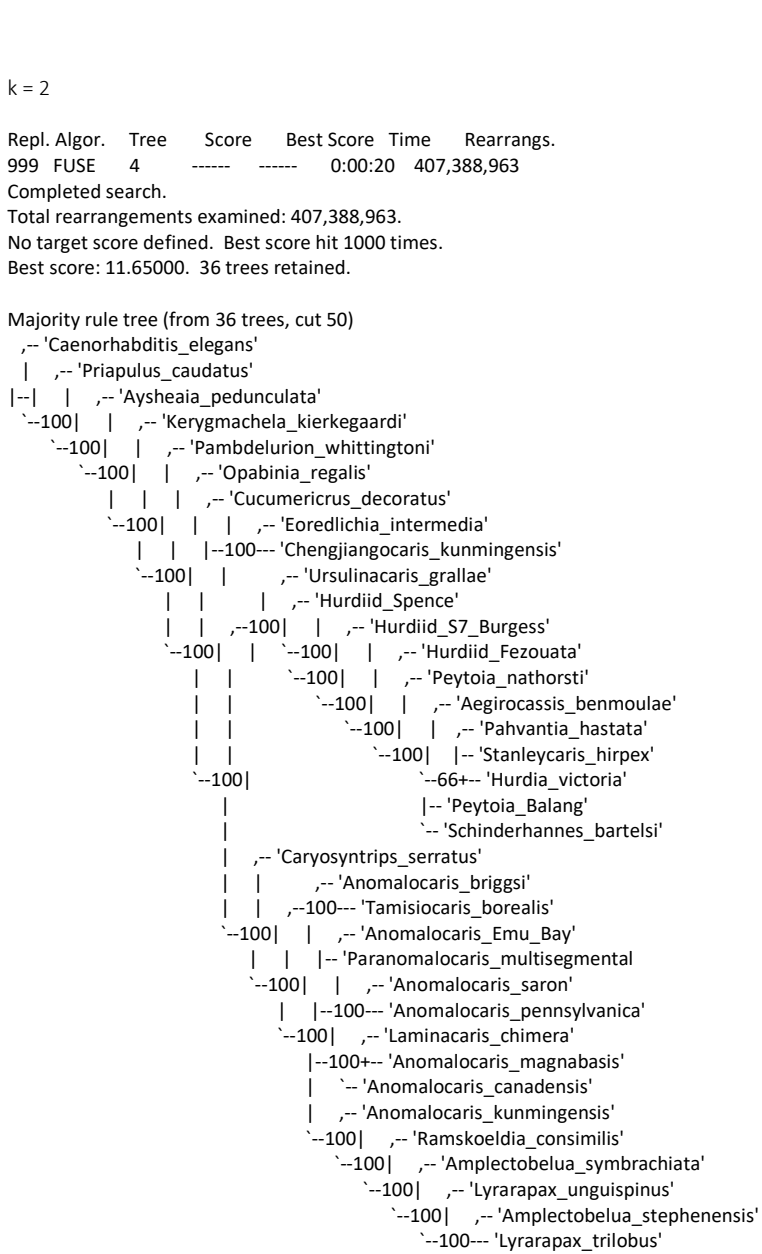

Reading from stats.run
Running stats.run with arguments: .run

Report is ON
Floating point printing uses 3 digits
Consistency index

	0	1	2	3	4	5	6	7	8	9
0	0.581	0.581	0.581	0.581	0.581	0.581	0.581	0.581	0.581	0.581
10	0.581	0.581	0.581	0.581	0.581	0.581	0.581	0.581	0.581	0.581
20	0.581	0.581	0.581	0.581	0.581	0.581	0.581	0.581	0.581	0.581
30	0.581	0.581	0.581	0.581	0.581	0.581				

Retention index

	0	1	2	3	4	5	6	7	8	9
0	0.779	0.779	0.779	0.779	0.779	0.779	0.779	0.779	0.779	0.779
10	0.779	0.779	0.779	0.779	0.779	0.779	0.779	0.779	0.779	0.779
20	0.779	0.779	0.779	0.779	0.779	0.779	0.779	0.779	0.779	0.779
30	0.779	0.779	0.779	0.779	0.779	0.779				

Again reading from thesismatrixscriptk1to10
Taxon names is ON

WARNING:
File "thesismatrixoutputk2.nex" already exists. It will be overwritten.

Saved data and trees (Nexus format) to file thesismatrixoutputk2.nex

k = 3

Repl. Algor. Tree Score Best Score Time Rearrangs.
999 FUSE 3 ------ ------ 0:00:19 433,875,949
Completed search.
Total rearrangements examined: 433,875,949.
No target score defined. Best score hit 1000 times.
Best score: 9.40952. 36 trees retained.

Majority rule tree (from 36 trees, cut 50)

```
  ,-- 'Caenorhabditis_elegans'
  |    ,-- 'Priapulus_caudatus'
|--|    |    ,-- 'Aysheaia_pedunculata'
  `--100|    |    ,-- 'Kerygmachela_kierkegaardi'
      `--100|    |    ,-- 'Pambdelurion_whittingtoni'
          `--100|    |    ,-- 'Opabinia_regalis'
              |    |    |    ,-- 'Cucumericrus_decoratus'
              `--100|    |    |    ,-- 'Eoredlichia_intermedia'
                  |    |    |--100--- 'Chengjiangocaris_kunmingensis'
                  `--100|    |         ,-- 'Ursulinacaris_grallae'
                      |    |         |    ,-- 'Hurdiid_Spence'
                      |    |    ,--100|    |    ,-- 'Hurdiid_S7_Burgess'
                      `--100|    |    `--100|    |    ,-- 'Hurdiid_Fezouata'
                          |    |         `--100|    |    ,-- 'Peytoia_nathorsti'
                          |    |              `--100|    |    ,-- 'Aegirocassis_benmoulae'
                          |    |                   `--100|    |    ,-- 'Pahvantia_hastata'
                          |    |                        `--100|    |-- 'Stanleycaris_hirpex'
                          `--100|                             `--66+-- 'Hurdia_victoria'
                              |                                  |-- 'Peytoia_Balang'
                              |                                  `-- 'Schinderhannes_bartelsi'
                              |    ,-- 'Caryosyntrips_serratus'
                              |    |         ,-- 'Anomalocaris_briggsi'
                              |    |    ,--100--- 'Tamisiocaris_borealis'
                              `--100|    |    ,-- 'Anomalocaris_Emu_Bay'
                                  |    |    |-- 'Paranomalocaris_multisegmental
                                  `--100|    |    ,-- 'Anomalocaris_saron'
                                      |    |--100--- 'Anomalocaris_pennsylvanica'
                                      `--100|    ,-- 'Laminacaris_chimera'
                                          |--100+-- 'Anomalocaris_magnabasis'
                                          |    `-- 'Anomalocaris_canadensis'
                                          |    ,-- 'Anomalocaris_kunmingensis'
                                          `--100|    ,-- 'Ramskoeldia_consimilis'
                                              `--100|    ,-- 'Amplectobelua_symbrachiata'
                                                  `--100|    ,-- 'Lyrarapax_unguispinus'
                                                      `--100|    ,-- 'Amplectobelua_stephenensis'
                                                          `--100--- 'Lyrarapax_trilobus'
```

Reading from stats.run
Running stats.run with arguments: .run

Report is ON
Floating point printing uses 3 digits
Consistency index

	0	1	2	3	4	5	6	7	8	9
0	0.581	0.581	0.581	0.581	0.581	0.581	0.581	0.581	0.581	0.581
10	0.581	0.581	0.581	0.581	0.581	0.581	0.581	0.581	0.581	0.581
20	0.581	0.581	0.581	0.581	0.581	0.581	0.581	0.581	0.581	0.581
30	0.581	0.581	0.581	0.581	0.581	0.581				

Retention index

	0	1	2	3	4	5	6	7	8	9
0	0.779	0.779	0.779	0.779	0.779	0.779	0.779	0.779	0.779	0.779
10	0.779	0.779	0.779	0.779	0.779	0.779	0.779	0.779	0.779	0.779
20	0.779	0.779	0.779	0.779	0.779	0.779	0.779	0.779	0.779	0.779
30	0.779	0.779	0.779	0.779	0.779	0.779				

Again reading from thesismatrixscriptk1to10
Taxon names is ON
Saved data and trees (Nexus format) to file thesismatrixoutputk3.nex

k = 4

Repl. Algor. Tree Score Best Score Time Rearrangs.
1001 FUSE 6 ------ ------ 0:00:29 635,312,294
Completed search.
Total rearrangements examined: 635,312,294.
No target score defined. Best score hit 1000 times.
Best score: 7.91429. 36 trees retained.

Majority rule tree (from 36 trees, cut 50)

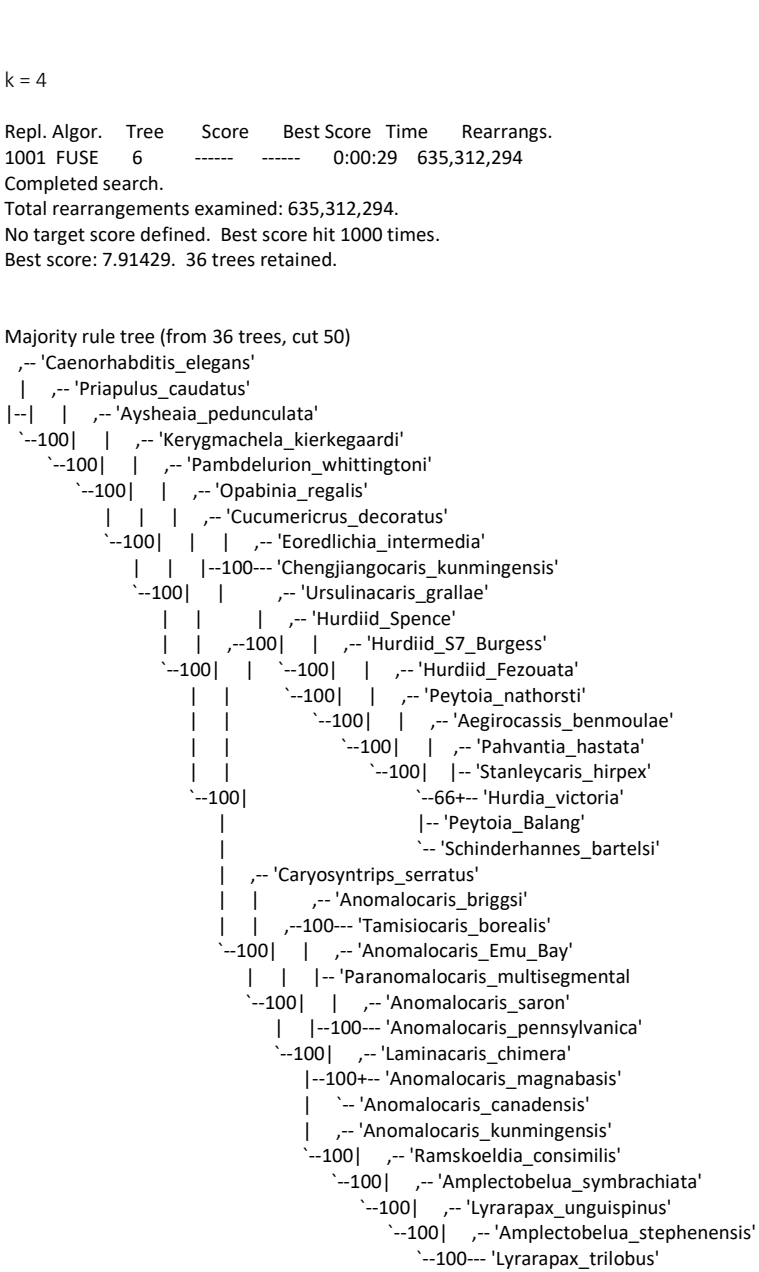

Reading from stats.run
Running stats.run with arguments: .run

Report is ON
Floating point printing uses 3 digits
Consistency index

	0	1	2	3	4	5	6	7	8	9
0	0.581	0.581	0.581	0.581	0.581	0.581	0.581	0.581	0.581	0.581
10	0.581	0.581	0.581	0.581	0.581	0.581	0.581	0.581	0.581	0.581
20	0.581	0.581	0.581	0.581	0.581	0.581	0.581	0.581	0.581	0.581
30	0.581	0.581	0.581	0.581	0.581	0.581				

Retention index

	0	1	2	3	4	5	6	7	8	9
0	0.779	0.779	0.779	0.779	0.779	0.779	0.779	0.779	0.779	0.779
10	0.779	0.779	0.779	0.779	0.779	0.779	0.779	0.779	0.779	0.779
20	0.779	0.779	0.779	0.779	0.779	0.779	0.779	0.779	0.779	0.779
30	0.779	0.779	0.779	0.779	0.779	0.779				

Again reading from thesismatrixscriptk1to10
Taxon names is ON
Saved data and trees (Nexus format) to file thesismatrixoutputk4.nex

k = 5

Repl. Algor. Tree Score Best Score Time Rearrangs.
999 FUSE 6 ------ ------ 0:00:37 854,408,245
Completed search.
Total rearrangements examined: 854,408,245.
No target score defined. Best score hit 1000 times.
Best score: 6.82738. 6 trees retained.

Majority rule tree (from 6 trees, cut 50)

Reading from stats.run
Running stats.run with arguments: .run

Report is ON
Floating point printing uses 3 digits
Consistency index

	0	1	2	3	4	5
0	0.595	0.595	0.595	0.595	0.595	0.595

Retention index

	0	1	2	3	4	5
0	0.791	0.791	0.791	0.791	0.791	0.791

Again reading from thesismatrixscriptk1to10
Taxon names is ON
Saved data and trees (Nexus format) to file thesismatrixoutputk5.nex

k = 6

Repl. Algor. Tree Score Best Score Time Rearrangs.
1000 FUSE 3 ------ ------ 0:00:47 1,074,754,892
Completed search.
Total rearrangements examined: 1,074,754,892.
No target score defined. Best score hit 1000 times.
Best score: 5.97835. 6 trees retained.

Majority rule tree (from 6 trees, cut 50)

Reading from stats.run
Running stats.run with arguments: .run

Report is ON
Floating point printing uses 3 digits
Consistency index

	0	1	2	3	4	5
0	0.595	0.595	0.595	0.595	0.595	0.595

Retention index

	0	1	2	3	4	5
0	0.791	0.791	0.791	0.791	0.791	0.791

Again reading from thesismatrixscriptk1to10
Taxon names is ON
Saved data and trees (Nexus format) to file thesismatrixoutputk6.nex

k = 7

Repl. Algor. Tree Score Best Score Time Rearrangs.
999 FUSE 4 ------ ------ 0:00:50 1,102,979,034
Completed search.
Total rearrangements examined: 1,102,979,034.
No target score defined. Best score hit 1000 times.
Best score: 5.31944. 6 trees retained.

Majority rule tree (from 6 trees, cut 50)

Reading from stats.run
Running stats.run with arguments: .run

Report is ON
Floating point printing uses 3 digits
Consistency index

	0	1	2	3	4	5
0	0.595	0.595	0.595	0.595	0.595	0.595

Retention index

	0	1	2	3	4	5
0	0.791	0.791	0.791	0.791	0.791	0.791

Again reading from thesismatrixscriptk1to10
Taxon names is ON
Saved data and trees (Nexus format) to file thesismatrixoutputk7.nex

k = 8

```
Repl. Algor.     Tree       Score      Best Score   Time      Rearrangs.
1002  FUSE       6          ------     ------       0:00:57   1,238,404,351
Completed search.
Total rearrangements examined: 1,238,404,351.
No target score defined.  Best score hit 1000 times.
Best score: 4.79270.  6 trees retained.

Majority rule tree (from 6 trees, cut 50)
  ,-- 'Caenorhabditis_elegans'
  |    ,-- 'Priapulus_caudatus'
|--|    |    ,-- 'Aysheaia_pedunculata'
  `--100|    |    ,-- 'Kerygmachela_kierkegaardi'
       `--100|    |    ,-- 'Pambdelurion_whittingtoni'
            `--100|    |    ,-- 'Opabinia_regalis'
                 `--100|    |    ,-- 'Cucumericrus_decoratus'
                      |    |    |-- 'Hurdiid_S7_Burgess'
                      `--100|    |    ,-- 'Eoredlichia_intermedia'
                           |    |--100--- 'Chengjiangocaris_kunmingensis'
                           `--100|    ,-- 'Hurdiid_Spence'
                                |    |        ,-- 'Hurdiid_Fezouata'
                                |    |        |    ,-- 'Peytoia_nathorsti'
                                |    |    ,--100|    |    ,-- 'Aegirocassis_benmoulae'
                                `--100|    |    `--100|    |    ,-- 'Pahvantia_hastata'
                                     |    |       `--100|    |-- 'Stanleycaris_hirpex'
                                     |    |             `--66+-- 'Hurdia_victoria'
                                     `--100|                |-- 'Peytoia_Balang'
                                          |                `-- 'Schinderhannes_bartelsi'
                                          |    ,-- 'Ursulinacaris_grallae'
                                          |    |        ,-- 'Anomalocaris_briggsi'
                                          `--100|    ,--100--- 'Tamisiocaris_borealis'
                                               |    |    ,-- 'Caryosyntrips_serratus'
                                               `--100|    |         ,-- 'Anomalocaris_kunmingensis'
                                                    `--100|    ,--100--- 'Anomalocaris_pennsylvanica'
                                                         |    |    ,-- 'Paranomalocaris_multisegmental
                                                         `--100|    |              ,-- 'Anomalocaris_Emu_Bay'
                                                              |    |        ,--100--- 'Anomalocaris_saron'
                                                              `--100|    ,--100|    ,-- 'Anomalocaris_magnabasis'
                                                                   |    |    `--100--- 'Anomalocaris_canadensis'
                                                                   `--100|    ,-- 'Laminacaris_chimera'
                                                                        `--100|    ,-- 'Ramskoeldia_consimilis'
                                                                             `--100|    ,-- 'Amplectobelua_symbrachiata'
                                                                                  `--100|    ,-- 'Lyrarapax_unguispinus'
                                                                                       `--100|    ,-- 'Amplectobelua_stephenen'
                                                                                            `--100--- 'Lyrarapax_trilobus'

Reading from stats.run
Running stats.run with arguments: .run

Report is ON
Floating point printing uses 3 digits
Consistency index

        0     1     2     3     4     5

   0 0.595 0.595 0.595 0.595 0.595 0.595

Retention index

        0     1     2     3     4     5

   0 0.791 0.791 0.791 0.791 0.791 0.791

Again reading from thesismatrixscriptk1to10
Taxon names is ON

WARNING:
File "thesismatrixoutputk8.nex" already exists.  It will be overwritten.

Saved data and trees (Nexus format) to file thesismatrixoutputk8.nex
```

k = 9

Repl. Algor. Tree Score Best Score Time Rearrangs.
999 FUSE 3 ------ ------ 0:01:04 1,516,012,498
Completed search.
Total rearrangements examined: 1,516,012,498.
No target score defined. Best score hit 1000 times.
Best score: 4.36169. 6 trees retained.

Majority rule tree (from 6 trees, cut 50)

Reading from stats.run
Running stats.run with arguments: .run

Report is ON
Floating point printing uses 3 digits
Consistency index

	0	1	2	3	4	5
0	0.595	0.595	0.595	0.595	0.595	0.595

Retention index

	0	1	2	3	4	5
0	0.791	0.791	0.791	0.791	0.791	0.791

Again reading from thesismatrixscriptk1to10
Taxon names is ON

WARNING:
File "thesismatrixoutputk9.nex" already exists. It will be overwritten.

Saved data and trees (Nexus format) to file thesismatrixoutputk9.nex

k = 10

Repl. Algor. Tree Score Best Score Time Rearrangs.
999 FUSE 7 ------ ------ 0:00:56 1,302,229,567
Completed search.
Total rearrangements examined: 1,302,229,567.
No target score defined. Best score hit 1000 times.
Best score: 4.00233. 6 trees retained.

Majority rule tree (from 6 trees, cut 50)

Reading from stats.run
Running stats.run with arguments: .run

Report is ON
Floating point printing uses 3 digits
Consistency index

	0	1	2	3	4	5
0	0.595	0.595	0.595	0.595	0.595	0.595

Retention index

	0	1	2	3	4	5
0	0.791	0.791	0.791	0.791	0.791	0.791

Again reading from thesismatrixscriptk1to10
Taxon names is ON

WARNING:
File "thesismatrixoutputk10.nex" already exists. It will be overwritten.

Saved data and trees (Nexus format) to file thesismatrixoutputk10.nex

Appendix 3

Supplemental material for Chapter 10

Analysis of the diversity and disparity of Radiodonta reveals two phases of evolution within the group

Supplemental 1

Time Bin	**Radiodont-bearing *Lagerstätten***
Div1	Zawiszyn Formation, Sirius Passet, Chengjiang biota, Shuijingtuo Formation
Div2	Poleta Formation, Emu Bay Shale, Balang Formation, Wulongquing Formation
Div3	Cranbrook Shale, Kinzers Formation, Latham Shale, Valdemiedes Formation, Jangle Limestone, Pioche Formation
Div4	Mantou Formation, Kaili biota, Pyramid Shale, Spence Shale, Mount Cap Formation, Burgess Shale, Stanley Glacier
Div5	Wheeler Formation, Marjum Formation, Jince Formation
	***Lagerstätten* not bearing radiodonts**
Div1	Paseky Shale, Nuititang Formation, Hetang Formation
Div2	Shipai Formation, Bianmachong Formation
Div3	Gibson Jack Formation, Tsingsutung Formation, Parker Shale
Div4	Bloomington Formation, Rennie Shale, Eldon Formation
Div5	Rockslide Formation, Vermilion/Duchesnay units

Accounting for uneven time length of Cambrian Stages

Stage	Age of base (Ma)	Length (Ma)
Guzhangian	500.5	
Drumian	504.5	4
Wuliuan	509	4.5
Stage 4	514	5
Stage 3	521	7

Solution: Split Stage 3 and Stage 4 into 3 time bins of ~4 million years each

Time Bin	Age of base (Ma)	Length (Ma)
Guzhangian	500.5	
Div5	504.5	4
Div4	509	4.5
Div3	513	4
Div2	517	4
Div1	521	4

Evaluation of Lagerstätten in Stage 3 and Stage 4 time bins

The Drumian and Wuliuan time bins remain unchanged. More precise ages for Lagerstätten in the Stage 3 and Stage 4 time bins were collated from the literature, to determine which of the three new time bins they should be assigned to.

Div1

Zawiszyn Formation: Older than 517 Ma. The oldest Cambrian fossil Lagerstätten, in the *Fallotaspis* Zone, Atdabanian (Dzik & Lendzion 1988; Daley & Legg 2015) Age approx. 521 Ma (Daley et al. 2018).

Sirius Passet biota: Older than 517 Ma. This Lagerstatte is *Nevadella* Zone in age (e.g. Williams et al. 1996; Peel 2010), and so older than 517 Ma through global correlations (Landing et al. 2013).

Chengjiang biota: Older than 517 Ma. U-Pb dataing on detrital zircons resolved a date of ~518 Ma for the Chengjiang biota (Yang et al. 2018). Soft-bodied fossils come from the *Wutingaspis-Eoredlichia* zone, which globally correlates to give an age older than 517 Ma (Landing et al. 2013).

Shuijingtuo Formation: Older than 517 Ma. This deposit is equivalent in age to the Chengjiang biota (Ma et al. 2017).

Div2

Poleta Formation: Between 513 and 517 Ma. Soft-bodied preservation is present at three levels, however 'Anomalocaridid' specimens are only known at the highest interval, 95 m above the base. The lower two levels (not containing 'Anomalocaridid' material) are Montezuman Stage, *Nevadella* Zone (English and Babcock 2010) which overlies the *Fallotaspis* Zone (Landing et al. 2013). The 'Anomalocaridid' level is lowermost Dyeran in age, which corresponds to the *'Olenellus'* trilobite zone (though this terminology has been superceded by a finer resolution trilobite zonation, see Webster 2011). This means that, through global correlations (Landing et al. 2013) this horizon is slightly younger than 517 Ma.

Emu Bay Shale: Between 513 and 517 Ma. This deposit is younger than the Chengjiang and Sirius Passet Lagerstatten, but approximately coeval with the Balang Formation and Guanshan biota (Wulongqing Formation) (Paterson et al. 2016), with a numerical age of 514Ma (+/- 1Ma) (Peng et al. 2012; Paterson et al. 2016). It belongs to the *Pararaia janeae* Zone, which in turn correlates to the upper Nangaoan-lower Duyunian stages (South China) and middle-upper Botoman (Siberia) (Landing et al. 2013).

Balang Formation: Between 513 and 517 Ma. This deposit contains trilobites including *Arthricocephalus chauveaui* and belongs to the lowermost Duyunian Stage (South China) (Liu 2013). This corresponds to the *Pararaia janeae* Zone (Australia) (Landing et al. 2013), and this deposit is coeval with the Emu Bay Shale (Paterson et al. 2016).

Wulongqing Formation: Between 513 and 517 Ma. Radiodont material from the Guanshan biota (Wulongqing Formation) was collected from the local *Palaeolenus* and *Megapalaeolenus* Zone (Wang et al. 2013), which spans the uppermost Nangaoan and lowermost Duyunian, including the *Arthricocephalus chauvenai* Zone (Landing et al. 2013) and is coeval with the *Pararaia janeae* Zone (Australia) (Landing et al. 2013). Thus this formation is coeval with the Emu Bay Shale (Paterson et al. 2016) and Balang Formation.

Div3

Cranbrook Shale: Between 509 and 513 Ma. The presence of *Wanneria* places the Cranbrook Shale in the middle '*Olenellus*' zone (Palmer & Repina 1993). This in turn places this deposit around the middle Dyeran, approximately 511 Ma through global correlations (Landing et al. 2013)

Kinzers Formation: Between 509 and 513 Ma. The soft-bodied fauna from the Kinzers Formation is restricted to the Emigsville Member which is Dyeran in age, as indicated by the presence of olenelloid trilobites, with six sub-faunules all within the '*Bonnia-Olenellus*' Zone (Campbell & Kauffman 1969; Skinner 2005). Radiodont material is known from the oldest of these, the *Wanneria Walcottana* Faunule (*sensu* Campbell & Kauffman 1969), where the presence of *Wanneria* suggests that this deposit is middle '*Olenellus'* Zone in age (Palmer & Repina 1993) and thus broadly coeval to the Cranbrook Shale.

Latham Shale: Between 509 and 513 Ma. The Latham Shale is slightly younger than the Cranbrook Shale, based on the presence of *Bristolia* (Briggs & Mount 1982; Palmer & Repina 1993; *This thesis Chapter 7*) but still belongs to the middle-upper '*Olenellus*' Zone (between *Bristolia mohavensis* and *Peachella iddingsi* Zones – Webster 2011; Pates et al. *submitted*).

Valdemiedes Formation: The single radiodont specimen known from this deposit is from the local upper Bilbilian Stage (Gámez-Vintaned et al. 2011; Pates & Daley 2017), older than the first paradoxidids in the area which indicate the start of the *Acadoparadoxides mureroensis* Zone (Álvaro et al. 2018). Thus the upper Bilbilian Stage broadly correlates to the *Hupeolenus* Zone in Morocco (Álvaro et al. 2018) and middle '*Olenellus*' Zone in Laurentia (Landing et al. 2013).

Jangle Limestone: Between 509 and 513 Ma. Soft-bodied material is known from the *Nephrolenellus multinodus* Zone in the Jangle Limestone (*This thesis Chapter 7*) which is near the top of the Dyeran (Webster 2011).

Pioche Formation: Between 509 and 513 Ma. Two soft-bodied horizons are known from the Pioche Formation, one in the *Nephrolenellus multinodus* (top of the 'Olenellus' Zone – Webster 2011) and one from the *Eokochaspsis nodosa* (Lieberman 2003; *This thesis Chapter 7*). These are immediately below the *Amecephalus arrojoensis* Zone, the top of which correlates to the base of the *Oryctocephalus indicus* Zone, likely to be defined as the base of the Wuliuan (Webster 2011).

Non-radiodont bearing BSTs

Div1

Paseky Shale: This unit yields an unusual assemblage reflecting a pecular environment possibly due to restricted marine conditions. Although many groups useful for stratigraphic correlations are absent, the Paseky Shale is likely older than 517 Ma, as it belongs to the Holsiny-Honce Formation, which itself correlates to the Issendalenian Stage in Western Gondwana (Geyer et al. 2008). The Issendalenian is older than the Banian Stage, which has trilobite zones either side of the 517 Ma boundary (Landing et al. 2013).

Niutitang Formation: The Nuititang immediately underlies the Hetang Formation (Pi et al. 2013), and thus also correlates to the Atdabanian in Siberia and is older than 517Ma.

Hetang Formation: This is Meishucunian-Quongzhusian in age (Zhou & Jiang 2009), which correlates to the Atdabanian in Siberia, which is older than 517 Ma (Landing et al. 2013).

Div2

Shipai Formation: The absolute age of the soft-bodied fauna in this formation is not exactly known. The Shipai Formation overlies the Shuijingtuo Formation (518 Ma approx. in age), and is itself overlain by the Tianheban Formation, which is upper Canglangpuan in age (Zhang & Hua 2005). The Shipai Formation is considered to be also Canglangpuan in age, and coeval to the Emu Bay Shale in South Australia (Zhang & Hua 2005). Correlations between Australia (Emu Bay Shale) and the platform of South China (Shipai Formation) make the Emu Bay Shale a youngest possible age for this site, but a Canglangpuan age places it in Div2, between 517 and 513 Ma (Landing et al. 2013).

Bianmachong Formation: Mei et al. (2007) place this unit at the lowermost point of the Canglangpuan Stage, which places it in the Div2 time bin, between 517 and 513 Ma, through global correlations (Landing et al. 2013).

Div3

Gibson Jack Formation: Robison (1984) reports *Naraoia compacta* from a site of poorly constrained upper Lower Cambrian age. The presence of *Olenellus* loosely places this site in the '*Olenellus*' Zone, which is Dyeran in age. The majority of the Dyeran is younger than 513 Ma, and so this deposit is treated tentatively as belonging to Div3 (513 - 509 Ma).

Tsingsutung Formation: The Tsingsutung Formation which is Duyunian local Stage and overlies the Balang Formation and underlies the Kaili Formation (Sun et al. 2014). The *Wiwaxia corrugata* sclerites come from the upper 50 meters of the Tsingsutung Formation, from the youngest trilobite zone in the Duyunian Stage (Sun et al. 2014). Globally this corresponds to the upper part of Stage 4 (Landing et al. 2013), and so this deposit is treated as belonging to Div3.

Parker Shale: The presence of *Olenellus crassimarginatus* in the Parker Shale and in two localities in the Kinzers Formation (including locality 22L, which bears radiodont material, see e.g. Pates & Daley 2018) means that these two sites are likely of a similar age (Webster & Landing 2016) and so this deposit is treated as belonging to Div3.

References

Álvaro, J. J., Esteve, J., & Zamora, S. (2018). Morphological assessment of the earliest paradoxidid trilobites (Cambrian Series 3) from Morocco and Spain. *Geological Magazine*, 155(7), 1566-1595.

Briggs, D. E., & Mount, J. D. (1982). The occurrence of the giant arthropod *Anomalocaris* in the Lower Cambrian of southern California, and the overall distribution of the genus. *Journal of Paleontology*, 56(5), 1112-1118.

Campbell, L., & Kauffman, M. E. (1969). *Olenellus* fauna of the Kinzers Formation, southeastern Pennsylvania. *Proceedings of the Pennsylvania Academy of Science*, 172-176.

Daley, A. C., & Legg, D. A. (2015). A morphological and taxonomic appraisal of the oldest anomalocaridid from the Lower Cambrian of Poland. *Geological Magazine*, 152(5), 949-955.

Dzik, J., & Lendzion, K. (1988). The oldest arthropods of the East European Platform. *Lethaia*, 21(1), 29-38.

English, A. M., & Babcock, L. E. (2010). Census of the Indian Springs Lagerstätte, Poleta Formation (Cambrian), western Nevada, USA. *Palaeogeography, Palaeoclimatology, Palaeoecology*, 295(1-2), 236-244.

Gámez-Vintaned, J. A., Linán, E., & Zhuravlev, A. Y. (2011). A new Early Cambrian lobopod-bearing animal (Murero, Spain) and the problem of the ecdysozoan early diversification. *In* Evolutionary Biology–Concepts, Biodiversity, Macroevolution and Genome Evolution (pp. 193-219). Springer, Berlin, Heidelberg.

Geyer, G., Elicki, O., Fatka, O., & Zylinska, A. (2008). Cambrian. *In* The Geology of Central Europe Volume 1: Precambrian and Palaeozoic. (Ed. McCann, T.). pp. 154-202. The Geological Society, London.

Landing, E., Geyer, G., Brasier, M. D., & Bowring, S. A. (2013). Cambrian evolutionary radiation: context, correlation, and chronostratigraphy—overcoming deficiencies of the first appearance datum (FAD) concept. *Earth-Science Reviews*, 123, 133-172.

Lieberman, B. S. (2003). A new soft-bodied fauna: the Pioche Formation of Nevada. *Journal of Paleontology*, 77(4), 674-690.

Liu, Q. (2013). The first discovery of anomalocaridid appendages from the Balang Formation (Cambrian Series 2) in Hunan, China. *Alcheringa*, 37(3), 338-343.

Ma, J., Liu, C., Lin, W., Sun, A., Wu, Y., & Fu, D. (2017). New Isoxys arthropod from Cambrian (Series 2, Stage 3) Qingjiang Biota, South China. *Korean Geological Society Conference*, 70-70.

Mei, M., Ma, Y., Zhang, H., Meng, X., & Chen, Y. (2007). From Basin Black Shales to Platform Carbonate Rocks: A Study on Sequence Stratigraphy for the Lower Cambrian of the Upper-Yangtze Region in South China. *Acta Geologica Sinica-English Edition*, 81(5), 739-755.

Palmer, A. R., & Repina, L. N. (1993). Through a glass darkly: taxonomy, phylogeny, and biostratigraphy of the Olenellina. *University of Kansas Paleontological Contributions,* 3, 1-35.

Paterson, J. R., García-Bellido, D. C., Jago, J. B., Gehling, J. G., Lee, M. S., & Edgecombe, G. D. (2016). The Emu Bay Shale Konservat-Lagerstätte: a view of Cambrian life from East Gondwana. *Journal of the Geological Society*, 173(1), 1-11.

Pates, S., & Daley, A. C. (2017). *Caryosyntrips*: a radiodontan from the Cambrian of Spain, USA and Canada. *Papers in Palaeontology*, 3(3), 461-470.

Pates, S., & Daley, A. C. (2018). The Kinzers Formation (Pennsylvania, USA): the most diverse assemblage of Cambrian Stage 4 radiodonts. *Geological Magazine*, Online early view: doi.org/10.1017/S0016756818000547.

Peel, J. S. (2010). Articulated hyoliths and other fossils from the Sirius Passet *Lagerstätte* (early Cambrian) of North Greenland. *Bulletin of Geosciences*, 85(3), 385-394.

Peng, J., Zhao, Y. L., & Sun, H. J. (2012). Discovery and significance of Naraoia from the Qiandongian (lower Cambrian) Balang Formation, Eastern Guizhou, South China. *Bulletin of Geosciences*, 87(1), 143-150.

Pi, D. H., Liu, C. Q., Shields-Zhou, G. A., & Jiang, S. Y. (2013). Trace and rare earth element geochemistry of black shale and kerogen in the early Cambrian Niutitang Formation in Guizhou province, South China: Constraints for redox environments and origin of metal enrichments. *Precambrian Research*, 225, 218-229.

Robison, R. A. (1984). New occurrences of the unusual trilobite Naraoia from the Cambrian of Idaho and Utah. *University of Kansas Paleontological Contributions,* 112, 1-8.

Skinner, E. S. (2005). Taphonomy and depositional circumstances of exceptionally preserved fossils from the Kinzers Formation (Cambrian), southeastern Pennsylvania. *Palaeogeography, Palaeoclimatology, Palaeoecology*, 220(1-2), 167-192.

Sun, H. J., Zhao, Y. L., Peng, J., & Yang, Y. N. (2014). New *Wiwaxia* material from the Tsinghsutung Formation (Cambrian Series 2) of Eastern Guizhou, China. *Geological Magazine*, 151(2), 339-348.

Wang, Y., Huang, D., & Hu, S. (2013). New anomalocardid frontal appendages from the Guanshan biota, eastern Yunnan. *Chinese Science Bulletin*, 58(32), 3937-3942.

Webster, M. (2011). Trilobite biostratigraphy and sequence stratigraphy of the upper Dyeran (traditional Laurentian 'Lower Cambrian') in the southern Great Basin, USA. *Museum of Northern Arizona Bulletin*, 67, 121-154.

Webster, M. & Landing, E. (2016). Geological context, biostratigraphy and systematic revision of late early Cambrian olenelloid trilobites from the Parker and Monkton formations, northwestern Vermont, USA. *Australasian Palaeontological Memoirs*, 49, 193-240.

Williams, M., Siveter, D. J., & Peel, J. S. (1996). Isoxys (Arthropoda) from the Early Cambrian Sirius Passet Lagerstätte, North Greenland. Journal of Paleontology, 70(6), 947-954.

Yang, C., Li, X. H., Zhu, M., Condon, D. J., & Chen, J. (2018). Geochronological constraint on the Cambrian Chengjiang biota, South China. *Journal of the Geological Society*, jgs2017-103.

Zhang, X. L., & Hua, H. (2005). Soft-bodied fossils from the Shipai Formation, lower Cambrian of the Three Gorge area, South China. *Geological Magazine*, 142(6), 699-709.

Zhou, C., & Jiang, S. Y. (2009). Palaeoceanographic redox environments for the lower Cambrian Hetang Formation in South China: evidence from pyrite framboids, redox sensitive trace elements, and sponge biota occurrence. *Palaeogeography, Palaeoclimatology, Palaeoecology*, 271(3-4), 279-286.

Analysis of the diversity and disparity of Radiodonta reveals two phases of evolution within the group

Supplemental 2

Ages of Cambrian BSTs, with justification for changes from Muscente et al. 2017

Age or unit	Reference	Edits from Muscente et al. 2017
Stage 3 (8)		
Niutitang Formation	Steiner 2005	
Hetang Formation	Zhou & Jiang 2009	Added
Sirius Passet	Daley & Peel 2010	
Zawiszyn Formation	Daley & Legg 2015	
Chengjiang biota	Hou et al. 1995	
Shuijingtuo Formation	Cui & Huo 2010; Daley et al. 2013	Added
Paseky Shale	Geyer et al. 2008	Moved from S4 to S3
Poleta Formation (lower levels)	English & Babcock 2010	
Stage 4 (15)		
Poleta Formation (upper level)	English & Babcock 2010	Moved from S3 to S4
Gibson Jack Formation	Robison 1984	Moved from S3 to S4
Cranbrook Shale	Briggs 1979	Moved from S3 to S4
Kinzers Formation	Briggs 1979	
Parker Slate	Conway Morris 1989; Muscente et al. 2017	
Latham Shale	Briggs & Mount 1982	
Jangle Limestone	*This thesis Chapter 7*	Added
Emu Bay Shale	McHenry & Yates 1993	
Bianmachong Formation	Steiner 2005	
Shipai Formation	Zhang & Hua 2010	
Balang Formation	Liu 2013	
Tsingsutung Formation	Sun et al. 2014	
Pioche Formation	Lieberman 2003	
Valdemiedes Formation	Pates & Daley 2017	Added
Wulongqing Formation	Weber et al. 2012; Wang et al. 2013	
Wuliuan (10)		
Kaili Formation	Zhao et al. 2005	Wuliuan only
Mantou Formation	Huang et al. 2012	Added
Bloomington Formation	Briggs & Robison 1984	

Rennie Shale	Conway Morris 1989; Muscente et al. 2017	
Pyramid Shale	*This thesis Chapter 8*	Added
Mount Cap Formation	Butterfield & Nicholas 1996	Wuliuan only
Spence Shale	Briggs & Robison 1984	
Burgess Shale	Collins et al. 1983	
Stanley Glacier	Caron et al. 2010	
Eldon Formation	Conway Morris 1989; Muscente et al. 2017	
Drumian (5)		
Wheeler Formation	Briggs & Robison 1984	
Marjum Formation	Briggs & Robison 1984	
Rockslide Formation	Kimmig & Pratt 2015	
Vermilion/Duchesnay units	Johnston et al. 2009	
Jince Formation	Fatka et al. 2011	Drumian only

Justification for moves:

Paskey Shale: this unit belongs to the Holsiny-Honce Formation, which itself correlates to the Issendalenian Stage (Western Gondwana) (Geyer et al. 2008). The Issendalenian globally correlates with for example the *Fallotaspis* Zone of Laurentia, and the *Schmidtiellus mickwitzi* zone in Baltica, and so is Stage 3 in age (Landing et al. 2013).

Poleta Formation: the radiodont bearing level is the uppermost of the three levels with exceptional preservation. This level is in the lowermost Dyeran (English & Babcock 2010). The other two levels are in the upper Montemezuman, and so are in Stage 3.

Gibson Jack Formation: the presence of *Olenellus* places this in the Dyeran (Robison 1984) which corresponds to Stage 4.

Cranbrook Formation: the presence of *Wanneria* trilobites means that this is middle '*Olenellus*' zone (Palmer & Repina 1993).

Kaili Formation: radiodont material is present in Wuliuan aged levels (Zhao et al. 2005).

Mount Cap Formation: radiodonts are only present in the Little Bear biota, which is Wuliuan in age (Harvey & Butterfield 2011).

Jince Formation: the Jince Formation stretches from uppermost Wuliuan to the Drumian, with radiodont material coming from high enough in the sequence that it is likely Drumian in age (Fatka et al. 2011; Fatka & Szabad 2014).

References

Briggs, D. E. (1979). *Anomalocaris*, the largest known Cambrian arthropod. *Palaeontology*, 22(3), 631-664.

Briggs, D. E., & Mount, J. D. (1982). The occurrence of the giant arthropod *Anomalocaris* in the Lower Cambrian of southern California, and the overall distribution of the genus. *Journal of Paleontology*, 56(5), 1112-1118.

Briggs, D. E., & Robison, R. A. (1984). Exceptionally preserved nontrilobite arthropods and *Anomalocaris* from the Middle Cambrian of Utah. *University of Kansas Paleontological Contributions*, 111, 1-23.

Butterfield, N. J., & Nicholas, C. J. (1996). Burgess Shale-type preservation of both non-mineralizing and 'shelly'Cambrian organisms from the Mackenzie Mountains, northwestern Canada. *Journal of Paleontology*, 70(6), 893-899.

Caron, J. B., Gaines, R. R., Mángano, M. G., Streng, M., & Daley, A. C. (2010). A new Burgess Shale–type assemblage from the "thin" Stephen Formation of the southern Canadian Rockies. *Geology*, 38(9), 811-814.

Collins, D., Briggs, D., & Morris, S. C. (1983). New Burgess Shale fossil sites reveal Middle Cambrian faunal complex. *Science*, 222(4620), 163-167.

Conway Morris, S. (1989). Burgess Shale faunas and the Cambrian explosion. *Science*, 246(4928), 339-346.

Cui, Z-L., & Huo, S-C., (1990). New discoveries of lower Cambrian crustacean fossils from western Hubei. *Acta Palaeontologica Sinica*, 3, 007.

Daley, A. C., & Peel, J. S. (2010). A possible anomalocaridid from the Cambrian Sirius Passet Lagerstätte, north Greenland. *Journal of Paleontology*, 84(2), 352-355.

Daley, A. C., Budd, G. E., & Caron, J. B. (2013). Morphology and systematics of the anomalocaridid arthropod *Hurdia* from the Middle Cambrian of British Columbia and Utah. *Journal of Systematic Palaeontology*, 11(7), 743-787.

Daley, A. C., & Legg, D. A. (2015). A morphological and taxonomic appraisal of the oldest anomalocaridid from the Lower Cambrian of Poland. *Geological Magazine*, 152(5), 949-955.

English, A. M., & Babcock, L. E. (2010). Census of the Indian Springs Lagerstätte, Poleta Formation (Cambrian), western Nevada, USA. *Palaeogeography, Palaeoclimatology, Palaeoecology*, 295(1-2), 236-244.

Fatka, O., Kraft, P., & Szabad, M. (2011). Shallow-water occurrence of Wiwaxia in the middle Cambrian of the Barrandian area, Czech Republic. *Acta Palaeontologica Polonica*, 56(4), 871-875.

Fatka, O., & Szabad, M. (2014). Cambrian biostratigraphy in the Pøíbram-Jince Basin (Barrandian area, Czech Republic). *Bulletin of Geosciences*, 89(2), 411-427.

Geyer, G., Elicki, O., Fatka, O., & Zylinska, A. (2008). Cambrian. *In* The Geology of Central Europe Volume 1: Precambrian and Palaeozoic. (Ed. McCann, T.). pp. 154-202. The Geological Society, London.

Harvey, T. H., & Butterfield, N. J. (2011). Great Canadian Lagerstätten 2. Macroand Microfossils of the Mount Cap Formation (Early and Middle Cambrian, Northwest Territories). *Geoscience Canada*, 38(4), 165-174.

Hou, X-G., Bergström, J., & Ahlberg, P. (1995). *Anomalocaris* and other large animals in the Lower Cambrian Chengjiang fauna of southwest China. *GFF*, 117(3), 163-183.

Huang, D., Wang, Y., Gao, J., & Wang, Y. (2012). A new anomalocaridid frontal appendage from the Middle Cambrian Mantou Formation of the Tangshan Area. *Acta Palaeontologica Sinica*, 51, 411-415.

Johnston, K. J., Johnston, P. A., & Powell, W. G. (2009). A new, Middle Cambrian, Burgess Shale-type biota, *Bolaspidella* Zone, Chancellor Basin, southeastern British Columbia. *Palaeogeography, Palaeoclimatology, Palaeoecology*, 277(1-2), 106-126.

Kimmig, J., & Pratt, B. R. (2015). Soft-bodied biota from the middle Cambrian (Drumian) Rockslide Formation, Mackenzie Mountains, northwestern Canada. *Journal of Paleontology,* 89(1), 51-71.

Landing, E., Geyer, G., Brasier, M. D., & Bowring, S. A. (2013). Cambrian evolutionary radiation: context, correlation, and chronostratigraphy—overcoming deficiencies of the first appearance datum (FAD) concept. *Earth-Science Reviews*, 123, 133-172.

Lieberman, B. S. (2003). A new soft-bodied fauna: the Pioche Formation of Nevada. *Journal of Paleontology*, 77(4), 674-690.

Liu, Q. (2013). The first discovery of anomalocaridid appendages from the Balang Formation (Cambrian Series 2) in Hunan, China. *Alcheringa*, 37(3), 338-343.

McHenry, B., & Yates, A. (1993). First report of the enigmatic metazoan *Anomalocaris* from the southern hemisphere and a trilobite with preserved appendages from the Early Cambrian of Kangaroo Island, South Australia. *Records of the South Australian Museum*, 26, 77-86.

Muscente, A. D., Schiffbauer, J. D., Broce, J., Laflamme, M., O'Donnell, K., Boag, T. H., Meyer, M., Hawkins, A. D., Huntley, J. W., McNamara, M., MacKenzie, L. A., Stanley Jr., G. D., Hunman, N. W., Hofmann, M. H., & Xiao, S. (2017). Exceptionally preserved fossil assemblages through geologic time and space. *Gondwana Research*, 48, 164-188.

Palmer, A. R., & Repina, L. N. (1993). Through a glass darkly: taxonomy, phylogeny, and biostratigraphy of the Olenellina. *University of Kansas Paleontological Contributions,* 3, 1-35.

Pates, S., & Daley, A. C. (2017). *Caryosyntrips*: a radiodontan from the Cambrian of Spain, USA and Canada. *Papers in Palaeontology*, 3(3), 461-470.

Robison, R. A. (1984). New occurrences of the unusual trilobite Naraoia from the Cambrian of Idaho and Utah. *University of Kansas Paleontological Contributions,* 112, 1-8.

Steiner, M., Zhu, M., Zhao, Y., & Erdtmann, B. D. (2005). Lower Cambrian burgess shale-type fossil associations of south China. *Palaeogeography, Palaeoclimatology, Palaeoecology*, 220(1-2), 129-152.

Sun, H. J., Zhao, Y. L., Peng, J., & Yang, Y. N. (2014). New *Wiwaxia* material from the Tsinghsutung Formation (Cambrian Series 2) of Eastern Guizhou, China. *Geological Magazine*, 151(2), 339-348.

Wang, Y., Huang, D., & Hu, S. (2013). New anomalocardid frontal appendages from the Guanshan biota, eastern Yunnan. *Chinese Science Bulletin*, 58(32), 3937-3942.

Weber, B., Hu, S., Steiner, M., & Zhao, F. (2012). A diverse ichnofauna from the Cambrian Stage 4 Wulongqing Formation near Kunming (Yunnan Province, South China). *Bulletin of Geosciences*, 87(1), 71-92.

Zhao, Y., Zhu, M., Babcock, L. E., Yuan, J., Parsley, R. L., Peng, J., Yang, X., and Wang, Y. (2005). Kaili Biota: a taphonomic window on diversification of metazoans from the basal Middle Cambrian: Guizhou, China. *Acta Geologica Sinica-English Edition*, 79(6), 751-765.

Zhou, C., & Jiang, S. Y. (2009). Palaeoceanographic redox environments for the lower Cambrian Hetang Formation in South China: evidence from pyrite framboids, redox sensitive trace elements, and sponge biota occurrence. *Palaeogeography, Palaeoclimatology, Palaeoecology*, 271(3-4), 279-286.

Analysis of the diversity and disparity of Radiodonta reveals two phases of evolution within the group

Supplemental 3

Characters for morphological character space analysis

#Overall organisation

1. Number of podomeres in the shaft
INTEGER, ORDERED

2. Number of podomeres in the medial region
INTEGER, ORDERED

3. Number of podomeres in the distal region
INTEGER, ORDERED

#Morphology of endite bases

4. Morphology of endite bases on the shaft podomeres
ORDERED
(0) none present
(1) shorter than the podomere to which they attach
(2) subequal in length to the podomere to which they attach
(3) subequal in length to the podomere to which they attach and thickened

5. Morphology of endite base on first medial podomere
(0) none present
(1) shorter than the podomere to which they attach
(2) subequal in length to the podomere to which they attach
(3) subequal in length to the podomere to which they attach and thickened
(4) at least twice the height of the podomere to which they attach

6. Morphology of endite bases on the medial podomeres
ORDERED
(0) none present
(1) shorter than the podomere to which they attach
(2) subequal in length to the podomere to which they attach
(3) at least twice the height of the podomere to which they attach

7. Arrangement of spinules on endite bases
(0) none present
(1) symmetric
(2) asymmetric, pointing distally

#Morphology of endites

8. Morphology of ventral endites on the shaft
ORDERED
(0) none present
(1) simple triangle
(2) elongate simple blade
(3) elongate blade with two flanking auxiliary blades
(4) elongate recurved blade
(5) elongate recurved blade with distally facing auxiliary spines

9. Morphology of endites on first medial podomere (sometimes 'hypertrophied endite')
(0) none present
(1) simple triangle
(2) elongate simple blade
(3) elongate blade with two flanking auxiliary blades
(4) thick central elongate blade with two flanking auxiliary blades
(5) elongate and recurved blade
(6) elongate and recurved blade with auxiliary spines on distal margin
(7) elongate and thickened recurved blade with auxiliary spines on distal margin
(8) elongate and thickened recurved blade with setae on distal margin

10. Morphology of endites on all other medial podomeres
(0) none present
(1) simple triangle
(2) elongate simple blade
(3) elongate blade with two flanking auxiliary blades
(4) thick central elongate blade with robust auxiliary blades on distal and proximal margins
(5) elongate recurved blade
(6) elongate recurved blade with auxiliary spines on distal margin
(7) elongate and thickened recurved blade with auxiliary spines on distal margin
(8) elongate and thickened recurved blade with setae on distal margin

11. Morphology of endites on distal podomeres
(0) none present
(1) mostly absent, one or two reduced endites present
(2) all present, but reduced in size, projecting from midpoint of ventral surface
(3) all present, but reduced in size, projecting from distal ventral surface

12. Relative lengths of endites on adjacent podomeres in medial region
(0) subequal
(1) alternate long/short

13. Length of endites in medial region
(0) all subequal in length
(1) general reduction distally, but endite on fifth podomere in medial region longer than that of third in medial region
(2) general reduction distally

14. Endites paired, and/or symmetric
(0) unpaired
(1) asymmetric
(2) symmetric

#Shape of podomeres

15. Morphology of flexible cuticle between podomeres
(0) simple line
(1) triangular

16. Shape of podomeres in medial region
ORDERED
(0) rectangular, longer than tall
(1) square
(2) rectangular, taller than long

17. Shape of podomeres in distal region
ORDERED
(0) rectangular, longer than tall
(1) square
(2) rectangular, taller than long

#Morphology of other (non-endite) spines

18. Composition of distalmost dorsal and terminal spines ('claw')
ORDERED
(0) none present
(1) single reduced straight spine
(2) single recurved spine
(3) two to four recurved spines
(4) five or more recurved spines

19. Morphology of 'claw' spines
(0) thin
(1) thick

20. Number and morphology of dorsal spines not included in 'claw'
(0) none present
(1) fewer than five, small spines
(2) five or greater, small spines
(3) single row of small spines
(4) single row of small spines with five or more large spines
(5) five or more large single pointed spines
(6) five or more large double pointed spines

Analysis of the diversity and disparity of Radiodonta reveals two phases of evolution within the group

Supplemental 4

Morphological character matrix

Character	1	2	3	4	5	6	7	8	9	10	11	12	13	14	15	16	17	18	19	20
Tamisocaris borealis	1	18	1	0	4	3	1	2	1	1	0	0	0	2	1	2	0	0	0	0
Tamisiocaris sp. Kinzers	?	?	1	?	4	3	0	?	1	1	?	0	0	2	1	1	1	0	0	0
Anomalocaris briggsi	1	11	2	3	4	3	1	5	1	1	2	0	0	2	1	2	0	4	0	0
Anomalocaris sp. Chengjiang	2	12	1	3	3	2	0	3	3	3	0	1	2	2	1	2	1	3	1	0
Anomalocaris saron	2	9	4	0	3	2	2	1	3	3	2	1	2	2	1	2	1	3	0	0
Anomalocaris pennsylvanica	1	12	1	2	2	2	0	2	2	2	2	1	2	2	1	2	2	4	0	0
Anomalocaris canadensis	1	9	4	0	1	1	0	1	3	3	3	1	2	2	1	2	1	4	0	0
Anomalocaris sp. EBS	1	9	4	3	3	1	0	3	3	3	?	1	2	2	1	2	1	4	0	0
Anomalocaris kunmingensis	1	9	4	0	3	1	2	1	4	3	2	1	2	2	1	2	2	4	1	0
Anomalocaris magnabasis	2	9	4	3	3	2	2	3	3	3	3	1	2	2	1	2	1	4	0	0
Paranomalocaris multisegmentalis	3	13	6	1	1	1	1	3	4	3	2	1	2	2	1	2	1	4	0	3
Ramskoeldia platyacantha	3	9	4	2	3	1	1	3	3	3	2	1	1	1	1	2	2	4	0	0
Ramskoeldia consimilis	3	9	4	0	3	1	1	1	4	3	2	1	1	1	1	2	2	3	0	0
Amplectobelua sp. Kinzers	?	11	1	0	3	0	0	?	4	2	3	1	1	1	1	2	2	3	1	1
Amplectobelua stephenensis	?	9	3	?	3	0	0	?	7	1	0	1	1	1	1	2	2	4	1	0
Amplectobelua symbrachiata	2	11	1	0	3	0	0	0	4	2	1	1	1	1	1	2	2	4	1	5
Lyrarapax trilobus	2	6	3	0	0	0	0	1	7	2	1	1	2	2	1	1	2	3	0	1
Lyrarapax unguispinus	?	6	6	?	0	0	0	0	7	3	0	1	2	2	1	1	2	4	0	1
Laminacaris chimera	2	12	1	0	0	1	2	2	7	3	2	1	2	?	1	2	2	4	1	2
Laminacaris? Kinzers	2	?	?	?	0	1	2	5	7	3	?	0	0	2	1	2	?	?	?	?
Caryosyntrips serratus	1	12	1	0	0	0	0	0	1	1	0	0	0	2	1	2	2	2	0	3
Caryosyntrips camurus	1	12	1	0	0	0	0	0	1	1	0	0	0	2	1	2	2	2	0	0
Caryosyntrips durus	1	?	1	0	0	0	0	0	1	1	0	0	0	2	1	2	2	2	0	4

Analysis of the diversity and disparity of Radiodonta reveals two phases of evolution within the group

Supplemental 4

Morphological character matrix

Hurdia victoria	2	5	5	0	0	0	0	2	7	7	1	0	0	0	0	2	1	1	0	2
Hurdia triangulata	2	5	5	0	0	0	0	0	7	7	0	0	0	0	0	2	1	1	0	2
Peytoia infercambriensis	?	?	?	0	0	0	0	?	7	7	?	0	2	0	0	1	1	0	0	0
Peytoia nathorsti	1	5	5	0	0	0	0	0	7	7	0	0	0	0	0	2	2	1	0	2
Peytoia sp. Balang	2	5	3	0	0	0	0	0	7	7	0	0	0	0	0	2	2	2	0	0
Stanleycaris hirpex	2	5	5	0	0	0	0	2	7	7	1	0	0	0	0	2	1	1	0	6
Stanleycaris sp. Wheeler	2	5	5	0	0	0	0	0	7	7	1	0	0	0	0	2	1	1	0	5
Hurdiid appendage Fezouata	3	5	4	0	0	0	0	0	7	7	1	0	0	0	0	2	1	0	?	2
Pahvantia hastata	5	5	?	2	0	0	0	5	8	8	0	0	0	0	0	0	?	0	?	1
Aegirocassis benmoulai	1	5	1	0	0	0	0	2	8	8	0	0	0	0	0	1	1	1	0	0
Schinderhannes bartelsi	3	5	1	0	0	0	0	0	7	7	0	0	0	0	0	2	1	?	0	0
Ursulinacaris grallae	2	5	5	0	0	0	0	4	6	6	1	0	0	2	0	2	2	0	0	0
Hurdiid body Spence	?	5	?	?	0	0	0	4	7	5	?	0	0	0	0	2	?	?	?	?
Peytoia? Burgess Shale	2	5	5	0	0	0	0	4	6	6	1	0	0	0	0	2	2	1	0	0

Analysis of the diversity and disparity of Radiodonta reveals two phases of evolution within the group

Supplemental 5

Results of Principal coordinate analysis

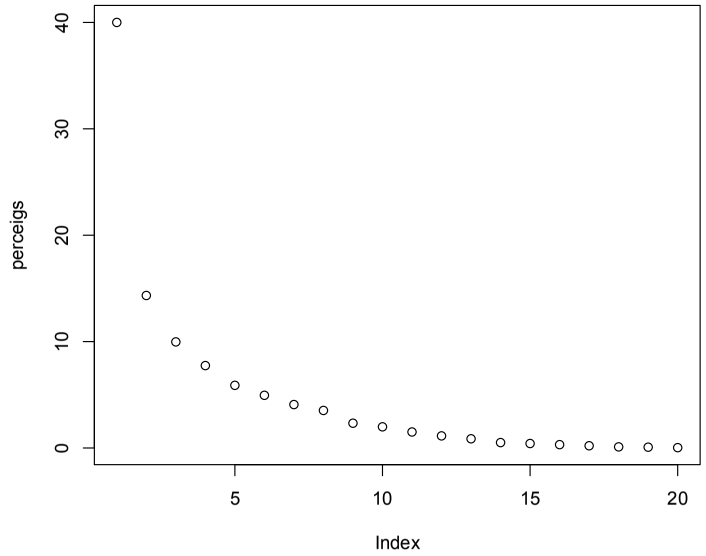

[Principal coordinate] eigenvalue percentage
[1] 40.00039099
[2] 14.33467701
[3] 9.97269144
[4] 7.74554790
[5] 5.88932192
[6] 4.95141844
[7] 4.08254843
[8] 3.52834010
[9] 2.32976406
[10] 1.98948539
[11] 1.50536473
[12] 1.13810324
[13] 0.86497177
[14] 0.50884410
[15] 0.42066068
[16] 0.31510500
[17] 0.20923958
[18] 0.10441832
[19] 0.07711926
[20] 0.03198766

Raw eigenvalues

[Principal coordinate] raw eigenvalue
[1] 2.120866e+00
[2] 7.600410e-01
[3] 5.287635e-01
[4] 4.106778e-01
[5] 3.122586e-01
[6] 2.625299e-01
[7] 2.164614e-01
[8] 1.870766e-01
[9] 1.235268e-01
[10] 1.054848e-01
[11] 7.981616e-02
[12] 6.034354e-02
[13] 4.586179e-02
[14] 2.697950e-02
[15] 2.230391e-02
[16] 1.670723e-02
[17] 1.109412e-02
[18] 5.536379e-03
[19] 4.088951e-03
[20] 1.696022e-03
[21] -1.110223e-16
[22] -2.152132e-03
[23] -6.357678e-03
[24] -8.715602e-03
[25] -9.319447e-03
[26] -1.509599e-02
[27] -1.865247e-02
[28] -2.503095e-02
[29] -3.166119e-02
[30] -3.788687e-02
[31] -4.366503e-02
[32] -5.444183e-02
[33] -6.561398e-02
[34] -7.073332e-02
[35] -8.231581e-02
[36] -9.396865e-02
[37] -1.257716e-01

Analysis of the diversity and disparity of Radiodonta reveals two phases of evolution within the group

Supplemental 6

Tabulated jackknifed sums of ranges and sums of variances

Sums of ranges

Low k value tree	Observed	SE	Mean	Bias
Amplectobeluidae	3.198671	0.1259419	3.057103	-0.9909759
Anomalocarididae	2.961597	0.2480762	2.826374	-0.9465676
Caryosyntrips	0.7509978	0.08046383	0.5006652	-0.5006652
Hurdiidae	3.293789	0.3556167	3.214232	-1.034236
Hurdiidae (Cambrian only)	3.163475	0.4252875	3.067435	-1.056442
Tamisiocarididae	1.65132	0.2411759	1.10088	-1.10088

High k value tree	Observed	SE	Mean	Bias
Amplectobeluidae	3.44054	0.2133562	3.260001	-1.263774
Anomalocarididae	2.701161	0.2015749	2.584612	-0.8158403
Caryosyntrips	0.7509978	0.08046383	0.5006652	-0.5006652
Hurdiidae	3.100947	0.3783444	3.006357	-1.040486
Hurdiidae (Cambrian only)	2.960572	0.4724859	2.838189	-1.101451
Tamisiocarididae	1.65132	0.2411759	1.10088	-1.10088

Sums of variances

Low k value tree	Observed	SE	Mean	Bias
Amplectobeluidae	0.1026578	0.008515231	0.1026578	0
Anomalocarididae	0.07265586	0.01568959	0.07265586	-9.714451e-17
Caryosyntrips	0.009625111	0.003306044	0.009625111	-1.040834e-17
Hurdiidae	0.05769855	0.01315587	0.05769855	1.804112e-16
Hurdiidae (Cambrian only)	0.06050845	0.01623711	0.06050845	-7.632783e-17
Tamisiocarididae	0.06224359	0.03193571	0.06224359	0

High k value tree	Observed	SE	Mean	Bias
Amplectobeluidae	0.1109499	0.008175538	0.1109499	0
Anomalocarididae	0.05997257	0.01134017	0.05997257	-4.857226e-17
Caryosyntrips	0.009625111	0.003306044	0.009625111	-1.040834e-17
Hurdiidae	0.05610464	0.01475174	0.05610464	7.632783e-17
Hurdiidae (Cambrian only)	0.05912189	0.0189336	0.05912189	-6.245005e-17
Tamisiocarididae	0.06224359	0.03193571	0.06224359	0

Cambrian stages comparisons

Sums of ranges

	Observed	SE	Mean	Bias
Stage 3	4.19917	0.2768078	4.028672	-1.534477
Stage 4	4.408217	0.3065069	4.316936	-1.186659
Wuliuan	3.431251	0.4003597	3.321054	-1.101979
Drumian	2.713944	0.6532828	2.472038	-1.209532

Sums of variances

	Observed	SE	Mean	Bias
Stage 3	0.1398429	0.02043504	0.1398429	0
Stage 4	0.1445472	0.01630093	0.144547	0
Wuliuan	0.09809832	0.0237831	0.09809832	-1.387779e-16
Drumian	0.08834116	0.02990401	0.08834116	-6.938894e-17

Time bin comparisons

Sums of ranges

	Observed	SE	Mean	Bias
Div1	4.19917	0.2768078	4.028672	-1.534477
Div2	3.14715	0.3322474	2.85162	-1.477647
Div3	4.038536	0.2307507	3.842928	-1.564866
Div4	3.431251	0.4003597	3.321054	-1.101979
Div5	2.713944	0.6532828	2.472038	-1.209532

Sums of variances

	Observed	SE	Mean	Bias
Div1	0.1398429	0.02043504	0.1398429	0
Div2	0.1277477	0.03970352	0.1277477	-1.387779e-16
Div3	0.1551345	0.02241526	0.1551345	2.220446e-16
Div4	0.09809832	0.0237831	0.09809832	-1.387779e-16
Div5	0.08834116	0.02990401	0.08834116	-6.938894e-17

Appendix 4

Supplemental material for Chapter 12

Quantitative analysis of repaired and unrepaired damage to trilobites from the Cambrian (Stage 4 – Drumian) Iberian Chains, NE Spain

Supplemental Information

Code for statistical calculations in Pates, Bicknell, Daley and Zamora.

```
#to be run in R

#binomial test to see if spines are adjacent more than expected by chance (10 adjacent injured spines, 15 injured spines total. Find probability of any spine adjacent to this injured spine)

binom.test(10,14,p=2/2207,alternative='two.sided')

#binomial to test asymmetry in injury location (8 right sided injuries, 16 injuries in total)

binom.test(8,16,p=0.5,alternative='two.sided')

#binomial to test selection for rear 3 thoracic segments (of 16 overall) (6 injuries on posterior 3, out of 10 injuries on complete trilobites in total)

binom.test(6,10,p=3/16,alternative = 'two.sided')

#Calculations of Bayesian Inference 5th and 95th percentile values (for R and F repair frequencies)
#general formula: qbeta(c(0.05,0.95),z+1,n-z+1) #z=number of injuries (for F)/number of injured trilobites (for R); n=number of trilobites

#to plot the curve to see shape of distribution, use dbeta and same general formula:

dbeta(x, z+1, n-z+1)
```

Posterior distributions from Bayesian inference analysis

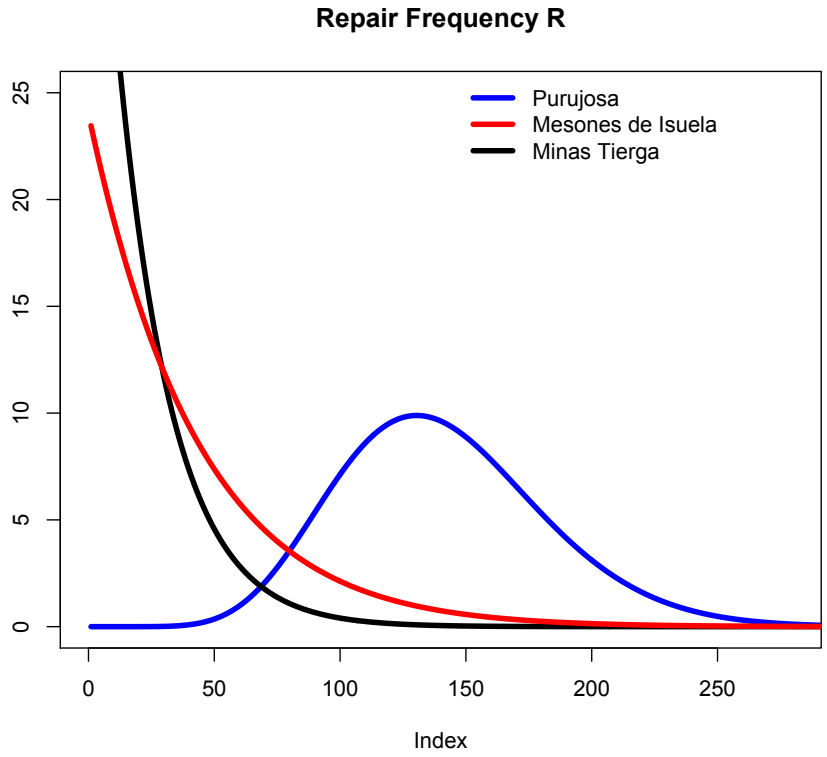

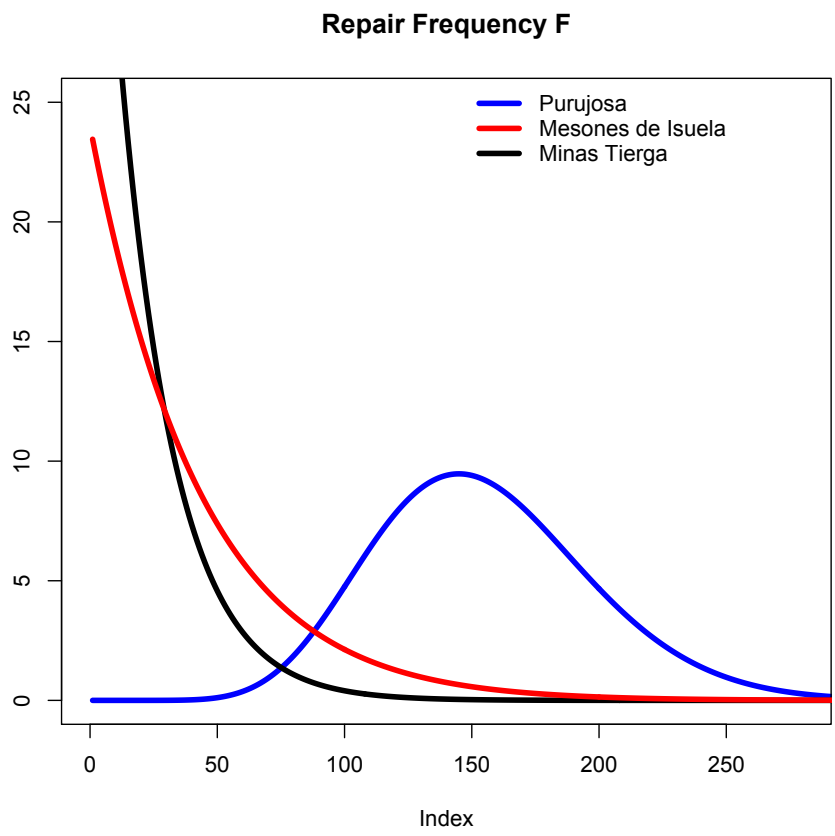

Images of trilobites from private collection studied for injuries

Histograms of specimen lengths from three sites

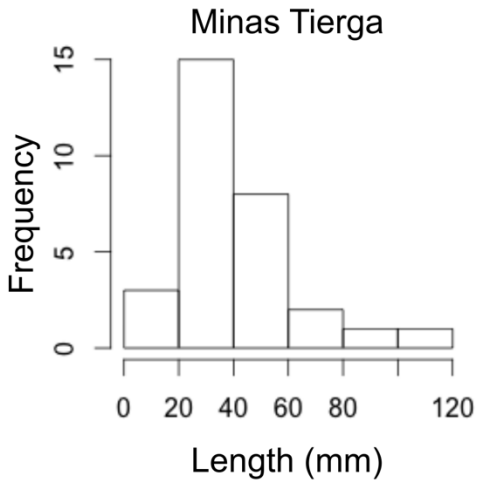
Minas Tierga
Frequency
0
5
10
15
0
20
40
60
80
120
Length (mm)

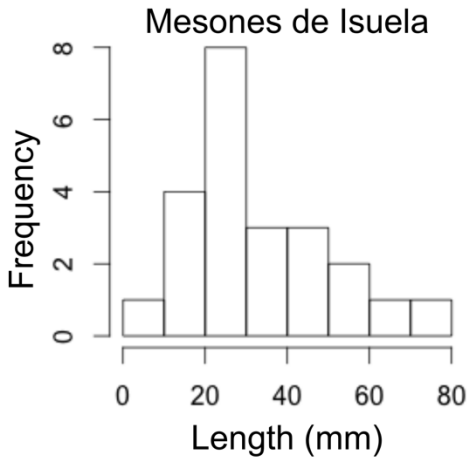
Mesones de Isuela
Frequency
0
2
4
6
8
0
20
40
60
80
Length (mm)

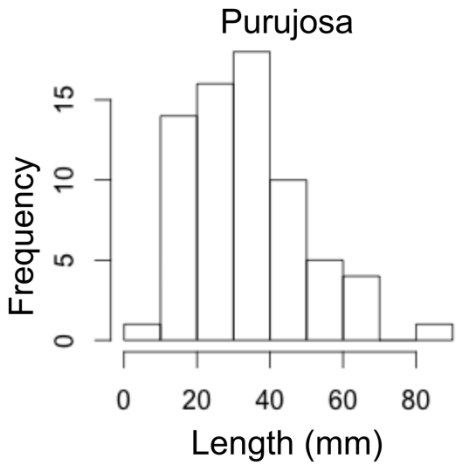
Purujosa
Frequency
0
5
10
15
0
20
40
60
80
Length (mm)